

This electronic version (PDF) was scanned by the International Telecommunication Union (ITU) Library & Archives Service from an original paper document in the ITU Library & Archives collections.

La présente version électronique (PDF) a été numérisée par le Service de la bibliothèque et des archives de l'Union internationale des télécommunications (UIT) à partir d'un document papier original des collections de ce service.

Esta versión electrónica (PDF) ha sido escaneada por el Servicio de Biblioteca y Archivos de la Unión Internacional de Telecomunicaciones (UIT) a partir de un documento impreso original de las colecciones del Servicio de Biblioteca y Archivos de la UIT.

هذه النسخة الإلكترونية (PDF) للاتصالات الدولي الاتحاد في والمحفوظات المكتبة قسم أجراه الضوئي بالمسح تصوير نتاج (ITU) والمحفوظات المكتبة قسم في المتوفرة الوثائق ضمن أصلية ورقية وثيقة من نقلاً.

此电子版（PDF版本）由国际电信联盟（ITU）图书馆和档案室利用存于该处的纸质文件扫描提供。

Настоящий электронный вариант (PDF) был подготовлен в библиотечно-архивной службе Международного союза электросвязи путем сканирования исходного документа в бумажной форме из библиотечно-архивной службы МСЭ.

© International Telecommunication Union

XVII A.P.
DÜSSELDORF
21.5-1.6 1990
CCIR

XVIIth PLENARY ASSEMBLY
DÜSSELDORF, 1990

INTERNATIONAL TELECOMMUNICATION UNION

REPORTS OF THE CCIR, 1990

(ALSO DECISIONS)

ANNEX TO VOLUME VI

PROPAGATION IN IONIZED MEDIA

CCIR INTERNATIONAL RADIO CONSULTATIVE COMMITTEE

ARCHIVES U.I.T. GENÈVE

Geneva, 1990

XVII A.P.
DÜSSELDORF
21.5-1.6 1990
CCIR

XVIIth PLENARY ASSEMBLY
DÜSSELDORF, 1990

INTERNATIONAL TELECOMMUNICATION UNION

REPORTS OF THE CCIR, 1990

(ALSO DECISIONS)

ANNEX TO VOLUME VI

PROPAGATION IN IONIZED MEDIA

CCIR INTERNATIONAL RADIO CONSULTATIVE COMMITTEE

92-61-04221-X

Geneva, 1990

© I.T.U.

ANNEX TO VOLUME VI

PROPAGATION IN IONIZED MEDIA

(Study Group 6)

TABLE OF CONTENTS

Page

Plan of Volumes I to XV, XVIIth Plenary Assembly of the CCIR (see Volume VI - Recommendations) .....

Distribution of texts of the XVIIth Plenary Assembly of the CCIR in Volumes I to XV (see Volume VI - Recommendations) .....

Table of contents I

Numerical index of texts V

Index of texts deleted VII

Section 6A - Ionospheric properties

Report 725-3 Ionospheric properties 1

Report 886-2 Special properties of the high latitude ionosphere affecting radiocommunications 16

Report 574-2 Ionospheric cross-modulation 41

Report 728-3 Ionospheric modification by ground-based, high-power radio transmissions 50

Report 893-1 Solar power satellites and the ionosphere 59

Report 1011-1 Artificial modification of the ionosphere by chemical injections 60

Report 887-2 Models of extraterrestrial plasmas 61

Section 6B - Radio noise

Report 258-5 Man-made radio noise 67

Report 322-3 Characteristics and applications of atmospheric radio noise data (Published separately) 75

Report 1151 Application of radio noise and interference data for system design 75

Report 342-6 Radio noise within and above the ionosphere 77

ARCHIVES U.I.T. GENÈVE

Page

Report 254-7 Measurement of atmospheric radio noise 93

Section 6C - Ionospheric propagation and operational forecasting

Report 726-2 Ground and ionospheric side- and back-scatter 103

Report 890-2 The operational use of side-scatter and back-scatter ... 109

Report 249-7 The use of oblique sounding for propagation analysis and optimization 112

Report 250-6 Long-distance ionospheric propagation without intermediate ground reflection 118

Report 262-7 ELF, VLF and LF propagation in and through the ionosphere 126

Report 727-3 Short-term prediction of solar-induced variations of operational parameters for ionospheric propagation 131

Report 888-2 Short-term forecasting of critical frequencies, operational maximum usable frequencies and total electron content 140

Report 889-2 Real-time channel evaluation of HF ionospheric radio circuits 149

Section 6D - Ionospheric propagation prediction at frequencies below about 1.6 MHz

Report 575-4 Methods for predicting sky-wave field strengths at frequencies between 150 kHz and 1705 kHz 167

Report 432-2 The accuracy of predictions of sky-wave field strength in bands 5 (LF) and 6 (MF) 185

Report 431-5 Analysis of sky-wave propagation measurements for the frequency range 150 to 1600 kHz 191

Report 265-7 Sky-wave propagation and circuit performance at frequencies between about 30 kHz and 500 kHz 212

Report 895-2 Radio propagation and circuit performance at frequencies below about 30 kHz 230

Section 6E - Ionospheric propagation prediction at frequencies between about 1.6 and 30 MHz

Report 340-6 CCIR atlas of ionospheric characteristics (Published separately) 259

Report 255-7 Long-term ionospheric propagation predictions 259

Page

Report 1012-1 Operational modelling of HF radio propagation conditions at high latitudes 268

Report 894-2 CCIR HF propagation prediction method 273

Report 252-2 CCIR interim method for estimating sky-wave field strength and transmission loss at frequencies between the approximate limits of 2 and 30 MHz (Published separately) 284

Supplement to Report 252-2 Second CCIR computer-based interim method for estimating sky-wave field strength and transmission loss at frequencies between 2 and 30 MHz (Published separately) 284

Report 729-3 Developments in the estimation of sky-wave field strength and transmission loss at frequencies above 1.5 MHz 285

Report 891-2 Antenna characteristics important for the analysis and prediction of sky-wave propagation paths 292

Report 266-7 Ionospheric propagation and noise characteristics pertinent to terrestrial radiocommunication systems design and service planning. (Fading) 298

Report 892-2 Computation of reliability for HF radio systems 316

Section 6F - Ionospheric propagation prediction and applications at frequencies above about 30 MHz

Report 263-7 Ionospheric effects upon Earth-space propagation 327

Report 259-7 VHF ionospheric propagation 358

Report 251-5 Communication by meteor-burst propagation 377

Report 260-3 Ionospheric scatter propagation 388

Section 6G - Ionospheric propagation measurements and data banks

Report 253-5 Measurement of sky-wave signal intensities at frequencies above 1.6 MHz 389

Report 1150 Standardized procedure for comparing predicted and observed HF sky wave signal intensities and results of such comparisons 409

Report 571-4 Comparisons between observed and predicted sky-wave signal intensities at frequencies between 2 and 30 MHz .. 418

Page

Report 1149 HF field strength measurements. Specifications for a field strength measurement campaign intended for future improvements in prediction methods, particularly those used for HF broadcasting 427

Report 430-5 Improvement in the world-wide ionospheric observing programme for numerical mapping purposes 444

Decisions

Decision 6-7 Sky-wave field strength and transmission loss at frequencies above 1.6 MHz 453

Decision 9-5 Radio propagation and circuit performance at frequencies below about 500 kHz 455

Decision 11-6 VHF and UHF propagation by sporadic E and other ionospheric regions 456

Decision 57-2 Sky-wave propagation at frequencies between 150 and 1700 kHz 458

Decision 83 HF measurements and data banks 460

Decision 84 The potential for an HF field-strength measurement campaign to provide a significant measurement data bank in time for preparations for a WARC HFBC in 1993 ... 462

Decision 85 Studies of the propagation prediction method for HF broadcasting 463

Decision 86 Preparation of a CCIR handbook on HF radio systems design 464

NUMERICAL INDEX OF TEXTS

ANNEX TO VOLUME VI

		Page
SECTION 6A:	Ionospheric properties	1
SECTION 6B:	Radio noise	67
SECTION 6C:	Ionospheric propagation and operational forecasting	103
SECTION 6D:	Ionospheric propagation prediction at frequencies below about 1.6 MHz	167
SECTION 6E:	Ionospheric propagation prediction at frequencies between about 1.6 and 30 MHz	259
SECTION 6F:	Ionospheric propagation prediction and applications at frequencies above about 30 MHz	327
SECTION 6G:	Ionospheric propagation measurements and data banks	389

REPORTS	Section	Page	REPORTS	Section	Page
249-7	6C	112	575-4	6D	167
250-6	6C	118	725-3	6A	1
251-5	6F	377	726-2	6C	103
252-2	6E	284	727-3	6C	131
253-5	6G	389	728-3	6A	50
254-7	6B	93	729-3	6E	285
255-7	6E	259	886-2	6A	16
258-5	6B	67	887-2	6A	61
259-7	6F	358	888-2	6C	140
260-3	6F	388	889-2	6C	149
262-7	6C	126	890-2	6C	109
263-7	6F	327	891-2	6E	292
265-7	6D	212	892-2	6E	316
266-7	6E	298	893-1	6A	59
322-3	6B	75	894-2	6E	273
340-6	6E	259	895-2	6D	230
342-6	6B	77	1011-1	6A	60
430-5	6G	444	1012-1	6E	268
431-5	6D	191	1149	6G	427
432-2	6D	185	1150	6G	409
571-4	6G	418	1151	6B	75
574-2	6A	41			

Note - Decisions which already appear in numerical order in the table of contents, are not reproduced in this index.

PAGE INTENTIONALLY LEFT BLANK

PAGE LAISSEE EN BLANC INTENTIONNELLEMENT

INDEX OF TEXTS WHICH HAVE BEEN DELETED AT THE END OF THE STUDY PERIOD 1986-1990

(In order to facilitate the retrieval of a given text, the page number of Volume VI of the XVIth Plenary Assembly, Dubrovnik 1986, is indicated.)

ANNEX TO VOLUME VI

Text	Title	Page No. Vol. VI Dubrovnik, 1986
Report 1013	Microcomputer-based methods for the estimation of HF radio propagation and circuit performance	268
Report 1014	Prediction of sky-wave field strength for broadcasting in Region 2 in the band 1605-1705 kHz	339
Report 1015	Sky-wave field strength prediction method for propagation to aircraft at 500 kHz	360
Decision 10-5	Operational parameters for ionospheric radio circuits	470
Decision 82	HF field strength measurement campaign	230*

*Conclusions of the Interim Meeting of Study Group 6 (Geneva, 1988).

SECTION 6A: IONOSPHERIC PROPERTIES

REPORT 725-3

IONOSPHERIC PROPERTIES

(Question 25/6)

(1978-1982-1986-1990)

1. Introduction

The ionosphere is the ionized region in the earth's atmosphere extending from about 50 km to roughly 2000 km above the surface. For reasons related to the historical development of ionosphere research, the ionosphere is divided into three regions (or layers) designated D, E and F, respectively, in order of increasing altitude (see Fig. 1). Subdivisions of these layers may exist under certain conditions, for example F1 and F2 layers. From the viewpoint of HF propagation, the E and F layers act principally as radio wave reflectors, and permit long range propagation between terrestrial terminals. The D region acts principally as an absorber, causing signal attenuation in the HF range, although VLF and ELF waves are reflected at D-region altitudes. The transition between reflection at D-region altitudes and E-region altitudes occurs in the medium frequency range. The ionosphere is also an important factor in space communications at VHF and higher frequencies, since the signal is modified and degraded to varying degrees in passing through the ionosphere.

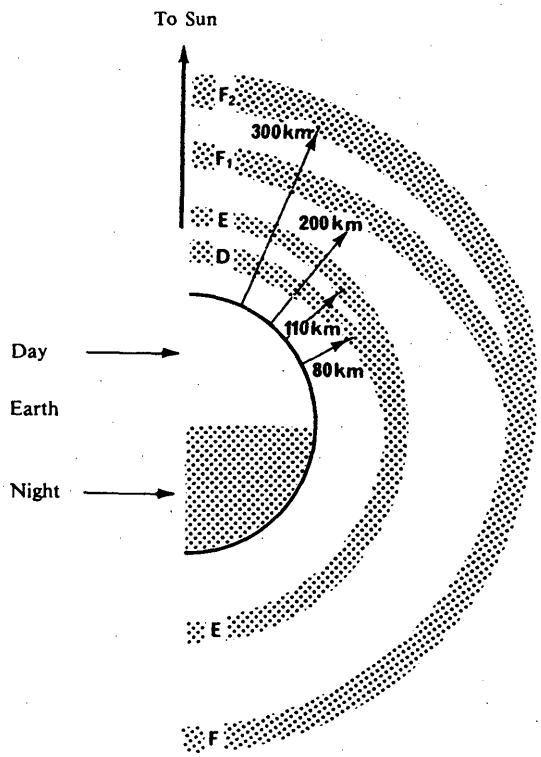


FIGURE 1 – *Ionospheric regions as a function of height above the Earth's surface*

ARCHIVES U.I.T. GENÈVE

2. Ionospheric production processes

The principal source of ionization in the ionosphere is electromagnetic radiation from the sun extending over the ultra-violet and X-ray portions of the spectrum. Other sources of ionization are however important, such as energetic charged particles of solar and magnetospheric origin and galactic cosmic rays. The ionization rate at various altitudes depends upon the intensity of the solar radiation as a function of wavelength, and the ionization efficiency of the neutral atmospheric gases. Since the Sun's radiation is progressively absorbed in passing through the atmosphere, its residual ionizing ability depends upon the length of the atmospheric path, and consequently upon the solar zenith angle (χ). The maximum ionization rate occurs when the Sun is overhead ($\chi = 0$), but geographic, diurnal and seasonal variations in the ionization density are found.

The production of free ionization by solar radiation (and charged particles) is counter-balanced by ionization loss processes, principally the collisional recombination of electrons and positive ions, and the attachment of electrons to neutral gas atoms and molecules. It is possible to determine, from physical principles, a reasonably realistic mathematical description of the altitude distribution of ionization, based on estimates of the solar ionizing flux, the vertical distribution of neutral atmospheric constituents and their absorption efficiency, and the solar zenith angle. This was first done by Chapman [1931] for a single constituent, isothermal atmosphere ionized by monochromatic solar radiation. This seems to be a reasonably good approximation for the formation of the E and F1 layers but is a poor representation for the D and F2 layers.

In the lowest part of the ionosphere, below about 65 km altitude, the dominant source of ionization is galactic cosmic rays. Consequently the variation of electron density at these altitudes is not dominated by the solar zenith angle dependence.

3. D region

The D region spans the approximate altitude range 50 to 90 km with electron density increasing rapidly with altitude. The D-region electron density exhibits large diurnal variations with maximum density shortly after local solar noon and small values at night. This diurnal variation is greatest in the altitude interval 70 to 90 km, with typical noon values of 10^8 to 10^9 electrons/m^3. There is a pronounced seasonal variation in D-region electron densities with a maximum in summer. In winter, although the solar zenith angle is greater, there often appears anomalously high electron density in the 70 to 90 km range, probably resulting from neutral atmosphere composition changes. The solar-cycle variation in D-region electron density is different at different altitudes. In the 70 to 90 km range, where solar X-rays are the dominant source, ionization is maximum at the peak of the solar cycle. Below 70 km, where production by cosmic rays dominates, maximum densities are found at solar minimum, because of reduced interplanetary scattering of galactic cosmic rays. For undisturbed days following a geomagnetic storm and associated with its recovery phase, the electron density in the 75 to 90 km range is enhanced in sub-auroral latitudes and mid-latitudes ($L = 4.5 - 2.0$) due to precipitation of energetic electrons from the outer radiation belt [Larsen *et al.*, 1976; Wagner *et al.*, 1982a and b].

4. E region

The altitude range from 90 to 130 km constitutes the E region and encompasses the so-called "normal" and "sporadic"-E layers. The former is a regular layer which conforms closely to the Chapman model, displaying a strong solar zenith angle dependence with maximum density near noon and a seasonal maximum in summer. The altitude of maximum density is about 110 km, with a value of approximately 10^{11} electrons/m^3, corresponding to a maximum plasma frequency of about 3 MHz. At night, only a small residual level of ionization remains in the E region, with typical plasma frequency of 0.4 to 0.6 MHz [Wakai, 1971]. The solar cycle dependence exhibits a maximum layer density at solar maximum, with a variation in daytime E-layer plasma frequency of about 30% over the solar cycle at a given location. The "sporadic"-E layer is discussed in § 8.1.

5. F region

The F region extends upward from about 130 km. At night the F region displays a different variation from the daytime F region which often is sub-divided into F1 and F2 layers, although the vertical electron density profile may display no clear stratification.

The F1 layer is the region between 130-210 km altitude, in which the maximum electron density is about $2 \times 10^{11}/m^3$. Like the E layer, the F1 layer follows the Chapman model approximately, but with a solar zenith angle dependence which is different from that of the E layer. The distinction between the F1 and F2 layers is not maintained at night.

The F2 layer is the highest ionospheric layer, and usually exhibits the greatest electron density, which may range typically from $10^{12}/m^3$ in daytime to about $5 \times 10^{10}/m^3$ at night. The F2 layer is not well represented by the Chapman formulation, since it is strongly influenced by winds, diffusion and other dynamic effects. In the early days of ionospheric research, when the Chapman model was thought to be valid, various significant departures from expected behaviour were termed "anomalies", although this term is now inappropriate.

The "diurnal anomaly" refers to the fact that maximum F2-layer electron density often occurs at times other than solar noon (typically 1300 to 1500 hours local time). Furthermore, the maximum F2-layer electron density shows a semi-diurnal variation with maxima around 10 h to 11 h (local time) and 22 h to 23 h (local time) [Matuura, 1980]. The "seasonal anomaly" is the observed tendency for maximum F2-layer densities, at around 1200 h (local time) in winter, to exceed the corresponding summer values. The "equatorial anomaly" refers to the marked departure from solar zenith angle dependence of F2-layer densities within 20° to 30° either side of the geomagnetic equator. At high latitudes, a variety of anomalous F2-layer features are observed, some of which are now associated with charged particle precipitation. The F-region "trough" is a pronounced depression in the F2-layer electron density resulting from magnetospheric convection, that extends from about 2° to 10° equatorward from the auroral oval in the late afternoon and night-time ionosphere.

Observations of electron density at altitudes above the height of maximum density determined from incoherent scatter radars, rockets and satellite-borne sounders indicate that the electron density decays approximately exponentially with height. At about 1,000 km, there is a change in electron density gradient caused by a transition from mainly O^+ to mainly H^+. The height at which this transition occurs increases with increasing latitude. The electron density is typically between 10^9 and 10^{10} electrons/m^3 at 1,000 km height, and about 10^9 electrons/m^3 at 5,000 km. Observations of electron densities determined from satellite-borne topside sounders in the upper ionosphere reveal that the equatorial anomaly can extend well beyond 500 km in altitude. In addition, these measurements show that the mid and high latitude F-region trough of depressed electron density in the night-time ionosphere is also a predominant feature of the topside ionosphere.

The special features of the F region near the equator and at high latitudes which have important effects on radio wave propagation are discussed in the following sections.

5.1 *Equatorial F region*

It is well known from both ground-based and satellite observations that significant latitudinal gradients exist in the F-layer ionization at low latitudes and that the form of the trans-equatorial distribution of foF2 changes markedly with local time [Awe, 1973]. Around sunrise a single maximum of ionization exists near the magnetic equator. Shortly thereafter, the latitudinal distribution of ionization changes sharply with the appearance of two crests separated by a narrow trough 2 to 5 degrees wide centred on the magnetic equator [Vila, 1971a; Walker and Chan, 1976]. By late morning the latitudinal separation of the crests has increased and the crests have increased in ionization density [Rastogi, 1959; Croom *et al.*, 1960; Lyon and Thomas, 1963; Rao and Malhotra, 1964]. Except in the northern winter, the northern crest is farther from the dip equator than is the southern, and in northern summer, the northern crest can reach its maximum latitude excursion several hours earlier than the southern crest [Sharma and Hewens, 1976]. The time at which the crests are farthest from the magnetic equator varies with solar activity occurring in the early afternoon during solar minimum and in the early evening during solar maximum [Rush *et al.*, 1969]. Later the crests move equatorward finally merging together to form a maximum of ionization above the equator.

It is now well established that the crest formation is explained by an "equatorial fountain" mechanism, connected with Hall drift, which is upwards when the electric field of the equatorial electrojet is in the eastward direction.

Considerable day-to-day variability is seen in the time of onset, decay and maximum development of the anomaly [Vila, 1971b; Rush and Miller, 1972]. Marked differences can occur between the latitudinal distributions of foF2 observed on a particular day at the same local time, but separated in longitude by only 30°.

The latitudinal variation of foF2 across the equator is often asymmetrical; that is the critical frequencies at the two crests are appreciably different [Lyon and Thomas, 1963]. This asymmetry appears to be due to thermospheric winds blowing across the equator from the sub-solar latitude [Bramley and Young, 1968]; in general, the crest which lies farther from the sub-solar latitude will be the greater. In the topside ionosphere, however, the situation is reversed with the crest of the anomaly being more pronounced in the summer hemisphere [Rush *et al.*, 1969].

Figure 2 shows an example of the structure of the topside ionosphere when the anomaly exists, together with the corresponding latitudinal variations of NmF2 and hmF2. It shows that the anomaly crests occur at the two points where a magnetically field-aligned arch of enhanced ionization intersects the peak of the layer; this arch extends into the topside ionosphere to altitudes of the order of 1000 km. The height of the layer peak is greatest (approximately 400 km) above the magnetic equator and decreases rapidly on either side to about 300 km near the location of the crests. During the development phase of the anomaly, the arch of enhanced ionization moves to higher magnetic field lines such that its top extends to greater altitudes and the crests move away from the equator. During the decay phase there is evidence [Eccles and King, 1969] which suggests that the top of the arch decreases in altitude and the crests move back towards the equator. The time at which the anomaly develops and decays in different longitude sectors varies appreciably [King *et al.*, 1964; Lockwood and Nelms, 1964]. The equatorial anomaly factor (the ratio of the mean foF2 at the two maxima north and south of the magnetic equator to foF2 at the magnetic equator) shows a longitude-dependent diurnal variation which appears as a difference between eastern hemisphere (60° E-150° W) and western hemisphere (120° W-30° E) [Matuura, 1980].

On magnetically disturbed days the anomaly crests are usually closer to the magnetic equator and the anomaly is not as well-developed as it is on quiet days. When the planetary magnetic index $K_p \geq 5_0$, the anomaly is absent [King *et al.*, 1967; Sharma and Hewens, 1976].

5.2 *High-latitude F region*

The high-latitude F-region is an extremely variable and dynamic region as exhibited by several quasi-permanent features. The most prominent feature is an area of severely depressed night-time F-region electron densities, referred to as the F-region trough equatorward of the auroral oval (see Figure 1, Report 886). The maximum electron density may be reduced by as much as an order of magnitude. Enhanced electron densities are observed on the dayside region immediately poleward of the auroral oval (see Figure 5, Report 886). The region in the vicinity of the magnetic pole is one of depleted electron density, sometimes referred to as the "polar cavity". Further discussion of high latitude variability is given in Report 886.

Results of several years of investigation of high-latitude F-region phenomenology and morphology are summarized by Hunsucker [1979].

6. Electron collision frequencies

Collisions between electrons and neutral particles are of great importance to some aspects of radio-wave propagation, particularly for the role they play in the attenuation of radio waves. The collision frequency/height profile in the D region, which is the region where the electron collision frequency is high ($\simeq 2 \times 10^6$ s^{-1} at 75 km), may be estimated from laboratory studies of the mobility of electrons in atmospheric gases [Smith, 1967], in combination with rocket-borne measurements of atmospheric temperature and number density (or pressure); or it may be determined quite independently from analysis of radio-wave propagation data [Belrose and Bourne, 1967; Thrane, 1968; Smith, 1967]. There is much evidence both in radio and pressure data, that the collision frequency in the D region changes with season, latitude, and on some occasions with solar activity. The variability from day to day is especially marked at high latitudes in winter.

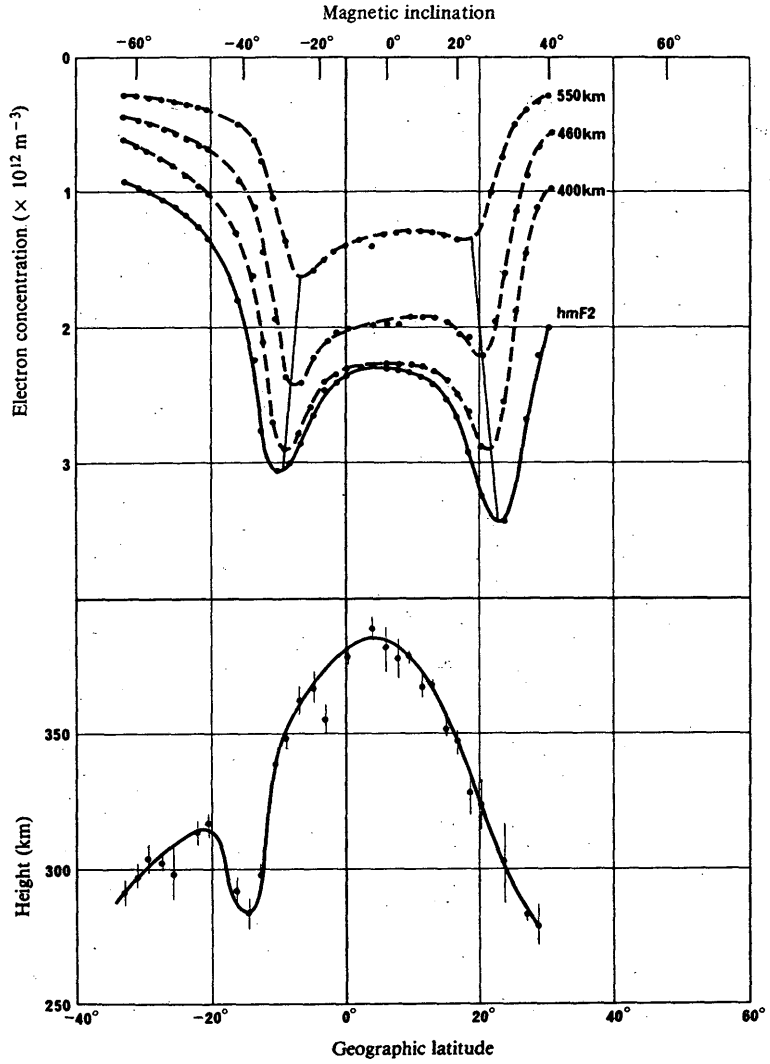


FIGURE 2 – *Data obtained from ISIS-1 ionograms recorded on 27 October, 1969, at 160° E longitude, 1505 LMT*

Upper section: latitudinal variations of NmF2 (continuous curve) and electron concentration at fixed heights in the topside ionosphere (broken curves). The thin lines join points which lie on a magnetic field line.

Lower section: the corresponding variation of hmF2

In the E and F regions collisions with ions become important; furthermore in the F region the electron and gas temperatures can be different. Collision frequency versus height profiles in the height range 100 to 200 km have been derived that are consistent with radio-wave propagation data. They are based on multi-frequency HF polarization and absorption measurements (with electron density versus height profiles determined in the same experiments) and on rocket probe measurements [Biryukov *et al.*, 1978; Gusev *et al.*, 1977; Vodolazkin *et al.*, 1983]. Day-time results show an exponential decrease in electron collision frequency with height, as expected according to the decrease in atmospheric pressure, to heights of about 140 km, but above that height the collision frequency increases with increasing height due to electron-ion collisions, reaching values that are 3 to 6 times the gas kinetic value. At night as compared to day, the effective collision frequency increases by six to seven times in summer and by three to four times in winter.

7. Total electron content

A single parameter of the ionization distribution which is very significant in determining trans-ionospheric propagation effects is the integral $\int N ds$, that is the integrated or total electron content (TEC) along the ray path from transmitter to receiver. When used without qualification TEC is usually taken to mean the content of a vertical column of unit cross-section, but for practical applications it is generally the content along a slant path that is required; thus in any particular case it is important to make clear whether slant or vertical values are being quoted. The slant TEC is greater than the vertical TEC by a factor that is often assumed to be equal to the secant of the zenith angle of the ray path at an ionospheric height in the vicinity of the F-layer maximum. The factor is usually less than this because of the preponderance of ionization in the topside of the layer.

7.1 *TEC measurements*

Measurements of TEC have been carried out since the mid-1960s ——— using primarily the Faraday rotation technique with VHF transmissions from either low-orbit (≈ 1000 km) or geostationary (35 800 km) satellites [Davies, 1980]. In practice, the vertical TEC, $\int N dh$, up to the height of the satellite, h_s, is estimated from the measured Faraday rotation Ω by use of:

$$\Omega = (KM/f^2) \int_0^{h_s} N \, dh \qquad (1)$$

where K is a constant, f is the frequency and M is the value of $B_L \sec(\mathrm{ZEN})$ at some suitable height. B_L is the longitudinal component of the Earth's magnetic induction and ZEN is the zenith angle of the ray [Rishbeth and Garriott, 1969].

It has been shown that, for a wide range of ionospheric profiles, the total content up to a height of 2000 km may be estimated to within 5% by using a value of M appropriate to a height of 420 km [Titheridge, 1972]. This TEC is usually referred to as the ionospheric or Faraday content N_I, as distinct from the total content N_T up to the geostationary satellite height. N_T can be measured by a VHF group delay method [Soicher, 1976] which is practically independent of the magnetic field, so that electrons at all points along the ray path have an equal effect. Measurements of the differential phase shift between coherent frequencies in the gigahertz range have also been used for this purpose [Awaka and Fujita, 1978]; in this method the effect of the geomagnetic field is entirely negligible. The difference between N_T and N_I is often called the protonospheric or plasmaspheric content (N_p). Generally, the ratio N_p/N_I varies from approximately 15% during the day to greater than 50% during the night [Soicher, 1977].

The ionospheric content N_I is in general closely related to the F2-layer critical frequency foF2, and depends strongly on latitude, local time, season, solar flux and geomagnetic activity. At low magnetic latitudes it exhibits the same equatorial anomaly as shown by foF2 (see § 5.1). Figure 3 gives examples of contours of N_I for the four seasons of the solar-minimum year 1966 [de Mendonca *et al.*, 1969], in which the behaviour of the southern crest of the anomaly is clearly shown. In middle latitudes N_I has been observed for many years at a number of stations, and its behaviour is relatively well documented. Latitude – local time contour maps for different seasons have been produced, for example in a European sector [Amayenc *et al.*, 1971] and in North America [Mendillo and Klobuchar, 1975]. In the latter study, the coverage extended northwards through and beyond the high latitude ionospheric trough, which is most marked during winter night-time. Other high-latitude TEC studies are described by Hargreaves *et al.* [1980].

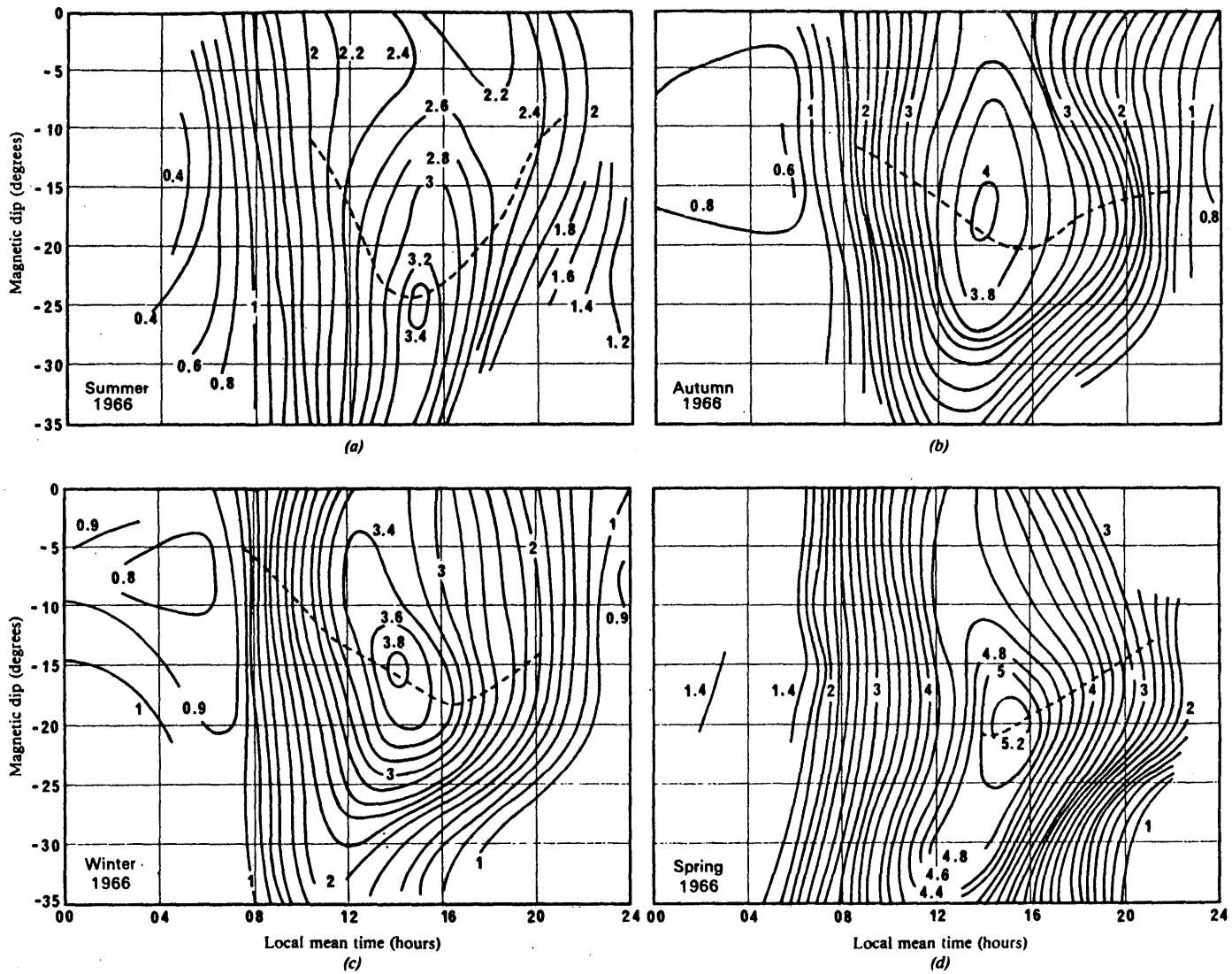


FIGURE 3 – *Example of ionospheric electron content (N_I) at low magnetic dip latitudes. The contours give N_I values in units of 10^{17} el/m² [de Mendonca et al., 1969]*

7.2 *TEC models*

Various groups have attempted to model N_I by one of the following approaches:

- predictions of N_I using extensive data bases at a small number of sites [Waldman and da Rosa, 1971] or using foF2 data and a model for the slab thickness N_I/NmF2, again derived from detailed studies at only a few sites [Klobuchar and Allen, 1970; Rao *et al.*, 1971; Minakoshi, 1987];
- calculation of N_I by integration of a predicted $N(h)$ profile [Bent *et al.*, 1975; Feen *et al.*, 1975; Lee and Nisbet, 1975].

Most of these models were derived, at least in part, from measurements made in the northern hemisphere, and they may be expected to apply best at mid-latitudes. A simplified model intended to give first-order accuracy (50% reduction in error for ionospheric time delay) on a world-wide basis has however been produced by a combination of the above methods [Klobuchar, 1975].

These simple models are able to predict monthly median TEC to within an r.m.s. error of 20-25% in daytime and 30-35% at night [Dulong, 1977]. A slab thickness model is useful for correction of TEC effects. The advantage is that day-to-day deviations of calculated TEC with a slab thickness model from daily observed TEC can be reduced if daily observed foF2 data are available [Minakoshi, 1988].

Greater accuracy can probably only be achieved by the use of near real-time systems, especially in difficult areas such as the equatorial and auroral regions. Studies of the spatial correlation of TEC by Klobuchar [1977] indicate that day-time TEC values are correlated with a coefficient of approximately 0.7 for separations of 2900 km east-west and 1800 km north-south.

8. Ionospheric irregularities

Various physical processes generate irregular structure in the ionosphere which displays strong temporal and geographical variations. Depending on the radio frequency being used, the method of observation, and the magnetic latitude of the observation, the irregularities produce a variety of qualitatively different effects. In regard to latitudinal variations it is convenient to consider three regions: the equatorial zone which extends approximately 20° on either side of the geomagnetic equator; the high latitude region which includes the auroral zone that extends equatorward of the auroral oval to approximately 57° corrected geomagnetic latitude and the polar cap that is poleward of the auroral oval; and the mid-latitude region which occupies the intermediate range of latitudes. There are well defined seasonal and diurnal variations in irregularity intensity in each of these regions.

8.1 *Sporadic E*

"Sporadic E" (Es) is the anomalous ionization which occurs at E-region altitudes, assumes various different forms, sometimes irregular and patchy, sometimes smooth and disk-like, and has little direct relationship to solar ionizing radiation. The properties of sporadic E are markedly different in three fairly well-defined regions — equatorial, high latitude and mid-latitude. A comprehensive world-wide survey of sporadic E has been prepared by Whitehead [1970]. Further progress is reviewed in a special issue of Radio Science [Matsushita and Smith, 1975].

8.1.1 *Equatorial sporadic E*

Sporadic-E layers are present during a high percentage of the daytime, but the latitude of maximum occurrence varies with longitude (Report 259).

In a narrow zone near the dip equator, a special type of sporadic E appears regularly during daylight hours [Matsushita, 1962; Knecht and McDuffie, 1962]. The width of this zone is approximately ± 6° in magnetic dip varying slightly with season, by approximately 1° towards the summer hemisphere [Giraldez *et al.*, 1981] and it is thus quite narrow in comparison with the width of the equatorial anomaly. This "equatorial" sporadic-E layer is usually observed during daylight, is highly transparent and gives high vertical incidence reflection frequencies; values of about 10 MHz are regularly observed using ionosondes near the dip equator. The structure of the sporadic-E irregularities, which are magnetically field-aligned, has been inferred by Cohen *et al.*, [1962] from radar observations at Jicamarca, Peru. It appears that the origin of the irregularities is associated with the equatorial electrojet [Mayaud, 1965]. Theories involving plasma instabilities have been proposed [Farley, 1963; Waldteufel, 1965] to account for their formation.

8.1.2 *High-latitude——sporadic E*

The morphology and dynamics of high-latitude Es are described by Bates and Hunsucker [1974] and Hunsucker [1975].

The auroral E region is characterized by several phenomena produced by auroral particle ionization and occurring almost continuously around the auroral oval. A relatively regular thick layer of ionization resembling the solar E-layer, referred to as auroral E, exists primarily at night and is a reflecting layer. Other auroral E region phenomena are referred to as sporadic E (Es) and are classified according to their appearance on vertical incidence ionograms /Piggott and Rawer, 1972; 1978/. These Es layers may be thin and patchy causing abrupt, mirror-like reflection as well as partial transmission. Auroral sporadic E can cause rapid fading and multipath problems on HF communications. Auroral sporadic E occurrence is positively correlated with the presence of visible aurora.

Sporadic E within the polar cap exhibits a different character from auroral Es. It is substantially weaker and displays a negative correlation with geomagnetic activity. Polar cap sporadic E extends in bands or ribbons across the polar cap, roughly in the direction of the sun and may be associated with weak sub-visual auroral optical emissions.

8.1.3 Mid-latitude *sporadic E*

The peak sporadic-E electron density at mid-latitudes may often reach a value many times that of the ambient E-region, the ionization being distributed in patches ranging in spatial extent from several kilometres to 1000 km and with thickness typically 500 to 2000 m. The height of the sporadic-E layer is usually in the range 95 to 135 km with a most probable value of 110 km. Kerblaï and Nosova [1980] and Minullin /1988/ have developed statistical models for prediction of Es parameters and reflection characteristics.

At mid-latitudes sporadic E occurs most frequently in summer daytime. The diurnal variation exhibits maxima in the mid-morning hours and near sunset, lagging the growth and decay of the regular-E region. The seasonal variation is complex and possibly related to the upper atmosphere winds; the seasonal minimum is usually near midwinter or the spring equinox. This seasonal behaviour changes abruptly at about 57° corrected geomagnetic latitude, the boundary of the auroral Es zone.

8.2 *F-region irregularities*

8.2.1 *Equatorial F region*

Ionization irregularities in the F region tend to develop in the evening about one hour or so after local sunset and possess scale-sizes from about 3 m to more than 10 km. The irregularities appear to be associated with the change in the height of F layer above the dip equator during the evening [Booker and Wells, 1938; Osborne, 1951; Wright, 1959; Lyon *et al.*, 1961; Aarons, 1982]. Generally the irregularities are more widespread in the equinoxes but may be different in different longitudes.

Topside soundings carried out during sunspot maximum revealed that equatorial spread F activity is high at longitudes from 0°W to 60°W in northern winter months and from 90°W to 180°W in northern summer months, while it tends to be widespread in the equinoxes [Maruyama and Matuura, 1984]. The occurrence probability of topside spread F shows two night-time peaks; one at post-sunset and the other pre-sunrise in

the low latitude region [Maruyama and Matuura, 1980]. Muldrew [1980a] found that the occurrence frequency of intense spread ("bubbles") maximizes near 23 hours local time. The occurrence of irregularities in the equatorial F region appears to decrease during times of geomagnetic disturbance [Fang and Liu, 1983].

The irregularities tend to be field-aligned with axial ratios of the order of 20 to 1 [Cohen and Bowles, 1961; Kent and Koster, 1967]. Calvert and Schmid [1964] have concluded from top-side sounder data that not only individual irregularities, but also entire patches of irregularities, are field-aligned. Patches of irregularities sometimes cover large areas. Kotadia [1959] has reported good day-to-day correlation of spread-F echoes between Ahmedabad, Kodaikanal and Singapore during the equinox, but not the solstice, months. Cohen and Bowles [1961] have studied the motion of irregularity patches using successive vertical incidence ionograms and concluded that they extend up to 1000 km in the E-W direction. Satellite data suggest patch sizes of 100 to 2000 km in the N-S direction and 500 to 3000 km in the E-W direction. On the other hand, HF back-scatter data [Clemesha, 1964] indicate patch sizes of 30 to 400 km, with a mean value of 100 km, in the E-W direction.

These earlier results have been corroborated and elaborated upon by the use of data from more detailed *in situ* satellite-borne measurements and ground-based scintillation observations. With the use of these data it has become fully appreciated that F-region ionization irregularities display significant longitudinal variability in addition to latitudinal and temporal dependencies. Details of these findings as well as the effect of equatorial irregularities on the performance of transionospheric propagation systems can be found in the review by Aarons [1977].

Equatorial irregularities were found by Lockwood and Petrie [1963], using Alouette-1 ionograms, to extend up to about 600-1000 km height in the topside ionosphere. Dyson and Benson [1978], using Alouette-2 and ISIS-1, found that radio waves were ducted by small-scale field-aligned irregularities (approximately 1 km length) which existed within large-scale field-aligned irregularity patches or bubbles (approximately 100 km extent). The electron density distribution within the ducts was not symmetrical with respect to the equator. Statistical studies of these ducts [Muldrew, 1980a and b] indicated that Cole's [1971] theory, of interchange of magnetic flux tubes due to field-aligned currents, can best explain the initial formation of the irregularities. When such regions are traversed by a probing radio wave, the associated Faraday rotation shows depletions of the electron content. Experimental evidence indicates that average depletions are of the order of 1.5 to 3.0 $\times$ 10^{16} el/m^2. Further, the amplitude scintillation rate may increase suddenly when these bubbles either form along or drift across the propagation path [Yeh *et al.*, 1979]. There is evidence that there are also isolated enhancements in the ambient electron content, and these are accompanied by simultaneous decrease in fading rate, scintillation index, and the signal's average amplitude level [Tyagi *et al.*, 1982]. The generation of a large-scale bubble can be very localized and the resulting large-scale irregularity patches may exist for several hours [Aarons and Buchau, 1978]. The irregularities maximize in the June solstice at Asian longitudes and in the December solstice at American longitudes.

8.2.2 *High latitude F region*

The F region in the auroral night-time ionosphere very often displays substantially lower electron densities than the E region, and is virtually always irregular in nature. Very large latitudinal gradients occur frequently at the equatorward and poleward edges of the auroral zone. Poleward of the auroral oval at magnetic noon, irregular F-region ionization of relatively high intensity is almost always observed. The irregularities in the structure of the high latitude ionosphere are discussed in more detail in Report 886 and in a special issue of Radio Science [Hunsucker and Greenwald, 1983].

9. Ionospheric disturbances

Ionospheric disturbances denote a temporary departure from the normal state of the ionosphere, and are associated with features in the solar wind or with solar flare events. These disturbances are important as they often result in marked changes in propagation conditions, including the interruption of ionospheric radiocommunications over wide areas for periods of a few minutes up to several days.

The occurrence of a solar flare event may be accompanied by the emission of electromagnetic radiation in the form of ultraviolet and X-rays, visible light and radio waves. Other emissions may be in the form of charged particles.

Ionospheric disturbances can be classified into several types, and these are discussed in the following sub-sections. More details are given in Report 886.

9.1 Sudden ionospheric disturbances

Occasionally a sudden outburst on the Sun, a Solar X-Ray flare event or more simply a solar flare, produces abnormally high ionization densities in the D region. This ionospheric phenomenon, called a Sudden Ionospheric Disturbance (SID), results in a sudden increase in the absorption of MF, HF, and VHF radio waves (VLF and LF field strength can be enhanced). Because SIDs are produced by direct X-ray and ultraviolet radiations from the Sun, they occur only on the sunlit side of the Earth, and are most frequent at solar maximum.

The increased extreme ultra-violet (EUV) and soft X-rays emitted from the Sun during a flare cause a sudden increase in the total electron content (SITEC) of the ionosphere. A SITEC generally occurs within minutes of the optical flare and causes N_I enhancements in the 5 to 30% range [Mendillo *et al.*, 1974]. The increase may partially decay away in 10 to 30 minutes but may simply raise the level of the normal N_I variation for the next few hours.

9.2 Ionospheric storms

Ionospheric storms, which may last for several days, are caused by streams of charged particles of solar origin, deflected by the Earth's magnetic field towards the auroral zones. They are accompanied by an increase in electron density in the D region and an expansion and diffusion of the F2 region which can result in decreased critical frequencies and increased layer heights. The effects of ionospheric storms are most severe at solar maximum but are more significant relative to communications at solar minimum.

The precise behaviour during an individual storm is a complex function of latitude, season, local time of sudden commencement, and many other factors still actively being studied. However a simplified general pattern may be represented by a positive phase of several hours, attributable primarily to electrodynamic lifting, in which N_I increases can be 100% or more, followed by a depression of 50 to 75% below normal values, which lasts for a day or more and is probably due to an enhanced loss rate arising from changes in the neutral atmosphere. Average storm patterns of the variations in TEC, as a function of season and invariant latitude, have been sufficiently defined in amplitude and resolved in local time to permit a realistic prediction technique for F-region disturbance effects [Mendillo and Klobuchar, 1980].

Geomagnetic disturbances, especially those of an intense global nature (storms) are associated with ionospheric disturbances with highly localized characteristics which are particularly intense during the main phase of the storm. Both types of disturbance exhibit recovery effects which can last for days. In particular some days after the main phase of a geomagnetic storm, the D-region ionization density is increased at sub-auroral and middle latitudes. This increase can last ten or more days [Lauter et al., 1977]. The effects of anomalous D-region ionization on radio-wave propagation are reviewed by Larsen [1979].

9.3 Auroral sub-storms

More common than geomagnetic storms, sub-storms are short (time scales of an hour or two), sometimes severe, geomagnetic disturbances primarily affecting the high latitude zones. Sub-storms are accompanied by intense charged particle precipitation, electric fields, plasma diffusion and heating of the neutral atmosphere. All radio propagation parameters may vary rapidly under the influence of an auroral sub-storm; those variations most frequently noted are found in D-region absorption and sporadic E. Total electron content can be significantly affected. Further discussion of the effects of high latitude ionospheric disturbances on propagation is given in Report 886.

9.4 Polar cap absorption

There are also infrequent but major disturbances which occur throughout the polar regions at corrected geomagnetic latitudes greater than 60 to 65°. These are called polar cap absorption (PCA) events and are caused by solar proton events (SPE) which almost always originate in major solar flares. This influx of high-energy solar protons into the relatively unshielded polar regions considerably increases D-region ionization resulting in strong absorption of HF and VHF radio waves. A total polar radio-wave blackout may exist for up to a day but the PCA as well as its effect on VLF and LF propagation can last for several days to a week or more. During solar maximum years, when SPEs are more prevalent, night-time LF propagation at latitudes greater than 75° can be dominated by SPE events since the recovery from one event may not be complete before another begins.

9.5 Man-made disturbances

Man, by altering the state of the upper atmosphere, may also cause ionospheric disturbances. These can result from any of the following activities:

- heating the ionosphere by powerful radio waves;
- releasing chemically active substances in the atmosphere;
- high altitude nuclear detonations releasing ionizing radiation and producing shock waves ;
- electron beam injection.

The effects of heating the ionosphere are described in Report 728 and Report 893. The effects of the chemical changes in the ionosphere are described in Report 1011. High altitude nuclear explosions have produced the strongest and most extensive ionospheric effects: e.g., black-outs, phase-deviations and travelling ionospheric disturbances over distances of thousands of kilometres [Baker and Davies, 1968].

10. Applications to radio communications

The ionosphere can support radio propagation to great ranges at very low frequencies. Reports 265 and 895 treat propagation in this frequency range. Propagation in the medium frequency range (150-1600 kHz) is discussed in Report 431, from which it is apparent that ionospheric (sky-wave) propagation is most important at night, since daytime absorption is high. The frequency range 3 to 30 MHz is the one in which ionospheric propagation is most important for long range terrestrial propagation. Report 252, the supplement to Report 252 and Report 894 deal with computation of field strengths of sky-waves at these frequencies. In the VHF range (30 to 300 MHz) and beyond, radio waves usually penetrate the ionosphere, but may, under certain conditions, support ground-to-ground propagation by scattering from ionospheric irregularities and sporadic E: Reports 259 and 263 deal with propagation in the VHF and UHF ranges.

REFERENCES

AARONS, J. [1977] Equatorial scintillations: A review. *IEEE Trans. Ant. Prop.*, **25**, 729-736.

AARONS, J. [1982] Global morphology of ionospheric scintillations. *Proc. IEEE*, Vol. 70, 360-378.

AARONS, J. and BUCHAU, J. [1978] The localized origin of equatorial F-region irregularity patches. *J. Geophys. Res.*, **83**, 1659-1664.

AMAYENC, P., BERTIN, F. and PAPET-LEPINE, J. [1971] Sur l'évolution latitudinale du contenu électronique de l'ionosphère. *Ann. de Géophys.*, **27**, 345-357.

AWAKA, J. and FUJITA, M. [1978] Measurement of total electron content by means of differential phase shift method using coherent SHF signals from a geostationary satellite. *J. Atmos. Terr. Phys.*, **39**, 1441-1446.

AWE, O. [1973] Behaviour of the F2 layer in the tropical region. Proc. 4th International Symposium on Equatorial Aeronomy, Ibadan. Ed. E. Oni, 682-690.

BAKER, D. M. and DAVIES, K. [1968] Waves in the ionosphere produced by nuclear explosions. *J. Geophys. Res.*, **73**, 448-451.

BATES, H. F. and HUNSUCKER, R. D. [1974] Quiet and disturbed electron density profiles in the auroral zone ionosphere. *Radio Sci.*, **9**, 455-467.

BELROSE, J. S. and BOURNE, I. A. [1967] The electron distribution and collision frequency height profile for the lower part of the ionosphere (The D- and lower E-regions): A review of Observational Data, Proc. of Conference on Ground Based Radio Wave Propagation Studies of the Lower Ionosphere, 79-96. Defence Res. Board, Ottawa, Canada.

BENT, R. B., LLEWELLYN, S. K., NESTERCZUK, G. and SCHMID, P. E. [1975] The development of a highly-successful world-wide empirical ionospheric model and its use in certain aspects of space communications and world-wide total electron content investigations. Proc. Symposium on the Effect of the Ionosphere on Space Systems and Communications, 23-38. Naval Research Laboratory, Arlington, Va., USA.

BIRYUKOV, A. V., DANILKIN, N. P., DENISENKO, P. F., KUCHERENKO, G. M., KNORIN, I. A., RUDAKOV, V. A., SOTSKY, V. V., FAER, Yu. N. and SHNYREVA, L. A. [1978] Measurements of electron density and collision rate during the flight of Vertikal '4. *Cosmic Res.*, USA., Vol. 16, **5**, 578-582.

BOOKER, H. G. and WELLS, H. W. [1938] Scattering of radio waves by the F-region of the ionosphere. *Terr. Magn. Atmos. Elect.*, **43**, 249-256.

BRAMLEY, E. N. and YOUNG, M. [1968] Winds and electromagnetic drifts in the equatorial F2-region. *J. Atmos. Terr. Phys.*, **30**, 99-111.

CALVERT, W. and SCHMID, C. W. [1964] Spread-F observations by the Alouette topside sounder satellite. *J. Geophys. Res.*, **69**, 1839-1852.

CHAPMAN, S. [1931] The absorption and dissociative or ionizing effect of monochromatic radiation in an atmosphere on a rotating earth. *Proc. Roy. Soc.*, **43**, 26.

CLEMESHA, B. R. [1964] An investigation of the irregularities in the F-region associated with equatorial spread-F. *J. Atmos. Terr. Phys.*, **26**, 91-112.

COHEN, R. and BOWLES, K. L. [1961] On the nature of equatorial spread-F. *J. Geophys. Res.*, **66**, 1081-1106.

COHEN, R., BOWLES, K. L. and CALVERT, W. [1962] On the nature of equatorial slant sporadic-E. *J. Geophys. Res.*, 67, 965-972.

COLE, K. D. [1971] Formation of field-aligned irregularities in the magnetosphere. *J. Atmos. Terr. Phys.*, **33**, 741-750.

CROOM, S., ROBBINS, A. and THOMAS, J. O. [1960] Variations of electron density in the ionosphere with magnetic dip. *Nature*, **185**, 902-903.

DAVIES, K. [1980] Recent progress in satellite radio beacon studies with particular emphasis on the ATS-6 radio beacon experiment. *Space Sci. Revs.*, Vol. 25, 357-430.

DE MENDONCA, F., KANTOR, I. J. and CLEMESHA, B. R. [1969] Low latitude ionospheric electron content measurements during half a solar cycle. *Radio Sci.*, **4**, 823-828.

DULONG, D. D. [1977] Reduction of the uncertainty of radar range correction. AFGL-TR-77-0125 (NTIS Accession No. AD A046166) National Technical Information Service, Springfield, Va. 22161, USA.

DYSON, P. L. and BENSON, R. F. [1978] Topside sounder observations of equatorial bubbles. *Geophys. Res. Lett.*, **5**, 795-798.

ECCLES, D. and KING, J. W. [1969] A review of topside sounder studies of the equatorial ionosphere. *Proc. IEEE*, **57**, 1012-1018.

FANG, D. J. and LIU, C. H. [1983] A morphological study of gigahertz equatorial scintillations in the Asian region. *Radio Sci.*, Vol. 18, 241-252.

FARLEY, D. T. [1963] A plasma instability resulting in field-aligned irregularities in the ionosphere. *J. Geophys. Res.*, **68**, 6083-6097.

FEEN, M. M., PISACANE, V. L. and STURMANIS, M. [1975] Prediction techniques for the effect of the ionosphere on ranging from satellites. Proc. Symposium on the Effects of the Ionosphere on Space Systems and Communications, 404-412. Naval Research Laboratory, Arlington, Va., USA.

GIRALDEZ, A. E., PUIG, L. and LAMA, I. [1981] Variabilidad de la ionización Es ecuatorial. *Geoacta*, Vol. XI.

GUSEV, V. D., DANILKIN, N. P., DENISENKO, P. F. and VODOLAZKIN, V. J. [1977] The determination of effective electron collision frequency profiles in the ionosphere on the basis of Volterra equation (in Russian). *Geomag. i Aeronom.*, Vol. 17, **4**, 645-648.

HARGREAVES, J. K., POULTER, E. M. and HUNSUCKER, R. D. [1980] ATS-6 electron content measurements from Alaska: recovery from a storm in summer 1979. Proc. Satellite Beacon Symposium, 119-140, Warsaw, Poland.

HUNSUCKER, R. D. [1975] Chatanika radar investigation of high latitude E-region ionization structure and dynamics. *Radio Sci.*, **10**, 277-288.

HUNSUCKER, R. D. [1979] Morphology and phenomenology of high-latitude E- and F-regions. *STPP**, Vol. II. Stock No. 003-017-00471-6. US Govt. Printing Office, Washington, DC 20402, USA.

HUNSUCKER, R. D. and GREENWALD, R. A. (Guest Eds.) [1983] Including special papers: Radio probing of the high-latitude ionosphere and atmosphere: new techniques and new results. *Radio Sci.*, Vol. 18, 6.

KENT, G. S. and KOSTER, J. R. [1967] Some studies of night-time F-layer irregularities at the equator using very high frequency signals radiated from earth satellites. *Spread-F and its Effect upon Radio Wave Propagation and Communication.* Eds. P. Newman and R. Penndorf Technivision, Maidenhead, UK.

KERBLAY, T. S. and NOSOVA, G. N. [1980] Statistical prediction of Es parameters and echo-signal characteristics. *STPP**, Vol. IV, C77 to C88. Stock No. 003-117-00479-1. US Govt. Printing Office Washington, DC 20402, USA.

KING, J. W., REED, K. C., OLATUNJI, E. O. and LEGG, A. J. [1967] The behaviour of the topside ionosphere during storm conditions. *J. Atmos. Terr. Phys.*, **29**, 1355-1363.

KING, J. W., SMITH, P. A., ECCLES, D., FOOKS, G. F. and HELM, H. [1964] Preliminary investigation of the structure of the upper ionosphere as observed by the topside sounder satellite Alouette. *Proc. Roy. Soc.*, **A.281**, 464-487.

KLOBUCHAR, J. A. [1975] A first-order, world-wide, ionospheric time-delay algorithm. Tech. Rep. 75-0502, Air Force Cambridge Research Labs., Bedford, MA., USA.

KLOBUCHAR, J. A. [1977] Correlation distance of mean daytime electron content. AFGL-TR-77-0185 (NTIS Accession No. AD A046166) National Technical Information Service, Springfield, Va. 22161, USA.

KLOBUCHAR, J. A. and ALLEN, R. S. [1970] A first-order model of total electron content group path delay for a midlatitude ionosphere. Tech. Rep. 70-0403, Air Force Cambridge Research Labs., Bedford, MA., USA.

KNECHT, R. W. and McDUFFIE, R. E. [1962] On the width of the equatorial Es belt. *Ionospheric Sporadic-E.*, 215-218. Eds. E. K. Smith and S. Matsushita, Pergamon Press, Oxford, UK.

KOTADIA, K. M. [1959] Spread-F in the ionosphere over Ahmedabad 1954-1957. *Proc. Indian Acad. Sci.*, **24**, 259-271.

LARSEN, T. R. [1979] Effects of D-region ionization on radio wave propagation. *STPP*, Vol. II, 617-654. Stock No. 003-017-00471-6. US Govt. Printing Office, Washington, DC 20402.

LARSEN, T. R., REAGAN, J. B., IMHOF, W. L., MONTBRIAND, L. E. and BELROSE, J. S. [May, 1976] A coordinated study of energetic electron precipitation and D region electron concentrations over Ottawa during disturbed conditions. *J. Geophys. Res.*, Vol. 81, **13**, 2200-2212.

LAUTER, E. A., BREMER, J., GRAFE, A., DETERS, I. and EVERS, K. [1977] The post-storm ionization enhancements in the mid-latitude D region and related electron precipitation from the magnetosphere. Heinrich-Hertz Institute STP Report No. 9.

LEE, M. K. and NISBET, J. S. [1975] Propagation predictions and studies using a ray-tracing programme combined with a theoretical ionospheric model. *IEEE Trans. Ant. Prop.*, Vol. AP-23, 132-136.

LOCKWOOD, G. E. K. and NELMS, G. L. [1964] Topside sounder observation of the equatorial anomaly at 75° W longitude. *J. Atmos. Terr. Phys.*, **26**, 569-580.

LOCKWOOD, G. E. K. and PETRIE, L. E. [1963] Low latitude field aligned ionization observed by the Alouette topside sounder. *Planet. and Space Sci.*, **11**, 327-330.

LYON, A. J., SKINNER, N. J. and WRIGHT, R. W. H. [1961] Equatorial spread-F at Ibadan, Nigeria. *J. Atmos. Terr. Phys.*, **21**, 100-119.

LYON, A. J. and THOMAS, L. [1963] The F2-region equatorial anomaly in the African, American and East Asian sectors during sunspot maximum. *J. Atmos. Terr. Phys.*, **25**, 373-386.

MARUYAMA, T. and MATUURA, N. [1980] Global distribution of occurrence probability of spread echoes based on Ionosphere Sounding Satellite-b observation. *J. Radio Res. Labs.*, (Japan), **27**, 201-216.

MARUYAMA, T. and MATUURA, N. [1984] - Longitudinal variability of annual changes in activity of equatorial spread F and plasma bubbles. J. Geophys. Res., 89, 10903-10912.

MATSUSHITA, S. [1962] Lunar tidal variations of sporadic-E. *Ionospheric Sporadic-E.*, 194-214. Eds. E. K. Smith and S. Matsushita, Pergamon Press, Oxford, UK.

MATSUSHITA, S. and SMITH, L. G. (Eds.) [1975] *Special issue of Radio Sci.*, Vol. 10, 3.

MATUURA, N. [1980] Characteristics of global distribution of foF2 based on topside sounding by ISS-b, Highlights of the Japanese IMS Programme. Institute of Space and Aeronautical Science, University of Tokyo, 239-247.

MAYAUD, P. N. [1965] Morphological analysis of the day-to-day variability in the "regular" daily variations S_r of the Earth's magnetic field. *Ann. de Géophys.*, **21**, 369-401.

MENDILLO, M. and KLOBUCHAR, J. A. [1975] Investigations of the ionospheric F-region using multi-station total electron content observations. *J. Geophys. Res.*, **80**, 643-650.

MENDILLO, M. and KLOBUCHAR, J. A. [1980] A morphology-based prediction scheme for the coupled latitudinal and local time development of F-region storms. *STPP.*, Vol. IV, C-15 to C-26. Stock No. 003-117-00479-1. US Govt. Printing Office, Washington, DC 20402.

* The abbreviation STPP refers to the Solar-Terrestrial Predictions Proceedings, published in four volumes by the National Oceanic and Atmospheric Administration (NOAA), US Department of Commerce and edited by R. F. Donnelly.

MENDILLO, M., KLOBUCHAR, J. A., FRITZ, R. B., DA ROSA, A. V., KERSLEY, L., YEH, K. C., FLAHERTY, B. J., RAGASWAMY, S., SCHMID, P. E., EVANS, J. V., SCHODEL, J. P., MATSOUKAS, D. A., KOSTER, J. R., WEBSTER, A. R. and SCHIN, P. [1974] Behaviour of the ionospheric F-region during the great solar flare of 7 August 1972. *J. Geophys. Res.*, 79, 665-672.

MINAKOSHI, H. [1988] - TEC observation and modelling in the Asian northern mid-latitutde region (to be published in J. Comm. Res. Lab (Japan)).

MINULLIN, R.G. [1988] - Periodichnosti v variatsiyakh mediannykh znacheny predelnykh chastot sloya Es (Periodicities in the variations of the median values of Es layer limiting frequencies). Geomagnetizm i aeronomiva, Vol. 28, 969-975.

MULDREW, D. B. [1980a] Characteristics of ionospheric bubbles determined from aspect-sensitive scatter spread F observed in Alouette-1. *J. Geophys. Res.*, **85**, 2115-2123.

MULDREW, D. B. [1980b] The formation of ducts and spread F and the initiation of bubbles by field-aligned currents. *J. Geophys. Res.*, **85**, 613-625.

OSBORNE, B. W. [1951] Ionospheric behaviour in the F-2 region at Singapore. *J. Atmos. Terr. Phys.*, **2**, 66-78.

PIGGOTT, W. R. and RAWER, K. [1972] URSI handbook of ionogram interpretation and reduction (2nd Ed.), World Data Center A for Solar-Terrestrial Physics. Report UAG 23. NOAA, Boulder, CO 80303, USA. Spanish text available from LIARA (Argentina), and French text available from CNET (France).

PIGGOTT, W. R. and RAWER, K. [1978] URSI handbook of ionogram interpretation and reduction (2nd Ed.). Revision of Chapters 1-4. World Data Centre A for Solar-Terrestrial Physics. Report UAG-23A, NOAA, Boulder, CO 80303, USA.

RAO, C. S. R. and MALHOTRA, P. L. [1964] A study of geomagnetic anomaly during I.G.Y. *J. Atmos. Terr. Phys.*, **26**, 1075-1085.

RAO, N. N., YOUAKIM, M. Y. and YEH, K. C. [1971] Feasibility study of correcting for the excess time delay of transionospheric navigational varying signals. Tech. Rep. No. 43, (SAMSO-TR-71-163), University of Illinois, Ionospheric Physics Lab., Urbana, IL, USA.

RASTOGI, R. G. [1959] The diurnal development of the anomalous equatorial belt in the F2-region of the ionosphere. *J. Geophys. Res.*, **64**, 727-732.

RISHBETH, H. and GARRIOTT, O. K. [1969] Introduction to ionospheric physics. *Int. Geophys. Series*, Vol. 14. Academic Press, New York and London.

RUSH, C. M. and MILLER, D. [1972] Some aspects of the day-to-day variability of the equatorial anomaly; American and Japanese sectors. *Radio Sci.*, **7**, 1085-1094.

RUSH, C. M., RUSH, S. V., LYONS, L. R. and VENKATESWARAN, S. V. [1969] Equatorial anomaly during a period of declining solar activity. *Radio Sci.*, **4**, 829-841.

SHARMA, R. P. and HEWENS, E. J. [1976] A study of the equatorial anomaly at American longitudes during sunspot minimum. *J. Atmos. Terr. Phys.*, **38**, 475-484.

SMITH, R. A. [1967] A survey of laboratory data for slow electrons in air, nitrogen and oxygen relevant to wave propagation and wave interaction in the lower ionosphere. Proc. Conference on Ground Based Radio Wave Propagation Studies of the Lower Ionosphere, Defense Research Board, Ottawa, Canada.

SOICHER, H. [1976] Comparative ionospheric and plasmaspheric electron contents from three world regions. *Nature*, Vol. 264, 46-48.

SOICHER, H. [1977] Ionospheric and plasmaspheric effects in satellite navigation sytems. *IEEE Trans. Ant. Prop.*, Vol. AP-25, 705-708.

THRANE, E. V. [1968] Collision frequency in the high latitude D-region. *Ionospheric Radio Communications*, 63-72. Ed. K. Folkestad, Plenum Press, New York, NY, USA.

TITHERIDGE, J. E. [1972] Determination of ionospheric electron content from the Faraday rotation of geostationary satellite signals. *Planet. and Space Sci.*, **20**, 353-369.

TYAGI, T. R., YEH, K. C., TAURIAINEN, A. and SOICHER, H. [1982] The electron content and its variation at Natal, Brazil. *J. Geophys. Res.*, Vol. 87, 2525-2532.

VILA, P. [1971a] Intertropical F2 ionization during June and July 1966. *Radio Sci.*, **6**, 689-698.

VILA, P. [1971b] New dynamic aspects of intertropical F2 ionization. *Radio Sci.*, **6**, 945-956.

VODOLAZKIN, V. I., DANILKIN, N. P., DENISENKO, P. F. and FAER, Yn. N. [1983] Empiricheskie vysotnye zavisimosti effektivnoi chastoty soudarenii v sredneshirotnoi ionosfere (Empirical altitude relations of effective collision frequency in the mid-latitude ionosphere). *Geomag. i Aeronom.*, Vol. 23, 1, 25-30.

WAGNER, C.-U., GRAFE, A. and NIKUTOWSKI, B. [1982a] Energetic electron fluxes and ionospheric absorption during the August 1972 event. *Gerlands Beitr. zur Geophys.*, Vol. 91, 457-479.

WAGNER, C.-U., RANTA, H. and RANTA, A. [1982b] Night-time ionospheric absorption during and after magnetospheric storms from auroral (L = 6.0) to medium (L = 2.5) latitudes. *J. Atmos. Terr. Phys.*, Vol. 44, 747-757.

WAKAI, N. [1971] Study on the night-time E region and its effect on the radio wave propagation. *J. Radio Res. Labs.* (Japan), **18**, 245-348.

WALDMAN, H. and DA ROSA, A. V. [1971] Prognostication of ionospheric electron content. Tech. Rep. SU-SEL-71-046 (SAMSO-TR-71-82), Stanford University, Radioscience Laboratory, Stanford, CA, USA.

WALDTEUFEL, P. [1965] Study of the instability associated with the equatorial sporadic-E layer. *Ann. de Géophys.*, **21**, 579-604.

WALKER, G. O. and CHAN, C. S. [1976] The diurnal variation of the equatorial anomaly in the topside ionosphere at Sunspot maximum. *J. Atmos. Terr. Phys.*, **38**, 699-706.

WHITEHEAD, J. D. [1970] Production and prediction of sporadic E. *Rev. Geophys. Space Phys.*, **8**, 65-144.

WRIGHT, R. W. H. [1959] Geomorphology of spread-F and characteristics of equatorial spread-F. *J. Geophys. Res.*, **64**, 2203-2207.

YEH, K. C., SOICHER, H. and LIU, C. H. [1979] Observations of equatorial ionospheric bubbles by radio propagation methods. *J. Geophys. Res.*, **84**, 6589-6594.

REPORT 886-2

SPECIAL PROPERTIES OF THE HIGH LATITUDE IONOSPHERE AFFECTING RADIOCOMMUNICATIONS

(Study Programme 25B/6)

(1982-1986-1990)

1. Introduction

The behaviour of the ionosphere at high latitudes differs from that at lower latitudes principally because it is exposed to the influence of disturbances in interplanetary space and in the magnetosphere. The pressure of the interplanetary plasma, which is in motion away from the Sun (the solar wind), confines the Earth's magnetic field to a finite volume, called the magnetosphere. At low latitudes, a magnetic field line, followed upward, passes horizontally over the magnetic equator not far from the Earth, and returns to the Earth in the opposite hemisphere, remaining everywhere deep within the magnetosphere. At high latitudes, on the other hand, field lines lead far from the Earth, either to the outer magnetosphere, or to interplanetary space. Since electrically charged particles can move easily along magnetic field lines, but across them only with difficulty, the low-latitude ionosphere is protected from events far from the Earth, while the high latitude ionosphere is not. Even when the interplanetary medium is in a steady state, the outer magnetosphere draws energy from the solar wind to create its own events (substorms), which may then perturb the high-latitude ionosphere.

1.1 *Influence of interplanetary and magnetospheric events*

There are two major types of influence in question:

- energetic particles (electrons and protons) from the sun and from the outer magnetosphere can penetrate to the atmosphere and create ionization at various altitudes, depending on the penetrating power (energy) of the particles;
- the solar wind blowing past the magnetic field of the Earth creates a dynamo which, besides accelerating some of the charged particles to high energy, induces an electric field perpendicular to the magnetic field, which causes ionization in high latitudes to drift horizontally and contributes to the formation of irregularities.

Progress has been reported on the development of models of the high latitude F region covering the polar cap and auroral zone latitudes for heights of 120 - 500 km that use interplanetary and magnetospheric parameters as input. [Akasofu, 1986; Watkins, et al., 1986; Quegan, et al., 1988; ——————— AGARD, 1989].

1.2 *Effects on the ionosphere*

The important effects of the high latitude ionosphere on the performance of communications systems are the following:

- electrons with energy greater than 20 keV and protons with energy of about 10 MeV penetrate to D-region heights and create extra ionization, thereby increasing the amount of radio-wave absorption, sometimes causing HF radio blackouts;
- electrons with energies of about 10 keV penetrate to E-layer altitudes and create reflecting layers. Whether these are useful for communication depends on their regularity in space and time, and on whether substantial D-region ionization is also present;

- electrons with energies from about 50 to 500 eV penetrate to F-region altitudes, and produce irregular enhancements of electron density, especially in the bottomside of the region;
- the high-latitude F region almost always contains small-scale irregularities that scatter HF waves and which cause scintillation on trans-ionospheric signals at higher frequencies. These irregularities are due to particle precipitation in some places, but elsewhere may be due to plasma instabilities associated with electric fields;
- variations of electron content affect the propagation delay, leading to errors in satellite ranging and navigation systems;
- the horizontal drift of ionization due to the magnetospheric electric field is important in the F region, where the recombination time is long;
- the magnetospheric electric field, along with aurorally produced ionization, gives rise to irregularities at E-region heights that scatter radio energy at HF, VHF, and UHF.

A brief review of ionospheric effects on high-latitude radio-wave propagation has been given by Hunsucker [1983] while more specific details are contained in the special issue of Radio Science [Hunsucker and Greenwald, 1983] and in an AGARD Lecture Series publication [AGARD, 1988]. Various radio probing techniques that provide measurements of the effects of high latitude ionospheric structure are reported by Soicher [1986a]. An idealized representation, in a north-south vertical plane of the main ionospheric features, is shown in Fig. 1 and is discussed in § 3.5 to 5.4.

2. Coordinate systems and auroral activity

2.1 *Magnetic coordinates*

Since the morphology of the high-latitude ionosphere is controlled to a great extent by the magnetic field, its properties are best described in terms of magnetic coordinates. The most useful orthogonal coordinate is local magnetic time, which is similar to ordinary local time, except that it is based on the geomagnetic pole rather than the geographic pole. For points well away from the region between the geographic and magnetic poles, the two types of local time are approximately equal. In each hemisphere, a "magnetic latitude – local time" frame of reference is fixed with respect to a line from the magnetic pole to the Sun. In this reference frame, the observer on Earth is on a moving platform that passes underneath phenomena that are stationary in space. One important exception is the solar terminator, which is fixed with respect to the geographic pole, at a given time of year. In the magnetic coordinates just described, the solar terminator moves diurnally towards and away from the Sun.

There are several forms of latitude connected with geomagnetism [Chapman, 1963]. The "dipole" latitude which is based on an approximation to a centred-dipole magnetic field, was used for ionospheric work and is adequate, provided that a great deal of precision is not required. "Corrected" geomagnetic latitude represents the real geomagnetic field more accurately, and is widely used in auroral studies. Conversion tables are given by Hakura [1965] and Gustafsson [1970]. Corrected geomgnetic latitude lines in the high latitude regions are displayed on Figures 2 and 3. A corresponding magnetic local time is defined, and the complete coordinate system is commonly referred to as CGLT (corrected geomagnetic-local time). "Invariant" latitude is a still more sophisticated coordinate [McIlwain, 1966], which is used primarily for studies of energetic trapped particles. At the Earth's surface, in high latitude regions, it is almost identical to corrected geomagnetic latitude.

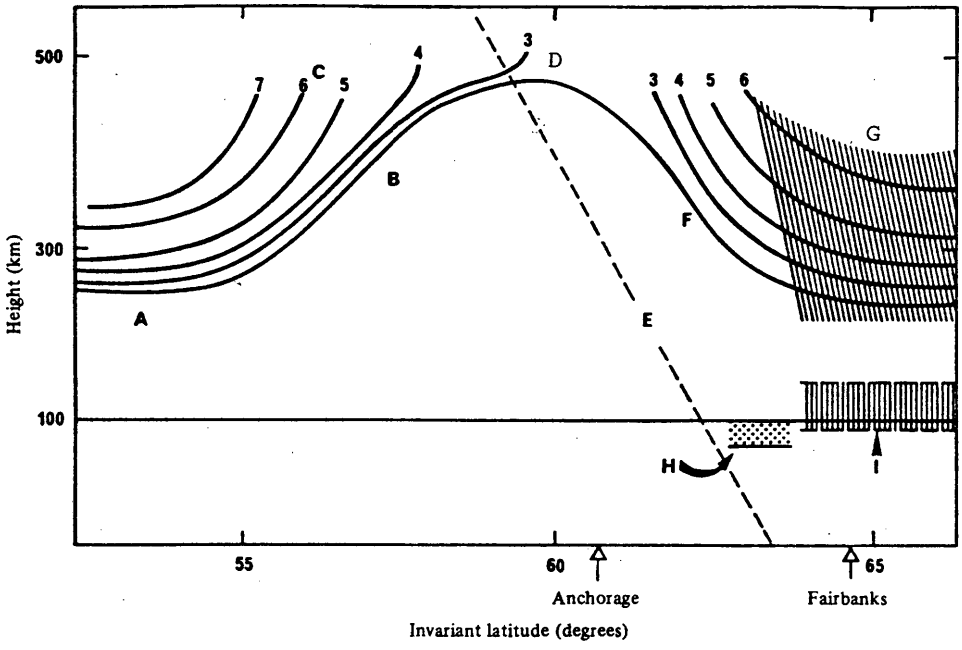


FIGURE 1 – *Idealized sketch of plasma frequencies in the vertical north-south plane through Fairbanks and Anchorage, Alaska.*
The salient ionospheric features which affect MF/HF sky wave propagation are illustrated [Hunsucker, 1983]

A: equatorward of trough
B: equatorward edge of trough
C: plasma frequency (MHz)
D: trough minimum
E: plasmapause field line
F: poleward edge of trough
G: F-region blobs
H: enhanced D-region absorption
I: E-region irregularities

2.2 *The auroral oval*

There are two kinds of aurora: visual aurora and radio aurora which can be further classified as discrete or diffuse. Discrete visual aurora and discrete radio aurora are believed to be closely correlated. No such temporal correlation is evident between diffuse visual aurora and diffuse radio aurora [Fremouw and Fang, 1975]. The auroral oval [Feldstein and Starkov, 1967], defined in the CGLT system, has been widely used as a reference domain for describing many high-latitude phenomena. It is an annular region in which the frequency of occurrence of visible discrete aurora is high. The oval for moderate magnetic activity ($Q = 3$, see § 2.3) is indicated by dotted lines in Figs. 4 to 8 inclusive. An analysis of magnetic activity data taken over an 11-year solar cycle reveals that $Q = 3$ corresponds to approximately the upper quartile value [Reilly, 1978]. The oval is eccentric with respect to the geomagnetic pole, being displaced about 4° toward the night side of the earth. Therefore an observer under the oval at midnight will be equatorward of it at noon. The polar cap is usually defined as the region poleward of the high-latitude boundary of the auroral oval. A method for determining the location of the oval as a function of space and time was developed by Whalen [1970], and a mathematical representation is given by Holzworth and Meng [1975].

The concept of an "auroral oval" as a band of luminosity encircling each of the geomagnetic poles was first deduced statstically. However, the auroral imaging photometry instrument on the Dynamics Explorer 1 satellite [Frank and Craven, 1988] clearly confirmed the omnipresence of auroral zone particle precipitation. In these images, the entire auroral oval is observed in visible and ultraviolet wavelength bands, permitting analysis of auroral featues such as the growth, expansion and recovery phases of substorms. The patterns of particle precipitation that produce the aurora are seen to be dynamic funtions of location. The details of the multispectral imaging allow extraction of the energy deposition rate and the characteristic energy of the precipitation over the entire auroral region at low spatial resolution [Rees et al., 1988]. Alternatively, statistical models of ionospheric parameters have been deduced from local measurements of electron precipitation by lower-altitude polar-orbiting satellites, averaged over long periods of time [Fuller-Rowell and Evans, 1987, and Hardy et al., 1985].

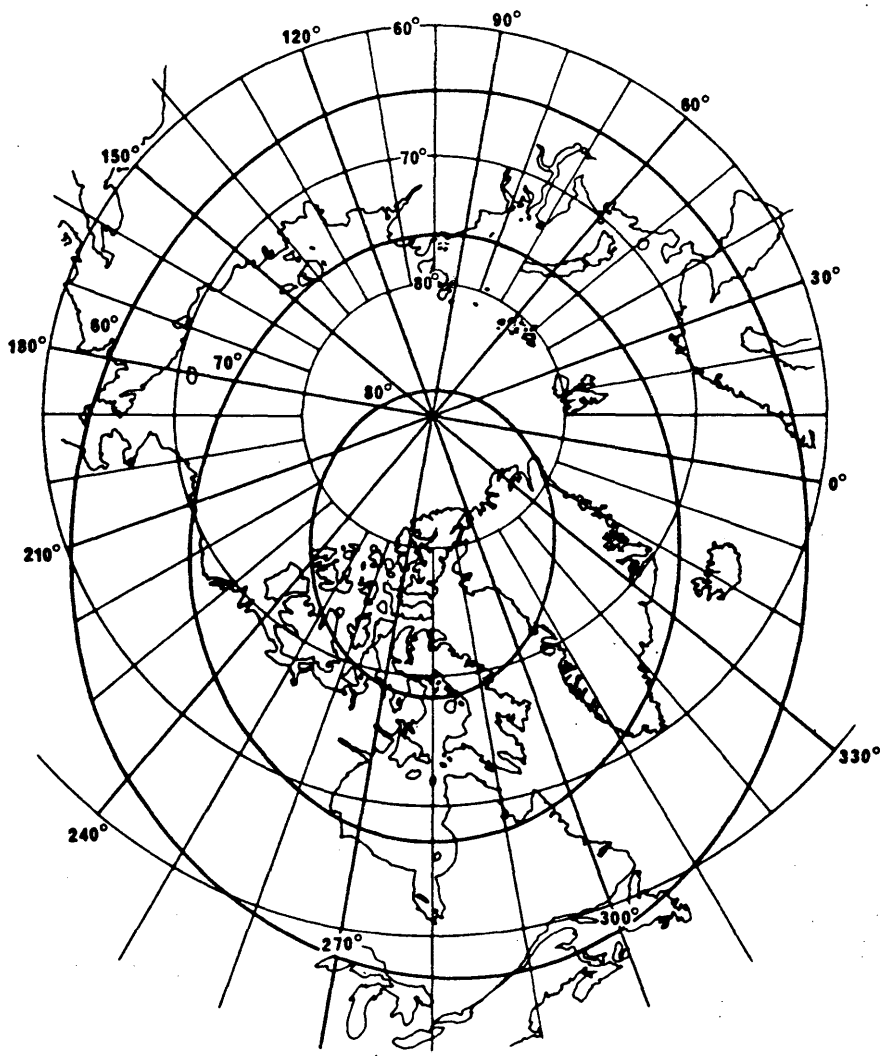


FIGURE 2 – *Corrected geomagnetic latitude in the northern hemisphere*

(Geographic latitude and longitude are also displayed for reference)

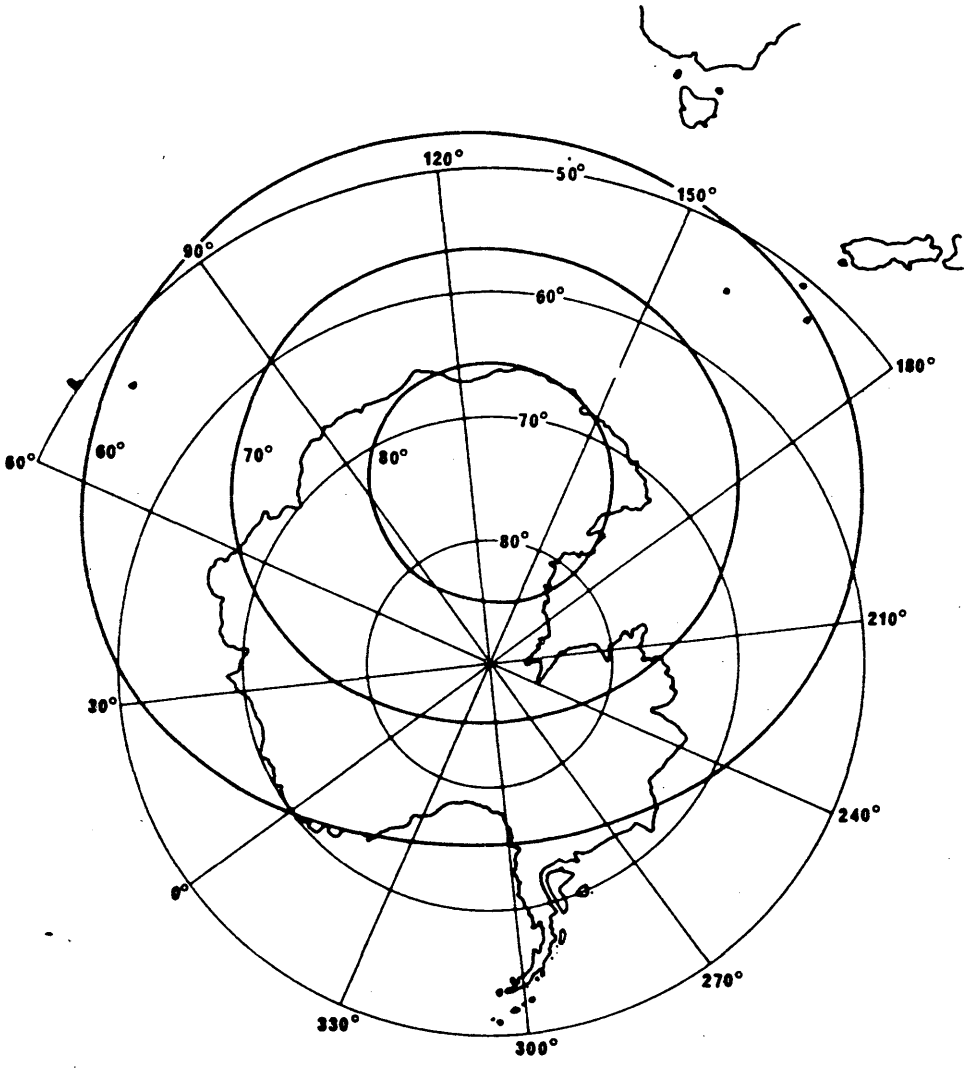


FIGURE 3 – *Corrected geomagnetic latitude in the southern hemisphere*

2.3 Magnetic activity and the size of the auroral oval

Feldstein labelled the ovals with a "Q" index of magnetic activity. There is a rough correspondence between Q and K_p index, which is widely available, although it is a planetary index, rather than an auroral one [Valley, 1965]. An auroral electrojet (AE) index has been defined as a measure of substorm activity [Allen et al., 1979]. The AE index is a widely accepted measure of global auroral electrojet activity based on 2.5 min readings of the H magnetic component trace from a ring of observatories located between 65° and 70° magnetic latitude [Davis and Sugiura, 1966].

By using electron precipitation data from hundreds of polar passes of Defense Meterological Satellite Programme (DMSP) satellites, Meng and Makita [1986] have determined the average locations of the equatorward and poleward boundaries of the precipitation region as a function of the hourly AE index of geomagnetic activity. Assuming a threshold number flux of 10^7 ——— el/cm^2/s/sr, Meng and Makita [1986] found that for quiet conditions (AE $\leqslant$ 150 nT), the poleward boundary of the low-energy electron precipitation (< 500 eV) is located at about 80° to 82° corrected geomagnetic latitude in both the evening and morning sectors, and the equatorward boundary of the high-energy precipitation (> 500 eV) is located at 61° to 71° in the evening sector and 67° to 69° in the morning sector. The transition boundary between the high- and low-energy regions is at about 73° to 75° in both the evening and morning sectors. During magnetically disturbed periods (AE > 400 nT), Meng and Makita [1986] found that the poleward boundary is located at about 73° to 75° in the evening sector and 76° to 77° in the morning sector; the transition and equatorward boundaries are located at about 70° to 72° and 64° to 66° respectively, in both the evening and morning sectors. Thus the extent of the polar cap varies from an equivalent latitude of approximately 84° during quiet conditions to further than 65° equivalent latitude during geomagnetic storms [Meng, 1984]. In general, as geomagnetic activity increases, the size of the polar cap increases, the width of the low-energy auroral electron precipitation region decreases, and the width of the high-energy auroral electron precipitation region increases.

2.4 *The outer precipitation zone*

Equatorward of the oval, there is a zone of precipitation that does not produce discrete aurora [Hartz and Brice, 1967; Hartz, 1971]. This zone is more circular than the oval and occupies the latitude range 60° to 70° geomagnetic. Phenomena related to the more energetic electron precipitation, such as diffuse aurora, auroral radio absorption, and X-rays, appear most strongly equatorward of the oval in the outer zone, which probably represents a sink of energy for the outer Van Allen belt of trapped energetic particles. The radio absorption in this zone is described in § 5 and absorption patterns are shown in Figs. 7 and 8.

2.5 Storms and substorms

Our understanding of the visual auroral event described by Akasofu [1968] as a substorm has evolved to include a variety of associated physical signatures that denote complex magnetospheric processes. Briefly, magnetospheric substorm is a transient process during which a significant amount of energy, derived from the interaction between the solar wind and the Earth's magnetic field, is deposited in the auroral ionoshere and magnetosphere [Rostoker et al., 1980; AGARD, 1989]. Isolated substorms last about an hour, but they may occur in rapid succession especially during major geomagnetic storms. Substorms are accompanied by intense charged particle precipitation, enhanced auroral electrojets, and heating of the neutral ionosphere. All radio propagation parameters for high latitude paths may vary rapidly under the influence of an auroral substorm; those variations most frequently noted are found in D-region absorption and sporadic E. Total electron content can be significantly affected.

3. The high-latitude F region

3.1 *Solar production*

The F region, when sunlit, owes its existence mainly to solar radiation. Even when the sun is close to the horizon, it produces ionization at a rate comparable with that due to precipitation in the noon sector of the auroral oval, where F-region particle production is greatest [Whitteker, 1977]. Horizontal drifting moves this ionization into the dark part of the polar cap. However, in general, the polar cap is a region of low ionospheric density compared with the auroral zone.

3.2 *F-region ionization drift within the polar cap*

Ionization drifts from the day side of the earth across the polar cap, to the midnight side, then returns on either side of the polar cap. A model of the drift pattern is shown in Fig. 4. This motion gives rise to a "tongue" of ionization extending across the polar cap from the sunlit side towards the dark side [Nishida, 1967]. An example from measurements made during the IGY in the northern hemisphere is shown in Fig. 5. Sato and Rourke [1964] give similar results for the southern hemisphere. The return flow has the converse effect of moving lower-density ionization from the night side of the earth sunward, contributing to the formation of a trough in electron density (see § 3.6). The "tongue" pattern is most pronounced near equinox when the solar terminator crosses the polar cap, but it exists also in summer and winter. The drift speed, and hence the density distribution, are variable. Hill [1963] describes "sporadic F" events in which anomalously high F-layer densities occur during equinox and winter months. During these events, the tongue of ionization is very pronounced.

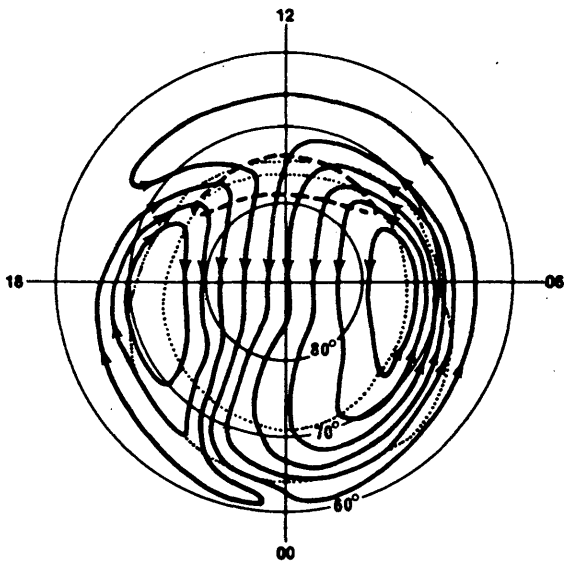


FIGURE 4 – *A model of the F-layer drift pattern, taking account of the rotation of the Earth [Heppner, 1977]*

The drift speed is proportional to the density of the flow lines; near the pole it is about 0.4 km/s. The coordinate system is invariant latitude and magnetic local time. A region of intense low-energy electron precipitation centred on magnetic noon is outlined by a dashed line. The boundaries of the auroral oval (Q = 3) are shown as dotted lines.

Combined measurements by the European Incoherent Scatter (EISCAT) UHF radar and the AMPTE UKS and IRM satellites have proved conclusively that the drift of ionospheric plasma at high latitudes is controlled by the interplanetary magnetic field [Rishbeth et al., 1985; Willis et al., 1986; Etemadi et al., 1988].

3.3 *Universal Time (UT) variation in the F region*

In the southern hemisphere, the density of the F region depends on Universal Time in a different way from its dependence on local time. In particular, there is an apparent diurnal variation at the south geographic pole, where local time has no meaning. Here, and elsewhere in the southern hemisphere, the electron density peaks at about 0700 UT, which, for the south geographic pole, is approximately magnetic midnight. The effect is usually ascribed to neutral-air winds which blow over the polar regions away from the Sun, lifting the ionization on the midnight side of the magnetic pole, thereby preventing rapid recombination [Hopkins *et al.*, 1973; Konnlein and Raitt, 1978]. However, since 0700 UT is also when the largest fraction of the southern (magnetic) polar cap is in sunlight, at high latitudes the UT effect may be partly due to the drifting described in § 3.2 above. In the northern hemisphere, there is a less obvious electron density maximum above 60° latitude at 1800 UT.

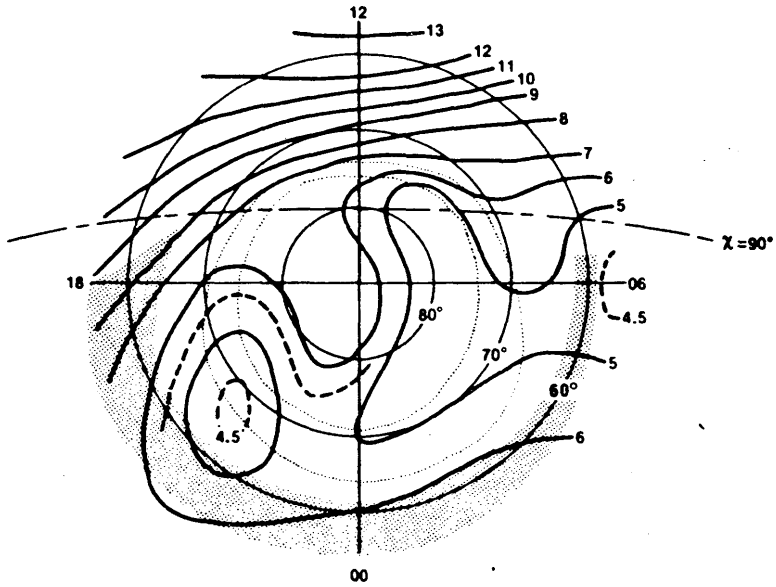


FIGURE 5 – *Median F-layer penetration frequencies in the northern hemisphere for March 1957 at 0600 UT*
[Hill and Penndorf, 1959]

Coordinates are CGLT. The labels on the contours of constant penetration frequency are in units of MHz. The broken line labelled $\chi = 90°$ is the solar terminator. The stippled area represents the position of the trough for $K_p = 3$ in the model of Halcrow and Nisbet [1977]. The boundaries of the auroral oval ($Q = 3$) are shown as dotted lines.

3.4 *The polar cap in darkness*

When most of the polar cap is in darkness (near winter solstice, and when the magnetic pole is on the side of the geographic pole away from the sun) the F region is much more variable in space and time than otherwise. Under these conditions, penetration frequencies are commonly 2 to 3 MHz [Whitteker *et al.*, 1978], but have occasionally been observed to go below 1 MHz, the lowest densities tending to occur at about local midnight in the polar cap [Timleck and Nelms, 1969; Nelms and Chapman, 1970; Brinton *et al.*, 1978].

3.5 *The F region in and near the poleward edge of the auroral oval*

An annular region including the poleward part of the oval and the part of the polar cap within a few degrees of the oval is characterized by precipitation of low-energy electrons, which deposit their energy at F-region altitudes. The precipitation is usually intense enough to prevent the penetration frequency in this part of the F layer from falling below about 3 MHz. Locally it can be much higher than this. There are large variations in electron density over short distances, making it difficult to obtain meaningful penetration frequencies from ionograms, which, however, have well defined characteristics [Wagner *et al.*, 1973; Pike *et al.*, 1974].

Of equal or possibly higher importance to the maintenance and structure of the night-time oval F-layer is the transport of plasma within the polar convection pattern. Modelling suggests that highly structured plasma enhancements in the night sector of the oval are the result of transport of polar cap plasma patches [see§3.7] into the oval midnight sector, where they are sheared into the observed narrow, latitudinally aligned structures in the flow separation and reversal region near midnight shown in Figure 4 [Robinson et al., 1985]. The non-auroral origin of such night oval F-region structures has been

confirmed by [Weber et al., 1985]. The strong longitudinal or UT dependence of the night-time oval F-layer measured by Incoherent Scatter Radars [de la Beaujardière et al., 1985] corresponds to the observed UT control of the polar cap patches and thereby relates the F-layer in the oval at least during magnetically active periods via the polar convection to the solar-produced F-layer equatorward of the cusp.

In the region near magnetic noon between about 75° and 80° magnetic latitude, soft (< 300 eV) particle precipitation is particularly intense and persistent, often increasing the penetration frequency of ionization in the altitude range 200 to 300 km by several MHz [Pike, 1971; Whitteker, 1976]. This region known as the day-time cusp or cleft, is indicated approximately in Fig. 4. The precipitation produces large-scale irregularities (tens of kilometres) which decay to smaller-scale sizes (tens of metres or less) as they drift equatorward in the midnight sector of the oval [Muldrew and Vickrey, 1982] or generally in a direction determined by the convection pattern [Kelley et al., 1982].

3.6 *The F-region trough in electron density*

Equatorward of the auroral oval, a trough is found in the electron density of the night-time F region [Muldrew, 1965, 1983; Dudeney et al., 1983]. The density can become low because ionization is not supplied by anti-sunward drifting or by precipitation or by the storage effect of permanently closed magnetic field lines.

The trough exists initially in the afternoon at high magnetic latitudes (about 70°) where it is only a few degrees wide. With increasing local time it shifts gradually to about 57° magnetic latitude (for moderate K_p) near local midnight when it can be about 10° or more in width. It may swing a few degrees poleward of this before disappearing near sunrise. According to Rycroft and Thomas [1970], the centre of the trough moves equatorward approximately 1.8° ± 0.4° per unit increase in K_p.

Very large latitudinal gradients of electron density exist at the equatorward and poleward edges of the ionospheric trough. These latitudinal gradients are even more strongly pronounced on the topside of the ionosphere, where the poleward boundary has been described as a "wall" of ionization. The latitudinal gradients at the low latitude boundary of the ionospheric trough are not as large as those at its high latitude boundary (the auroral oval edge) but are nevertheless often considerably larger than the gradients encountered at mid-latitudes. The ratio of densities inside and outside the trough can vary between less than 0.1 to almost 1, but there is no known dependence on magnetic activity. A model of the trough has been given by Halcrow and Nisbet [1977]. In the model, the density in the trough is taken to be 0.25 of the density outside. In Fig. 5 is shown the model trough for K_p = 3, which is approximately the median index for the F-layer data that are shown.

3.7 *F-region irregularities*

Irregularities are found more or less continuously throughout the high latitude region starting at about 60° corrected geomagnetic latitude [Clark and Raitt, 1975]. Theories of the formation of high latitude irregularities are discussed by Keskinen and Ossakow [1983]. Associated with the auroral oval is an "irregularity zone" in the bottomside of the F layer (see § 3.5). The propagation effects of F-layer irregularities are discussed in § 8.1.

Sun-aligned polar cap F-layer auroral arcs (radio auroras) drifting from dawn to dusk have been observed in the winter polar cap by Weber and Buchau [1981] and Buchau et al., [1983]. During years of enhanced solar activity they constitute substantial (5 to 8 fold) enhancements above a nominal 10^5 el cm^{-3} background density (foF2 ~ 3 MHz) and occupy the polar cap mainly during quiet geomagnetic conditions. Near solar minimum the density enhancements are rarely

more than a factor of 2 above the background. During more disturbed conditions ($K_p > 4$), large, structured electron density patches are observed moving at high speed in the anti-sunward direction. The occurrence of these patches is under strong UT control. There is also evidence for solar cycle dependence of the maximum densities within the patches (observed foF2 max ≈ 6 MHz for $R_I = 33$).

These and other observations suggest that the origin of the patches is the sunlit ionosphere equatorward of the noonsector of the oval [Buchau et al., 1985]. A mechanism involving substantial changes in the Interplanetary Field B_z component, which may generate these patches and inject them into the polar cap plasma convection pattern [Heelis et al., 1982] has been suggested by Anderson et al., [1987]. The diameter of these patches is greater than 1,000 km and they can therefore affect HF communications on circuits with reflection points in the polar cap.

3.8 *The F1 layer*

In the summer, during sunspot minimum years, the F1-layer maximum observed frequency (MOF) often exceeds the F2-layer MOF on polar propagation paths from 2000 to 3500 km in length [Hunsucker and Bates, 1969]. This is because, in the morning at least, foF2 decreases more quickly with increasing latitude than foF1. An F1-prediction method useful for radio propagation predictions is given by Ducharme *et al.* [1971] (see Report 340).

4. The high-latitude E region

At high latitudes, as elsewhere, the sun produces an E region when it is above the horizon, but ionization is also produced in the same altitude range by the precipitation of energetic particles, principally electrons. The precipitation layers are particularly important in the —— winter, when the solar E layer vanishes.

4.1 *Auroral* ——— *E* region

A steady flux of electrons precipitating at auroral latitudes produces a relatively, thick layer of ionization at E region altitudes with penetration frequencies at night between 1.5 - 2.5 MHz [Elkins, 1980]. This layer is referred to as "night" E or Ea [Piggott and Rawer, 1972]. In the daytime, Ea exists together with the solar E-layer. ——— A model suggested by Wagner [1972] contains auroral E in a belt 4° to 5° wide, with its poleward boundary at the centre of the auroral oval. This is illustrated in Fig. 6. In this belt, foEa > 2 MHz, with the maximum foEa near the equatorward boundary. For active magnetic condition, the width increases to 7°. For quiet conditions, the maximum foEa is 2.5 MHz at a virtual height of 130 km. For magnetically active conditions, the corresponding values are 4 MHz and < 110 km. The probability of occurrence is from 92% to 95%. According to Gassmann [1970], the occurrence of auroral E is less frequent in the late afternoon and early evening hours.

Also associated with auroral precipitation is a sporadic E layer referrred to as type r (Esr) since it increases in virtual height at the high frequency end similar to group retardation. Esr blankets over part or nearly all of its frequency range and usually shows spreading. Besprozvannaya, et al., [1979] determined the space-time distribution of auroral E in winter by combining the v.i. observations of foEa and foEsr for 1958 and 1964. The occurrence of these auroral E layers closely follows the auroral oval and the poleward and equatorward boundaries of occurrence tend to move to lower latitudes by 2° to 3° with increasing magnetic activity. During quiet magnetic conditions at solar minimum, the auroral E region diminishes greatly in width and extent.

In addition to Esr, there are two other types of sporadic E associated with visible aurora: auroral Es (Esa) and flat Es (Esf). Esr is often associated with quiet diffuse auroras while Esa and Esf are associated most often with active auroras [Elkins and Rush, 1973]. Sporadic E types similar to those observed at mid-latitudes occur during the daytime but with relatively low frequency. The space-time distribution of the probability of occurrence of auroral Es > 3 MHz changes significantly with magnetic activity. Under quiet magnetic conditions, a region of enhanced Es occurrence is located within the auroral zone with a maximum occurrence at the poleward edge, and extending over the polar cap at solar minimum. With increased magnetic activity, sporadic E appears to be confined to two ring-shaped maxima, ~ 60° and 72° geomagnetic latitude encircling the geomagnetic pole and separated by a minimum at ~ 65° geomagnetic latitude [Besprozvannaya, et al., 1979; Elkins, 1980]. Auroral sporadic E with a high penetration frequency is associated with substorms. It is less common in winter than in summer by a factor of about 1.6 [Gassmann, 1972], but is more important for communications in the winter. Hunsucker and Bates [1969] report that it is most important for communications at sunspot minimum, when Es modes can occur more than 50% of the time on paths between Alaska and either Greenland or Norway, with typical MOFs of 16 to 18 MHz. The occurrence rate in the Canada-Alaska sector seems to be higher than in the Siberia sector (80% and 60% in summer according to Gassmann [1972]).

4.2 Polar cap E region

Sporadic E within the polar cap exhibits a different character from auroral Es although the same current-driven plasma instability is active in both regions. In general it is substantially weaker and displays a negative correlation with geomagnetic activity related to auroral substorms. Polar cap sporadic E extends in bands or ribbons across the polar cap, roughly in the direction of the sun and may be associated with weak sub-visual auroral optical emissions.

5. The D region and radio absorption

For frequencies above LF, the D region does not reflect radio waves, but absorbs them, because the electron-neutral collision frequency is high. Because of the close connection between the electron density in the D region and the absorption of radio energy, the D region is here described in terms of its absorbing properties.

There are two main categories of absorption events: auroral absorption, which is due to electrons precipitating at auroral latitudes, and polar cap absorption, due to protons precipitating over the whole polar region.

Absorption changes can be measured by "riometers", which use galactic radio noise as a source. Riometers are usually operated at a frequency of about 30 MHz, and employ polar or vertically directed directional antennas [Hargreaves, 1969]. An absorption of 1 dB measured by a 30 MHz riometer is considered important, since it translates to 10 dB or more on an HF circuit, depending on obliquity and frequency [Agy, 1970]. Absorption has also been measured on VHF ionospheric forward-scatter circuits [Bailey, 1964]. The frequency variations of auroral and polar cap absorption depend on conditions. At sufficiently high frequencies the absorption varies as $1/f^2$; below some limiting frequency it is constant. This limiting frequency depends on path obliquity and lies in the lower HF band for auroral absorption and the upper HF band for polar cap absorption. At LF and lower frequencies, absorption becomes less important (see § 9).

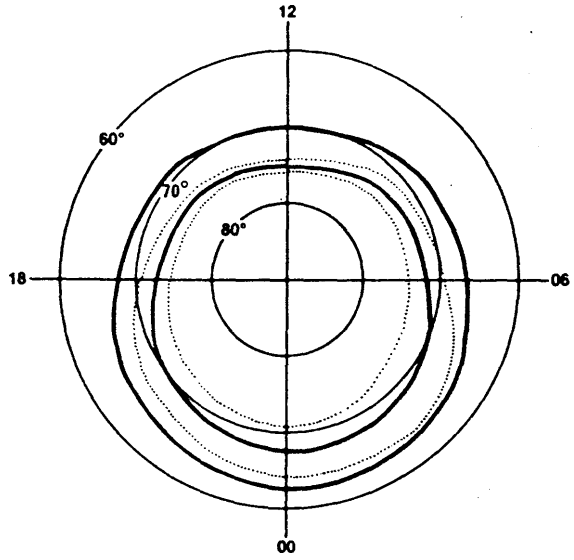


FIGURE 6 – *A model of the distribution of auroral E for moderate (Q = 3) magnetic activity [Wagner, 1972]*

The region over which the penetration frequency exceeds 2 MHz is bounded by heavy lines. Coordinates are geomagnetic latitude and time. The maximum penetration frequency of 3.2 MHz occurs near the low-latitude boundary of this region. The boundaries of the auroral oval (Q = 3) are shown as dotted lines.

5.1 *Absorption increases after geomagnetic storms (the post-storm effect)*

Increased D-region absorption is observed regularly after geomagnetic storms from sub-auroral latitudes ($\leqslant$ 62° invariant latitude) to mid-latitudes ($\simeq$ 45° invariant latitude). The increased absorption in this belt is distinct from the auroral absorption zone and is caused by precipitation of energetic electrons from the radiation belt [Larsen et al., 1976; Wagner and Ranta, 1983].

The zone of increased absorption starts to develop shortly after the main phase of the storm and exists during the whole recovery phase, i.e., up to 10 days or more. [Belrose and Thomas, 1968].

The amplitude and duration of the absorption increase are closely correlated with the D_{st}-index [Lauter *et al.*, 1977], but also depend on the polarity of the interplanetary magnetic field [Lauter *et al.*, 1977, 1978]. At the beginning of the recovery phase after a geomagnetic storm, the poleward boundary of the belt is found around 55-58° invariant latitude in Europe; it moves slowly poleward reaching about 62° invariant latitude at the end of the recovery phase [Wagner *et al.*, 1982]. A notable feature of the post-storm events studied by Larsen et al. [1976] was the large spread in the deduced effective electron-loss rates, which was greater at 80 km than at higher or lower heights. This effect is addressed in the paragraphs below.

5.2 Winter variability of ionospheric absorption

On some days in winter marked increases in ionization densities are observed throughout the D region. This phenomenon has been extensively studied in Europe and has long been thought due to some sort of meteorology in the lower ionosphere [Dieminger, 1955].

Evidence for the meteorological change hypothesis has been found by a Western European 1975/76 D-region winter anomaly campaign (refer to Offerman [1979] and several papers in this special issue of the J. Atmos Terr. Phys.). The enhanced electron densities were attributed to increases in the number densities of normal ionizable constituents, and to decreases in electron loss rates. Attempts to study the phenomenon at similar geographic but higher magnetic latitudes in Canada, however, have been frustrated by high energy particle electron "drizzle" associated with post-storm effects, which dominate the winter variability of absorption at Canadian latitudes. It is now clear that both "post-storm" effects and "meteorological" changes affect ionization densities, and that these phenomena can occur together [Belrose, 1981].

5.3 *Auroral absorption*

Auroral absorption is a substorm phenomenon, related to the occurrence of luminous aurorae and magnetic disturbances. The occurrence pattern is zonal (in contrast with the polar cap events) with a statistical width of 5°-8° of latitude for a Gaussian absorption zone [Hargreaves and Cowley, 1967]. At a fixed site the observer sees absorption events typically from a minute to several tens of minutes in duration. Absorption has two maximums, one near midnight, and the other in the morning. As seen from a fixed site, the midnight absorption occurs in brief, intense events, which are associated directly with the local substorm (breakup) aurora. The morning absorption commences about an hour after a substorm, and is more spread out in space and time. It is not associated with the local aurora.

Figure 7 shows the percentage of time for which absorption exceeds 1 dB. The midnight absorption region does not appear because the events are brief. However, if the median intensity of individual events is plotted (Fig. 8), the midnight maximum appears. Plots of this sort assume that longitude is irrelevant, but work of Agy [1975] has indicated a longitudinal dependence of absorption, with a maximum over Alaska, and possibly also over northern Europe. As the level of magnetic intensity increases, the absorption zone moves toward the equator, reaching 60° geomagnetic latitude when K_p is about 7.

It is not usual for the whole of the absorption zone to be active simultaneously, for both latitudinal and longitudinal movements are seen within the total pattern. In the night sector, absorption regions appear to move both towards and away from the pole [Hargreaves, 1974], though at the onset of a substorm the motion is always poleward at high latitude and typically equatorward at low latitude, there being an origin near geomagnetic latitude 65° [Jelly, 1970]. In longitude, the substorm onset propagates both eastward and westward from the midnight sector, to appear in the day side of the zone 30 to 60 minutes later [Jelly and Brice, 1967; Hargreaves, 1968]. Overall pictures of the substorm behaviour have been given by Berkey *et al.* [1974] and Zhulina *et al.* [1983].

The energetic electrons causing absorption come directly from the tail of the magnetosphere as the result of a substorm, or from the outer Van Allen belt. Electrons over a wide energy band contribute to the absorption with the range 40 to 80 keV making an important contribution [Penman *et al.*, 1979]. According to rocket measurements, the height of greatest absorption is 90 to 95 km by night and about 75 km by day, the absorption layer having a vertical thickness of 15 to 20 km [Hargreaves, 1969].

5.4 *Polar cap events*

Polar cap absorption (PCA) events which are often called solar proton events (SPE), are caused by the eruption of solar X-ray flares that emit energetic (MeV) protons which reach the Earth. The absorption occurs between about 45 and 75 km altitude [Hargreaves, 1969]. At HF, attenuation can be greater than 100 dB. The occurrence of such a flare may be announced by a Sudden Ionospheric Disturbance (a brief absorption event) on the sunlit side of the Earth, at all latitudes, caused by X-rays from the flare. The PCA event can occur from 15 minutes to several hours later. The delay time represents the travel time of the protons from the sun to the vicinity of the Earth. Whereas it is not possible to predict the occurrence of a sudden ionospheric disturbance, once a flare has been observed there is a good chance of forecasting the occurrence, time of arrival, and severity of a PCA event [Cliver *et al.*, 1978; Akinyan and Chertok, 1980; Akinyan *et al.*, 1980]. Unlike X-rays, the protons are guided by the Earth's magnetic field, and appear only above about 60° magnetic latitude, whether sunlit or not. (Note that the area covered by "Polar Cap Absorption" is usually larger than the "polar cap" as defined in § 2.2.) However absorption in the sunlit part of the polar cap is about 4 times stronger (at 30 MHz) than in the

dark part, where many of the electrons are immobilized by attachment to air molecules to form negative ions. Depending on the phase of the sunspot cycle there may be from 0 to 14 PCA events per year [Collins *et al.* 1961]. The average duration of a PCA event is about 2 days, but it may be as long as 4 days. A survey of PCA events from 1952 to 1963 is given by Bailey [1964], who tabulates events giving rise to daylight absorption of 2.5 dB or more on a 30 MHz riometer at 70° magnetic latitude, or 20 dB on a 1575 km VHF-scatter link at 32.2 MHz with the scatter point at the same latitude. His table is given in Report 263. A statement summarizing these data is that the number N of hours of PCA per year is given approximately by $N = -70 + 4.4\,R$, where R is the mean smoothed Zurich sunspot number. For the worst year in the survey, this is 780 hours, representing about 9% of the year. Since absorption is greatly reduced during dark hours, any given circuit will be blacked out for a smaller fraction of the time than this. Zmuda and Potemra [1972] give a table of events from 1965 to 1969. Larsen [1974] plots events from 1965 to 1973.

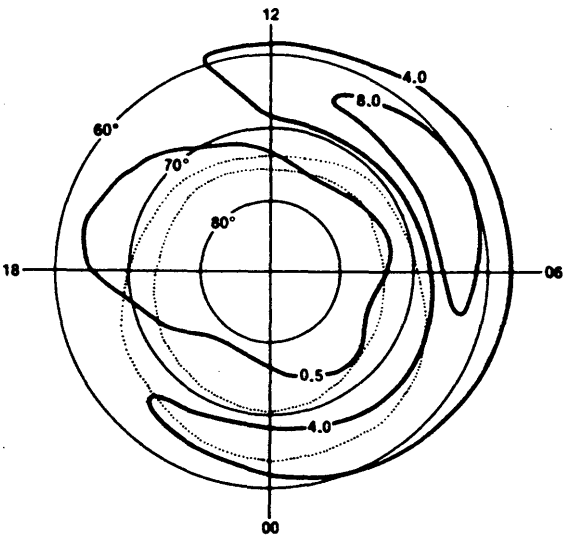


FIGURE 7 – *Percentage of time for which auroral absorption was at least 1 dB [Hartz et al., 1963]*

Coordinates are geomagnetic latitude and time. The boundaries of the auroral oval (Q = 3) are shown as dotted lines.

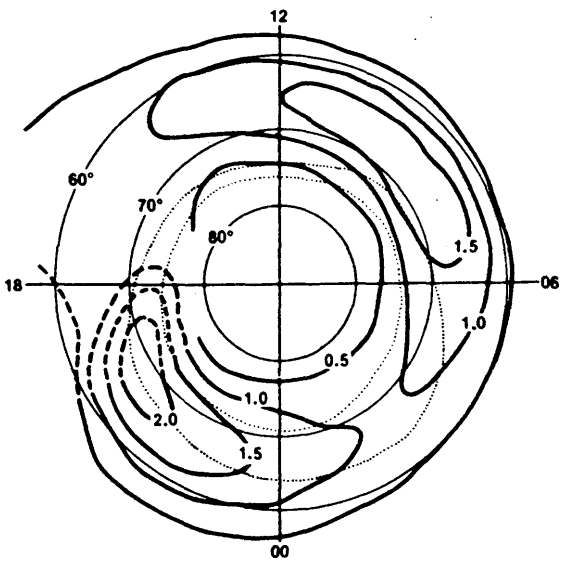


FIGURE 8 – *Median intensity of auroral absorption events in dB [Hargreaves and Cowley, 1967]*

Coordinates are geomagnetic latitude and time. The boundaries of the auroral oval (Q = 3) are shown as dotted lines.

Magnetic storms may occur from 20 to 60 hours after a major flare. If the PCA still exists when a storm commences, the absorption can spread to lower latitudes, to about 55°, due to the distortion of the geomagnetic field. It has been observed that the PCA absorption increases at about the time of the beginning of a storm, then decreases for an hour or more [Holt and Landmark, 1964; Lied, 1967].

5.5 *Effect of absorption on radio circuits*

During large absorption events HF signals may be attenuated or completely blacked out, depending on the path and on the severity of the disturbance. In general, propagation paths crossing the auroral absorption zone are affected by storms and substorms, while paths within the polar cap are affected only by PCA events. Since a PCA event affects preferentially the lower HF frequencies, while the higher frequencies are more affected by the storm-induced disturbance of the F region, a viable frequency management strategy can be to use a high frequency during the absorption event, and a low one during the following storm [Herman and Penndorf, 1964]. Other suggestions for rerouting HF traffic during absorption events are given by Lied [1967] and Hunsucker and Bates [1969].

VHF ionospheric scatter circuits are affected, for the most part, not by auroral absorption, but only by PCA events [Bailey, 1964]. This is thought to be because the scattering levels lie below the altitudes usually affected by auroral precipitation. In sunlight, these circuits experience absorption during PCA events. However, in darkness, signal levels are frequently higher than in the absence of PCA events, because of increased electron density at the scattering levels.

6. HF propagation in the irregular polar ionosphere

The polar cap ionosphere, consisting mostly of ionization transported from the sunlit hemisphere, is usually a better reflector for HF propagation than the oval that surrounds it. However it is less regular than the mid-latitude F layer, and much less so when in darkness. From the point of view of HF propagation, the ionosphere associated with the auroral oval is the most irregular of all, with large variations in time and space. The equatorward edge of the oval corresponds approximately to the poleward edge of the trough. The trough can give rise to large horizontal gradients in electron density.

6.1 *Horizontal gradients*

Horizontal gradients can produce azimuthal deviations of the ray paths from the great-circle (GC) direction, as large as 10° to 20° [Millman, 1978]. The most severe angular deviation occurs when the propagation path is tangential to the auroral oval. Scattering from irregularities can also lead to non-great-circle (NGC) modes. Azimuthal refraction can result in multipath fading and inefficient reception by directional antennas. In northern summer, normal ionospheric modes dominate, but in northern winter, NGC modes dominate [Lomax, 1972].

Gradients along the path have the effect of making the path asymmetric between transmitter and receiver, with the reflection point shifted to a point of higher density, increasing the effective MOF.

6.2 *F-layer predictions*

Buchau [1972] has pointed out that for propagation prediction in the high latitude ionosphere, it is inappropriate to use a model of an average ionosphere since the steep gradients in electron density are generally smoothed out. This applies particularly in winter, when the distribution of electron density is characterized by large and irregular variations in density.

6.3 *Rapid temporal variations*

The auroral ionosphere exhibits great variability, much of which is due to substorms. All radio propagation parameters may vary rapidly under the influence of an auroral substorm, particularly D-region absorption and sporadic E.

6.4 *Frequency and time spreading of signals*

The irregularities in the polar ionosphere are usually in motion, and therefore ionospherically reflected signals are subject to Doppler shifts. Basler *et al.* [1973] deduced drifts in the polar cap of from 0.5 to 1.0 km/s. The roughness of the ionosphere also gives rise to multipath and time spreading.

For great-circle paths, the frequency spread is not much different from that at mid-latitudes, 0.1 to 0.5 Hz. For non-great-circle paths, however, it is 5 to 10 Hz [Lomax, 1972]. Basler *et al.* [1973] quote 2 Hz under quiet conditions and 3.5 Hz under disturbed conditions. They also observed events at the rate of about 2 per hour in which the received frequency drifted at about 2 Hz/min for a few minutes. Hunsucker and Bates [1969] show a typical spectrum with a width of about 8 Hz. The time-delay spread is 100 to 200 μs for great circle paths, and 1 to 2 ms for non-great circle paths [Lomax, 1972].

Distortion of AM transmissions is common because of destructive interference between the two side bands. Single side band (SSB) and CW transmissions are less affected [Hunsucker and Bates, 1969].

6.5 *Fading*

F-region propagation paths in the polar region almost invariably experience fading due to F-region irregularities. Hunsucker and Bates [1969] quote a fading correlation bandwidth greater than 1 kHz for 90% of the time. Paths near the poleward boundary of the auroral oval, particularly in the noon sector, may be the most severely affected.

6.6 *Polarization*

At high latitudes, where the magnetic field is almost vertical, the X-mode waves have horizontal polarization for near grazing incidence. However, since X-mode waves are strongly absorbed, a vertical HF antenna, receiving the O-mode waves, should theoretically have an advantage over a horizontal antenna. A discussion of polarization matching to the ionosphere is given by Davies [1969]. In practice this advantage does not seem to have been observed, and horizontal dipoles are usually employed for convenience, and operate satisfactorily.

6.7 *Two-hop modes*

The ice caps of Greenland and Antarctica are particularly poor reflectors of radio energy [Hunsucker and Bates, 1969]. This results in greater path loss for multi-hop modes over the ice-caps than multi-hop paths elsewhere. The irregular terrain and the large variation in ground electrical properties in high latitude regions, such as Alaska, can also increase signal loss at the ground reflection point [Hunsucker, 1983].

7. HF-UHF scattering from electron density irregularities

Electron density irregularities in the ionosphere scatter radio waves over a wide range of frequencies from HF to UHF. In the case of oblique HF transmissions, backscatter extending up to F-region heights, i.e., 300-400 km, has been observed as well as in the E region [Malik and Aarons, 1964; Bates and Albee, 1970]. Backscatter from the E-region auroral and F-region irregularities is aspect angle sensitive with the maximum reflectivity occurring when the propagation direction is normal to the magnetic field lines. The aspect sensitivity decrease of the cross-section of F-region backscatter echoes in the 6 to 15 MHz band appears to be of the order of 5 dB/degree of off-perpendicularity from the magnetic field line [Bates and Albee, 1970].

Scattering from auroral ionization at VHF and UHF is normally confined to E-region heights of about 110 km [Leadabrand *et al.*, 1965; Abel and Newell, 1969]. However, 106 MHz auroral backscatter has been detected at altitudes of the order of 300 km [Schlobohm *et al.*, 1959]. Based on radio scattering from auroral ionization conducted in the frequency range from 50 to 3000 MHz, Chesnut [1972] has reported that:

- the aspect sensitivity is nearly independent of frequency,
- the scattering cross-section decreases about 10 dB/degree of aspect angle,
- the scattering cross-section varies exponentially with frequency, the slope being time-variant with an average of 33 dB/1000 MHz, and
- there is a moderate spatial correlation between the radio aurora and the visual aurora.

A comprehensive review of VHF-UHF radio auroral scattering is given by Chesnut [1972].

It is hypothesized that radio auroral reflections occur where both the (aurorally produced) electron density and the electric field (drift rate) are great enough to trigger the formation of ion-acoustic waves. This implies that the auroral echoes are associated with E-region currents, in particular with the auroral electrojet. The structure of the ion-acoustic waves gives rise to the aspect sensitivity.

Radio auroral echoes have a large Doppler spread, and the signal amplitude decorrelates in a very short time [Leadabrand *et al.*, 1965]. Such echoes have been used for VHF communication [Lange-Hesse, 1968], but the fading occurs at several hundred Hertz, and voice communications are accompanied by a characteristic growl or hiss. The path geometry must allow for specular reflection from surfaces parallel to the magnetic field, and even where the geometry is correct, communications are not available for a large fraction of the time.

The phenomenon is probably more important in terms of VHF interference due to scattering of unwanted signals from distant transmitters. At UHF, such interference is unimportant for low power circuits, but can cause clutter in high-power radars, for directions in which the magnetic orthogonality condition is satisfied.

Large enhancements may be observed on VHF links due to sporadic-E mode support, but usually such signals fluctuate with frequent deep fades. UHF tropospheric scatter links may be overloaded by intense specularly reflected signals.

8. Transionospheric propagation

Transionospheric propagation is of ———importance because of the ———traffic of communications to and from artificial earth satellites. Signals from geostationary satellites pass through the high latitude ionosphere at a low angle, encountering more ionization than would a vertical signal. For a more general treatment of transionospheric propagation, see Report 263.

8.1 *Scintillations of transionospheric signals*

Scintillations of signals passing through the ionosphere are due mainly to field-aligned irregularities in the F region [Liszka 1972]. ———Two reviews of the global morphology of ionospheric scintillation and scattering mechanisms [Yeh and Liu, 1982; Aarons, 1982] have been published. Numerical models of scintillation distribution are given by Aarons et al. [1980] and by Singleton [1980].———
Various methods of deducing the scale sizes of the irregularities that cause scintillations lead to values in the range 0.4 to 3 km. A phenomenon called "radio star visibility fade" is due to smaller irregularities, with scale sizes of the order of 100 m. Measured altitudes are all within the range 200 to 500 km. During disturbed conditions, relative density variations have been deduced in the range 10 to 40%. At auroral latitudes, the scintillation index approximately doubles as the K_p index goes from 0 to 4. The scintillation rate can be up to 50 Hz during periods of intense ionospheric disturbance.

Scintillations occur over the whole high latitude ionosphere with distinctly different morphologies being observed in the auroral oval [Basu and Aarons, 1980] and polar cap [Basu et al., 1987]. In the auroral oval, diurnal and magnetic activity variations are the major controlling factors while in the northern polar cap a pronounced minimum is observed during the June solstice when the polar ionosphere is sunlit, as shown in Figure 9. Both regions show a pronounced solar cycle effect. Clark and Raitt [1975] made direct in-situ measurements of high latitude irregularities and their measurements are in accord with the high latitude scintillation morphology study of Basu and Aarons [1980].

Martin and Aarons [1977], using 136 MHz transmissions primarily at low elevation angles, found that scintillations were most intense for propagation paths through the aurora. The rocket measurements of Frihagen and Jacobsen [1971] also showed strong variations in electron density just poleward of auroral forms. However, Buchau *et al.* [1978], monitoring 250 MHz signals from aircraft at high elevation angles, found that, during periods of quiet to moderate magnetic activity at least, the strongest scintillations occurred in the polar cap. Nevertheless, they found the highest rate of occurence of scintillations to be near the poleward boundary of the auroral oval, at least twice the rate as near the equatorward boundary. Discrete aurora embedded in the diffuse aurora (a phenomenon found in the equatorward half of the oval) did not affect the signals.

E-layer scintillations may also occur, but they tend to be masked by the stronger F-layer scintillations. In measuring signal amplitudes, rather than phase, there is a bias toward the F layer, because it is farther away from the receiver, and therefore the amplitude variations are more fully developed [Forsyth, 1972].

8.2 *Propagation delay of transionospheric signals*

For transionospheric paths, the propagation delay, which depends on total electron content, can be important. For example, the propagation path to a polar orbiting satellite can experience rapid changes in phase path due to large horizontal gradients in electron density. Sometimes variations in total content may be assumed to follow variations in the peak density of the F layer. For example, correponding to the F-layer trough there is also a trough in total content. Representative high latitude values of total electron content have been given by Klobuchar et al. [1986] and Soicher [1986b].

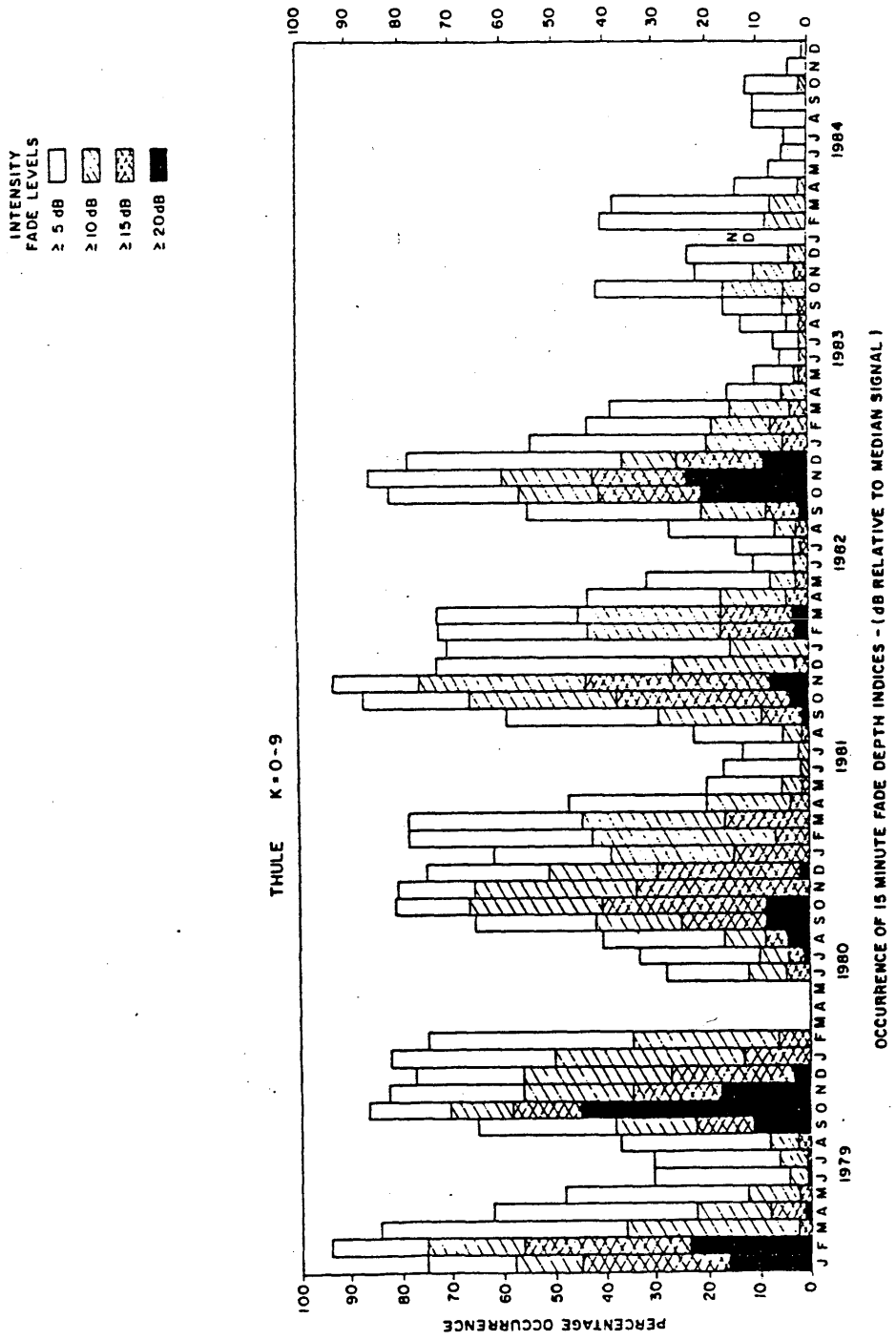


Figure 9. Variation of the occurrence of 250 MHz scintillations of various fade levels (20dB, 15dB, 10dB, 5dB) at Thule, Greenland during sunspot minimum. [From Basu et al., 1987].

However, there is likely to be considerable variation in other parameters such as the equivalent slab thickness (ratio of total content to peak density). The slab thickness in darkness is likely to be much smaller than at mid latitudes because of the escape of ionization in the topside ionosphere along open magnetic field lines. Any source of heating in the topside ionosphere, such as sunlight or low-energy electron precipitation, will increase the slab thickness. During intense auroral events, much of the ionization in a vertical column can be located below the F layer. The electron content responds to substorm activity in a complex manner depending on the season and on the time of onset of the activity [Mikkelsen and Dangaard, 1976].

9. Effects at LF/VLF

The principal features affecting the propagation of LF skywaves at high latitudes are sporadic E during night-time and D-region reflection and absorption during day-time. While the effects qualitatively can be similar to those at HF, there are marked differences. In this frequency range, the absorption decreases with decreasing frequency and with increase in the electron-density height gradient at the base of the ionosphere where the waves are reflected. Thus, during a severe disturbance, caused for example by a solar X-ray flare, HF absorption increases markedly, whereas LF "reflection height" and absorption decrease. There is a corresponding decrease in the phase delay of the signal traversing the region. LF is useful for distances of up to about 3000 km for point-to-point communications, since severe ionospheric disturbances to HF circuits in Arctic regions have only a small effect on LF signal amplitudes [Belrose, 1968; Bury, 1964].

At VLF, sky-wave absorption is small but important phase changes affect the use of these waves for navigation and positioning systems. Ionizing precipitation into the D region causes a reduction of the effective height of the ionosphere inside polar regions, which in turn causes a phase advance in any signal traversing the region. The effects of electron auroral precipitation are described by Belrose [1968], Westerlund and Reder [1973a], Larsen [1974], Kikuchi and Evans [1983] and Kikuchi *et al.*, [1983]. Even during quiet times, in the auroral zone, the night-time VLF reflection height is about 80 km, and thus markedly below that at middle and low latitudes (85 to 90 km). For signals traversing the latitude of auroral particle precipitation, VLF anomalies occur but they are not well correlated with riometer and magnetic variations. Such effects are in general stronger by night than by day, since at these latitudes few of the precipitating electrons have energies great enough to penetrate below the normal day-time D-region reflection heights. In the magnetic latitude range of about 60° to 65°, where electrons with energies greater than 200 keV precipitate, VLF anomalies are pronounced, and occur at all times of the day with maximum occurrence in the evening [Kikuchi *et al.*, 1983]. The correlation with riometer absorption and magnetic field changes is however poor, due in part to the differing sensitivities of the observed phenomena to energetic particle precipitation, and the localized nature of the precipitation. A close correlation can be found for the case of controlled experiments i.e., a path is so chosen that a once reflected sky-wave is the dominant mode, and the riometer and magnetometer are located near path mid-point [Belrose, 1968]. In the case of long-range propagation, a close correlation has been observed between absorption and magnetic field changes during global scale geomagnetic field variations such as magnetospheric substorms [Kikuchi and Evans, 1983].

Solar proton events (SPE) on the other hand have effects that are more marked, widespread and long lasting. An SPE can cause a decrease in phase delay of up to about 1.5 cycles at 10 kHz [Kasper and Hutchinson, 1978]. The events begin suddenly (onset times of 10 to 60 minutes), and decrease slowly with a return to normal over several days (up to a fortnight for strong events affecting high latitude propagation). This decrease is usually modulated by the diurnal variation in D-region electron density [Larsen, 1974], but the diurnal variation (i.e., change from night-to-day) is usually less than normal and on at least one occasion disappeared entirely [Belrose and Ross, 1962].

The low ground conductivities in Arctic regions also have a marked effect on LF and VLF propagation, particularly if the propagation path traverses the Greenland or Antarctic ice-caps. Attenuation rates for signals propagating across the Greenland ice-cap are 1.3 dB/1000 km by night and 22 dB/1000 km by day [Morfitt, 1977]. (Normal attenuation rates for mixed land-sea paths for circuits which do not traverse ice-caps are 2 dB/1000 km and 3 dB/1000 km respectively.) Since day-time proton disturbances lead to a further lowering of the ionospheric reflecting boundary, this results in attenuation rates that are markedly greater; up to 30 dB attenuations have been measured for paths traversing the Antarctic ice-cap [Crary and Crombie, 1972]. The waveguide mode structure may also change from transverse magnetic (TM) to transverse electric (TE). The severity of VLF anomalies associated with SPE therefore strongly depends on whether the transmission path crosses an ice-cap [Westerlund and Reder, 1973b].

REFERENCES

AARONS, J. [1982] Global morphology of ionospheric scintillations. *Proc. IEEE*, Vol. 70, 360-378.

AARONS J., MACKENZIE, E. and BHAVNANI, K., [1980] - High Latitude Analytical Formulas for Scintillation Levels. Radio Sci., Vol. 15, 115-127.

ABEL, W. G. and NEWELL, R. E. [1969] Measurements of the afternoon radio aurora at 1295 MHz. *J. Geophys. Res.*, Vol. 74, 231-245.

AGARD [1988] Media effects on electronic systems in the high latitude region. AGARD Lecture Series 162 (ISBN 92-835-0478-X).

AGARD [1989] Ionospheric structure and variability on a global scale and interactions with the atmosphere, AGARD CP441.

AGY, V. [1970] HF radar and auroral absorption. *Radio Sci.*, Vol. 5, 1317-1324.

AGY, V. [1975] On the geographic distribution of auroral absorption. *J. Atmos. Terr. Phys.*, Vol. 37, 681-685.

AKASOFU, S.-I. [1968] *Polar and Magnetospheric Substorms.* Springler-Verlag, New York, NY, USA.

AKASOFU, S.I. [1986] - Solar-Terrestrial Relationship in the High Latitude Region. AGARD-CP-382, 1.1-1 - 1.1-17. Avail: NTIS Ref. NASA access No. N86-27566.

AKINYAN, S. T. and CHERTOK, I. M. [1980] Determination of PCA values using integral parameters of solar microwave flares. *Geomag. i Aeronom.*, Vol. 20, 192-196.

AKINYAN, S. T., CHERTOK, I. M. and ZHULINA, E. M. [1980] Determination of PCA value from the characteristics of solar radio bursts. *Solar Terrestrial Predictions Proc.*, Vol. III, Ed. R. F. Donnelly, D27 to D33, US Govt. Printing Office, Stock No. 003-017-00473-2; Washington, DC 20402.

ALLEN, J. H., ABSTON, C. C., SALAZAR, J. E. and McKINNON, J. A. [1979] Auroral Electrojet Magnetic Activity Indices AE (11-12) for January-June 1975. World Data Center A for Solar-Terrestrial Physics, Report UAG-73, NOAA Boulder, CO., USA.

ANDERSON, D.N., BUCHAU, J. and HEELIS, R.A. [1987] - Origin of Density Enhancement in the Winter Polar Cap Ionosphere. The Effect of the Ionosphere on Communication, Navigation and Surveillance Systems, Ed. John M. Goodman, NTIS Order No. AD-191855.

BAILEY, D. K. [1964] Polar cap absorption. *Planet. and Space Sci.*, 12, 495-541.

BASLER, R. P., SCOTT, T. D. and DUPUY, R. L. [1973] Irregularity motions in the polar ionosphere. *Radio Sci.*, Vol. 8, 745-751.

BASU, S. and AARONS, J. [1980] - The Morphology of High-Latitude VHF Scintillation Near 70° W., Radio Sci., Vol. 15, 59-70.

BASU, S., MACKENZIE, E.M., BASU, S., COSTA, E., FOUGERE, P.F., CARLSON, H.C. and WHITNEY, H.E. [1987] - 250 MHz/GHz Scintillation Parameters in the Equatorial Polar and Auroral Environments. IEEE Journal on Selected Areas in Communications Vol. SAC-5, 102.

BATES, H. F. and ALBEE, P. R. [1970] Aspect sensitivity of F-layer HF backscatter echoes. *J. Geophys. Res.*, Vol. 75, 165-170.

BELROSE, J. S. [1968] Low and very low frequency radio wave propagation. AGARD Lecture Series XXIX, NTIS Accession No. AD 676788. National Technical Information Service, Springfield, Va, 22161, USA.

BELROSE, J.S. [1981] - The Propagation Medium: An Overview. AGARD Conf. Proc. No. 305 on Medium, Long and Very Long Wave Propagation (at Frequencies less than 3 000 kHz), pp. 1.1 - 1.18. Ed. J.S. Belrose. Avail: NTIS (Ref. NASA Access. No. N82-27613).

BELROSE, J. S. and ROSS, D. B. [1962] Observations of unusual LF propagation made during polar cap (PCA) events, *J. Phys. Soc.*, Japan, 17, Supplement A-11 (International Conference on Cosmic Rays and the Earth Storm), 126-130.

BELROSE, J.S. and THOMAS, L. [1968] - Ionization changes in the middle latitude D region associated with geomagnetic storms. J. Atmos. Terr. Phys., 30, 1397-1413.

BERKEY, F. T., DRIATSKIY, V. M., HENRIKSEN, K., HULTQVIST, B., JELLY, D. H., SCHUKA, T. I., THEANDER, A. and YLINIEMI, J. [1974] A synoptic investigation of particle precipitation dynamics for 60 substorms in IQSY (1964-65) and IASY (1969). *Planet. and Space Sci.*, Vol. 22, 255-307.

BESPROZVANNAYA, A.S., SHIROCHKOV, A.V. and SHCHUKA, T.I. [1979] - On the approach to forecasting polar ionospheric conditions. Solar Terrestrial Predictions Proc., Vol. II, 528-542, Ed. R.F. Donnelly, U.S. Government Printing Office, Stock No. 003-017-00471-6, Washington, D.C. 20402.

BRINTON, H. C., GREBOWSKY, J. M. and BRACE, L. H. [1978] The high latitude winter F-region at 300 km: thermal plasma observations from AE-C. *J. Geophys. Res.*, Vol. 83, 4767-4776.

BUCHAU, J. [1972] Instantaneous versus averaged ionosphere. Arctic ionosphere modelling – five related papers, AFCRL-72-0305, 1-7. Air Force Cambridge Research Laboratories, Bedford, MA., USA.

BUCHAU, J., AARONS, J., MULLEN, J. P., WEBER, E. J., WHALEN, J. A. and WHITNEY, H. E. [1978] Amplitude scintillation studies in the polar region on 250 MHz. *Effect of the Ionosphere on Space and Terrestrial Systems*, 17-24 Ed. John M. Goodman, US Govt. Printing Office 1978 0-277-182, Washington, DC 20402.

BUCHAU, J., REINISH, B. W., WEBER, E. J. and MOORE, J. G. [1983] Structure and dynamics of the winter polar cap F region. *Radio Sci.*, Vol. 18, 995-1010.

BUCHAU, J., WEBER, E.J., ANDERSON, D.N., CARLSON, JR., H.C., MOORE, J.F., REINISH, B.W. and LIVINGSTON, R.C. [1985] - Ionospheric Structures in the polar cap: Their origin and relation to 250 MHz scintillation. Radio Sci., Vol. 20, 325-338.

BURY, G. J. [1964] Military communications in the Canadian Arctic. *Arctic Communications*, 67-71 Ed. B. Landmark, AGARDograph 78, Pergamon Press, Oxford, UK.

CHAPMAN, S. [1963] Geomagnetic nomenclature. J. Geophys. Res., 68, 1174.

CHESNUT, W. G. [1972] Polar propagation effects on VHF-UHF radars. *Radar propagation in the Arctic.* Ed. J. Frihagen, AGARD-CP-97, 5-1 to 5-38.

CLARK, D. H. and RAITT, W. J. [1975] Characteristics of the high-latitude ionospheric irregularity boundary, as monitored by the total ion current probe on ESRO-4. *Planet. and Space Sci.*, Vol. 23, 1643-1647.

CLIVER, E. W., SECAN, J. A., BEARD, E. D. and MANLEY, J. A. [1978] Prediction of solar proton events at the Air Force Global Weather; Space Environmental Forecasting Facility. *Effect of the Ionosphere on Space and Terrestrial Systems.* Ed., John M. Goodman, US Govt. Printing Office 0-277-182, 393-400, Washington, DC 20402.

COLLINS, C., JELLY, D. H. and MATTHEWS, A. G. [1961] High-frequency radio-wave black-outs at medium and high latitudes during a solar cycle. *Can. J. Phys.*, 39, 35-52.

CRARY, J. H. and CROMBIE, D. D. [1972] Antarctic ice cap attenuation rates of VLF signals determined from short and long great circle paths. *Radio Sci.*, Vol. 7, 233-238.

DAVIES, K. [1969] *Ionospheric Radio Waves.* Blaisdell, Waltham, MA., USA.

DAVIS, T. N. and M. Sugiura [1966] Auroral electrojet index AE and its Universal Time variations. J. Geophys. Res., 71, 785-801.

DE LA BEAUJARDIERE, O., CAUDAL, O.G., HOLT, J., CRAVEN, J., WICKWAR, V.B., BRACE, L., EVANS, D and WINNINGHAM, J.D. [1985] - Universal Time Dependence of Night-time F-Region densities at High Latitudes. J. Geophys. Res., Vol. 90, 4319.

DIEMINGER, W. [1955] - Short wave echoes from the lower ionosphere. Conference on the Physics of the Ionosphere, Phys. Soc. (London), 53-57.

DUCHARME, E. D., PETRIE, L. E. and EYFRIG, R. [1971] A method for predicting the F1 critical frequency. *Radio Sci.*, Vol. 6, 369-378.

DUDENEY, J.R., RODGER, A.S. and JARVIS, M.J. [1983] - Radio studies of the main F-region trough in Antarctica. Radio Sci., Vol. 18, 927-936.

ELKINS, T.J. [1980] - A model for high frequency solar auroral clutter. RADC-TR-80-122. Rome Air Development Center, Grifiss Air Force Base, N.Y., NTIS Order No. AD-A091049.

ELKINS, T.J. and RUSH, C.M. [1973] - A statistical predictive model of the polar ionosphere. An Empirical Model of the Polar Ionosphere. Ed. T. Elkins, AFCRL-TR-73-0331. Air Force Cambridge Research Laboratories, Hanscom Air Force Base, MA 01731, NTIS Order No. AD-766-240.

ETEMADI, A., COWLEY, S.W.H., LOCKWOOD, M., BROMAGE, B.J.I., WILLIS, D.M. and LUHR, H. [1988] - The dependence of high latitude dayside ionospheric flows on the north-south component of the IMF: a high time resolution correlation analysis using EISCAT "POLAR" and AMPTE UKS and IRM data, Planet Space Sci., 36, 471-498.

FELDSTEIN, Y. I. and STARKOV, G. V. [1967] Dynamics of auroral belt and polar geomagnetic disturbances. *Planet. and Space Sci.*, Vol. 15, 209-229.

FORSYTH, P. A. [1972] (In discussion on polar scintillation) *Radar Propagation in the Arctic*, Ed. J. Frihagen AGARD-CP-97, IV-2.

FRANK, L. A. and J. D. CRAVEN [1988] Imaging results from Dynamics Explorer 1, Rev. Geophys., 26, 249-283.

FREMOUW, E. J. and FANG, D. J. [1975] An All-Sky-Camera format for radar auroral studies. *Radio Sci.*, Vol. 10, 891-904.

FRIHAGEN, J. and JACOBSEN, T. [1971] *In situ* observations of high latitude F-region irregularities. *J. Atmos. Terr. Phys.*, Vol. 33, 519-522.

FULLER-ROWELL, T. J. and D. S. EVANS [1987] Height-integrated Pedersen and Hall conductivity patterns inferred from the TIROS-NOAA satellite data. J. Geophys. Res., 92, 7606-7618.

GASSMANN, G. J. [1970] An ionospheric model for the arctic. AFCRL-70-0562, Air Force Cambridge Research Laboratories, Bedford, Mass., USA.

GASSMANN, G. J. [1972] Model of arctic sporadic E. Arctic ionosphere modelling – five related papers. AFCRL-72-0305, 21-28. Air Force Cambridge Research Laboratories, Bedford, MA., USA.

GUSTAFSSON, G. [1970] A revised corrected geomagnetic coordinate system. *Arkiv för Geofysik*, 5, 595-617.

HAKURA, Y. [1965] Tables and maps of geomagnetic coordinates corrected by the higher order spherical harmonic terms. *Rep. Ion. and Space Res. Japan*, Vol. 19, 121-157.

HALCROW, B. W. and NISBET, J. S. [1977] A model of F2 peak electron densities in the main trough region of the ionosphere. *Radio Sci.*, Vol. 12, 815-820.

HARDY, D.A., GUSSENHOVEN, M.S. and HOLEMAN, E. [1985] - A Statistical Model of Auroral Electron Precipitation. J. Geophys. Res., Vol. 90, A5, 4229-4248.

HARGREAVES, J. K. [1968] Auroral motions observed with riometers: latitudinal movements and a median global pattern. *J. Atmos. Terr. Phys.*, Vol. 30, 1461-1470.

HARGREAVES, J. K. [1969] Auroral absorption of HF radio waves in the ionosphere: a review of results from the first decade of riometry. *Proc. IEEE*, Vol. 57, 1348-1373.

HARGREAVES, J. K. [1974] Dynamics of auroral absorption in the midnight sector – the movement of absorption peaks in relation to the substorm onset. *Planet. and Space Sci.*, Vol. 22, 1427-1441.

HARGREAVES, J. K. and COWLEY, F. C. [1967] Studies of auroral radio absorption events at three magnetic latitudes-I occurrence and statistical properties of the events. *Planet. and Space Sci.*, Vol. 15, 1571-1583.

HARTZ, T. R. [1971] Particle precipitation patterns. *The radiating atmosphere*, 225-238, Ed. B. M. McCormac, D. Reidel, Publishing Co., Dordrecht, Netherlands.

HARTZ, T. R. and BRICE, N. M. [1967] The general pattern of auroral particle precipitation. *Planet. and Space Sci.*, Vol. 15, 301-329.

HARTZ, T. R., MONTBRIAND, L. E. and VOGAN, E. L. [1963] A study of auroral absorption at 30 MHz. *Can. J. Phys.*, **41**, 581-595.

HEELIS, R.A., LOWELL, J.K. and SPIRO, R.W. [1982] - A Model of the High Latitude Ionosphere Convection Pattern. J. Geophys. Res., Vol. 87, 2873-2880, 1984.

HEPPNER, J. P. [1977] Empirical models of high-latitude electric fields. *J. Geophys. Res.*, Vol. 82, 1115-1125.

HERMAN, J. R. and PENNDORF, R. B. [1964] Reception of mid-latitude transmissions in northern Canada. *Arctic Communications*, 97-119. Ed. B. Landmark, AGARDograph 78, Pergamon Press, Oxford, UK.

HILL, G. E. [1963] Sudden enhancements of F-layer ionization in polar regions. *J. Atmos. Sci.*, Vol. 20, 492-497.

HILL, G. E. and PENNDORF, R. B. [1959] Research concerning forecasting of anomalous propagation at high latitudes. Tech. Rep. RAD-TR-59-19, AVCO Corp., Wilmington, MA., USA.

HOLT, O. and LANDMARK, B. [1964] Some experimental studies of the arctic D-region. *Arctic Communications*, 3-25. Ed. B. Landmark AGARDograph 78, Pergamon Press, Oxford, UK.

HULZWORTH, R. H. and C.-I. MENG [1975] Mathematical representation of the auroral oval. Geophys. Res. Letters, 2, 377-380.

HOPKINS, H. D., O'AREY, R. J. and SAYERS, J. [1973] UT control of the topside polar ionosphere. *Planet. and Space Sci.*, Vol. 21, 1459-1462.

HUNSUCKER, R. D. [1983] Anomalous propagation behaviour of radio signals at high latitudes. AGARD Conf. Proc. No. 332, *Propagation Aspects of Frequency Sharing, Interference and System Diversity*, 11-1 to 11-15. Ed. H. Soicher. NASA Accession No. N83-30873. National Technical Information Service, Springfield, VA 22161, USA.

HUNSUCKER, R. D. and BATES, H. F. [1969] Survey of polar and auroral region effects on HF propagation. *Radio Sci.*, Vol. 4, 347-365.

HUNSUCKER, R. D. and GREENWALD, R. A. (Guest Eds.) [1983] Including special papers: radio probing of the high-latitude ionosphere and atmosphere: new techniques and new results. *Radio Sci.*, Vol. 18, 6.

JELLY, D. H. [1970] On the morphology of auroral absorption during substorms. *Can. J. Phys.*, **48**, 335-345.

JELLY, D. H. and BRICE, N. M. [1967] Changes in Van Allen radiation associated with polar substorms. *J. Geophys. Res.*, Vol. 72, 5919-5931.

KASPER, J. F. and HUTCHINSON, C. E. [1978] The Omega navigation system, an overview. *IEEE Comm. Soc. Mag.*, Vol. 16, 3, 23-35.

KELLEY, M. C., VICKREY, J. F., CARLSON, C. W. and TORBERT, R. [1982] On the origin and spatial extent of high latitude F region irregularities. *J. Geophys. Res.*, Vol. 87, 4469-4475.

KESKINEN, M. J. and OSSAKOW, S. L. [1983] Theories of high latitude ionospheric irregularities: a review. *Radio Sci.*, Vol. 18, 1077-1091.

KIKUCHI, T. and EVANS, D. S. [1983] Quantitative study of substorm-associated VLF phase anomalies and precipitating energetic electrons on November 13, 1979. *J. Geophys. Res.*, Vol. 88, 871-880.

KIKUCHI, T., NOZAKI, K. and OHTANI, A. [1983] Simultaneous observation of VLF phase and absorption anomalies at Showa station, Antarctica in association with magnetospheric substorms. *Memoirs of Nat. Inst. Polar Res.*, Special Issue **26**, 113-123. National Institute of Polar Research, Tokyo, Japan.

KLOBUCHAR, J.A., BISHOP, G.J. and DOHERTY, P.H. [1986] - Total Electron Content and L-Band Amplitude and Phase Scintillation Measurements in the Polar Cap Ionosphere. AGARD CP-382, Ed. H. Soicher, 2.1-1 - 2.1-8. Avail: NTIS Ref. NASA access No. N86-27566.

KONNLEIN, W. and RAITT, W. J. [1978] ESRO-1 and ESRO-4: A model of the UT effect in electron density at middle latitudes of the southern hemisphere. *Planet. and Space Sci.*, Vol. 26, 1179-1184.

LANGE-HESSE, G. [1968] VHF auroral backscatter communication. *Ionospheric Radio Communications*, 174-206, Ed. K. Folkestad, Plenum Press, New York, NY. 10011, USA.

LARSEN, T. R. [1974] Irregular variations in the high latitude ionosphere and their effects on propagation. *ELF-VLF Radio Wave Propagation*, 171-185, Ed. J. A. Holtet, D. Reidel Publishing Co., Dordrecht, Netherlands.

LARSEN, T.R., REGEAN, J.B., IMHOF, W.L., MONTBRIAND, L.E. and BELROSE, J.S. [1976] - A coordinated study of energetic electron precipitation and D-region electron concentrations over Ottawa during disturbed conditions. J. Geophys. Res., 81, 2200-2212.

LAUTER, E. A., BREMER, J., GRAFE, A., DETERS, I. and EVERS, K. [1977] The post-storm ionization enhancements in the mid-latitude D region and related electron precipitation from the magnetosphere. Heinrich-Hertz Institute STP Report No. 9.

LAUTER, E. A., LASTOVICKA, J. and RAPOPORT, Z. T. [1978] Mid-latitude post-storm events and interplanetary magnetic field. *Phys. Solariterr.*, **1**, 13-82.

LEADABRAND, R. L., SCHLOBOHM, J. C. and BARON, M. J. [1965] Simultaneous very high frequency and ultra high freqency observations of the aurora at Fraserburgh, Scotland. *J. Geophys. Res.*, Vol. 70, 4235-4284.

LIED, F., Ed. [1967] *High Frequency Radio Communications with Emphasis on Polar Problems.* AGARDograph 104, Technivision, Maidenhead, UK.

LISZKA, L. [1972] Polar propagation effects on radio-astronomical and satellite transmissions. *Radar Propagation in the Arctic.* AGARD-CP-97, 16-1 to 16-8.

LOMAX, J. B. [1972] Frequency distortion in auroral HF propagation. *Radar Propagation in the Arctic*, AGARD-CP-97, 22-1 to 22-12.

MALIK, C. and AARONS, J. [1964] A study of auroral echoes at 19.4 megacycles per second. *J. Geophys. Res.*, Vol. 69, 2557-2564.

MARTIN, E. and AARONS, J. [1977] F layer scintillations and the aurora. *J. Geophys. Res.*, Vol. 82, 2717-2722.

McILWAIN, C. E. [1966] Magnetic coordinates. *Space Sci. Rev.*, **5**, 585-598.

MENG, C.-I. [1984] Dynamic variation of the auroral oval during intense magnetic storms. J. Geophys. Res., 89, 227-235.

MENG, C.-I. and K. MAKITA [1986] Dynamic variations of the polar cap. Solar Wind-Magnetosphere Coupling, edited by Y. Kamide and J. A. Slavin, Terra Scientific, Tokyo, 605-631.

MIKKELSEN, I. S. and DANGAARD, K. [1976] Behavior of auroral zone total electron content during substorms. Proc. COSPAR Symposium on the geophysical Use of Satellite Beacon Observations, 384, Boston, MA., USA.

MILLMAN, G. H. [1978] Ionospheric propagation effects on HF backscatter radar measurements. *Effect of the Ionosphere on Space and Terrestrial Systems*, 211-218. Ed. John M. Goodman. US Govt. Printing Office, 0-277-182, Washington, DC 20402.

MORFITT, D. G. [1977] Effective electron density distributions describing VLF/LF propagation data. Report NOSC TR141, Naval Ocean Systems Centre, San Diego, CA., USA.

MULDREW, D.B. [1965] - F-layer ionization troughs deduced from Alouette data. J. Geophys. Res., 70, 2635-2650.

MULDREW, D.B. [1983] - Alouette - ISIS radio wave studies of the cleft, the auroral zone and the main trough and of their associated irregularities. Radio Sci., Vol. 18, 1140-1150.

MULDREW, D. B. and VICKREY, J. F. [1982] High-latitude F region irregularities observed simultaneously with ISIS-1 and the Chatanika radar. *J. Geophys. Res.*, Vol. 87, 8263-8272.

NELMS, G.L. and CHAPMAN, J.H. [1970] - The high latitude ionosphere: results from the Alouette/ISIS topside sounders. The Polar Ionosphere and Magnetospheric Processes, 233-269. Ed. G. Skovli, Gordon Breach Publishing Co., New York, NY, USA.

NISHIDA, A. [1967] Average structure and storm-time change of the polar topside ionosphere at sunspot minimum. *J. Geophys. Res.*, Vol. 72, 6051-6061.

OFFERMAN, D. [1979] - An integrated GBR Campaign for Study of the D-region in Western Europe 1975/76. J. Atmos. Terr. Phys., 41, 1047-1050.

PENMAN, J. M., HARGREAVES, J. K. and McILWAIN, C. E. [1979] The relation between 10 to 80 keV electron precipitation observed at geosynchronous orbit and auroral radio absorption observed with riometers. *Planet. and Space Sci.*, Vol. 27, 445-451.

PIGGOTT, W.R. and RAWER, K. [1972] - URSI Handbook of ionogram interpretation and reduction. World Data Center A for Solar-Terrestrial Physics, Report UAG-23, NOAA, Boulder, CO. 80303.

PIKE, C. P. [1971] A latitudinal survey of the daytime polar F layer. *J. Geophys. Res.*, Vol. 76, 7745-7753.

PIKE, C. P., MENG, C.-I., AKASOFU, S.-I. and WHALEN, J. A. [1974] Observed correlations between interplanetary magnetic field variations and the dynamics of the auroral oval and the high-latitude ionosphere. *J. Geophys. Res.*, Vol. 79, 5129-5142.

QUEGAN, S., GILL, R.S. and LOCKWOOD, M. [1988] - Comparisons between EISCAT observations and model calculations of the high latitude ionosphere, J. Atmos, Terr. Phys., 50, 1057-1076.

REES, M. H., D. LUMMERZHEIM, R. G. ROBLE, J. D. WINNINGHAM, J. D. CRAVEN, and L. A. FRANK [1988] Auroral energy deposition rate: characteristic electron energy and ionospheric parameters derived from Dynamics Explorer 1 images. J. Geophys. Res., 93, 12841-12860.

REILLY, A. E. [1978] The geomagnetic index Q-its persistence, predictability and other pertinent properties, AFGL-TR-78-0223. National Technical Information Service, Springfield, VA. 22161, USA.

RISHBETH, H., SMITH, P.R., COWLEY, S.W.H., WILLIS, D.M. VAN EYKEN, A.P., BROMAGE, B.J.I and CROTHERS, S.R. [1985] - Ionospheric response to changes in the interplanetary magnetic field observed by EISCAT and AMPTE UKS, Nature, 318, 451-452.

ROBINSON, R.M., TSUNODA, R.T., and VICKEREY, J.F. [1985] - Sources of F-region Ionization Enhancements in the Night-time Auroral Zone. J. Geophys. Res., Vol. 90, 7533-7546.

ROSTOKER, G., S.-I. AKASOFU, J. FOSTER, R. A. GREENWALD, Y. KAMIDE, K. KAWASAKI, A. T. Y. LUI, R. L. McPHERRON, and C. T. RUSSELL [1980] Magnetospheric substorms - definitions and signatures. J. Geophys. Res., 85, 1663-1668.

RYCROFT, M.J., and THOMAS, J.O. [1970] - The magnetospheric plasmapause and the electron density trough at the Alouette 1 orbit. Planet and Space Sci., Vol. 18, 6580.

SATO, T. and ROURKE, G. F. [1964] F-region enhancements in the Antarctic. *J. Geophys. Res.*, Vol. 69, 4591-4607.

SCHLOBOHM, J. C., LEADABRAND, R. L., DYCE, R. B., DOLPHIN, L. T. and BERG, M. R. [1959] High-altitude 106.1 – Mc radio echoes from auroral ionization detected at a geomagnetic latitude of 43°. *J. Geophys. Res.*, Vol. 64, 1191-1196.

SINGLETON, D. C. [1980] Improving the ionospheric irregularity model. *Solar Terrestrial Predictions Proc.*, Vol. IV, Ed. R. F. Donnelly, D1-1 to D1-15, US Govt. Printing Office, Stock No. 003-117-00479-1, Washington, DC 20402.

SOICHER, H., EDITOR [1986a] - Propagation Effects on Military Systems in the High Latitude Region. AGARD-CP-382. Avail: NTIS Ref. NASA Access. No. N86-27566.

SOICHER, H. [1986b] - Variability of Transionospheric Time Delay at Subauroral Latitudes. IEEE Transactions on Antennas and Propagation, Vol. AP-34, No. 11, 1313-1319.

TIMLECK, J.E. and NELMS, G.L. [1969] - Electron densities less than 100 cm^{-3} in the topside ionosphere. Proc. IEEE, 57, 1164-1171.

VALLEY, S. L., Ed. [1965] *Handbook of Geophysics and Space Environment*, McGraw-Hill Book Co., New York, NY, USA.

WAGNER, R. A. [1972] Modelling the auroral E-layer. Arctic Ionospheric Modelling – Five Related Papers. AFCRL 72-0305, 9-20. Air Force Cambridge Research Laboratories, Bedford, MA., USA.

WAGNER, C.-U. and RANTA, H. [December, 1983] The midlatitudinal post-storm electron precipitation belt. *J. Atmos. Terr. Phys.*, Vol. 45, 12, 811-822.

WAGNER, C.-U., RANTA, H. and RANTA, A. [1982] Night-time ionospheric absorption during and after magnetospheric storms from auroral (L = 6.0) to medium (L = 2.5) latitudes. *J. Atmos. Terr. Phys.*, Vol. 44, 747-757.

WAGNER, R. A., SNYDER, A. L. and AKASOFU, S.-I. [1973] The structure of the polar ionosphere during exceptionally quiet periods. *Planet. and Space Sci.*, Vol. 21, 1911-1922.

WATKINS, B.J., AKASOFU, S.I., FRY, C.D. [1986] - Progress in Modelling the Polar Ionosphere from Solar and Magnetosphere Parameters. AGARD-CP-382, 7.2-1 - 7.2-4. Avail: NTIS Ref. NASA Access. No. N86-27566.

WEBER, E. J. and BUCHAU, J. [1981] Polar cap F layer auroras. *Geophys. Res. Lett.*, 8, 125.

WEBER, E.J., TSUNODA, R.T., BUCHAU, J., SHEEHAN, R.E., STRICKLAND, D.J., WHITING, W. and MOORE, J.G. [1985] - Coordinated Measurements of Auroral Zone Plasma Enhancements. J. Geophys. Res. Vol. 90, 6497-6513.

WESTERLUND, S. and REDER, F. H. [1973a] VLF propagation at auroral latitudes. *J. Atmos. Terr. Phys.*, Vol. 35, 1453-1474.

WESTERLUND, S. and REDER, F. H. [1973b] VLF signals propagating over the Greenland ice-sheet. *J. Atmos. Terr. Phys.*, Vol. 35, 1475-1491.

WHALEN, J. A. [1970] Auroral oval plotter and monograph for determining corrected geomagnetic local time, latitude and longitude for high latitudes in the Northern Hemisphere. Air Force Cambridge Research Laboratories, Report No. AFCRL-70-0422, Environmental Research Paper, No. 327, AD 713170 (available from Defense Technical Information Center, Cameron Station, Alexandria, VA. 22314, USA).

WHITTEKER, J. H. [1976] The magnetospheric cleft – ionospheric effects. *J. Geophys. Res.*, Vol. 81, 1279-1288.

WHITTEKER, J. H. [1977] The transient response of the topside ionosphere to precipitation. *Planet. and Space Sci.*, Vol. 25, 773-786.

WHITTEKER, J. H., SHEPHERD, G. G., ANGER, C. D., BURROWS, J. R., WALLIS, D. D., KLUMPAR, D. M. and WALKER, J. R. [1978] The winter polar ionosphere. *J. Geophys. Res.*, Vol. 83, 1503-1518.

WILLIS, D.M., LOCKWOOD, M., COWLEY, S.W.H., VAN EYKEN, A.P., BROMAGE, B.J.I., RISHBETH, H., SMITH, P.R., and CROTHERS, S.R. [1986] - A survey of simultaneous observations of the high-latitude ionosphere and interplanetary magnetic field with EISCAT and AMPTE UKS, J. Atmos. Terr. Phys., 48, 987-1008.

YEH, K. C. and LIU, C. H. [1982] Radio wave scintillation in the ionosphere. *Proc. IEEE*, Vol. 70, 324-360.

ZHULINA, E. M., KISCHA, D. V., LUKASKIN, V. M. and SCHIRACHKOV, A. V. [1983] *Additional energy losses in high-latitude radio links.* Nauka Publishing House, Moscow, USSR.

ZMUDA, A. J. and POTEMRA, T. A. [1972] Bombardment of the polar-cap ionosphere by solar cosmic rays. *Rev. Geophys. Space Phys.*, Vol. 10, 981-991.

REPORT 574-2

IONOSPHERIC CROSS-MODULATION

(Study Programme 28F/6)

(1974–1978–1986)

1. Introduction

The basic theory of non-linear phenomena in a plasma as developed by Ginzburg and Gurevich [1960] and Gurevich [1971] extends the earlier work of Bailey [1937] on wave interaction or "cross-modulation". Briefly stated, the propagation of strong modulated waves through a plasma produces perturbations in the plasma which cause changes to take place in the electron temperatures which in turn affect the collision frequency, ion chemistry and electron density; and therefore the conductivity and permittivity of the medium. The result of these changes in the medium produced by one modulated intense radio wave is the superimposition of its modulation on the carrier of another wave propagating through the same region. Because of the large number of transmissions using the HF, MF and LF bands which propagate through the D and E regions, this wave interaction or ionospheric cross-modulation is difficult to distinguish from co-channel interference and even more difficult to measure [Huxley, 1950, 1955; Fejer, 1955; Ratcliffe and Shaw, 1948; Shaw, 1951; Bell, 1966; Hibberd, 1964; Cutolo, 1964, etc.].

Measurements made when the bands were less crowded have been summarized by Knight [1973] and show cross-modulation depths less than 7% when standardized to a power of 100 kW. The standardized measurements are shown in Fig. 1 of Annex I to Recommendation 498.

2. The simple theory of cross-modulation

For the communications engineer concerned with estimating the interference caused by cross-modulation, the main features of a treatment given by Huxley and Ratcliffe [1949] in a paper designed to give a simple physical explanation of the phenomenon are presented.

2.1 *The electron collisional process*

The free electrons which are mainly responsible for the reaction of the ionosphere on radio waves are located in D and lower E regions and may be regarded as a gaseous constituent statistically in thermal equilibrium with the far more numerous molecules in the atmosphere. Each electron may be considered to have a thermal energy Q_0 and a velocity V_0 related to the temperature θ_0 of the atmosphere by the gas equation:

$$Q_0 = \frac{1}{2} m V_0^2 = \frac{3}{2} k\theta_0 \tag{1}$$

where m is the mass of the electron (9.1×10^{-31} kg), k is the Boltzmann's constant (1.37×10^{-23} joules per Kelvin) and θ_0 is in Kelvin, Q_0 and V_0 being in MKS units.

If at the point under consideration the equilibrium is disturbed by increasing the velocity of the electrons to V, Q_0 and θ_0 change to Q and θ in accordance with (1), the temperature of the surrounding atmosphere being unchanged. There is no conclusive evidence as to how the electron collision frequency depends upon V in the lower ionosphere, but it will be assumed here that the mean free path of electrons is independent of electron velocity, so that the collisional frequency ν is increased from its equilibrium value ν_0 proportionately with V. Thus:

$$\frac{Q}{Q_0} = \frac{\nu^2}{\nu_0^2} = \frac{\theta}{\theta_0} \tag{2}$$

At each collision some energy is transferred to the surrounding atmosphere, the amount being proportional to the energy excess and equal to $G(Q - Q_0)$ where G is a constant that from laboratory experiments on nitrogen is found to have a value of about 10^{-3}. The equilibrium is disturbed by the passage of a radio wave, and if the energy extracted from the wave by an electron in a collision at the time t is Q_e, the energy equation for the electron is:

$$\frac{dQ}{dt} = \nu Q_e - \nu G(Q - Q_0)$$

which from (2) may be written

$$\frac{d\nu}{dt} = \frac{Q_e \nu_0^2}{2 Q_0} - \frac{G}{2}(\nu^2 - \nu_0^2) \tag{3}$$

If Q_e were constant ν would ultimately take up a value $\bar{\nu}$ given by:

$$\bar{\nu} = \nu_0 \left(1 + \frac{Q_e}{G Q_0}\right)^{1/2} \tag{4}$$

except possibly for very strong fields, $Q_e \ll G Q_0$ and therefore $\nu - \nu_0 \ll \nu_0$.

Thus with the removal of Q_e, $\nu - \nu_0$ decays exponentially to zero with a time-constant of $1/G\nu_0$. In the region of the ionosphere under consideration ν_0 is of the order of 10^6 collisions per sec, so that this time constant is about 10^{-3} seconds corresponding to a frequency of 1000 Hz. It therefore follows that the collisional frequency is unable to respond to the changes at radio frequency in the wave.

As, however, Q_e is proportional to the power density in the wave and hence to the square of the electric field E, the collisional frequency can respond to the r.m.s. value of the field. If this r.m.s. value is amplitude-modulated at audio frequency, the collisional frequency will in some measure be able to follow the modulation for frequencies not greatly in excess of 500 Hz.

2.2 *The modulation process*

In general the modulation on the radio wave will contain many audio frequencies, but to estimate the level of cross-modulation it is sufficient to consider a single frequency $\omega/2\pi$ and only the component of this frequency in the square of the field. Thus writing the r.m.s. radio field as:

$$E = E_0 (1 + M \cos \omega t) \tag{5}$$

the square will be taken as:

$$E^2 = E_0^2 \left(1 + \frac{M^2}{2}\right) + E_0^2\ 2M\ \cos \omega t \tag{6}$$

where $M = 1$ for 100% modulation.

The mean value of E^2 is thus significantly above E_0^2, and it is this increased value that determines the mean value of ν in (4) while ν takes the form:

$$\nu = \bar{\nu} (1 + M_\nu) \tag{7}$$

where M_ν is the modulation derived from the modulation term in (6).

Writing Q_e as

$$Q_e = CE^2 \tag{8}$$

where the constant of proportionality C will be found by considering the attenuation of the radio wave by the electron collisions as it passes through the ionosphere, and taking the modulation component of ν in (7) as $\nu_0 M_\nu$, the modulation equation derived from (3), (6) and (8) becomes:

$$\nu_0 \frac{dM_\nu}{dt} = \frac{\nu_0^2\ CE_0^2\ 2M\ \cos \omega t}{2Q_0} - \frac{G}{2}\ 2\nu_0\ (\nu_0 M_\nu)$$

or

$$\frac{dM_\nu}{dt} + G\nu_0 M_\nu = \frac{\nu_0\ CE_0^2 M \cos \omega t}{Q_0}$$

whence

$$|M_\nu| = \frac{CE_0^2\ M}{Q_0\ G\left[1 + \left(\frac{\omega}{G\nu_0}\right)^2\right]^{1/2}} \tag{9}$$

The denominator shows how the response drops off at higher audio frequencies.

2.3 *The absorption process*

As the radio wave passes through the ionosphere, the loss of the energy extracted by the electrons in the collisional process causes the wave to be exponentially attenuated according to an amplitude reduction factor $\exp(-\int \alpha ds)$ where the integral is taken over the transmission path and α is an absorption coefficient. By considering the absorption of the wave passing through a thin slab of unit cross-section, it can be shown that the energy Q_e extracted by each electron in a collision is:

$$Q_e = \frac{2\alpha\mu E^2}{N\nu\ Z_0} \tag{10}$$

where μ is the real part of the refractive index of the ionosphere given by the Appleton-Hartree equation, N is the electron density (number of electrons per m^3) and Z_0 is the impedance of free space, the field E being in V/m.

As the radio frequency may be in the neighbourhood of the gyromagnetic frequency f_H, it is important to include the effect of the Earth's magnetic field by considering the case for which it is greatest, when the propagation is along the direction of the earth's field. The value of α is then known to be:

$$\alpha = \frac{Ne^2 Z_0 \nu}{2\mu m [4\pi^2 (f \pm f_H)^2 + \nu^2]} \tag{11}$$

where e is the electron charge (1.60×10^{-19} coulomb), f is the radio frequency in Hz, and the + and − signs refer to the ordinary and extraordinary waves respectively.

Thus from (8), (10) and (11):

$$C = \frac{e^2}{m [4\pi^2 (f \pm f_H)^2 + \nu^2]} \tag{12}$$

The ν^2 term in the denominator can be neglected in the present estimate of cross-modulation if, say $4\pi^2 (f \pm f_H)^2 > 10\nu^2$ or $(f \pm f_H) > \nu/2$. This criterion is well enough obeyed at high and medium frequencies, except for the extraordinary wave near to the gyrofrequency, which is of the order of 1 MHz, where a resonance occurs increasing the value of C. Under these resonance conditions, especially for high power transmissions, the value of $\nu - \nu_0$ may be comparable with ν_0, and (4) from (8) and (12) should be regarded as a quadratic equation in $(\bar{\nu})^2$. At lower frequencies where f is of the order of or less than ν, a much more sophisticated full-wave treatment of the whole problem is really needed.

The value of C in (12) used in (9) gives

$$|M_\nu| = \frac{2e^2 E_0^2 M}{3 m k \theta_0 \left[4\pi^2 (f \pm f_H)^2 + \nu_0^2\right] G \left[1 + \left(\frac{\omega}{G\nu_0}\right)^2\right]^{1/2}} \tag{13}$$

where Q_0 has been given its value in (1) and in the denominator ν^2 has been approximated by ν_0^2, in keeping with the assumption made in deriving (9) that C is a constant for a given carrier frequency.

2.4 *Demodulation and cross-modulation*

As the attenuation of the wave has the form of an amplitude reduction factor, the direct dependence of α in (11) upon ν implies that the modulation transferred from the wave to the collisional frequency reacts back on the amplitude of the wave. Actually this produces some demodulation of the wave, which is a phenomenon of considerable interest when using modulation experiments to investigate the physical structure of the lower regions of the ionosphere. For this purpose it is really necessary to make a much more detailed statistical analysis of the electron motion than has been adopted here which includes a close study of the gyromagnetic resonance.

More importantly here, however, the modulation imposed on α can similarly be transferred to the amplitude reduction factor of another wave of different frequency passing through the modulation region, giving rise to cross-modulation. Apart from its physical significance, this phenomenon is a source of interference which it is here the purpose to assess. In principle the effect is mutual, each wave to some extent being demodulated and modulating the other, but it is now desirable to distinguish between the frequencies and to regard one transmission as wanted, with its own modulation on to which some modulation is imposed from an unwanted or disturbing transmission. Calling the frequencies f_W and f_D respectively, the frequency f in (13) must now be interpreted as f_D.

If the amplitude reduction factor for the wanted wave is ρ, from (7) and (11) it is then given by

$$\rho = \exp\left(-\int \frac{Ne^2 Z_0 \bar{\nu} (1 + M_\nu)\, ds}{2\mu m [4\pi^2 (f_W \pm f_H)^2 + \nu^2]}\right) \tag{14}$$

The integration is extended over the region of cross-modulation, which is of limited size because of the attenuation suffered by the disturbing wave in passing through the ionosphere, whereby the modulation in (13) imposed on the collisional frequency decreases with the decrease in E_0. The region may, however, be sufficiently extended for the increase of N and the decrease of ν with height in the ionosphere to be significant in estimating ρ in (14). Eventually the product $N\nu$ decreases, but initially it can increase with height.

The time of passage of a wave-front through the region is so short that (14) may be regarded as an integration across the region at a moment of time on the audio-frequency time scale. Thus M_v is held constant with respect to time during the integration, and the consideration of the time variation of M_v at the audio frequency shows that ρ becomes modulated and may be written in terms of a mean value and modulation M_ρ by:

$$\rho = \bar{\rho}\,(1 + M_\rho) \tag{15}$$

Thus

$$\log_e \rho = \log_e \bar{\rho} + \log_e (1 + M_\rho)$$

or since it may be anticipated that $M_\rho \ll 1$

$$\log_e \rho = \log_e \bar{\rho} + M_\rho \tag{16}$$

As $M_\rho = 0$ when $M = 0$, it follows from (14) and (16) that

$$\log_e \bar{\rho} = -\int \frac{Ne^2\, Z_0\, \bar{\nu}\, ds}{2\mu m\,[4\pi^2\,(f_W \pm f_H)^2 + \bar{\nu}^2]} \tag{17}$$

$$M_\rho = -\int \frac{Ne^2\, Z_0\, \bar{\nu}\, M_v\, ds}{2\mu m\,[4\pi^2\,(f_W \pm f_H)^2 + \bar{\nu}^2]} \tag{18}$$

where in the denominators the modulation on ν^2 has been neglected by using the mean value.

The integral for M_ρ in (18) may now be estimated by taking M_v outside as a mean value while formally retaining the dependence of N and ν on position inside the integral, so that from (17) in terms of amplitudes

$$|M_\rho| = -|M_v| \log_e \bar{\rho} \tag{19}$$

and hence from (13)

$$|M_\rho| = -\frac{2e^2 E_0^2\, M \log_e \bar{\rho}}{3mk\theta_0 \left[4\pi^2\,(f_D \pm f_H)^2 + \nu_0^2\right] G \left[1 + \left(\frac{\omega}{G\nu_0}\right)^2\right]^{1/2}} \tag{20}$$

with an estimated mean value of E_0^2 within the modulation region. This is essentially the result given by Huxley and Ratcliffe [1949].

The determination of $\log_e \bar{\rho}$ from (17) implies a knowledge of the distribution of N and ν in the modulation region for an assumed model of the ionosphere. Huxley and Ratcliffe point out that the reduction factor $\bar{\rho}$ may be derived from measurements of the reflection coefficient of the ionosphere for the frequency of the wanted wave on the assumption that there is no deviative absorption near to the reflection point in the ionosphere, the absorption all occurring at the level of cross-modulation, remembering that the modulation may not occur on both the upgoing and downcoming paths. If $\bar{\rho}$ is expressed in terms of a positive decibel loss D, then

$$D = -20 \log_{10} \bar{\rho} = 8.7 \log_e \bar{\rho} \tag{21}$$

If also the cross-modulation region is at a distance d km from the disturbing transmitter which has an e.i.r.p. of P kW in the direction of the region, then

$$E_0 = \frac{0.1732}{d}\sqrt{P} \qquad \text{V/m} \tag{22}$$

It will then be found from (20), (21) and (22) that with the numerical values of e, m and k already given, the value $G = 1.3 \times 10^{-3}$ quoted by Huxley and Ratcliffe and the value $\theta_0 = 300$ K of the atmosphere at the modulation level:

$$|M_p| = \frac{0.31\ PDM}{d^2\left[(f_D \pm f_H)^2 + 0.025\nu_0^2\right]\left[1 + \frac{2.34 \times 10^{-5}}{\nu_0^2} f_M^2\right]^{1/2}} \qquad (23)$$

where f_D, f_H and ν_0 are in MHz and the modulation frequency $f_M = \omega/2\pi$ is in Hz.

3. Improved theory

Although a useful guide, the simple theory of Huxley and Ratcliffe may not always be adequate to assess the probable levels of cross-modulation to be expected. By classifying a given situation into one of five basic categories, Table I [Maslin, 1976c] has shown under what conditions the simple theory may be expected to fail and how it may be amended easily to achieve more reliable predictions. For example, calculations borne out by experimental results show how the transferred modulation is greater than expected when the wanted wave reflection level is located within the disturbed region [Maslin, 1976b]. If the disturbed region is very low down in the ionosphere, however, an increase in the average power of the disturbing wave does not necessarily imply an increase in the modulation transferred to the wanted wave [Maslin, 1976a]. These are examples of cases III and I respectively, of Table I.

4. Discussion

A simple derivation of an approximate cross-modulation equation is given in symbolic form in (20) and in numerical form in (23). It is based on the concept of the change in absorption caused by the change in collision frequency as the link between the modulation on the disturbing wave and that transferred to the wanted wave. Section 3 and Annex I to Recommendation 498 list some of the factors on which the depth of the cross-modulation depends.

As is to be expected, the cross-modulation is directly proportional to the depth of modulation on the disturbing wave and on the radiated power in the direction of the modulation region in the ionosphere from the disturbing transmitter. The dependence upon the decibel loss suffered by the wanted wave in the modulation region stresses the fact that not only must the wave pass through the modulation region on its passage to the receiving point on the Earth, but that it must also suffer absorption in the process. Thus although the cross-modulation does not depend intrinsically on the power of the wanted transmission, this power must be sufficient for the received signal to survive the loss by absorption in the region. A typical value of D would be 10 dB if the loss is not to be excessive, while it is clear that the phenomenon will not be observed on sufficiently high frequencies where the absorption is very small because of the large value of f_W in (14).

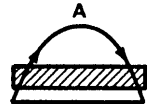
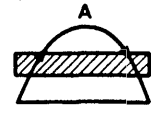
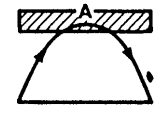
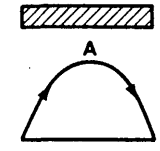
The direct effect of the Earth's magnetic field on the wanted wave is implicit in determining the value of D from $\bar{p}$. It is greatest for the extraordinary wave for which, under some conditions, the absorption may be effectively complete, leaving only the cross-modulation on the ordinary wave. The reception of cross-modulated signals therefore depends on the polarization characteristics of the transmitting and receiving antennas and on the time of day.

As shown in (23) the part played by the Earth's field is more significant for the disturbing wave. The transmission may be intended for medium or low frequency ground wave propagation on the basis that the wave entering the ionosphere is heavily absorbed. It is evident that the extraordinary wave is particularly effective in modulating the collisional frequency when the disturbing frequency is near to the gyrofrequency. On the other hand the absorption of the wave restricts the volume of the cross-modulation region and hence the decibel loss of the wanted wave in traversing the region. In a more rigorous investigation of the power absorbed by the medium from the disturbing wave, the combined effect of the ordinary and extraordinary waves must be used [Maslin, 1974, 1975a and 1975b].

The relation between M_p and M_v in (19) is based on a mean value of M_v and this implies a mean value of ν_0 in (23) and a power P somewhat less than the actual e.i.r.p. of the disturbing transmitter. The collisional frequency has a controlling influence at the gyromagnetic resonance for the extraordinary wave, but otherwise the rapid decrease of ν_0 with increasing height mainly restricts the audio-frequency range over which cross-modulation is obtained. Values for ν_0 decrease exponentially with height and typically at night there are 10^6 collisions per second at 81 km and 10^5 at 94 km. Knight [1968] has reviewed details of the ionospheric parameters and the related attenuation characteristics at different heights and frequencies, and also has given a very useful discussion of the gyromagnetic effect.

TABLE I – *Categories for cross-modulation estimation*

The path of the wanted wave is shown in relation to the disturbed region

Case	I	II	III	IV	V
Configuration					disturbing wave frequency close to gyrofrequency
Location of disturbed region	far below A	below A	near to or at A	above A	anywhere
M_ρ (relative)	small	medium	large	small	large (if geometry suitable)
Simple theory	not adequate	adequate	not adequate	not adequate	not adequate
Examples	$f_W \approx 10 f_D$ or $f_W > 10 f_D$	$C_D f_D < C_W f_W$	$f_W > f_D$ $(C_D f_D \approx C_W f_W)$	$10 f_W < f_D$ or $f_D \approx f_W$ $(C_D f_D > C_W f_W)$	disturbing transmitter close to wanted wave trajectory

where C_D C_W are the cosines of the angles of incidence on the ionosphere of the disturbing and wanted waves respectively.

As the frequency of the disturbing wave is increased above the gyrofrequency, the cross-modulation eventually varies as f_D^{-2}.

Then (23) can be put in the simple approximate form:

$$P = \frac{3.2 \mid M_p \mid d^2 f_D^2}{MD} \quad \text{kW} \tag{24}$$

In order to assess the nuisance value of interference on the wanted wave, it is assumed that $| M_p | = 0.03$, that the disturbing wave is 40% modulated so that $M = 0.4$, and that $D = 10$ dB. Then at 1.6 MHz for $d = 150$ km, corresponding to a wave incident on the ionosphere at about 45°, the power of the disturbing wave should not exceed 1.4 MW if cross-modulation is to be acceptable. With the e.i.r.p. values now obtainable at MF, it seems likely that cross-modulation interference troubles may arise, especially as the simplified form in equation (24) excludes possible gyromagnetic resonance effects. However, a study for the same conditions for frequencies above 5 MHz shows that even the very high values of e.i.r.p. currently associated with HF broadcasting are unlikely to cause sufficient modulation to be a nuisance.

5. Experimental measurements of cross-modulation imposed upon signals with frequencies as low as 20 kHz have been made by Jones *et al.* [1972] using transmissions from WWVL at Fort Collins, Colorado (United States of America) as the wanted signal and transmissions from Platteville, Colorado (United States of America) as the modifying signal. The Platteville transmitter has an e.i.r.p. of 50 MW [Utlaut, 1970]. Figure 1 shows some results of extensions of that experiment using the 60 kHz transmission from WWVB from Fort Collins, Colorado (United States of America) as the wanted signal, and a 7.4 MHz transmission from Platteville as the modifying signal [Utlaut, 1974]. The measurements were made at Bennett, Colorado. Both ordinary and extraordinary polarizations of the Platteville signals were used. The cross-modulation effects are, as expected, much stronger for extraordinary that the ordinary polarization.

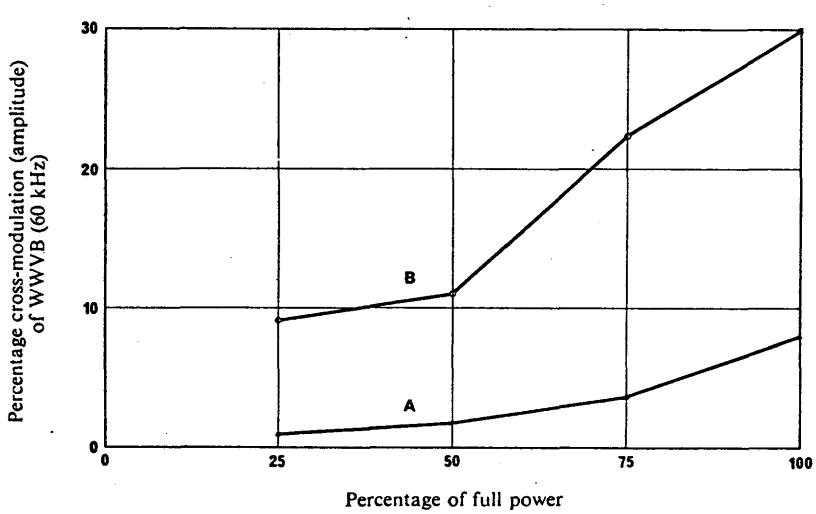


FIGURE 1 – *Cross-modulation of the 60 kHz signal from WWVB (received at Bennett, Colorado) by the Platteville transmitter operating at 7.4 MHz with a maximum e.i.r.p. of 50 MW, and 100% modulated at 10 Hz*

Curve A: ordinary wave
Curve B: extraordinary wave polarizations of the Platteville antenna

6. Interpretation of cross-modulation effects has been largely confined to the changes in conductivity (i.e., modulation transfer as a result of changes in wanted signal attenuation) and has not considered changes in permittivity. The changes in permittivity that can result from the presence of signals from high power transmitters suggests that wanted signals involving modulation other than amplitude modulation may also be affected by a cross-modulation phenomenon.

REFERENCES

BAILEY, V. A. [1937] On some effects caused in the ionosphere by electric waves. Part I, *Phil. Mag.*, **23**, 929-960.

BELL, C. D. [1966] Investigation of problems encountered in wave interaction experiments at high power. Ionosphere Research Lab. Scientific Report No. 262, Ionosphere Research Lab., Pennsylvania State University.

CUTOLO, M. [1964] On some resonance phenomena near the gyrofrequency obtained during the propagation of a radio wave in plasma. NBS Technical Note No. 211, **2**, 1-69.

FEJER, J. A. [1955] The interaction of pulsed radio waves in the ionosphere. *J. Atmos. Terr. Phys.*, **7**, 322-332.

GINZBURG, V. L. and GUREVICH, A. V. [1960] Non-linear phenomena in plasma situated in an alternating magnetic field (in Russian). *Usp. Soviet Fiz.*, **3**, 175-195.

GUREVICH, A. V. [1971] Disturbance of the ionosphere by radio waves (in Russian). *Geomag. i Aeronom.*, **11**, 953 (English translation, 803).

HIBBERD, F. H. [1964] Wave interactions at oblique incidence near the gyrofrequency. NBS Technical Note No. 211, **4**, 45-64.

HUXLEY, L. G. H. [1950] Ionospheric cross-modulation at oblique incidence. *Proc. Roy. Soc.* Vol. A200, 486-511.

HUXLEY, L. G. H. [1955] Comment on the theory of radio wave interaction. *Proc. Roy. Soc.*, Vol. A229, 405-407.

HUXLEY, L. G. H. and RATCLIFFE, J. A. [1949] A survey of ionospheric cross-modulation. *Proc. IEE*, Part III, **96**, 433-440.

JONES, T. B., DAVIES, K. and WIEDER, B. [1972] Observations of D region modifications at low and very low frequencies. *Nature*, **238**, 33-34.

KNIGHT, P. [1968] Ionospheric non-linearity. BBC Research Department, Report No. RA-17.

KNIGHT, P. [1973] LF and MF propagation: A study of ionospheric cross-modulation measurements. *BBC Eng.* **94**, 12-21.

MASLIN, N. M. [1974] Theory of energy flux and polarization changes of a radio wave with two magnetoionic components undergoing self demodulation in the ionosphere. *Proc. Roy. Soc.*, Vol. 341A, 361-381.

MASLIN, N. M. [1975a] Theory of the modifications imposed on the ionospheric plasma by a powerful radio wave reflected in the D or E region. *Proc. Roy. Soc.*, Vol. 343A, 109-131.

MASLIN N. M. [1975b] Theory of heating in the lower ionosphere by obliquely incident waves from a powerful point transmitter. *Proc. Roy. Soc.*, Vol. 346A, 37-57.

MASLIN, N. M. [1976a]. The effect of a time varying collision frequency on a radio wave obliquely incident on the lower ionosphere. *Proc. Roy. Soc.*, Vol. 348A 245-263.

MASLIN, N. M. [1976b]. Theory of the modulation imposed on an obliquely incident radio wave reflected in a disturbed region of the lower ionosphere. *Proc. Roy. Soc.*, Vol. 349A 555-570.

MASLIN, N. M. [1976c] Estimating ionospheric cross-modulation. *Proc. Roy. Soc.*, Vol. 351A, 277-293.

RATCLIFFE, J. A. and SHAW, I. J. [1948] A study of the interaction of radio waves. *Proc. Roy. Soc.*, Vol. A193, 311-343.

SHAW, I. J. [1951] Some further investigations of ionospheric cross-modulation. *Proc. Phys. Soc.*, Vol. B64, 1-20.

UTLAUT, W. F. [1970] An ionospheric modifications experiment using very high power, high frequency transmission. *J. Geophys. Res.*, Vol. 75, 6402-05.

UTLAUT, W. F. [1974] A survey of ionospheric modification effects produced by high-power HF radio waves. AGARD Conf. Proc. 138, 3-1 to 3-16 (Conference on Non-linear Effects in Electromagnetic Wave Propagation). National Technical Information Service, Springfield, Va. 22161, USA.

REPORT 728-3

IONOSPHERIC MODIFICATION BY GROUND-BASED, HIGH-POWER RADIO TRANSMISSIONS

(Question 39/6)

(1978-1982-1986-1990)

1. Introduction

The modification of the ionospheric plasma by high-power radio transmissions divides into ohmic ionospheric heating, a non-linear but classical process, and into the generation of parametric instabilities by non-linear wave interaction processes. One aspect of the former, ionospheric cross-modulation, is dealt with in Report 574.

Most ionospheric modification activities have been conducted at HF and these are most often concerned with producing changes in the upper ionosphere (150-400 km) using purpose-built transmitters operating at frequencies close to the F-region critical frequencies. If the modifying frequency is less than the critical frequency, the modification is termed overdense; if however, the modifying frequency is greater than the critical frequency, the modification is said to be underdense.

Experimental investigations [Bochkarev —— et al., 1979; Bochkarev —— et al., 1982; Borisov —— et al., 1987] have shown that the ionosphere can be appreciably modified by an oblique high power radio emission at frequencies considerably in excess of the critical frequency of the F region of the ionosphere.

Experiments have also been conducted using transmitters operating from VLF to UHF, giving rise to modifications in all regions of the ionosphere. These experiments have provided a new understanding of plasma physics. Perhaps more importantly they have shown that the modified region can have a significant effect on radio signals, used for communications purposes, which pass through it.

Collections of papers on ionospheric modification experiments have appeared in special issues of Radio Science [1974], — the Journal of Atmospheric and Terrestrial Physics [1982], — ESA [1983] and Suzdal/Moscow Conference proceedings [1986].

2. Ohmic heating theory

2.1 *Introduction*

Theoretical work by Ginzburg and Gurevich [1960], Farley [1963], Meltz and Lelevier [1970], Stubbe and Kopka [1977], Gurevich [1978], and Perkins and Roble [1978] have suggested that plasma heating by ohmic dissipation should produce large-scale changes in the electron temperature and as a result in the electron density and other parameters. Many non-linear phenomena arise from the fact that the collision frequency depends on the electron temperature.

2.2 *A simple theory of ohmic heating*

The following simplified theory illustrates how ohmic heating can occur. A wave with electric field E, and angular frequency ω, is considered to pass through a slab of ionospheric plasma with effective collision frequency ν between electrons and ions or neutrals. This field acts upon the electrons, of mass m, and charge e and accelerates them. Collisions, however, retard them and energy is extracted from the wave, resulting in an increase in electron temperature. Although the electrons become hotter, they transfer only a small part of their excess energy to the ions or neutrals during collisions because the electron mass is so much smaller than the ion or neutral mass. In the F-region, the electron-ion collision frequency is $\leqslant 10^3$/s, the fractional energy loss per collision is $\leqslant 10^{-4}$, and the time constant for energy loss is therefore, ~ 10 s. This low loss rate makes appreciable heating of the electrons possible. Heating of the E-region is less easy. Here the electron-neutral collision frequency is $\sim 2 \times 10^5$/s, the fractional energy loss per collision is 5×10^{-3} and consequently the time constant for energy loss is only ~ 1 ms. Strong absorbsion of the incident radio wave occurs in the region where the electron plasma frequency is near the radio frequency. This is because the wave is slowed near this natural resonance, and the electrons have a greater opportunity to collide with the heavy particles.

For simplicity, consider radio frequencies sufficiently greater than the local electron cyclotron frequency ($\sim$ 1.3 MHz) to render the geomagnetic field effects negligible.

Since the ion motions can be neglected, application of Newton's second law of motion gives for the electron directional velocity, $\underline{V}$:

$$m\frac{\mathrm{d}\underline{V}}{\mathrm{d}t} = -e\underline{E} - m\nu\underline{V} \tag{1}$$

The change in electron temperature due to the incident wave is found by considering the conservation of energy. In unit time, the wave electric field performs work

$$\underline{J} \cdot \underline{E} = -eN\underline{V} \cdot \underline{E} \tag{2}$$

on the plasma, where:

N: electron number density; and

$\underline{J}$: current density.

Conversely, during this time, electrons lose energy via collisions and thus:

$$\frac{\mathrm{d}}{\mathrm{d}t}\left(\frac{3}{2}NkT_e\right) = eN\underline{V} \cdot \underline{E} - \frac{3}{2}G\nu Nk(T_e - T) \tag{3}$$

where:

G: average fractional electron energy loss in one collision;

T: temperature of the collision species;

T_e: electron temperature; and

k: Boltzmann's constant.

ARCHIVES U.I.T. GENÈVE

If the electric field is described by:

$$\underline{E} = \underline{E}_0 \exp(- j\omega t) \tag{4}$$

the electron velocity is from equation (1):

$$\underline{V} = \underline{V}_0 \exp(- j\omega t) \tag{5}$$

where:

$$\underline{V}_0 = - eE_0 / m \left(\frac{\nu + j\omega}{\nu^2 + \omega^2} \right) \tag{6}$$

To a first approximation, the oscillatory part of the heating can be ignored and the solution of equation (3) gives:

$$\Delta T = T_e - T = \left(\frac{E_0}{E_p} \right)^2 T \tag{7}$$

where:

$$E_p^2 = \frac{3kTmG}{e^2} (\omega^2 + \nu^2) \tag{8}$$

E_p is the electric field needed to cause large thermal perturbation of the ionospheric plasma temperature and for $\omega \gg \nu$ it varies from about $3 \times 10^{-4} f$ (mV/m) in the D and E-regions to about $10^{-4} f$ (mV/m) in the F-region [Walker, 1979]. f is the frequency of the perturbing wave in Hz. Such fields imply equivalent isotropically radiated powers of approximately 100 MW.

3. Parametric instability theory

The parametric wave-plasma instability generally involves a three-wave interaction. In the context of ionospheric modification, a high power HF electromagnetic wave provides the initial driving or pump field whose energy cascades into a lower frequency electrostatic electron plasma wave and a lower frequency ion-acoustic wave.

The non-linear mechanism responsible for most parametric instabilities in the ionosphere is the thermal pressure force [Perkins, 1974; Fejer, 1979] rather than the so-called ponderomotive force [Chen, 1974]. The ponderomotive force arises from non-linear convective and Lorentz force terms in the electron equation of motion, and is applicable to a collisionless plasma. The electron temperature perturbations caused by wave heating give rise to an additional thermal pressure force in the electron equation of motion. The thermal pressure force dominates over the ponderomotive force in generating field-aligned ionospheric irregularities.

Fuller details of theory have been provided by Meltz and Perkins [1974], Perkins *et al.* [1974], Fejer and Leer [1972a and b] and Lee and Kuo [1983]. This subject is reviewed by Fejer [1979].

4. Modification effects

Many HF modification experiments have been conducted since 1970 using purpose-built facilities [Utlaut, 1975; Stubbe *et al.*, 1982a; Gurevich and Migulin, 1982]. These typically use transmitter powers of 1 or 2 MW together with antenna gains which give a resultant e.i.r.p. of between approximately 100 and 250 MW. Significant ionospheric modification has also been produced however, using 160 kW of power and a cross-dipole antenna with a gain of only 8 dBi (providing an e.i.r.p. of about 0.5 MW at 50% efficiency) [Utlaut *et al.*, 1974]. The power flux-densities in the F-region of the ionosphere for e.i.r.p. of 100 MW and 0.5 MW are, at most, about 100 μWm^{-2} and 0.5 μWm^{-2} respectively, if lower altitude ionospheric absorption is neglected. These values may be reduced by 6 dB, or more, when absorption occurring in the lower ionosphere is considered.

Some of the copious modification effects caused by HF (and other frequencies) heating radio waves are described below.

At altitudes of less than 200 km, electrons collide primarily with neutrals, the collision frequency increases with temperature and strong radio waves are absorbed more than weak radio waves. Auto-demodulation [King, 1959] is one result. Above 200 km, where electrons collide primarily with ions, the collision frequency decreases with temperature and strong radio waves are absorbed less than weak radio waves: in this case, auto-modulation results.

The mechanism of D-region ionospheric cross modulation is dealt with in Report 574, and the effects in Annex I of Recommendation 498.

In addition to modification of the upper ionosphere by high power HF waves, it is possible to generate ELF and VLF waves as a result of modification of the lower ionosphere by use of pulsed high power HF waves. Getmansev *et al.* [1974, 1977] have shown that powerful HF radio transmissions can excite electromagnetic radiation at the modulation frequency of the HF heater wave and Kapustin *et al.* [1977] found that this effect was enhanced in auroral regions. Ferraro *et al.* [1982] and Stubbe *et al.* [1981, 1982b] have reported the reception on the ground of ELF waves resulting from the ionospheric detection of ELF modulated HF waves transmitted by a transmitter near Tromsø, Norway. The theoretical aspects of such an experiment have been addressed in detail by Stubbe and Kopka [1977]. James et al. [1984] observed simultaneous ELF waves on the ground and in the topside ionosphere generated by modulation of the Tromsø transmitter.

Cannon [1982] and Cannon *et al.* [1982] have found evidence of ELF/VLF generation apparently due to LF and MF broadcast emissions. Cannon [1982] has shown how LF and MF broadcast signals can heat the auroral D or E region, modulating the auroral electrojet which then emits ELF/VLF signals. The modulation of the auroral electrojet by HF heater waves was not expected to cause significant geomagnetic field perturbations [Willis and Davis, 1973]. However, experiments performed at Tromsø, Norway, with the EISCAT facilities produced geomagnetic field perturbations as large as 10.8 γ [Stubbe and Kopka, 1981]. Kuo and Lee [1983] suggested that they were excited by the thermal filamentation instability of high-power HF waves. Integral harmonics of the ELF modulating frequencies can be produced nonlinearly in the auroral D and E regions [James, 1985]. Controlled injection of VLF signals from ground-based transmitters causes electron precipitation from the radiation belts which increases ionization at ionospheric heights [Imhof et al., 1985]. Naturally occurring electron precipitation varies greatly from much lower to much higher than observed artificially produced precipitation.

Perturbations in electron density occur if heating is maintained for a sufficiently long time. At altitudes below about 200 km an increase in electron density occurs because the dissociative recombination coefficient decreases with increasing temperature [Gurevich, 1971]. Tomko *et al.* [1980a] have developed a theoretical model of the D-region ion chemistry that is applicable to ionospheric heating conditions. The model provides a quantitative estimate of the increased attachment rate and decreased recombination coefficient. The changes in attachment rates and recombination coefficients in the lower ionosphere are important in interpreting absorption data [Tomko *et al.*, 1980b], incoherent scatter data [Matthews and Bekeny, 1978], and ionosonde data [Meltz *et al.*, 1982]. At higher altitudes, in the F region, high electron temperatures correspond to an increase in pressure causing plasma to stream out of the heated region along the geomagnetic field line. Electromagnetic energy is then focused into the region of reduced electron density leading to further heating and expansion. This results in large scale irregularities in the F-region electron density, aligned along the geomagnetic field and with transverse dimensions of approximately 1 km. One result of this thermal self-focusing process is the production of artificial spread F (see § 5). Perkins and Roble [1978] have described the changes in the electron density and temperature that are expected in the D, E and F regions during ionospheric heating. From the height of the plasma line [Muldrew and Showen, 1977], Muldrew [1978, 1981, 1988] proposes that the parametric decay instability responsible for the observed decay plasma line occurs in field-aligned ducts about 25 m in diameter. When the HF transmitter is turned on for the first time in on-off cycling, naturally occurring ducts slowly become larger, growing quickly during the on period but not decaying completely during the off period. This explains many plasma line observations, including the "plasma-line overshoot", identified by Showen and Kim [1978], where the plasma line intensity increases rapidly after heater turn-on, reaches a maximum in a couple of seconds and then decreases to a much lower fluctuating level.

One of the unexpected effects of the early HF ionospheric modification experiments was the generation of small scale (approximately 1 m) field-aligned irregularities which cause back-scatter to VHF and UHF waves. Theories to explain their development have been proposed by Perkins [1974], Vaskov and Gurevich [1977], Lee and Fejer [1978], Das and Fejer [1979], Inhester *et al.*, [1981], Dysthe et al., [1983] and Lee and Kuo [1983]. These irregularities are probably generated about 200 m below the reflection height of the HF heating wave where its heating effect is greatest. Due to the importance of these irregularities to the radio communicator they are dealt with in more detail in § 5.

Another important result of the early work was the discovery that the reflectivity of the ionosphere to a low power diagnostic wave was greatly reduced in the reflection region of a high-power heating signal, [Utlaut and Violette, 1974]. Since this occurred over a wide diagnostic frequency range it was termed wide-band absorption. This phenomenon has been attributed to the scattering of the diagnostic radio waves into Langmuir Waves [Graham and Fejer, 1976].

Kopka *et al.*, [1982] also report absorption of the heating wave itself and for transmitted powers greater than a threshold value, the received signal was found to decrease with an increase in e.r.p. This may have implications for communication systems since it suggests an optimum transmitted power level.

New important results have been obtained on single hop oblique sounding ionospheric paths using high power radio waves [Bochkarev ——— et al,. 1979; Bochkarev ——— et al., 1982; Borisov ——— et al., 1987]. It was found that in the field of an obliquely incident high power wave with a frequency near to the MUF of the F2 layer a modification occurs in the regular ionosphere which can have a considerable effect on the characteristics of radio signals passing through this perturbation.

Appreciable changes were recorded experimentally in the spectrum, the amplitude and the angles of arrival of the test signal at the point of reception due to the effect of a high power oblique radio emission, and these changes may be of considerable interest from the point of view of propagation over various distances.

5. Scattering of radio signals from artificially induced irregularities

With an e.i.r.p. of 0.5 MW or greater, large scale (seen as spread-F on ionograms) and small scale irregularities of electron density aligned with the Earth's magnetic field develop within seconds of the transmitter turn-on, as a result of ohmic heating and development of parametric instabilities and plasma waves. The consequence to radio signals passing through the disturbed region for paths with both terminals on the ground as well as Earth-space paths is that both the depth and rate of fading increase. In addition, because of the field-aligned irregularities, an effective reflector of large radar cross section ($\approx 10^5$ to 10^9 m^2) at altitudes of 250 to 300 km in the ionosphere is produced. These effects are produced when the heating transmitter frequency is below the critical frequency of the F-region ($\leq$ 12 MHz) but on a frequency which matches the plasma frequency at some height in the ionosphere.

The scattering properties of the field-aligned irregularities have been used to transmit voice, teletype, facsimile and pulsed transmissions between ground terminals separated by thousands of kilometres and using frequencies, ranging from HF to UHF, which would not otherwise have been useful for these paths. A fairly high degree of aspect sensitivity is associated with the F-region scattering. Thus, the locations on the Earth at which signals are received by this scattering mechanism depend in part upon the geomagnetic position and the altitude of the modified ionospheric region. In general, the signals can be received in an area on the equatorial side of the modified region which has a large east-west extent, ranging up to about 4000 km, but only 200 to 500 km in north-south extent. The location of the area on the ground is determined by geometrical considerations as are illustrated in Figs. 1 and 2. Figure 3 illustrates potential areas of coverage from this mechanism for different geomagnetic latitudes of the modified region. Details of the irregularity model and the geometrical consideration of the scattering have been provided by Rao and Thome [1974], Stathacopoulos and Barry [1974], and Utlaut [1975].

A strong scattering region near 110 km altitude in the E-region can also be produced when the heating transmitter is operating on frequencies below the E-region critical frequency ($\approx$ 3 MHz) [Fialer, 1974]. Fewer observations have been made of the E-region scattering during modification, but the limited evidence suggests that the scattering is less aspect sensitive than that from the F-region and, thus, signals may be received on the ground in areas having a greater north-south extent than that found for the F-region.

From the evidence obtained in the studies mentioned above, it appears that there is a potential, both for beneficial use of intentional ionospheric modification and as a possible source of increased interference due to signals scattered from intended or unintended modified regions, at frequencies ranging from HF to UHF. It may also be expected that under proper conditions, interference between earth terminals and satellites could exist, since as shown in Fig. 1, scattering occurs in all directions defined by the scattering cone and thus an earth transmitter will have energy scattered into space, and *vice-versa*, by the irregularities in the modified region.

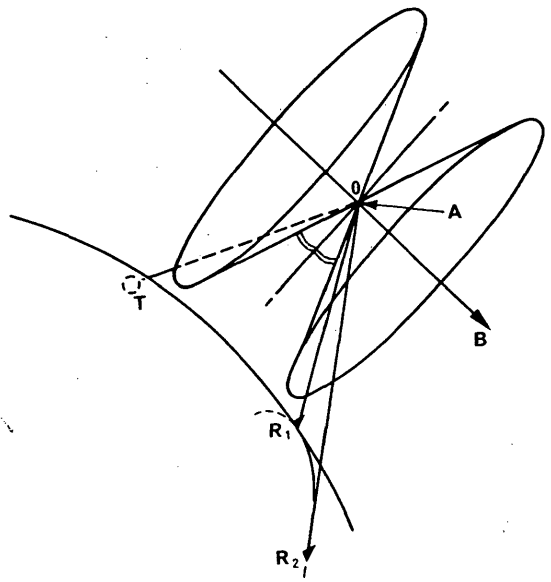


FIGURE 1 – *Conical surfaces illustrate possible signal paths to and from field-aligned specular scatter. Curve formed by intersection of cone and spherical Earth defines points where signals from a transmitter can be received on Earth*

A: scattering point
B: Earth's magnetic field
R_1 R_2: receiver sites
T: transmitter site

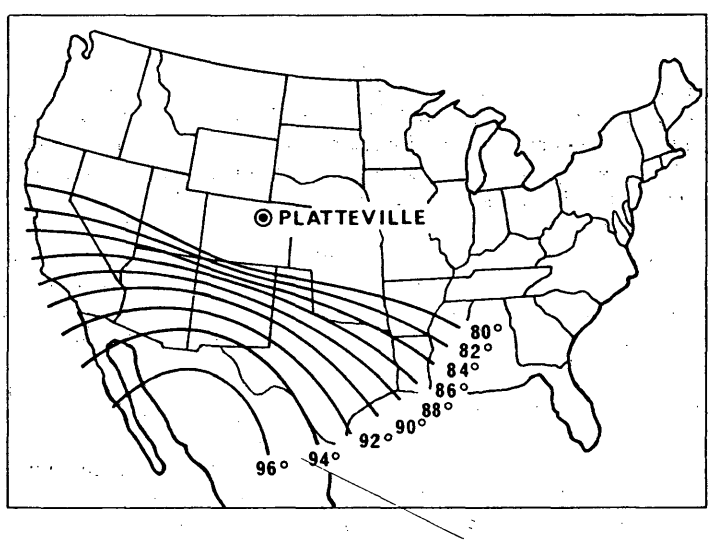


FIGURE 2 – *Contours of earth intersections of rays originating at point 230 km above Platteville and meeting geomagnetic field at angle indicated*

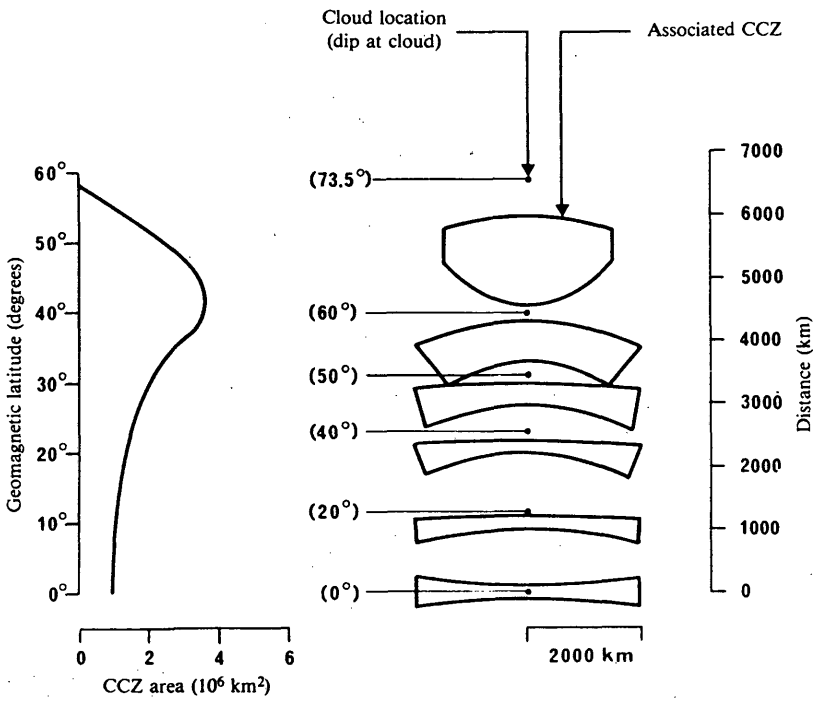


FIGURE 3 – *Common communication zone (CCZ) versus latitude*

An illustration of communication zones on the Earth's surface in which signal paths between any two points might be established by way of the scattering region of the modified ionosphere. Communication paths between pairs of points outside these zones are also possible and are determined by specular reflection processes. The extent of the scatterers is taken to be 100 km along the field line centred at an altitude of 270 km. Scattering is assumed to be limited to within ± 5° of specular reflection

REFERENCES

BOCHKAREV, G.S., EREMEHKO, V.A., LOBACHEVSKY, L.A., LYANNOI, B.E., MIGULIN, V.V. and CHERKASHIN, Y.N. [1982] Non linear interaction of decametre radio waves at close frequencies in oblique propagation. J. Atmos. Terr. Phys., 44, No. 12, 1137-1141.

BOCHKAREV, G.S., KIM, V.Y., LOBACHEVSKY, L.A., LYANNOI, B.E., MIGULIN, V.V., SERGEENKO, O.S. and CHERKASHIN, Y.N. [1979] Interaction of decametre radio waves at frequencies close to the F2 MUF in oblique propagation. Geomag. i. Aeronom., Vol. 19, 5, 830-833.

BORISOV, B.B., BOCHKAREV, G.S., BULATOVA, N.N., GORDIENKO, O.Y., ZHILTSOV, A.U., KISELEV, V.F., KISHCHA, P.V., LOBASHEVSKY, L.A., MITROFANOVA, T.A., NAGORSKY, P.M., PETROV, M.S., TARASHCHUK, Y.E., TROSHKINA, K.A., KHMELYUK, Y.A., CHERKASHIN, Y.N.CHERNOV, Y.A. [1987] - Spektralnye kharakteristiki signalov NZ pri vozdeistvii na ionosferu moshchnogo naklonnogo radioizlucheniya (Spectral characteristics of oblique incidence signals when the ionosphere is subject to the influence of a high-power oblique radio emission). Tezisy dokladov XV Vsesoyuznoi konferentsii po rasprostraneniyu radiovoln, Alma-Ata, Nauka, 121.

CANNON, P. S. [1982] Ionospheric ELF radio signal generation due to LF and/or MF radio transmissions – I. Experimental results. *J. Atmos. Terr. Phys.*, Vol. 44, 819-829.

CANNON, P. S., TURUNEN, T. and RYCROFT, M. J. [1982] Ionospheric ELF radio signal generation due to LF and/or MF radio transmissions – II. Interpretation. *J. Atmos Terr. Phys.*, Vol. 44, 831-841.

CHEN, F. F. [1974] *Introduction to Plasma Physics.* Plenum Press, New York, NY 10011, USA.

DAS, A. C. and FEJER, J. A. [1979] Resonance instability of small-scale field-aligned irregularities. *J. Geophys. Res.*, Vol. 84, 6701-6704.

DYSTHE, K.B., MJOLHUS, E., PECSELI, H.L. and RYPDAL, K. [1983] - A thermal oscillating two-stream instability, Phys. Fluids, Vol. 26(1), 146-157.

ESA [1983] Proceedings of the International Conference on Active Experiments in Space. Special Publication 195. Agence spatiale européenne, Neuilly, France.

FARLEY, D. T., Jr. [1963] Artificial heating of electrons in the F-region of the ionosphere. *J. Geophys. Res.*, Vol. 68, 2, 401-413.

FEJER, J. A. [1979] Ionospheric modification and parametric instabilities. *Rev. Geophys. Space Phys.*, Vol. 17, 135-153.

FEJER, J. A. and LEER, E. [1972a] Purely growing parametric instability in an inhomogeneous plasma. *J. Geophys. Res.*, Vol. 77, 700-708.

FEJER, J. A. and LEER, E. [1972b] Excitation of parametric instability by radio waves in the ionosphere. *Radio Sci.*, Vol. 4, 7, 481-491.

FERRARO, A. J., LEE, H. S., ALLSHOUSE, R., CARROLL, K., TOMKO, A. A., KELLY, F. J. and JOINER, R. G. [December, 1982] VLF/ELF radiation from the ionospheric dynamo current system modulated by powerful HF signals. *J. Atmos. Terr. Phys.*, Vol. 44, 12, 1113-1122.

FIALER, P. A. [1974] Field-aligned scattering from a heated region of the ionosphere – Observations at HF and VHF. *Radio Sci.*, Vol. 9, 11, 923-940.

GETMANSEV, G. G., GULELMI, A. V., KLAIN, B. I., KOTIK, D. S., KRYLOV, S. M., MITYAKOV, N. A., RAPOPORT, V. O., TRAKHTENGERTS, V. Yu. and TROITSKAYA, V. A. [1977] Excitation of magnetic pulsations under the action on the ionosphere of radiation of a powerful short-wave transmitter. *Radiophys. Quant. Electron.*, Vol. 20, 703-705.

GETMANSEV, G. G., ZUIKOV, N. A., KOTIK, D. S., MIRONENKO, L. F., MITYAKOV, N. A., RAPOPORT, V. O., SAZONOV, Yu. A., TRAKHTENGERTS, V. Yu. and EIDMAN, V. Yu. [1974] Combination frequencies in the interaction between high-power short-wave radiation and ionospheric plasma. *JETP Lett.*, Vol. 20, 101-102.

GINZBURG, V. L. and GUREVICH, A. V. [1960] Nonlinear phenomena in a plasma located in an alternating electromagnetic field. *Usp. Soviet Fiz.*, 3, 115-146 and 175-194.

GRAHAM, K.N. AND FEJER, J.A. [1976] - Anomalous radio wave absorption due to ionospheric heating effects. Radio Sci., Vol. 11, No. 12, 1057-1063.

GUREVICH, A. V. [1971] Disturbance of the ionosphere by radio waves. *Geomag. i Aeronom.*, Vol. 11, 803-809.

GUREVICH, A. V. [1978] *Non-linear Phenomena in the Ionosphere.* Springer-Verlag, New York, NY, USA.

GUREVICH, A. V. and MIGULIN, V. V. [1982] Investigations in the USSR of non-linear phenomena in the ionosphere. *J. Atmos. Terr. Phys.*, Vol. 44, 12, 1019.

IMHOF, W.L., GAINES, E.E., VOSS, H.D., REAGAN, J.B., DATLOWE, D.W., MOBILIA, J., HELLIWELL, R.A., INAN, U.S., KATSUFRAKIS, J. and JOINER, R.G., [1985] - Results from the SEEP Active Space Plasma Experiment: Effects on the Ionosphere. Radio Science, Vol. 20, No. 3, 511-518.

INHESTER, B., DAS, A. C. and FEJER, J. A. [1981] Generation of small-scale, field-aligned irregularities in ionospheric heating experiments. *J. Geophys. Res.*, Vol. 86, 9101-9106.

JAMES, H.G. [1985] - The ELF spectrum of artificially modulated D/E region conductivity. J. Atmos. Terr. Phys., 47, 1129-1142.

JAMES, H.G., DOWDEN, R.L., REITVELD, M.T., STUBBE, P. and KOPKA, H. [1984] - Simultaneous observations of ELF waves from an artificially modulated auroral electrojet in space and on the ground. J. Geophys. Res., 89, 1655-1666.

JOURNAL OF ATMOSPHERIC AND TERRESTRIAL PHYSICS [December, 1982] Special issue: Ionospheric modification. Papers from the Twentieth General Assembly of the International Union of Radio Science. Vol. 14, 12.

KAPUSTIN, I. N., PERTSOVSKY, R. A., VASILEV, A. N., SMIRNOV, V. S., RASPOPOV, O. M., SOLOVENA, L. E., ULYACHENKO, A. A., ARYKOV, A. A. and GALAKHOVA, N. V. [1977] Generation of radiation at combination frequencies in the region of the auroral electrojet. *JETP Lett.*, Vol. 25, 228-231.

KING, J. W. [1959] Ionospheric self demodulation and self distortion of radio waves. *J. Atmos. Terr. Phys.*, Vol. 14, 44.

KOPKA, H., STUBBE, P., JONES, T. B. and ROBINSON, T. [1982] Non-linear reflectivity of high-power radio waves in the ionosphere. *Nature*, Vol. 195, 5851, 680.

KUO, S. P. and LEE, M. C. [1983] Earth magnetic field fluctuations produced by filamentation instabilities of electromagnetic heater waves. *Geophys. Res. Lett.*, Vol. 10, 979-981.

LEE, M. C. and FEJER, J. A. [1978] Theory of short-scale field-aligned density striations due to ionospheric heating. *Radio Sci.*, Vol. 13, 893-899.

LEE, M. C. and KUO, S. P. [1983] Excitation of upper hybrid waves by a thermal parametric instability. *J. Plasma Phys.*, Vol. 30, 463-478.

MATHEWS, J. D. and BEKENY, F. S. [1978] The effect of negative ions on Thompson scattering in the presence of electron heating. *Geophys. Res. Lett.*, **5**, 925-927.

MELTZ, G. and LELEVIER, R. E. [1970] Heating the F-region by deviative absorption of radio waves. *J. Geophys. Res.*, Vol. 75, 6406-6416.

MELTZ, G. and PERKINS, F. W. [1974] Ionospheric modification theory: past, present, and future. *Radio Sci.*, Vol. 9, 885-888.

MELTZ, G., RUSH, C. M. and VIOLETTE, E. J. [1982] Simulation of D and E region high-power microwave heating with HF ionospheric modification experiments. *Radio Sci.*, Vol. 17, 701-715.

MULDREW, D. B. [1978] The role of field-aligned ionization irregularities in the generation of the HF-induced plasma line at Arecibo. *J. Geophys. Res.*, Vol. 83, 2552-2560.

MULDREW, D. B. [1981] Generation of ionospheric irregularities associated with plasma lines induced by an HF wave. *Radio Sci.*, Vol. 16, 121-125.

MULDREW, D.B. [1988] - Duct model explanation of the plasma line overshoot observed at Arecibo, J. Geophys. Res., 93, 7598-7604.

MULDREW, D. B. and SHOWEN, R. L. [1977] Height of the HF-enhanced plasma line at Arecibo. *J. Geophys. Res.*, Vol. 82, 4793-4804.

PERKINS, F. W. [1974] A theoretical model for short-scale field-aligned plasma density striations. *Radio Sci.*, Vol. 9, **11**, 1065-1070.

PERKINS, F. W., OBERMAN, C. and VALEO, E. J. [1974] Parametric instabilities and ionospheric modification. *J. Geophys. Res.*, Vol. 79, 1478-1496.

PERKINS, F. W. and ROBLE, R. G. [1978] Ionospheric heating by radio waves: Predictions for Arecibo and the satellite power station. *J. Geophys. Res.*, Vol. 83, 1611-1624.

RADIO SCIENCE [1974] Special issue: Ionospheric modification by high power transmitters. *Radio Sci.*, Vol. 9, **11**.

RAO, P. B. and THOME, G. S. [1974] A model for RF scattering from field-aligned heater-induced irregularities. *Radio Sci.*, Vol. 9, 987-996.

SHOWEN, R.L. and KIM, D.M. [1978] - Time variation of the HF-induced plasma waves, J. Geophys. Res., 83, 623-628.

STATHACOPOULOS, A. D. and BARRY, G. H. [1974] Geometric considerations in the design of communications circuits using field-aligned ionospheric scatter. *Radio Sci.*, Vol. 9, 1021-1024.

STUBBE, P. and KOPKA, H. [1977] Modulation of the polar electrojet by powerful HF waves. *J. Geophys. Res.*, Vol. 82, 2319-2325.

STUBBE, P. and KOPKA, H. [1981] Generation of Pc5 pulsations by polar electrojet modulation: first experimental evidence. *J. Geophys. Res.*, Vol. 86, 9073.

STUBBE, P., KOPKA, H. and DOWDEN, R. L. [1981] Generation of ELF and VLF waves by polar electrojet modulation. Experimental results. *J. Geophys. Res.*, Vol. 86, 9073-9078.

STUBBE, P., KOPKA, H., LAUCHE, H., RIETVELD, M. T., BREKKE, A., HOLT, O., JONES, T. B., ROBINSON, T., HEDBERG, A., THIDE, B., CROCHET, M. and LOTZ, H. J. [1982a] Ionospheric modification experiments in northern Scandinavia. *J. Atmos. Terr. Phys.*, Vol. 44, **12**, 1025-1041.

STUBBE, P., KOPKA, H., RIETVELD, M. T. and DOWDEN, R. L. [1982b] ELF and VLF wave generation by modulated HF heating of the current carrying lower ionosphere. *J. Atmos. Terr. Phys.*, Vol. 44, 1123-1136.

SUZDAL/MOSCOW [1986] - Conference proceedings of the International Conference on Ionospheric Modifications by Powerful Radio Waves, USSR.

TOMKO, A. A., FERRARO, A. J., LEE, H. S. and MITRA, A. P. [1980a] A theoretical model of D-region ion chemistry modifications during high power radio wave heating. *J. Atmos. Terr. Phys.*, Vol. 42, 275-285.

TOMKO, A. A., FERRARO, A. J. and LEE, H. S. [1980b] D-region absorption effects during high-power radio wave heating. *Radio Sci.*, Vol. 15, 675-681.

UTLAUT, W. F. [1975] Ionospheric modification induced by high-power HF transmitters – A potential for extended range VHF-UHF communications and plasma physics research. *Proc. IEEE*, Vol. 63, 7, 1022-1043.

UTLAUT, W. F. and VIOLETTE, E. J. [1974] A summary of vertical incidence radio observations of ionospheric modification. *Radio Sci.*, Vol. 9, 895-903.

UTLAUT, W. F., VIOLETTE, E. J. and MELANSON, L. L. [1974] Radar cross section measurements and vertical incident effects observed with Platteville at reduced power. *Radio Sci.*, Vol. 9, 1033-1040.

VASKOV, V. V. and GUREVICH, A. V. [1977] Resonance instability of small-scale plasma perturbations. *Sov. Phys. JETP*, Vol. 46, 487-494.

WALKER, J. C. G. [1979] Active experimentation with the ionospheric plasma. *Rev. Geophys. Space Phys.*, Vol. 17, 4, 534-544.

WILLIS, J. W. and DAVIS, J. R. [1973] Radio frequency heating effects on electron density in the lower E region. *J. Geophys. Res.*, Vol. 78, 5710.

REPORT 893-1*

SOLAR POWER SATELLITES AND THE IONOSPHERE

(Question 39/6) (1982-1990)

In the late 1970s and early 1980s, solar power satellites (SPS) were viewed as possibly providing a significant contribution to the Earth's future energy requirements. A typical concept of such a system involved collecting solar energy by a large array of solar cells in geostationary orbit, converting to RF power at microwave frequencies and beaming the microwave energy to earth collectors for conversion into a d.c. power grid. Details of a conceptual design are given in Report 679. Because the power levels involved with SPS systems far exceed those normally encountered in radio transmission, it is possible that the interaction of the microwave beam with the ionosphere and troposphere could produce serious effects on existing radio services.

The impact of the operation of solar power satellites on the ionosphere may be separated into two broad categories: those in which the ionospheric plasma influences the propagation characteristics of the microwave power beam and those whereby the ionospheric plasma itself is modified. In the former case, electron density gradients and irregularities may affect the propagation of the power beam. Refraction effects may cause the apparent position of the power beam to change. Ionospheric irregularities could cause scintillation and scattering of the power beam possibly giving rise to co-channel interference to other radio systems.

The modification of the ionospheric plasma by the passage of a high power microwave beam through it results from the ohmic heating of the electrons by the power beam. This ohmic heating can cause increased absorption of radio waves transversing the same region as the microwave power beam. Also the ohmic heating could produce thermal self-focusing leading to the formation of electron density irregularities that could scatter radio waves at much lower frequencies if they encountered the scattering volume. Fortunately the region of the ionosphere in which these effects are likely to occur is generally confined to the vicinity where the power beam passes through the ionosphere.

Secondary effects on the ionosphere and the troposphere could also arise as the result of the rocket exhausts associated with the numerous launches that would be required to support the construction and maintenance of a complete SPS system.

Solar power satellites are no longer viewed as a viable alternative to meet the future energy needs of the world and hence the extensive discussion contained in earlier versions of this report [Dubrovnik, 1986] has been abbreviated in this document. The bibliography contains the pertinent citations from the previous text.

* This Report is brought to the attention of Study Group 2.

A description of ionospheric effects and their ramifications on radio systems arising from high power transmissions at HF and lower frequencies is discussed in Reports 728 and 574.

BIBLIOGRAPHY

GLASER, P. E. [1977] The potential of satellite solar power. *Proc. IEEE*, Vol. 658, 1162-1176.

GRANT, W., RUSH, C. M. and MORRISON, E. [1980] Studies of the potential impact of the solar power systems on the ionospheric and telecommunications systems; Propagation effects in space/Earth paths. AGARD Conf. Proc. No. 284, 41-1 to 41-19, Technical Editing and Reproductions House, London, UK.

HUGHES, K. A. [1980] The interactions of a solar power satellite transmission with the ionosphere and troposphere; Propagation effects in space/Earth paths. AGARD Conf. Proc. No. 284, 38-1 to 38-7, Technical Editing and Reproductions House, London, UK.

US DEPT. OF ENERGY [1980c] Environmental Assessment for the Satellite Power System (SPS) Concept Development and Evaluation Program (CDEP), Office of Energy Research DOE/ER-0069, 93-115.

REPORT 1011-1

ARTIFICIAL MODIFICATION OF THE IONOSPHERE BY CHEMICAL INJECTIONS

(Question 25/6)

(1986-1990)

Typical rocket exhaust products such as H_2, H_2O and CO_2 can cause large-scale depletions of the electron density in the ionospheric F region. This results from these products transforming the F region plasma which is usually dominated by atomic ion processes to a plasma that is dominated by molecular ion processes. Once the molecular ions associated with these products are formed, they dissociatively recombine with the ambient electron density at a rate that is 100 to 1000 times faster than the recombination of electrons with the naturally occurring molecules of nitrogen (N_2) and oxygen (O_2). The result of this is the creation of an "ionospheric hole" in the F region. The lack of large-scale effects due to chemical injections in the lower ionosphere is due to the high neutral densities and molecular ion chemistry that dominates at D- and E- region heights.

The ionospheric depletion that results from chemical injections has been observed using measurements of total electron content and HF radio signals. The theory explaining the physical mechanisms involved in the creation of ionospheric depletions by chemical injections is well-developed. Hence the extensive discussion contained in an earlier version of this report (Dubrovnik, 1986) has been abbreviated in this document. The bibliography contains a list of relevant citations from the previous text.

BIBLIOGRAPHY

FORBES, J. M. [1980] Upper atmosphere modifications due to chronic discharges of water vapour from space vehicle exhausts. *Space Systems and their Interactions with Earth's Space Environment.* Eds. H. B. Garrett and C. P. Pike. AIAA, New York, NY, USA.

MacDOUGALL, J. W., FULFORD, J. A. and FORSYTH, P. A. [1981] Ionospheric electron content measurements during "Waterhole". *Can. J. Phys.*, Vol. 59, 1170-1174.

MENDILLO, M. [1981] The effect of rocket launches on the ionosphere. *Adv. Space Res.*, 1, 275-290.

MENDILLO, M., HAWKINS, G. S. and KLOBUCHAR, J. A. [1975] A sudden vanishing of the ionospheric F-region due to the launch of Skylab. *J. Geophys. Res.*, Vol. 80, 2217-2228.

PONGRATZ, M. B. and SMITH, G. M. [1978] The LAGOPEDO experiments – and overview. *EOS Trans. Amer. Geophys. Union*, Vol. 59, 334.

ZINN, J. and SUTHERLAND, C. D. [1980] Effects of rocket exhaust products in the thermosphere and ionosphere. *Space Solar Power Rev.*, 1, 109.

REPORT 887-2 *

MODELS OF EXTRATERRESTRIAL PLASMAS

(Question 25/6)

(1982-1986-1990)

1. Introduction

The three most important characteristics of extraterrestrial plasma that affect radio signals propagating in the interplanetary medium are the electron density N, the one-dimensional spectrum of r.m.s. electron density fluctuations V_{ne} and the velocity of the plasma motion (ordered and thermal). Table I provides values of plasma characteristics pertinent to interplanetary space, to the solar corona and to the earth's ionosphere, and magnetosphere.

2. The solar corona and solar wind

The solar wind is a complex, time-dependent, low density mixture of particles and fields which continually emanates from the sun. Since Parker's [1958] theoretical prediction and subsequent conformation by satellite observation, the solar wind has become an entire scientific discipline with significant implications for solar-terrestrial studies. Primarily as a result of research in the 1970's, using solar X-ray photography, it has been determined that most of the solar wind originates from coronal holes, which are regions in the upper solar atmosphere exhibiting an open magnetic field topology. The coronal plasma cannot be confined by this magnetic configuration and freely expands into the interplanetary medium. Recurrent high-speed, low-density solar-wind streams have been specifically identified with coronal holes [e.g. Zirker, 1977]. In addition, solar flares and possibly other solar phenomena result in the release of solar plasma into the interplanetary medium. Brandt [1970] and Hundhausen [1972] review the primary topic of solar wind flows, while Holzer [1978] updates and extends these reviews to include the context of coronal holes. Models of coronal hole flows are surveyed by Suess [1979].

2.1 *Plasma density*

The electron density from the Sun out to the distance of the Earth is given by the extended corona term of the Allen-Baumbach relation [Allen, 1976].

Berman et al. [1982] have analyzed 2.3 GHz signal phase fluctuations and columnar electron density measurements inferred from Viking spacecraft signals and recommend the following model where R, the distance from the Sun, is expressed in units of a solar radius (6.96×10^8 m):

$$N(R) \approx \frac{2.21 \times 10^{14}}{R^6} + \frac{1.55 \times 10^{12}}{R^{2.3}} \qquad (1)$$

---

* This Report is brought to the attention of Study Group 2.

In this model, the inner corona is modelled by the first term, which gives a value of $N = 1.25 \times 10^{14}$ m^{-3} at $R = 1.1$, which agrees with Allen's [1976] model and becomes equal to the second term at $R = 3.8$. (For electron densities at lower solar altitudes, tabulated values should be used.) It yields a value at the distance of the Earth of $N = 6.70 \times 10^6$ electrons · m^{-3} which is a typical value for observed solar wind densities. However, solar wind density can be highly variable on a time scale of minutes to hours. Values have been seen to range from less than 1 to greater than 75×10^6 m^{-3} [King, 1979].

Expression (1) is appropriate to low heliographic latitudes (± 15°). Allen [1976] and Saito *et al.*, [1977] both find a decrease in electron density by a factor of 4 to 5 between the Equator and pole for the inner corona. Tyler *et al.*, [1977] propose a model including a simple expression to account for variation with heliographic latitude (θ), which has been modified slightly here to fit the above observations:

$$N(R,\theta) \approx \left[\cos^2\theta + \frac{1}{25}\sin^2\theta\right]^{\frac{1}{2}} \tag{2}$$

This expression may be used in connection with (1) if desired. Its appropriateness is questionable for $R > 5$.

2.2 *Inhomogeneities*

Fluctuations in radial electron density have been characterized in terms of the one-dimensional frequency spectrum V_{ne} (measured *in situ* by spacecraft) by Woo and Armstrong [1979]. Their determination is:

$$V_{ne}(f) = 0.052\, R^{-3.45} f_s^{-1.65} v^{-1} \frac{(\text{electrons/m}^3)^2}{\text{Hz}} \tag{3}$$

and, if the solar wind speed v is assumed to be 3×10^5 m/s and constant:

$$V_{ne}(f) = 1.7 \times 10^{-7}\, R^{-3.45} f_s^{-1.65} \frac{(\text{electrons/m}^3)^2}{\text{Hz}} \tag{4}$$

where R is in solar radii ($20 \leq R \leq 215$), f_s is in Hz, and v is in m/s.

2.3 *Plasma velocity and magnetic field*

The solar wind expands radially away from the sun achieving speeds at the Earth ranging from approximately 300 up to values in excess of 1000 km/s. Solar magnetic fields are dragged along with the flow. Because the sun rotates, a solar magnetic field line from a given area element on the sun will be drawn out along the path followed by the fluid particles emanating from that area. Thus to an observer at the Earth (not rotating with the solar surface), the magnetic field theoretically maps along an Archimedean spiral tracing from the Earth back to its point of origin on the sun. Observations indicate that, on average, the inter-planetary magnetic field at the Earth does tend to cluster along this direction, which is approximately 45° to the west of the Earth-sun line. However, the inter-planetary magnetic field direction and magnitude are highly variable, with total magnitudes ranging from a few to tens of gammas.

3. Planetary ionospheres and magnetospheres

As planetary exploration continues, more and better data are being obtained about the other members of our solar system. Three, and possibly four, of the planets have rings (Jupiter, Saturn, Uranus, and possibly Neptune). Some planets and even their satellites have significant atmospheres, and some have intrinsic magnetic fields large enough to form a protective magnetosphere about the planet, shielding it from direct impact by solar wind plasma. Since a planetary atmosphere or magnetosphere could distort a radio signal propagating in the interplanetary medium, Table II summarizes pertinent atmospheric, ionospheric, and magnetospheric parameters as they are now known, for each of the planets of the solar system. More detailed information is given in the references cited in Table II.

TABLE I — *Characteristics of the plasma state in interplanetary space, in the solar corona and in the Earth's ionosphere with respect to a 2.3 GHz radio-wave [Smith and Edelson, 1980]*

Item	Parameter	Units	*a*) Deep space Location (extraterrestrial)		*b*) Near-Earth space Location (terrestrial)		
			A	B	C	D	E
			Interplanetary space 1 AU from the Sun	Solar corona 4 R_S (1) from Sun's centre	Magnetosphere 1 6.6 R_T (1) (geostationary orbit)	Magnetosphere 2 4 R_T (1) (Inside plasmapause)	Ionosphere 300 km altitude
1.	Electron density, N	(m^{-3})	7.5×10^6	1.2×10^{11}	3×10^7	3×10^8	10^{12}
2.	Effective temperature, T	(K)	1.5×10^5	1.5×10^6	5000	10^4	1200
3.	Flow speed, v	(km/s)	450	72	—	—	—
4.	Magnetic field, B_0	(gauss)	5×10^{-5}	0.14	10^{-3}	5×10^{-3}	0.4
5.	Collision frequency, ν	(s^{-1})	1.2×10^{-5}	5.9×10^{-3}	2.3×10^{-3}	5.9×10^{-2}	1100
6.	Plasma frequency, f_N	(Hz)	2.5×10^4	3.1×10^6	4.9×10^4	1.6×10^5	9×10^6
7.	Electron gyrofrequency, f_H	(Hz)	140	3.9×10^5	2.8×10^3	1.4×10^4	1.1×10^6
8.	$X = (\omega_N/\omega)^2$		2.9×10^{-12}	1.8×10^{-6}	4.5×10^{-10}	4.8×10^{-9}	1.5×10^{-5}
9.	$Y = \omega_H/\omega$		6.1×10^{-8}	1.7×10^{-4}	1.2×10^{-6}	6.1×10^{-6}	4.9×10^{-4}
10.	$Z = \nu/\omega$		8.5×10^{-16}	4.1×10^{-13}	1.6×10^{-13}	4.1×10^{-12}	7.9×10^{-8}
11.(1)	$n_0 = (1 - X)^{1/2}$		$1 - 1.4 \times 10^{-12}$	$1 - 9.2 \times 10^{-7}$	$1 - 2.2 \times 10^{-10}$	$1 - 2.4 \times 10^{-9}$	$1 - 7.7 \times 10^{-6}$
12.(1)	$n_{QL} = [1 - X/(1-Y)]^{1/2}$		$1 - 1.4 \times 10^{-12}$ $+ [8.8 \times 10^{-20}]$	$1 - 9.2 \times 10^{-7}$ $+ [1.6 \times 10^{-10}]$	$1 - 2.2 \times 10^{-10}$ $+ [2.7 \times 10^{-16}]$	$1 - 2.4 \times 10^{-9}$ $+ [1.5 \times 10^{-14}]$	$1 - 7.7 \times 10^{-6}$ $+ [7.5 \times 10^{-9}]$
13.(1)	$n_g = 1/n_0$		$1 + 1.4 \times 10^{-12}$	$1 + 9.2 \times 10^{-7}$	$1 + 2.2 \times 10^{-10}$	$1 + 2.4 \times 10^{-9}$	$1 + 7.7 \times 10^{-6}$
14.(1)	$n_g n_{QL}$		$1 + 8.8 \times 10^{-20}$	$1 + 1.6 \times 10^{-10}$	$1 + 2.7 \times 10^{-16}$	$1 + 1.5 \times 10^{-14}$	$1 + 7.5 \times 10^{-9}$
15.	Debye length, λ_D	(m)	9.8	0.24	21.8	0.40	2.4×10^{-3}
16.	Plasma state, λ_D/λ		75 (warm)	1.8 (lukewarm)	168 (warm)	3.1 (lukewarm)	1.8×10^{-2} (cold)
17.	Critical magnetic field, B_c	(gauss)	7.6×10^{-5}	3.1×10^{-2}	2.3×10^{-5}	1.25×10^{-4}	2.5×10^{-3}
18.	Magnetic control B/B_c		0.66 (weak)	4.6 (moderate)	43.5 (strong)	40 (strong)	160 (very strong)

(1) R_S is the solar radius, R_T is the Earth radius, n_0 is the isotropic refractive index, n_{QL} is the quasi-longitudinal approximation to the refractive index, n_g is the group refractive index for an isotropic medium. The numerical values in square brackets in item 12 are the differences $n_{QL} - n_0$ which are seen to be negligible.

TABLE II – *Properties of planetary atmospheres and ionospheres* *

Item	Planets								
	Mercury	Venus	Earth (2)	Mars	Jupiter	Saturn	Uranus	Neptune	Pluto
Mean distance from Sun astronomical unit (1)	0.387	0.723	1	1.524	5.203	9.539	19.28	30.06	39.72
Main atmospheric components	None (traces of He, H)	Carbon dioxide (96%)	Nitrogen (78%) Oxygen (21%)	Carbon dioxide (95%)	Hydrogen (89%) Helium (11%)	Hydrogen (94%) Helium (6%)	Hydrogen (85%) Methane (10%)	Hydrogen Helium Methane	Methane
Mean day-time temperature at visible surface (°C)	427	460	22	−60	−100	−180	−210	−220	−230
Atmospheric pressure at surface (mbars)	$< 2 \times 10^{-10}$	93 000	1000	7-9	1000	> 1000	>10 000	$> 10^6$	< 50
Surface gravity (Earth = 1)	0.37	0.88	1.0	0.38	2.64	1.32	0.85	1.4	?
Ionosphere	None detected	Well developed but variable	D, E, F1, F2	F1	Yes	Yes	Yes	Yes	Unknown
Maximum electron density (electrons per m^3)	$< 4 \times 10^9$	10^{11} to 10^{12}	2×10^{12}	10^{11}	2×10^{11}	2.3×10^{10}	10^{11}	$< 10^{11}$	?
Height of maximum electron density (km)		150-200	250-400	125	1600	2500	500	?	?
Magnetic field	Yes-weak	None detected	Yes-strong	Yes-weak	Yes-strong	Yes-strong	Yes-weak	None detected	None likely
Magnetic dipole moment (G cm^3)	1.8 to 6×10^{22}	$< 4.3 \times 10^{16}$	8×10^{25}	$< 1.0 \times 10^{22}$	1.55×10^{30}	4.3×10^{28}	?		

* [Allen, 1976; Smith and West, 1983].

(1) The astronomical unit (the mean distance from the Earth to the Sun) is 1.496×10^8 km.

(2) See Reports 725 and 263.

REFERENCES

ALLEN, C. W. [1976] *Astrophysical Quantities.* The Athlone Press, University of London, London, United Kingdom.

BERMAN, A.L., WACKLEY, J.A. and HIETZKE, W.H. [1982] - Direct comparison of Viking 2.3-GHz signal phase fluctuation and columnar electron density between 2 and 160 solar radii. The Telecommunications and Data Acquisition Progress Report 42-71, July-September 1982, pp. 117-128. Jet Propulsion Laboratory, California Institute of Technology, Pasadena. CA, USA."

BRANDT, J. C. [1970] *Introduction to the Solar Wind.* W. H. Freeman and Co., San Francisco, CA, USA.

HOLZER, T. E. [1978] The solar wind and related astrophysical phenomena. *Solar System Plasma Physics: A Twentieth Anniversary Overview.* Eds. C. F. Kennel, L. J. Lanzerotti, and E. N. Parker, North-Holland Publishing Co., New York, NY, USA.

HUNDHAUSEN, A. J. [1972] *Coronal Expansion and Solar Wind.* Springer-Verlag, New York, Heidelberg, Berlin.

KING, J. H. [1979] *Interplanetary Medium Data Book.* Supplement 1, NASA NSSDC/WDC-A-R&S 79-08-Suppl-1.

PARKER, E. N. [1958] Dynamics of the Interplanetary Gas and Magnetic Fields. *Astrophys. J.*, Vol. 128, 664-676.

SAITO, K., POLAND, A. J. and MUNRO, R. H. [1977] A study of the background corona near solar minimum. *Solar Phys.*, Vol. 55, 121-234.

SMITH, E. K. and EDELSON, R. E. [1980] Radio propagation through solar and other ionized media. JPL Publication 79-117, NASA-JPL, California Institute of Technology, Pasadena, CA 91103, USA.

SMITH, R. E. and WEST, G. S. (Compilers) [1983] Space and planetary environment criteria guidelines for use in space vehicle development. 1982 Revision, Vols. I and II. NTIS N83-18816/9 and N83-28061/0. National Technical Information Service, Springfield, VA 22161, USA.

SUESS, S. T. [1979] Models of coronal hole flows. *Space Sci. Revs.*, Vol. 23, **2**, 159-200.

TYLER, G. L., BRENKLE, J. P., KOMAREK, T. A. and ZYGIELBAUM, A. I. [1977] The Viking solar corona experiment. *J. Geophys. Res.*, Vol. 82, 4335-4340.

WOO, R. and ARMSTRONG, J. W. [1979] Spacecraft radio scattering observations of the power spectrum of electron density fluctuations in the solar wind. *J. Geophys. Res.*, Vol. 84, **12**, (Paper 9A0771), 7288-7296.

ZIRKER, J. B. [1977] Coronal holes and high speed wind streams. *Rev. Geophys. Space Phys.*, Vol. 15, 257-269.

PAGE INTENTIONALLY LEFT BLANK

PAGE LAISSEE EN BLANC INTENTIONNELLEMENT

SECTION 6B: RADIO NOISE

REPORT 258-5

MAN-MADE RADIO NOISE

(Study Programme 29C/6)

(1963-1970-1974-1978-1982-1990)

1. Introduction

In the solution of telecommunication problems, it is highly desirable to be able to estimate the radio noise at any location as caused by different types of noise sources. At certain locations, unintended man-made noise may be dominant. Since such noise can arise from a number of sources, such as power lines, industrial machinery, ignition systems, etc., it varies markedly with location and time [Hagn, 1973, 1981; Herman, 1971, 1979; Horner, 1971; Skomal, 1978; URSI, 1975, 1978 and 1981].

Current information is not available for estimating man-made noise intensities under all conditions but from limited observations [JTAC, 1968; Spaulding and Disney, 1974; and Spaulding *et al.*, 1975] it is possible to derive typical values.

2. Reference values of noise power

Median values of man-made noise power expressed in terms of F_a (dB above thermal noise at T_0 = 288 K, see Reports 322 and 670) attributed to man-made sources are shown in Fig. 1 as curves A to D, for business, residential, rural, and quiet rural areas, respectively, in the United States of America [Spaulding and Disney, 1974]. Measurements from 103 areas during 1966-1971 inclusive were used in the determination of the upper three curves. Business areas are defined as any area where the predominant usage thoughout the area is for any type of business (e.g. stores and offices, industrial parks, large shopping centres, main streets or highways lined with various business enterprises, etc.). Residential areas are defined as any area used predominantly for single or multiple family dwellings with a density of at least five single family units per hectare and no large or busy highways. Rural areas are defined as areas where dwellings are no more than one every two hectares. Attached to the use of these area classifications is the qualification that localized, intense noise sources are excluded. Curve D (for quiet rural areas) corresponds to the values of man-made noise at carefully selected quiet receiving sites as reported in Report 322. The dashed curve E, for galactic-noise obtained from Report 322, is included for reference. Further limited measurements in the USA reported by Spaulding and Disney [1974] relate to parks and university campuses (which generally have less vehicular traffic, electrical equipment and other types of noise source than business or residential areas) and relate to interstate highways (where the main source is ignition noise).

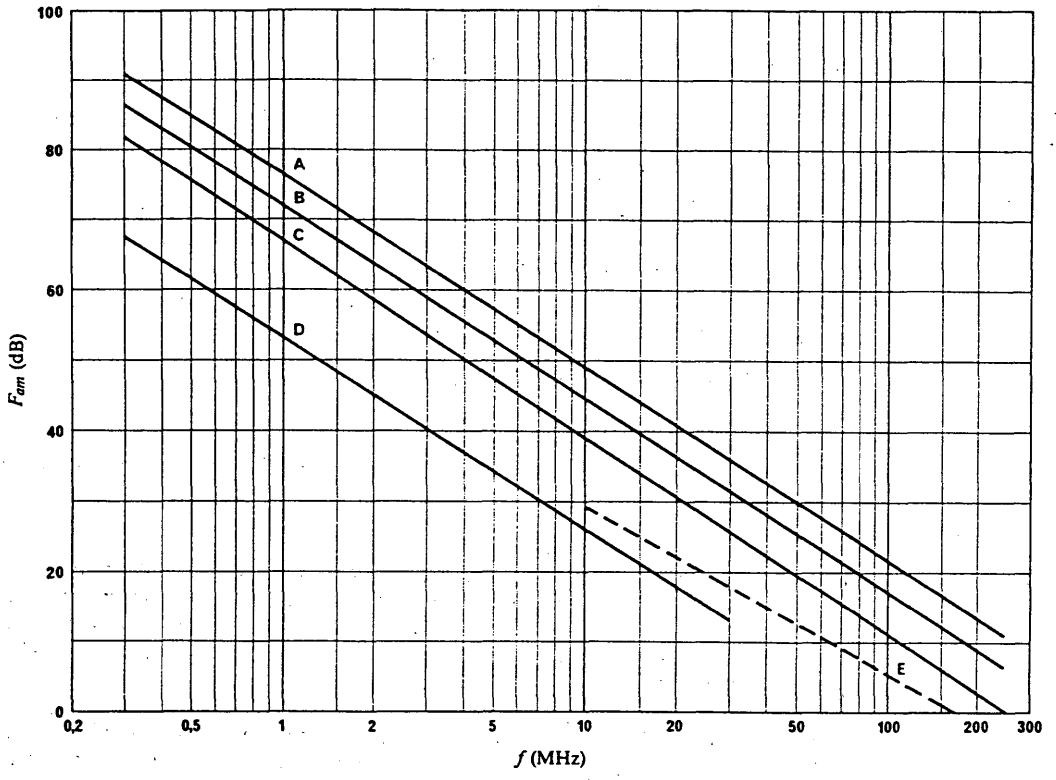


FIGURE 1 – *Median values of man-made noise power for a short vertical lossless grounded monopole antenna*

Environmental category:
A: business
B: residential
C: rural
D: quiet rural
E: galactic

In all cases, as with the data of Fig. 1, results are consistent with a linear variation of the median value, F_{am}, with frequency f of the form:

$$F_{am} = c - d \log f \qquad (1)$$

With f expressed in MHz, c and d take the values given in Table I. Note that equation (1) is valid in the range 0.3 to 250 MHz for all the environmental categories except those of curves D and E as indicated on the figure.

TABLE I — *Values of the constants c and d*

Environmental category	c	d
Business (curve A)	76.8	27.7
Inter-state highways	73.0	27.7
Residential (curve B)	72.5	27.7
Parks and university campuses	69.3	27.7
Rural (curve C)	67.2	27.7
Quiet rural (curve D)	53.6	28.6
Galactic noise (curve E)	52.0	23.0

Table II gives the variations measured within an hour about the hourly median value of noise power at a specified location. Upper and lower decile values D_u and D_l respectively are quoted for a selection of frequencies and for three types of environmental category.

An indication of the variation encountered from location to location within each environmental category is given by Spaulding and Disney [1974]. For all frequencies combined these authors quote the standard deviation of the median value as 7.5 and 6.5 dB, respectively, for business, residential and rural areas. A better estimate of the location variability of F_{am} for these environmental categories for a specific frequency may be obtained from the standard deviations σ_{NL} given in Table II for the measurement frequencies used.

Hagn and Sailors [1979] have presented four statistical-distribution models of increasing complexity (simple Gaussian, composite Gaussian, χ-square, Gaussian from χ-square) which utilize the time and location variability of F_a to predict the exceedence probabilities of man-made radio noise available power levels for short, vertically-polarized antennas located near the ground. The models are useful in predicting the probability that the short-term signal-to-noise ratio for a given communication system equals or exceeds a value required for successful communications [Hagn, 1980]. The parameters for these models at each of the measurement frequencies are summarized in Table III. For the simple Gaussian model, the mean is approximated by F_{am} and the standard deviation is σ_N where:

$$\sigma_N = \sqrt{\sigma_{NL}^2 + \sigma_{NT}^2} \tag{2}$$

assuming that the temporal and spatial variabilities are uncorrelated. The parameter σ_{NT} is the standard deviation of the temporal variability and values are obtained from D_u and D_l of Table II using:

$$\sigma_{NT} = \frac{1}{1.28}\left[\frac{D_u^2 + D_l^2}{2}\right]^{\frac{1}{2}} \tag{3}$$

For the composite Gaussian model, the standard deviations for the upper and lower halves of the distribution are given by σ_{Nu} and σ_{Nl}, respectively, and the mean is given by F_{am}. The corresponding upper and lower deciles are given by D_{Nu} and D_{Nl}. The composite Gaussian model is the simplest model which takes into account skewness ($D_{Nu} \neq D_{Nl}$) in the distribution. The χ-square model also takes into account skewness. In the χ-square model, the parameter ν is the number of degress of freedom. The χ-square model satisfies the relationship $F_a = a + b\chi^2$. The mean noise $\overline{F}_a = a + b\nu$, and the standard deviation $\sigma_{N_{\chi^2}} = b\,(2\nu)^{1/2}$, where a, b, and ν are given in Table III for ten discrete frequencies between 0.25 MHz and 250 MHz. For details of fitting data with a χ-square distribution and the use of the parameters ν, a, and b of Table III, see Zacharisen and Crow [1970]. A second Gaussian model is given in Table III using parameters estimated from the χ-square approximations. For this model, the mean is given by $F_{a_{\chi^2}}$ and the standard deviation by $\sigma_{N_{\chi^2}}$. When the skew is not too great, all four models predict similar values between the deciles; however, the χ-square model gives the best fit to the entire distribution. The simple Gaussian model should be used when the skew is not too high ($\nu \geqslant 10$) and when a simple model is required as in interference analysis [Sailors, *et al.*, 1977] (Report 657). The composite Gaussian model (which accounts for skewness) is the choice when a means is available to determine the appropriate half of the distribution. To date it has not been possible to choose one of these four models as consistently being the best. The above description may be used as a guideline for picking the appropriate model for a specific case.

TABLE II — *Representative values of selected measured noise parameters for business, residential and rural environmental categories*

Frequency (MHz)	Environmental category											
	Business				Residential				Rural			
	F_{am} (dB (kT_0))	D_u (dB)	D_l (dB)	σ_{NL} (dB)	F_{am} (dB (kT_0))	D_u (dB)	D_l (dB)	σ_{NL} (dB)	F_{am} (dB (kT_0))	D_u (dB)	D_l (dB)	σ_{NL} (dB)
0.25	93.5	8.1	6.1	6.1	89.2	9.3	5.0	3.5	83.9	10.6	2.8	3.9
0.50	85.1	12.6	8.0	8.2	80.8	12.3	4.9	4.3	75.5	12.5	4.0	4.4
1.00	76.8	9.8	4.0	2.3	72.5	10.0	4.4	2.5	67.2	9.2	6.6	7.1
2.50	65.8	11.9	9.5	9.1	61.5	10.1	6.2	8.1	56.2	10.1	5.1	8.0
5.00	57.4	11.0	6.2	6.1	53.1	10.0	5.7	5.5	47.8	5.9	7.5	7.7
10.00	49.1	10.9	4.2	4.2	44.8	8.4	5.0	2.9	39.5	9.0	4.0	4.0
20.00	40.8	10.5	7.6	4.9	36.5	10.6	6.5	4.7	31.2	7.8	5.5	4.5
48.00	30.2	13.1	8.1	7.1	25.9	12.3	7.1	4.0	20.6	5.3	1.8	3.2
102.00	21.2	11.9	5.7	8.8	16.9	12.5	4.8	2.7	11.6	10.5	3.1	3.8
250.00	10.4	6.7	3.2	3.8	6.1	6.9	1.8	2.9	0.8	3.5	0.8	2.3

F_{am}: median value

D_u, D_l: upper, lower decile deviations from the median value within an hour at a given location

σ_{NL}: standard deviation of location variability

TABLE III — *Summary of noise model parameters*

Environmental category	Freq. (MHz)	Simple Gaussian		Composite Gaussian				χ-square			Gaussian from χ-square	
		F_{am} (dB (kT_0))	σ_N (dB)	σ_{Nu} (dB)	σ_{Nl} (dB)	D_{Nu} (dB)	D_{Nl} (dB)	v	*a*	*b*	$F_{a\chi^2}$ (dB (kT_0))	$\sigma_{N\chi^2}$ (dB)
Business	0.25	93.5	8.3	8.8	7.8	11.3	9.9	92.16	37.51	0.61	93.9	8.3
	0.50	85.1	11.6	12.8	10.3	16.4	13.2	32.12	39.26	1.46	86.1	11.7
	1.00	76.8	6.3	8.0	3.9	10.2	5.0	3.51	69.77	2.46	78.4	6.5
	2.50	65.8	12.4	13.0	11.8	16.7	15.1	142.29	−38.56	0.74	66.3	12.4
	5.00	57.4	9.2	10.5	7.8	13.5	10.0	16.58	31.70	1.62	58.5	9.3
	10.00	49.1	7.7	9.5	5.3	12.1	6.8	4.95	38.38	2.49	50.7	7.8
	20.00	40.8	8.7	9.6	7.7	12.3	9.9	32.66	6.18	1.08	41.5	8.7
	48.00	30.2	11.1	12.5	9.5	16.0	12.2	20.91	− 4.69	1.73	31.4	11.2
	102.00	21.2	11.4	12.8	9.8	16.4	12.6	21.95	−15.62	1.73	22.3	11.5
	250.00	10.4	5.6	6.4	4.5	8.3	5.8	12.28	− 2.80	1.13	11.1	5.6
Residential	0.25	89.2	6.8	8.1	5.3	10.3	6.8	8.67	75.88	1.66	90.3	6.9
	0.50	80.8	8.5	10.5	5.7	13.5	7.4	4.67	69.42	2.84	82.7	8.7
	1.00	72.5	6.5	8.2	4.3	10.5	5.5	4.02	64.49	2.37	74.0	6.7
	2.50	61.5	10.4	11.3	9.4	14.4	12.0	45.36	12.58	1.09	62.2	10.4
	5.00	53.1	8.4	9.6	7.1	12.3	9.1	17.11	29.28	1.45	54.1	8.5
	10.00	44.8	6.1	7.2	4.9	9.2	6.2	10.38	31.57	1.36	45.7	6.2
	20.00	36.5	8.3	9.5	6.9	12.2	8.8	14.80	14.75	1.54	37.5	8.4
	48.00	25.9	8.8	10.4	6.8	13.3	8.7	8.90	8.53	2.11	27.3	8.9
	102.00	16.9	7.9	10.1	4.6	13.0	5.9	3.09	8.98	3.35	19.0	8.2
	250.00	6.1	4.9	6.1	3.2	7.8	4.1	4.13	0.00	1.74	7.2	5.0
Rural	0.25	83.9	7.2	9.1	4.5	11.7	5.7	3.52	75.82	2.80	85.7	7.4
	0.50	75.5	8.5	10.7	5.4	13.7	6.9	3.78	65.57	3.17	77.6	8.7
	1.00	67.2	9.5	10.1	8.8	13.0	11.3	75.34	9.41	0.77	67.7	9.5
	2.50	56.2	10.2	11.2	9.0	14.4	11.5	28.78	18.36	1.35	57.1	10.2
	5.00	47.8	9.4	9.0	9.7	11.5	12.4	260.87	154.61	0.41	47.6	9.4
	10.00	39.5	6.8	8.1	5.1	10.4	6.5	7.49	27.37	1.78	40.7	6.9
	20.00	31.2	6.9	7.6	6.2	9.7	8.0	39.08	0.87	0.79	31.7	7.0
	48.00	20.6	4.5	5.2	3.5	6.7	4.5	9.84	11.27	1.02	21.3	4.5
	102.00	11.6	7.1	9.0	4.5	11.6	5.8	3.72	3.25	2.71	13.3	7.4
	250.00	0.8	3.0	3.5	2.3	4.5	3.0	9.20	− 5.29	0.71	1.2	3.0

3. Dependence on location

Measurements made at HF in the United Kingdom indicate that curve D is appropriate for rural areas and that the man-made noise powers in business and residential areas are below those given by curves A and B. Measurements made at VHF in business and residential areas indicate man-made noise powers some 10 dB below those of curves A and B.

These results seem to suggest that differences in patterns of utilization of electrical and mechanical appliances or in the national statutory regulation of interference can lead to differing values of man-made noise power and that, until further evidence is available, the curves in Fig. 1 should be treated with caution.

Measurements made in the MF and HF range to determine the propagation attenuation coefficient of man-made noise α, as a function of residential density ρ, have in Poland led to the empirical relationship

$$\log \alpha = -3.47 + 0.690 \log \rho$$

where α is in dB/m and ρ is residential density in inhabitants/hectare. The influence of frequency on the value of attenuation coefficient was found to be insignificant [Rymarowicz, 1974 and 1975].

An unexpected result of measurements made in the MF range was lower man-made noise intensity in the residential areas of cities in the highly industrialized parts of the country. This is contrary to the generally held opinion about increase in the man-made noise power with increase of industrialization. This may probably be due to greater attenuation over paths through dense settlement patterns in highly industrialized regions, while the density of noise sources remained sensibly unchanged [Morón and Rymarowicz, 1975]. Further investigations are necessary to confirm these results.

4. Measurements at frequencies above 250 MHz

Skomal [1973, 1978] has reviewed man-made noise data collected in a range of countries at various distances from metropolitan areas. Results over the frequency range 500 kHz to 1 GHz are summarized. In the frequency range of about 300 to 800 MHz there is evidence that the rate of decrease of noise power with frequency is significantly less than that at lower frequencies as given in Table I. This is consistent with the presence of a localized maximum in the UHF-band emission spectrum of vehicular ignition interference.

At four sites in downtown Ottawa, Canada, measurements of the UHF-VHF radio environment were carried out over a 17-day period in November, 1976 by Lauber and Bertrand [1977]. A linear regression equation of the median values of F_a data for all four sites for the frequencies 200 to 500 MHz is given as $F_{am} = -15.8 \log f + 48.4$ (f in MHz). In the frequency range from 200 to 300 MHz, the results using this equation compare favourably with those using the business area equation of Spaulding and Disney [1974]. The standard deviation σ_N and upper and lower deciles, D_u and D_l, for these data are given in Table IV for the measurement frequencies 200, 300, 400 and 500 MHz.

TABLE IV — *F_{am} distribution parameters for business areas*

Frequency (MHz)	Standard deviation σ_N (dB)	D_u (dB)	D_l (dB)
200	4.7	5.0	6.0
300	4.6	7.0	4.5
400	4.2	5.5	4.5
500	4.1	6.5	2.5

Man-made noise level measurements have been made of the UHF radio environment over a four-month period (1982-1983) in and around Ottawa by Lauber and Bertrand [1984]. The antenna noise temperature T_a has been measured at a number of sites typical of business, residential and rural areas at 600, 700, 800, 900 and 950 MHz. For each of the areas a minimum of 1800 one-second measurements have been combined to form a cumulative probability distribution which shows the time and location variability of the noise. The highly skewed shape of the distributions, especially those from the business areas, shows that the UHF radio environment is composed of a background noise level upon which is superimposed a highly variable man-made noise level from vehicle ignition noise.

Beyond 1 GHz for business areas and 250 MHz for residential and rural areas, the measurement of man-made noise has been difficult because the available receivers have been internal noise-limited. In such a receiver system, the external noise does not affect its operating noise-threshold appreciably (Reports 413, (Oslo, 1966) and 670). Man-made noise measurements in an urban environment at frequencies between 1.7 and 35 GHz have been reported by Pratt *et al.* [1978] using radiometer techniques; however, the results were always below the reference temperature of 288 K.

5. Amplitude probability distributions

Measurements of the amplitude probability distributions (APD's) of man-made noise both from the overall environment and from specific sources have been made at many locations [Spaulding *et al.*, 1971, Lauber and Bertrand, 1979; Hagn, 1981].

The results of mathematical modelling of amplitude statistics using empirical and theoretical models have been reported by Lauber and Bertrand [1979]. A summary of a wide selection of mathematical models, mostly designed for atmospheric noise, has been given by Spaulding [1981]. A new series of statistical-physical models which use the characteristics of the physical processes to derive expressions for the amplitude statistics have been developed by Middleton [1979a, b]. To date, these models have been applied to a number of measured APD's with excellent agreement.

6. Combination of powers from different types of noise

There are certain situations (particular geographic locations, times and frequencies, especially HF) where man-made noise, atmospheric noise and galactic noise intensities are comparable. In these circumstances a method needed for summing the powers to yield estimates of the median seasonal time-block F_{am} values and percentile values of the resultant distribution has been developed [Spaulding and Stewart, 1987]. This assumes, for the man-made noise component, combination of temporal and locational variability and also assumes that the individual types of noise each follow log normal distributions. Computer routines are available from the CCIR Secretariat giving F_{am} and other parameters of the resultant distribution as defined in Report 322 (D_u, D_ℓ, σD_u, σD_ℓ and σF_{am}). See also Resolution 63.

REFERENCES

HAGN, G. H. [1973] Radio noise of terrestrial origin. *Radio Sci.*, Vol. 8, 6, 613-621.

HAGN, G. H. [1980] VHF radio system performance model for predicting communications operational ranges in irregular terrain. *IEEE Trans. Comm.*, Vol. COM-2B, 1637-1644.

HAGN, G. H. [1981] Man-made electromagnetic noise. *Handbook of Atmospherics.* Ch. 7, Ed. H. Volland, CRC Press, Boca Raton, Fla., USA.

HAGN, G. H. and SAILORS, D. B. [1979] Empirical models for probability distributions of short-term mean environmental man-made radio noise levels. 3rd Symposium and Technical Exhibition on Electromagnetic Compatibility, Rotterdam, 355-360 (available from EMC Symposium 1979, Postbus 5810, NL-2280 Rijswijk (ZH)), Netherlands.

HERMAN, J. R. [1971] Survey of man-made radio noise. *Progress in Radio Science*, Vol. I, 315-348, URSI, Brussels, Belgium.

HERMAN, J. R. [1979] *Electromagnetic Ambients and Man-Made Noise*, Vol. III, Multi-Volume EMC Encyclopedia Series. Don White Consultants, Inc., Gainsville, Va. 22065, USA.

HORNER, F. [1971] Techniques used for the measurement of atmospheric and man-made noise. *Progress in Radio Science*, Vol. II, 177-182, URSI, Brussels, Belgium.

JTAC [1968] Unintended radiation. *Suppl. 9 to Spectrum Engineering – The Key to Progress.* IEEE, New York, NY, USA.

LAUBER, W. R. and BERTRAND, J. M. [1977] Preliminary urban VHF/UHF radio noise intensity measurements in Ottawa, Canada. 2nd Symposium and Technical Exhibition on Electromagnetic Compatibility, Montreux, Switzerland, 357-362. (IEEE No. 77CH1224-5 EMC).

LAUBER, W. R. and BERTRAND, J. M. [1979] Statistical measurements and modelling of HVDC powerline noise. IEEE International Symposium on Electromagnetic Compatibility, 9-11 October, San Diego, Calif., USA, 224-231 (IEEE 79CH1383-9 EMC).

LAUBER, W.R. and BERTRAND, J.M. [1984] - Man-made noise level measurements of the UHF radio environment, IEEE National Symposium on Electromagnetic Compatibility, 24-26 April, San Antonio, Texas, USA, 185-192 (IEEE No. 84CH2035-4).

MIDDLETON, D. [1979a] Canonical non-Gaussian noise models: their implications for measurements and for prediction of receiver performance. *IEEE Trans. Electromag. Compt.*, Vol. EMC-21, 3, 209-220.

MIDDLETON, D. [1979b] Procedures for determining the parameters of the first-order canonical models for class *A* and class *B* electromagnetic interference. *IEEE Trans. Electromag. Compt.*, Vol. EMC-21, 3, 190-208.

MORÓN, W. and RYMAROWICZ, Z. [1975] Urban man-made noise in high industrialized and low industrialized regions in the medium wave range. 1st Symposium and Technical Exhibition on Electromagnetic Compatibility, Montreux, Switzerland, 284-287.

PRATT, T., BROWNING, D. J. and RAHHAL, Y. [1978] Radiometric investigations of the urban microwave noise environment at 1.7, 8.8 and 35 GHz. Proc. IEE International Conference on Antennas and Propagation, Part 2 – Propagation, London, UK, 28-30 November (IEE Conf. Publ. No. 169).

RYMAROWICZ, Z. [1974] Man-made noise in the medium frequency range in the cities of Lower Silesia and its dependence on population and industrialization of the city (in Polish). Institute of Telecommunications, Ph.D. thesis.

RYMAROWICZ, Z. [1975] Noise propagation in urban areas in medium and short wave range. 1st Symposium and Technical Exhibition on Electromagnetic Compatibility, Montreux, Switzerland, 281-283.

SAILORS, D. B., KUGEL, C. P. and HAYDON, G. W. [1977] Predicting the compatibility of high frequency skywave communication systems. *IEEE Trans. Electromag. Compt.*, Vol. EMC-19, 331-342.

SKOMAL, E. N. [1973] An analysis of metropolitan incidental radio noise data. *IEEE Trans. Electromag. Compt.*, Vol. EMC-15, 45-57.

SKOMAL, E. N. [1978] *Man-made Radio Noise.* Van Nosrand Reinhold, Co., New York, NY, USA.

SPAULDING, A. D. [1981] *Handbook of Atmospherics*, Ch. 6. Ed. H. Holland. CRC Press, Boca Raton, Florida, USA.

SPAULDING, A. D., AHLBECK, W. H. and ESPELAND, L. R. [1971] Urban residential man-made radio analysis and predictions. OT Telecommunications Research and Engineering Rep. 14, US Govt. Printing Office, Washington, DC 20402.

SPAULDING, A. D. and DISNEY, R. T. [1974] Man-made noise: Part I, OT Rep. 74-38. US Govt. Printing Office, Washington, DC 20402.

SPAULDING, A. D., DISNEY, R. T. and HUBBARD, A. G. [1975] Man-made noise: Part II, OT Rep. 75-63. US Govt. Printing Office, Washington, DC 20402.

SPAULDING, A.D. and STEWART, F.G. [1987] - An updated noise model for use in IONCAP. National Telecommunications and Information Administration (NTIA) Report 87-212 (NTIS Order No. PB 87-1650007/AS).

URSI [1975] *Rev. of Radio Sci.* 1972-1974, 128-132. International Union of Radio Science, Brussels, Belgium.

URSI [1978] *Rev. of Radio Sci.* 1975-1977, 57-64. International Union of Radio Science, Brussels, Belgium.

URSI [1981] *Rev. of Radio Sci.* 1978-1980, E1-E13, International Union of Radio Science, Brussels, Belgium.

ZACHARISEN, D. H. and CROW, E. L. [1970] Fitting distributions of telecommunication variables with Chi-square distributions. *Radio Sci.*, Vol. 5, 1307-1315.

REPORT 322-3*

CHARACTERISTICS AND APPLICATIONS OF ATMOSPHERIC RADIO NOISE DATA

(Question 29/6)

(1963-1974-1982-1986)

In accordance with decisions of the XVIth Plenary Assembly this Report replaces Report 322 (Geneva, 1963) as well as its Supplement No. 1, and is published separately in the form of a booklet.

REPORT 1151

APPLICATION OF RADIO NOISE AND INTERFERENCE DATA FOR SYSTEM DESIGN

(Question 29/6)

(1990)

In sound broadcasting there are difficulties in relating current CCIR statistical noise parameters to listener annoyance. Also, to date it has not been found possible to generate the temporal statistics of the noise but only to determine the amplitude probability distributions (APD). Existing noise parameters derived from the ADPs should be complemented with the corresponding temporal distributions. This would involve measurements of the durations that the noise exceeds each of a series of amplitude thresholds. Example sets of measurements are contained in Spaulding [1976].

Studies of the unwanted emission characteristics of electrical equipment are undertaken within CISPR, primarily to set limits for acceptable radiation. CISPR classifies interference as continuous or discontinuous on the basis of whether this lasts for more or less than 200ms. The sound broadcast listener is concerned both with impairments to intelligibility as with speech and those which affect the aesthetic enjoyment of music. It is suggested that the CISPR duration classification offers a convenient approach that could be used in first CCIR efforts to generate noise duration statistics relevant to sound broadcasting. Results of measurements could be provided separately for continuous and discontinuous interference. Whereas the APD is of interest for continuous interference, for discontinuous interference the peak value is probably the most useful measure, together with the duration and repetition rate.

Existing noise models relate to median values over an hour. Often in sound broadcasting there is interest in intelligibility over shorter periods, particularly in listener channel selection. It would be useful to produce complementary data on within-an-hour variability. These types of data over short averaging periods are also likely to become of increasing importance in assessing the impairments of digital broadcasting resulting from noise causing burst errors.

---

* This new version of Report 322 was adopted by the XVIth Plenary Assembly (Dubrovnik, 1986) for the purpose of facilitating further studies to be carried out by Study Group 6 (see Recommendation 372).

Noise intensities are currently expressed in terms of available power from a lossless short vertical monopole above a perfectly conducting ground plane and as equivalent horizontally incident vertically polarised field strengths. There may be a case instead for expressing noise intensities appropriate to reception on an isotropic antenna to ease the computation of signal/noise ratios since signal amplitudes use this reference.

It should also be noted that in many situations the background to satisfactory signal reception comes from co-channel and adjacent channel emissions rather than from atmospheric and man-made noise. Whilst the texts of Study Group 1 concerned with spectrum monitoring contain details of how to measure such signals, no composite measurement data are presented despite the known surveys that have been carried out in several countries. It would be helpful to have available such information, particularly for the HF broadcasting bands.

REFERENCES

SPAULDING, A.D. [1976] - Man-made noise; The problem and recommended steps toward solution, Office of Telecommunications Report 76-85 (National Technical Information Service Order PB253745).

REPORT 342-6

RADIO NOISE WITHIN AND ABOVE THE IONOSPHERE

(Study Programme 29A/6)

(1966-1970-1974-1978-1982-1986-1990)

1. Introduction

Radio noise levels, observable at a satellite in the ionosphere, depend on the properties of the medium surrounding the spacecraft in several different ways. The local ionization controls the propagation of radio waves in such a way as to determine whether emissions may reach the satellite and, if so, the effective angular antenna aperture for radiations from distant sources; it also modifies the antenna impedance and thus controls the observed noise level. The local ionospheric conditions also enter into the mechanisms for noise generation. Accordingly, ionospheric influences are usually of paramount importance in considerations of radio noise levels at satellite heights, and the present Report has been prepared with this in mind. Thus the spacecraft location in the ionosphere or the magnetosphere is of primary importance in describing the noise environment, particularly when the electron number density and magnetic field strength are included in the location parameters. For convenient reference throughout the Report, the variation of these two parameters with height is illustrated in Fig. 1 in terms of plasma frequency and electron gyro-frequency for a representative high-latitude ionosphere and magnetosphere. This figure also shows the variation with height of the x and z mode critical frequency, the upper-hybrid resonance frequency, the plasma frequency and the electron gyro-frequency that will be referred to from time to time. For the lower latitudes the situation is qualitatively quite similar to that illustrated, save that some of the curves are shifted somewhat in frequency. Subsequent sections of this Report will describe the radio noise bands in terms of frequency domains whose boundaries correspond to limits for particular propagation modes. The relevant modes depend on latitude (and particularly the invariant magnetic latitude at the Earth's surface for the relevant L shell [McIlwain, 1961]) at which the spacecraft is located.

This Report covers mainly the frequency range of potential interest for radio services above the F-layer maximum for which ionospheric shielding from the Earth is desirable. Generally speaking, this includes the frequencies between about 10 kHz and 20 MHz. The factors discussed are also important for many research investigations using satellites in the ionosphere. Noise will also be a limiting factor in some services using frequencies which penetrate the ionosphere; in this case, terrestrial noise and transmissions need to be considered as possible sources of interference. This Report does not discuss in any detail the sources of noise on frequencies much higher than the critical frequency, but a few comments on noise from terrestrial sources are included.

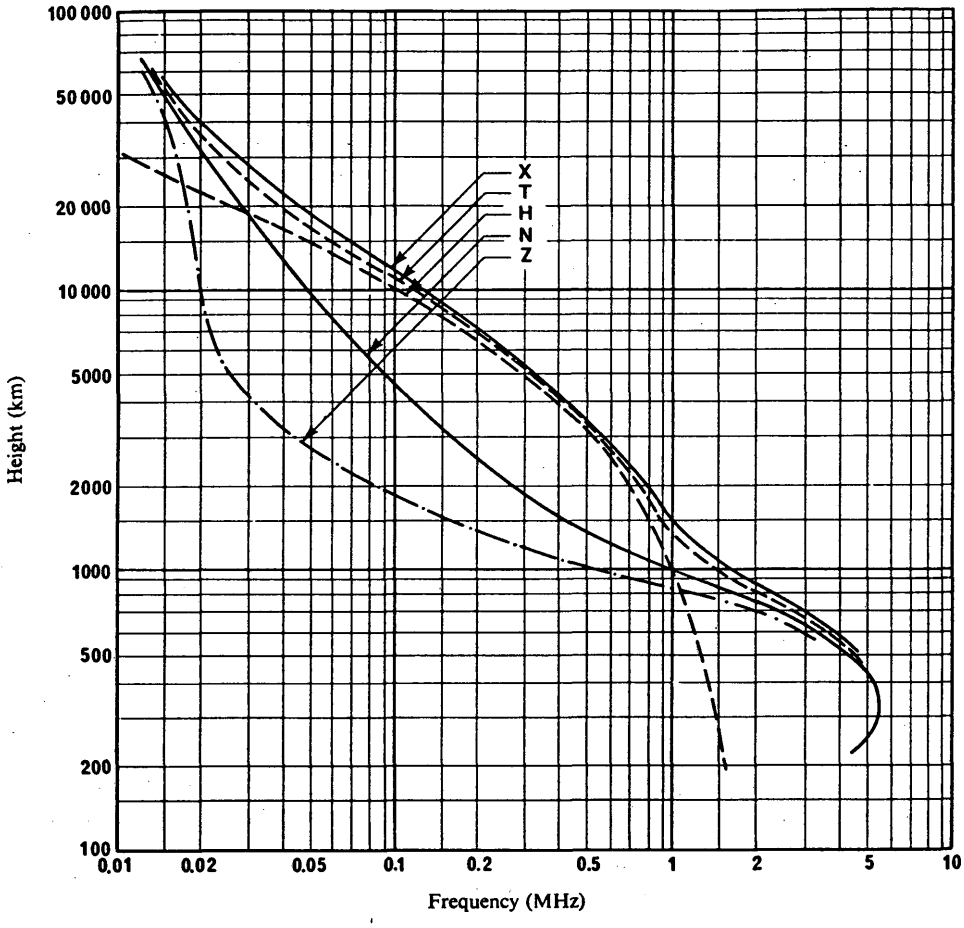


FIGURE 1 – *The variation with height, in a representative high-latitude ionosphere and magnetosphere, of the following:*

- electron gyro-frequency, $f_H = eB_0/2\pi m$, represented by the curve labelled H.
- plasma frequency, $f_N = (N_e^2/4\pi^2\varepsilon_0 m)^{1/2}$, represented by the curve labelled N.
- z-mode critical frequency, $f_Z = [(f_H^2/4) + f_N^2]^{1/2} - f_H/2$, represented by the curve labelled Z.
- upper-hybrid resonance frequency, $f_T = (f_N^2 + f_H^2)^{1/2}$, represented by the curve labelled T.
- x-mode critical frequency, $f_X = [(f_H^2/4) + f_N^2]^{1/2} + f_H/2$, represented by the curve labelled X.

2. Cosmic noise

Included here are galactic, and possibly extra-galactic, noise emissions which are observable above the limiting frequency for extraordinary wave propagation at the spacecraft. This limiting frequency is termed fxS and is defined by:

$$\text{fxS} = \left[(f_H^2/4) + f_N^2\right]^{1/2} + f_H/2 \qquad (1)$$

In the usual ionospheric terminology, this corresponds to the condition $X = 1 - Y$, where $X = f_N^2/f^2$; $Y = f_H/f$; f_N (the plasma frequency) $= (Ne^2/4\pi^2\varepsilon_0 m)^{1/2}$; f_H (the electron gyro-frequency) $= eB_0/2\pi m$; and $f =$ the observing frequency.

At frequencies above about 10 MHz, cosmic noise levels are fairly well established on the basis of measurements made with ground-based equipment [Andrew, 1966; Getmantsev *et al.*, 1968]. Measurements have been made from a number of rockets and satellites at fixed frequencies below 10 MHz [Walsh *et al.*, 1964; Huguenin *et al.*, 1964; Alexander and Stone, 1965; Benediktov *et al.*, 1965; Slysh, 1965 and 1966; Chapman, 1961] and fixed-frequency and sweep-frequency receiver measurements have been made from the Ariel, Alouette, ISIS, RAE, Zond, Luna and ISS-b satellites to determine the galactic noise spectrum [Smith, 1965; Hartz, 1964a and 1969a; Alexander *et al.*, 1969a; Hakura *et al.*, 1969, Clark *et al.*, 1970; Grigorieva and Slysh, 1970; Kotaki *et al.*, 1981]. These results are consistent with those obtained by Ellis *et al.* [1962] with ground-based equipment during selected ionospheric conditions. Some variation of the noise level from different regions of the galaxy has been noted in the satellite and rocket results, but, since the antenna aperture in most cases exceeded 2π steradians, the variations are not large and probably comparable with the experimental uncertainties.

Some results of the measurements of cosmic noise in rockets and satellites are plotted in Fig. 2 in terms of effective noise temperatures and some selected values from the smooth curve are listed in Table I. Measurements from the RAE satellite [Alexander *et al.*, 1969a] agree with the values shown in Fig. 2 within the limits of experimental error. The portion of the curve below about 0.6 MHz is based on IMP-6 satellite measurements between 130 and 2600 kHz and represents the minimum values for cosmic noise observed by that satellite [Brown, 1973]. The maximum cosmic noise values measured were about 1.5 to 2.0 dB above those shown and tabulated.

These values can be converted to brightness by means of the relation:

$$\text{brightness } B = 2kT_A/\lambda^2 \text{ W m}^{-2} \text{ Hz}^{-1} \text{ sterad}^{-1} \quad (2)$$

where T_A is the effective antenna temperature, λ is the wavelength (m) and k is Boltzmann's constant (1.38×10^{-23} Joules/K). The flux density can also be derived from

$$\text{flux density } S = 4\pi kT_A/\lambda^2 \text{ W m}^{-2} \text{ Hz}^{-1} \quad (3)$$

This relationship has been established on the assumption that typical antennas on spacecraft have effective apertures of 4π steradians, that they receive only one component of polarization and that the noise is nearly randomly-polarized. Flux densities are also listed in Table I. For comparison with values given in other Reports in which the effective antenna noise factor is used, for example Report 322 on atmospheric noise, the results are listed also in this form in Table I. The values in the HF range agree with those given in Report 322 for cosmic noise within 2 dB.

For the indicated frequency range and for a spacecraft antenna with a broad effective aperture [Hartz and Roger, 1964], the noise temperatures shown in Table I are the minimum galactic values that are observable within or above the ionosphere. In those cases where values significantly higher than these have been observed in this same frequency range, some additional source of noise or interference is to be sought. A number of such sporadic or occasional emission types are recognized, and they are discussed in the following sections.

Using fixed-frequency receivers on the ISS-b satellite, the average galactic radio noise has been measured at the frequencies 5, 10 and 25 MHz [Kotaki *et al.*, 1981]. These results expressed as effective temperature, are shown in Fig. 2 along with previous results. The receiving system of the ISS-b satellite employs two dipole antennas mounted on the plane of rotation spaced 90° apart. Table II lists the observational results obtained by ISS-b at these three frequencies. F_a is the mean value observed at each frequency. The parameters σ_u and σ_l are the upper and lower standard deviations from the mean value. GC/AC is the ratio in decibels of the radio brightness in the directions of the galactic centre and anti-centre. Most of the variation in the cosmic noise is due to the direction of a receiver relative to the galactic centre. The values of F_a agree with those given in Report 670 for cosmic noise.

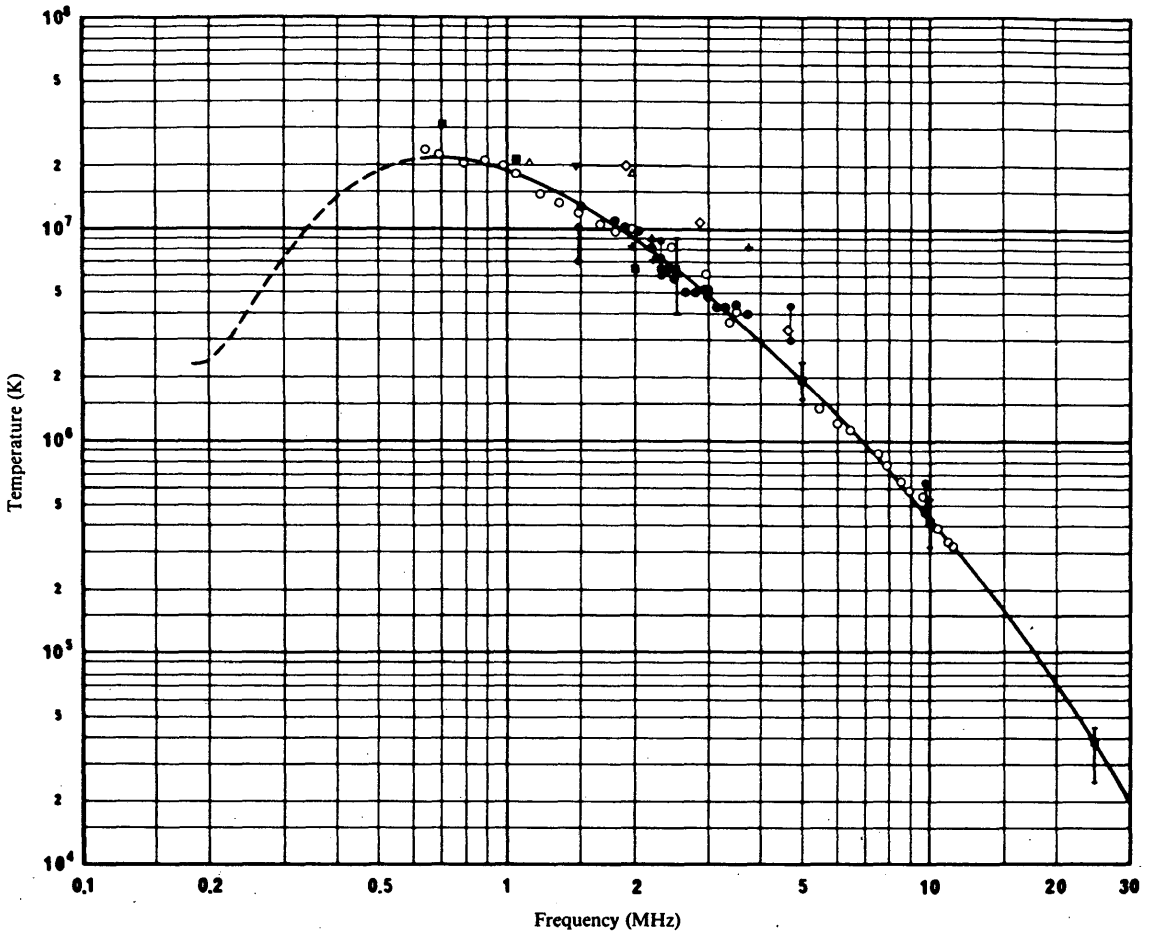


FIGURE 2 – *Effective temperature of an antenna receiving galactic noise*

- ▲ Walsh *et al.*, 1964
- ▲ Huguenin *et al.*, 1964
- ◇ Alexander and Stone, 1965
- ■ Benediktov *et al.*, 1965
- ▽ Slysh, 1965 and 1966
- + Chapman, 1961
- ▼ Smith, 1965
- Ellis *et al.*, 1962
- ● Alouette-1
- ○ Alouette-2
- Brown, 1973
- ISS-b

TABLE I — *Cosmic background noise observed with receivers in spacecraft*

f (MHz)	*T* (× 10⁶ K)	Power flux-density in one polarization component (10^{-21} W m^{-2} Hz^{-1})	Effective antenna noise factor (1) (dB)
0·2	2·4	0·18	39
0·4	14	4·3	47
0·6	21	15	49
0·8	21	26	49
1·0	19	37	48
2·0	9	69	45
3·0	5·0	86	42
5·0	1·8	86	38
10·0	0·42	80	31

(1) Reference temperature 288 K.

TABLE II – *Cosmic radio noise intensity measured by ISS-b*
[Kotaki *et al.*, 1981]

	Frequency (MHz)		
	5	10	25
F_a (dB/KT_0)	37.7	31.6	20.8
σ_u (dB)	1.1	1.0	1.2
σ_l (dB)	1.4	1.3	1.6
GC/AC (dB)	3.1	2.2	3.3

3. Solar noise

Radio noise emissions of solar origin, or which can be clearly associated with solar activity, have been observed sporadically at frequencies greater than fxS with various spacecraft [Hartz, 1964b and 1969b; Hakura *et al.*, 1969 and 1970; Alexander *et al.*, 1969b; Slysh, 1967; Benediktov *et al.*, 1968a; Grigorieva and Slysh, 1970, Haddock and Graedel, 1970]. During intervals of enhanced solar activity, short-duration noise bursts have been observed consistently at frequencies as low as 200 kHz and, occasionally, down to 50 kHz or even lower, though some of the observations at frequencies as low as 20 kHz are not always easily identified as solar related [Slysh, 1967; Dunckel *et al.*, 1970; Malitson *et al.*, 1973; Fainberg *et al.*, 1972]. At the higher frequencies, a clear association with ground observations of solar bursts can often be made. Long duration noise storms and type-IV events have also been observed with satellites and the maximum noise level observed for solar events is approximately 10^{-16} W m^{-2} Hz^{-1} [Hartz, 1969b].

4. Magnetospheric noise

Satellite-borne receivers operating in the outer regions of the magnetosphere at frequencies that exceed the local plasma frequency often observe noise levels substantially greater than those attributable to cosmic noise. At least two and probably three distinct types of broad-band emission are recognized, and their origin is associated, through direction-finding measurements and measurements of the spatial distribution of intensity, with the denser plasma regions closer to the Earth. The first, highly sporadic in character, with short time-scale variations, was probably first observed on some of the earlier Soviet space probes [Benediktov *et al.*, 1965, 1968a, 1968b, 1969; Slysh 1965, 1966, 1967]. Subsequent observations have led to a better definition of this noise type (see also [Huguenin *et al.* 1964]), and it has been variously described as "highpass", "midfrequency", "terrestrial kilometric", and "auroral kilometric" noise [Dunckel *et al.*, 1970, Brown, 1973; Gurnett, 1974; Kurth *et al.*, 1975; Benson, 1975]. It occurs in the frequency range from about 30 kHz to 1.0 MHz, with an intensity peak near 200 kHz which may, on occasion, exceed 10^{-14} W m^{-2} Hz^{-1}. Studies carried out on several satellites have localized the source of such emissions to altitudes of the order of two Earth radii in the auroral latitudes on the night side of the Earth, primarily near 22 hours local time. This noise type is strongly associated with the occurrence of aurora and geomagnetic disturbances, and is thought to be linked to the influx into the atmosphere of energetic electrons [Stone, 1973; Kaiser and Stone, 1975]. It has been reported at frequencies as low as 20 kHz and in excess of 1.5 MHz on occasions, but its main characteristic is its occurrence and/or intensity variability.

The second type, identified as continuum radiation, is also in the VLF and LF range, but it is much weaker and slowly-varying or quasi-continuous in nature. Its lower frequency limit, of the order of 1 kHz, apparently corresponds to the local plasma frequency at the observing spacecraft. It exhibits an intensity peak near 30 kHz, and for higher frequencies the noise intensity decreases with a spectral index of approximately -2.8. Thus it is usually below the cosmic noise level at frequencies above about 100 kHz though it has on occasion been

detected up to 300 kHz. Intensity variations which appear to be correlated with geomagnetic activity are observed, but it is not always clear that such reports pertain to only one noise type; nevertheless the intensity at 30 kHz has been found to approximate 10^{-17} W m^{-2} Hz^{-1} during high K_p conditions [Brown, 1973; Stone, 1973; Gurnett, 1975; Frankel, 1973]. This type seems to correspond to the "broadband" emissions reported by Dunckel *et al.* [1970]. It appears to be generated in a broad region that extends through the morning sector from about 0400 h to 1400 h local time, immediately beyond the plasmapause boundary. One possible source for this radiation is gyrosynchrotron emission from energetic electrons in the outer radiation zone, though the observed localization in time of the noise and its dependence on K_p index appear to be inconsistent with this explanation. Another possible source is precipitating particles from the trapped population or from the magnetospheric cleft [Stone, 1973], though again the local times do not correspond too well. An alternative source proposed by Gurnett and Frank [1976] as more likely, is from relatively low-energy electrons that are being injected into the outer radiation zone, in which case the noise generation can probably be linked with a coherent plasma instability.

This second noise type has been further subdivided [Gurnett and Shaw, 1973; Gurnett, 1975] into a trapped radiation component, which includes those frequencies below the plasma frequency of the magnetosheath or solar wind, and an escaping component consisting of those frequencies that may propagate freely outward into interplanetary space.

Kaiser and Stone [1975] have reported an emission type, also above the local plasma frequency, that appears to be generated more or less continuously in the day-side auroral oval. They describe the radiation as being very weak, with intensities only about a factor of ten above the cosmic noise background, and occurring in a narrow frequency band with a peak intensity slightly below 200 kHz. Apparently, this is a different type than the continuum emission discussed above and further definition of its characteristics particularly the local time of occurrence, of the day-side auroral-region emissions appears necessary. Kaiser and Stone have suggested that this type results from auroral particle precipitation that is peculiar to the day-time sector of the auroral oval, and which therefore is quasi-continuous in contrast to the sporadic night-time auroral kilometric noise. It is known that this region is one of intense low-energy electron precipitation on a fairly continuous basis, and noise emissions rather analogous to the sporadic night-time auroral kilometric radiation seem quite likely.

In addition to these broad-band emissions, satellite receivers in the magnetosphere have observed a number of relatively narrow-band emissions that can be associated with characteristic frequencies of the local medium, and which appear to be electrostatic in nature. The first of these is a band bounded by the local upper-hybrid (f_T) and plasma (f_N) frequencies, where

$$f_T^2 = f_N^2 + f_H^2. \tag{4}$$

This noise type has been studied more extensively at lower heights and in the ionosphere, and will be discussed in more detail in a later section. It is also observable over a wide range of heights in the plasmasphere and magnetosphere where it has been referred to as upper-hybrid resonance noise [Shaw and Gurnett, 1975; Mosier *et al.*, 1973].

The second type consists of intense narrow-band electrostatic emissions at frequencies between harmonics of the local electron cyclotron frequency. These are identified as $(n + \frac{1}{2}) f_H$ harmonics [Kennel *et al.*, 1970; Fredricks and Scarf, 1973], though the emissions do not appear precisely at the half integral harmonics. They are thought to arise from an electrostatic instability driven by a non-Maxwellian electron velocity distribution. The harmonics can be observed both above and below f_N, and while they can be found throughout much of the outer magnetosphere, they appear most intense and persistent in the vicinity of the base of the plasma sheet. The narrow-band electromagnetic hisses have been often observed in the vicinity of the plasmapause below the local electron cyclotron frequency. They seem to be generated in the vicinity of the equatorial plasmapause [Ondoh *et al.*, 1980].

Two variations of the above electrostatic noise types have been identified by Shaw and Gurnett from recordings made by the IMP-6 satellite in the magnetosphere as "narrow-band" and "diffuse" electrostatic emissions. These emissions appear most often between f_H harmonics that are near f_N; they are found to occur from well inside the plasmapause to radial distances as great as ten earth radii and appear to be a permanent feature of the magnetosphere. Typically they have small electric field amplitudes, with broad-band field strengths of the order of 2 μV/m. These bands appear to merge continuously into the two previous types of plasma wave emissions, into upper-hybrid-resonance noise inside the plasmasphere and into $(n + \frac{1}{2}) f_H$ harmonics in the outer magnetosphere.

5. Ionospheric noise

5.1 *Whistler-mode noise*

A number of measurements have been made with VLF receivers in rockets and satellites and the results show considerable variation both with time and with position of the spacecraft. In this section, consideration will be given to whistler-mode frequencies which are less than the lower of f_H and f_N at the spacecraft and greater than the local lower-hybrid resonance f_{LHR}.

This latter frequency is defined by:

$$f_{LHR}^{-2} = 1836\,(f_N^{-2} + f_H^{-2})\,\bar{m}_{eff} \qquad (5)$$

where $\bar{m}_{eff} = (\Sigma A_i m_p / m_i)^{-1}$, in which A_i and m_i are respectively the fractional abundance and mass of each ionic constituent, and m_p is the proton mass. In general, f_{LHR} is less than 10 kHz for the main regions of the ionosphere.

In the VLF band, the observed noise intensities vary by orders of magnitude and definite trends are now beginning to emerge. Most of the reported values are for frequencies near 10 kHz, and range from peak values of about 10^{-11} W m^{-2} Hz^{-1} to less than 10^{-16} W m^{-2} Hz^{-1} [Oelberman, 1964; Leiphart *et al.*, 1962; Gurnett, 1966; Jørgensen, 1968; Shawhan and Gurnett, 1968; Dunckel and Helliwell, 1969; Hughes *et al.*, 1971, Gurnett and Frank, 1972]. Various authors have arrived at typical or average intensities of about 10^{-14} W m^{-2} Hz^{-1}; but this must be viewed with some caution because of the very large variance. It is now becoming clear that the highest values are found in a fairly restricted range of latitudes in association with the influx, into the upper atmosphere, of energetic charged particles from the solar wind and from the magnetosphere. The work of Gurnett [1966], Hughes and Kaiser [1971], Barrington *et al.* [1971] and others, indicates that on the average the most intense noise is found in the midday, afternoon and evening sectors of the auroral oval, where the average noise intensity is of the order of 2×10^{-13} W m^{-2} Hz^{-1}. The noise is usually described as broad-band; it is often most intense at frequencies greater than f_{LHR} and because of this has been termed "lower hybrid-resonance noise" by some authors [Brice and Smith, 1964; McEwen and Barrington, 1967]. However, there seems to be little reason to believe that this noise differs fundamentally from what some authors have termed "VLF hiss" [Gurnett, 1966], or what is now becoming known, at least at the higher latitudes, as "auroral hiss".

The occurrence map of this broadband hiss [Ondoh, 1988] shows two regions of high occurrence probability (above 0.5) in the afternoon sector at invariant latitudes from 76° to 78°S and in the midnight-morning sector from 78° to 81°S. The high-latitude contour of occurrence probability 0.3 lies along a latitudinal circle of about 82°S. The low-latitude contour of 0.3 lies at 74°S on the meridian corresponding to 10 hours geomagnetic local time (MLT) and extends down to 67°S on the meridian corresponding to 22 hours MLT. At frequencies between 10 kHz and 20 kHz riser emissions or VLF hisses with fine rising structures have been observed in the topside mid-latitude ionosphere in the recovery phase of a magnetic substorm [Ondoh , 1985].

The whistler-mode noise is observed at frequencies well above 10 kHz, and appears to be continuous up to the lower of f_H and f_N [Walsh *et al.*, 1964; Harvey, 1968; Hartz, 1969a]. The noise intensity appears to drop steeply with increasing frequency [Jørgensen, 1968; Shawhan and Gurnett, 1968]. At frequencies greater than 100 kHz, the noise intensities have been found in the noon and evening portions of the auroral oval, where the average intensity is about 4×10^{-17} W m^{-2} Hz^{-1} [Barrington *et al.*, 1971; Laaspere *et al.*, 1971]. At lower latitudes the values are of the order of 10^{-19} W m^{-2} Hz^{-1} or less. At 540 kHz a value 1.7×10^{-18} W m^{-2} Hz^{-1} has been quoted as typical for auroral hiss [Laaspere *et al.*, 1971]. However, at this frequency and at 200 kHz, peak values have been observed that exceed the typical auroral hiss levels by some three orders of magnitude.

A one-to-one relationship appears to have been demonstrated between incoming electrons with energies of the order of 100 eV and the intensity of whistler-mode emissions [Hartz, 1971; Gurnett and Frank, 1972, Hoffman and Laaspere, 1972; Whitteker *et al.*, 1972; Walsh *et al.*, 1975]. This type of noise is thought to be generated in some coherent particle process, i.e. one in which collective interactions play a determining role. Above about 100 kHz the emissions appear to be predominantly longitudinal electric waves, in contrast with their electromagnetic character at VLF [James, 1973a, b].

Various attempts have been made to explain the whistler-mode noise intensities in terms of the Cerenkov radiation produced by such electrons [Lim and Laaspere, 1972; James, 1973b; Maeda, 1973; English and Hughes, 1974; Taylor and Shawhan, 1974; Smith, 1975]. Cyclotron instabilities of energetic electrons in the outer plasmasphere are also an important radiation process for explaining the plasmaspheric hiss of the electrostatic whistler mode. The plasmaspheric hiss is the strongest noise of all ionospheric noises at mid- and low-latitudes and it occurs persistently in both geomagnetically disturbed and quiet periods [Thorne *et al.*, 1973; Ondoh *et al.*, 1983]. The auroral LF/MF hiss is frequently observed in the topside ionosphere of the night-time auroral zone and its upper-cutoff frequency is approximately half the local electron gyrofrequency [Benson, 1985; Benson and Wong, 1987; Aikyo et al., 1987]. An analysis of arrival angles suggests that the cyclotron maser instability driven by precipitating auroral electrons with upward loss cone [Wu et al., 1983] is the most probable source mechanism, and also the most effective process at low altitudes ($f_N > f_H$) in the topside ionosphere [Benson and Wong, 1987; Aikyo et al., 1987].

In addition to noise associated with whistler-mode emissions and other noise in the frequency range between f_N and f_T, the Ariel-4 satellite at a height of 500 km detected noise of two further types, both of a wideband nature [Walsh *et al.*, 1975]. One consisted of sporadic noise over the full range of measuring frequencies (0.25 to 4 MHz) with an intensity some 80 dB above that of cosmic noise.

This wide frequency range extends through many regions of the Clemmow, Mullaly and Allis (CMA) diagram [Stix, 1962], but in many cases involves the non-propagating Region 5: hence the noise is attributed to some unknown interaction between the satellite and the surrounding plasma. The same applies to the second type of noise, which occurred when the local f_N exceeded about 6 MHz, and which decreased by 40 dB or more with increasing frequency over the range of measurement.

5.2 *Ionospheric noise associated with the upper-hybrid resonance*

Walsh *et* al., [1964] observed unexpectedly high noise levels at 0.75, 1.225 and 2.0 MHz, during the course of a rocket flight, and were able to link these to certain properties of the ionosphere. In particular, they showed that intense noise enhancements occurred when the receiver frequency was between the local plasma frequency, f_N, and the local upper-hybrid frequency, f_T. They associated the enhanced noise with a particular domain in the CMA diagrams, namely Region 3, and this noise type is often identified as "Region-3 noise". That frequency domain is bounded by the greater of f_N and f_H on the one hand and by f_T on the other; it is also a region where wave-particle interactions are expected to generate electrostatic radiation. As already noted, such electrostatic Region-3 emissions are observed in the magnetosphere and have been designated as "upper-hybrid resonance" emissions. In the ionosphere such emissions are observed routinely. Harvey [1965 and 1968] reported observations for the Ariel-2 satellite that were similar to those of Walsh *et al.* [1964], and showed that the intensity of the noise was related to the energetic particle flux in the inner Van Allen radiation belt. He reported, as well, that another anomalously intense noise band, also related to the energetic particle flux, was observable in the frequency range below the local plasma frequency and above the extraordinary wave cut-off frequency, fzS, at the satellite. fzS corresponds to the conditions $X = 1 + Y$ in the usual ionospheric terminology; it is defined by the relation:

$$\text{fzS} = \left[(f_H^2/4) + f_N^2\right]^{1/2} - f_H/2 \qquad (6)$$

This second band of noise is thought to originate as "Region-3" noise and likely to appear in the other spectral region as a result of mode coupling and propagation at frequencies below the local f_N.

Similar results have been reported by Hartz [1967, 1969a], Burenin *et al.*, [1968], Bauer and Stone [1968], Gregory [1969 and 1971] and Walsh *et al.* [1975]. The more recent of these indicate that the greatest intensities occur at high latitudes, and that there is a relationship between the noise intensities and energetic particle influx. It is noted that Gregory's results were obtained with a loop antenna, which would indicate that this noise type is not entirely electrostatic in nature.

5.3 *Noise at frequencies above f_T*

Narrow bands of noise near 2 and 4 MHz have been observed occasionally by James *et al.* [1973] in the ISIS-1 and 2 recordings. Such emissions appear in a latitude band centred approximately on the auroral oval, and, at least at times, their intensity exceeds that of the cosmic noise background by several orders of magnitude. This type of noise is thought to originate in an electrostatic process in the auroral latitudes below the satellite in a region where $f_T = 2f_H$, followed by mode conversion and upward propagation so that the satellite can observe electromagnetic radiation in a narrow frequency band and at its first harmonic.

On occasions the lower-frequency band, i.e. that near 2 MHz, extends down in frequency to an apparent cut-off frequency that is double the local f_H. On other occasions this band appears broader still and extends down in frequency to the local f_T. Such instances occur during ionospheric disturbances when the satellite is over the nightside auroral oval. This type of noise would then appear to be analogous to the auroral kilometric radiation at VLF that is observed by satellites at greater heights.

5.4 *Ionospheric noise in other spectral regions*

For a substantial portion of the ionosphere f_N is comparable to f_H, being greater or less than that frequency within a factor of about ten. One very convenient way of designating the spectral regions in terms of propagation modes and possible generation mechanisms is by means of the CMA diagram [Stix, 1962]. Experience with noise observations on ionospheric satellites, and notably on the Alouette and ISIS satellites, has shown that noise emissions may be observed on suitable occasions in all spectral regions. Those described above are the most prevalent types, and are clearly associated with the auroral latitudes and with charged particle interactions. Other spectral types probably arise from these basic types and are observable (as such) as a consequence of mode conversion and propagation from the region of origin.

One exception appears to be the Region-3 noise. This noise band appears in a great many of the Alouette-2 and ISIS recordings at frequencies below fzS and above f_N (although this latter limit is not always a firm one) in those situations where fzS is greater than f_H [Hartz, 1967 and 1969a]. This frequency range will not support electromagnetic wave propagation, and consequently the observations could perhaps be viewed as arising in a local source, for example, one involving the interaction of the satellite itself and the medium.

It is difficult to arrive at estimates of the absolute intensities of the various types of noise included in this section because of uncertainties regarding the antenna impedance and the exact nature of the phenomenon that is being observed. Nevertheless, the reported values are several orders of magnitude above the expected cosmic noise level and must be taken into account.

6. Interference of terrestrial origin

Interference from ground-based HF transmitters can be received at a spacecraft at frequencies above the ionospheric penetration frequency or critical frequency as it is more conventionally termed. This critical frequency varies with geographic region, time of day, season, and solar activity; it may be as low as 0.5 MHz at night in certain latitudes, or greater than 15 MHz in equatorial regions by day. As a consequence, a receiver in a high altitude satellite can be subjected to strong interference from the ground within and above this frequency range. Measurements on such signals have shown them to exceed the cosmic noise level by more than 50 dB [Huguenin and Papagiannis, 1965]. Even in relatively narrow frequency gaps between terrestrial transmitters, the peak values of interference from atmospherics may exceed the galactic level by significant amounts over major thunderstorm areas of the globe [Huguenin and Papagiannis, 1965; Horner, 1965; Aksenov *et al.*, 1970; Horner and Bent, 1969; Herman *et al.*, 1973]. A previous survey of noise from terrestrial sources has been made by Rawer [1967]. Herman *et al.*, [1975] on the basis of RAE-1 data have made a more recent survey of transmissions from the Earth that are associated with thunderstorms and with other man-made origins. ——————The composite intensity of noise and interference of terrestrial origin within the standard radio wave guard bands at 2.5, 5.0, 10.0 and 25 MHz derived from ISS-b observations shows a maximum of 25 dB above the galactic noise level [Iwama et al., 1989].——————The occurrence of ground reflected echoes observed by Alouette-1 were used as a qualitative measure of the HF noise level in the topside ionosphere [Muldrew *et al.*, 1967].

On frequencies greater than foF2, the terrestrial noise power above the ionosphere exhibits a frequency dependence which is related to the magnitude of foF2 below the spacecraft. For a constant foF2, the noise power increases with increasing observing frequency (f) due to the expanding effective source size whose radius is a function of the ratio foF2/f [Herman *et al.*, 1975; Horner and Bent, 1969]. Going from 5 MHz to 10 MHz the increase is typically about 20 dB. In the absence of interfering ground-based signals, maximum noise power is observed at a frequency (typically in the range 10 to 15 MHz) where the ionosphere ceases to limit the effective source size. At lunar distances noise on frequencies a few megahertz above foF2 arriving from the direction of the Earth can be 6 to 12 dB greater than cosmic-noise background [Herman, 1974]; the interference level from Earth-based transmitters can be much greater than this.

The Appleton-Hartree magneto-ionic theory predicts that interference from ground-based transmitters can be received at a spacecraft orbiting above the F layer peak when:

$$\text{foF2} < \sqrt{2} f_{HF2} \tag{7}$$

at frequencies between fzF2 and fzI if fzI > fzF2

where foF2 is the ordinary wave critical frequency of the F layer, f_{HF2} is the gyro-frequency at the peak of the F layer, fzF2 is the extraordinary-wave critical frequency of the F layer and is given by:

$$\text{fzF2} = \left[\frac{(f_{HF2})^2}{4} + (\text{foF2})^2\right]^{\frac{1}{2}} - \frac{f_{HF2}}{2} \tag{8}$$

and where fzI is the z mode frequency at the spacecraft, corresponding to the condition where the index of refraction for the vertical incidence z mode of propagation becomes infinite and is given by:

$$\text{fzI} = \left[\frac{f_T^2}{2} + \left[\frac{f_T^4}{4} - f_N^2 f_H^2 \cos^2\theta\right]^{\frac{1}{2}}\right]^{\frac{1}{2}} \tag{9}$$

where z refers to the lower branch extraordinary wave as described by the Appleton-Hartree equation [Budden, 1961]; f_N, f_H, and f_T are as defined above, and θ is the angle between the vertical and the direction of the Earth's magnetic field.

For the condition foF2 < $\sqrt{2} f_{HF2}$, the main source of interference is the standard MF broadcast transmissions from 0.54 up to about 1.3 MHz [Hagg *et al.*, 1969]. Loran transmissions at 2 MHz also are frequently observed by satellite receivers at times of low foF2 [Legg and Newman, 1967]. Such forms of interference are fairly common in the winter months at night, over the region of the main F layer trough [Muldrew, 1965].

The Appleton-Hartree theory also predicts interference from ground-based transmitters at frequencies less than fwI, where fwI is the whistler wave infinity at the spacecraft, corresponding to the condition where the vertical incidence whistler mode of propagation becomes infinite and is given by:

$$\text{fwI} = \left[\frac{f_T^2}{2} - \left[\frac{f_T^2}{4} - f_N^2 f_H^2 \cos^2\theta\right]^{\frac{1}{2}}\right]^{\frac{1}{2}} \tag{10}$$

where w refers to the lower branch ordinary wave and f_N, f_H, f_T and θ are as defined previously. The highest frequency at which whistler mode breakthrough can be detected at the spacecraft is equal to:

$$f_N \text{ if } f_N < f_H \text{ and} \tag{11}$$

$$f_H \text{ if } f_H < f_N \tag{12}$$

Interference propagating through the peak of the F layer via the whistler mode is the result of coupling of signals from the z mode to the whistler mode in the D and E regions of the ionosphere. Such coupling may also occur in the F region when foE < f_{HF2} (foE is the upper branch ordinary wave critical frequency of the E layer) but such coupling will be inefficient because of low collision frequency in the F region.

The main sources of whistler mode interference on the ionograms obtained by the Alouette-2 and ISIS satellites are the Loran C pulse transmissions at 0.1 MHz, long wave broadcast transmissions from 0.15 to 0.3 MHz and the standard MF broadcast transmissions from 0.54 to about 1.3 MHz.

A second type of man-made interference for satellite reception is now recognized. Because of the non-linear behaviour of the ionospheric plasma surrounding the spacecraft, discrete radio signals can give rise to beat frequencies or intermodulation products. The beat mechanism may involve various combinations of the frequencies of these discrete signals which may be radiated by the satellite itself and at frequencies harmonically related to such radiations, or which may occur at ionospheric resonance frequencies that are excited in some non-linear fashion by satellite emissions; the signals may even come from ground-based transmissions. Numerous examples of this form of interference appear in the Alouette and ISIS records at frequencies well below the ionospheric critical frequency. Some of these effects can perhaps be attributed to very oblique propagation from the ground at the observed frequency, or to beats produced in the receiving equipment itself. However, in many cases such explanations are implausible and it has been concluded that a significant portion of the observed beat frequencies is produced in the ionospheric plasma near the spacecraft [Barrington and Hartz, 1968 and 1969; Hagg, 1967; Hartz and Barrington, 1969].

Another subject that requires further consideration in this regard involves parametric processes in the ionospheric plasma. Considerable current interest is being devoted to this topic, and a separate study in this area might be appropriate [Tzoar, 1969].

A third type of interference involves VLF emissions from the ground that can propagate to the satellite by way of the whistler mode, mainly at night [Bullough *et al.*, 1971]. The observed signal intensities appear to depend on latitude, D-region absorption and F-region structure, but further studies should be made.

7. Resonances observed with ionospheric sounders

Ionospheric sounders aboard rockets and satellites transmit short radio-wave pulses and record the subsequent response of the ionosphere with a radio receiver on the spacecraft [Knecht *et al.*, 1961; Warren, 1962]. Discrete signals or resonances are observed which can persist from a fraction of a millisecond to many milliseconds after the termination of the transmitted pulse. The most frequent and predictable of these resonances occur when the operating frequency is at about the local plasma frequency, f_N, the local upper-hybrid frequency, f_T, and its harmonic $2f_T$, and harmonics of the electron gyro-frequency, nf_H [Lockwood, 1963; Calvert and Goe, 1963]. Other resonance responses can be found at lower frequencies that bear a fractional relationship to one or more of the principal resonances of the ambient plasma [Hartz and Barrington, 1969], at frequencies corresponding to the electrostatic or Bernstein resonances of the local medium [Warren and Hagg, 1968], and at a frequency that corresponds to $2f_H$ at a location in the ionosphere remote from the spacecraft [Muldrew and Hagg, 1966]. At times, and notably during disturbed ionospheric conditions, a number of these resonances may be observed in the receiver recordings when the sounder transmitter is not operating [Hartz, 1969a; Mosier *et al.*, 1973]. Resonances have also been observed when the pulse transmitter is fixed and the receiver is swept in frequency [Lockwood, 1973]. These various resonant responses may have to be considered in the design of electronic circuitry for spacecraft.

Matuura and Nishizaki [1969] found pulse echoes, named proton cyclotron echoes, on the Alouette-2 ionograms which may be attributed to the interaction of repeated pulse signals emitted by the topside sounder with the ionospheric plasma surrounding the spacecraft. The delay-time between the pulse signal emission and the reception of the pulse echoes is equal to the gyration time of protons around the magnetic field at the satellite position and independent of the frequency of the emitted waves.

Many of the characteristics of the principal resonances can be explained by the theory of the propagation of electrostatic waves [McAfee, 1968, 1969a, 1969b, 1970; Muldrew, 1972a, 1972b]. The electrostatic waves launched obliquely at frequencies within several kilohertz of the plasma frequency or upper hybrid-frequency propagate short distances from the spacecraft, are reflected by the ionized medium and returned to the satellite,

producing a signal with a given delay. The delay of this signal is so extremely sensitive to frequency that the frequency spectrum of a transmitted pulse can produce echoes over a wide range of delays, thus producing a long receiver response. Other resonances may be related to non-linear effects in the local plasma [Hartz and Barrington, 1969], to the radiation of sidebands of the transmitter pulse [Lockwood, 1973], and to the generation of electrostatic waves with possibly a subsequent conversion to and propagation of electromagnetic radiation in the case of some remote resonances [Oya, 1971].

8. Conclusion

This Report deals mainly with noise at frequencies below the critical frequency of the ionosphere and, although cosmic noise values can be extrapolated to higher frequencies (see Report 322 and Andrew [1966]), noise from lightning discharges and man-made sources on the ground will need to be taken into account, probably up to a frequency of approximately 500 MHz, depending on the antenna characteristics. Noise arising from the non-linear properties of the plasma needs much more study. Measurements of noise being made at the present time in various satellites should provide useful additional data. Consideration should be given to turbulence generated in the ionosphere plasma by the vehicles moving through it. In general, the subject of kinetics of plasmas and the generation of noise should be investigated more extensively and more carefully.

Note. – Contributions from URSI have been used in the preparation of this Report.

REFERENCES

AIKYO, K. , ONDOH, T and OHTAKA, K. [1987] - Some characteristics and propagation of whistler-mode LF/MF emissions as observed at low altitudes above the antarctic region with ISIS-1, Proc. Natl. Inst. Pol. Res. Symp. Upper Atmos. Phys. (Japan), Vol. 1, pp. 173 - 184.

AKSENOV, V. I., DUBINSKǏ, B. A., ZHEKULIN, L. A., KISELEVA, Z. Y., LISHIN, I. V., MAKAROV, V. A. and MIKAILOV, L. N. [1970] Investigation of transmission of ultralong radio waves through the Earth's ionosphere: preliminary results from the Cosmos 142 satellite. (in Russian). *J. Cosmic Res.* (USSR), **8**, 571.

ALEXANDER, J. K., BROWN, L. W., CLARK, T. A., STONE, R. G. and WEBBER, R. R. [1969a] The spectrum of the cosmic radio background between 0.4 and 6.5 MHz. *Astrophys. J. (Lett.)*, Vol. 157, L163.

ALEXANDER, J. K., MALITSON, H. H. and STONE, R. G. [1969b] Type III radio bursts in the outer corona. *Solar Phys.*, **8**, 388-397.

ALEXANDER, J. K. and STONE, R. G. [1965] Rocket measurements of cosmic-noise intensities below 5 Mc/s. *Astrophys. J.*, Vol. 142, 1327-1332.

ANDREW, B. H. [1966] The spectrum of low radio frequency background radiation. *Monthly Notices Roy. Astron. Soc.*, Vol. 132, 79-86.

BARRINGTON, R. E. and HARTZ, T. R. [1968] Satellite ionosonde records: resonances below the cyclotron frequency. *Science*, Vol. 160, **3824**, 181-183.

BARRINGTON, R. E. and HARTZ, T. R. [1969] Resonances observed by the Alouette topside sounders. *Plasma Waves in Space and in the Laboratory*, 55. Ed. J. O. Thomas and B. J. Landmark, Edinburgh University Press, Edinburgh, UK.

BARRINGTON, R. E., HARTZ, T. R. and HARVEY, R. W. [1971] Diurnal distribution of ELF, VLF and LF noise at high latitudes as observed by Alouette II. *J. Geophys. Res.*, Vol. 76, 5278-5291.

BAUER, S. J. and STONE, R. G. [1968] Satellite observations of radio noise in the magnetosphere. *Nature*, Vol. 218, 1145-1147.

BENEDIKTOV, E. A., GETMANTSEV, G. G., MITYAKOV, N. A., RAPOPORT, V. O., SAZONOV, J. A. and TARASOV, A. F. [1965] Intensity measurements of radiation on frequencies 725 and 1525 kHz by means of receivers on the Electron-2 satellite (in Russian) *Cosmic Space Research* (All-Union Conference on Space Physics, Moscow, 581-606).

BENEDIKTOV, E. A., GETMANTSEV, G. G., MITYAKOV, N. A., RAPOPORT, V. O. and TARASOV, A. F. [1968a] Type III solar bursts recorded by the Electron-4 satellite (in Russian). *J. Cosmic Res.* (USSR), **6**, 950.

BENEDIKTOV, E. A., GETMANTSEV, G. G., MITYAKOV, N. A., RAPOPORT, V. O. and TARASOV, A. F. [1968b] Relation between geomagnetic activity and the sporadic radio emission recorded by the Electron satellites (in Russian). *J. Cosmic Res.* (USSR), **6**, 946.

BENEDIKTOV, E. A., GETMANTSEV, G. G., MITYAKOV, N. A., RAPOPORT, V. O. and TARASOV, A. F. [1969] Variations in the mean level of radio emission at the frequencies 1.1 and 2.3 MHz according to measurements made by the artificial earth satellite "Electron-4" (in Russian). *J. Cosmic Res.* (USSR), **7**, 156.

BENSON, R. F. [1975] Source mechanism for terrestrial kilometric radiation. *Geophys. Res. Lett.*, Vol. 2, **2**, 52-55.

BENSON, R. [1985] - Auroral kilometric radiation: wave modes, harmonics, and source region electron density structures, J. Geophys. Res., 90, pp. 2753 - 2784.

BENSON, R. and WONG, H.K. [1987] - Low-altitude ISIS-1 observations of auroral radio emissions and their significance to the cyclotron maser instability, J. Geophys. Res., 92, pp. 1218 - 1230.

BRICE, N. M. and SMITH, R. L. [1964] A very-low-frequency plasma resonance. *Nature*, Vol. 203, **4948**, 926-927.

BROWN, L. W. [1973] The galactic radio spectrum between 130 and 2600 kHz. *Astrophys. J.*, Vol. 180, 359-370.

BUDDEN, K. G. [1961] *Radio Waves in the Ionosphere*, 59. Cambridge University Press, Cambridge, UK.

BULLOUGH, K., SAGREDO, J. L., HUGHES, A. R. W. and KAISER, T. R. [1971] Ariel 3 observations of the GBR (16 kHz) wavefield above the winter night-time ionosphere. *Space Research XI*, 1305-1312.

BURENIN, A. N., GETMANTSEV, G. G., MITYAKOV, N. A., RAPOPORT, V. O., SIZMIN, A. M. and TYUKIN, V. N. [1968] Radio radiation intensity at 1.68 MHz as measured by "Cosmos-142" (in Russian). *J. Cosmic Res.* (USSR), **6**, 313.

CALVERT, W. and GOE, G. B. [1963] Plasma resonances in the upper ionosphere. *J. Geophys. Res.*, Vol. 68, 6113-6120.

CHAPMAN, J. H. [1961] Effects of the ionosphere on radio noise measurements from an earth satellite. *Space Research II*, 597. Eds. H. C. van de Hulst, C. de Jager and A. F. Moore. North-Holland Publishing Co., Amsterdam, Netherlands.

CLARK, T. A., BROWN, L. W. and ALEXANDER, J. K. [1970] Spectrum of the extragalactic background radiation at low radio frequencies. *Nature*, Vol. 228, 847-848.

DUNCKEL, N., FICKLIN, B., RORDEN, L. and HELLIWELL, R. A. [1970] Low-frequency noise observed in the distant magnetosphere with OGO 1. *J. Geophys. Res.*, Vol. 75, **10**, 1854-1862.

DUNCKEL, N. and HELLIWELL, R. A. [1969] Whistler-mode emissions on the OGO 1 satellite. *J. Geophys. Res.*, Vol. 74, **26**, 6371-6385.

ELLIS, G. R. A., WATERWORTH, M. D. and BESSELL, M. [1962] Spectrum of the galactic radio emission between 10 Mc/s and 1.5 Mc/s. *Nature*, Vol. 196, **4859**, 1079.

ENGLISH, H. W. and HUGHES, A. R. W. [1974] An attempt to explain satellite observations of high latitude VLF hiss in terms of generation by incoherent Cerenkov radiation. *Space Research XIV*, 359-367.

FAINBERG, J., EVANS, L. G. and STONE, R. G. [1972] Radio tracking of solar energetic particles through interplanetary space. *Science*, Vol. 178, **4062**, 743-744.

FRANKEL, M. S. [1973] LF radio noise from the Earth's magnetosphere. *Radio Sci.*, Vol. 8, **11**, 991-1005.

FREDRICKS, R. W. and SCARF, F. L. [1973] Recent studies of magnetospheric electric field emissions above the electron gyro-frequency. *J. Geophys. Res. (Lett.)*, Vol. 78, **1**, 310-314.

GETMANTSEV, G. G., KARAVANOV, V. S., KOROBKOV, Y. S. and TARASOV, A. F. [1968] Frequency spectrum of the distributed cosmic radio emission in the range from 6.3 to 40 MHz (in Russian). *Astron. J.*, **45**, 936.

GREGORY, P. C. [1969] Radio emission from auroral electrons. *Nature*, Vol. 221, 350.

GREGORY, P. C. [1971] Satellite observations of magnetospheric radio noise-1. Emissions between the plasma and upper hybrid resonance frequencies. *Planet. and Space Sci.*, Vol. 19, 813-820.

GRIGORIEVA, V. P. and SLYSH, V. I. [1970] Long wave cosmic radio radiation in circumlunar space (in Russian). *J. Cosmic Res.* (USSR), **8**, 284.

GURNETT, D. A. [1966] A satellite study of VLF hiss. *J. Geophys. Res.*, Vol. 71, 5599-5615.

GURNETT, D. A. [1974] The Earth as a radio source: terrestrial kilometric radiation. *J. Geophys. Res.*, Vol. 79,**28**, 4227-4238.

GURNETT, D. A. [1975] The Earth as a radio source: the non-thermal continuum. *J. Geophys. Res.*, Vol. 80, 2751-2763.

GURNETT, D. A. and FRANK, L. A. [1972] VLF hiss and related plasma observations in the polar magnetosphere. *J. Geophys. Res.*, Vol. 77, 172-190.

GURNETT, D. A. and FRANK, L. A. [1976] Continuum radiation from low-energy electrons in the outer radiation zone. *J. Geophys. Res.*, Vol. 81, 3875-3885.

GURNETT, D. A. and SHAW, R. R. [1973] Electromagnetic radiation trapped in the magnetosphere above the plasma frequency. *J. Geophys. Res.*, Vol. 78, 8136-8149.

HADDOCK, F. T. and GRAEDEL, T. E. [1970] Dynamic spectra of Type III solar burst from 4 to 2 MHz observed by OGO-III. *Astrophys. J.*, Vol. 160, 293-300.

HAGG, E. L. [1967] Electron densities of 8-100 electrons/cm^3 deduced from Alouette II high latitude ionograms. *Can. J. Phys.*, Vol. 45, 27-36.

HAGG, E. L., HEWENS, E. J. and NELMS, G. L. [1969] The interpretation of topside sounder ionograms. *Proc. IEEE*, Vol. 57, **6**, 949-960.

HAKURA, Y., NISHIZAKI, R. and TAO, K. [1969] Analysis of observational data obtained by Alouette II. IV. Galactic noise spectrum and solar radio bursts in hecto-decametric wave region. *J. Radio Res. Labs.* (Japan), Vol. 16, **87/88**, 215-226.

HAKURA, Y., NISHIZAKI, R., TAO, K. and YAMASHITA, F. [1970] Results of special observations for the Proton Flare Project 1969. III. Observation of solar radio bursts by satellite Alouette II during the PFP interval May-July, 1969. *J. Radio Res. Labs.* (Japan), Vol. 17, **89**, 21-32.

HARTZ, T. R. [1964a] Observations of the galactic radio emission between 1.5 and 10 MHz from the Alouette satellite. *Ann. Astrophys.*, Vol. 27, 823-830.

HARTZ, T. R. [1964b] Solar noise observations from the Alouette satellite. *Ann. Astrophys.*, Vol. 27, 831-836.

HARTZ, T. R. [1967] Satellite observations of ionospheric radio noise. *Progress in Radio Science*, URSI. 1963-1966, 1109.

HARTZ, T. R. [1969a] Radio noise levels within and above the ionosphere. *Proc. IEEE*, Vol. 57, **6**, 1042-1050.

HARTZ, T. R. [1969b] Type III solar radio bursts at hectometer wavelengths. *Planet. and Space Sci.*, Vol. 17, 267-287.

HARTZ, T. R. [1971] Particle precipitation patterns. *The Radiating Atmosphere*, 225. Ed. B. M. McCormac. D. Reidel Publishing Co., Dordrecht, Netherlands.

HARTZ, T. R. and BARRINGTON, R. E. [1969] Nonlinear plasma effects in the Alouette recordings. *Proc. IEEE*, Vol. 57, **6**, 1108-1113.

HARTZ, T. R. and ROGER, R. S. [1964] The effective antenna beam width for a satellite-borne radio telescope. *Can. J. Phys.*, Vol. 42, 2146-2152.

HARVEY, C. C. [1965] Results from the UK-2 satellite. *Ann. Astrophys.*, Vol. 28, 248-254.

HARVEY, C. C. [1968] Radio emission from geomagnetically trapped particles. *Nature*, Vol. 217, **5123**, 50-51.

HERMAN, J. R. [1974] Earth as a planetary radio noise source. Final Report on Contract NAS5-24007-Mod 4 (Avco Corp., 201 Lowell St., Wilmington, Ma 01887, USA).

HERMAN, J. R., CARUSO, J. A. and STONE, R. G. [1973] Radio Astronomy Explorer (RAE)-I. Observations of terrestrial radio noise. *Planet. and Space Sci.*, Vol. 21, **3**, 443-461.

HERMAN, J. R., STONE, R. G. and CARUSO, J. A. [1975] Radio detection of thunderstorm activity with an Earth-orbiting satellite. *J. Geophys. Res.*, Vol. 80, 665-672.

HOFFMAN, R. A. and LAASPERE, T. [1972] Comparison of very low-frequency auroral hiss with precipitating low-energy electrons by the use of simultaneous data from two OGO 4 experiments. *J. Geophys. Res.*, Vol. 77, 640-650.

HORNER, F. [1965] Radio noise in space originating in natural terrestrial sources. *Planet. and Space Sci.*, Vol. 13, 1137-1150.

HORNER, F. and BENT, R. B. [1969] Measurement of terrestrial radio noise. *Proc. Roy. Soc.*, Vol. 311, 527-542.

HUGHES, A. R. W. and KAISER, T. R. [1971] VLF radio emissions and the aurora. *The Radiating Atmosphere*, 336. Ed. B. M. McCormac, D. Reidel Publishing Co., Dordrecht, Netherlands.

HUGHES, A. R. W., KAISER, T. R. and BULLOUGH, K. [1971] The frequency of occurrence of VLF radio emissions at high latitudes. *Space Research XI*, 1323-1330.

HUGUENIN, G. R., LILLEY, A. E., McDONOUGH, W. H. and PAPAGIANNIS, M. D. [1964] Measurements of radio noise at 0.7 and 2.0 Mc/s from a high-altitude rocket probe. *Planet. and Space Sci.*, Vol. 12, 1157-1167.

HUGUENIN, G. R. and PAPAGIANNIS, M. D. [1965] Spaceborne observations of radio noise from 0.7 to 7.0 MHz and their dependence on the terrestrial environment. *Ann. Astrophys.*, Vol. 28, 239-247.

IWAMA, M., MARUBASHI, K. and KATOH, C. [1989] Radio noise intensity at guard bands for HF standard waves in the topside ionosphere measured by ISS-b. J. Comm. Res. Lab. (Japan), Vol. 36, 148, 55-67.

JAMES, H. G. [1973a] Spin modulation of high-latitude hiss measured by an electric dipole. *Radio Sci.*, Vol. 8, **12**, 1133-1147.

JAMES, H. G. [1973b] Whistler-mode hiss at low- and medium-frequencies in the dayside-cusp ionosphere. *J. Geophys. Res.*, Vol. 78, 4578-4599.

JAMES, H. G., HAGG, E. L. and STRANGE, D. L. P. [1973] Narrow-band radio noise in the topside ionosphere. Proc. AGARD Conf. on Non-Linear Effects in Electromagnetic Wave Propagation.

JØRGENSEN, T. S. [1968] Interpretation of auroral hiss measured on OGO 2 and at Byrd Station in terms of incoherent Cerenkov radiation. *J. Geophys. Res.*, Vol. 73, 1055-1069.

KAISER, M. L. and STONE, R. G. [1975] Earth as an intense planetary radio source: similarities to Jupiter and Saturn. *Science*, Vol. 189, 285-287.

KENNEL, C. F., SCARF, F. L., FREDRICKS, R. W., McGEHEE, J. H. and CORONITI, F. V. [1970] VLF electric field observations in the magnetosphere. *J. Geophys. Res.*, Vol. 75, 6136-6152.

KNECHT, R. W., VANZANDI, T. E. and RUSSEL, S. [1961] First pulsed radio soundings of the top side of the ionosphere. *J. Geophys. Res.*, Vol. 66, 3078-3081.

KOTAKI, M., KURIKI, I., KATOH, C. and SUGIUCHI, H. [1981] Cosmic radio noise at high radio frequencies as observed with ISS-b. *J. Radio Res. Labs.* (Japan), Vol. 28, **125/126**, 35-48.

KURTH, W. S., BAUMBACK, M. M. and GURNETT, D. A. [1975] Direction-finding measurements of auroral kilometric radiation. *J. Geophys. Res.*, Vol. 80, 2764-2770.

LAASPERE, T., JOHNSON, W. C. and SEMPREBON, L. C. [1971] Observations of auroral hiss, LHR noise and other phenomena in the frequency range 20 Hz-540 kHz on OGO 6. *J. Geophys. Res.*, Vol. 76, 4477-4492.

LEGG, A. J. and NEWMAN, W. S. [1967] The reception of ground-based loran transmissions by the fixed-frequency topside sounder satellite. *J. Atmos. Terr. Phys.*, Vol. 29, 1383-1386.

LEIPHART, J. P., ZEEK, R. W., BEARCE, L. S. and TOTH, E. [1962] Penetration of the ionosphere by very-low-frequency radio signals. Interim results of the LOFTI I experiment. *Proc. IRE*, Vol. 50, Part I, 6.

LIM, T. L. and LAASPERE, T. [1972] An evaluation of the intensity of Cerenkov radiation from auroral electrons with energies down to 100 eV. *J. Geophys. Res.*, Vol. 77, 4145-4157.

LOCKWOOD, G. E. K. [1963] Plasma and cyclotron spike phenomena observed in top side ionograms. *Can. J. Phys.*, Vol. 41, 190-194.

LOCKWOOD, G. E. K. [1973] Side band and harmonic radiation from top side sounders. *J. Geophys. Res.*, Vol. 78, 2244-2250.

MAEDA, K. [1973] VLF hiss from electrons in the Earth's magnetosphere. Rep. X-646-73-111, Goddard Space Flight Center, Greenbelt, Md., USA.

MALITSON, H. H., FAINBERG, J. and STONE, R. G. [1973] A density scale for the interplanetary medium from observations of a Type II solar radio burst out to 1 A.U. *Astrophys. J. (Lett.)*, Vol. 183, L35.

MATUURA, N. and NISHIZAKI, R. [1969] Proton cyclotron echoes in the top side ionosphere. *J. Geophys. Res.*, Vol. 74, 5169-5172.

McAFEE, J. R. [1968] Ray trajectories in an anisotropic plasma near plasma response. *J. Geophys. Res.*, Vol. 73, 5577-5584.

McAFEE, J. R. [1969a] Top side resonances as oblique echoes. *J. Geophys. Res.*, Vol. 74, 802-808.

McAFEE, J. R. [1969b] Top side ray trajectories near the upper hybrid resonance. *J. Geophys. Res.*, Vol. 74, 6403-6408.

McAFEE, J. R. [1970] Top side plasma frequency resonance below the cyclotron frequency. *J. Geophys. Res.*, Vol. 75, 4287-4290.

McEWEN, D. J. and BARRINGTON, R. E. [1967] Some characteristics of the lower hybrid resonance noise bands observed by the Alouette I satellite. *Can. J. Phys.*, Vol. 45, 13-19.

McILWAIN, C. E. [1961] Co-ordinates for mapping the distribution of magnetically trapped particles. *J. Geophys. Res.*, Vol. 66, 3681-3691.

MOSIER, S. R., KAISER. M. L. and BROWN, L. W. [1973] Observations of noise bands associated with the upper hybrid resonance by the IMP-6 radio astronomy experiment. *J. Geophys. Res.*, Vol. 78, 1673.

MULDREW, D. B. [1965] F layer ionization troughs deduced from Alouette data. *J. Geophys. Res.*, Vol. 70, 2635-2650.

MULDREW, D. B. [1972a] The electrostatic resonances associated with the maximum frequencies of cyclotron harmonic waves. *J. Geophys. Res.*, Vol. 77, 1794-1801.

MULDREW, D. B. [1972b] Electron resonances observed with top side sounders. *Radio Sci.*, Vol. 7, 779-789.

MULDREW, D. B. and HAGG, E. L. [1966] A novel ionospheric cyclotron resonance phenomenon observed on Alouette I data. *Can. J. Phys.*, Vol. 44, 925-939.

MULDREW, D. B., LITWACK, M. D. and TIMLECK, P. L. [1967] Interpretation of the statistics of occurrence of Alouette-1 earth echoes. *Planet. and Space Sci.*, Vol. 15, 611-618.

OELBERMAN, E. J. [1964] Expected radio noise levels in the upper atmosphere from 100 cps to 100 kMc/s. IEEE International Convention Record, **12**, Part 6, 331.

ONDOH, T. [1985] - Characteristics of riser emissions observed by ISIS satellites, edited by H. Kikuchi, pp. 53 - 64, Elsevier Science Publishers, B. V. Amsterdam.

ONDOH, T. [1988] - Polar occurrence map of broadband auroral hiss observed by ISIS satellites, J. Radio Research Laboratory (Japan), Vol. 35, No. 144, pp. 1 - 14.

ONDOH, T., NAKAMURA, Y., WATANABE, S., AIKYO, K. and MURAKAMI, T. [1983] Plasmaspheric hiss observed in the topside ionosphere at mid- and low-latitudes. *Planet. and Space Sci.*, Vol. 31, **4**, 411-422.

ONDOH, T., NAKAMURA, Y., WATANABE, S. and MURAKAMI, T. [1980] Narrow-band VLF hiss observed in the vicinity of the plasmapause. *J. Radio Res. Labs.* (Japan), Vol. 27, **124**, 131-139.

OYA, H. [1971] Conversion of electrostatic plasma waves into electromagnetic waves: numerical calculation of the dispersion relation for all wavelengths. *Radio Sci.*, Vol. 6, **12**, 1131-1141.

RAWER, K. [1967] Noise produced by terrestrial sources in the near-earth space. *Propagation Factors in Space Communications*, 383-408. Ed. W. T. Blackband, McKay and Co., London, UK.

SHAW, R. R. and GURNETT, D. A. [1975] Electrostatic noise bands associated with the electron gyro-frequency and plasma frequency in the outer magnetosphere. *J. Geophys. Res.*, Vol. 80, 4259-4271.

SHAWHAN, S. D. and GURNETT, D. A. [1968] VLF electric and magnetic fields observed with the Javelin 8.45 rocket experiment. *J. Geophys. Res.*, Vol. 73, 5649-5664.

SLYSH, V. E. [1965] The measurement of cosmic radiation on frequencies 210 and 2200 kHz at heights to 8 earth radii on Zond 2 (in Russian). *J. Cosmic Res.* (USSR), **3**, 760.

SLYSH, V. E. [1966] Measurements of kilometre radio-emission in inter-planetary space (in Russian). *J. Cosmic Res.* (USSR), **6**, 923.

SLYSH, V. E. [1967] Solar radio emission at 2 and 0.2 MHz (in Russian). *Astron. J.*, **44**, 94.

SMITH, F. G. [1965] Cosmic radio noise as measured in the satellite Ariel II; Part II, Analysis of the observed sky brightness. *Monthly Notices Roy. Astron. Soc.*, Vol. 131, 145-153.

SMITH, P. A. [1975] Cerenkov relations between r.f. noise and energetic particles on Ariel 4. *Proc. Roy. Soc.*, Vol. 343A, 241-255.

STIX, T. H. [1962] *The Theory of Plasma Waves.* McGraw-Hill, New York, NY, USA.

STONE, R. G. [1973] Radio physics of the outer solar system. *Space Sci. Rev.*, Vol. 14, 534-551.

TAYLOR, W. W. L. and SHAWHAN, S. D. [1974] A test of incoherent Cerenkov radiation for VLF hiss and other magnetospheric emissions. *J. Geophys. Res.*, Vol. 79, 105-117.

THORNE, R. M., SMITH, E. J., BURTON, R. and HOLZER, R. E. [1973] Plasmaspheric hiss. *J. Geophys. Res.*, Vol. 78, 1581.

TZOAR, N. [1969] Parametric excitations in plasma in a magnetic field. *Phys. Rev.*, Vol. 178, **1**, 356-362.

WALSH, D., HADDOCK, F. T. and SHULTE, H. F. [1964] Cosmic radio intensities at 1.225 and 2.0 Mc/s measured up to an altitude of 1700 km. *Space Research IV*, 935. Ed. P. Muller, North-Holland Publishing Co., Amsterdam, Netherlands.

WALSH, D., HAYES, A. P. and HARRISON, V. A. W. [1975] Observations of radio frequency noise from Ariel 4. *Proc. Roy. Soc.*, Vol. 343A, 227-240.

WARREN, E. S. [1962] Sweep frequency radiation sounding of the top side of the ionosphere. *Can. J. Phys. (Lett.)*, Vol. 40, 1692.

WARREN, E. S. and HAGG, E. L. [1968] Observation of electrostatic resonances of the ionospheric plasma. *Nature*, Vol. 220, 466-468.

WHITTEKER, J. H., BRACE, L. H., BURROWS, J. R., HARTZ, T. R., HEIKKILA, W. J., SAGALYN, R. C. and THOMAS, D. M. [1972] ISIS I observations of the high-latitude ionosphere during a geomagnetic storm. *J. Geophys. Res.*, Vol. 77, 6121-6128.

WU, C.S., DILLENBURG, D., ZIEBELL, L.F. and FREUND, H.P. [1983] - Excitation of whistler waves by reflected auroral electrons, Planet, Space Sci., 31, pp. 499 - 507.

REPORT 254-7

MEASUREMENT OF ATMOSPHERIC RADIO NOISE

(Study Programme 29B/6)

(1959-1963-1966-1970-1974-1978-1982-1986-1990)

1. Noise measurements and results

An extensive series of measurements of noise has been made since 1957 using standard equipment (ARN-2) at a network of stations throughout the world [Crichlow *et al.*, 1959-67]. All these stations have measured noise power (effective antenna noise figure, Reports 670 and 322) but some stations were additionally equipped for the measurement of other noise parameters descriptive of the noise structure. An account of this measurement programme has been prepared by URSI [1962]. Using the measurement data from this network of measurement stations from July 1957 to October 1961, world-wide estimates of atmospheric noise levels and other characteristics were prepared [Report 322 (Geneva, 1963)]. The regular forwarding of data from the ARN-2 network to the Data Collecting Center at Boulder, Colorado, United States, ceased in November 1966, although some stations continued to make sporadic measurements past that date. From 1958 to 1965, the USSR operated a network of ten noise measurement stations within the USSR, and the measurement data from this network were supplied to the World Data Center. Parameters different from the ARN-2 noise parameters were measured, but these Soviet data could be transformed to the ARN-2 format [Likhter and Terina, 1960]. Using all the data from the ARN-2 and Soviet networks with the addition of other available appropriate data, the noise estimates of Report 322 were updated [Spaulding and Washburn, 1985]. These new estimates are contained in Report 322-3 (Dubrovnik, 1986). Computer routines that produce all the noise estimates from Report 322-3 (Dubrovnik, 1986) (and also man-made noise estimates from Report 258) are available from the CCIR Secretariat.

At some frequencies systematic differences, up to 4 dB in noise power, have been obtained by different techniques at the same site.

Reports of measurements at high frequencies have suggested that the noise intensity estimates in the original Report 322 were too low during daytime in some tropical regions [CCIR, 1963-66a, b, and c; CCIR, 1966-69a], with the discrepancies being up to 10 dB or more in the lower part of the HF band. The most recent version of Report 322 does indicate such an increase in the noise estimates for tropical regions. Other early published comparisons between predicted and measured noise values are also taken into account in the most recent version of Report 322 [e.g. Herman, 1961; Ibukun, 1964].

Results of a special study of atmospheric noise at VLF have been published in the form of charts and curves [Watt, 1967]. Results for VLF and ELF are also available [Maxwell, 1967; Remizov *et al.*, 1971]. In addition, work towards the development of an improved VLF noise-prediction model has been reported [CCIR, 1970-74a]. Data from a new global network of eight computer-controlled receiving systems for the measurement of electromagnetic noise in the 10 - 32 000 Hz (ELF/VLF) frequency band are available [Fraser-Smith et al., 1987; Fraser-Smith and Helliwell, 1985]. Balloon measurements of low frequency transverse electric (TE) and transverse magnetic (TM) atmospheric noise field strengths have been reported by Turtle et al. [1989], for altitudes varying between 1.5 km and 21 km. In general, the horizontal electric field strength increases as the altitude increases, becoming 8 to 10 dB below the vertical electric field strength at 21 km. At aircraft elevations (10 km), the horizontal field is approximately 15-20 dB below the vertical field.

Results of measurements of noise over a nine-month period at a quiet rural site in Southern England over the frequency range 5 - 20 MHz have been compared with predictions based on Reports 322-2 (Geneva, 1982) and 322-3 (Dubrovnik, 1986) [Gibson, 1989]. The mean difference between the measured and predicted values is about 1.5 dB (measured values larger in both cases). The r.m.s. difference is 3.7 dB using Report 322-2 (Geneva, 1982) and 3.2 dB using Report 322-3 (Dubrovnik, 1986).

A comprehensive series of measurements of atmospheric noise levels in Central Australia [Ward, 1989] shows consistent discrepancies between measured and predicted levels of atmospheric noise in the middle of the HF band during daytime conditions. The observed noise levels between 10 and 30 MHz are consistent with predicted levels of galactic noise and are as much as 10 dB below predicted atmospheric noise levels between 10 and 20 MHz. The measurements also demonstrate that there are systematic differences in noise level associated with the use of directional antennas relative to those measured with an omnidirectional antenna. Preliminary results indicate that there is a very marked solar cycle dependence in noise levels in the middle portion of the HF band. Both of these features can be readily explained in terms of variations in radio wave propagation conditions.

In a report from India it has been stated that, in tropical countries, atmospheric noise at VHF is of practical importance [Aiya, 1979]. Data are furnished which should be useful to designers of VHF communication systems in the tropical regions.

2. Statistical characteristics of noise

Measurements of amplitude-probability distributions of noise have been made at many locations [URSI, 1962] and the data have been used in Report 322. It has been shown that allowance can be made for the noise structure in estimating required signal-to-noise ratios.

Statistical noise data for bands 5 (LF), 6 (MF) and 7 (HF) have become available from measurements made in India over two decades. They are based on a technique which emphasizes the importance of the bursts of noise which are the main source of noise interference to many services. The influence of the noise on voice communication, broadcasting and data transmission has been studied [CCIR, 1966-69b; URSI, 1981; Spaulding, 1981]. Some information is available on the short- and long-term statistical variations of noise [Crichlow *et al.*, 1960; Remizov *et al.*, 1967; Watt, 1967; Watt and Maxwell, 1957; Spaulding *et al.*, 1962]. Methods for obtaining the wide-band atmospheric noise characteristics from narrow-band measurements have been investigated [Remizov, 1977; Remizov *et al.*, 1979].

The results of some measurements of the amplitude and time statistics and of the mathematical modelling of these statistics have been reported by Disney and Spaulding [1970]. A summary of a wide selection of mathematical models of the atmospheric noise process has been given by Spaulding and Middleton [1975], Spaulding [1977] and Middleton [1979]. In addition, attempts to produce laboratory simulators of atmospheric noise have been reported by Bolton [1971].

3. Measurements with directional antennas

Measurements have been made with directional antennas of the type used in high-frequency, long-distance communication. There are insufficient data for a full report to be made, but the results of some investigations have been published [Kronjäger and Vogt, 1959; Bradley and Clarke, 1964] and some preliminary information is contained in Report 322. In addition, more recent measurements carried out in Canada are reported in CCIR [1970-74b].

4. Lightning-flash counters and direction-finding networks

The object of lightning-flash counter observations, in so far as they are required for noise studies, is to determine the number of lightning discharges occurring per unit area of the Earth's surface, in different places and at different times. Although the expansion of counter networks has proceeded rather slowly, further experience has been gained in their use, and in the comparison between the CCIR types and other types. Data from counters of a type which has been adopted by CIGRE (Conférence internationale des grands réseaux électriques) and which has been used extensively, can be correlated with data from the CCIR counters provided that appropriate sensitivities have been used; work has been in progress to establish the effective range of the CIGRE counter with improved accuracy [Frühauf *et al.*, 1966]. Experiments with another counter, operating on the high-frequency energy from atmospherics have led to similar conclusions, regarding the incidence of discharges, as those from the CCIR counter.

Experiments in the United Kingdom [Horner, 1960] and others, reported in a CCIR document from Sweden [CCIR, 1963] have resulted in different estimates of the effective range of the CCIR counter, and further investigation is required. However, the more precise evaluation of this quantity need not delay the collection of further data which will show at least the relative values in different geographical locations.

A lightning-flash counter operating in the high frequency band has been developed in India and is claimed to be cheap, compact and portable, and to have a well-defined range of detection [Aiya and Hari Shankar, 1969].

An analysis has been made of data from lightning-flash counters of the CCIR recommended design, used in the United Kingdom and in Singapore. The results, which have been published [Horner, 1967] include comparisons between counter data and noise data which are particularly relevant to the work of the CCIR. These comparisons illustrate the conditions under which estimated noise intensities, based on counts and on the known electrical characteristics of lightning flashes, agree or disagree with the direct measurements of noise which are mentioned in § 1.

In broad terms agreement is good when the measured noise can reasonably be expected to originate mainly in relatively near storms, provided that these are sufficiently numerous to produce a continuing succession of atmospherics. Conditions which give rise to discrepancies between the two methods of estimating noise are:

- at VLF, when the hourly count is less than 30, the measured noise is higher than would be calculated from the counts. The difference is presumably due to the reception of noise from an area larger than that for which the counter records can be regarded as representative;
- at MF and the lower parts of the HF band, when the hourly count is less than 500 per hour, the measured noise is lower, sometimes by up to 30 dB, than the value expected from the counts. This is believed to occur because the dynamic range of the noise measuring equipment, though large, is still insufficient for the recording of the mean power of the most impulsive type of noise.

The errors in the measurements of noise at MF and HF occur only during local storms and when the hourly count is less than 500. They therefore affect only a small proportion of the data in Report 322. However, in tropical regions the measured monthly median and the upper and lower decile values of noise can all be affected, depending on the intensity of storm activity during the month. The data in Report 322 need to be used with caution in any application in which noise from local storms may be important. Counter data, if available, probably provide a better guide in such circumstances than do measurements of noise intensity.

The work has shown that counters are at least a valuable supplement to noise measurements and help to distinguish genuine high levels of noise from those caused by interference.

Although a large volume of data from atmospherics direction-finding networks exists, no reports are at hand which show how these data could be used in noise studies. The problems involved are considerable, but, since these networks are potentially capable of providing information leading to knowledge of the noise generated in oceanic areas, where adequate networks of lightning-flash counters cannot be established, early attention should be given to a study of whether the potentialities are likely to be realized in practice.

Some work bearing on results obtained by direction-finding on atmospherics is contained in CCIR [1963-66d] and Horner [1971].

5. Intensity and nature of noise from individual lightning discharges

Atmospherics from near storms have been recorded, in such a way that the effects of propagation can be allowed for, and an energy spectrum derived, which is effectively a characteristic of the source alone [Watt and Maxwell, 1957; Taylor and Jean, 1959; Horner, 1964; Horner and Bradley, 1964; Pierce, 1967]. The spectrum has been used in conjunction with lightning-flash counters and propagation data, to give estimates of integrated noise at certain locations [Horner, 1967]. These have been compared with measured noise intensities and the agreement is sufficiently close to justify further investigation of this method of approach.

6. World distribution of thunderstorms

Estimates of the probability of a thunderstorm occurring at any location for each hour of the day for each of the four seasons have been prepared [Crichlow *et al.*, 1971] based on the WMO thunderstorm day reports.

Using four satellite-borne receivers operating in the HF band, the global distribution of lightning rate per 10° of latitude and longitude has been mapped every six hours in local time, 0000-0600, 0600-1200, 1200-1800 and 1800-2400 for the four seasons [Kotaki *et al.*, 1981]. The results for 1200-1800 for the northern summer June-August are illustrated in Fig. 1. The global distribution of lightning rate per 10° of latitude and longitude has also been mapped every four hours (UTC) for the four seasons [Kotaki *et al.*, 1981; RRL, 1981]. One of these maps is shown in Fig. 2.

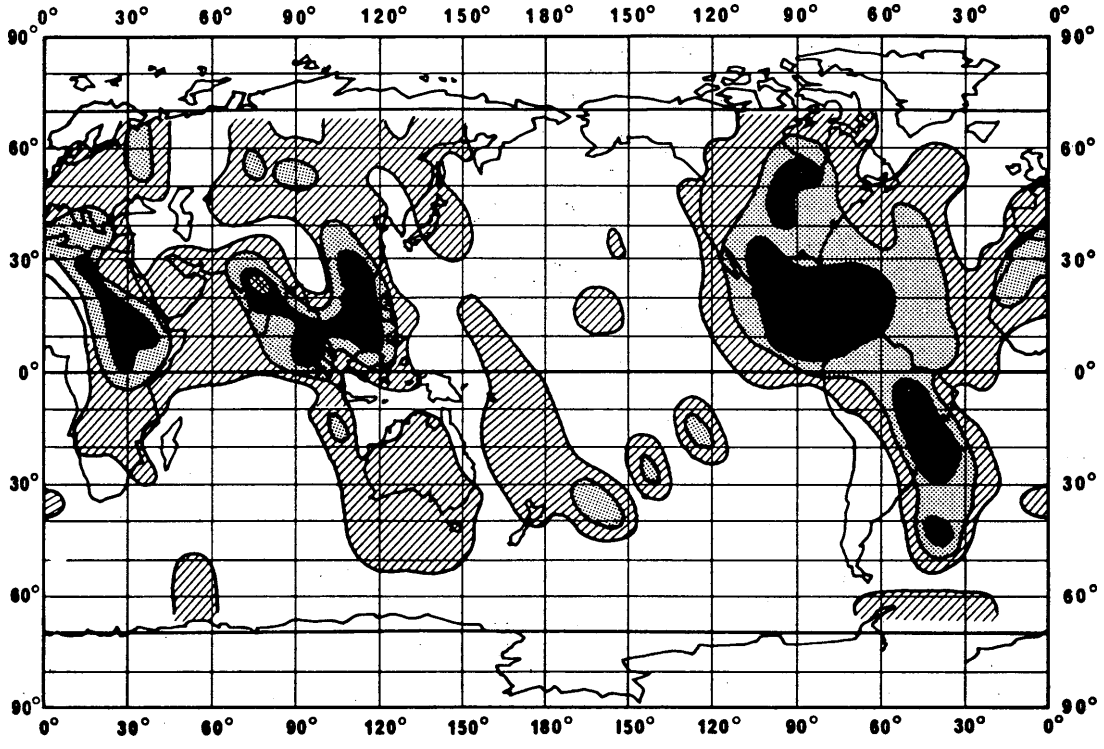


FIGURE 1 – *Lightning occurrence rate in northern summer June-August, 1978, 1200-1800 (local time)*

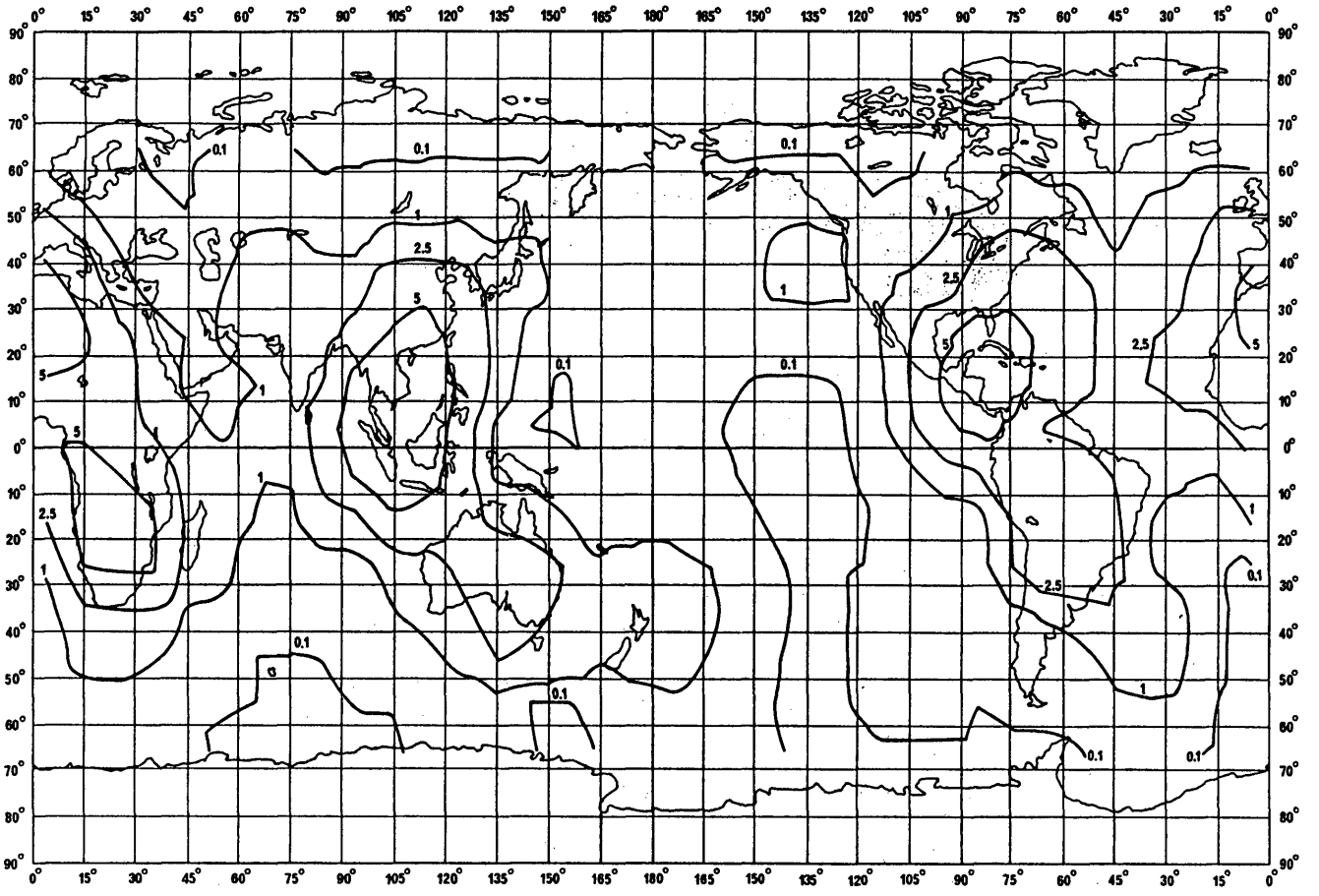


FIGURE 2a – *Global distribution of the occurrence rate of lightning discharges.*
September, October, November: 2200-0200 h UTC

(Frequency of lightning discharges occurring within 100 km^2 per second is obtained by multiplying the contour value by 10^{-5})

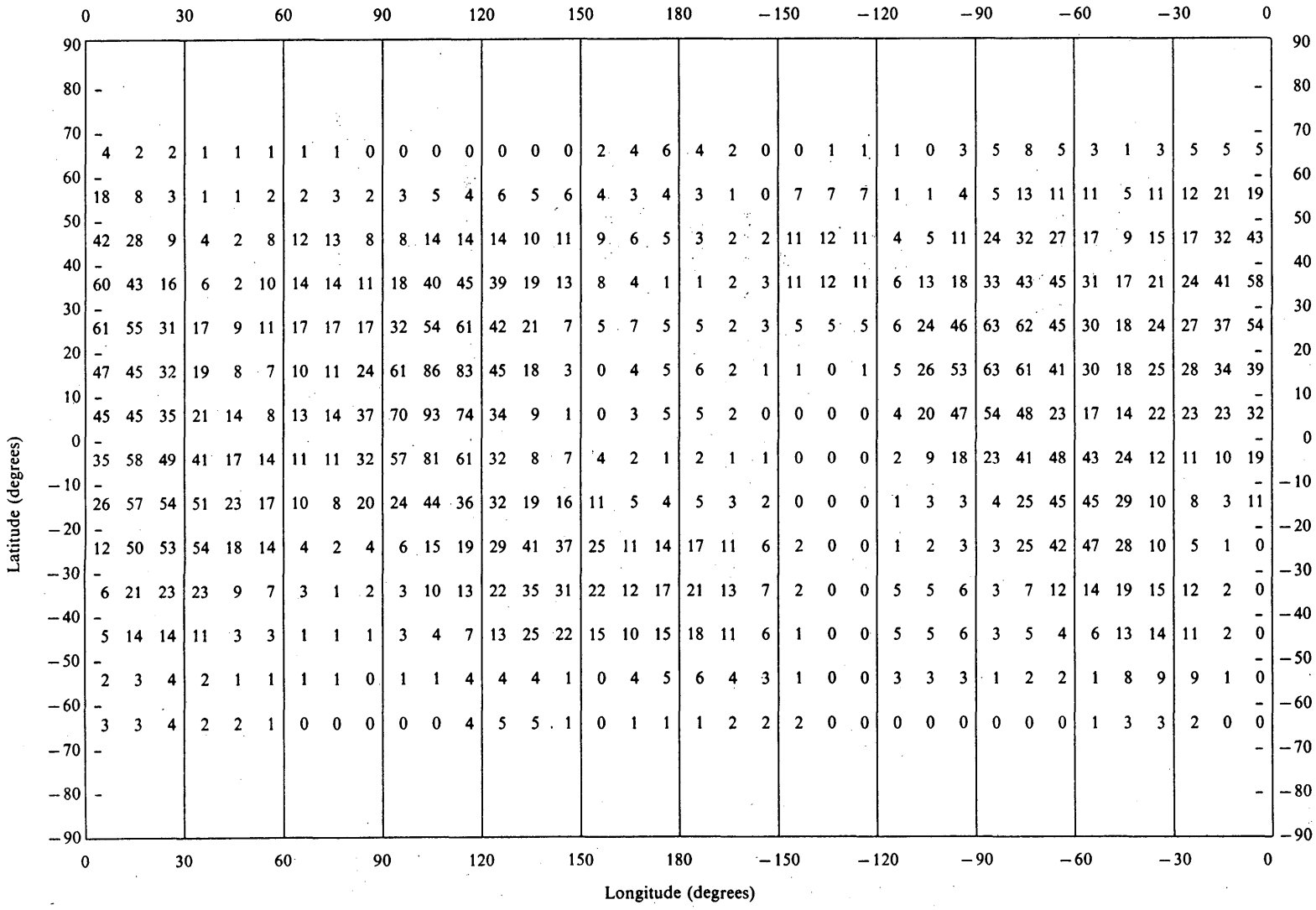


FIGURE 2b – *Numerical map of the occurrence rate of lightning discharges*
September, October, November: 2200-0200 h UTC

(Frequency of lightning discharges occurring within 100 km^2 per second
is obtained by multiplying the numerical value by 10^{-6})

REFERENCES

AIYA, S. V. C. [1979] Atmospheric noise data for tropical regions. *Radio Sci.*, Vol. 14, 1001-1010.

AIYA, S. V. C. and HARI SHANKAR, M. [1969] A lightning flash density gauge. *ITE J.*, XV, **10**.

BOLTON, E. [1971] Simulating atmospheric radio noise from low frequency through high frequency. *Rev. Sci. Instr.*, Vol. 42, **5**, 574-577.

BRADLEY, P. A. and CLARKE, C. [1964] Atmospheric radio noise and signals received on directional aerials at high frequencies. *Proc. IEE*, Vol. 111, 1534-1540.

CRICHLOW, W. Q., DAVIS, R. C., DISNEY, R. T. and CLARK, M. W. [1971] Hourly probability of world-wide thunderstorm occurrences. Telecommunications Research Report OT/ITS RR 12, US Dept. of Commerce, Washington, DC 20402.

CRICHLOW, W. Q., DISNEY, R. T. and JENKINS, M. A. [1959-67] Quarterly radio noise data. NBS Tech. Notes Nos. 18 and 18-2 to 18-26, and ESSA Tech. Reps. IER 18-27 to 18-32, Institute for Environmental Research, Boulder, Colo., USA.

CRICHLOW, W. Q., SPAULDING, A. D., ROUBIQUE, C. J. and DISNEY, R. T. [1960] Amplitude probability distributions for atmospheric radio noise. NBS Monograph 23, US Govt. Printing Office, Washington, DC 20402.

DISNEY, R. T. and SPAULDING, A. D. [1970] Amplitude and time statistics of atmospheric and man-made radio noise. ESSA Tech. Rep. ERL 150-ITS-98, US Dept. of Commerce, Washington, DC 20402.

FRASER-SMITH, A. C. and R. A. HELLIWELL [1985] The Stanford University ELF/VLF radiometer project: Measurement of the global distribution of ELF/VLF electromagnetic noise. Proc. 1985 IEEE Internat. Symp. on Electromagn. Compatibility, IEEE Cat. No. 85CH2116-2, 305-311.

FRASER-SMITH, A. C., R. A. Helliwell, B. R. FORTNAM, P. R. McGILL, and C. C. TEAGUE [1987] A new global survey of ELF/VLF radio noise, AGARD Conference Proceedings No. 470, Effect of Electromagnetic Noise and Interference on Performance of Military Radio Communication Systems, Lisbon, Portugal, [illegible] (NTIS, 5285 Port Royal Road, Springfield, VA 22161, USA or ESA/Information Retrieval Service, 10, rue Mario Nikis, 75015 Paris, France).

FRÜHAUF, G., AMBERG, H. and WÜRSTER, W. [1966] Wirkungsweise und Reichweite von Blitzzählern (Functioning and range of lightning flash counters). Beihefte (Supplement) der *ETZ*, **6**.

GIBSON, A.J. [1989] - NRPP Research Note No. 113, Measurements of noise at HF in Southern England.

HERMAN, J. R. [1961] Reliability of atmospheric radio noise predictions. *NBS J. Res.*, Vol. 65D, **6**, 565-574.

HORNER, F. [1960] The design and use of instruments for counting local lightning flashes. *Proc. IEE*, Vol.107B, 321-330.

HORNER, F. [1964] Radio noise from thunderstorms. *Advances in Radio Research.*, **2**, 121. Ed. J. A. Saxton, Academic Press. London, UK.

HORNER, F. [1967] Analysis of data from lightning flash counters. *Proc. IEE*, Vol. 114, 916-924.

HORNER, F. [1971] Scientific activities of (URSI) Commission VIII. *Progress in Radio Science*, 1966-69, Part I, 253-257, Gen. Ed. C. M. Minnis, URSI, Brussels, Belgium.

HORNER, F. and BRADLEY, P. A. [1964] The spectra of atmospherics from near lightning discharges. *J. Atmos. Terr. Phys.*, Vol. 26, 1155-1166.

IBUKUN, O. [1964] Measurements of atmospheric noise levels. *Radio and Electron. Engr.*, Vol. 28, 405.

KOTAKI, M., KURIKI, I., KATOH, C. and SUGIUCHI, H. [1981] Global distribution of thunderstorm activity observed with ISS-b. *J. Radio Res. Labs.* (Japan), Vol. 28, **125/126**, 49-71.

KRONJÄGER, W. and VOGT, K. [1959] Über das Aussengeräusch kommerzieller Antennenanlagen (On the external noise of commercial antenna installations). *NTZ*, Vol. 12, 7, 371-373.

LIKHTER, YA. I. and G. I. TERINA [1960] Some results of an investigation of the intensity of atmospheric radio noise in Moscow. Byulleten Mezhdunarodnogo Geofizich eskogo Goda, Vol. V, No. 3, pp. 91-97.

MAXWELL, E. L. [1967] Atmospheric noise from 20 Hz to 30 kHz. *Radio Sci.*, **2**, 637-644.

MIDDLETON, D. [1979] Canonical non-Gaussian noise models: their implications for measurements and prediction of receiver performance. *IEEE Trans. Electromag. Compt.*, Vol. EMC-21, **3**, 209-220.

PIERCE, E. T. [1967] Atmospherics – their characteristics at the source, and propagation. *Progress in Radio Science*, 1963-66, Part 1, Proc. XV, General Assembly of URSI.

REMIZOV, L. T. [1977] Relationship between the characteristics of the random natural field strength in the VLF band recorded with the narrowband and wideband methods (in Russian). Doklady Akademii Nauk SSSR, Vol. 235, **2**, 306.

REMIZOV, L. T., OLEINIKOVA, I. V., KOROLIEV, A. N., VISKREVTSOV, I. G. and TCHERNIAVSKY, A. F. [1971] Statistical characteristics of atmospheric noise at VLF (in Russian). *Radiotekhnika i Elektronika*, **16**, 1191-1199.

REMIZOV, L. T. PASKUAL, A. G. and APRAKSIN, L. B. [1979] The interrelationship of statistical models of atmospheric radio noise using narrowband and wideband reception in the VLF band. *Radiotekhnika i Elektronika*, Vol. XXIV, **3**, 498-510.

REMIZOV, L. T., POTAPOV, A. V. and VIKHROV, B. R. [1967] Probability distribution of time intervals between atmospherics (in Russian). *Radiotekhnika i Elektronika*, **12**, 706-708.

RRL [1981] World Distribution of Thunderstorm Activity Obtained from Ionosphere Sounding Satellite-b Observations, June 1978 to May 1980. *Radio Res. Labs.*, Japan.

SPAULDING, A. D. [1977] Stochastic modelling of the electromagnetic interference environment. IEEE International Conference on Communications (ICC '77), 12-15 June, Chicago, Ill., USA, Conf. Record, 42.2-115 – 123 (IEEE Catalogue No. 77CH1209-6CSCB).

SPAULDING, A. D. [1981] Atmospheric Radio Noise and its Effects on Telecommunication Systems. *Handbook of Atmospherics*, Ch. 6. Ed. H. Volland, CRC Press, Boca Raton, Fla., USA.

SPAULDING, A. D. and MIDDLETON, D. [1975] Optimum reception in an impulsive interference environment. OT Report 75-67, US Govt. Printing Office, Washington, DC 20402.

SPAULDING, A. D., ROUBIQUE, C. J. and CRICHLOW, W. Q. [1962] Conversion of the amplitude-probability distribution function for atmospheric radio noise from one bandwidth to another. *NBS J. Res.*, Vol. 66D, **6**, 713-720.

SPAULDING, A. D. and J. S. WASHBURN [1985] Atmospheric radio noise: Worldwide levels and other characteristics. National Telecommunications and Information Administration (NTIA) Report 85-173 (NTIS Order No. PB 85-212942).

TAYLOR, W. L. and JEAN, A. G. [1959] Very low frequency radiation spectra of lightning discharges. *NBS J. Res.*, Vol. 63D, **2**, 119-204.

TURTLE, J. P., E. C. FIELD, C. R. WARBER, and P. R. McGILL [1989] Low frequency TE atmospheric noise: Measurement and Theory. Radio Science, 24, No. 3, pp 325-329.

URSI [1962] The measurement of characteristics of terrestrial radio noise. Special Report No. 7. Elsevier, London, UK.

URSI [1981] *Review of Radio Science* 1978-1981, E1-E13, International Union of Radio Science, Brussels, Belgium.

WARD, B.D. [1989] - Atmospheric noise measurements in Central Australia - Comparison with CCIR noise models, SRL Technical Report, SRL-0037-TR.

WATT, A. D. [1967] *VLF Radio Engineering*. Pergamon Press, New York, NY, USA.

WATT, A. D. and MAXWELL, E. L. [1957] Characteristics of atmospheric noise from 1 to 100 kcs. *Proc. IRE*, Vol. 45, **6**, 787-794.

CCIR Documents

[1963]: 183 (Sweden).

[1963-66]: **a.** VI/79 (India); **b.** VI/201 (India); **c.** VI/202 (India); **d.** VI/67 (Rev.1) (Germany (Federal Republic of)).

[1966-69]: **a.** VI/86 (India); **b.** VI/173 (India).

[1970-74]: **a.** 6/184 (URSI); **b.** 6/270 (Canada).

ARCHIVES U.I.T. GENÈVE

PAGE INTENTIONALLY LEFT BLANK

PAGE LAISSEE EN BLANC INTENTIONNELLEMENT

SECTION 6C: IONOSPHERIC PROPAGATION AND OPERATIONAL FORECASTING

REPORT 726-2

GROUND AND IONOSPHERIC SIDE- AND BACK-SCATTER

(Question 32/6)

(1978-1986-1990)

1. Introduction

Radio waves propagated via the ionosphere have been observed to arrive from azimuths which differ considerably from the great circle direction. Many of the off-path signals exhibit the characteristics of a scatter signal with a typical fading period less than one second. The angle of arrival of these scatter signals is quite variable and the signal strength gradually decreases to a level 25 to 40 dB less than the great circle mode of propagation as the propagation path deviates from the great circle path [Goddard, 1939; Feldman, 1939; Dieminger, 1951; Hagg and Rolfe, 1963; Edward and Jansky, 1941; Silberstein and Dickson, 1965].

A radio wave propagated via the ionosphere is partially scattered by the irregularities of the ground or sea, and even to some extent by those of the ionosphere itself. Scattering coefficients of the Earth's surface may be quite variable depending upon the nature of the surface and the elevation angle [Steel, 1964]. Some of the scattered energy is returned over the same propagation path to the vicinity of the transmitter [Villard and Peterson, 1952a; Shearman, 1956; Silberstein, 1954; Peterson, 1957; Kono, 1950; Dieminger, 1951] and, by measuring the time delay of the echo, the slant range to the scattering source may be inferred. By employing a directional antenna rotating slowly around the vertical, the azimuth of the echoing region can be estimated. A comprehensive review has been published by Croft [1972].

2. Ground and ionospheric side-scatter

The side-scatter mode of propagation has also been studied using CW field strength data together with bearing and oblique incidence sounding data. The side-scatter mode of propagation is evident on the oblique ionograms but exact identification is only possible if the ionogram data are used in conjunction with CW field strength data.

2.1 *Ground side scatter*

Non great-circle signals are predominantly the result of multi-hop modes of propagation in which side-scatter occurs from irregularities at the surface of the Earth. The lowest path loss occurs for the bearing of an intersection of the skip distances around the transmitter and receiver because of skip distance focusing. The directivity of the transmitting antenna influences the bearing of the maximum received signal strength [Miya and Ueno, 1960]. The ground side-scatter mode of propagation accounts for the southerly deviation of BBC television signals received in North America [Hagg and Rolfe, 1963], the southerly deviation of HF signals received in both directions between England and Japan [Wilkins, 1960; Kanaya and Yokoi, 1960a], the large deviations of radio signals from European and American stations observed in Japan [Miya and Kanaya, 1956; Miya *et al.*, 1957; Kanaya and Yokoi, 1960b and 1960c] and the wide range of azimuths over which the signals are received on short paths [Dieminger, 1951]. Several workers have suggested that non great-circle signals are produced by scatter from land areas; the signal strength of sea scatter is believed to be negligible in comparison with the signal strength of land scatter [Miya and Kanaya, 1955; Miya *et al.*, 1951]. However, observations in North America at 41 MHz and 20 MHz indicate little difference in signal strength between scatter signals arriving from the land and from the sea [Hagg and Rolfe, 1963].

2.2 *Ionospheric side-scatter*

Ionospheric side-scatter from irregularities located in the auroral region have been reported by several workers. In some cases the non great-circle signals were attributed to direct scatter from ionospheric irregularities without an ordinary type of ionospheric reflection [Bates *et al.*, 1966a]. In other cases, they were attributed to multi-hop modes of propagation in which the strongest scatter signals were produced by irregularities in the ionospheric region where the radio waves are focused [Hagg and Rolfe, 1963]. On transmissions between Europe and southern Africa, azimuthal deviations of up to ± 50° were observed. By additional time delay measurements it was shown that these great-circle deviations are caused by F-layer inhomogeneities near the Earth's magnetic equator [Röttger, 1973a; Crochet, 1972; Nielson and Crochet, 1974] and in the auroral region [Röttger, 1973b]. Crochet assumes scatter from weak field aligned irregularities while Röttger assumes that the strongest non great-circle signals result from specular reflections at horizontal gradients of electron density.

Rice [1973] has shown that at a given time the signal for a particular mode arrived from several directions and that each mode was composed of components where the ray paths deviated from the great circle path by as much as 9° (indicating that the ray paths had different effective reflection points).

2.3 *Practical applications*

The ground and ionospheric side-scatter modes of propagation can lead to an extension of time beyond that which a given frequency can be used on the great-circle path and also leads to the use of frequencies higher than the basic MUF. Communication circuits may, however, be degraded by the interference caused by strong side-scatter signals. The ground scatter mode could maintain communication during disturbances; this mode often avoids propagating through regions of abnormally high absorption. Transmission experiments in the United States of America show that in the case of side-scatter both the average azimuth spread of direction of arrival and the fading spectrum width are greatly enhanced compared to great-circle propagation [Blair, 1971].

The direction from which the ground side-scatter signals are received can be predicted from skip distance data deduced from monthly predictions of basic MUF [Hagg and Rolfe, 1963]. The non great-circle path MUF and also the direction from which ground side-scatter signals are received can be predicted by the two control-circles method using ionospheric prediction maps [Miya and Kanaya, 1955].

The seasonal variations of large scale great circle path deviations on a North Atlantic path have been investigated using the HF broadcast transmissions of Deutsche Welle. The signal on the great circle path is attenuated by ionospheric absorption during the summer and by a decrease of the MUF during the winter. During these periods the ray paths are regularly deviated toward the equator. Deviations of the order of 50 degrees from true azimuth have been observed with signal intensities up to 15 dB above those on the great circle path. Around the equinoxes, however, the signal on the great circle path dominates [Hortenbach, 1979].

In 1961 and 1962, measurements of azimuthal angles of arrival of transmissions from WWV, WSL, MSF and JJY were made at Moscow by means of a direction finder. As a result of measurements of WWV and WSL transmissions in autumn and winter from 1800 to 0500 UT, it has been established that the deviations from the great circle:

- in 14% of the cases vary between ± 5°;
- in 33% of the cases vary between +6° and +25°;
- in 53% of the cases vary between −6° and −100°.

3. Ground back-scatter

To establish the bearing of a back-scatter echo, the combined azimuthal directivity of the transmitting and receiving antennas must be sufficient to discriminate against off-bearing echoes. However, because of ionospheric tilts, the possible errors in azimuthal information become progressively greater with the number of hops involved.

To estimate the range of back-scatter sources from oscilloscope records it is necessary to postulate the active modes. Their identification is assisted by a knowledge of the combined vertical directivity of the antennas, but unless vertical-incidence data are available, caution is needed in drawing conclusions. In one experiment, however, when the ionospheric height data were not available, the ground range was inferred using an antenna with a vertical pattern split into two distinct lobes: by showing an overlapping of the echoes from these two lobes the phenomenon of focusing has been demonstrated [Ranzi, 1961].

Information concerning elevation angle versus back-scatter delay, such as can be obtained with a vertical angle scanning antenna, can be processed to provide ionospheric model parameters, including the longitudinal component of tilt in the direction of interest. Such information and measurement of the elevation angle of arrival of a specific back-scatter source allow a quite accurate determination of the range to the source [Tveten, 1971].

The focusing effect is characteristic of F-layer echoes near the skip distance, and the probability of occurrence of this effect appears to be greatest in the evening in winter and at night in summer. The absence of focusing can be used to identify Es modes [Bibl, 1960]. Elevation angle measurements of back-scatter by Es modes also identify them clearly and unambiguously [Tveten and Hunsucker, 1969]. Another method of identifying Es modes is the use of the azimuth-sweeping back-scatter sounder; motion of isolated Es patches can be easily traced and a general westward drift has been noted around 40° North latitude [Villard and Peterson, 1952b; Clark, 1956; Harwood, 1961; Egan and Peterson, 1962; Bibl, 1961; Shearman and Harwood, 1960].

This type of sounder occasionally observes slight changes in range of the skip-zone echo, these changes in range being a function of the azimuth. These are consistent with a large-scale single wave of altered F-region ionization, the wave sweeping over the observing station at speeds of the order of 1000 km/h [Tveten, 1961]. In addition, when sufficiently short pulses are used for back-scatter sounding, irregularities in signal amplitude which may change range with time are seen. These signal enhancements appear to be caused by moving irregularities in the ionosphere which cause signal focusing [Tveten, 1961; Shearman, 1963] or by certain special conditions [Dueno, 1963]. Georges and Stephenson [1969] have studied the effects of F-region travelling disturbances on back-scatter sounding records by numerical simulation, and have shown that in some instances, conventional methods of estimating speeds and direction from actual records may be erroneous.

A lack of correlation was often observed between the transmission loss in a given radiocommunication link and the total loss in the back-scatter soundings performed along the same path as the radio link. This is due to the fact that the intensity of the back-scatter echoes strongly depends upon the presence of focusing F2-region irregularities, which have no detectable influence on the transmission loss in a radiocommunication link. It is also observed that this focusing effect is stronger when the back-scatter sounding in temperate latitudes is performed in the direction of the Earth's magnetic field. The amplitude of the back-scatter signals shows a negative correlation with the occurrence of spread-F.

Other work at 40.3 MHz has shown echoes with delay up to 50 times greater than those for E reflections [Maynard, 1961]; they involve off-path auroral echoes as well as one- and two-hop F2 ground-scatter reflections from as far as 6000 km. During winter daytime, F2 reflections were nearly always involved.

In China, the propagation delays of the first signals to arrive by sky-wave have been measured at several locations at distances less than 1,000 km from the BPM transmitting station (35°,00'N, 109°,31'E). When the receiving carrier frequency is higher than the basic MUF of the transmitter-receiver circuit, the first signal propagated via the non great-circle path is usually received with a propagation delay about 5 ms greater than when the carrier frequency is lower than the basic MUF. Comparison and analysis of the measured results with ionospheric data show that these large delay-time signals are probably caused by the ground back- and side-scatter echo due to skip distance focusing [Chen 1983; Ning and Li 1988].

The Doppler spectrum for back-scatter from the ocean surface is characterized by two dominant first-order echoes surrounded by a second-order continuum. The dominant wave direction and hence surface wind direction, can be estimated from the first-order echoes. Estimation of other sea-state parameters such as wind speed and wave height requires that the second-order back-scatter spectrum is free from ionospheric contamination. The degree of Doppler broadening and multi-mode can be ascertained [Ward, 1985] in areas where there are islands or coastline in the field of view. Jiao and Zhang (1985) have studied 3-dimensional (time delay-power-Doppler frequency) spectrograms of HF sky-wave back-scatter echoes and have derived the rate of change of the equivalent reflection height of the ionosphere from Doppler spectrograms. The values of the rate of change are in conformity with the results derived from vertical soundings. The speed, the vertical amplitude and the wavelength of the travelling ionospheric disturbance (TID) can be obtained from the Doppler spectra for two different bearings [Bradley et al., 1983].

As a result of investigations carried out in the USSR in 1987-1988 into the variation of back-scatter signals with azimuth, it was possible to determine the probability of signals being received from various directions as a function of the time of day and the season, and also to determine the effects of ionospheric disturbances and the terminator [Lobachevsky et al., 1988, CCIR, 1986-90].

4. Ionospheric back-scatter

Irregularities and gradients have been observed experimentally in the ionosphere, which are capable of giving direct back-scatter echoes at frequencies well above the frequencies normally reflected from an overdense ionosphere.

Near the auroral zone the irregularities in ionization density in the E region associated with auroral disturbance are capable of scattering HF, VHF and even UHF waves. Comprehensive reviews have been given [Little *et al.*, 1956; Presnell *et al.*, 1959; Fricker *et al.*, 1957; Bagaryatskii, 1961; Unwin and Baggaley, 1972].

The intensity and probability of occurrence of auroral back-scatter has a pronounced diurnal variation, with peaks in the evening and early morning; however, their occurrence in local time is dependent both on magnetic latitude and the level of magnetic disturbance [Unwin, 1967; Greenwald *et al.*, 1973]. There is a seasonal variation which maximizes at the equinoxes. Studies indicate that critical reflection may occur at frequencies as high as 100 MHz during auroral disturbances, supporting the use of a theoretical model which includes both weak scattering and critical reflection [Moorcroft, 1961] to explain echoes at these frequencies. From a six-frequency experiment (50 MHz-3000 MHz) Chesnut [1969] deduced that the volume scattering coefficient could be approximated by an exponential frequency function. The Doppler effects observed on auroral scatter signals present complications for communication [Czechowsky, 1974; Tsunoda, 1976].

The auroral ionospheric irregularities which are responsible for radar back-scatter, over a very wide range of frequencies, are related to the visible aurora and to the electric fields and energetic particle precipitation associated with the aurora [Bates *et al.*, 1966b; Bates, *et al.*, 1969]. The high degree of aspect sensitivity exhibited by the magnetic field-aligned irregularities results in an apparent concentration of echoes in the E region at VHF and UHF [Unwin, 1958]. Auroral echoes from the night-time ionosphere are spatially discrete in nature, while those from the sunlit ionosphere are spatially diffuse [Presnell *et al.*, 1959].

Direct back-scatter from irregularities in the F region at heights of 250 to 400 km apparently unrelated to visual aurora have been obtained [Bates, 1959], with winter daytime echoes appearing more "patchy" than those seen at night [Bates, 1960]. At HF there is sufficient ionospheric refraction to permit strong echoes from the F region; Bates [1966], on the basis of HF back-scatter data obtained near the geomagnetic pole, proposed a back-scatter auroral monitoring system.

REFERENCES

BAGARYATSKII, B. A. [1961] Radar reflections from aurorae. *Usp. Soviet. Fiz. Nauk*, **73**, 197-241.

BATES, H. F. [1959] The height of irregularities in the arctic atmosphere. *J. Geophys. Res.*, **64**, 1257-1265.

BATES, H. F. [1960] Direct HF back-scatter from the F-region *J. Geophys. Res.*, **65**, 1993-2002.

BATES, H. F. [1966] A proposed polar auroral radar system. *J. Atmos. Terr. Phys.*, **28**, 903-907.

BATES, H. F., ALBEE, P. R. and HUNSUCKER, R. D. [1966a] On the relationship of the aurora to non great-circle high frequency propagation. *J. Geophys. Res.*, **71**, 1413-1420.

BATES, H. F., BELON, A. E., ROMICK, G. J. and STRINGER, W. J. [1966b] On the correlation of optical and radio auroras. *J. Atmos. Terr. Phys.*, **28**, 439-446.

BATES, H. F., SHARP, R. D., BELON, A. E. and BOYD, J. S. [1969] Spatial relationships between HF radar aurora, optical aurora and electron precipitation, *Planet. Space Sci.*, **17**, 83-95.

BIBL, K. [1960] Experimental proof of focusing at the skip distance by back-scatter records. *Proc. IRE*, **48**, 956-957.

BIBL, K. [1961] Neuartige Back-scatter-Registrierungen und Ergebnisse (A new method of recording back-scatter and presenting the results). From the reports of the meeting on ionospheric physics and wave propagation. *FTZ*, Darmstadt, Kleinheubacher Berichte, **8**, 111-114.

BLAIR, J. C. [1971] The effectiveness of spectrum and azimuth spread measurements in detecting side scatter. Proc. 4th Allerton Conference on DF, University of Illinois, Urbana, IL., USA.

BRADLEY, P.A., GIBSON, A.J. and KING, J.W. [1983] - HF Radar Doppler Studies of the Effects of Ionospheric Motions on Radio Wave Propagation in Different Modes, IEE Conference Publ. No. 219, 191-195.

CHEN, H.Q. [1983] - A preliminary study of the abnormal phenomenon in shortwave time-signals, Kexue Tongbao Vol. 28 No. 4 pp. 497-501.

CHESNUT, W. G. [1969] Low-frequency waves and irregularities in the auroral ionosphere as determined by radar measurements, in *Low Frequency Waves and Irregularities in the Ionosphere*, edited by N. d'Angelo, D. Riedel Pub. Co., Dordrecht, Holland, 173-191.

CLARK, C. [1956] Motion of sporadic-E patches determined from high-frequency back-scatter records. *Nature*, **178**, 486-487.

CROCHET, M. [1972] Propagation transéquatoriale en dehors du grand cercle en ondes décamétriques. Part I: Mise en évidence et morphologie, *Ann. de Géophys.* **28**, 27-35. Part II: Application à l'étude par diffusion des irrégularités. *Ann. de Géophys.* **28**, 381.

CROFT, T. A. [1972] Sky-wave back-scatter: A means for observing our environment at great distances. *Rev. Geophys. Space Phys.*, **10**, 73-155.

CZECHOWSKY, P. [1974] Doppler shift of auroral back-scatter signals. *J. Geophys. Res.*, **40**, 229-237.

DIEMINGER, W. [1951] The scattering of radio waves. *Proc. Phys. Soc.*, **64-B**, 142-158.

DUENO, B. [1963] Interpretation of some sweep-frequency back-scatter echoes. *J. Geophys. Res.*, **68**, 3603-3610.

EDWARD, C. F. and JANSKY, K. G. [1941] Measurement of the delay and direction of arrival of echoes from nearby short wave transmitters. *Proc. IRE*, **29**, 322.

EGAN, R. D. and PETERSON, A. M. [1962] Back-scatter observations of sporadic-E. *Ionospheric Sporadic E*, 89-109. Ed. Smith, E. K. and Matsushita, S., Pergamon Press.

FELDMAN, C. B. [1939] Deviations of short radio waves from the London-New York great circle path. *Proc. IRE*, **27**, 625.

FRICKER, S. J., INGALLS, R. P., STONE, M. L. and WANG, S. C. [1957] UHF auroral observations. *J. Geophys. Res.*, **62**, 527-546.

GEORGES, T. M. and STEPHENSON, J. J. [1969] HF radar signatures of travelling ionospheric irregularities, 3D ray-tracing simulation. *Radio Sci.*, **4**, 679-699.

GODDARD, D. R. [1939] Transatlantic reception of London television signals. *Proc. IRE*, **27**, 692.

GREENWALD, R. A., ECKLUND, W. L. and BALSLEY, B. B. [1973] Auroral currents, irregularities and luminosity. *J. Geophys. Res.*, **78**, 8193-8204.

HAGG, E. L. and ROLFE, W. [1963] A study of transatlantic radio propagation modes at 41.5 Mc/s. *Can. J. Phys.*, **41**, 220.

HARWOOD, J. [1961] Some observations of the occurrence and movement of sporadic-E ionization. *J. Atmos. Terr. Phys.*, **20**, 243-262.

HORTENBACH, K. J. [1979] Über das jahreszeitliche Verhalten beträchtlicher Grosskreisabweichungen auf Nordatlantikstrecken (On the seasonal variations of large-scale great circle deviations on North-Atlantic paths). *Kleinheubacher Berichte*, Vol. 22, 327-334.

JIAO, P.N. and ZHANG, X.J. [1985] - Measurement of the HF Backscatter Echo Spectra, (in Chinese, abstract in English), Chinese J. Space Science, 5, 191-198.

KANAYA, S. and YOKOI, H. [1960a] Simultaneous measurements of azimuthal arrival angles of signals in cooperation with United Kingdom – Determination of scattering area. *KDD Tech. J.*, **25**, 38-43.

KANAYA, S. and YOKOI, H. [1960b] The lateral deviation of radio waves propagated along the longer great circle path from Europe. *Rep. Ion. and Space Res. Japan*, **14**, 192-195.

KANAYA, S. and YOKOI, H. [1960c] The bearings of WWV signals, Washington, DC, observed at Tokyo. *Rep. Ion. and Space Res. Japan*, **14**, 435-440.

KONO, T. [1950] Experimental study on scattered echoes (II). *Rep. Ion. Res. Japan*, **4**, 189-199.

LITTLE, C. G., RAYTON, W. M. and ROOF, H. B. [1956] Review of ionospheric effects at VHF and UHF. *Proc. IRE*, **44**, 992-1018.

LOBACHEVSKY, L.A., MARCHENKO, N.P., RUBTSOV, L.N., TUSHENTSOVA, I.A. and TSEDILINA, E.E. [1988] - Issledoyanie azimutalnykh zavisimostei vysokochastotnykh radiovoln metodom VNZ (Investigations of the variation of high frequency radio waves as a function of azimuth by means of the backscatter sounding method), Vzaimodeistvie radiovoln s ionosferoi, (Interaction between radio waves and the ionosphere), Institut zemnogo magnetizma, ionosfery i rasprostranemniya radiovoln Akademii nauk SSSR, (IZMIRAN) Moscow, 121.

MAYNARD, L. A. [1961] Propagation of meteor-burst signals during the polar disturbance of November 12-16, 1960. *Can. J. Phys.*, **39**, 628.

MIYA, K., ISHIKAWA, M. and KANAYA, S. [1957] On the bearing of ionospheric radio waves. *Rep. Ion. Res. Japan*, **11**, 130-144.

MIYA, K. and KANAYA, S. [1955] Radio propagation prediction considering scattering wave on the Earth's surface. *Rep. Ion. Res. Japan*, **9**, 1.

MIYA, K., and KANAYA, S. [1956] On the lateral deviation of radio waves coming from Europe. *Rep. Ion. Res. Japan*, **10**, 1-8.

MIYA, K., KOBAYASHI, T. and WAKAI, N. [1951] Field intensity of scattered wave in radio wave propagation. *Rep. Ion. Res. Japan*, **5**, 55.

MIYA, K. and UENO, K. [1960] Influence of directivity of the transmitting antenna on the bearing of HF signals. *Rep. Ion. and Space Res. Japan*, **14**, 187.

MOORCROFT, D. R. [1961] Models of auroral ionization. *Can. J. Phys.*, **39**, 677-715.

NIELSON, D. L. and CROCHET, M. [1974] Ionospheric propagation of HF and VHF radio waves across the geomagnetic equator. *Rev. Geophys. Space Phys.* **12**, 688-702.

NING, B.Q. and LI, J. [1988] - Propagation delay observations of BPM standard time-signal with a continuous display system (in Chinese). ACTA Geophysica Sinica, Vol. 31, 4, 300-308.

PETERSON, A. M. [1957] Ionospheric back-scatter. *Annals of the IGY III*, Part IV, 361-381, Pergamon Press.

PRESNELL, R. I., LEADABRAND, R. L., PETERSON, A. M., DYCE, R. B. SCHLOBOHM, J. C. and BERG, M. R. [1959] VHF and UHF radar observations of the aurora at College, Alaska, *J. Geophys. Res.*, **64**, 1179-1190.

RANZI, I. [1961] Back-scatter echo pattern and vertical radiation diagram. Centro radioelettrico sperimentale G. Marconi, Rome, Note 8.

RICE, D. W. [1973] Phase characteristics of ionospherically propagated radio waves. *Nature, Physical Science*, **244**, 86-88.

RÖTTGER, J. [1973a] Wave-like structures of large-scale equatorial spread-F irregularities. *J. Atmos. Terr. Phys.* **35**, 1195-1206.

RÖTTGER, J. [1973b] Seitenscatter durch polares spread-F beobachtet auf der Strecke Lindau-Tsumeb (Side-scatter due to polar spread-F observed on the path Lindau-Tsumeb). *Kleinheubacher Berichte*, **16**, 155-157.

SHEARMAN, E. D. R. [1956] A study of ionospheric propagation by means of ground back-scatter. *Proc. IEE*, **103**, 203-209.

SHEARMAN, E. D. R. [1963] The amplitude and spectrum of ground back-scatter echoes. *Proc. International Conference on the Ionosphere* 1962, 293-300. Ed. A. C. Stickland, Bartholomew Press.

SHEARMAN, E. D. R. and HARWOOD, J. [1960] Sporadic-E observed by back-scatter techniques in the United Kingdom. *J. Atmos. Terr. Phys.*, **18**, 29-42.

SILBERSTEIN, R. [1954] Sweep-frequency back-scatter – Some observations and deductions. *Trans. IRE*, AP-2, 56-63.

SILBERSTEIN, R. and DICKSON, F. H. [1965] Great circle and deviated path observations on CW signals using a simple technique. *IEEE Trans. Ant. Prop.*, AP-13, 52-63.

STEEL, J. G. [1964] The effect of the ground back-scatter coefficient on observations of sporadic-E over sea, land and mountains. *J. Atmos. Terr. Phys.*, **26**, 323-324.

TSUNODA, R. T. [1976] Doppler velocity maps of the diffuse radar aurora. *J. Geophys. Res.*, **81**, 425-435.

TVETEN, L. H. [1961] Ionospheric motions observed with high-frequency back-scatter sounders. *NBS J. Res.*, **65-D**, 115-127.

TVETEN, L. H. [1971] Range estimation based on back-scatter measurements. Proc. of 4th Allerton-House Conference on HF Radio Direction Finding and Radio Location Research, RRL Publication No. 389, University of Illinois, Urbana, IL, USA.

TVETEN, L. H. and HUNSUCKER, R. D. [1969] Remote sensing of the terrestrial environment with an HF radio high-resolution azimuth and elevation scan system, *Proc. IEEE*, **57**, 487-493.

UNWIN, R. S. [1958] The geometry of auroral ionization. *J. Geophys. Res.*, **63**, 501-506.

UNWIN, R S. [1967] The morphology of the radio aurora at sunspot maximum: I Diurnal and seasonal variations. *J. Atmos. Terr. Phys.*, **28**, 1167-1181.

UNWIN, R. S. and BAGGALEY, W. J. [1972] The radio aurora. *Ann. de Géophys.*, **28**, 111-127.

VILLARD, O. G. and PETERSON, A. M. [1952a] Scatter-sounding: a technique for study of the ionosphere at a distance. *Trans. IRE*, PGAP-3, 186-201.

VILLARD, O. G. and PETERSON, A. M. [1952b] A method for studying sporadic-E clouds at a distance. *Proc. IRE*, **40**, 992-994.

WARD, B. D. [1985] Doppler characteristics of HF back-scatter – the Jindalee mini-radar. Proc. URSI-IPS Conference on the Ionosphere and Radio-wave Propagation. Eds. D. G. Cole and L. F. McNamara. IPS Radio and Space Services Tech. Rep. TR-85-04, Ionospheric Prediction Service, Sydney, Australia.

WILKINS, A. F. [1960] HF propagation – its present and future use for communications purposes. *J. Brit. Inst. Radio Engrs.*, **20**, 939.

CCIR Documents

[1986-90] : 6/199 (USSR).

REPORT 890-2

THE OPERATIONAL USE OF SIDE-SCATTER AND BACK-SCATTER

(1982-1986-1990)

(Question 32/6)

1. Introduction

This Report is concerned with the operational use of side-scatter and back-scatter techniques to determine propagation conditions and unusual types of propagation. The physical bases of scatter techniques have been outlined in Report 726. The operational use of scatter techniques has in fact been severely limited to date because of high equipment costs and the difficulty in the interpretation and analysis of scattered echoes.

2. Side-scatter

Practical applications of side-scatter by the ground and the ionosphere have been reviewed in Report 726. Utilizing side-scatter, the following factors can be obtained:

- an extension of the time for which a given frequency can be used, beyond the time when the frequency fails on the great-circle path,
- the use of frequencies higher than the basic MUF, and
- the orientation of the antenna beam axis for maximum signal.

The ground side-scatter mode could also be used to maintain communications during disturbances since this mode often avoids propagating through regions of abnormally high absorption.

3. Back-scatter

Practical applications of ground back-scatter data for evaluating MUF, transmission loss and ground reflectivity have been reviewed by Croft [1972] and Chernov [1971]. There are three main fields in which back-scatter could play a role in predicting propagation conditions:

- skip distance mapping,
- monitoring of ionospheric structure, and
- monitoring of irregularities.

3.1 *Skip distance mapping*

The accuracy in determining skip distance by means of back-scatter techniques appears to be adequate for many applications [Blair *et. al.*, 1970]. High resolution back-scatter measurements have been found to be very useful in determining area ground coverage for HF broadcasts. This is accomplished by means of the addition of a virtually inaudible modulation to the broadcasts and the subsequent reception of the modulated energy via sky-wave back-scatter [Fenwick, 1962].

Croft [1972] describes a case in which the problem of poor reception in some parts of South America of broadcasts from the United States was solved using backscatter techniques. One of the main target areas was found to lie within the skip zone of the transmitter because of defocusing effects of the equatorial anomaly.

Back-scatter data may, therefore, be used to determine the optimum elevation angle for a specified HF broadcast service. With this information a suitable antenna array can be selected from those available, thus overcoming changes in the geometry of the ionospheric reflection caused by day-to-day variations of the ionosphere.

Jiao and Zhu [1985] have deduced a semi-empirical equation with which the skip distance corresponding to a minimum group path can be determined by using the backscatter ionogram from a single sounding station. With this method, the ground distance of discrete scattering sources or moving targets can also be determined in principle [Jiao and Du, 1987; Du and Jiao, 1987].

The strength of the back-scatter echo unfortunately is not a useful indicator of the transmission loss on a co-located communications circuit, even when antenna differences are taken into account. This is due to the fact that the intensity of the back-scatter echo depends strongly on the presence of focusing F2 irregularities, which have no detectable influence on the transmission loss on the communications link, and on the scattering coefficient of the surface being illuminated.

3.2 *Monitoring of ionospheric structure*

Numerous attempts have been made to infer remote ionospheric structure directly from the observed back-scatter, since knowledge of this structure would allow more accurate communications predictions to be made. The most common method of approach has been the measurement of the frequency-time locus of the leading edge of a swept frequency back-scatter echo and the subsequent deduction of ionospheric structure from this leading edge by means of simplifying approximations. Usually, these approximations involve the assumption that the ionosphere consists of only a single F layer, and, furthermore, that the layer has some particular shape. Du Broff *et al.* [1979] describe one method of backscatter inversion and give references to earlier papers. A solution to the general problem of back-scatter ionogram inversion has been proposed by Goutelard *et al.* [1979a]; based on a simple but adequate ionospheric layer model for establishing transmission parameters, the method consists of using analytical relations for rapid calculation of profile parameters. Bagwell [1978] also suggests there may be some scope for the determination of ionospheric structure using Doppler techniques.

The characteristics of the F-layer profile obtained by backscatter inversion can be compared with vertical incidence sounders down-range in the region of the ionosphere being sampled. The results have shown some correlation between the two sets of profiles, but the general consensus is that the method does not work well enough to justify an operational application [Croft, 1972].

Sources of error in plasma frequency mapping using backscatter have been discussed by Blair *et al.* [1970]. The accuracy of the technique depends mainly on the magnitude of ionospheric ionization gradients, which can cause plasma frequency estimates to be applied at the wrong heights and ranges. The effect of gradients can be corrected for, at least partly, by measuring delays and elevation angles from fixed targets of known range. One such target is a coastline where the land-sea interface can be identified by Doppler techniques [Blair *et al.*, 1969].

3.3 *Monitoring of irregularities*

Backscatter has proved to be of value as a means for monitoring irregularities in the ionosphere. Patches of sporadic E are easiest to understand because they behave much like localized flat mirrors in the lower regions of the ionosphere and produce localized patches of backscatter on a plan-position indicator (PPI) display. Sporadic E modes may also been identified by the absence of focusing (which is characteristic of F-layer echoes near the skip distance [Bibl, 1960]), and by their elevation angles [Tveten and Hunsucker, 1969]. Once a sporadic E mode has been identified, consideration can be given to taking advantage of its superior communications properties.

If used in conjunction with sampling against time and frequency applied to both the transmitted and the received signal [Goutelard *et al.*, 1979b], the backscatter technique reveals small inhomogeneities in the ionospheric plasma as well as certain short-term local modifications such as ionized trails caused by meteors.

Travelling disturbances in the ionosphere cause a variety of observed localized moving irregularities in the backscatter echoes. However it is not possible to deduce the nature of a disturbance from its backscatter appearance – it is necessary to formulate hypothetical models of the disturbance and then to calculate the backscatter, hoping to match observed forms.

REFERENCES

BAGWELL, D. J. [1978] Doppler processing of HF back-scatter radar and mode structures of ionospheric propagation. IEE Conf. Proc. No. 169, Part 2, 56-59.

BIBL, K. [1960] Experimental proof of focussing at the skip distance by backscatter records. *Proc. IRE*, Vol. 48, 956-957.

BLAIR, J. C., MELANSON, L. L. and TVETEN, L. H. [1969] HF-ionospheric radar ground-scatter map showing land-sea boundaries by a spectral-separation technique. *Electron. Lett.*, Vol. 5, 4, 75-76.

BLAIR, J. C., HUNSUCKER, R. D. and TVETEN, L. H. [1970] Ionospheric mapping by backscatter. *Ionospheric Forecasting.* Ed. V. Agy, AGARD Conf. Proc. No. 49, Paper 17.

CHERNOV, Y. A. [1971] Vozvratno-Naklonnoe Zondirovanie Ionosferi (Ionospheric backscatter sounding) (in Russian). Sviaz, Moscow, USSR.

CROFT, T. A. [1972] Sky-wave backscatter: a means of observing our environment at great distances. *Rev. Geophys. Space Phys.*, Vol. 10, 1, 73-156.

DU, J.H. and JIAO, P.N. [1987] - Determination of the Radial Track of Moving Objects' on the Ground by the HF Backscatter Technique, Chinese J. Space Science 7, 229-233.

DU BROFF, R. E., RAO, N. N. and YEH, K. C. [1979] Backscatter inversion in a spherically symmetric ionosphere. *Radio Sci.*, Vol. 14, 5, 837-842.

FENWICK, R. B. [1962] A test of the frequency-shift-pulse backscatter sounding technique in short-wave broadcasting. Final Rep. Contract IA-8513, 72. Stanford Electronic Lab., Stanford University, Stanford, Calif., USA.

GOUTELARD, C., CARATORI, J., COATANHAY, J. L., and ROLLAND, R. [1979a] Application de la technique backscatter aux prévisions de transmission ionosphériques à très court terme. AGARD Conf. Proc. No. 244, *Aspects of Electromagnetic Wave Scattering in Radio Communications*, Paper No. 14. Ed. A. N. Ince. NASA Accession No. N79-10299. National Technical Information Service, Springfield, VA 22161, USA.

GOUTELARD, C., CARATORI, J. and JOISEL, A. [1979b] Technique de sondage électromagnétique par échantillonnage spatio-fréquentiel des signaux de réception. Applications à l'étude des inhomogénéités du plasma ionosphérique. AGARD Conf. Proc. No. 244, *Aspects of Electromagnetic Wave Scattering in Radio Communications*, Paper No. 13. Ed. A. N. Ince. NASA Accession No. N79-10299. National Technical Information Service, Springfield, VA 22161, USA.

JIAO, P.N. and DU, J.H. [1987] - A Method of Determining Ground Distance of the Separate Scatterer Echo in HF Backscatter Ionograms, IEE Conference Publication Number 274, ICAP-87, Part 2, 186-189.

JIAO, P.N. and ZHU, Q.C. [1985] - A New Method of Determining Ground Distance Corresponding to Minimum Time-Delay in HF Backscattering. Fourth International Conference on Antennas and Propagation, IEE ICAP-85, Part 2, 555-558.

TVETEN, L. H. and HUNSUCKER, R. D. [1969] Remote sensing of the terrestrial environment with an HF radio high-resolution azimuth and elevation scan system. *Proc. IEEE*, Vol. 57, 4, 487-493.

REPORT 249-7

THE USE OF OBLIQUE SOUNDING FOR PROPAGATION ANALYSIS AND OPTIMIZATION

(Study Programme 27B/6)

(1959-1963-1966-1970-1974-1978-1982-1986-1990)

1. Introduction

This report is concerned with the use of oblique sounding for the analysis of propagation conditions on a fixed point-to-point circuit, and for the real-time selection of the optimum working frequency (OWF). Evaluation of an HF circuit benefits from knowledge of the propagation modes, and the time delay and Doppler spread on each mode, as a function of frequency. Applications of the techniques described in this Report for real-time circuit evaluation are contained in Report 889.

2. Techniques

Measurement of mode structure can be achieved by step-frequency pulse or swept-frequency (FMCW) transmissions, the latter offering the advantage of low peak power requirements [Fenwick and Barry, 1965]. Oblique sounding is a very powerful technique for the study of propagation conditions along a fixed point-to-point circuit, and has been used to provide test data for the validation of MUF prediction techniques, for the identification of unusual propagation modes, and other purposes which rely on the large amount of detailed information shown on an oblique ionogram. Long-range propagation experiments using oblique digital ionosondes have measured polarization, amplitude, phase, Doppler frequency and incidence angle [Reinisch et al., 1985].

The conventional oblique incidence ionosonde does not measure Doppler characteristics. Although it is possible to measure Doppler spread on a CW transmission, it is generally not possible to resolve the contribution from individual modes. The time-delay spread and Doppler spread on each mode can be measured using narrow-band FMCW [Earl and Ward, 1987] or a coded-pulse sounder utilizing a real-time correlation receiver [Wagner and Goldstein, 1985].

3. Results of propagation analyses

Oblique incidence pulse tests have been undertaken in Canada [Hatton, 1961], France [Delobeau *et al.*, 1955], Federal Republic of Germany [Möller, 1960], Japan [Aono, 1962], the United States of America [Agy and Davies, 1959; Tveten, 1961] and in Africa [Davies and Barghausen, 1966].

Many oblique measurements have been made, some of which have been scaled for the maximum observed frequency (MOF), over HF circuits in various parts of the world during a range of solar activity conditions between 1981 and 1988 [Goodman and Daehler, 1988].

3.1 MUF versus MOF comparison

Care must be exercised when comparing maximum observed frequencies (MOF) with predicted MUFs to establish whether any differences arise due to the ionospheric mapping or from the application of the obliquity factor. Comparison of maximum observed frequencies with predicted MUFs has shown that the existing theories of propagation generally seem to be adequate for calculating the basic MUF for distances up to several thousands of kilometres.

McNamara [1975] found that for two 2000-km circuits within Australia, monthly median predicted 1-hop MUFs were within about 5% of the MOF. For 2- and 3-hop propagation modes, the discrepancies were larger, partially as a result of the simplifying assumptions in the method used for MUF calculations (equal hop length, no tilts).

The maximum and lowest observed frequencies (MOF and LOF), as well as the parts of the spectrum having the least multipath propagation and the active propagation modes, were observed on 5 paths in the USSR with ranges between 1000 km and 10 000 km [Smirnov, 1972]. In quiet ionospheric conditions the MOF usually exceeded the basic MUF, which was calculated using the USSR prediction method [Zhulina *et al.*, 1969], by 10 to 35%. The increase in the MOF caused by scatter amounted to about 10%. In periods of magnetic disturbance the MOF was less than the basic MUF and the LOF increased. Additional studies have been reported [Rose *et al.*, 1978] using 132 path-months of hourly median MOF.

Measurements of MUF over HF circuits in the north-eastern United States of America have been made during part of the solar cycle maximum and agree well with values predicted by ITS-78 and IONCAP prediction programs [Teters *et al.*, 1983; Millman and Swanson, 1985]. Daehler et al., [1987] and Roy and Sailors [1987] have compared MUFs predicted by several propagation models with MOFs for numerous paths.

There can be notable departures between calculated and observed results if calculations are made using simple theoretical models. This agreement can be improved by the inclusion of electron density gradients in ray tracing [Röttger, 1967]

and modelling horizontal gradients [Davies and Rush, 1985]. Angle of arrival measurements may, in principle, determine the extent to which gradients must be taken into account.

It is extremely important when comparing MUFs and MOFs for each propagation mode be scaled separately so that MOFs and MUFs are compared for the same propagation mode. If the MOF data are tabulated without regard to mode, they should be analysed in terms of histograms of count versus MOF. This allows the identification of the propagation modes present. Median values calculated without regard to the number of propagation modes present in the observed data can be very misleading [McNamara, 1974].

3.2 Study of anomalous propagation modes

The presence of anomalous propagation modes on a given circuit can be established either by comparing the observed oblique ionograms with simulated ionograms for all the usual propagation modes, or by comparing reliable MUFs with the hourly histograms of the MOF. Either method can reveal a propagation mode with an MOF higher than the highest predicted MUF. The extra propagation mode could correspond, for example, to Es modes, to combination modes involving equatorial Es [McNamara, 1974] or to either of the two trans-equatorial propagation (TEP modes) [Nielson and Crochet, 1974; McNamara, 1974].

In an experiment carried out in 1970 and 1971 between Japan and Australia, for the path distances of 5873 km [Kuriki et al., 1974] and 7374 km [Tanohata et al., 1975], the dominant mode of propagation involves two reflections from the F layer with an intervening reflection at the surface of the Earth (2F mode). However, signals at frequencies higher than the maximum observed frequency of the 2F mode were frequently received during the period around 1000 to 2000 h local time. The occurrence was about 40% for each hour of observation and the MOF of this mode was about 4 ± 2MHz higher than the MOF of the 2F mode propagating at the same time.

At low latitudes anomalously high operational MUFs associated with F scatter are encountered at night [Davies and Barghausen, 1966; Nielson and Crochet, 1974].

For high-latitude paths, the basic MUF for transmission distances at the 2000-3400 km range is normally controlled by the F1 layer in the summer [Petrie and Stevens, 1965]. For long paths, the one hop F2 (Pedersen ray) is the principal mode [Hagg and Rolfe, 1963] under certain conditions over a wide range of latitudes. The maximum observed frequency (MOF) may however be controlled by an Es mode on some occasions. Further results of high latitude soundings were presented in a survey paper [Hunsucker and Bates, 1969].

The reflection coefficient of Es and the ionosonde equipment characteristics must be considered in estimating the usefulness of Es as a reflector at oblique incidence [Stevens, 1968a]. Sporadic-E MOFs for one-hop auroral region paths as high as 72 MHz are implied from simultaneous incoherent scatter radar and ionosonde data [Hunsucker, 1975].

Anomalous propagation modes affecting VHF propagation are described in Report 259.

3.3 Magneto-ionic splitting

Magneto-ionic splitting of x and o components was studied by Kopka and Möller [1968] using ray tracing. Results are given for a 2000 km path as a function of both magnetic latitude and magnetic azimuth. In general, the magneto-ionic splitting is less for an east-west path than a north-south path. Aono [1962] and Davies and Barghausen [1966] found this separation to be nearly equal to the longitudinal value of the gyrofrequency f_H on north-south paths. Agy and Davies [1959] found that there was a separation of about 0.2 MHz on a 2400 km east-west path and that the separation decreased with an increase in distance.

3.4 Characteristics of multipath propagation

Sweep-frequency pulse sounding results show that the spread of time delays due to multipath propagation decreases with increasing ratio, K (working frequency/basic MUF). Numerical data are given, for a variety of paths, by Davies [1965]. Measurements in China [Chen and Zhou, 1984] on a 1340 km path show that for $K \leq 1$, the mean spread exhibits a parabolic decrease as K increases, with a minimum value at $K = 1$, while for $K > 1$ up to the operational MUF the mean spread is unchanged. Theoretical analysis [Dai, 1985] shows that for a given value of K, the spread is normally distributed and that the expectation and variance vary with the value of K. This was confirmed by the above measurements.

Propagation experiments conducted during the period November-December 1981, along a great-circle path from north to south over 11 000 km, show that the frequency range of single-mode propagation becomes widest at a propagation distance of about 2000-3500 km, and then decreases gradually with an increase in distance. Single mode propagation at distances greater than about 8000 km is difficult to identify because many complex modes appear at the same frequency [Ichinose *et al.*, 1985].

The time-delay data necessary to simulate the HF channel (see Report 549) in the design of wideband communications systems can be obtained from oblique-incidence ionograms. However, the resolution in time delay in some sounder systems may not be adequate to allow the data to be used effectively [Sailors and Hill, 1977].

3.5 Channel scattering function

A wideband, step frequency coded pulse channel probe has been used to evaluate propagation conditions on high latitude paths [Wagner et al., 1987]. Pulse response time ———— diagrams and channel scattering functions constructed from the data permit individual propagating modes to be classified as specular, multipath-specular, or diffuse multipath. Short range propagation experiments using a coherent, coded-pulse oblique sounder designed to probe the HF communication channel to a bandwidth of 1 MHz, have been conducted [Wagner and Goldstein, 1985]. Such experiments yield measurements of the amplitude, the phase, the delay dispersion and the group delay.

Other high latitude channel probe measurements [Basler et al., 1987] have been used in conjunction with a theoretical model to determine the characteristics of the ionosphere responsible for the observed time-delay and Doppler spread.

4. Application to practical HF communication links

Results from oblique incidence sounding studies have shown that such equipments may be used in parallel with communications systems to determine optimum, short-term operating frequencies. A number of studies have now been carried out which are designed to determine the improvements that can be achieved from the use of oblique sounding information [Probst, 1968; Stevens, 1968b; Slutz *et al.*, 1969].

Improvement in radiocommunications during disturbed propagation conditions has been achieved due to effective selection and use of available operating frequencies when predictions or prearranged operating frequency schedules are inaccurate [Jull *et al.*, 1962].

It has been found that oblique sounding information can be a valuable aid in assessing the performance of the communication system. With propagation removed as an unknown variable, any defects in, or limitations of, the communication system performance or operation can be more readily discovered.

However, experiments involving ionospheric sounding at oblique incidence disclose a number of problems when the sounding equipment is used in parallel with the communications equipment or when the communications equipment is used to perform the sounding. The following must be considered:

- any differences in operational sensitivity between communication and sounding equipment parameters;
- inaccuracies which result from sounding over an ionospheric path separated from the communications path (particularly when the sounding data are used for quantitative prediction of signal levels). Studies [Jull, 1968] suggest that for a separation of 32 km, the r.m.s. differences in signal levels amounted to 5 dB when the sounding information was averaged over eight minutes;
- that ionospheric non-reciprocity results in unequal levels of signals travelling in opposite direction between linear antennas. The path non-reciprocity which arises when polarization fading was present can be appreciably reduced by averaging signal levels for eight minutes [Jull, 1968];
- any differences of performance of the sounder and communication equipment in the presence of interference;
- the difficulty in determining the sounding repetition rate required to ensure the validity of the information when ionospheric conditions begin to vary, as during disturbed periods;
- the difficulty in determining a sounding signal that is representative of the modulation of the communications system;

Operational applications of the HF oblique incidence sounding are treated by Study Group 3 (see Report 357). Oblique ionosondes are the most widely used form of class I real-time channel evaluation systems (see Report 889). However, other techniques offer considerable potential.

REFERENCES

AGY, V. and DAVIES, K. [1959] Ionospheric investigations using the sweep-frequency pulse technique at oblique incidence. *NBS J. Res.*, Vol. 63D, 151-174.

AONO, Y. [1962] Study of radio wave propagation in sweep frequency pulse transmission tests in Japan. *J. Radio Res. Labs.* (Japan), Vol. 9, 42, 127-200.

BASLER, R.P., PRICE, G.H., TSUNODA, R.T. and WONG, T.L. /1987/ - HF channel probe. "The effect of the ionosphere on communication, navigation and surveillance systems", Eds J M Goodman, J.A. Klobuchar, H Soicher, G. Joiner, Government Printing Office, Washington, DC 20402.

CHEN, Y. C. and ZHOU, G. N. [1984] Frequency dependence of parameters for the ionospheric channels (in Chinese). *J. China Inst. Comm.*, Vol. 5, 2, 48-56.

DAEHLER, M., REILLY, M.H., RHOADES, F J and GOODMAN, J.M. /1987/ Comparison of measured MOFs with propagation model forecasts. Page 4A-12. "The effect of the ionosphere on communication, navigation and surveillance systems", Eds. J.M. Goodman, J.A. Klobuchar, H. Soicher, G. Joiner, Government Printing Office, Washington, DC 20402.

DAI, Y. S. [1985] HF time-varying channel (in Chinese). Publishing House of People's Posts and Telecommunications, Beijing, People's Republic of China.

DAVIES, K. [1965] Ionospheric radio propagation. NBS Monograph 80, 181, US Govt. Printing Office, Washington, DC 20402.

DAVIES, K. and BARGHAUSEN, A. F. [1966] The effect of spread F on the propagation of radio waves near the equator. *Spread F and its effects upon radiowave propagation.* 437-466. AGARDograph 95, Ed. P. Newman, Technivision, Maidenhead, UK.

DAVIES, K. and RUSH, C.M. /1985/ - Reflection of high-frequency radio wave in inhomogeneous ionospheric layers. Radio Science, Vol. 20, pp. 303-309.

DELOBEAU, F., EYFRIG, R. and RAWER K. [1955] Résultats expérimentaux de transmission ionosphérique d'impulsions à incidence oblique (Experimental results of ionospheric pulse transmissions at oblique incidence). *Ann. des Télécomm.*, Vol. 10. 55-64.

EARL, G.F. and WARD, B D. /——— 1987 The frequency management system of the JINDALEE OTH Radar. Radio Science, 22, 275-291.

FENWICK, R. B. and BARRY, G. H. [1965] Step by step to a linear frequency sweep. *Electronics*, Vol. 38, 66-70.

GOODMAN, J.M. and DAEHLER, M. [1988] - The NRL data base of oblique-incidence soundings. Naval Research Laboratory Report 6337 (NTIS Accession N° AD-A199 777) National Technical Information Service, Springfield, VA 22161, USA.

HAGG, E. L. and ROLFE, W. [1963] A study of transatlantic radio propagation modes at 41.5 MHz. *Can. J. Phys.*, 41, 220-233.

HATTON, W. L. [1961] Oblique-sounding and HF radiocommunication. *IRE Trans. Comm. Systems*, Vol. PGCS-9, 275.

HUNSUCKER, R. D. [1975] Chatanika radar investigation of high latitude E-region ionization structure and dynamics. *Radio Sci.*, Vol. 10, 277-288.

HUNSUCKER, R. D. and BATES, H. F. [1969] Survey of polar and auroral region effects on HF propagation. *Radio Sci.*, Vol. 4, 347-365.

ICHINOSE, M., KURATANI, Y. and YAMAZAKI, I. [1985] HF propagation experiments made with a Chirp sounder aboard a ship. *J. Radio Res. Labs.* (Japan), Vol. 32, 136, 61-71.

JULL, G. W. [1968] HF spatial and temporal propagation characteristics and sounding assisted communications. *Ionospheric Radio Communications*, 225-241. Ed. K. Folkestad, Plenum Press, New York, NY 10011, USA.

JULL, G. W., DOYLE, D. J., IRVINE, G. W. and MURRAY, J. P. [1962] Frequency sounding techniques for HF communications over auroral zone paths. *Proc. IRE*, Vol. 50, 1676-1682.

KOPKA, H. and MÖLLER, H. G. [1968] MUF calculations including the effect of the earth's magnetic field. *Radio Sci.*, Vol. 3, 53-56.

KURIKI, I., KASUYA, I., HOJO, H. and TANOHATA, K. [1974] Analysis of maximum observed frequencies on oblique ionograms by ray tracing technique. *J. Radio Res. Labs.* (Japan), Vol. 21, 161-190.

McNAMARA, L.F. /1974/ - Ionospheric predictions on trans-equatorial circuits. Proc IREE (Australia), 35, 117-126.

McNAMARA, L.F. /1975/ - The accuracy of MUF predictions within Australia. Ionospheric Prediction Service Series R Reports, IPS-R28, Sydney.

MILLMAN, G. H. and SWANSON, R. W. [1985] Comparison of HF oblique transmissions with ionospheric predictions. *Radio Sci.*, Vol. 20, 3, 315-318.

MÖLLER, H. G. [1960] Ergebnisse der Impulsübertragung mit veränderlicher Frequenz auf der Strecke Sodankylä-Lindau (Results of variable frequency pulse transmissions over the path Sodankylä-Lindau). *Kleinheubacher Berichte*, 7, 115-123.

NIELSON, D. L. and CROCHET, M. [1974] Ionospheric propagation of HF and VHF radio waves across the geomagnetic equator. *Rev. Geophys. Space Phys.*, 12, 688-702.

PETRIE, L. E. and STEVENS, E. E. [1965] An F1 layer MUF prediction system for northern latitudes. *IEEE Trans. Ant. Prop.*, Vol. AP-13, 542-546.

PROBST, S. E. [1968] The CURTS concept and current state of development. *Ionospheric Radio Communications*, 370-379. Ed. K. Folkestad, Plenum Press, New York, NY 10011, USA.

REINISCH, B. W., BIBL, K., AHMED, M., SOICHER, H., GORMAN, F. J. and JODOGNE, J. C. [1985] Multipath and Doppler observations during transatlantic digital HF propagation experiments, propagation influences on digital transmission systems – problems and solutions. AGARD Conf. Proc. No. 363, *Propagation Influences on Digital Transmission.* Ed. J. H. Blythe. NASA Accession No. N85-19269. National Technical Information Service, Springfield VA 22161, USA.

ROSE, R. B., MARTIN, J. N. and LEVINE, P. H. [1978] MINIMUF-3: a simplified HF MUF prediction algorithm. Naval Ocean Systems Center Tech. Rep. 186, NTIS Accession No. AD A0522052. National Technical Information Service, Springfield, Va. 22161, USA.

RÖTTGER, J. [1967] Messung des Erhebungswinkels von Kurzwellen bei schrägem Einfall in die Ionosphäre (Measurement of the angle of HF radiation at oblique incidence in the ionosphere). Thesis at the Institute of Geophysics and Meteorology of the Technische Hochschule Braunschweig.

ROY, T.N. and SAILORS, D.B. [1987] - HF maximum usable frequency (MUF) model uncertainty assessment. Naval Ocean Systems Center Technical Report 1184 (NTIS ACCESSION N° AD-A189 132) National Technical Information Service, Springfield, VA 2161, USA.

SAILORS, D. B. and HILL, J. R. [1977] Simulation and measurement of the HF channel. Naval Ocean Systems Center Tech. Rep. 111, NTIS Accession No. A043384. National Technical Information Service, Springfield, Va. 22161, USA.

SLUTZ, R. J., GAUTIER, T. N. and LEFTIN, M. [1969] Short-term radio propagation forecasts in Southeast Asia. ESSA Tech. Rep. ERL-97-ITS-72. US Govt. Printing Office, Washington, DC 20402.

SMIRNOV, V. B. Ed. [1972] Naklonnoe zondirovanie ionesfery (Oblique-incidence sounding of the ionosphere) Collection of articles, No. 1, published by Gidrometizdat, Leningrad, USSR.

STEVENS, E. E. [1968a] The significance of sporadic E propagation in determining the MUF. *Ionospheric Radio Communications*, 289-293. Ed. K. Folkestad, Plenum Press, New York, NY, USA.

STEVENS, E. E. [1968b] The CHEC sounding system. *Ionospheric Radio Communications*, 359-369. Ed. K. Folkestad, Plenum Press, New York, NY, USA.

TANOHATA, K., YAMAOKA, M., NAKAJIMA, M., SAKAMOTO, T., IGUCHI, M. and YAMASHITA, K. [1975] Some consideration of maximum observed frequencies on the path between St. Kilda and Yamagawa. *Rev. Radio Res. Labs.* (Japan), Vol. 21, 33-41.

TETERS, L. R., LLOYD, J. L., HAYDON, G. W. and LUCAS, D. L. [1983] Estimating the performance of telecommunication systems using the ionospheric transmission channel – ionospheric communications analysis and prediction program user's manual. NTIA Report 83-127. US Govt. Printing Office, Washington, DC 20402.

TVETEN, L. H. [1961] Long-distance one-hop F1 propagation through the auroral zone. *J. Geophys. Res.*, Vol. 66, 1683-1684.

WAGNER, L.S and GOLDSTEIN, J.A. [1985] - High resolution probing of the HF ionospheric sky wave channel: F2 layer results. Radio Science, Vol. 20, pp. 287-302.

WAGNER, R.P., PRICE, G.H., TSUNODA, E.T. and WONG, T.L. [1987] - HF channel probe. "The effect of the ionosphere on communication navigation and surveillance systems", Eds. J.M. Goodman, J.A. Klobuchar, H. Soicher, G. Joiner, Government Printing Office, Washington, DC 20402.

ZHULINA, E. M., KERBLAÏ, T. S., KOVALEVSKAYA, E. M. and co-workers [1969] *Osnovy dolgosrochnogo radioprognozirovaniya* (Fundamentals of long-term radio forecasting) 172 pages. Nauka Publishing House, Moscow, USSR.

REPORT 250-6

LONG-DISTANCE IONOSPHERIC PROPAGATION WITHOUT INTERMEDIATE GROUND REFLECTION

(Study Programme 25D/6)

(1959-1963-1966-1970-1974-1978-1982-1986)

1. Introduction

There are modes of propagation controlled by the regular ionospheric regions by which HF and VHF radio-waves can travel to great distances in or below the ionosphere over low absorption paths without intermediate ground reflection. The distances in question extend from the maximum distance at which the classical one-hop low-angle ray can exist to all around the world. Modes of propagation which are now recognized include: one-hop propagation by high-angle rays, commonly called Pedersen-rays; propagation in the presence of ionospheric tilts by modes which do not return to the ground, sometimes called chordal hop propagation; and guided propagation in the ionosphere by modes, commonly called whispering-gallery modes and double-walled modes.

In addition to long-range propagation controlled by the regular ionosphere, MF and HF propagation can result from ducting by field-aligned ionospheric irregularities above the ionization maximum of the F region.

2. Pedersen-ray propagation

One-hop propagation is usually ignored in ionospheric predictions for circuits longer than 4000 km. However, single-hop propagation over distances greater than 10 000 km may arise [Fulton *et al.*, 1960]. The experimental evidence presented by Muldrew and Maliphant [1962] showed that:

- one-hop Pedersen propagation to 5600 km occurs regularly during the summer day-time;
- the range of useful communication frequencies may be extended by several MHz;
- in theory, for frequencies less than the maximum frequency that can be reflected, the upper limit to the one-hop Pedersen propagation distance is set by the signal-to-noise ratio and the limit of this mode of propagation may well be in excess of 7500 km in temperate regions and 10 000 km in equatorial regions.

According to Sazhin and Tinin [1975], favourable conditions for long-distance propagation by means of the Pedersen-ray occur as a result of the diffusion of the layer maximum. The attenuation of the wave associated with the Pedersen-ray decreases with increasing flatness of the extreme in electron density $N(Z)$. The presence of various kinds of inhomogeneities and of several layers makes the extreme $N(Z)$ even flatter. The convergence of critical frequencies and of the heights of maxima of the various layers are examples. Such a situation prevails most frequently in the day-time in summer.

3. Ionospheric tilt-supported propagation

Long-distance HF propagation by modes supported by longitudinal ionospheric tilts is possible. Such gradients may be caused by:

- variations in layer heights and/or
- variations in layer critical frequency.

An ionospheric layer tilt can cause a ray to be either refracted back to the earth or refracted so as to travel above the earth's surface before re-entering the ionosphere to undergo further refraction back to the ground. Titheridge [1958] derived a general relation which may be used to calculate the bearing and elevation angle deviations caused by a ray encountering particular forms of stratified layers having different tilts. Folkestad [1968] derived a set of formulae giving exact expressions for group paths and ground distances to the impact points for rays propagated in an ionosphere eccentric to the Earth. Rao [1968a, 1968b, 1968c] used a three-dimensional ray-tracing computer programme to calculate the expected direction of arrival and changes in bearing of radio waves resulting from temporal variations in the electron density distribution and seasonal variations in sunrise tilts. This type of propagation had often been observed on long-range transequatorial paths [Stein, 1958; Southworth, 1960; Kerblaï and Kovalevskaya, 1967; Gerson, 1968; Tao *et al.*, 1970].

Observations of HF signals propagating to the antipodal point of a transmitter [Bold, 1969; Albrecht, 1957, 1959] have demonstrated the importance of chordal-hop propagation supported by longitudinal ionospheric tilts. Bold [1972] observed over an antipodal path a large and sudden pre-sunrise increase in signal strength not predicted by a computer model previously used successfully for the same path on a lower frequency. Fenwick and Villard [1963] found this type of propagation attractive for explaining measurements of round-the-world (RTW) echoes which, under certain conditions, showed remarkably low dispersion and attenuation between successive echoes. The interpretations of their observations showed that for a substantial number of paths in the night-time hemisphere, RTW echoes consisted of successive reflections from the ionosphere but that, in the daylight hemisphere, the waves were usually refracted back to ground.

Observations by Hortenbach and Rogler [1979] on a trans-antipodal path (Wertachtal, Federal Republic of Germany to Melbourne, Australia) revealed unexpectedly high signal intensities resulting from tilt-supported propagation modes. Coupling into and out of the duct evidently was via layer tilts existing in the twilight regions near both terminals of the path.

4. Guided propagation in the ionosphere

Certain modes of propagation have been attributed to channelling in the ionosphere as in a waveguide, instead of just skywave multi-hop path propagation. These arise for:

- an electron density profile characterized by a monotonic increase of the electron density with height. The waveguide has an upper boundary, usually within the F layer, but no lower boundary. Guided waves propagate inside the concavity of the reflecting sphere; the Earth's lower ionosphere acts as a spherical whispering-gallery path (the limiting case of chordal propagation) for radio waves;

- an electron density profile characterized by relative minima, like the one between the E and F layers. The waveguide possesses an upper and lower wall, and ducting occurs in the space between the two concentric spheres, a double-walled duct. The propagation mechanism of whispering-gallery and double-walled ducts is indistinguishable observationally; the electron density profile that supports the former is observed more often than the profile required by the latter.

A method to estimate the maximum frequency of the guide, taking into account the height of the F2 layer, the maximum electron density and gradient, has been developed by Shlionsky [1979, 1980].

4.1 *Geometric optics analysis of guided propagation in the ionosphere*

Since it is desirable to distinguish ionospheric-guided modes from other kinds of propagation, such as multi-hop, the geometric analysis (ray-tracing) has usually been restricted to frequencies near or above the basic MUF for multi-hop propagation. The ray-tracing analysis of this phenomenon was performed with ionospheric models including those with spherical asymmetry, day-to-night transitions, irregularities and discontinuities [Barker and Grossi, 1966; Grossi and Langworthy, 1966; Grossi and Langworthy, 1968; Chvojková, 1965, 1974a, 1974b, 1976; Tsedilina, 1975].

The results of the analyses show:

4.1.1 whispering-gallery propagation is possible in any phase of the solar cycle;

4.1.2 at the most favourable frequency, a ray must make an angle not larger than 7° to 8° with the tangent to the layer for guidance to occur, and a ray leaving a ground-located source, and even grazing the horizon, arrives at ionospheric altitudes with too small an angle of incidence or too large a grazing angle for guidance;

4.1.3 the guided paths are not reachable from the ground unless scattering or refracting (or reflecting) centres perform as wave couplers between ground and whispering-gallery;

4.1.4 the MUF in the whispering-gallery is roughly twice the basic MUF of an equivalent multi-hop path, between ground-based terminals;

4.1.5 there can be joint existence of multi-hop and whispering-gallery both on the day and night sides of the earth; and

4.1.6 the total calculated losses, inclusive of absorption, are relatively insensitive to terminal separation and are of the order of magnitude of 125 dB to 138 dB from 25 MHz to 45 MHz.

4.2 *Full wave analysis of guided propagation in the ionosphere*

Using full wave mode theory, many features of RTW propagation echoes of signals from satellites below the horizon have been explained [Chang, 1971a, 1971b]. The theoretical results indicate:

4.2.1 the MUF for F-layer whispering-gallery propagation is approximately six times the vertical incidence frequency;

4.2.2 as the ratio of wave frequency to vertical penetration frequency increases above six, energy leaks and attenuation increases;

4.2.3 for day-time F region assumed to have a maximum plasma frequency of 9 MHz, leakage is enough to make a signal travelling around the world have an attenuation of about 11 dB;

4.2.4 since the maximum oblique-incidence penetration frequency for the F region is about four times the vertical penetration frequency, the MUF for F-layer whispering-gallery propagation is more than 1.5 times the MUF for ground-to-ground communications;

4.2.5 for both transmitter and receiver located where the least attenuated mode has the highest field strength, the field strength in the F-layer whispering-gallery at a distance of 11 000 km from the transmitter is about 3 to 4 dB higher than the field strength in free space;

4.2.6 the MUF for E-layer whispering-gallery is 14.9 times the vertical penetration frequency;

4.2.7 for a day-time E region, the MUF for whispering-gallery propagation is more than 2.6 times higher than the MUF for ground-to-ground communications;

4.2.8 collisions cause serious attenuation of trapped whispering-gallery modes associated with the E-region whispering-gallery, unlike communication along the F-region whispering-gallery, communication is practical only for a distance of a few thousand kilometres and is ineffective for propagation around the world.

The field strength of ionospheric guided modes has been estimated by Vsekhsvyatskaya and Kalinin [1979] and the use of the adiabatic invariant method to study guided modes has been developed by Gurevich and Tsedilina [1979, 1985].

4.3 *Wave coupling into ionospheric guided propagation modes*

Natural mechanisms able to perform injection/extraction of HF radio waves into/from the ionospheric ducted modes are:

- ionospheric tilts,
- sporadic-E ionization,
- auroral columns and curtains,
- meteor trails,
- equatorial F-region ionization troughs.

Artificial scattering centres are also conceivable, such as rocket-launched trails, rocket-launched ionospheric seeding, or an RF-induced ionized cloud. The basic parameters which characterize a wave coupler are:

- injection/extraction losses,
- time spread and doppler spread,
- geometry of utilization, and
- time availability of geophysical mechanisms.

The injection/extraction losses of ionospheric tilts are considerably less than the other couplers. Barker and Grossi [1966] illustrate the conversion of a multi-hop skywave into a whispering-gallery mode through a day-night transition; lack of symmetry constitutes the only chance for such guided paths to be excited from the ground.

The global properties of ionospheric wave ducts have been investigated [Tushentsova *et al.*, 1975]. Toman and Miller [1977] have shown that ionospheric ducting of HF rays does not require but is facilitated by the continued presence of an ionization valley in the plane of the ray trajectory. Burtnyk *et al.* [1962] observed that F-layer sunset tilts last longer, are larger in maximum amplitude, and are seen more often than sunrise tilts. Gerson *et al.* [1969] noted a decline before and an ascent after sunrise in antipodal reception.

Satellite soundings have shown the existence of significant sheets of ionization irregularities above the height of maximum electron density of the F region. These sheets probably extend below the height of maximum electron density and may be responsible for long-distance propagation of frequencies above the basic MUF [Hagg and Rolfe, 1963].

Gurevich and Tsedilina [1975] have investigated the trapping of energy in the ionosphere interlayer duct and its escape during specular scattering of radio waves by irregularities created by ionospheric heating.

4.4 *Satellite experiments*

In the OV4 satellite-to-satellite experiment [Barker and Grossi, 1970], leakage of the guided wave down to the Earth's surface and reception aboard a high-altitude flying aircraft were rare except for line-of-sight, antipodal and local sunrise-sunset configurations. The results also indicate that:

- the horizontal electron density gradient near the regions of sunrise and sunset can create the tilts necessary to convert multi-hop propagation in the day hemisphere into whispering-gallery propagation in an elevated guide in the night hemisphere, and that,

- a whispering-gallery in the north-south direction near the twilight girdle line might be very effective for long-range communications between elevated points.

The reception at the ground of HF signals radiated by a satellite orbiting above the F2 region of the ionosphere from long ranges, beyond the horizon, has been discussed by Beni *et al.*, [1978]. Satellite signals from the 1970-34A satellite were received in Florence, Italy, over ranges greater than 10 000 km. High propagation probability from the North Atlantic zone occurred when the satellite was above the F2 maximum (445-1500 km altitude) and when the sunset transition was near the receiving sation. Another favourable situation occurred when the satellite was high (800-1600 km) in the night zone south of the receiving station; both the satellite and receiving station were situated along the twilight zone. Free-space propagation losses were reduced by as much as 6 dB over ranges of 12 000 km, and up to 8 dB for nearly antipodal satellite passes. This tends to confirm the existence and the importance of guided propagation for long range communications between satellites and ground terminals.

5. HF propagation by ducting along field-aligned ionization

5.1 *Existence of HF propagation by ducting along field-aligned ionization*

High frequency propagation along ionization irregularities aligned with the Earth's magnetic field was suggested at almost the same time by Wagner [1928] and by Pedersen [1929]. Later, Obayashi [1959] and then Gallet and Utlaut [1961] made a similar interpretation of observations of long-delay echoes in HF radar. Further observations with HF radar seemed to confirm the interpretation [du Castel, 1963, 1965a; Petit, 1966], while others appeared to contradict it [Budden and Yates, 1952; Thomas *et al.*, 1963]. A special investigation in the region of the magnetic conjugate on the Earth's surface has demonstrated the possibility of field-aligned propagation over a broad range of frequencies in the HF band [Bukin, 1978, 1981]. A review of HF ionospheric ducting is given by Toman [1979]. One type of long-delay echo (frequency $\leqslant$ 4 MHz, delay $\leqslant$ 0.4 s) can be explained by field-aligned ducting [Muldrew, 1979; Villard *et al.*, 1980].

In the development of space techniques, rocket observations were also interpreted in terms of propagation by ducting [Knecht and Russel, 1962]. Then satellite observations brought more extensive confirmation [Muldrew, 1963; Calvert and Schmid, 1964; du Castel, 1965b; Dyson, 1967; Loftus *et al.*, 1966; Ramasastry and Walsh, 1969].

5.2 *Analyses and interpretations of observations*

The theory of propagation along field-aligned irregularities was developed by several authors [Voge, 1961, 1962; Booker, 1962; Muldrew, 1963; du Castel, 1965c; Walker, 1966]. The excess electron density in the irregularities is a few percent of the ambient ionization density, and the dimensions perpendicular to the magnetic field are a few kilometres [Loftus *et al.*, 1966].

A maximum in the frequency of occurrence of these irregularities observed by radar is found near sunrise, and a secondary maximum near sunset [Loftus *et al.*, 1966; Muldrew, 1967; Petit, 1966; du Castel, 1965c]. Initial studies using data gathered over a large region indicate that the occurrence of ducting seems to be independent of the level of geomagnetic disturbance [Muldrew, 1967; Loftus *et al.*, 1966]. However, a positive correlation with geomagnetic disturbance was found at northern midlatitudes (around 45° to 55° invariant latitude) for medium solar activity [Nishizaki and Matuura, 1972].

An analysis of satellite data from five low-latitude telemetry stations indicates that the frequency of occurrence of ducting has a lunar semi-monthly oscillation with a maximum at about 6 and 21 days after a new Moon [Sharma and Muldrew, 1973].

Another analysis of satellite data (Alouette-2, ISIS-1 and ISIS-2) from nine telemetry stations located at various longitudes and latitudes (in the western zone 58° W to 82° W, in the eastern zone 104° E to 149° E and intermediate zones 01° W to 28° E and 160° W) [Sharma and Muldrew, 1975] indicates that:

- averaged over all longitudes, the minimum frequency occurrence of echoes is about 2% around March and September, and the maxima are 7.8% in December-January and 6.2% in July;

- only a single maximum in frequency of occurrence exists in both the western and eastern zones, which are observed near the December solstice and near the June solstice respectively. Stations in the intermediate zone show a seasonal variation very similar to the average picture obtained from all the data, i.e. the frequency of occurrence is minimum in the equinoctial months and is maximum in the solstitial months.

In the above analysis, the observation of ducts were usually obtained at frequencies between 1 MHz and 2 MHz and none have been noted above 7 MHz.

Ducts are formed after sunset and before the formation of the E-F valley. E-region irregularities formed by field-aligned currents produce perpendicular electric fields which cause interchange of magnetic flux tubes [Cole, 1971; Muldrew, 1980].

REFERENCES

ALBRECHT, H. J. [1957] Investigations on Great Circle Propagation between Eastern Australia and Western Europe. *Geof. Pura e Applicata*, **38**, 169-180.

ALBRECHT, H. J. [1959] Further studies on the chordal-hop theory of ionospheric long range propagation. *Arch. Met. Geoph. Bioklim.*, **11**, 383-391.

BARKER, J. I. and GROSSI, M. D. [1966] Design of a satellite-to-satellite communication experiment to explore HF/VHF guided propagation in the lower ionosphere. *Radio Sci.*, Vol. 1, 1229-1234.

BARKER, J. I. and GROSSI, M. D. [1970] Results of the OV4-1 dual satellite experiment on guided ionospheric propagation. *Radio Sci.*, Vol. 5, 983-996.

BENI, P., BERTINI, F. and PELLEGRINI, P. F. [1978] HF transionospheric long range propagation from satellite observed at Florence. *Planet. and Space Sci.*, Vol. 26, **1**, 37-49.

BOLD, G. E. J. [1969] Power distribution near the antipode of a short-wave transmitter. *J. Atmos. Terr. Phys.*, Vol. 31, 1391-1411.

BOLD, G. E. J. [1972] The influence of chordal paths on signals propagating to the near antipode of an HF radio transmitter. *IEEE Trans. Ant. Prop.*, Vol. AP-20, 741-746.

BOOKER, H. G. [1962] Guidance of radio and hydromagnetic waves in the magnetosphere. *J. Geophys. Res.*, Vol. 67, **11**, 4135-4162.

BUDDEN, K. G. and YATES, G. G. [1952] A search for radio echoes of long delay. *J. Atm. Terr. Phys.*, **2**, 272.

BUKIN, G. V. [1978] Eskperimentalnye issledovaniya magnitosfernogo rasprostraneniya KV signalov na trasse zemlya-zemlya (Experimental studies of magnetospheric propagation of SW signals on an Earth-Earth path). *Geomag. i Aeronom.*, Vol. 18, **3**, 440.

BUKIN, G. V. [1981] Magnitosferny signal v prisutstvii nagreva ionosfery (Magnetospheric signal in the presence of ionospheric heating). *Geomag. i Aeronom.*, Vol. 21, **3**, 561.

BURTNYK, N., McLEISCH, C. W. and WOLFE, J. [1962] Ionospheric layer tilts at Ottawa, Canada, *Can. J. Phys.*, **40**, 1614-1619.

CALVERT, W. and SCHMID, C. W. [1964] Spread F observations by the Alouette topside sounder satellite. *J. Geophys. Res.*, Vol. 69, 1839-1852.

CHANG, H. [1971a] The waveguide mode theory of whispering-gallery propagation in the F-region of the ionosphere. *Radio Sci.*, Vol. 6, 475-482.

CHANG, H. [1971b] Whispering-gallery propagation in the E-region of the ionosphere at HF and VHF. *Radio Sci.*, Vol. 6, 465-473.

CHVOJKOVÁ, E. [1965] Analytical formulae for radio path in spherically stratified ionosphere. *NBS J. Res.*,Vol. 69D, 453-457.

CHVOJKOVÁ, E. [1974a] Radio-path formula: 1-theory, circumterrestrial echo and other singularities. *Geomagn. i Aeronom.*, Vol. 14, 57-66 (in Russian); 46-53 (in English).

CHVOJKOVÁ, E. [1974b] Radio-path formula: 2 practical applications. *Geomag. i Aeronom.*,Vol. 14, 466-494 (in Russian); 392-399 (in English).

CHVOJKOVÁ, E. [1976] Multiple propagation paths between satellites situated in the ionosphere below the F-layer peak. *J. Atmos. Terr. Phys.*, Vol. 38, 329-331.

COLE, K. D. [1971] Formation of field-aligned irregularities in the magnetosphere. *J. Atmos. Terr. Phys.*, Vol. 33, 741-750.

DU CASTEL, F. [1963] Recherche expérimentale sur le guidage géomagnétique d'ondes décamétriques (Experimental research on geomagnetic ducting of HF radio waves). *Ann. des Télécomm.*, Vol. 18, **9-10**, 177-184.

DU CASTEL, F. [1965a] Mise en évidence expérimentale d'un guidage géomagnétique d'ondes décamétriques (Experimental evidence of geomagnetic ducting of HF radio waves). *C.R. Acad. Sci.*, Paris, Vol. 261, 1057-1060.

DU CASTEL, F. [1965b] Sur certains échos guidés observés par sondages ionosphériques en satellite. (Concerning certain ducted echoes observed by means of satellite ionospheric soundings). *Space Res. V*, **216**. North-Holland Publ. Co., Amsterdam, Holland.

DU CASTEL, F. [1965c] Projet d'observation par satellite des irrégularités d'ionisation alignées sur le champ magnétique dans la magnétosphère (Plan for the observation by satellite of ionospheric irregularities in the magnetosphere, aligned with the magnetic field). *Planet. and Space Sci.*, Vol. 13, 1255-1271.

DYSON, P. L. [1967] Magnetic field aligned irregularities at mid geomagnetic latitudes. *J. Atmos. Terr. Phys.*, Vol. 28, 857-869.

FENWICK, R. B. and VILLARD, O. G., Jr. [1963] A test of the importance of ionosphere-ionosphere reflections in long-distance and around-the-world high frequency propagation. *J. Geophys. Res.*, Vol. 68, 5659-5666.

FOLKESTAD, K. [1968] Exact ray computations in a tilted ionosphere with no magnetic field. *Radio Sci.*, Vol. 3, 81-84.

FULTON, B., SANDOZ, O. and WARREN E. [1960] The lower frequency limits for F-layer radio propagation. *J. Geophys. Res.*,Vol. 65, 177-183.

GALLET, R. M. and UTLAUT, W. F. [1961] Evidence of the laminar nature of the exosphere obtained by means of guided high frequency wave propagation. *Phys. Rev. Lett.*, **6**, 591-594.

GERSON, N. C. [1968] Ray tracing over a trans-equatorial path. Scatter propagation of radio waves. AGARD Conf. Proc. No. 37 (NATO, Neuilly-sur-Seine).

GERSON, N. C., HENGEN, J. G., PIPP, R. M. and WEBSTER, J. B. [1969] Radio wave propagation to the antipode. *Can. J. Phys.*, 2143-2159.

GROSSI, M. D. and LANGWORTHY, B. M. [1966] Geometric optics investigation of HF and VHF guided propagation in the ionospheric whispering-gallery. *Radio Sci.*, Vol. 1, 877-886.

GROSSI, M. D. and LANGWORTHY, B. M. [1968] Short-wave ionospheric whispering-gallery. IEEE International Convention Digest, 88, March 18-21, New York, N.Y., USA.

GUREVICH, A. G. and TSEDILINA, E. E. [1975] Trapping of radiation in the ionospheric duct during scattering on artificial inhomogeneities. *Geomag. i Aeronom.*, Vol. 15, 713-715.

GUREVICH, A. G. and TSEDILINA, E. E. [1979] *Sverkhdalnee rasprostranenie korotkikh radiovoln* (Ultra long distance propagation of short waves). Nauka Publishing House, 246, Moscow, USSR

GUREVICH, A. G. and TSEDILINA, E. E. [1985] *Long-distance Propagation of HF Radio Waves.* Springer, Heidelberg, Federal Republic of Germany.

HAGG, E. L. and ROLFE, W. [1963] Study of transatlantic radio propagation modes at 41.5 Mc/s. *Can. J. Phys.*, **41**, 220-233.

HORTENBACH, K. J. and ROGLER, F. [1979] On the propagation of short waves over very long distances: predictions and observations. *Telecomm. J.*, Vol. 46, 320-329.

KERBLAÏ, T. and KOVALEVSKAYA, E. [1967] Computation of the MUF in the presence of horizontal ionospheric inhomogeneity. *Geomag. i Aeronom.*, Vol. 7, 92-96.

KNECHT, R. W. and RUSSEL, S. [1962] Pulsed radio soundings of the topside ionosphere in the presence of spread F. *J. Geophys. Res.*, Vol. 67, 1178-1182.

LOFTUS, B. T., VAN ZANDT, T. E. and CALVERT, W. [1966] Observations of conjugate ducting by the fixed-frequency topside sounder satellite. *Ann. de Géophys.*, Vol. 22, 530.

MULDREW, D. B. [1963] Radio propagation along magnetic field aligned sheets of ionization observed by the Alouette topside sounder. *J. Geophys. Res.*, Vol. 68, 5355-5370.

MULDREW, D. B. [1967] Medium-frequency conjugate echoes observed on topside-sounder data. *Can. J. Phys.*, **45**, 3935-3944.

MULDREW, D. B. [1979] Generation of long-delay echoes. *J. Geophys. Res.*, Vol. 84, 5199-5215.

MULDREW, D. B. [1980] The formation of ducts and spread F and the initiation of bubbles by field-aligned currents. *J. Geophys. Res.*, Vol. 85, 613-625.

MULDREW, D. B. and MALIPHANT, R. G. [1962] Long-distance one-hop ionospheric radio propagation. *J. Geophys. Res.*, Vol. 67, 1805-1815.

NISHIZAKI, R. and MATUURA, N. [1972] Conjugate ducted echoes observed on Alouette 2 ionograms. *J. Radio Res. Labs.* (Japan), **19**, 99.

OBAYASHI, T. [1959] A possibility of the long distance HF propagation along the exospheric field aligned ionization. *Rep. Ion. Res.*, Japan, **13**, 177.

PEDERSEN, P. O. [1929] Wireless echoes of long delay. *Proc. IRE*, Vol. 17, 1750-1785.

PETIT, M. [1966] Etude du guidage géomagnétique d'ondes décamétriques entre points conjugués au sol (Study of the geomagnetic ducting of HF radio waves between conjugate points on the Earth's surface). Diplôme E. S., Fac. des Sc., Paris.

RAMASASTRY, J. and WALSH, E. J. [1969] Conjugate echoes observed by Alouette 2 topside sounder at the longitudes of Singapore. *J. Geophys. Res.*, Vol. 74, **24**, 5665-5674.

RAO, N. N. [1968a] Ray-tracing investigation of direction of arrival observation of HF radio waves. *Radio Sci.*, Vol. 3, 796-802.

RAO, N. N. [1968b] Bearing deviation in HF transionospheric propagation. I. Exact computations for some ionospheric models with no magnetic field. *Radio Sci.*, Vol. 3, 1113-1118.

RAO, N. N. [1968c] Bearing deviation in HF transionospheric propagation. II. Application of exact computations. *Radio Sci.*, Vol. 3, 1119-1123.

SAZHIN, V. I. and TININ, M. V. [1975] Long-distance propagation by means of the Pedersen-ray. *Geomag. i Aeronom.*, Vol. 15, 564-567.

SHARMA, R. P. and MULDREW, D. B. [1973] A lunar effect in the occurrence of conjugate echoes on topside sounder ionograms. *J. Geophys. Res.*, Vol. 78, 8251-8260.

SHARMA, R. P. and MULDREW, D. B. [1975] Seasonal and longitudinal variations in the occurrence frequency of magnetospheric ionization ducts. *J. Geophys. Res.*, Vol. 80, 977-984.

SHLIONSKY, A. G. [1979] *Dalnee rasprostranenie radiovoln v ionosfere* (Long-distance propagation of radio waves in the ionosphere). Nauka Publishing House, Moscow, USSR.

SHLIONSKY, A. G. [1980] Prediction of waveguide propagation of radio waves using the extremalparametric method based on predicted ionosphere parameters. *Solar-Terrestrial Predictions Proc.*, Vol. IV, D-3, 60-70, Boulder, CO, USA.

SOUTHWORTH, M. P. [1960] Night-time equatorial propagation at 50 MHz: First results from an IGY amateur observing programme. *J. Geophys. Res.*, Vol. 65, 601-607.

STEIN, S. [1958] The role of ionospheric layer tilts in long-range high frequency radio propagation. *J. Geophys. Res.*,Vol. 63, 217-241.

TAO, K., OCHI, F., YAMAOKA, M., WATANABE, S., WATANABE, C. and TANOHATA, K. [1970] Experimental results of VHF transequatorial propagation. *J. Radio Res. Labs.*, (Japan), **17**, 83-101.

THOMAS, J. A., McINNES, B. A. and CROUCHLEY, J. [1963] High frequency exospheric duct propagation experiments. *J. Atmos. Terr. Phys.*, Vol. 25, 613-619.

TITHERIDGE, J. E. [1958] Variations in the direction of arrival of high-frequency radio waves. *J. Atmos. Terr. Phys.*, **13**, 17-25.

TOMAN, K. [1979] High-frequency ionospheric ducting – a review. *Radio Sci.*, Vol. 14, 447-453.

TOMAN, K. and MILLER, D. C. [1977] Computation study of long-range high-frequency ionospheric ducting. *Radio Sci.*, Vol. 12, 467-476.

TSEDILINA, E. E. [1975] Round-the-world radio wave propagation in ionospheric wave ducts. *Geomag. i Aeronom.*, Vol. 15, 371-374.

TUSHENTSOVA, I. A., FISHCHUK, D. I. and TSEDILINA, E. E. [1975] Investigation of the global properties of ionospheric wave ducts. II. *Geomag. i Aeronom.*, Vol. 15, 62-66.

VILLARD, O. G. Jr., MULDREW, D. B. and WAXHAM, F. W. Jr. [1980] The magnetospheric echo box – A type of long-delayed echo explained. *QST*, Vol. 64, **10**, 11-14.

VOGE, J. [1961, 1962] Propagation guidée le long d'un feuillet atmosphérique ou exosphérique. (Propagation by ducting along a thin atmospheric or exospheric layer.) *Ann. des Télécom.*, Vol. 16, **11-12**, 288-295 and Vol. 17, **1-2**, 34-44.

VSEKHSVYATSKAYA, I. S. and KALININ, Yu. K. [1979] Ob interferentsii dekametrovykh voln vblizi antipoda (Interference of HF waves near the antipode). *Geomag. i Aeronom.*, Vol. 19, **3**, 470-473.

WAGNER, K. W. [1928] Beobachtungen über die Reflexion von Hertzschen Wellen im Weltraum, weit ausserhalb der Erde (Observations on the reflection of radio waves in space, distant from the Earth). *Elekt. Nachr. Techn.*, **5**, 483.

WALKER, A. D. [1966] The theory of guiding of radio waves in the exosphere. *J. Atmos. Terr. Phys.*, Vol. 28, 1039-1056.

REPORT 262-7

ELF, VLF AND LF PROPAGATION IN AND THROUGH THE IONOSPHERE

(Question 25/6)

(1963-1966-1970-1974-1978-1982-1986-1990)

1. Introduction

Transmitted radio frequencies in the range from 30 Hz to 300 kHz, which are typically reflected from the lowest ionospheric layers, are useful for a wide range of applications in addition to radiocommunication. In particular, the stability of propagation of frequencies in the VLF range (3-30 kHz) makes them useful for navigation and time comparison purposes. (For terrestrial paths, a discussion of the propagation characteristics of frequencies below about 30 kHz is found in Report 895, and Report 265 contains circuit performance information for the frequency range from 30 to 500 kHz.) However, it has been known for many years that very low frequencies can be propagated through the ionosphere by a mode which for historical reasons has been called the "whistler mode". Signals originating in lightning flashes were observed at frequencies within the audio range and were termed "musical atmospherics" [Eckersley, 1925; Barkhausen, 1919]. These frequencies are subject to dispersion such that the velocity of propagation decreases with frequency. The received signal therefore has a characteristic whistle of decreasing frequency over a period of a second or more. They also consist of a series of well-separated echoes with increasing frequency dispersions. These remarkable properties have been explained theoretically in terms of propagation, by an extraordinary mode of low velocity and small attenuation, along a path closely confined around a line of the Earth's magnetic field, the signals travelling to and fro between conjugate points on the surface of the Earth [Storey, 1953; Morgan *et al.*, 1956; Helliwell and Morgan, 1959]. A comprehensive survey of the history of whistler research has been published [Helliwell, 1965].

The whistler mode is classified into a ducted mode propagating along field aligned irregularities of enhanced ionization [Smith, 1961; Cerisier, 1974] and a non-ducted mode with large wave normal angles to geomagnetic field lines [Kimura, 1966; Smith and Angerami, 1968; Aikyo *et al.*, 1972]. Ray-tracing results of VLF waves in model magnetospheres [Aikyo and Ondoh, 1971; Walter and Scarabucci, 1974] have suggested a density gradient wave trapping in the plasmapause and a VLF wave trapping of non-ducted modes in the plasmasphere or plasma trough as observed by satellites [Burtis and Helliwell, 1969; McPherson and Koons, 1970; Gurnett and Shaw, 1973]. The whistler duct width increases with corrected geomagnetic latitude in the plasmasphere [Ondoh, 1976].

2. Use of VLF and LF transmitters

The whistler mode of propagation has been studied by using high-power VLF and LF transmitters. With the increasing interest being shown in the problem of transmission on various frequencies for terminal points on the surface of the Earth and in or above the ionosphere, it is now preferable to think of ELF, VLF and LF propagation in general and to restrict the term "whistler" to transmissions covering a frequency spectrum such as is originated by a lightning flash for which the frequency dispersion characteristic of whistlers can be observed.

It is interesting to note that the times when relatively strong signals have been obtained between conjugate points with VLF transmitters have shown only poor correlation with the times when whistlers were prevalent. Thus, although experiments using natural sources are of great scientific interest in unravelling some of the complexities of VLF propagation through the ionosphere, they must be supplemented with experiments directly related to propagation on given frequencies from chosen transmitting points.

3. Frequency limits and intensity considerations

It has been found that when both terminals are on the surface of the Earth, the whistler mode is effective at frequencies as low as 400 Hz and as high as 35 kHz. There is a well-defined cut-off frequency which is approximately 0.6 of the minimum gyro-frequency for electrons along the path. Satellite-borne receivers, which extend the observations to non-ducted signals, show the presence of whistler-mode signals at frequencies as high as 0.9 of the local electron gyro-frequency [Dunckel and Helliwell, 1977]. Whistler-mode propagation has been observed at most locations between geomagnetic latitudes 20° and 80°, and during the winter night even at Okinawa and Varanasi where the geomagnetic latitude is as low as 15° [Ondoh *et al.*, 1979; Singh and Singh, 1977]. Observations at middle latitudes show that, at night, signals by a single traverse between conjugate points can be obtained by the whistler mode for more than half the time and can approach in strength on occasion to within 10 dB of the conventional waveguide signal between the Earth and the ionosphere. Little is known about the intensity of daytime whistler-mode signals, but it appears that they are severely attenuated in the D region of the ionosphere.

Factors important in the calculation of intensity are:

- the polarization and directivity of the radiator,
- the properties of the path between the end-points of the duct in the ionosphere and the terminal points on the ground,
- the transmission coefficient for the propagation through the lower regions of the ionosphere,
- the spatial divergence in the duct,
- multipath effects resulting from the presence of more than one duct,
- the amplification, or absorption, of signal energy through interaction with charged particles in the plasma.

4. Propagation analysis

A full-wave computer program has been developed for studying the fields in a horizontally stratified ionosphere for waves incident from above or below for a wide range of the relevant parameters [Pitteway, 1965; Pitteway and Jesperson, 1966]. In some models studied, the effects of sporadic-E layers have been included. Sporadic E can give very high internal reflection coefficients for waves incident from above. This is important when only the distant end of the guiding magnetic field line is in daylight, since very efficient two-hop whistler-propagation may then be possible. It has also been shown that a large part of the whistler wave energy can be reflected in the absence of sporadic E provided the wave-normal direction is outside the acceptance cone for penetration to the Earth's surface [Thomas and Smeathers, 1971]. This is important in the interpretation of rocket measurements of whistlers.

Near 14 kHz the transmission coefficient for upgoing waves varies only slowly with angles of incidence between $\pm$ 85° at middle latitudes, whereas at 100 kHz efficient transmission is possible only at angles within a cone having its axis along the direction of the magnetic field; this influence of the magnetic field is more noticeable at all frequencies at lower latitudes [Thomas and Horowitz, 1971]. Both by day and night, the transmission coefficient is mainly determined by losses in the ionosphere, provided that steep gradients of electron density, similar to those in a sporadic-E layer, are absent. The whistler-wave absorption, which occurs chiefly in the lower ionosphere, increases with frequency and with decrease in latitude [Thomas and Horowitz, 1971; Wieder, 1967].

In the auroral zone, the whistler wave absorption is considerably influenced by particle precipitation, that is, several tens of dB for polar black-out events, and 10 to 20 dB at a sunlit noon or auroral night, whereas it is only a few dB in the quiet ionosphere during a winter night [Ondoh, 1963; Harang, 1968].

At the lower ELF frequencies Galejs [1972] and Pappert [1973] found that excessive dipole moments were required for effective excitation of the terrestrial waveguide mode by satellite-borne sources. De Witt *et al.*, [1976] calculated the propagation characteristics of ELF/VLF waves through the ionosphere from a source in the magnetosphere. Expressions were developed which gave the ratio of the power transmitted to the Earth's surface to the power incident on the top of the ionosphere, as a function of the number of wave-hops in the earth-ionosphere waveguide. The wave polarization was calculated as a function of the number of hops. In addition, in calculating the signal power budget for a magnetospheric source of ELF or VLF waves, it was necessary to calculate the geometric spreading factor of the waves as they propagated from the source to a receiver at the Earth's surface [Kelly *et al.*, 1976a]. In all low altitude transmitter cases (below about 2200 km) the spreading factor decreased rapidly in magnitude as distance from the maximum point of the hot spot power pattern increased. The spreading factor was shown to be smaller and less sensitive to receiver location for a fixed

high-altitude transmitter location. The satellite power required to provide a S/N ratio in excess of 0 dB in a 1 Hz bandwidth at a ground range of 1000 km from the ionospheric exit point of the waves was evaluated for several cases [Kelly *et al.*, 1976b]. The power requirement (in the megawatt range) exceeds that available on current spacecraft missions, but it is within the realm considered possible for future space electric power systems.

5. Satellite observations

The study of VLF propagation in and through the ionosphere has been considerably advanced by using satellites. For a terminal point within the ionosphere, the effect of a highly anisotropic medium on the antenna characteristics and thus on the transmission loss must be considered. A useful review of satellite observations of VLF phenomena in the magnetosphere has been published [Rycroft, 1967].

An interesting series of experiments has been undertaken in the Lofti satellite programme. Lofti-I indicated that useful amounts of VLF radio energy can penetrate the atmosphere/ionosphere interface and, in particular, that 18 kHz signals from ground-based transmitters were detected as far as 16 000 km away in the ionosphere with substantially less attenuation at night than by day, as expected. The observed time delays ranged from 10 to 200 ms, indicating that the VLF propagation velocity in the ionosphere is much lower than in free space [Leiphart *et al.*, 1962]. In the Lofti-II experiment, in addition to signal strength, measurements were made of dipole impedance in the ionosphere. The measured impedance was found to be radically different from that in free space. This is also in accordance with theoretical analyses.

Alouette-1 contained a receiver covering the frequency range 0.4 to 10 kHz using an electric dipole. The VLF signals received at the satellite were very strong. Short fractional hop (SFH) whistlers, i.e. those which have been propagated from a lightning flash only once through the ionosphere often overloaded the receiver. Transmissions were received from high-power ground-based transmitters and even from low-power transmitters (100 W) at 10 kHz, but no study has yet been made of these signals. Long fractional hop (LFH) whistlers, i.e. those thought to be propagating down the line of force from the opposite hemisphere, were often observed having the same dispersion characteristics during a full ten-minute telemeter recording. This implied that a particular duct was active throughout this period in propagating the whistlers which, after leaving the duct, travelled some thousands of kilometres transversely to reach the satellite receiver. Horizontal propagation of SFH whistlers can lead to reflection of these signals near the height of the satellite [Barrington and Belrose, 1963; Carpenter *et al.*, 1964; Smith, 1964].

However, simultaneous ground and satellite reception of whistlers [Thomson and Dowden, 1977a] show that most whistlers are received in satellites after reflection near the base of the ionosphere. Since downgoing whistlers usually exit from ducts at altitudes well above 1000 km [Thomson and Dowden, 1977b], whistlers from a given duct can be received on satellites over a wide range along the path of a satellite (up to 2000 km for ISIS-2 at an altitude of 1400 km). Even wider reception ranges, without change in dispersion characteristics, occur for non-ducted "pro-longitudinal" whistlers [Thomson and Dowden, 1977c]. While in both cases those effects are due to deviation ($\approx 20°$) from strictly field-aligned propagation, transverse propagation is not involved.

While theoretically one would expect ions to strongly influence ELF propagation, the effects of ions were not directly observed prior to the satellite experiments. The importance of ions is demonstrated by the identification of ioncyclotron whistlers [Smith *et al.*, 1964; Barrington *et al.*, 1966a and b], which have been studied to provide a measure of mean ionic mass at the height of the satellite [Gurnett *et al.*, 1965; Barrington and McEwen, 1967]. Moreover, a VLF plasma reasonance, the lower hybrid resonance for the transverse mode of propagation, was identified in Alouette VLF data as a cut-off frequency for VLF noise [Brice *et al.*, 1964]. This identification also provided information on the mean ionic mass at the height of the satellite [Barrington *et al.*, 1965]. Solar cycle variations of the occurrence rate of trans-equatorial proton and deuteron ion whistlers were obtained from ISIS observations [Watanabe and Ondoh, 1984].

6. Conclusions

The study of ELF, VLF and LF propagation in and through the ionosphere began with ground based observations of whistlers, which are dominantly influenced by their long propagation path through the magnetosphere. Satellite-borne observations have greatly advanced our knowledge about propagation within the ionosphere – these observations have revealed the importance (at the lowest frequencies) both of propagation transverse to the direction of the Earth's magnetic field and of ions on propagation. As might be expected, the ionosphere strongly affects the propagation of ELF, VLF and LF radio waves, which can penetrate it by the

whistler mode of propagation. This propagation is possible for Earth-space and space-Earth systems. The propagation is characterized by large group delays, highly variable attenuations, very indirect transmission paths, and also by a complicated interaction between the propagated waves and energetic particles present in the ionosphere. Because of this latter observation, proposals have been made for employing high-power VLF and LF transmitters in satellites. While such transmissions may give rise to significant amounts of noise and interference, they are likely to be limited by the difficulty in providing high power for satellite-borne transmitters.

REFERENCES

AIKYO, K. and ONDOH, T. [1971] Propagation of non-ducted VLF-waves in the vicinity of the plasmapause. *J. Radio Res. Labs.*, (Japan), **18**, 153-182.

AIKYO, K., ONDOH, T. and NAGAYAMA, M. [1972] Non-ducted whistlers observed in the plasmasphere. *J. Radio Res. Labs.*, (Japan), **19**, 151-174.

BARKHAUSEN, H. [1919] Zwei mit Hilfe der neuen Verstärker entdeckte Erscheinungen (Two phenomena discovered with the use of new amplifiers). *Phys. Z.*, **20**, 401-403.

BARRINGTON, R. E. and BELROSE, J. S. [1963] Preliminary results from the very low frequency receiver aboard Canada's Alouette satellite. *Nature*, Vol. 198, **4887**, 651-656.

BARRINGTON, R. E., BELROSE, J. S. and NELMS, G. L. [1965] Ion composition and temperature at 1000 km as deduced from simultaneous observations of a VHF plasma resonance and topside sounding data from the Alouette I satellite. *J. Geophys. Res.*, **70**, 1647-1664.

BARRINGTON, R. E., BELROSE, J. S. and MATHER, W. E. [1966a] A helium whistler observed in Canadian satellite Alouette II. *Nature*, Vol. 210, 80-81.

BARRINGTON, R. E., BELROSE, J. S. and NELMS, G. L. [1966b] Ion composition and temperature at 1000 km as deduced from VLF plasma resonances and topside ionograms. *Electron density distributions in the ionosphere and exosphere.* Edited by J. Frihagen, North-Holland Publ. Co., Amsterdam, Holland.

BARRINGTON, R. E. and McEWEN, D. J. [1967] Ion composition from VLF phenomena observed by Alouette I and II. *Space Res.* **VII**, 624-633.

BRICE, N. M. SMITH, R. L., BELROSE, J. S. and BARRINGTON, R. E. [1964] Recordings from satellite Alouette I – a very low frequency plasma resonance. *Nature*, Vol. 203, **4948**, 926-927.

BURTIS, W. J. and HELLIWELL, R. A. [1969] Banded chorus – A new type of VLF radiation observed in the magnetosphere by OGO 1 and OGO 3. *J. Geophys. Res.*, Vol. 74, 3002-3010.

CARPENTER, D. L., DUNCKEL, N. and WALKUP, J. F. [1964] A new very low frequency phenomenon – whistlers trapped below the protonosphere. *J. Geophys. Res.*, Vol. 69, **23**, 5009-5017.

CERISIER, J. C. [1974] Ducted and partly ducted propagation of VLF waves through the magnetosphere. *J. Atmos. Terr. Phys.*, **36**, 1443-1467.

DE WITT, R. N., KELLY, F. J. and CHAYT, G. A. [1976] Lower ionospheric effects on the propagation of waves from an ELF/VLF source in the magnetosphere. *Radio Sci.*, **11**, 189-197.

DUNCKEL, N. and HELLIWELL, R. A. [1977] Spacecraft observations of man-made whistler-mode signals near the electron gyrofrequency. *Radio Sci.*, Vol. 12, **5**, 821-829.

ECKERSLEY, T. L. [1925] A note on musical atmospheric disturbances. *Phil Mag.*, **49**, 1250-1260.

GALEJS, J. [1972] Stable solutions of ionospheric fields in the propagation of ELF and VLF waves. *Radio Sci.*, 7, 549-561.

GURNETT, D. A. and SHAW, R. R. [1973] Electromagnetic radiation trapped in the magnetosphere above the plasma frequency. *J. Geophys. Res.*, Vol. 78, **34**, 8136-8149.

GURNETT, D. A., SHAWAN, S. D., SMITH, R. L. and BRICE, N. M. [1965] Ion cyclotron whistlers. *J. Geophys. Res.*, Vol. 70, 1665-1688.

HARANG, L. [1968] VLF emissions observed at stations close to the auroral zone and at stations on lower latitudes. *J. Atmos. Terr. Phys.*, **30**, 1143-1160.

HELLIWELL, R. A. [1965] *Whistlers and Related Ionospheric Phenomena.* Stanford University Press, Stanford, CA, USA.

HELLIWELL, R. A. and MORGAN, M. G. [1959] Atmospheric whistlers, *Proc. IRE*, **47**, 200-208.

KELLY, F. J., BAKER, D. J. and CHAYT, G. A. [1976a] Spreading of waves emitted from an ELF/VLF source in the magnetosphere. *Radio Sci.*, **11**, 93-106.

KELLY, F. J., CHAYT, G. A. and BAKER, D. J. [1976b] Waveguide-mode power budget for an ELF/VLF transmitting satellite. Naval Research Laboratory Report No. 8032 (NTIS Accession AD A002287) National Technical Information Service, Springfield, VA., USA.

KIMURA, I. [1966] Effect of ions on whistler-mode ray tracing, *Radio Sci.*, **1**, 269-283.

LEIPHART, J. P., ZEEK, R. W., BEARCE, L. S. and TOTH, E. [1962] Penetration of the ionosphere by very low frequency radio signals. Interim results of the LOFTI I experiment. *Proc. IRE*, **50**, 6-17.

McPHERSON, D. A. and KOONS, H. C. [1970] Dependence of ELF emissions on the location of the plasmapause. *J. Geophys. Res.*, **75**, 5559-5564.

MORGAN, M. G., DINGER, H. E. and ALLCOCK, G. McK. [1956] Observations of whistling atmospherics at geo-magnetically conjugate points. *Nature*, Vol. 177, 29-31.

ONDOH, T. [1963] The ionospheric absorption of the VLF emissions at the auroral zone. *J. Geomag. Geoelect.*, **15**, 90-108.

ONDOH, T. [1976] Magnetospheric whistler ducts observed by ISIS satellites. *J. Radio Res. Labs.*, (Japan), **23**, 139-147.

ONDOH, T., KOTAKI, M., MURAKAMI, T., WATANABE, S., and NAKAMURA, Y. [1979] Propagation characteristics of low-latitude whistlers. *J. Geophys. Res.*, **84**, 2097-2104.

PAPPERT, R. A. [1973] Excitation of the earth-ionosphere waveguide by point dipoles at satellite heights. *Radio Sci.*, **8**, 535-545.

PITTEWAY, M. L. V. [1965] The numerical calculation of wave fields reflection coefficients and polarizations for long waves in the lower ionosphere. Part I, *Phil. Trans. Roy. Soc.*, Series A, **257**, 219-242.

PITTEWAY, M. L. V. and JESPERSON, J. L. [1966] A numerical study of the excitation, internal reflection and limiting polarization of whistler waves in the lower ionsophere. *J. Atmos. Terr. Phys.*, **28**, 17-43.

RYCROFT, M. J. [1967] A review of satellite observations of VLF phenomena in the magnetosphere, in MF, LF and VLF propagation. IEE Conf. Publ., **36**, 267-294.

SINGH, R. N. and SINGH, R. P. [1977] Whistlers recorded at Varanasi. *Nature*, Vol. 266, 40-41.

SMITH, R. L. [1961] Propagation characteristics of whistlers trapped in field-aligned columns of enhanced ionization. *J. Geophys. Res.*, Vol. 66, 3699-3716.

SMITH, R. L. [1964] An explanation of subprotonospheric whistlers. *J. Geophys. Res.*, Vol. 69, **23**, 5019-5021.

SMITH, R. L. and ANGERAMI, J. J. [1968] Magnetospheric properties deduced from OGO 1 observations of ducted and non-ducted whistlers. *J. Geophys. Res.*, Vol. 73, 1-20.

SMITH, R. L., BRICE, N. M., KATSUFRAKIS, J., GURNETT, D. A., SHAWAN, S. D., BELROSE, J. S. and BARRINGTON, R. E. [1964] An ion gyrofrequency phenomenon observed in satellites. *Nature*, Vol. 204, 274-275.

STOREY, L. R. O. [1953] An investigation of whistling atmospherics. *Phil. Trans. Roy. Soc.*, Series A, **246**, 113-141.

THOMAS, L. and HOROWITZ, S. [1971] The ionospheric absorption of downgoing whistler waves during night-time. *J. Atmos. Terr. Phys.*, **33**, 879-888.

THOMAS, L. and SMEATHERS, J. R. [1971] The internal reflection of whistler waves in the lower ionosphere. *J. Atmos. Terr. Phys.*, **33**, 959-962.

THOMSON, R. J. and DOWDEN, R. L. [1977a] Simultaneous ground and satellite reception of whistlers: 1. Ducted whistler. *J. Atmos. Terr. Phys.*, **39**, 869-878.

THOMSON, R. J. and DOWDEN, R. L. [1977b] Ionospheric propagation of whistlers, *Planet. and Space Sci.*, **25**, 1037-1043.

THOMSON, R. J. and DOWDEN, R. L. [1977c] Simultaneous ground and satellite reception of whistlers: 2. PL whistlers. *J. Atmos. Terr. Phys.*, **39**, 879-890.

WALTER, F. and SCARABUCCI, R. R. [1974] VLF ray trajectories in a latitude-dependent model of the magnetosphere. *Radio Sci.*, **9**, 7-15.

WATANABE, S. and ONDOH, T. [1984] - Solar activity dependence of trans-equatorial ion whistler. Planet. Space Sci., 32, 955-964.

WIEDER, B. [1967] Transmission of VLF radio waves through the ionosphere. *Radio Sci.*, **2**, 595-605.

REPORT 727-3

SHORT-TERM PREDICTION OF SOLAR-INDUCED VARIATIONS OF OPERATIONAL PARAMETERS FOR IONOSPHERIC PROPAGATION

(Study Programme 27A/6)

(1978-1982-1986-1990)

1. Introduction

This Report considers the short-term prediction of solar activity and prediction of magnetic, ionospheric and radiocommunications disturbances which follow certain kinds of solar activity. It then references available short-term prediction services. The prediction of day-to-day variations in ionospheric parameters (mainly foF2 and total electron content) is considered in Report 888.

2. Solar-terrestrial relations: Background and sources

The literature in this field is mainly to be found in two independent series of publications: those of the Special Committee on Solar-Terrestrial Physics (SCOSTEP) which, in cooperation with the Committee on Space Research (COSPAR), organizes every four years symposia on the subject, and those of the International Ursigram and World Days Service (IUWDS) which has initiated a series of periodic workshops devoted more especially to techniques for predicting solar-terrestrial relationships [Simon *et al.*, 1986; Donnelly, 1979].

3. Short-term prediction of solar activity

Prediction of solar activity has three applications to short-term prediction of ionospheric parameters: firstly, as an indicator of the likelihood of solar flares causing increased D-region absorption; secondly, as an indicator of possible occurrence of those solar events and situations likely to be followed by magnetic/ionospheric disturbances, and thirdly as an indicator of short-term changes in the sun's ionizing radiation leading to variations in ionospheric critical frequencies and basic MUFs.

There is also the need, for scientific and other purposes, to recognize the active regions likely to produce proton flares, as well as to identify proton flares in their early stages.

The optical, radio and X-ray emission from the Sun is assessed each day at the IUWDS Regional Centres [IUWDS, 1973]. The observations made at and received at these centres are used in the prediction of solar activity and the associated effects on radiocommunication system performance.

Solar observations can be used to indicate, a few hours to a few days in advance, the regions on the solar disk which produce flares observed in the Hα line and the likely effects of such flares. The basic data for the predictions are solar spectro-heliograms (Hα, calcium), solar magnetograms, radio maps in millimetric and centimetric wavelengths and daily reports of the flares observed in the Hα line /Simon et al., 1969; Martres et al., 1973; Bleiweiss et al., 1977; Stasiewicz et al., 1979; Severny et al., 1979; Cook and Davies, 1979; Heckman, 1979/. Solar active regions that are likely to produce flares are marked by magnetic complexity, including high magnetic gradients and shears /Sawyer et al., 1986/.

Some of the data on Hα flares are such that one can predict the onset of a polar cap absorption event (PCA) a few tens of minutes in advance. These data are the position of the flare on the solar disk relative to the position of the sunspots, centimetric bursts, spectral radio bursts and hard X-ray bursts [Croom, 1971; Lange-Hesse and Rinnert, 1970; Tanaka and Enome, 1975; Cook and Davies, 1979; Heckman, 1979; Smart and Shea, 1979].

The prediction of short-term solar activity is largely subjective and is based usually on the behaviour of previous active regions with similar characteristics [Heckman, 1979]. Objective techniques are being developed [Hirman, *et al.*, 1980] but with limited success. Sources of information dealing with the subject of the prediction of solar activity and solar flares are given by McIntosh and Dryer [1972] , Cook and McCue [1975] and Sawyer et al. (1986).

4. Short-term prediction of magnetic and ionospheric disturbances

The short-term prediction of magnetic and ionospheric disturbances is closely related to observing those solar and geophysical phenomena that relate to these disturbances and to forwarding warnings to regional centres.

Such observations include:

- satellite and ground-based measurements of X-ray, optical, and radio signatures of significant solar flares [Heckman, 1979; Cook and Davies, 1979];
- ground-based optical and radio measurements of solar coronal holes [Heckman, 1979; Cook and Davies, 1979; Marubashi *et al.*, 1979];
- satellite and ground-based measurements of proton fluxes at energies greater than 10 MeV [Bailey, 1964; Larsen, 1979];
- measurements of inter-planetary scintillations of radio sources to identify disturbances propagating through the inter-planetary medium [Hewish, 1972; Coles *et al.*, 1974; Cronyn *et al.*, 1975];
- spacecraft measurements of solar wind plasma and magnetic field data. This specifically includes the magnitude of the southward component of the inter-planetary field and the general strength and direction of the field (either toward or away from the sun) [Akasofu *et al.*, 1973; Foster *et al.*, 1971; Svalgaard, 1975; Russell *et al.*, 1975; Tsurutani, 1979].

4.1 *Sudden ionospheric disturbances* (SID)

The enhanced flux of X-ray radiation accompanying large flares may cause sudden ionospheric disturbances (SID). Two of these solar flare effects are the immediate increase in ionization densities throughout the D region and the lowering of the base of that region. The increased ionization density results in increased absorption of radio waves, which causes short-wave fade-outs (SWF). The lowering of the layer, on the other hand, is not significant at HF, but causes sudden phase anomalies (SPA) on VLF circuits. Other immediate effects are sudden absorption of cosmic noise (SCNA), sudden enhancement of atmospherics (SEA) on very low frequencies, sudden increases in total electron content and sudden changes in field strength at long wavelength [Mitra and Goyal, 1984]. The subject has been reviewed by Larsen [1979]. A simple expression for the probability of an SWF within a 24-hour period is given by Milsom [1985].

Forecasting the quantitative aspects of the SID arising from a given flare can be done with some success using models of the D region which consider in detail the ionization changes induced by X-rays of given amplitude and spectral distribution. Once the modified D-region electron density profile has been calculated, it is a relatively straight-forward matter to determine the effects on selected communication circuits. Such methods are described by Klos and Stasiewicz [1979] and by Argo and Rothmuller [1979].

The increase in the lowest observed frequency (LOF) following a solar flare has been found to be proportional to X-ray enhancement and solar zenith angle [Rose *et al.*, 1974]. Real-time measurements of X-ray flux between 1 and 8 Å have been used to predict the duration of HF spectrum outage due to a short-wave fade-out [Argo *et al.*, 1978a]. By use of event rise characteristics, the outage time of short-wave fade events was directly related to the peak of the solar X-ray event. The decay slope was accurately depicted as having one of four exponential time constants, the chosen constant being associated with the ratio of the flux change to the rise time.

4.2 *Polar cap absorption* (PCA) and solar proton events

Solar proton events can cause polar cap absorption events (PCA) which lead to complete radiocommunications blackouts at high latitudes due to greatly increased absorption. The so-called proton flares have distinctive characteristics which allow reasonable success in forecasting their eruption and consequent terrestrial effects [Cook and Davies, 1979; Heckman, 1979; Smart and Shea, 1979].

Using observations of radio frequency solar noise and *in situ* measurements of high energy protons, it is now possible to predict:

- whether or not polar cap absorption can be expected from a particular solar flare-burst and
- the maximum absorption to be expected from a particular solar storm [Castelli and Guidice, 1976].

Cliver [1976], Akinyan *et al.*, [1979] and Akinyan and Chertok [1980] have developed methods for predicting the intensity of principal PCA events using 10.7 cm solar flux observations.

Smart and Shea [1979] have developed a procedure to generate a computerized time-intensity profile of the solar proton intensity expected at the Earth after the occurrence of a significant solar flare. The presence of type II and type IV radio bursts is a critical feature of proton acceleration [Cliver *et al.*, 1985]. The observed association between U-shaped special signatures of radio emissions and proton events probably results from the "big flare syndrome" [Kahler, 1982].

At VLF the effect may be greater than normal phase advance on navigational and positioning systems. An Omega navigational system correction model [Argo and Hill, 1976] translates high energy (E > 10MeV) proton flux measured at satellite altitudes into phase error corrections. The model is derived from measurements of Omega phase errors. The parameters of the model are: integrated proton flux (E > 10MeV), time of day and path length through the polar cap region.

4.3 *Geomagnetic storms*

Solar activity often leads to geomagnetic disturbances through the interaction of the solar wind and the Earth's magnetic field. This modifies the existing system of ionospheric and magnetospheric currents and gives rise to geomagnetic and, indirectly, ionospheric storms.

The probability of a solar flare causing a geomagnetic storm depends on the position of the flare on the solar disk and on the energy of the flare as indicated by the accompanying optical brightening, X-ray enhancement and centimetric and metric radio bursts. The magnitude of the type IV spectral radio event is also an important precursor [McNamara, 1980].

The Comprehensive Flare Index is a useful indicator of the probability that a flare will cause a geomagnetic storm [Dodson-Prince *et al.*, 1978] as is the time-integrated X-ray flux between 1 and 8 Å (a measure of flare energy) [Heckman, 1979]. The time delay between the flare and the storm is typically 2-3 days but is very difficult to forecast accurately without *in situ* satellite measurements [Cook and Davies, 1979; Heckman, 1979].

As well as geomagnetic and ionospheric storms caused by solar flares, there exists a class of storms known as recurrent storms because of their marked tendency to recur after one solar rotation (27 days). These storms are associated with features of the solar corona known as coronal holes.

Coronal holes are the source of high speed solar wind streams (HSSWS) which travel at several times the velocity of the background solar wind [Sheeley and Harvey, 1978; Nolte *et al.*, 1976]. As an HSSWS sweeps over the Earth, typically 3 to 4 days after central meridian passage of the associated coronal hole, the changes induced in the Earth's magnetosphere and ionosphere can lead to geomagnetic and ionospheric storms. These storms can last up to about 7 days. Not all HSSWS are found to produce storms, their effectiveness in this regard being related to parameters of the solar wind and interplanetary field.

Recurrent storms are a feature of the declining phase of a solar cycle, when both the coronal holes and their associated HSSWS can last up to 10 solar rotations [Bohlin, 1977]. Forecasts of recurrent storms have historically been based on a 27 day recurrence pattern, with some account being taken of active regions near the supposed coronal hole [Cook and Davies, 1979]. The reliability of these forecasts is enhanced when direct observations of the holes themselves are possible at X-ray, XUV, EUV or radio wavelengths [Timothy *et al.*, 1975; Bohlin, 1977; Neupert and Pizzo, 1974; Dulk and Sheridan, 1974]. However, the observations of most relevance are *in situ* observations of relevant solar wind parameters and their changes as the HSSWS sweeps past.

Geomagnetic storms have also been attributed to ejections from the Sun associated with sudden disappearing filaments (SDF) [Joselyn and McIntosh, 1981; McNamara and Wright, 1982]. The time delay is 4 to 5 days, and the delay is least for large filaments and for filaments close to the central meridian [Wright and McNamara, 1983]. Magnetic field variations in the solar wind associated with SDF which directly control magnetic storms can be predicted from the solar magnetic field in the region surrounding the disappearing filaments. The filament produces a cylindrical magnetic structure (called the magnetic flux rope) the axis of which has a direction corresponding to that of the filament. The magnetic field configuration of the rope is right-handed for disappearing filaments in the southern hemisphere and left-handed for filaments in the northern hemisphere of the sun [Marubashi, 1986].

Studies of large-scale heliospheric transients using the method of interplanetary scintillation of radio sources, indicate that some non-recurrent geomagnetic activity usually ascribed to solar flares, can be attributed to intermittent eruptions of high speed solar wind from coronal holes [Hewish and Bravo, 1986; Houminer and Hewish, 1988].

4.4 *Ionospheric storms*

The geomagnetic storm is often a good indication of the simultaneous existence of an ionospheric storm, i.e. of disturbances in the ionosphere which are more severe than the normal day-to-day variability.

From the point of view of communications, the most important ionospheric storm effects are those imposed on the F2 layer, which is in fact the layer most affected by storms. In terms of the maximum plasma frequency in the F2 layer, foF2, storm effects can be either an increase of foF2 (called a positive phase) or a decrease of foF2 (called a negative phase). The negative phase is the more important to the communicator because it reduces the available bandwidth. Physical mechanisms used to explain the features of ionospheric storms are discussed by Evans [1973] and Rishbeth [1975].

At mid-latitudes, a typical storm starts with a positive phase, which lasts for a few hours, and is followed by a negative phase which lasts for one or two days. However, the amplitude of each phase is a complicated function of the starting time of the storm, latitude and season, and only one type of phase may in fact occur for a given storm. Variations of ionospheric storm effects with the last three parameters have been described [Mendillo, 1973; Matuura, 1972; Mendillo and Klobuchar, 1980; Cander, 1985].

The ionospheric effects of recurrent storms seem to be essentially the same as those of flare-induced storms except that they tend to be somewhat less severe and to last longer [McNamara, 1977a, b]. A limited study of ionospheric storms associated with SDF indicates that the effects of SDF are not distinguishable from the effects of flares and HSSWS.

Changes in the basic MUF at low latitudes during magnetic storms tend to be less than the day-to-day fluctuations in foF2 observed during quiet days. The low-latitude increase in foF2 is compensated for by an accompanying increase in hmF2 so that the actual changes are not very significant [Aggarwal and Reddy, 1974].

At high latitudes there exist significant changes in both the basic MUF and the lowest usable frequency (LUF) during geomagnetic disturbances. The changes in the absorption associated with magnetic substorms display longitudinal and latitudinal variations in the region of the auroral oval [Jelly, 1970]. The use of the Auroral Electrojet index ——— is of value in estimating certain features of auroral substorm absorption [Elkins, 1972]. Verdile and Puig [1977] have studied storm effects which seem to correlate with auroral magnetic indices (AU, AL) and which appear to be due to the propagation of disturbances originating in the auroral oval.

4.5 *Practical methods for short- and medium-term forecasting*

Forecasts of the duration and extent of an ionospheric storm are mainly based on climatological models of storm effects, little success being reported in forecasting the behaviour of a particular storm [Argo *et al.*, 1978b]. Kuleshova *et al.* [1980] have however achieved some success in forecasting basic MUF changes during storms by carefully analysing past storms in terms of the presence or absence of positive and negative phases, sudden or gradual commencement geomagnetic storms, and the severity of foF2 changes.

Accurate, quantitative, circuit parameter forecasts are not possible using only monthly median predictions and the probability of magnetic disturbances [Cook and McCue, 1975]. Such forecasts, however, are useful for many users, especially if backed up by confirmation when a disturbance has begun.

The behaviour of the ionosphere during an ionospheric storm attributable to a feature or event on the Sun (flare, coronal hole, sudden disappearing filament) can be considered as a special case of the normal day-to-day variability of the ionosphere, and can be forecast in practice using the same techniques [see § 2.5 of Report 888].

5. Geomagnetic storm effects on total electron content (TEC)

The major source of variation in TEC from monthly mean conditions is due to geomagnetic activity. Since theoretical modelling capabilities are not sufficiently advanced to predict the behaviour of the TEC during magnetic storms, morphology-based prediction schemes represent the only viable method currently available. The major needs for the transionospheric propagation community pertain to the daytime period when the greatest absolute differences in TEC from monthly mean conditions occur.

Mendillo and Klobuchar [1980] have outlined the state-of-the-art of TEC prediction capabilities during magnetic storms, while Mendillo [1973] has described how one could predict whether or not a storm in progress would be expected to produce a positive phase at mid-latitudes. Mendillo finds that a geomagnetic storm sudden commencement (SC) will produce an enhancement in total electron content at mid-latitudes during the afternoon period following the SC unless there is an intervening post-midnight period with a strong depression of the geomagnetic field. Operationally, this is taken to be a depression in the field of at least 100 gammas near 0300 h (local time), and provides a limited prediction ability with a lead-time of about 12 hours.

The major uncertainty encountered in attempting to apply morphology-based corrections to TEC during magnetic storms is the requirement to predict the storm commencement time, for both sudden storm commencements and for gradual storm commencements.

The world regions where the morphologies, and therefore prediction capabilities, of TEC behaviour during magnetic storms are lacking are the low and equatorial latitude regions and the entire southern hemisphere. Correlations between ionospheric variations and various geomagnetic disturbance indices (e.g. TEC versus K_p or D_{st}) appear to be of little value in predicting the effects of magnetic storms on TEC.

6. Usefulness and reliability of short-term forecasts

Verification techniques have involved consideration of both the number of storm days for which correct forecasts were issued and the number of quiet days for which storm forecasts or false alarms were issued. Radio propagation quality figures for specific geographic areas have been prepared by the United States of America, the Federal Republic of Germany and Japan for use in forecasts and their verification.

Descriptions of different types of verification procedures are given by Heckman [1979], Marubashi *et al.* [1979], Minnis [1977] and Sawyer et al. [1986].

7. Operational short-term forecasting systems

This section lists the administrations and their organizations which currently issue short-term forecasts, including an outline of the services available. Further information on Regional Warning Centres (RWC) of the International Ursigram and World Days Service is published elsewhere [IUWDS, 1973]. Reports on current operations of most of the IUWDS-RWCs are given in Volume I of Solar-Terrestrial Predictions Proceedings [Donnelly, 1979].

7.1 *Australia*

Ionospheric Prediction Service, Department of Science, Sydney (IUWDS-RWC)

Daily operation, forecasts issued as required.

Shortwave fadeout (SWF) and magnetic disturbance in three grades of probability and three levels of intensity, with background notes on solar and geophysical activity.

Supplementary forecasts to users according to circuit path latitudes.

7.2 *France*

7.2.1 *Observatoire de Paris and Centre National d'Etudes des Télécommunications, Meudon (IUWDS-RWC)*

Closed Sundays and public holidays.

Solar activity and magnetic storm forecasts.

7.2.2 *CNET, Service des Prévisions Ionosphériques, Lannion*

Closed weekends and public holidays.

Daily and weekly forecasts of operational MUF and LUF.

7.3 *Federal Republic of Germany*

Forschungsinstitut der Deutschen Bundespost beim Fernmeldetechnischen Zentralamt (IUWDS-RWC)

Closed weekends and public holidays.

Review for past 24 hours and forecast for next 24 hours of solar and magnetic activity, foF2, and propagation conditions between the Federal Republic of Germany and five main regions.

7.4 *India*

National Physical Laboratory, New Delhi (IUWDS Associate RWC)

Closed Sundays and holidays.

Prediction for circuits within India.

7.5 *Japan*

Ministry of Posts and Telecommunications, Radio Research Laboratories, Koganei and Hiraiso Branch (IUWDS-RWC)

Daily operation.

Daily radio disturbance warnings (N = normal, U = unstable, W = disturbed) broadcast 6 times per hour by JJY.

Weekly propagation forecasts for next 7 days, issued by post.

Automated Radio Disturbance Warning Issuance System (RADWIS).

7.6 *United Kingdom*

Marconi Research Centre, Great Baddow

Closed weekends and public holidays.

Coded forecast of likely operational MUF and LUF deviations from predicted values in the European area for the next four 6-hour periods with assessment of likely quality figures. Plain language summary of likely conditions and report on past 24 hours.

7.7 *USA*

7.7.1 *National Oceanic and Atmospheric Administration, Space Environment Services Center (NOAA-SESC) Boulder*

(IUWDS-RWC and World Warning Agency).

Daily 24 hours.

Twice daily reports of solar and geophysical activity – current observation of the optical, radio and X-ray Sun, solar wind and magnetic field, and forecasts of trends in all of these. Immediate alerts of major events.

7.7.2 *United States Air Force Global Weather Center (AFGWC)*

Space environment forecasts.

7.8 *USSR*

Hydrometeorological Service, Institute of Applied Geophysics, Moscow (IUWDS-RWC)

Daily 24 hours.

Short-term predictions of ionospheric and magnetic disturbances (monthly, five-days, two-days and semi-diurnal) for five regions of the USSR (Polar, Auroral zone, European, Central Asia, Far East).

7.9 *The IUWDS Centres*

Each IUWDS-RWC issues daily a Geoalert giving the activity level to be expected in each active solar region during the forecast day and its advice on expected geomagnetic activity. The IUWDS World Warning Agency (the Boulder USA Centre) collates these advices and issues a daily WWA Geoalert based on the advice from each Centre including its own. This Geoalert is of use mainly in programming scientific investigations but it is also of use to Centres which issue disturbance forecasts of various kinds. This system has been in continuous operation since 1957 [IUWDS, 1973].

8. International cooperation

Attention is drawn to Recommendation 313 and its Annex on exchange of information for short-term forecasts and the transmission of ionospheric disturbance warnings.

REFERENCES

AGGARWAL, S., and REDDY, B. M. [1974] Effects of magnetic and solar activity on HF communications via F2 region. *Indian J. Radio and Space Phys.*, Vol. 3, **4**, 401-406.

AKASOFU, S. I., PERREAULT, P. D., YASUHARA, F. and MENG, C. I. [1973] Auroral substorms and the interplanetary magnetic field. *J. Geophys. Res.*, Vol. 78, 7490-7508.

AKINYAN, S. T. and CHERTOK, I. M. [1980] Determination of PCA values using integral parameters of solar microwave flares. *Geomag. i Aeronom.*, **20**, 192-196.

AKINYAN, S. T., CHERTOK, Z. M. and ZHULINA, E. M. [1979] Determination of PCA values from the characteristics of solar radio bursts. *STPP**, Vol. III, D27-D33.

ARGO, P. E. and HILL, J. R. [1976] Omega Navigation disturbance correction tables. Naval Electronics Laboratory Center TR 480, NTIS Accession No. AD A028 972. National Technical Information Service, Springfield, Va. 22161, USA.

ARGO, P. E., HILL, J. R. and ROTHMULLER, I. J. [1978a] X-ray flare and short-wave fade duration model. Naval Ocean Systems Center TR 255, NTIS Accession No. AD A057 284. National Technical Information Service, Springfield, Va. 22161, USA.

ARGO, P. E., HILL, J. R. and ROTHMULLER, I. J. [1978b] Magnetic substorms and ionospheric storms. Naval Ocean Systems Center TR 256, NTIS Accession No. AD A057 975. National Technical Information Service, Springfield, Va. 22161, USA.

ARGO, P. E. and ROTHMULLER, I. J. [1979] PROPHET: An application of propagation forecasting principles. *STPP*, Vol. I, 312-321.

BAILEY, D. K. [1964] Polar cap absorption. *Planet. and Space Sci.*, **12**, 495-541.

BLEIWEISS, M. P., WEFER, F. L. and KONIGES, A. E. [1977] Emission and absorption at wavelengths of 8.6 mm and 2.0 cm as determining factors of T_e and N_e in the filament. Naval Ocean Systems Center TR 136, NTIS Accession No. AD A044 559. National Technical Information Service, Springfield, Va., 22161, USA.

BOHLIN, J. D. [1977] Extreme ultraviolet observations of coronal holes. 1. Locations, sizes and evolution of coronal holes, June 1973-January 1974. *Solar Phys.*, Vol. 51, 377-398.

CANDER, L. R. [1985] A morphology-based study of ionospheric storms as seen at Grocka ionospheric station. Solar-Terrestrial Predictions: Proceedings of a Workshop at Meudon, France, June 18-22, 1984, 559, Ed. P. A. Simon, G. Heckman and M. A. Shea, published by National Oceanic and Atmospheric Administration, 325 Broadway, Boulder, CO 80303, USA, and Air Force Geophysics Laboratory; Hanscom AFB, Bedford, MA 01731, USA.

* The abbreviation STPP refers to the Solar-Terrestrial Predictions Proceedings, published in four volumes by the National Oceanic and Atmospheric Administration (NOAA), US Department of Commerce and edited by R. F. Donnelly (see [Donnelly, 1979 and 1980]).

CASTELLI, J. P. and GUIDICE, D. A. [1976] Impact of current solar radio patrol observations. *Vistas in Astron.*, **19**, 355.

CLIVER, E. W. [1976] Parent-flare emission at 2.8 GHz as a predictor of the peak absorption of polar-cap events. Naval Electronics Laboratory Center TR 2015, NTIS Accession No. AD A037 552 1761. National Technical Information Service, Springfield, Va. 22161, USA.

CLIVER, E. W., McNAMARA, L. F. and GENTILE, D. C. [July, 1985] Peak-flux-density spectra of large solar radio bursts and proton emission from flares. *J. Geophys. Res.*, Vol. 90, A7, 6251-6266.

COLES, W. A., RICKETT, B. J. and RUMSEY, V. H. [1974] Interplanetary scintillations in *Solar Wind Three*, 351-367. Ed. C. T. Russell, Institute of Geophysics and Planetary Physics, University of California, Los Angeles, Calif., USA.

COOK, F. E. and DAVIES, P. [1979] A review of the operation of the IUWDS Regional Warning Centre at the Ionospheric Prediction Service, Sydney. *STPP*, Vol. I, 229-238.

COOK, F. E. and McCUE, C. G. [1975] Solar-terrestrial relations and short-term ionospheric forecasting. *Radio and Electron. Engr.* (UK), Vol. 45, 11-30.

CRONYN, W. M., ERSKINE, F., SHAWHAN, S. D., GOTWALS, B. L. A. and ROELOF, E. C. [1975] Prediction of ionospheric effects associated with solar wind disturbances using interplanetary scintillation observations at 34.3 MHz. Proc. Symposium on the Effects of the Ionosphere on Space Systems and Communications, Naval Research Laboratory, Arlington, Va., USA.

CROOM, D. L. [1971] Forecasting the intensity of solar proton events from the time characteristics of solar microwave bursts. *Solar Phys.*, **19**, 171-185.

DODSON-PRINCE, H. W., HEDEMAN, E. R. and MOHLER, D. C. [1978] Studies of geomagnetic storms and solar flares in the years of increasing solar activities, cycles 19 and 20 (1955-1957, 1965-1968). Report AFGL-TR-78-0267, Air Force Geophysical Lab., Hanscom AFB, Mass., USA.

DONNELLY, R. F. [1979] Ed. Solar Terrestrial Predictions Proceedings:

Vol. I [1979] Prediction Group Reports. US Dept. of Commerce, US Govt. Printing Office, No. 003-023-00041-9, Washington, DC 20402.

Vol. II [1979] Working Group Reports and Reviews, US Dept. of Commerce, US Govt. Printing Office, No. 003-017-00471-6, Washington, DC 20402.

Vol. III [1980] Solar Activity Predictions. US Dept. of Commerce, US Govt. Printing Office, No. 003-017-00473-2, Washington, DC 20402.

Vol. IV [1980] Predictions of Terrestrial Effects of Solar Activity. US Dept. of Commerce, US Govt. Printing Office, No. 003-017-00479-1, Washington, DC 20402.

DULK, G. A. and SHERIDAN, K. W. [1974] The structure of the middle corona from observations at 80 and 160 MHz. *Solar Phys.*, **36**, 191-202.

ELKINS, T. J. [1972] A model of auroral substorm absorption. AFCRL Environmental Research Paper, No. 404, AFCRL-TR-72-0413. Air Force Cambridge Research Laboratories, Bedford, Mass., USA.

EVANS, J. V. [1973] The causes of storm-time increases of the F-layer at mid-latitudes. *J. Atmos. Terr. Phys.*, Vol. 35, 593-616.

FOSTER, J. C., FAIRFIELD, D. H., OGILVIE, K. W. and ROSENBERG, T. J. [1971] Relationship of interplanetary parameters and occurrence of magnetospheric substorms. *J. Geophys. Res.*, Vol. 76, 6971-6975.

HECKMAN, G. [1979] Predictions of the Space Environment Services Center. *STPP*, Vol. I, 322-349.

HEWISH, A. [1972] Observations of the solar plasma using radio scattering and scintillation methods. *Solar Wind*, Eds. C. P. Sonett *et al.*, NASA SP-308, 477-485 (and discussion, 485-493).

HEWISH, A. and BRAVO, S. [1986] - The sources of large-scale heliospheric disturbances. Solar Phys. 106, 185.

HIRMAN, J., NEIDIG, D. F., SEAGRAVES, P. M., FLOWERS, W. E. and WIBORG, P. M. [1980] The application of multivariate discriminant analysis to solar flare forecasting. *STPP*, Vol. IV, C-64 to C-75.

HOUMINER, Z. and HEWISH, A. [1988] - The solar origin of the 2-9 August 1972 events. Planet. Space Sci. 36, 301.

IUWDS (INTERNATIONAL URSIGRAM AND WORLD DAYS SERVICE) [1973] Synoptic Codes for Solar and Geophysical Data, third revised edition, IUWDS Secretariat, Boulder, Colo., USA.

JELLY, D. H. [1970] On the morphology of auroral absorption during substorms. *Can. J. Phys.*, **48**, 335-345.

JOSELYN, J. A. and McINTOSH, P. S. [1981] Disappearing solar filaments: A useful predictor of geomagnetic activity. *J. Geophys. Res.*, Vol. 86, 4555-4564.

KAHLER, S. W. [1982] The role of the big flare syndrome in correlations of solar energetic proton fluxes and microwave burst parameters. *J. Geophys. Res.*, Vol. 87, 3439-3448.

KŁOS, Z. and STASIEWICZ, K. [1979] Estimation of solar flare influence on radio circuit transmission loss. *STPP*, Vol. I, 67-71.

KULESHOVA, V. P., LAVROVA, E. V. and LYAKHOVA, L. N. [1980] Forecasting of δfoF2 variation for ionospheric disturbance. *STPP*, Vol. IV, C-37 to C-40.

LANGE-HESSE, G. and RINNERT, K. [1970] The reliability of transpolar VLF measurements as a method to forecast HF propagation disturbances. AGARD Conf. Proc. No. 49, *Ionospheric Forecasting*, Paper No. 30, Ed. V. Agy. NASA Accession No. N70-23112. National Technical Information Service, Springfield, VA 22161, USA.

LARSEN, J. R. [1979] Effects of D-region ionization on radio wave propagation. *STPP*, Vol. II, 617-654.

MARTRES, M. J., SORU-ESCAUT, I. and RAYROLE, J. [1973] Relationship between some photospheric motions and the evolution of active centres. *Solar Phys.*, **32**, 365-378.

MARUBASHI, K. [1986] - Structure of the interplanetary magnetic clouds and their solar origins, Adv. Space Res., Vol. 6, No. 6, 335-338.

MARUBASHI, K., MIYAMOTO, Y., KIDIKORO, T. and ISHII, T. [1979] Forecasts of geomagnetic activities and HF radio propagation conditions made at Hiraiso, Japan. *STPP*, Vol. I, 182-204.

MATUURA, N. [1972] Theoretical models of ionospheric storms. *Space Sci. Revs.*, **13**, 124-189.

McINTOSH, P. S. and DRYER, M. (Eds.) [1972] Solar Activity Observations and Predictions, Vol. 30, *Progress in Astronautics and Aeronautics*, MIT Press, Cambridge, Mass., USA.

McNAMARA, L. F. [1977a] Recurrent storms and their effects on HF radio communications. *Monitor-Proc.* IREE Australia, 48-55.

McNAMARA, L. F. [1977b] Ionospheric storm effects on maximum usable frequencies on circuits around Australia. Ionospheric Prediction Service, Series R reports, IPS-R35, Sydney, Australia.

McNAMARA, L. F. [1980] Geomagnetic effects of solar flares observed during 1968-1978. Ionospheric Prediction Service Series R Reports, IPS-R37, Sydney, Australia.

McNAMARA, L. F. and WRIGHT, C.S. [1982] Disappearing solar filaments and geomagnetic activity. *Nature*, Vol. 299, **5883**, 537-538.

MENDILLO, M. [1973] A study of the relationship between geomagnetic storms and ionospheric disturbances at mid-latitudes. *Planet and Space Sci.*, Vol. 21, 349-358.

MENDILLO, M. and KLOBUCHAR, J. A. [1980] A morphology based prediction scheme for the coupled latitudinal and local-time development of F-region storms. *STPP*, Vol. IV, C-15 to C-26.

MILSOM, J. D.[1986]Towards improving a short-term ionospheric forecasting service. Solar-Terrestrial Predictions: Proceedings of a Workshop at Meudon, France, June 18-22, 1984, 524, Ed. P. A. Simon, G. Heckman and M. A. Shea, published by National Oceanic and Atmospheric Administration, 325 Broadway, Boulder, CO 80303, USA, and Air Force Geophysics Laboratory; Hanscom AFB, Bedford, MA 01731, USA.

MINNIS, C. M. [1977] Ionospheric storm forecasts: Assessment of their economic value. *Telecomm. J.*, Vol. 44, 328-330.

MITRA, S. N. and GOYAL, R. K. [1984] Study of solar-terrestrial relationship through SCL. Paper presented at the "Workshop on Solar-Terrestrial Predictions", Meudon, France. 18-22 June, 1984.

NEUPERT, W. M. and PIZZO, V. [1974] Solar coronal holes as sources of recurrent geomagnetic disturbances. *J. Geophys. Res.*, Vol. 79, 3701-3709.

NOLTE, J. T., KRIEGER, A. S., TIMOTHY, A. F., GOLD, R. E., ROELOF, E. C., VAIANA, G., LAZARUS, A. J., SULLIVAN, J. D. and McINTOSH, P. S. [1976] Coronal holes as sources of solar wind. *Solar Phys.*, **46**, 303-322.

RISHBETH, H. [1975] F-region storms and thermospheric circulation. *J. Atmos. Terr. Phys.*, Vol. 37, 1055-1064.

ROSE, R. B., HILL, J. R. and BLEIWEISS, M. P. [1974] Sudden ionospheric disturbance grid. Naval Electronics Laboratory Center Tech. Rep. 1938, NTIS Accession No. A006567, National Technical Information Service, Springfield, Va. 22161, USA.

RUSSELL, C. T., BURTON, R. K. and McPHERRON, R. L. [1975] Some properties of the Svalgaard A/C index. *J. Geophys. Res.*, Vol. 80, 1349-1351.

SAWYER, C., WARWICK, J.W. and DENNETT, J.T. /1986/ - Solar flare prediction. Colorado Associated University Press, Boulder, Colorado.

SEVERNY, A. B., STEPENYAN, N. N. and STESHENKO, N. V. [1979] Soviet short-term forecasts of active region evolution and flare activity. *STPP*, Vol. I, 72-88.

SHEELEY, N. R., Jr. and HARVEY, J. W. [1978] Coronal holes, solar wind streams and geomagnetic activity during the new sunspot cycle. *Solar Phys.*, **59**, 159-178.

SIMON, P., HECKMAN, G. and SHEA, M. A. [1986] Solar-Terrestrial Predictions: Proceedings of a Workshop at Meudon, France, June 18-22, 1984, published by National Oceanic and Atmospheric Administration, 325 Broadway, Boulder, CO 80303, USA, and Air Force Geophysics Laboratory; Hanscom AFB, Bedford, MA 01731, USA.

SIMON, P., MARTRES, M. J. and LEGRAND, J. P. [1969] Flares forecasting. *Symposium on Solar Flares and Space Research*, North-Holland Publishing Co., New York, NY, USA.

SMART, D. F. and SHEA, M. A. [1979] PPS76 – A computerized "event-mode" solar proton forecasting technique. *STPP*, Vol. I, 406-427.

STASIEWICZ, K., MAKSYMIENKO, M. and JAKIMIEC, M. [1979] KAZIA – A computer system for solar-terrestrial data processing and objective prediction. *STPP*, Vol. I, 61-66.

SVALGAARD, L. [1975] An atlas of interplanetary sector structure, 1957-1974, Stanford University, Institute for Plasma Research, Report No. 629, Stanford, Calif., USA.

TANAKA, H. and ENOME, S. [1975] The microwave structure of coronal condensations and its relation to proton flares. *Solar Phys.*, **40** (1), 123-131.

TIMOTHY, A. F., KRIEGER, A. S. and VAIANA, G. S. [1975] The structure and evolution of coronal holes. *Solar Phys.*, **42**, 135-156.

TSURUTANI, B. [1979] Substorm warnings: an ISEE-3 real time data system. *EOS Trans.*, **60**, 702-703.

VERDILE, J. L. and PUIG, L. I. [1977] Propagación hacia latitudes medias de perturbaciones aurorales. Report C-30, LIARA, Laboratorio Ionosférico de la Armada, República Argentina.

WRIGHT, C. S. and McNAMARA, L. F. [1983] The relationships between disappearing solar filaments, coronal mass ejections, and geomagnetic activity. *Solar Phys.*, Vol. 87, 401-417.

REPORT 888-2 *

SHORT-TERM FORECASTING OF CRITICAL FREQUENCIES, OPERATIONAL MAXIMUM USABLE FREQUENCIES AND TOTAL ELECTRON CONTENT

(Study Programme 27C/6)

(1982-1986-1990)

1. Introduction

Daily values of foF2 are known to vary by about 15 to 20% from the monthly median value of foF2 during quiet times as well as during magnetic storms. These variations may be superimposed on slower upward or downward drifts in values over several days. It is desirable to predict all these variations for the purpose of efficient radiocommunications.

The need for forecasts of day-to-day variations of the ionosphere has been pointed out by King and Slater [1973], who show that at middle latitudes the monthly quartile range of observed daily values of foF2 at a particular place and local time is twice as great, on average, and five times as great in summer, as the error in the corresponding median value predicted by Report 340. The diagrams given by Wilkinson [1979] clearly illustrate the spread in foF2 at Australian ionospheric stations from low to high latitudes. Rush *et al.* [1974] have considered the implications of the daily variability of the F2 region to oblique HF communication circuits by simulating circuit performance using ray tracing techniques.

Forecasting the daily variations of the E and F1 regions presents little difficulty since they can be represented by monthly median values of foE and foF1 [Rush and Gibbs, 1973].

The basic method used in short-term forecasting of ionospheric parameters is extrapolation of a time series of past observations, on the assumption that the current trend will be maintained for at least the near future. Extrapolation can be done on the ionospheric parameter itself (e.g. foF2), on an index derived from ionospheric parameters or on a physical parameter known to possess a suitably high correlation with the ionospheric parameter.

Forecasts can be made with different lead-times, depending on how closely the variations in the ionosphere need to be tracked, and the sampling interval must match that lead-time. For example, if significant variations of the ionosphere occur within an hour, observations would be required every 5 to 10 minutes and forecasts made with similar lead-times.

The usefulness of, and the requirements for, a network of ground-based and satellite-borne ionospheric observations whose measurements are to be used for short-term prediction of radio propagation conditions, have been described in detail by Rush [1976]. However, it should be noted that the relatively high correlations found by Rush correspond to very disturbed days (that is, ionospheric storm days) and these same high correlations are not always obtained for days when the deviations from the median values are relatively small (McNamara and Wilkinson, 1986; Milsom, 1986).

* This Report is brought to the attention of Study Groups 3 and 8.

2. Short-term forecasting of foF2 and operational MUF

2.1 *Causes of short-term MUF variations*

Short-term variations in ionospheric conditions due to solar flares, high speed solar wind streams emanating from coronal holes and due to changes in the ionizing flux from the Sun are discussed in Report 727. In general the variations due to solar flares and coronal holes have a fairly well defined start time, can be related to the solar event causing them and can be forecast with some success.

Even under magnetically quiet conditions, the ionosphere exhibits day-to-day variations due to changes in the ionizing ultraviolet (UV) flux from the Sun and to changes in the solar wind and its interaction with the magnetosphere and ionosphere. The total effect for the latter is very complex and the complete causal chain has not been established. The former also presents unsolvable problems because the UV flux can be measured only with great difficulty.

Superimposed on these variations are variations with a time scale of the order of 10 minutes to a few hours due to travelling ionospheric disturbances (TIDs), which are in fact the ionospheric signature of gravity waves in the neutral atmosphere [Hines, 1974]. Large TIDs have been found to originate at high latitudes in association with large geomagnetic disturbances [Francis, 1975; Richmond and Roble, 1979], while smaller ones would seem to be of local meteorological origin [Bertin *et al.*, 1978].

TIDs can change foF2 by 1 or 2 MHz and introduce multiple Doppler components which result in long period fading and consequent decrease in circuit quality. However the effects of TIDs can often be removed by the use of either space or polarization diversity.

2.2 *Forecasts using solar and geophysical parameters*

Short-term forecasts of foF2 have been made by relating changes in foF2 to corresponding changes in selected geophysical variables such as the 10.7 cm solar flux and the geomagnetic index, K_p [Bennett and Friedland, 1970; Ichinose *et al.*, 1980]. The disadvantage of this type of approach is that the independent geophysical variables upon which changes in foF2 are assumed to depend must themselves first be predicted. Even if this were done successfully, only limited succes in forecasting foF2 is possible [McNamara, 1976a; Wilkinson, 1979].

The high correlation between long-term average values of the solar 10.7 cm radio flux with ionospheric parameters is well established and has led to the use of ionospheric prediction indices based on the 10.7 cm flux (Recommendation 371). Although this high correlation suggests the possibility of developing a short-term forecasting system based on a forecast of the 10.7 cm flux, days to weeks ahead, in reality the correlation between 10.7 cm flux and foF2 over short time scales is limited. This is probably because it is the solar UV flux which ionizes the ionosphere and the relationship between the two fluxes is not known on short time scales [Hall *et al.*, 1969; Hall and Hinteregger, 1970].

Some success has been reported using long-term averages of the 10.7 cm flux [McNamara, 1976a; Da Rosa *et al.*, 1973], but in general the correlation between daily values of flux and foF2 or TEC is not high enough to provide useful forecasts of the latter parameters.

Zevakina and Lavrova [1980] report a correlation between the direction of the interplanetary magnetic field (IMF) and the sense of the departure of foF2 from its median value. On days when the IMF points away from the Sun the values of foF2 at high and mid latitudes are in most cases higher than the median values, whereas on days when the IMF is towards the Sun, the values are lower. The direction of the component of the IMF at right angles to the ecliptic also affects the sense of the departures of foF2 from its median values.

These relationships between the direction of the IMF and deviations of foF2 offer some forecasting capability but measurements of the IMF are usually not available in real-time and inferences of its direction from high latitude magnetograms [Svalgaard, 1972; Fougere, 1974; Wilcox, 1972] are not always correct.

A method which combines forecasts using associated geophysical parameters and sounder information has been developed [Reilly and Daehler, 1986]. In this method, the statistical monthly median model which is typically based on either an average sunspot number or 10.7 cm solar radio flux, is adjusted to fit sounder observations on a given path, thus defining an updated solar parameter which may be used to predict HF properties for other paths.

Kiseliova and Zevakina [1984] have reported some success in relating positive disturbances in foF2 to changes in solar wind parameters, the sector structure of the IMF, and geomagnetic activity indices. A review of recent progress made by the USSR on short-term forecasting of ionospheric disturbances has been prepared by Zevakina [1986].

2.3 *Forecasts using ionospheric parameters*

A more successful approach to the short-term forecasting of foF2 or alternatively of an operational MUF on a given circuit, is a prediction scheme based directly upon immediate past observations of foF2 or operational MUF. Such prediction schemes for foF2 are described, for example, by Rush and Gibbs [1973], Lyakhova and Kostina [1973], McNamara [1976b] and Wilkinson [1979].

Rush and Gibbs [1973] used a five-day weighted mean value of foF2 to predict daily and hourly values of that parameter. The method of Lyakhova and Kostina [1973] is based on the observation that correlation coefficients between the deviations of foF2 from median values remain greater than 0.5 for up to four hours. The high correlation between hour-to-hour variations of foF2 has been discussed by Lyakhova [1960], Radinov [1963], Gautier and Zacharisen [1965] and Rush [1972].

McNamara [1976b] made predictions of foF2 at a particular location up to 3 hours ahead by projecting forward the trend in the departures of the last few hours' observations from a 15-day running median. Wilkinson [1979] on the other hand, simply projected forward in time the deviation of an observed foF2 value from the predicted monthly median value of foF2. He found this technique to be effective for lead times of up to about 3 hours.

Similar techniques have been applied to oblique circuits by Ames and Egan [1967], Ames *et al.* [1970], Krause *et al.* [1970; 1973a and b] and D'Accardi [1978].

The success of any of these forecasting schemes will depend on the particular circumstances of its intended use, especially as regards the required accuracy of the forecast and the lead-time required. Most schemes are reasonably successful in forecasting an operational MUF which is closer to the actual value than is the predicted monthly median value, but only for lead-times of the order of an hour or less.

2.4 *Forecasts using ionospheric indices*

To make short-term forecasts for circuits for which no real-time observations exist, the behaviour of the ionosphere must be inferred from such data as are available, using these observations to infer the values along the required circuit.

Numerous studies have reported correlation coefficients which illustrate the degree to which hourly deviations of ionospheric parameters at two or more locations are related [Gautier and Zacharisen, 1965; Zacharisen, 1965; Zevakina *et al.*, 1967a; Rush, 1972].

McNamara [1979] used observations at nearby ionospheric stations to determine an effective ionospheric index which was then used in conjunction with synoptic monthly median maps of foF2 to predict the value of foF2 at the reflection point of the given circuit.

Forecasts were made by projecting the index forward in time. Lead-times of 0 to 3 hours and 24 hours were considered and it was found that forecasts 24 hours ahead were in general no more inaccurate than those made 0 to 3 hours ahead. Errors in forecast values of foF2 at two mid-latitude stations were less than 10% on 50 to 70% of occasions for the periods considered. Whether or not this is an acceptable level of error would depend on its intended application.

Other, more complicated, methods based on the updating of synoptic maps of ionospheric parameters in real-time are described by Thompson and Secan [1979] and Tascione *et al.* [1979]. A forecasting scheme based on the use of daily ionospheric indices has been described by Wilkinson [1986].

In the limit of zero lead-time, the "forecast" in fact becomes a real-time assessment of the ionosphere.

2.5 *Practical schemes for short- and medium-term forecasts*

Practical schemes for short- and medium-term forecasting of the ionosphere and radio propagation conditions rely on various combinations of the three approaches described above.

Forecasts based upon ionospheric data only a few hours old, and intended to cover only the next few hours, can take account of both the day-to-day deviations from long-term predictions and those due to magnetic disturbance in progress if the magnetic disturbance is not too severe. A difficulty which still remains is that the deviations vary not only with time, but between different places at the same time so that observations near or along the particular circuit path are necessary, using either vertical- or oblique-incidence or back-scatter

techniques. Uffelman [1982] and Uffelman et al. [1982] have described a successful technique for applying oblique incidence sounder observations on one circuit to MUF forecasting on a nearby circuit. Another approach is to make forecasts for zones, within which the deviations are less than between zones, e.g. the method of Zevakina *et al.* [1967b]. Investigation of topside sounding data for forecast purposes by Piggott [1970] served to point out the spatial anomalies, including the very large differences between the northern and southern hemispheres. Advanced digital ionosonde techniques [Bibl and Reinisch, 1978] offer the possibility of identification and interpretation of complex ionospheric conditions in near real-time [Reinisch and Huang, 1982; Wright and Pitteway, 1982]. A world-wide network of such ionosondes [Wright, 1981], sounding obliquely and vertically, could provide a global forecasting system.

The Deutsche Bundespost method relies on continuous recording of 20 European and overseas radio circuits in addition to the solar activity and magnetic disturbance forecasting techniques already described. Each 24 hours, percentage deviations from predictions are examined in relation to current solar/geophysical events and in relation to conditions at the same stage of past solar rotations. Since the forecasts are intended mainly for the circuits already being monitored, the effect of spatial anomalies is avoided, and the method is then subject to the same kind of uncertainties as those already mentioned. This method has been developed from the earlier techniques described by Ochs [1970]. A prediction approach based on solar-geophysical data and on real-time field strength measurements of distant HF transmitters on 26 frequencies has been reported by Damboldt [1979]. The distinctive feature of the predictions is that they are forecast in the form of a quality figure which is related to the daily expected field strength.

Some forecasting schemes are based on particular models. For example, the model of Obayashi and Matuura, [1972] which describes the distribution of electron density variations with height, latitude and season during the main phase of a geomagnetic storm has been used by Barclay [1976].

The method of short-term forecasting described by Barclay [1976] includes comparison of hourly foF2 values from two stations in Western Europe with the corresponding predictions. Operational MUFs are then forecast as low for the next period if magnetic disturbance above a given level is current, otherwise normal, unless spot number and radio flux are significantly different from their predicted values. LUFs are forecast high in winter if magnetic activity is high, and high or low depending again on predetermined deviations in sunspot numbers and radio flux level. Instructions of this nature enable unskilled persons to make up forecasts which have some utility, especially during quiet periods.

In the USSR, statistical studies of the changes in foF2 have indicated "forbidden" time intervals for storm commencements at their ionospheric stations [USSR, 1957]. Relatively stable communications have been predicted in the USSR in the auroral zone utilizing real-time monitoring since it has been observed that strong fluctuations in foF2 do not take place over periods of 15 to 30 minutes when F2 layer reflections exist. In the United States of America the deviations of the daily foF2 from the computed monthly median have been analysed for all stations for selected months in 1958. Systematic world-wide patterns are observed in the deviations, particularly during ionospheric disturbances [Jones *et al.*, 1973]. A review of the major progress made in the USSR in short-term forecasting of ionospheric disturbances is given by Zevakina [1986].

The medium-term (one week) forecasting method used by the French Administration is based on mathematical models established by the application of the theory of systems, models and their identification [Le Roux, 1980]. These models, which take into account the geomagnetic Ak and solar Φ indices, are sufficiently effective to enable the hourly basic MUFs to be predicted weekly for various geographical regions. Messages giving percentage basic MUF deviations in relation to previously published monthly forecasts are issued each week, one week in advance. A daily forecast of the expected MUF and LUF levels for the next 24 hours, divided into six-hourly intervals, is also made for a North European zone and a European zone, based on observations at Uppsala and Lannion [Bourdila *et al.* 1984].

3. Short-term forecasting of total electron content

General methods of predicting transionospheric effects on radio waves have been reported in the Solar-Terrestrial Predictions Proceedings [Klobuchar, 1979] and are also described in Report 263, whereas the relevant ionospheric parameters are described in Report 725.

Predictions of monthly average values of total electron content (TEC) are normally derived from electron density profiles, which are constructed from models of foF2 and M(3000)F2 [Jones *et al.*, 1969; Jones and Obitts, 1970]. They therefore include the errors inherent in both these empirical models.

Comparisons of median observed TEC with predicted values at mid- and low-latitude stations [McNamara and Wilkinson, 1983; McNamara, 1984] have shown that an error of 10% is not unusual at mid-latitudes, with a 20% to 30% error often occurring at low latitudes.

Short-term variability of TEC about the monthly average values is approximately 25% r.m.s., with a nearly normal distribution [Johanson *et al.*, 1978; Soicher *et al.*, 1982]. At mid-latitudes this is several times the error in predicted median values. The plasmaspheric (or protonospheric) contribution to TEC could be assumed to be 15% of TEC during the day [Donnelly, 1979 and 1980].

3.1 *Geomagnetic storm effects on TEC*

The major source of variation in TEC from monthly mean conditions is due to geomagnetic activity associated with events on the Sun. These variations are discussed in Report 727.

3.2 *Use of near-real-time TEC measurements to improve short-term predictions*

Monthly mean time-delay values, even with corrections for average magnetic storm-induced changes in TEC, may not be sufficiently accurate for certain systems or for some classes of users of systems. They may instead require near-real-time measurements of the local ionosphere, either of foF2 or of TEC, to up-date median models. Alternatively, the use of two, widely-spaced, frequencies to actually measure and correct for the first order ionospheric time-delay error in real-time should be considered. Up-dating techniques include producing improved weekly or monthly median values to serve as a basis for predicting values for the following several hours.

Studies of adaptive techniques that use real-time observations to reduce average monthly r.m.s. errors in predictions have been conducted using foF2 data [Wilkinson, 1979] and TEC data [Donatelli and Allen, 1978, 1981; Leitinger *et al.*, 1978]. In order to appreciably reduce the residual error (about 50%) when using observations at the same location, the prediction intervals should be less than the following:

- solar maximum
  - day-time: 3 h
  - night-time: 1 h
- solar minimum
  - day-time: 1 h
  - night-time: 30 min.

The intervals for useful up-dating during solar minimum should be shorter to effect the same percentage reduction. The residual error is much less during solar minimum conditions.

3.3 *Spatial projections of near-real-time measurements*

Spatial projection of observations has been discussed in correlation studies using foF2 [Rush, 1976] and TEC [Klobuchar and Johanson, 1977; Soicher, 1978, 1979]. The work by Klobuchar and Johanson [1977] indicates a latitudinal correlation distance that is approximately one-half the longitudinal correlation distance. This must be considered with the time effects for any adaptive technique in which real-time observations are used for up-dating at a location other than that from which the observation was made. This has been examined using TEC data from mid-latitude stations [Allen *et al.*, 1977]. The increased error growth rate represents a superposition of spatial and temporal fluctuations. By reducing the space-time interval to an equivalent time interval, a usable updating interval may be estimated. A good approximation for mid-latitude stations can be made with the following equation [Klobuchar, 1979]:

$$\Delta ET = \frac{1}{15}\left[(\Delta LON)^2 + (2\Delta LAT)^2\right]^{\frac{1}{2}} + \left\{\begin{array}{c}\Delta T \\ \text{or} \\ |\Delta T - \Delta LT|\end{array}\right\} \quad (1)$$

where:

ΔLON: longitudinal separation (degrees)

ΔLAT: latitudinal separation (degrees)

ΔT: time interval between observation and up-date (hours)

ΔLT: $\Delta LON/15$ (hours)

ΔET: equivalent time interval (hours)

{}: refers to choice for east or west direction from observing to up-dating location; ΔT if W → E, $|\Delta T - \Delta LT|$ if $E \rightarrow W$

4. Forecasts of other parameters

The short-term forecasting of the operational MUF on a circuit is generally all that would be required for voice and low-speed telegraphy circuits. For medium-speed data links, other parameters such as fading periods and Doppler frequency spread become important, since these affect the error rates. While short-term forecasting of these parameters may be possible, it is generally agreed that real-time frequency management is essential for the operation of medium-speed data links [Clarke, 1979]. Sporadic E is especially important in this regard since it cannot be successfully forecast but can provide highly stable communications.

Because of the highly variable nature of the occurrence and intensity of sporadic-E ionization, predictions must be statistical in character.

Forecast possibilities of sporadic E "openings" based on measured E-region drifts were described by Harnischmacher and Rawer [1970] who described series of measurements of Es appearing day-by-day at the same local time plus one hour per day, with increased absorption at the end of such a sequence. Zevakina *et al.* [1967a] take account of seasonal Es variations in the USSR Manual.

In a study made over a solar cycle in South America, Giráldez and Mesterman [1973] have indicated that the occurrence of Es during a day depends upon the virtual height of the Es observed near sunrise.

Conditions in the magnetosphere, such as electron density and temperature, appear to be controlling factors in the basic pattern of particle dumping and electric fields and thus the most useful way of predicting auroral Es may be via satellites in operation for magnetospheric studies.

The high latitude ionosphere presents special problems because of its variability and complexity (Report 886). Besprozvannaya *et al.* [1979] suggest that the methods used for mid-latitude forecasting are unsuitable for high latitudes and that a more suitable method could be based on monitoring of large-scale features of ionization distribution that are the projections on the upper ionosphere of large-scale structural characteristics of magnetospheric plasma. This could be done using ground-based ionosondes at suitable locations or by using satellites.

Real-time assessment of the high latitude trough and its effects on communications can, for example, be made using DMSP (Defense Meteorological Satellite Programme) auroral photographs to indicate the poleward edge of the trough and then using the model of the trough described by Halcrow and Nisbet [1977].

REFERENCES

ALLEN, R. S., DONATELLI, D. E., HARTMANN, G. K. and LEITINGER, R. [1977] Adaptive mapping of mid-latitude ionosphere. Report AFGL-TR-77-0176, Air Force Geophysical Lab., Hanscom AFB, Mass., USA.

AMES, J. W. and EGAN, R. D. [1967] Digital recording and short-term prediction of oblique ionospheric propagation. *IEEE Trans. Ant. Prop.*, Vol. AP-15, 3, 382-389.

AMES, J. W., EGAN, R. D. and McGINTIE, G. F. [1970] Short-term prediction of HF communication circuit performance *Ionospheric Forecasting*. Ed. V. Agy, AGARD Conf. Proc. No. 49, Paper No. 22.

BARCLAY, L. W. [1976] An ionospheric storm model used for forecasting. AGARD Conf. Proc. 173, Radio Systems and the Ionosphere, Athens, Greece.

BENNETT, S. M. and FRIEDLAN, A. B. [1970] Prediction of daily fluctuation of the F-region plasma frequency. *Ionospheric Forecasting.* Ed. V. Agy, AGARD Conf. Proc. No. 49, Paper No. 31.

BERTIN, F., TESTUD, J., KERSLEY, L. and REES, P. R. [1978] The meteorological jet stream as a source of medium scale gravity waves in the thermosphere: an experimental study. *J. Atmos. Terr. Phys.*, Vol. 40, 1161-1184.

BESPROZVANNAYA, A. S., SHIROCHKOV, A. V. and SHOHUKA, T. I. [1979] On the approach to forecasting ionospheric problems. *STPP**, Vol. II, 528-542.

BIBL, K. and REINISCH, B. W. [1978] The universal digital ionosonde. *Radio Sci.*, Vol. 13, 519-530.

BOURDILA, A. M., FLEURY, R. and LE ROUX, Y. M. [1984] Short-term radio propagation predictions in the HF range. Paper presented at the "Workshop on Solar-Terrestrial Predictions", Meudon, France. 18-22 June, 1984.

CLARKE, R. H. [1979] Influence of ionospheric irregularities on HF skywave communications. *Abstracts of the Sydney Ionospheric Propagation Conference of May 14-17, 1979.* Eds. D. G. Cole and L. F. McNamara, Ionospheric Prediction Service Series X Reports, IPS-X9, Sydney, Australia.

D'ACCARDI, R. J. [1978] Time-series modelling and analysis of high frequency (HF) vertical and short-path oblique incidence ionospheric soundings. US Army Communications R&D Command Research and Development Tech. Rep. CORADCOM 78-7, NTIS Accession No. AD A058 630. National Technical Information Service, Springfield, Va. 22161, USA.

DAMBOLDT, T. [1979] HF short-term field strength predictions and their agreement with observations. AGARD Conf. Proc. No. 238, Vol. 1, *Operational Modelling of the Aerospace Propagation Environment.* Ed. H. Soicher. NASA Accession No. N79-18094. National Technical Information Service, Springfield, VA 22161, USA.

DA ROSA, A. V., WALDMAN, H., BENDITO, J. and GARRIOTT, O. K. [1973] Response of the ionospheric electron content to fluctuations in solar activity. *J. Atmos. Terr. Phys.*, Vol. 35, 1429-1442.

DONATELLI, D. E. and ALLEN, R. S. [1978] Temporal variability of ionospheric refraction correction. *Effect of the Ionosphere on Space and Terrestrial Systems*, 490-496. Ed. J. M. Goodman, US Govt. Printing Office, Stock No. 008-051-00069-1, Washington, DC 20402.

DONATELLI, D. E. and ALLEN, R. S. [1981] Time cells for adaptive prediction of total electron content. *Radio Sci.*, Vol. 16, 2, 261-270.

DONNELLY, R. F. Ed. Solar-Terrestrial Predictions Proceedings:

Vol. I [1979] Prediction Group Reports. US Dept. of Commerce, US Govt. Printing Office, No. 003-023-00041-9, Washington, DC 20402.

Vol. II [1979] Working Group Reports and Reviews. US Dept. of Commerce, US Govt. Printing Office, No. 003-017-00471-6, Washington, DC 20402.

Vol. III [1980] Solar Activity Predictions. US Dept. of Commerce, US Govt. Printing Office, No. 003-017-00473-2, Washington, DC 20402.

Vol. IV [1980] Predictions of Terrestrial Effects of Solar Activity. US Dept. of Commerce, US Govt. Printing Office, No. 003-017-00479-1, Washington, DC 20402.

FOUGERE, P. F. [1974] Dependence of inferred magnetic sector structure upon geomagnetic and solar activity. *J. Atmos. Terr. Phys.*, Vol. 22, 8, 1173-1184.

FRANCIS, S. [1975] Global properties of atmospheric gravity waves: A review. *J. Atmos. Terr. Phys.*, Vol. 37, 1011-1054.

GAUTIER, T. N. and ZACHARISEN, D. H. [1965] Use of space and time correlation in short-term ionospheric predictions. First IEEE Annual Communications Convention, 7-9 June, Boulder, Colo., USA, Conf. Record, 671-676.

GIRALDEZ, A. E. and MESTERMAN, I. [1973] Physical processes and guides for predicting Es (in Spanish). LIARA, Report C-21. Laboratorio Ionosférico de la Armada, República Argentina.

HALCROW, B. W. and NISBET, J. S. [1977] A model of F2 peak electron densities in the main trough of the ionosphere. *Radio Sci.* Vol. 12, 5, 815-820.

HALL, L. A., HIGGINS, J. E., CHAGNON, C. W. and HINTEREGGER, H. E. [1969] Solar cycle variation of extreme ultraviolet radiation. *J. Geophys. Res.*, Vol. 74, 4181-4183.

HALL, L. A. and HINTEREGGER, H. E. [1970] Solar radiation in the extreme ultraviolet and its variation with solar rotation. *J. Geophys. Res.*, Vol. 75, 6959-6965.

HARNISCHMACHER, E. and RAWER, K. [1970] Precursor events for possible forecasting of sporadic-E and increased absorption. *Ionospheric Forecasting.* Ed. V. Agy. AGARD Conf. Proc. No. 49, Paper No. 32.

HINES, C. O. [1974] *The Upper Atmosphere in Motion.* American Geophysical Union, Washington, DC, USA.

ICHINOSE, M., MAEDA, R. and ITO, S. [1980] Short-term prediction of maximum usable frequency for radio communications over the Japan area. *J. Radio Res. Labs.* (Japan), Vol. 27, 124, 179-185.

JOHANSON, J. M., BUONSANTO, M. J. and KLOBUCHAR, J. A. [1978] The variability of ionospheric time delay. *Effect of the Ionosphere on Space and Terrestrial Systems*, 479-485. Ed. J. M. Goodman, US Govt. Printing Office, Stock No. 008-051-00069-1, Washington, DC 20402.

* The abbreviation STPP refers to the Solar-Terrestrial Predictions Proceedings, published in four volumes by the National Oceanic and Atmospheric Administration, US Department of Commerce and edited by R. F. Donnelly (see [Donnelly, 1979 and 1980].

JONES, W. B., GALLET, R. M., LEFTIN, M. and STEWART, F. G. [1973] Analysis and representation of the daily departures of the foF2 from the monthly median. Office of Telecommunications. Report 73-12. US Dept. of Commerce. Supt. of Documents, US Govt. Printing Office, Washington, DC 20402.

JONES, W. B., GRAHAM, R. P. and LEFTIN, M. [1969] Advances in ionospheric mapping by numerical methods. ESSA Tech. Reprint ERL 107-ITS-75. US Govt. Printing Office, Washington, DC 20402.

JONES, W. B. and OBITTS, D. L. [1970] Global representation and solar cycle variation of foF2 monthly median 1954-1958. Telecomm. Res. Rep. OT/ITS/TRR3. Office of Telecommunications, Supt. of Documents, US Govt. Printing Office, Washington, DC 20402.

KING, J. W. and SLATER, A. J. [1973] Errors in predicted values of foF2 and hmF2 with the observed day-to-day variability. *Telecomm. J.*, Vol. 40, 766-770.

KISELIOVA, M. V. and ZEVAKINA, R. A. [1984] Forecasting of positive ionospheric disturbances. Paper presented at the "Workshop on Solar-Terrestrial Predictions", Meudon, France. 18-22 June, 1984.

KLOBUCHAR, J. A. [1979] Transionospheric propagation predictions. *STPP*, Vol. II, 213-245.

KLOBUCHAR, J. A. and JOHANSON, J. M. [1977] Correlation distance of mean daytime electron content. Report AFGL-TR-77-0185, DCA No. ADA 048117, Air Force Geophysical Lab., Hanscom AFB, Mass., USA.

KRAUSE, G. E., D'ACCARDI, R. J. and ROSWELL, E. L. [1970] Field test of a near-real-time ionospheric forecasting scheme (60 km). US Army Electronics Command Research and Development Tech. Rep. ECOM-3345.

KRAUSE, G. E., D'ACCARDI, R. J. and ROSWELL, E. L. [1973a] Field test of a near-real-time ionospheric forecasting scheme (200 km). US Army Electronics Command Research and Development Tech. Rep. ECOM-4144.

KRAUSE, G. E., D'ACCARDI, R. J. and ROSWELL, E. L. [1973b] Field test of a near-real-time ionospheric forecasting scheme (500 km). US Army Electronics Command Research and Development Tech. Rep. ECOM-4145.

LEITINGER, R., ALLEN, R. S., DONATELLI, D. E. and HARTMANN, G. K. [1978] Adaptive mapping of ionospheric features. *Effect of the Ionosphere on Space and Terrestrial Systems*, 530-537. Ed. J. M. Goodman, US Govt. Printing Office, Washington, DC 20402.

LE ROUX, Y. M. [1980] Prévisions ionosphériques à court terme par modélisation mathématique prédictive. *Ann. de Géophys.*, Vol. 36, 251-261.

LYAKHOVA, L. N. [1960] Short-range forecasting of the state of the ionosphere. *Trudy IZMIRAN*, 17, 240-281.

LYAKHOVA, L. N. and KOSTINA, L. I. [1973] On quantitative ionospheric forecasting. *Geomag. i Aeronom.*, Vol. 13, 1, 50-53.

McNAMARA, L. F. [1976a] The correlation of individual values of foF2 and M(3000)F2 with the solar 10.7 cm flux under magnetically quiet conditions. Ionospheric Prediction Service, Series R Reports, IPS-R30, Sydney, Australia.

McNAMARA, L. F. [1976b] Short-term forecasting of foF2. Ionospheric Prediction Service Series R Reports, IPS-R33, Sydney, Australia.

McNAMARA, L. F. [1979] The use of ionospheric indices to make real- and near-real-time predictions of foF2 around Australia. *STPP*, Vol. I, 249-258.

McNAMARA, L. F. [1984] Prediction of total electron content using international reference ionosphere. *Adv. Space Res.*, 4, 25-50.

McNAMARA, L. F. and WILKINSON, P. J. [1983] Prediction of total electron content using the international reference ionosphere. *J. Atmos. Terr. Phys.*, Vol. 45, 169-174.

McNAMARA, L.F. and WILKINSON, P.J. /1986/ - A cautionary note on the use of F2 region correlation coefficients for short-term forecasting purposes. Solar-Terrestrial Predictions: Proceedings of a Workshop at Meudon, France, June 18-22, 1984, 529, Ed. P.A. Simon, G. Heckman and M.A. Shea, published by National Oceanic and Atmospheric Administration, 325 Broadway, Boulder, CO 80303, USA, and Air Force Geophysics Laboratory, Hanscom AFB, Bedford, MA 01731, USA.

MILSOM, J.D. /1986/ - Towards improving a short-term ionospheric forecasting service. Solar-Terrestrial Predictions: Proceedings of a Workshop at Meudon, France, June 18-22, 1984, 524, Ed. P.A. Simon, G. Heckman and M.A. Shea, published by National Oceanic and Atmospheric Administration, 325 Broadway, Boulder, CO 80303, USA, and Air Force Geophysics Laboratory, Hanscom AFB, Bedford, MA 01731, USA.

OBAYASHI, T. and MATUURA, N. [1972] Theoretical model of F-region storm. *Solar-terrestrial Physics*, 1970, Part IV, 199-211.

OCHS, A. [1970] The forecasting system of the Fernmeldetechnisches Zentralamt AGARD Conf. Proc. No. 49, *Ionospheric Forecasting*, Paper No. 43. Ed. V. Agy. NASA Accession No. N70-23112. National Technical Information Service, Springfield, VA 22161, USA.

PIGGOTT, W. R. [1970] The use of satellite data for prediction purposes. AGARD Conf. Proc. No. 49, *Ionospheric Forecasting*, Paper No. 19. Ed. V. Agy. NASA Accession No. N70-23112. National Technical Information Service, Springfield, VA 22161, USA.

RADINOV, Ya. S. [1963] Autocorrelative characteristics of critical frequency and ionization-density fluctuations. *Geomag. i Aeronom.*, Vol. 3, 985-990.

REILLY, M.H., DAEHLER, M. [1986] - Sounder updates for statistical model predictions of maximum usable frequencies on HF sky wave paths. Radio Science, Vol. 21, No. 6, 1001-1008.

REINISCH, B. W. and HUANG, X. [1982] Automatic calculation of electron density profiles from digital ionograms, 3. Processing of bottomside ionograms. *Radio Sci.*, Vol. 17, 837-844.

RICHMOND, A. D. and ROBLE, R. G. [1979] Dynamic effects of aurora-generated gravity waves on the mid-latitude ionosphere. *J. Atmos. Terr. Phys.*, Vol. 41, 7-8, 841-852.

RUSH, C. M. [1972] Improvements in ionospheric forecasting capability. Report AFCRL-72-0138. Air Force Cambridge Research Lab., Bedford, Mass., USA.

RUSH, C. M. [1976] An ionospheric observation network for use in short-term propagation predictions. *Telecomm. J.*, Vol. 43, 544-548.

RUSH, C. M. and GIBBS, J. [1973] Predicting the day-to-day variability of the mid-latitude ionosphere for application to HF propagation predictions. Report AFCRL-TR-73-0335. Air Force Cambridge Research Labs., Bedford, Mass., USA, Air Force Surveys in Geophysics, No. 268.

RUSH, C. M., MILLER, D. and GIBBS, J. [1974] The relative daily variability of foF2 and hmF2 and their implications for HF radio propagation. *Radio Sci.*, Vol. 9, 749-756.

SOICHER, H. [1978] Spatial correlation of transionospheric signal time delays. *IEEE Trans. Ant. Prop.*, Vol. AP-26, 311-314.

SOICHER, H. [1979] Correlation of satellite signal time delays at widely separated locations. *IEEE Trans. Ant. Prop.*, Vol. AP-27, 888-890.

SOICHER, H., HOUMINER, Z. and SHUVAL, A. [1982] Total electron content structure in the Middle East. *Radio Sci.*, Vol. 17, 1623-1631.

SVALGAARD, L. [1972] Interplanetary magnetic-sector structure 1926-1971. *J. Geophys. Res.*, Vol. 77, 4027-4034.

TASCIONE, T. F., FLATTERY, T. W., PATTERSON, V. G., SECAN, J. A. and TAYLOR, J. W., Jr. [1979] Ionospheric modelling at Air Force Global Weather Central. *STPP*, Vol. I, 367-377.

THOMPSON, R. L. and SECAN, J. A. [1979] Geophysical forecasting at AFGWC. *STPP*, Vol. I, 350-366.

UFFELMAN, D. R. [1982] HF propagation assessment studies over paths in the Atlantic. IES 1981, *Effects of the Ionosphere on Radiowave Systems.* Eds. J. M. Goodman, F. D. Clarke and J. Aarons. US Govt. Printing Office, Washington DC 20402.

UFFELMAN, D. R., HARNISH, L. O. and GOODMAN, J. M. [1982] The application of real-time model update by oblique ionospheric sounders to frequency sharing. AGARD Conf. Proc. No.332, *Propagation Aspects of Frequency Sharing, Interference and System Diversity*, 12-1 to 12-11. Ed. H. Soicher. NASA Accession No. N83-30873. National Technical Information Service, Springfield, VA 22161, USA.

USSR [1957] Annals of the corpuscular conference of the Academy of Sciences of the USSR, Moscow (in Russian).

WILCOX, J. M. [1972] Inferring the interplanetary magnetic field by observing the polar geomagnetic field. *Rev. Geophys. Space Phys.*, Vol. 10, 1003-1014.

WILKINSON, P. J. [1979] Prediction limits for foF2. *STPP*, Vol. I, 259-278.

WILKINSON, P. J. [1986] Short-term forecasting using daily ionospheric indices. Solar-Terrestrial Predictions: Proceedings of a Workshop at Meudon, France, June 18-22, 1984, 509, Ed. P. A. Simon, G. Heckman and M. A. Shea, published by National Oceanic and Atmospheric Administration, 325 Broadway, Boulder, CO 80303, USA, and Air Force Geophysics Laboratory, Hanscom AFB, Bedford, MA 01731, USA.

WRIGHT, J. W. [1981] Global real-time ionospheric monitoring. *Effects of the Ionosphere on Radiowave Systems.* Ed. J. M. Goodman, US Govt. Printing Office, Library of Congress, Catalog No. 82-600510.

WRIGHT, J. W. and PITTEWAY, M. L. [1982] Application of dopplionograms and goniogram to atmospheric gravity wave disturbances in the ionosphere. *J. Geophys. Res.*, Vol. 87, 1719.

ZACHARISEN, D. H. [1965] Space-time correlation coefficients for use in short-term ionospheric predictions. NBS Report 8811. National Technical Information Service, Springfield, Va. 22161, USA.

ZEVAKINA, R. A. [1986] Development of short-term ionospheric predictions. A review. Solar-Terrestrial Predictions: Proceedings of a Workshop at Meudon, France, June 18-22, 1984, 519, Ed. P. A. Simon, G. Heckman and M. A. Shea, published by National Oceanic and Atmospheric Administration, 325 Broadway, Boulder, CO 80303, USA, and Air Force Geophysics Laboratory, Hanscom AFB, Bedford, MA 01731, USA.

ZEVAKINA, R. A. and LAVROVA, E. V. [1980] On the possibility of predicting variations in the F2-region parameters as a function of the IMF direction. *STPP*, Vol. IV, C-27 to C-36.

ZEVAKINA, R. A., LAVROVA, E. V. and LYAKHOVA, L. N. [1967a] Manual on short-term prediction of ionospheric geomagnetic storms and radio-propagation forecasting service. Nauka Publishing House, Moscow, USSR.

ZEVAKINA, R. A., LAVROVA, E. V. and LYAKHOVA, L. N. [1967b] *Principles for Predicting Ionospheric and Magnetic Disturbances* (in Russian). Nauka Publishing House, Moscow, USSR.

BIBLIOGRAPHY

TCHERNOV, Y. A. [1971] *Back-scatter Sounding of the Ionosphere* (in Russian). Sviaz, Moscow, USSR.

REPORT 889-2*

REAL-TIME CHANNEL EVALUATION OF HF IONOSPHERIC RADIO CIRCUITS

(Study Programme 27B/6)

(1982-1986-1990)

Contents

1 INTRODUCTION
- 1.1 Long-term prediction
- 1.2 Short-term forecasting
- 1.3 Real-time channel evaluation (RTCE)

2 FACTORS AFFECTING CHANNEL QUALITY
- 2.1 Time and frequency dispersion
  - 2.1.1 Time dispersion
  - 2.1.2 Frequency dispersion
- 2.2 External noise and interference
- 2.3 Parameters indicating channel quality

3 METHODS OF MEASURING CHANNEL QUALITY
- 3.1 Swept-frequency ionospheric sounding
  - 3.1.1 Oblique-incidence sounding
  - 3.1.2 Vertical incidence sounding
  - 3.1.3 Backscatter sounding
  - 3.1.4 Transionospheric sounding
- 3.2 Passive channel evaluation
  - 3.2.1 Frequency monitoring
  - 3.2.2 Noise and interference monitoring
- 3.3 In-Channel sounding
  - 3.3.1 Signal strength monitoring
  - 3.3.2 Signal-to-noise ratio monitoring
  - 3.3.3 Error-ratio measurement
  - 3.3.4 Pseudo-error counting
  - 3.3.5 Phase-error measurement
  - 3.3.6 Spectral broadening of CW tones
  - 3.3.7 Pulse shape
  - 3.3.8 Automatic repetition (ARQ)
  - 3.3.9 Channel estimation/equalisation

4 CURRENT TRENDS

5 CONCLUSIONS

6 REFERENCES

* This Report is brought to the attention of Study Groups 3 and 8.

1. Introduction

In order to take full advantage of the HF communications potential of the ionosphere and to overcome its inherent variability, frequency management should be implemented in three stages, namely long-term prediction, short-term forecasting and real-time channel evaluation (RTCE).

1.1 Long-term prediction

Long-term prediction of monthly median parameters is the traditional approach to frequency management and system design. Frequency planning predictions based on historical ionospheric data are made using methods such as described in Reports 252 and 894. Frequencies are selected which are aimed at the achievement of at least a 90 per cent reliability for communications at all times of day, during any season, and at all parts of the solar cycle. Engineering decisions such as transmitter power and suitable antennas are also made at this stage.

Optimum working frequencies (OWF) for a particular circuit are derived for each hour of the day, usually for a month at a time, based on empirically derived algorithms. Use of predictions in this manner continues to yield acceptable, though not necessarily high quality, communications for many purposes such as voice and telegraph transmissions.

Difficulties associated with long-term predictions include:

a) The optimum working frequencies may provide communications for only 90% of the days of the month.

b) The predictions do not take into account the effects of ionospheric storms and other short-term changes of the ionosphere.

c) The signal and noise estimates are not always accurate and signal-to-noise ratio is not necessarily a sufficient criterion for choosing frequencies for some types of communication.

d) Reliable long-term predictions of sporadic E are not available.

e) No account is taken of interference from other users.

f) Discrepancies between the observed values of foF2 and the values obtained from the CCIR maps (see Report 430) lead to errors in predicted propagation modes and maximum usable frequencies (MUF).

1.2 *Short-term forecasting*

The next stage of sophistication in communications planning is to specify which of the assigned frequencies are actually available at a given time, taking into account the short-term variability of the ionosphere. Techniques based on real-time observations of the sun, of the ionosphere and of frequencies actually being supported on a given circuit are described in Reports 727 and 888. Real-time monitoring of the ionosphere and forecasts on the time scale of minutes to days are possible, overcoming points a) and b) above. Short-term forecasting techniques at HF have not been fully tested due to lack of suitable solar monitoring systems. Rothmuller [1978] found in operational tests using solar data from the Solrad HI satellite, that HF outages due to propagation were reduced by 15% and that the duration of outages was reduced by 15 to 20%.

These techniques do not, however, indicate which of the assigned frequencies propagating at a given time would be the best to use for a given form of communication. Nor is the forecast frequency range completely accurate because of inevitable errors in the forecasting techniques.

1.3 Real-time channel evaluation (RTCE)

RTCE is the process of measuring appropriate parameters of a set of channels in real time and of employing the data thus obtained to describe quantitatively the states of those channels and hence their relative capabilities for passing a given class, or classes, of communication traffic.

RTCE is potentially capable of yielding high quality HF communications under even the most adverse propagation conditions. It is at this stage that all potentially useful assigned frequencies are examined in real time to see which is the best to use for the given communications purpose.

It is not necessary for the communicator to know what detailed, fundamental, physical principles create the distortions imposed by the ionospheric medium on a particular signal, but rather that he, or the automatic management portions of the radio system, should have access to the values of the parameters of an appropriate real-time model which describes the path behaviour adequately. Once these have been obtained, the model can be used to adapt optimally the signal format and signal processing algorithms for the associated communications link.

RTCE can be used to overcome the problems c), d), e) and f) listed in § 1.1. RTCE systems have no need to rely on synoptic models of atmospheric and man-made noise, since the systems can measure the noise at the working frequency in real time. Alternatively, the system may measure parameters more relevant to the type of signal modulation in use. They can also take advantage of sporadic-E propagation modes which often support propagation at frequencies above the basic MUF of the F layer and offer very low error ratios. Interference is taken directly into account in RTCE systems. Because of their ability to select frequencies above the predicted basic MUF, this allows use of higher frequencies which tend to suffer from lower levels of interference.

2. Factors affecting channel quality

2.1 *Time and frequency dispersion*

In general, there are two basic sources of signal distortion associated with HF paths – time dispersion and frequency dispersion. The effects of these mechanisms are presented conveniently by the "channel propagation function", an illustrative example of which is given in Fig. 1. This is a composite function showing the dispersive effects of the path on an ideal impulse in the time-domain and a single CW tone in the frequency domain.

In the example, three distinct propagation modes are shown: these may be due to reflections from different ionospheric layers and/or multiple reflections by the same layer. In practice, often both the time dispersions and the frequency dispersions of different modes are liable to overlap, particularly when F-scatter propagation, high and low-angle rays or magnetoionic splitting is involved. Any given propagation function is a valid description of the path behaviour only for a specified RF carrier frequency and over a period in which the ionosphere remains sensibly constant. It is also a function of the combined transmitting and receiving antenna directivities and gains. In the longer term, time variations of the path parameters will cause changes in the number of modes, mode amplitudes and delays, and the shape of the distributions associated with each of the modes.

Most path models employed in RTCE systems are related to the propagation function and tend to fall into either a time or frequency domain category, depending on the nature of the signals to be transmitted over the corresponding communications link.

ARCHIVES U.I.T. GENÈVE

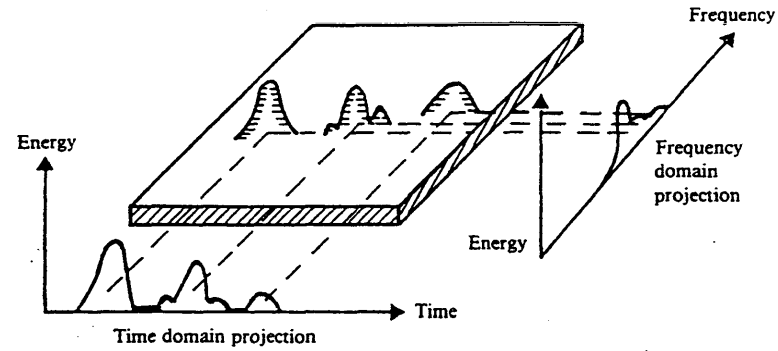


FIGURE 1 – *Typical channel propagation function [Darnell, 1975]*

2.1.1 *Time dispersion*

The time-domain projection of the propagation function yields mode amplitude and relative delays of the multi-mode propagation. Such propagation has been widely recognised as a major source of error in phase-shift-keyed (PSK) digital data transmissions, usually evident as an irreducible error-ratio, not improved by increasing signal-to-noise ratio. This effect, called intersymbol interference, arises when the spread in propagation delays becomes comparable with the duration of the digital-data frame period.

2.1.2 *Frequency dispersion*

The consequences of frequency dispersion are less widely recognized. It almost invariably accompanies time dispersion but the converse is not necessarily true – frequency dispersion can exist in the absence of significant time dispersion [Clarke and Tibble, 1978]. Frequency dispersion arises because the components of an ionospheric skywave pass through different regions of the ionosphere and therefore suffer different Doppler frequency shifts. The resultant wavefield fades at a rate dependent on the Doppler frequency spread. An analysis of a 75-baud parallel tone DPSK transmission between Townsville and Sydney demonstrated a pronounced positive correlation between the bit error ratio and the Doppler frequency spread of a CW tone within the 3 kHz passband of the data signal [Clarke, 1979].

2.2 External noise and interference

In addition to the influence of ionospheric variability and the channel propagation function on HF sky-wave channel quality, external noise and interference from other users of the radio spectrum are also important considerations. Interference is the more troublesome to the normal operations of a properly planned radio system. The characteristics of interfering signals depend on the services which they provide. Strong broadcast signals are relatively predictable in their behaviour while the multitude of short-lived narrow-band data transmissions are, individually, unpredictable. One of the major roles of RTCE techniques in modern radio systems is to adapt the signal transmission and processing algorithms so that interference is minimized while the required ionospheric channel is maintained.

Quantitative information on the character of HF interference at locations in the United Kingdom is available [Gott et al., 1982; Gibson and Arnett, 1988].

2.3 *Parameters indicating channel quality*

There are many different forms of RTCE systems and many different measurable parameters on which a particular RTCE scheme can be based. Examples of time and frequency dependent parameters which might be measured at the RTCE receiver are:

- ionospheric mode of propagation;
- spread in signal propagation time;
- signal amplitude;

- background noise intensity;
- background interference intensity;
- signal-to-noise ratio;
- signal phase stability;
- Doppler frequency spread;
- signal pulse shape;
- quality of the received signal, e.g. speech intelligibility, bit error ratio.

These measures and some other potentially useful channel assessment techniques are addressed in the following sections.

3. Methods of measuring channel quality

Several different approaches to the problem of channel assessment have been made. Some of the earliest methods involved swept-frequency ionospheric sounders and these techniques are still widely used. More recently RTCE systems have been fully integrated with the traffic carrying radio system so that more detailed appraisals for specific assigned frequencies are possible. Consequently, the role of the radio operator is changing and for a fully adaptive radio system, he no longer needs to concern himself with frequency management matters.

3.1 Swept-frequency ionospheric sounding

3.1.1 *Oblique-incidence* sounding

A widely used form of RTCE is oblique-incidence sounding of which several forms are available. The simplest type is a pulse sounder employing time and frequency synchronized transmission and reception [Darnell, 1978] (Report 249). Another form of oblique incidence ionosonde is the "chirp" or Frequency Modulated Continuous Wave (FMCW) sounder [Barry and Fenwick, 1975]. An oblique-incidence ionogram, shown in Fig. 2, can be used to avoid interference bands and to select frequency ranges where single-mode propagation exists. Alternatively, if no regions of single-mode propagation exist, a figure of merit for a particular channel might be derived by considering the relative powers of the individual propagation modes at that frequency. This method of channel evaluation is based on the premise that single-moded propagation will yield the best communications channel since this limits the total time dispersion for the path and thus limits intersymbol interference [Darnell, 1978].

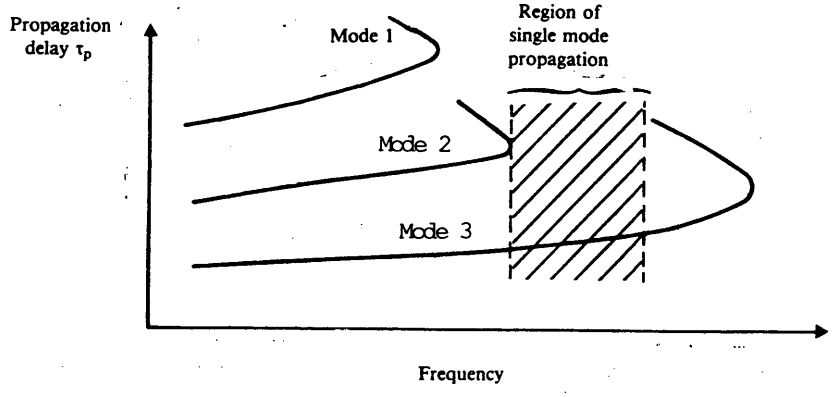


FIGURE 2 – *Idealized oblique – incidence ionogram showing the frequency range over which only one ray path is supported [Darnell, 1978]*

In Japan, a network of five ionosondes operates with coordinated starting times to provide real-time channel evaluation for common users at remote sites by means of synchronized reception [Kuriki and Takeuchi, 1986]. This system is similar to the United States' concept of a Common User Radio Transmission System (CURTS) [Probst, 1968].

From oblique incidence ionograms it is possible to identify propagation modes, to measure the maximum observed frequency (MOF) and to determine the range of frequencies over which only one propagation mode is supported. Antenna and frequency channels appropriate to the prevailing conditions can then be selected [Barry and Fenwick, 1975]. Signal-to-noise data may also be used if they are available.

Transmissions of Kineplex data between Townsville and Sydney revealed that the number of propagation modes present at a given frequency is not a good indicator of associated circuit quality [Clarke, 1979]. The best reception was obtained during summer months, when propagation was via the sporadic-E layer at frequencies above the F-layer MOF. During winter and equinoctial months, when there was usually no sporadic E, and propagation was via the F layer, no overall correlation was found between data quality and the number of modes, although on individual occasions the error-ratio was reduced by two orders of magnitude by changing from multi-moded to single-mode F-layer propagation. Data errors tended to occur in bursts which coincided with amplitude fades greater than about 20 dB [Clarke, 1979]. However this may not apply to modern systems given adequate bit interleaving and receiver dynamic range.

The lack of overall correlation between data quality and number of modes presumably resulted from the fact that even when several modes were present, the lowest order was typically at least 10 dB stronger than the other modes at the same frequency. Propagation is thus effectively single-moded even though the ionogram shows the presence of several modes.

Even when an ionogram indicates single-moded F-layer propagation, the propagation in fact may comprise multipath components which are not resolvable on the ionogram. These may be magnetoionic components, the result of ionospheric curvature caused by travelling ionospheric disturbances or still smaller scale irregularities such as spread F [Clarke and Tibble, 1978]. These effects, particularly spread F, can cause severe amplitude fading and a consequent reduction in data quality even though the oblique incidence ionogram indicates that propagation is single-moded [Clarke, 1979].

Under certain circumstances it may be possible for some propagation parameters (e.g., fading) over a point-to-point circuit to be non-reciprocal [Jull and Pettersen, 1964; Budden and Jull, 1964].

One problem associated with the use of an oblique incidence ionosonde for RTCE is that interpretation of ionograms is required to make maximum use of the instrument, whereas the ideal RTCE system would be automatic. Work is in progress to develop efficient algorithms to allow automatic interpretation of ionograms but this is a major task involving complex pattern recognition techniques. Another potential difficulty with oblique incidence sounding is any difference which might exist between the sounding system sensitivity and antenna performance and those of the main communication system.

An important consideration when oblique incidence soundings are used to infer conditions on a different path or at a different time is the spatial and temporal correlation of the chosen RTCE parameter. Goodman and Daehler [1988] discuss these factors for measurements of the maximum observed frequency.

3.1.2 *Vertical incidence sounding*

A vertical incidence sounder emits a sounding signal which can take any of the forms previously described for oblique sounding. The reflected signals are processed by a synchronized sounder receiver to produce a vertical incidence ionogram. One of the more important developments of recent years is the digital ionosonde [Bibl and Reinisch, 1978; Wright and Pitteway, 1979] and the automated scaling of ionograms that it affords [Reinisch and Huang, 1982].

The vertical incidence data can be used directly in propagation model formulation for short distance sky-wave paths, e.g., out to about 300 km. For longer paths, geometrical factors can be applied to the ionogram data to calculate oblique incidence properties. The value of such calculations depends on how closely the ionosphere at the circuit reflection points match the ionosphere at the sounder station. The extent to which an observation at one point can be used to infer ionospheric conditions at another has been discussed by Rush [1976], McNamara and Wilkinson [1986] and by Milsom [1986].

3.1.3 *Backscatter sounding*

Backscatter sounding can be carried out at a single site, with the transmitted energy radiated obliquely. The received signal is due to energy which has propagated via the ionosphere and has been scattered either from the ground or directly from the ionosphere back to the sounder following a similar ionospheric path.

Attenuation in such a system is large because of the very high losses at the ground and much higher transmitter powers are required than for vertical or oblique incidence ionosondes. The definition in the backscatter ionogram is also inferior to that in oblique or vertical incidence ionograms. However, backscatter sounding does give a good indicator of usable frequency ranges for single-hop paths. The multi-hop case tends to produce excessive path losses. The forms of modulation used for oblique incidence sounders can be employed in backscatter systems. Backscatter sounding has been reviewed by Croft [1972] and is also covered briefly in Report 726. It can be performed either at a fixed frequency or swept frequencies and is usually performed with highly directional antenna arrays both to improve received signal/noise ratios and to limit surveillance areas.

Backscatter sounding has been used operationally in the fields of HF radar and HF broadcasting. In the latter, this is accomplished by means of the addition of a virtually inaudible modulation to the broadcasts and the subsequent reception of the modulated energy via backscatter. Such soundings could help the transmitter personnel determine the optimum broadcasting band and transmitting antenna for each desired area of coverage. This process is made more accurate by deploying transponders in the coverage area so that a ground range calibration can be performed.

In practice the transmitted frequency is not generally changed in the short-term and any operational changes in real-time would be to use an alternative transmitting antenna with more appropriate beam elevation characteristics. The bulk of the energy reflected from the ionosphere is then directed on to the target area overcoming the day-to-day variations of the circuit geometry due to the corresponding variations of the ionosphere.

The significance of backscatter sounding with regard to HF radar has been described by Headrick and Skolnik [1974]. David *et al.* [1976] have studied a process for ensuring that reception conditions on a radio-channel pre-selected in accordance with an appropriate operational schedule are satisfactory. Earl and Ward [1986] have described a backscatter sounding system used in conjunction with an HF radar. This system yields real-time estimates of calibrated backscatter power levels and simultaneous estimates of HF noise intensities.

Backscatter sounding can also be used to monitor sporadic-E propagation on a circuit since the backscatter echoes have a characteristic signature [Croft, 1972]. Sporadic-E propagation modes often yield exceedingly low error ratios. However, interpretation of the backscatter echoes is a very complex problem and requires an operator, whereas frequency monitoring systems (section 3.2.1) can detect sporadic-E modes more simply by virtue of their almost-zero Doppler shift.

3.1.4 Transionospheric sounding

Transionospheric sounding is based on measurements of group delay at frequencies close to the critical frequency [Avdyushin et al., 1983]. Observations with the Intercosmos-19 and Cosmos-1809 satellites have demonstrated the following capabilities:

- measurement of bottomside electron density profiles;
- determination of the MUF;
- measurement of horizontal electron density gradients;
- measurement of the presence, location and concentration of ionospheric inhomogeneities.

This method supplements the capabilities of ground-based vertical incidence and oblique incidence sounding and satellite-based topside sounding [Danilkin, 1985]. A large volume of the ionosphere can be probed by utilizing the motion of the satellite in conjunction with simultaneous measurements from multiple ground stations. It may be used either to complement conventional sounders or in a stand-alone capacity.

3.2 Passive channel evaluation

Information on the behaviour of the ionosphere and the interference present on assigned radio channels can be collected using transmitters of opportunity and passive receiver-monitoring methods. Also channels which are unusable owing to high noise and interference levels can be logged.

3.2.1 *Frequency monitoring*

The original form of single-site RTCE is that in which the frequency band is scanned manually with a receiver in order to assess which identifiable transmissions are propagating from a given site, together with their relative qualities. The assumption of reciprocity allows an estimate of the frequency which should be used for transmission to a specified location. This procedure might now be made more comprehensive by the use of adaptive or steerable receiving antenna arrays which would enable "pencil beam" steering to be carried out in both azimuth and elevation. Such a procedure would allow non-identifiable transmissions to be included in the passive RTCE process since their positions could be computed approximately by measurements of azimuthal and vertical angles of arrival.

Darnell et al., [1988] propose a global common-user system in which agencies equipped with suitable receiving equipment will be able to acquire RTCE information at various levels of sophistication.

3.2.2 Noise and interference monitoring

Cottrell [1979] gathered noise statistics which indicated that one 3 kHz channel from ten should be adequate for an operational system during daytime. For night-time operation, when HF channel occupancy is higher, it is likely that more candidate channels will be needed to ensure that at least one is usable. The optimum channel will not vary significantly over a period of one minute.

Interference measurement to a resolution of 3 kHz can be a useful criterion for channel selection. Assessment of the availability of an ionospheric path by means of long term predictions and short term forecasting can also form part of the selection procedure. Test signals on the actual circuit of concern are a reliable means of deducing the prevailing ionospheric conditions and provide a means of conveying information about interference conditions to distant sites in a network.

Gott et al., [1983] have indicated the existence of important interference components within a 3 kHz bandwidth. Interference monitoring within a 3 kHz bandwidth is highly desirable so that it can be avoided or excised.

The above observations clearly demonstrate the benefit of passive noise and interference monitoring in RTCE.

3.3 In-channel sounding

3.3.1 Signal strength monitoring

A measure of signal strength available within a sky-wave channel is not in its own right a good indication of link quality. Trials of both high speed and 75-baud modems have eliminated this channel characteristic from the list of viable channel quality measures.

3.3.2 Signal-to-noise ratio monitoring

Signal-to-noise (including interference) ratio has been used as a link quality measure in several past systems [Probst, 1968; Stevens, 1968]. In each case the addition of this feature proved advantageous. This option appears to be a viable RTCE criterion for systems which are intended to carry low-speed data. A single channel 75-baud tone exchange link falls in this class. For medium or high speed links a measure of signal-to-noise ratio alone is probably inadequate. Under these circumstances time dispersion in the form of discrete multipath will play a critical role in determining channel quality.

In one of the most comprehensive comparisons of rival link quality measures, Humphreys and Shearman [1985] show signal-to-noise ratio to be a good choice for low-speed data links. This selection was especially valuable under high error ratio conditions.

While the time-average signal level at frequencies within a 3 kHz bandwidth will not vary significantly the same is not true of underlying interference which will often be present. Careful consideration should be given to the bandwidth in which the noise part of this ratio is measured. If potentially useful channels are first assessed in a 3 kHz bandwidth and those with a low signal-to-noise ratio discounted, then the remainder can be searched for optimum tone placements to a higher resolution. In this way the time lost in searching for a satisfactory channel can be minimized.

Devices have been developed [Darbyshire and Gott, 1986] to excise narrow-band interference within a normal 3 kHz voice channel. Similarly, the benefits of in-band tone agility have been widely discussed [Darnell, 1978, 1979; Gott and Hillam, 1979; Sloggett, 1979].

A practical RTCE system which has been developed in Canada is termed CHEC (Channel evaluation and calling) [Stevens, 1968]. This is an "in-channel" sounding system, i.e. it sounds in the frequency channels actually assigned to the user. On each of a relatively small number of channels, the CHEC base transmitter emits a signal of several seconds duration which is encoded with a selective calling code, data on the base station interference level in that channel and a CW section. At the remote receiver specified by the selective call, the base station interference level in each of the alternative channels is decoded and a measurement of signal strength made using the CW section of the transmission. Assuming reciprocity, a processor at the remote station computes the optimum channel for transmission to the base using the criterion of predicted signal-to-noise ratio at the base due to the remote transmitter. The CHEC technique yields a significant improvement in channel availability.

The original CHEC system is no longer operational. A microprocessor controlled system of the CHEC type has been developed [Chow et al., 1981; McLarnon, 1982], termed RACE (Radiotelephone with automatic channel evaluation).

3.3.3 Error-ratio measurement

The error-counting technique discussed by Darnell [1978] employs a test signal with essentially the same parameters as the traffic signal. The test signal occupies each of the assigned channels in turn and a bit error-ratio established for each channel. This technique has obvious merit in that a direct measure is made of digital-data quality. With some forms of traffic, it is possible to derive the RTCE data from the normal operating system, i.e. a channel may be evaluated while it is actually passing traffic. Darnell [1978] has described results of tests of an RTCE system based on error-counting techniques which used ten possible channels carrying two types of traffic on two European paths.

The circuit peformance using two frequencies selected during traditional frequency prediction techniques was compared with that obtained using frequency selection based on the RTCE data. The former technique was restricted to the use of one "day" and one "night" frequency. The results of the tests indicated that for the two types of traffic considered, a substantial percentage increase in circuit reliability on average about 45%, can be achieved by the RTCE rather than 2-frequency selection techniques.

3.3.4 Pseudo-error counting

A technique aimed at accelerating the accumulation of error counting has been developed which is usually referred to as "pseudo-error" counting. Rather than use a system's normal detection circuit, the operation is degraded in some way so that the final error count becomes more sensitive to flaws in the channel quality [Leon, 1973].

One method of pseudo-error generation might be implemented by relaxing the detection thresholds for the identification of digital "zeros" and "ones". Another approach is to use the margins of "soft decisions" and this too should be regarded as another form of error ratio acceleration [Darnell, 1978; Chase, 1973; Humphreys and Shearman, 1985]. McLarnon [1982] describes the use of pseudo-error ratio monitoring in the design of an automatic HF radiotelephone system.

3.3.5 Phase-error measurement

Circuit quality for tone exchange modulation links may be assessed by sampling the phase stability of a pilot tone transmitted with the communication traffic. Usually the pilot tone would lie between the "mark" and "space" frequencies. The phase of the pilot tone is sampled at a synchronous rate of approximately 100 Hz. The frequency with which the phase difference between consecutive sample phases exceeds some predetermined threshold can be used as a measure of channel integrity [Darnell, 1978; Betts and Darnell, 1975].

Betts and Darnell [1975] described an experiment to verify the theoretically derived relationships between a pilot-tone phase error ratio and the frequency-shift keying (FSK) data error ratio. A set of three trials was performed, for circuit lengths of 850, 1700 and 9800 km.

The results of all trials have confirmed the predicted relationships between FSK data error ratio and pilot-tone phase error ratio. Significant deviations occurred for less than 1% of the total duration of the recorded data. These deviations were attributable to two main causes: the first was very fast fading (greater than 1 fade/s) and the second some unusual and very intense man-made interference.

Betts and Suleiman [1979] suggest from theoretical analysis, laboratory simulation and field trials that phase-error information can be used to support any form of digital modulation. Betts and Suleiman also outline a second generation pilot-tone technique in which the multipath time delay difference between signals in a two-path multipath circuit is made. The method uses more than one pilot tone and a correlation technique to determine the structure of frequency selective fading.

A disadvantage of the phase-error method is the lengthy period of time required to evaluate a channel.

3.3.6 Spectral broadening of CW tones

Clarke [1980] describes a RTCE scheme which applies to a 2400 bit/sec Kineplex modulation format. Experiments have shown that the error ratio on such circuits shows a pronounced positive correlation with the broadening of spectral components within the data signal. A frequency management technique based on the spectral width of CW tones at each allocated frequency is under consideration. A hybrid approach has been adopted in which channels are classified on the basis of measured signal-to-noise ratio, fading statistics, and tone width. According to Clarke, ten channels can be evaluated every 5-10 minutes.

3.3.7 Pulse shape

Gott and Dutta [1979] describe a diversity combiner which adapts its combining method according to the quality of each propagation path where circuit quality is analysed depending on the regularity of the FSK signal transitions (jitter). A similar scheme can be adapted to perform frequency selection rather than diversity branch selection. Shaw et al., [1988] present a theoretical appraisal of zero-crossing filter RTCE. The technique has the advantage that channel evaluation can take place during the transmission of ordinary traffic.

Humphreys and Shearman [1985] on comparing rival circuit quality measures for low-speed HF data links identify telegraph distortion as useful but not as important as signal-to-noise ratio.

3.3.8 Automatic repetition (ARQ)

Many HF systems utilize the error-control technique called ARQ. The method is very successful and several workers have suggested that the rate at which repeat requests are made might be used to assess channel quality during the normal passage of traffic [Darnell, 1978; Elvy, 1985; Borgmann, 1988]. Others [see for example Reed and Hopkinson [1988]] use information gained from the error control code correction rate to assess link quality.

3.3.9 Channel estimation/equalization

The conventional means of transmitting data at rates of order 2400 bit/sec is multiplexing data between several separate channels in the frequency domain each carrying low-speed data. George and Halligan [1985] have described a practical "channel quality sounder" for use on such data circuits at rates of 2400 to 4800 bit/s. New HF transmission techniques are emerging which enable high-speed data to be carried on a single modulated tone. One modem using such a technique has been described by Currie and Weale [1985], but there are several others. Opinions vary over the best signal processing approach, the two general schemes are referred to as "channel estimation" [Clark, 1981] and "channel equalization". Both methods require that the receiving signal processor holds a great deal of information about the channel impulse response, or its inverse. Under these circumstances, there is clear potential for sophisticated circuit quality analyses based on overall time dispersion, proportion of energy in the dominant sky-wave mode, measured fading of individual modes, a measure of phase stability and statistical measures of "confidence" in the channel model. Pennington [1983] discusses RTCE for this class of modem.

4. Current trends

Over the past few years microcomputer and sophisticated signal processors are increasingly becoming an integrated part of radio communication systems for exploiting or mitigating electromagnetic propagation effects, and so improving their operational performance [AGARD, 1989]. RTCE circumvents the problems encountered with oblique incidence sounding techniques (see section 3.1.1). These new systems are becoming fully integrated with the traffic-carrying radio equipment. This offers considerable cost advantages compared with stand-alone systems.

With the increasing use of RTCE there is a need for equipment from various manufacturers to be compatible. This entails the standardization of protocols for the sounding process and the subsequent establishment of communication. It is likely that such protocols will need to be standardized for each application (i.e. point-to-point link protocols are likely to be different to tactical network protocols).

5. Conclusions

Given the uncertainties inherent in forecasting, RTCE can be regarded as the best available technique for choosing an operating frequency for HF communications. The allocated frequencies are tested in real time, the "best" one selected and the communications link changed accordingly. In principle any of the parameters of the link can be adjusted but at the present time practical RTCE schemes deal almost exclusively with the choice of operating frequency.

The potential advantages accruing from the use of RTCE techniques have been summarized by Darnell [1975, 1986]:

- the effect of man-made noise and interference can be measured and specified quantitatively [Darnell 1979];
- the facility for real-time, on-line measurement of propagation and interference allows the use of relatively transient propagation modes e.g. sporadic-E layer propagation;
- RTCE evaluation allows a more efficient use of the frequency spectrum by tending to select frequency channels higher than those which would be chosen via prediction techniques. Thus spectrum congestion is reduced;
- RTCE will provide a means of automatically selecting the best frequency and simultaneously indicating preferred stand-by channels;
- transmitter power can be minimized, consistent with providing an acceptable quality of received traffic;
- RTCE data can be used to adapt other parameters of a communication system optimally for the prevailing path conditions, e.g. bandwidth, data rate, modulation type, start time and duration of the transmission, signal processing algorithm at the receiver, elevation angles for antenna array beams, diversity type and adaptive equalization;
- the provision of off-line propagation analysis requirements can be eliminated for fixed link operations; however, these will still be valuable for system planning purposes.

The selection of which frequencies to evaluate should be made on the basis of long-term predictions updated by short-term forecasts. Also, with a communications network, the full range of assigned frequencies must be parcelled out according to some overall plan, in order to avoid unnecessary interference between members of the network.

REFERENCES

AGARD [1989] - Operational aids for exploiting or mitigating electromagnetic propagation effects - Conference Proceedings No. 453

AVDYUSHIN, S.I., DANILKIN, N.P., IVANOV, I.I., IPATOV, E.B., KUSHNEREVSKY, YU.V., LUKIN, D.S. and MIGULIN, V.V. [1983] - "Transionosfernoe zondirovanie na granitse radioprozrachnosti ionosfery ("Transionospheric sounding at the limit of ionospheric transparency") - Geomagnetizm i Aeronomiya, Vol. 23, No. 4, pages 567-572.

BARRY, G. H. and FENWICK, R. B. [1975] Techniques for real-time HF channel measurement and optimum data transmission. AGARD Conf. Proc. No. 173, *Radio Systems and the Ionosphere*. Ed. W. T. Blackband. NASA Accession No. N77-20302. National Technical Information Service, Springfield, VA 22161, USA.

BETTS, J. A. and DARNELL, M. [1975] Real-time HF channel estimation by phase measurements on low-level pilot tones. AGARD Conf. Proc. No. 173, *Radio Systems and the Ionosphere*, Paper 18. Ed. W. T. Blackband. NASA Accession No. N77-20302. National Technical Information Service, Springfield, VA 22161, USA.

Betts, J.A. and Suleiman, Z.A. [1979], "Real-Time Channel Estimation of Data circuits", IEE Coll Dig. 1979/48. Recent Advances in HF Communications Systems and Techniques, February.

BIBL, K. and REINISCH, B. W. [1978] The universal digital ionosonde. *Radio Sci.*, Vol. 13, 519-530.

Borgmann, D. [1988], "An HF Radio Link Processor with Adaptive Frequency Management", IEE Conf. Pub. No. 284, pp. 81-85. Fourth International Conference on HF Radio Systems and Techniques, 11-14 April, (London UK).

BUDDEN, K.G. and JULL, G.W. [1964] - Reciprocity and non-reciprocity with magnetoionic rays. Can. J. Phys., No. 42, pp. 113-130.

Chase, D. [1973], "A Combined Coding and Modulation Approach to Communications over Dispersive Channels", IEEE Trans., Vol. COM-21, No. 3, March, pp. 159-174.

CHOW, S. M., IRVINE, G. W., McLARNON, B. D. and KAYE, A.R. [1981] Communications for small communities in developing countries. Proc. Pacific Telecommunications Conference, Pacific Telecommunications Council, Honolulu, Hawaii.

Clark, A.P. [1981], "Channel Estimation for an HF Radio Link", Proc. IEE, Vol. 128, Part F, No. 1, February, pp. 33-42.

CLARKE, R. H. [1979] Influence of ionospheric irregularities on HF skywave communications. Paper presented at the Sydney Ionospheric Propagation Conference, 14-17 May. Abstract published in IPS-X10, Ionospheric Prediction Service, Sydney, Australia.

Clarke, R.H. [1980], "A Frequency Management Technique for HF Sky-Wave Communications Based on CW Soundings", Australian DOD Rpt. ERL-0138-tr, May.

CLARKE, R. H. and TIBBLE, D. V. [1978] Measurement of the elevation angles of arrival of multicomponent HF skywaves. *Proc. IEE*, Vol. 125, 1, 17-24.

Cottrell, R.A. [1979], "An Automatic HF Channel Monitoring System", IEE Colloquium Digest 1979/48. Recent Advances in HF Communications Systems and Techniques, February.

CROFT, T. [1972] Sky-wave backscatter: a means of observing our environment at great distances. *Rev. Geophys. Space Phys.*, Vol. 10, 1, 73-156.

Currie, J.C. and Weale, J.R. [1985], "Studies of Inverse Filtering and Channel Estimation Techniques for HF Serial Modems", IEE Conf. Pub. No. 245, pp. 151-155, Third International conference on HF Communications Systems and Techniques, 26-28 February, (London, UK).

DANILKIN, N.P. [1985] - "Prosvechivanie ionosfern na granitse diapazona radioprozrachnosti" ("Illumination of the ionosphere at the limit of the radiotransparency range") - Radiotekhnika, No. 9, page 3.

Darbyshire, E.P. and Gott, G.F., [1986], "Robust Data Transmission at HF", IEE Conf., Pub. No. 68, pp. 63-69, Fourth International Conference on Radio Receivers and Associated Systems, 1-4 July.

DARNELL, M. [1975] Channel estimation techniques for HF communications. AGARD Conf. Proc. No. 173, *Radio Systems and the Ionosphere*, Paper 16.

DARNELL, M. [1978] Channel evaluation techniques for dispersive communications paths. *Communications Systems and Random Process Theory*. Ed. J. K. Skwirzynski, Sijthoff and Noordhoff, The Netherlands, 425-460.

DARNELL, M. [1979] An HF data modem with in-band frequency agility. IEE Conference on Recent advances in HF communications systems and techniques.

DARNELL, M. [1986] Embedded Real-Time Channel Evaluation Techniques, AGARD LS-145, 6-1 to 6-16 (ISBN 92-835-1521-8).

Darnell, M., Hague, J. and Chan, A., [1988], "A Global Common-User System for the Provision of HF Propagation Data", AGARD EPP Symposium, Oct., Paris.

DAVID, P., GOUTELARD, C. and VAN UFFELEN, J. P. [1976] Procédé de sélection de la fréquence optimale pour une transmission de données sur canal ionosphérique. AGARD Conf. Proc. No. 173, *Radio Systems and the Ionosphere*, Paper 17. Ed. W. T. Blackband. NASA Accession No. N77-20302. National Technical Information Service, Springfield, VA 22161, USA.

EARL, G. F. and WARD, B. D. [1986] Frequency management support for remote sea-state sensing using the Jindalee sky-wave radar. *Proc. IEEE*, Special Issue – Oceanic Engineering.

Elvy, S.J. [1985], "A Design for an Automatic HF Radio System", Radio Science, Vol. 20, No. 3, May-June, pp. 261-268.

GEORGE, P. L. and HALLIGAN, R. J. [1985] Techniques for real-time HF channel evaluation in aid of optimized data transmission. Proc. URSI-IPS Conference on the Ionosphere and Radio Wave Propagation. Eds. D. G. Cole and L. F. McNamara. Technical Report TR-85-04. Ionospheric Prediction Service, Sydney, Australia.

Gibson, A.J. and Arnett, L. [1988], "New HF Spectrum Occupancy Measurements in Southern England", IEE Conf. Pub. No. 284, pp. 159-164, Fourth International conference on HF Radio Communications Systems and Techniques, 11-14 April, (London UK).

Goodman, J.M. and Daehler, M. [1988], "Use of Oblique-Incidence-Sounders in HF Frequency Management", IEE Conf. Pub. No. 284, pp. 66-70. Fourth International conference on HF Radio Communications Systems and Techniques, 11-14 April, (London UK).

Gott, G.F. and Dutta, S. [1979], "Improved diversity Combiner in HF Interference", IEE Coll. Dig. 1979/48. Recent Advances in HF Communications Systems and Techniques, February.

GOTT, G.F., DUTTA, S. and DOANY, B.E. [1983] - Analysis of HF interference with application to digital communications, Proc. IEE, 130 Part F, pp. 452-458.

Gott, G.F. and Hillam, B. [1979], "The Improvement of Slow Rate FSK by Frequency Agility and Coding", IEE Coll. Dig. 1979/48. Recent Advances in HF Communications Systems and Techniques, February 1979.

GOTT, G.F., WONG, N.F. and DUTTA, S. [1982] - "Occupancy Measurements Across the Entire HF Spectrum", AGARD Conf. Proc. No. 332. "Propagation Aspects of Frequency Sharing Interference and System Diversity", Ed. H. Soicher. NASA Accession No. N83-30873. National Technical Information Service, Springfield, VA 22161, USA.

HEADRICK, J. M. and SKOLNIK, M. I. [1974] Over the horizon radar in the HF band. *Proc. IEEE*, Vol. 62, 6, 664-673.

Humphreys, J.A. and Shearman, E.D.R. [1985], "Propagation and Performance Assessment on a Working HF Data Link", IEE Conf. Pub. No. 245, pp. 32-36. Third International conference on HF Communications Systems and Techniques, 26-28 February, (London UK).

JULL, G.W. and PETTERSEN, G.W.E. [1964] - Origin of non-reciprocity on high frequency ionospheric paths. Nature, Vol. 201, pp. 483-484.

KURIKI, I. and TAKEUCHI, T. [1986] Vertical/oblique incidence ionospheric sounding, *J. Radio Res. Labs.* (Japan), Vol. 33.

Leon, B.J. [1973], "Bit Error ratio Amplification", National Telecommunications Conf., Nov. 26-28, Atlanta GA, IEEE p. 4A/1, Vol. 1.

McLARNON, B. D. [1982] Real-time channel evaluation in an automatic HF radio telephone system. Proc. Second IEE Conference on HF Communication Systems and Techniques, London, United Kingdom.

McNAMARA, L.F. and WILKINSON, P.J. [1986] - A cautionary note on the use of F2 region correlation coefficients for short-term forecasting purposes. Solar-Terrestrial Predictions: Proceedings of a Workshop at Meudon, France, June 18-22, 1984, 529, Ed. P.A. Simon, G. Heckman and M.A. Shea, published by National Oceanic and Atmospheric Administration, 325 Broadway, Boulder, CO 80303, USA, and Air Force Geophysics Laboratory, Hanscom AFB, Bedford, MA 01731, USA.

MILSOM, J.D. [1986] - Towards improving a short-term ionospheric forecasting service. Solar-Terrestrial Predictions: Proceedings of a Workshop at Meudon, France, June 18-22, 1984, 524, Ed. P.A. Simon, G. Heckman and M.A. Shea, published by National Oceanic and Atmospheric Administration, 325 Broadway, Boulder, CO 80303, USA, and Air Force Geophysics Laboratory, Hanscom AFB, Bedford, MA 01731, USA.

Pennington, J. [1983], "HF Channel Evaluation Measurements for 2.4 kbits/sec Modems", IEEE International Conf. on Communications, pp. 1116-1120, Vol. 2, 19-22 June, Boston MA.

PROBST, S. E. [1968] The CURTS concept and current state of development. *Ionospheric Radio Communications*, 370-379. Ed. K. Folkstad, Plenum Press, New York, NY, USA.

Reed, A.P.C. and Hopkinson, J.N. [1988], "Adaptive Data Link Protocols: Design and Performance over Automated HF Skywave Links", IEE Conf. Pub. No. 284, pp. 6-11. Fourth International Conference on HF Radio Communications Systems and Techniques, 11-14 April, (London UK).

REINISCH, B.W. and HUANG, X. [1982] - Automatic calculation of electron density profiles from digital ionograms, 1. Automatic 0 and X trace identification for topside ionograms, pp. 421-434, 3. Processing of bottomside ionograms, pp. 837-844, Radio Sci., Vol. 17.

ROTHMULLER, I. J. [1978] Real-time propagation assessment: initial test results. IES 1978, *Effect of the Ionosphere on Space and Terrestrial Systems.* Ed. J. M. Goodman. US Govt. Printing Office, Washington DC 20402.

RUSH, C. M. [1976] An ionospheric observation network for use in short-term propagation conditions. *Telecomm. J.*, Vol. 43, 544-548.

Shaw, M., Honary, B. and Darnell, M. [1988], "An RTCE-assisted ARQ Transmission Scheme: Design and Performance", IEE Conf. Pub. No. 284, pp. 43-50. Fourth International Conference on HF Communications Systems and Techniques, 11-14 April.

Sloggett, C.D.R. [1979], "Improving the Reliability of HF Data Transmissions", IEE Coll. Dig. 1979/48. Recent Advances in HF Communications Systems and Techniques, February 1979.

STEVENS, R. W. [1968] The CHEC sounding system. *Ionospheric Radio Communications.* Ed. K. Folkstad, Plenum Press, New York, NY, USA.

WRIGHT, J.W. and PITTEWAY, M.L.V. [1979] - Real-time data acquisition and interpretation capabilities of the Dynasonde. 1. Data acquisition and real-time display, pp. 815-825, and 2. Determination of magnetoionic mode and echo-location using a small spaced receiving array, pp. 827-835. Radio Sci., Vol. 14, 5.

SECTION 6D: IONOSPHERIC PROPAGATION PREDICTION AT FREQUENCIES BELOW ABOUT 1.6 MHz

REPORT 575-4

METHODS FOR PREDICTING SKY-WAVE FIELD STRENGTHS AT FREQUENCIES BETWEEN 150 kHz AND 1705 kHz

(Study Programme 31D/6)

(1974-1978-1982-1986-1990)

1. Introduction

Several sky-wave field-strength prediction methods have been proposed for various parts of the world. The aim of this Report is to describe those methods which are currently in use. The analysis of the corresponding measurement results is given in Report 431.

In all these methods the field strengths are expressed by their logarithms, in dB(μV/m), in order to simplify the introduction of correction factors.

The general form of a propagation formula where the field strength is expressed in dB(μV/m) is:

$$E = E_0 + P + \Delta_A - \Delta_t \qquad (1)$$

where

E: annual median value of the field strength at a place and a given hour. The field strength E is that which would be measured by a loop antenna aligned in the vertical plane of the great circle path, at heights of less than 0.1 λ. Thus, the field strength is the resultant of the downcoming wave and the ground-reflected wave.

E_0: value of E under standard conditions. These relate to an effective monopole radiated power (e.m.r.p.) of 1 kW which is equivalent, to a cymomotive force (c.m.f.) of 300 V. E_0 also relates to a given reference time and to certain ground conductivities at the ends of the path. The reference time, and the conductivities, may be different in different prediction methods. The way of calculating E_0 is different in each method.

P: correction accounting for the power actually fed to the antenna.

Δ_A: correction accounting for the gain of the transmitting antenna in the direction of propagation considered. It covers both the horizontal and vertical radiation pattern. In the case of an omnidirectional vertical transmitting antenna the correction factor Δ_A is identical to the transmitting antenna gain factor due to vertical directivity, G_V, given in Fig. 1 of Annex I to Recommendation 435. The calculation of P and Δ_A is common to all methods.

Δ_t: correction accounting for the hour of the day. The computation of Δ_t may vary with the reference hour adopted; it may alternatively be replaced by the computation of a correction factor depending on the position of the sun at the point of the propagation path under consideration.

The field-strength value E_0 for standard conditions can be expressed in a general way by the following equation:

$$E_0 = C - f(d) + \Sigma\Delta_K \quad (2)$$

where

C: constant, different from one method to the other, which may vary, however, for a particular method with the region of the world.

$f(d)$: represents the main influence of the length of the propagation path.

$\Sigma\Delta_K$: sum of correction coefficients accounting for the influence of the frequency or of spatial or temporal parameters depending on the propagation path and the time considered.

The computation of $f(d)$ and $\Sigma\Delta_K$ varies from one method to the other, but some of the elements may be common to several methods.

The various propagation formulae based on this general model permit the computation of the sky-wave field strength and do not take account of the ground wave. In real cases, at short distances, the ground wave is important and particular caution has to be exercised to take into account both the ground wave and the sky wave.

The expression "annual median of the field strength" requires some further explanation. It is, in principle, and by agreement, the annual median (i.e. the value exceeded during 50% of the nights of a year) of the half-hourly medians of the field strength recorded every night of the year during half an hour centred on the hour considered. A smaller number of nights may, in fact, be taken into account, provided this number remains sufficiently great and the nights are regularly distributed over the course of the year (e.g. every second or third night).

2. Method using the Cairo north-south curve

2.1 *Propagation curve*

The first propagation curves used were the so-called Cairo curves (see Report 431), [ITU, 1938], one of which applies to north-south paths and the other to east-west paths. They result from measurements made in 1937 and 1938 on north-south paths on the American continent, on east-west paths across the North Atlantic and on paths between Europe and South America. The original curves were not based on annual medians of half-hourly medians, but were "quasi-peak" values of the field strength. The presentation given here, and showing curves 9 dB below the original ones, is that which was adopted by the Regional Administrative LF/MF Broadcasting Conference (Geneva, 1975) for use in the Asian part of Region 3 [ITU, 1975] and is such that predictions made on the basis of these curves are equivalent to those based on annual medians of half-hourly medians.*

When using the concept of excess polarization coupling loss (see § 2.3) which takes into account the path orientation, the field strength may be calculated on the basis of one single curve, the north-south curve (Fig. 1), by adding to the field strength so derived a correction term $-L_p$ called excess polarization coupling loss. Thus:

$$E_0 = E_c - L_p \quad (3)$$

where

E_0: the annual median value of the field strength at the reference time.

E_c: the field strength value derived from the Cairo north-south curve; it is only applicable at distances greater than 300 km.

L_p: the excess polarization coupling loss.

The curve of Fig. 1 can be approximated mathematically by

$$E_c = \frac{231}{3 + 0.001\,d} - 18 \quad (4)^{**}$$

d being the distance in km, measured along the great-circle path.

---

* Measurements made in India and Japan are described in Report 431.

** In planning exercises at medium frequencies, the EBU has made use of the following empirical formula, known as the Minne formula:

$$E_0 = \frac{396}{4 + 0.001\,d} - 40$$

The corresponding curve is situated between the north-south and east-west Cairo curves reduced to median values.

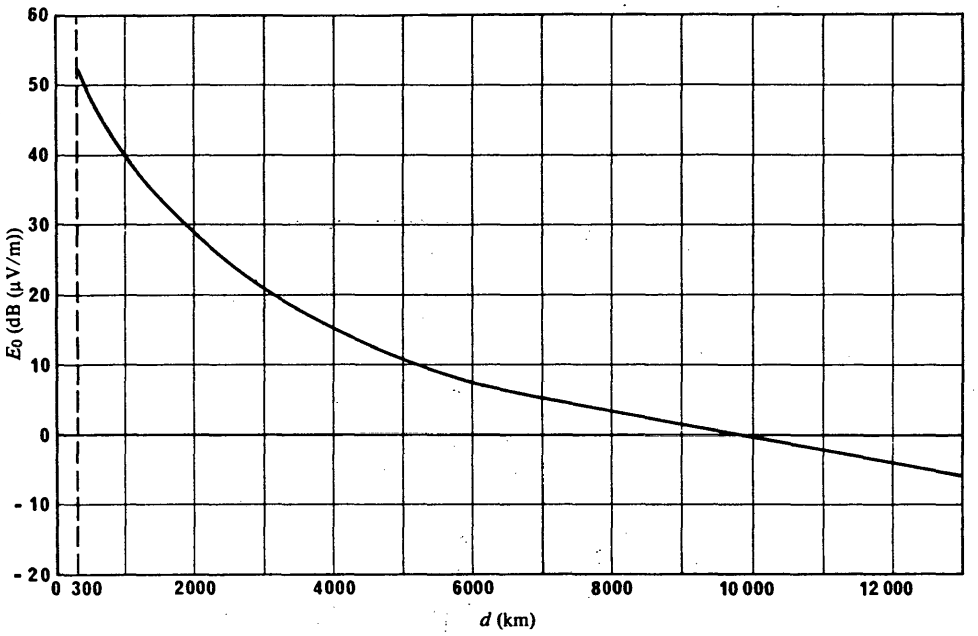


FIGURE 1 – *Annual midnight median value of sky-wave field strength of Cairo north-south curve*

2.2 *Reference time*

Midnight at the mid-point of the propagation path is taken as the reference time.

2.3 *Excess polarization coupling loss, L_p*

Polarization coupling loss occurs when waves enter the ionosphere, because some of the incident power passes into the extraordinary wave, which is then absorbed. Further loss occurs when the wave leaves the ionosphere, because it is elliptically polarized and only its vertical component normally couples with the receiving antenna.

Polarization coupling loss is small in temperate latitudes and is included as a constant in propagation curves and formulae. In tropical latitudes, however, it is larger and depends on the direction of propagation relative to that of the Earth's magnetic field. Account must therefore be taken of the amount by which the polarization coupling loss exceeds that occurring in temperate latitudes.

A detailed description of the determination of the excess polarization coupling loss, L_p, is given in § 2.4 of Annex I to Recommendation 435.

Manual calculation of this correction is tedious but there are certain simplifying factors:

- the correction is required only between dip latitudes 45° N and 45° S; hence no correction is required for terminals in Europe, North America, the U.S.S.R., southern Africa, Australia, and New Zealand;
- although it is necessary to estimate the bearing of the great circle path relative to the magnetic meridian rather than the geographic meridian, the difference between these (the magnetic declination) is small over much of the area of Africa, South America, and Asia in which the correction must be applied.

Figure 2 represents a map of Regions 1 and 3 using a conic projection based on standard parallels at 28° N and 9° S, i.e. a projection centred approximately on the magnetic dip equator in this area. Great circle paths represented, approximately, by straight lines on this map measured from any one terminal near this dip equator, have bearing errors less than 2° for distances up to 4000 km.

Although bearing errors become somewhat greater as the distance of the terminal from the dip equator increases, this is associated with a reduction in the value of the predicted polarization coupling loss and, hence, of the possible absolute error in prediction.

Superimposed on Fig. 2 is the extent of the area within which errors in coupling loss prediction exceeding 1 dB can result from neglecting magnetic declination. In the remaining part of Africa and the Asian mainland, bearings may be referred to the geographic rather than the magnetic meridian with negligible error.

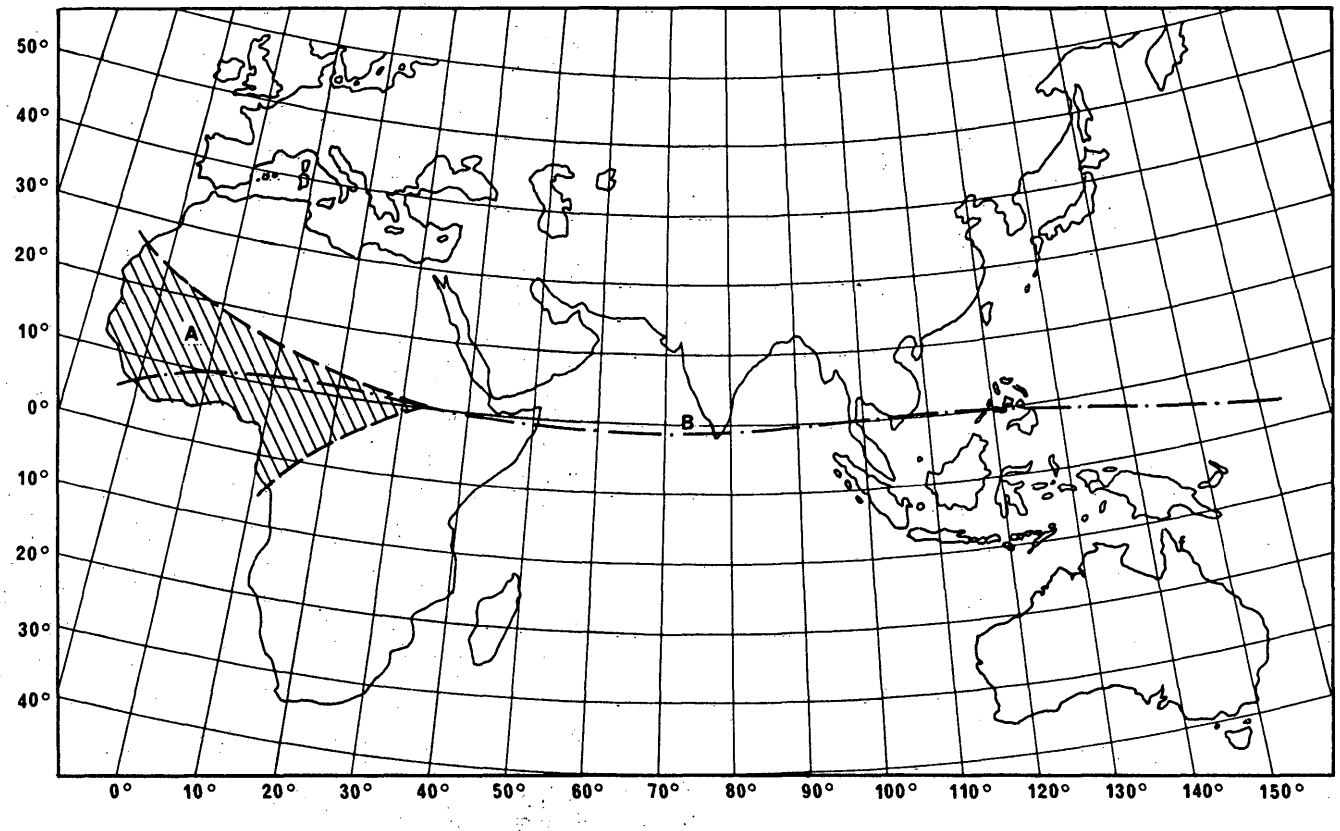


FIGURE 2 – *Map for facilitating the manual calculation of excess polarization coupling loss (§ 2.3)*

Conic projection
Standard parallels 28° N and 9° S
Central meridian 80° E

A: area within which errors in estimating excess coupling loss can exceed 1 dB if magnetic declination is neglected
B: magnetic dip equator

2.4 *Hourly loss factor, L_t*

The correction factor Δ_t that accounts for the hour of the day when applied to the Cairo N-S curve is identical to the hourly loss factor L_t described in § 2.7 of Annex I to Recommendation 435.

2.5 *Day-to-day and short-period variations of field strength*

See § 3 of Annex I to Recommendation 435.

3. Method proposed by the U.S.S.R.

The measurements described in Report 431 were carried out with the object of drawing up sky-wave propagation curves usable for field-strength prediction in the U.S.S.R. Statistical analysis of these measurements enabled an empirical formula which gives the dependence of field strength on distance and frequency to be derived, as follows [Ivanov-Kholodny and Nikolsky, 1969; Udaltsov and Shlyuger, 1972; Vilenski *et al.*, 1970; CCIR, 1970-74]:

$$E_0 = 105.3 - 20 \log d - 1.9 \times 10^{-3} f^{0.15} d - 0.24 \times 10^{-3} f^{0.4} d (\tan^2 \Phi - \tan^2 37°) \quad (5)$$

where

E_0 : the annual median field strength (dB(μV/m)) for 1 kW e.m.r.p.

d: the ground distance (km)

f: the frequency (kHz)

Φ : geomagnetic latitude at the path mid-point.

This formula is valid for values of Φ between 37° and 60°. It gives the annual median field strength for midnight local time at the path mid-point. To calculate field strengths for other times of day and for particular seasons, Fig. 2 of Report 431 should be taken into account.

4. Method proposed by Interim Working Party 6/4

Interim Working Party 6/4 was able to show that the range of validity of the U.S.S.R. method can be extended to distances less than 300 km and to regions beyond the U.S.S.R. if the following modifications are made to the U.S.S.R. formula:

- the ground distance d is replaced by the slant-propagation distance p;
- a correction for sea-gain is added where applicable;
- a correction for excess polarization-coupling loss is applied in tropical regions;
- paths longer than 3000 km are divided into two equal sections and the loss factors for the two sections calculated separately and averaged;
- the variation with geomagnetic latitude is made an asymmetrical function of Φ, to take account of differences between the northern and southern hemispheres.

Full details of the modified method are given in Annex I of Recommendation 435. The modifications have a negligible effect on field-strength predictions within the U.S.S.R. Outside the U.S.S.R., the modified formula gives results which agree reasonably well with field strengths measured in most parts of the world.

Further measurements in equatorial regions are desirable, as the accuracy of the method of Recommendation 435 has not been sufficiently tested in these areas. Field strengths in these regions appear to differ to some extent from those predicted by the method. Suitable correction factors may need to be introduced, as has been done for Australia and New Zealand.

Field strengths measured on paths between North America and Europe are 15 to 20 dB higher than those predicted by the method of Recommendation 435. Further measurements on paths near and across the auroral zone are therefore desirable.

5. Wave-hop methods

A theoretical method was proposed by the BBC [Knight, 1973]. In this method, called the wave-hop method, estimated losses due to all the ionospheric and terrestrial factors which affect a wave as it propagates from transmitter to receiver are subtracted from the field strength which would arise if losses were absent. This process is carried out for each propagation mode which is likely to make a significant contribution to the received signal, the contributions are then added on a power basis. This method is applicable for any path length and for the whole world, except for the auroral zones. Field strengths have been predicted for 152 paths in different parts of the world and compared with measured values. On paths shorter than 3000 km, 84% of the differences are less than 10 dB and on longer paths 66% of the differences come within this range.

The wave-hop method described in Report 265 can be used for paths up to 2000 km for frequencies above 150 kHz. The range of frequencies for which the method can be used can be increased by using versions of Figs. 10 and 11 of Report 265 which extend up to equivalent vertical frequencies of 1000 kHz [Belrose, 1968]. The method can be used for the calculation of both day-time and night-time sky-wave field strengths.

6. Simplification proposed by IWP 6/4 for planning purposes in Region 2

In preparation for a Regional Administrative Broadcasting Conference (535-1605 kHz, Region 2), Interim Working Party 6/4 considered available prediction methods and measurements taken in various parts of Region 2. In order to meet this requirement, some simplifications were made to the method described in the Annex I of Recommendation 435.

For planning purposes, the following formula may be used in Region 2:

$$E = V + G_S - L_p + A - 20 \log p - 10^{-3} k_R p \qquad (6)$$

The only differences between equation (6) and the basic formula (1) of the method described in Annex I to Recommendation 435 are in the following terms:

- because in Region 2 the reference hour is traditionally two hours after sunset, the constant A is 103;
- the effect of solar activity may be neglected for planning purposes (i.e., $k_R = k$);
- the basic loss factor k is given by

$$k = 0.067 \, |\Phi| + 0.2 + 3 \tan^2(\Phi + 3°) \qquad (7)$$

When $\Phi > 59°$, equation (7) should be evaluated using $\Phi = 59°$. When $\Phi < -59°$, equation (7) should be evaluated using $\Phi = -59°$. Whenever equation (7) gives a value of $k < 3$, then set $k = 3$. Figure 3 shows values of k calculated from equation (7) according to these rules.

These modifications are applicable to the MF band only.

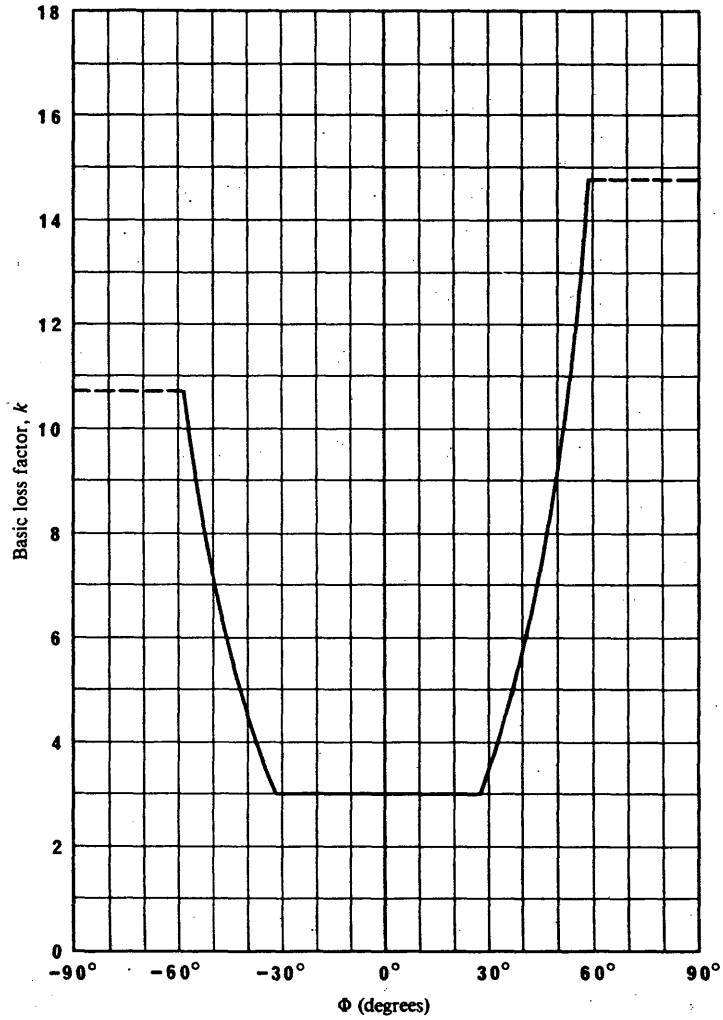


FIGURE 3 – *Basic loss factor k*

$$-59° \leq \Phi \leq 59°$$

$$k \geq 3$$

$$k = 0.067 \mid \Phi \mid + 0.2 + 3 \tan^2 (\Phi + 3°)$$

7. The Region 2 Method

The Regional Administrative MF Broadcasting Conferences (Region 2; 535 - 1 605 kHz; Buenos Aires, 1980; Rio de Janeiro, 1981) decided that the calculation of sky-wave field strength two hours after sunset shall be conducted in accordance with the provisions which follow. No account is taken in the Agreement of sea gain or of excess polarization coupling loss.

List of symbols

d: short great-circle path distance (km)

E_c: characteristic field strength, mV/m at 1 km for 1 kW

$f(\theta)$: radiation as a fraction of the value $\theta = 0$ (when $\theta = 0$, $f(\theta) = 1$)

f: frequency (kHz)

F: unadjusted annual median sky-wave field strength, in dB(μV/m)

F_c: field strength read from Fig. 7 for a characteristic field strength of 100 mV/m

P: station power (kW)

θ: elevation angle from the horizontal (degrees)

General procedure

Radiation in the horizontal plane of an omnidirectional antenna fed with 1 kW (characteristic field strength, E_c) is known either from design data or, if the actual design data are not available, from Figs. 4 and 5.

Elevation angle θ is given by

$$\theta = \arctan\left(0.00752 \cot \frac{d}{444.54}\right) - \frac{d}{444.54} \quad \text{degrees} \quad \text{for } 0° < \theta < 90° \tag{8}$$

It is assumed that the Earth is a smooth sphere with an effective radius of 6367.6 km and that reflections occur from an ionospheric height of 96.5 km.

The radiation $f(\theta)$ expressed as a fraction of the value at $\theta = 0$ at a pertinent elevation angle θ can be determined from Fig. 6.

The product $E_c f(\theta)\sqrt{P}$ is thus determined for an omnidirectional antenna. For a directional antenna, $E_c f(\theta)\sqrt{P}$ can be determined from the antenna radiation pattern. $E_c f(\theta)\sqrt{P}$ is the field strength at 1 km at the appropriate elevation angle and azimuth.

The unadjusted sky-wave field strength F is given by:

$$F = F_c + 20 \log \frac{E_c f(\theta)\sqrt{P}}{100} \quad \text{dB}(\mu\text{V/m}) \tag{9}$$

where F_c is the direct reading from the field strength curve in Fig. 7.

Note. – Values of F_c in Fig. 7 ——————are normalized to 100 mV/m at 1 km corresponding to an effective monopole radiated power (e.m.r.p.) of −9.5 dB(kW).

For distances greater than 4250 km, it should be noted that F_c can be expressed by:

$$F_c = \frac{231}{3 + d/1000} - 35.5 \quad \text{dB}(\mu\text{V/m}) \tag{10}$$

The Regional Administrative Radio Conference to Establish a Plan for the Broadcast Service in the Band 1605-1705 kHz in Region 2 (Geneva, 1986; Rio de Janeiro, 1988) adopted this method for intra-regional use with one modification. The modification, which applies to the band 1605-1705 kHz only, states that if the distance, d, is less than 200 km, F_c is evaluated for d=200 km. However, the actual value of d is to be used in determining angle of departure.

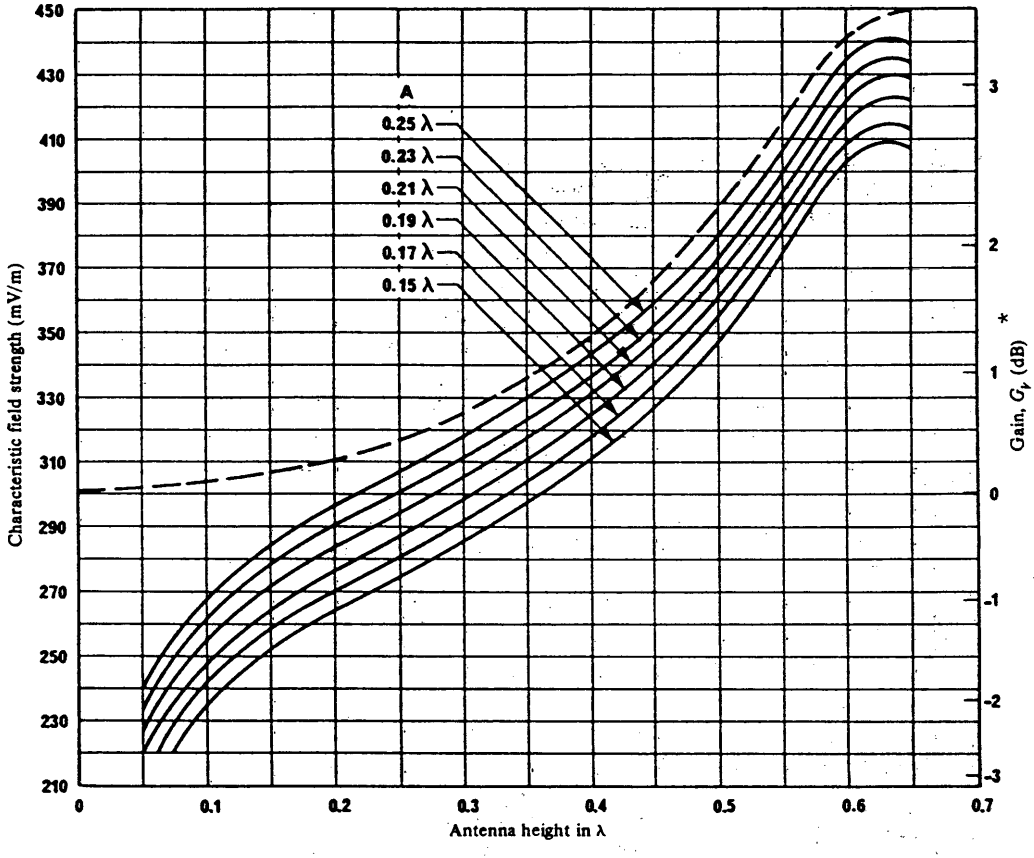


FIGURE 4 – *Characteristic field strengths for simple vertical antennas, using 120-radial ground systems*

A: radius of ground system

——— Real antenna correctly designed

– – – Ideal antenna on a perfectly conducting ground

*Gain is relative to a short vertical monopole on the surface of a perfectly conducting ground.

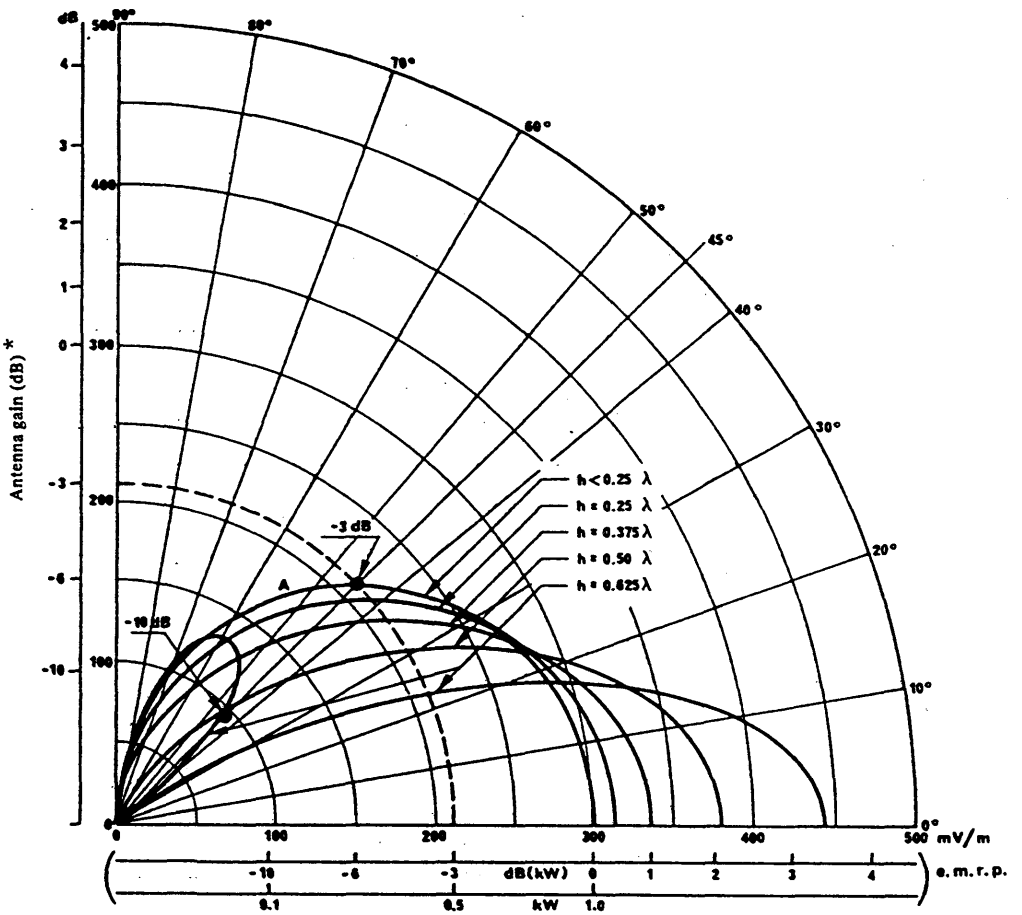


FIGURE 5 – *Effective monopole radiated power (e.m.r.p.) and field strength at a distance of 1 km as a function of elevation angle, for different heights of vertical antennas assuming a transmitter power of 1 kW*

A: Short vertical antenna

*Gain is relative to a short vertical monopole on the surface of a perfectly conducting ground.

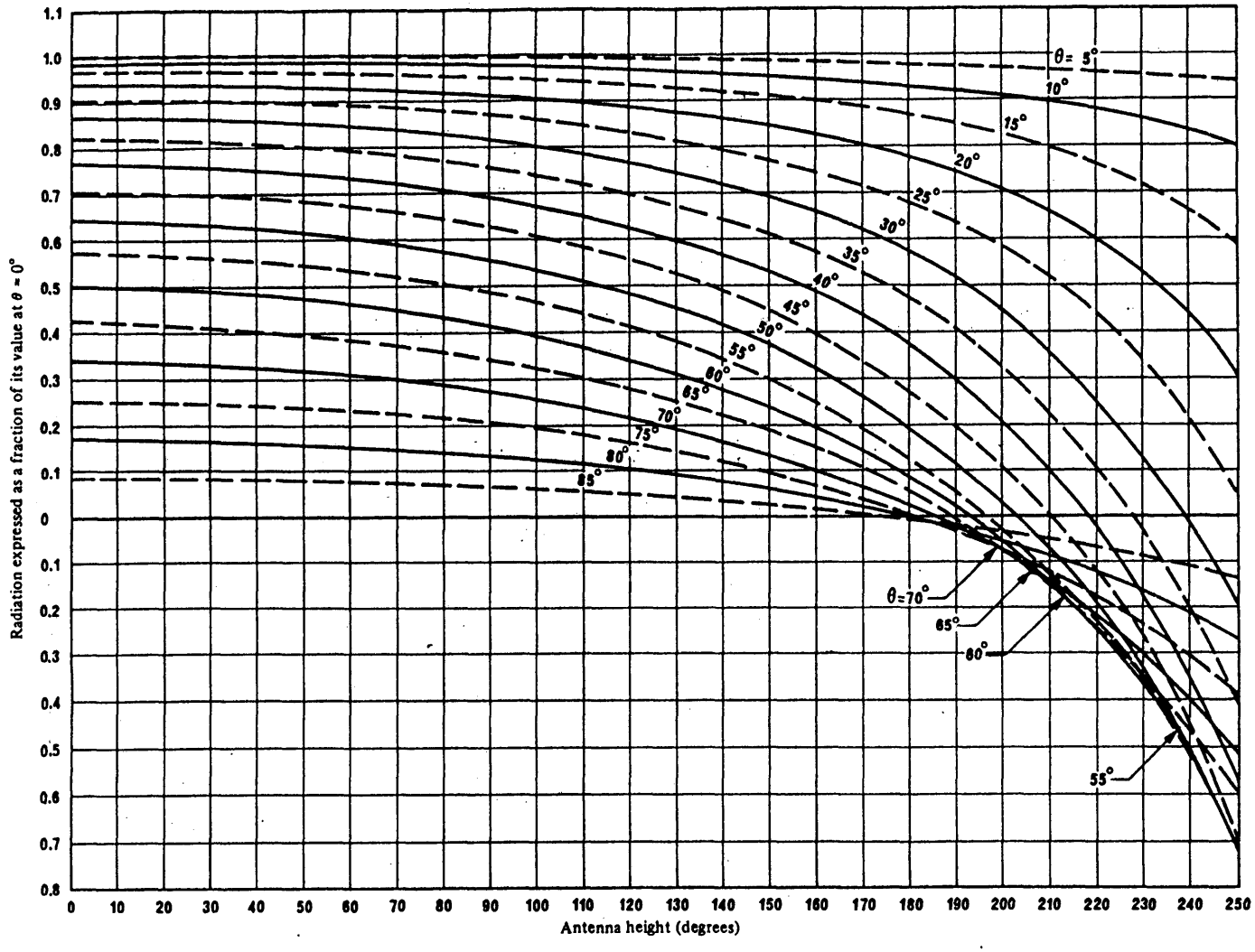


FIGURE 6 – *Vertical plane radiation of simple vertical antennas as a function of electrical tower height for various values of elevation angle (θ)*

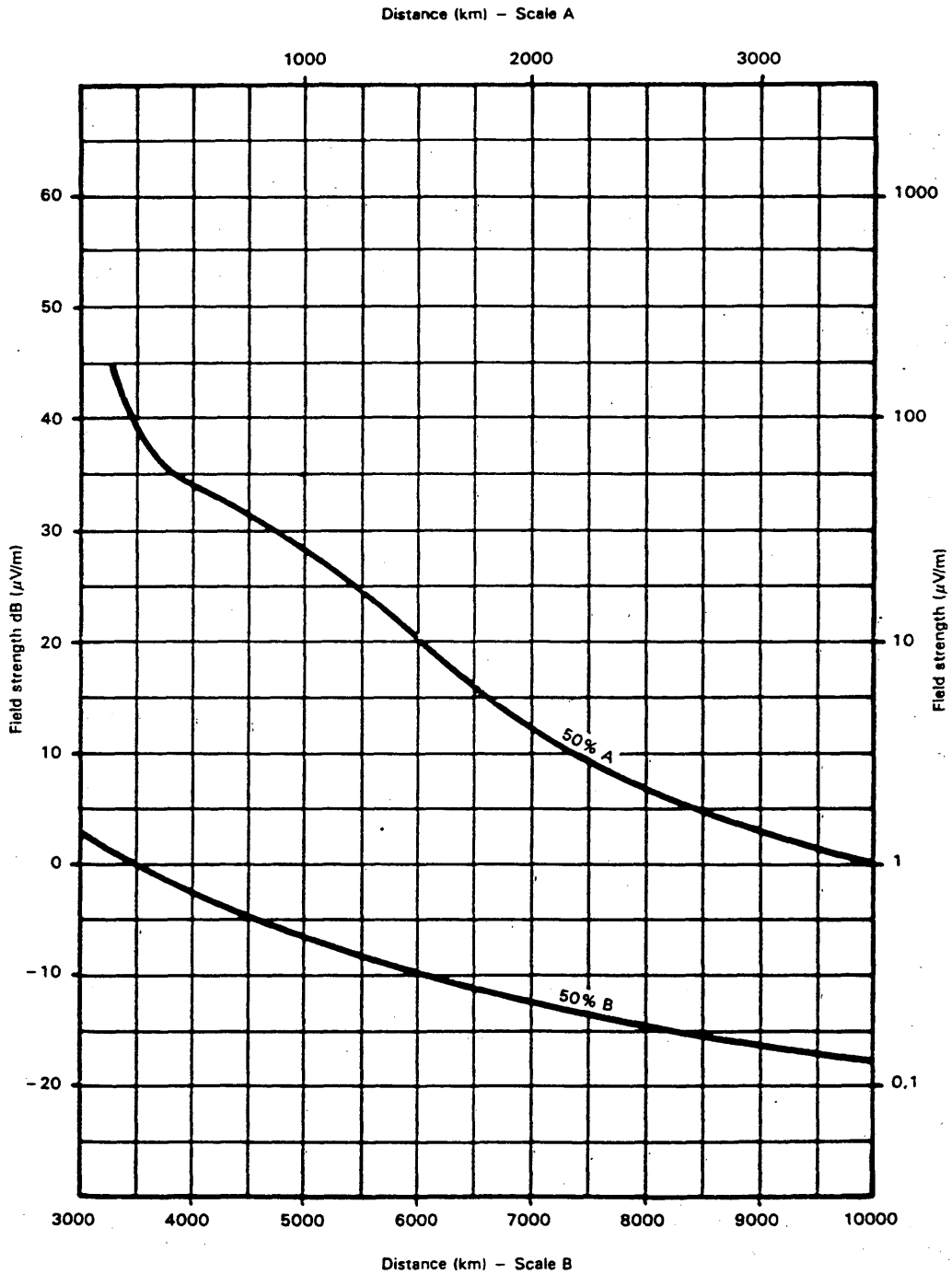


FIGURE 7– *Skywave field strength vs distance for a characteristic field strength of 100 mV/m*

8. Considerations related to the band 1605-1705 kHz

Study Group 6 at its Interim Meeting in August-September, 1983 decided (Decision 57) to reactivate Interim Working Party 6/4 to consider sky-wave propagation matters related to the First Session of the Regional Administrative Radio Conference to establish a plan ——— for the Broadcasting Service in the Band 1605-1705 kHz in Region 2, Geneva, 1986. The resulting studies concluded, inter alia that:

Based on the latest study on frequency dependence, the Region 2 method for calculating night-time sky-wave field strengths in the band 535-1605 kHz as described in ——— § 7, ——— can be extended to 1705 kHz without introducing significant additional errors. If administrations in Region 2 prefer a somewhat more advanced approach to improve accuracy of prediction, there are two alternative methods. The simplified CCIR method for planning purposes in Region 2 (see §6 of the present Report) and the modified FCC method [Wang, 1985] should be considered.

The modified FCC method suggests that for great-circle distances (d) greater than 200 km, F_c in equation (9) be given by:

$$F_c = (95 - 20 \log d) - (2\pi + 4.95 \tan^2 \Phi)\,(d/1000)^{\frac{1}{2}} \qquad (11)$$

where Φ is the arithmetic mean of the geomagnetic latitude of the transmitter (Φ_T) and that of the receiving site (Φ_R) of a path. Northern latitudes are considered positive, southern latitudes negative. If $|\Phi|$ is greater than 60°, equation (11) is evaluated for $\Phi = 60°$. If d is less than 200 km, F_c is evaluated for $d = 200$ km. However, the actual value of d is to be used in determining angle of departure. ——— Figure 16 of Annex I to Recommendation 435 ——— may be used in determining Φ. Figure 8 shows F_c for selected latitudes according to this method. It should be mentioned that this method can be used for frequencies between 535 - 1 705 kHz. Accuracy of the method can be improved if slant distance is used instead of great-circle distance.

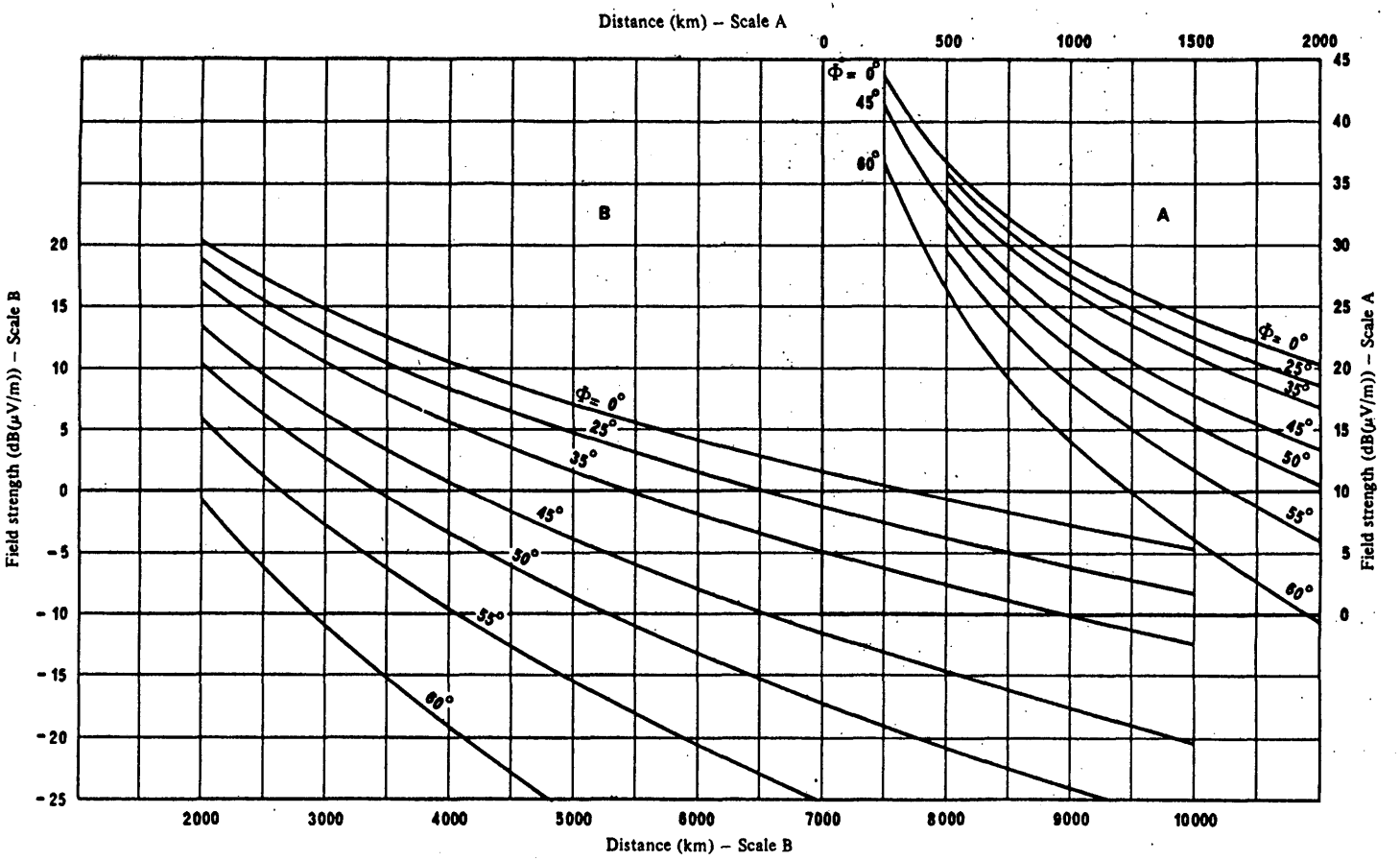


FIGURE 8– *Sky-wave field strength vs distance (100 mV/m at 1 km, 50%, 2 hours after sunset)*

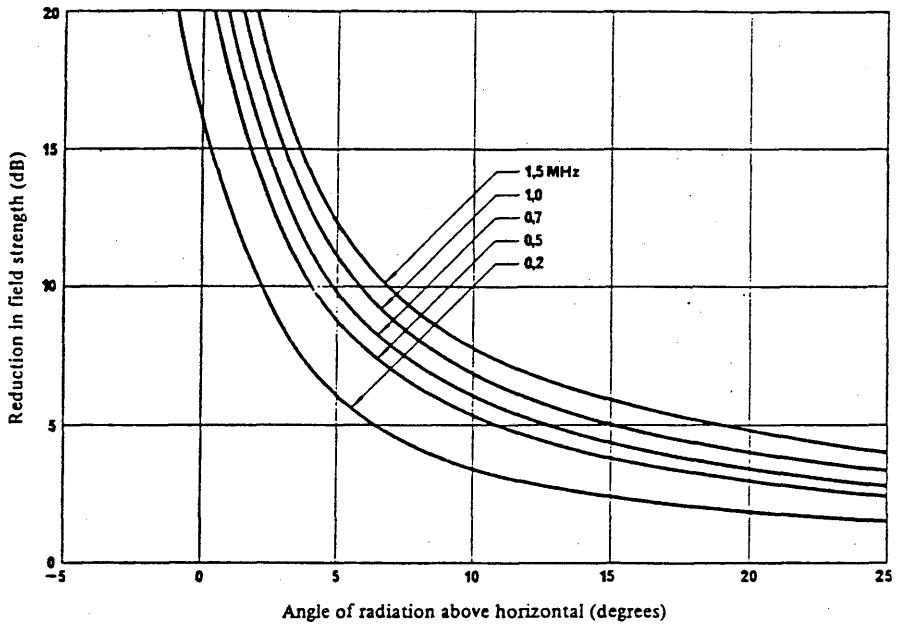
$$F_c = (95 - 20 \log d) - (2\pi + 4.95 \tan^2 \Phi)\,(d/1000)^{1/2}$$

9. Influence of the ground on radiation towards the ionosphere

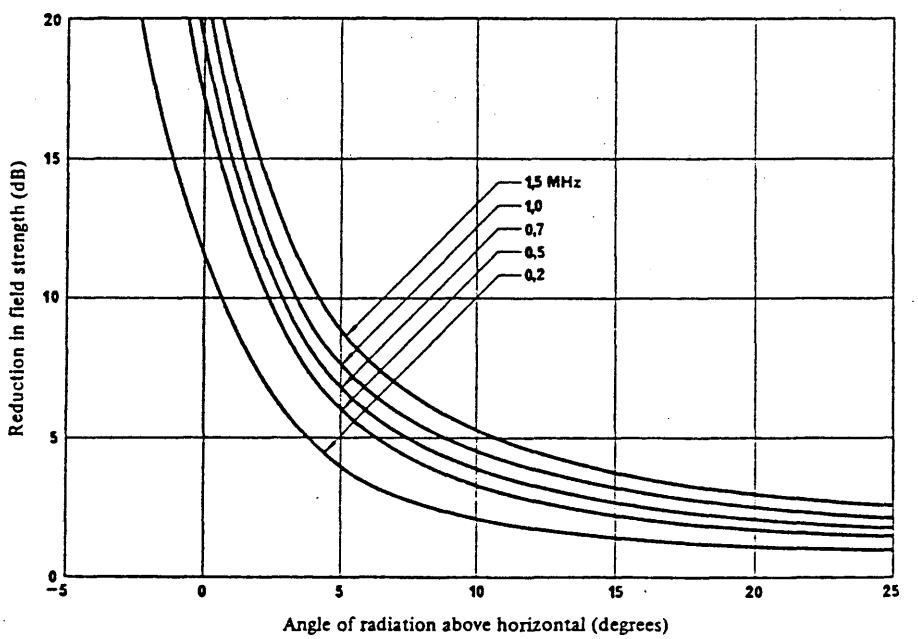
Figure 9 shows the variation of field strength with elevation angle for antennas on an imperfectly conducting curved Earth compared with the case where the antennas are located on flat perfectly conducting ground [Knight 1973]. Report 879 Section 3 gives the effective ground conductivity for various types of terrain. The curves in Figure 9 apply to vertical transmitting antennas up to 0.6 λ high. They also extend to negative angles of radiation which apply when waves diffract around the curvature of the Earth (defined as the angular distance between the antenna and the tangent point of the wave, as described in Report 265 Section 2.1). It is convenient to describe the variation of field strength with ground conductivity in terms of the ground loss, defined as a reduction in field strength which occurs above a curved Earth when land replaces sea water. This may be derived from Figure 9 by subtracting field strength reductions for sea water from those for ground of the appropriate conductivity. It is also convenient at times to use the corresponding inverse term "sea gain" which occurs when land is replaced by sea water. Ground loss and sea gain apply equally to transmitting and receiving antennas.

Note that the Annex to Recommendation 435, together with many of the results quoted in Report 431, are derived from measurements made with transmitting and receiving antennas located on typical imperfectly-conducting ground (3 - 10 mS/m). Thus the results and predictions implicitly include a ground loss term. For antenna locations near the sea, it is necessary to take account of sea gain; and, contrary to the signal enhancement which occurs in such a situation, if the ground conductivity is an order of magnitude smaller than 10 mS/m, it is necessary to take account of the additional ground loss that will occur.

An example which shows the effectiveness of sea gain as a function of the propagation path length for single and multi-hop propagation has been calculated and is shown in Figure 10. A frequency of 1 MHz and E-layer propagation has been assumed.

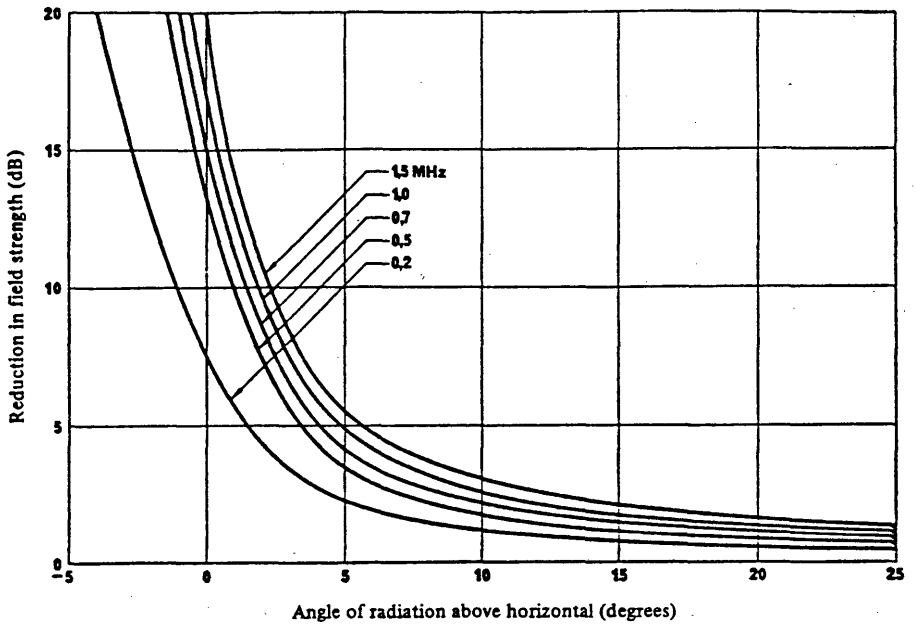


a) Ground conductivity, 10^{-3} S/m;
Relative permittivity, 5

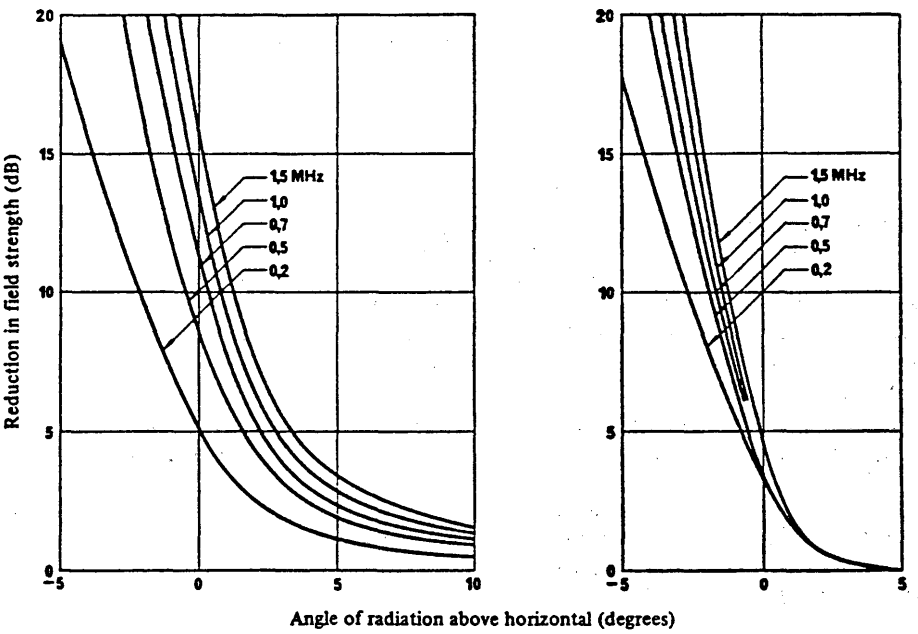


b) Ground conductivity, 3 x 10^{-3} S/m;
Relative permittivity, 10

FIGURE 9 – *Reduction in field-strength for vertical antennae up to 0.6 λ high, including the effect of the curvature of the Earth*



c) Ground conductivity, 10^{-2} S/m;
Relative permittivity, 20



d) Ground conductivity, 3 x 10^{-2} S/m;
Relative permittivity, 30

e) Ground conductivity 4 S/m (sea water);
Relative permittivity, 80

FIGURE 9 (continued)

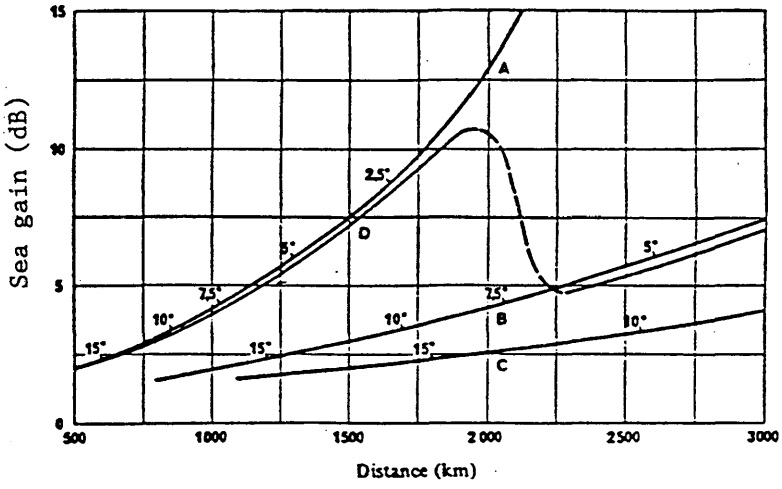


FIGURE 10 - Sea gain for multi-hop propagation

The curves show the sea gain which occurs when ground of conductivity 5×10^{-3} S/m is replaced by sea water at one end of the path. E-layer reflection (layer height 90 km) is assumed and the numbers against the curves denote angles of radiation.

Curve A: single-hop mode
B: two-hop mode
C: three-hop mode
D: effective sea gain for all modes

REFERENCES

BELROSE, J. S. [1968] Low and very low frequency radio wave propagation. AGARD Lecture Series XXIX, NTIS Accession No. AD676788, National Technical Information Service, Springfield, Va. 22161, USA.

ITU [1938] Documents of the International Radiocommunications Conference at Cairo, Vol I, 425-433, Fig. 3 (See also Report of Committee on Radio-Wave Propagation. *Proc. IRE*, Vol. 26, 1193-1234, Fig. 3).

ITU [1975] Final Acts of the Regional Administrative LF/MF Broadcasting Conference (Regions 1 and 3), Geneva, 1975.

IVANOV-KHOLODNY, G. S. and NIKOLSKY, G. M. [1969] *Solntse i ionosfera* (The Sun and the Ionosphere), 338-351, Nauka Publishing House, Moscow, U.S.S.R.

KNIGHT, P. [1973] MF propagation: a wave-hop method for ionospheric field-strength prediction. *BBC Eng.*, Vol. 100, 22-34.

UDALTSOV, A. N. and SHLYUGER, I. S. [1972] Propagation curves of the ionospheric wave at night for the broadcasting range. *Geomag. i Aeronom.*, **10**, 894-896.

VILENSKI, I. M., UDALTSOV, A. N. and SHLYUGER, I. S. [1970] Field strength of radio waves in the 150-1600 kHz range that propagate to great distances from the transmitter. *Geomag. i Aeronom.*, **10**, 204-207.

WANG, J. C. H. [March, 1985] A skywave propagation study in preparation for the 1605-1705 kHz broadcasting conference. *IEEE Trans. Broadcasting*, Vol. BC-31, 10-17.

CCIR Documents

[1970-74]: 10/82 (USSR).

REPORT 432-2

THE ACCURACY OF PREDICTIONS OF SKY-WAVE FIELD STRENGTH IN BANDS 5 (LF) AND 6 (MF)

(Study Programme 31A/6)

(1970-1978-1986)

1. Introduction

The field strength of sky-wave signals in bands 5 (LF) and 6 (MF) observed at the surface of the Earth varies continuously with time and may be predicted only in terms of statistical methods. It has become common practice to base predictions on field-strength measurements without prior knowledge of all the factors influencing the measurement. If instrumental and processing errors are small, the accuracy of such predictions depends upon the reception site environment and the assumption that conditions in the propagation medium will follow much the same pattern as in the past. Although this is a reasonable assumption, it does not permit the accuracy of prediction to be identified completely with the accuracy of determining a field-strength statistic, until the morphology of the propagation medium and the source of variations within the medium are better understood, or until measurements are made over a very long period. Provided these limitations are recognized, it may be said that the accuracy of prediction is determined by the spread of statistics around a common characteristic.

There have been numerous contributions to Study Programme 31A/6 from the EBU, OIRT, United States of America, India, Australia, Japan and the Federal Republic of Germany. As detailed results are readily available for the EBU, OIRT, Japanese, USA, and Australian field-strength measuring campaigns, these sources of data are used in this Report to determine the accuracy of low frequency and medium frequency sky-wave field-strength predictions.

Field-strength measurements from Europe are available for numerous receiving sites, propagation paths and transmitting stations, whereas Australian results are available for numerous transmitting stations and propagation paths but for very few receiving sites. Data made available by Japan are part of a regular MF sky-wave field-strength measurement survey conducted by members of the ABU and includes many long distance paths. These different approaches do not prevent a comparison of the results either with respect to field-strength values or the variance inherent in the measurement. It is not the purpose of this Report to enquire into the difference in predictions for various parts of the world, but rather to study the accuracy of predictions, the information required to achieve this accuracy, and the significance of different variances. Ultimately, account will be taken of the differences referred to above, in a single prediction method applicable in all regions, as indicated in § 4 of this Report.

2. General aspects of the prediction of sky-wave field strength in band 6 (MF)

The nature of fading of the sky-wave field strength in band 6 (MF) suggests that the distribution of instantaneous values may be determined with sufficient precision from observations of half an hour to one hour duration, except during periods of rapid general change, such as that following sunset and that preceding sunrise when a period of one quarter hour is more appropriate. The distribution of instantaneous values is not constant but is appreciably more stable than other field-strength statistics from night to night. A convenient indication of this distribution is obtained by extracting the hourly median, upper decile and lower decile values from recordings. In the medium frequency band, the ratio of upper decile to median has a mean value of 5 dB and a standard deviation* of 1.1 dB to 2 dB.

---

* Standard deviation and standard error values, in decibels, refer respectively to the ratios (standard deviation + mean)/mean and (standard error of mean + mean)/mean.

If median or upper decile values are plotted against the time of night, a general characteristic pattern will be evident for any particular frequency, distance and month of the year. Hourly median values for any one transmission and reception site at a given time of night and month are distributed with a standard deviation of 2.0 dB to 4.5 dB. The standard error* of a mean determined from such hourly medians is 0.6 dB to 1.4 dB for a sample of 15 values or 1.1 dB to 2.6 dB for a sample of 4 values. Monthly means of hourly medians may therefore be determined with considerable accuracy and are used to study the variation of field strength throughout a year.

If the measurement is made independent of sunset or sunrise variations, hourly median values for any one transmitting station and any one reception site are distributed throughout a year with a standard deviation ranging from 3.0 dB to 5.0 dB. The former value refers to some transmission paths observed at the second hour after sunset in Australia which display a normal distribution of hourly median field strength in μV/m. The latter value refers to measurements made at midnight in Europe where the distribution is excessively skew. In order to apply normal statistical methods, it is necessary to transform these values into a form which will produce a normal distribution. A satisfactory transformation is obtained if hourly median values are given in dB(μV/m). Results from some paths observed in Australia also display an excessively skew distribution which on a dB scale has a standard deviation of 4.2 dB. This represents a significant departure from that observed in Europe. The standard error of the annual mean of hourly medians at the second hour after sunset or at midnight is therefore between 0.5 dB and 0.7 dB for a sample of 52 values.

If annual mean values for several transmissions are plotted against distance, a single characteristic may be drawn for each transmission frequency about which annual means are distributed with a standard deviation varying between 1.0 dB, 2.5 dB or 5 dB. The first value refers to observations made in Australia during 1958/1959 in which there was no significant variation with transmission frequency. The second figure refers to weighted annual means used to compute EBU predictions. The third figure refers to measurements made by ABU members. At any one distance the standard error of the characteristic derived from annual means is therefore 0.5 dB, 1.25 dB, 2.5 dB for a sample of 4 values and 0.7 dB, 1.8 dB, 3.5 dB for a sample of 2 values.

More importance is attached to the distribution of annual mean values as these include errors of measurement associated not only with receiving sites, but also with transmitting sites. It should be understood that, with our present knowledge of sky-wave signal variations, such a statement relates to the error of a sample mean derived from an assumed single population. An examination of the statistics will show that this assumption is incorrect, but in determining propagation curves, the variance of annual means (between sample variance) represents an error. On the other hand, this error is very much a part of sky-wave field strength prediction if it is primarily due to the reception site environment.

A particular feature of the EBU results is the extent of the variation between samples as indicated by the spread of weighted annual means. The significance of these variations can be gauged by comparing the standard deviation between samples (2.5 dB) with the standard error of individual means, which for a sample of 52 values would be 0.7 dB. A departure of 2.5 dB by a sample mean from a population would occur only once in a thousand trials if the departure occurred purely by chance. The origin of this variance has not been determined, but it is probably associated with several factors, including the influence of the reception site environment.

In order to reduce the amount of work involved in future propagation tests, methods of measurement should be employed which reduce the standard error of estimate to a minimum. The possibility of reducing the influence of the reception site environment has been demonstrated by applying corrections to the measurement.

While field strength predictions in various forms have been made since sound broadcasting services were first established, it has become the practice to predict the annual median of hourly medians for a particular time of night or for a specified interval after sunset. For some purposes, however, it may be necessary to have a more detailed knowledge of sky-wave field strength variation with time and location. Instantaneous values vary in unison to a limited degree at locations separated by less than about 3 km. The correlation becomes quite poor for locations separated by more than 6 km. In addition to these variations with time and location, the general level of sky-wave field strength (hourly median) varies over the surface of the Earth in an urban area forming a standing

* Standard deviation and standard error values, in decibels, refer respectively to the ratios (standard deviation + mean)/mean and (standard error of mean + mean)/mean.

wave pattern. This pattern either changes or moves from hour to hour and from night to night. There are also residual or long term differences in field strength from site to site which tend to be obscured by the larger variations between sites from hour to hour and from night to night.

Superimposed on all these variations are changes from night to night and from week to week common to all sites over an extensive area. These variations exceed the between-site variations with time. Consequently, hourly median values are fairly well correlated for locations with a separation up to and possibly beyond 350 km.

From the limited information available, an indication of the extent of these variations is given in Table I.

The above deals with night-time field strengths only. Statistical aspects of day-time field strengths collected in the United States of America have also been studied. It has been reported that day-time, as well as night-time, field-strength distributions display appreciable skewness. The median value of day-time field strengths has a strong tendency to be closer to the lower-decile value than to the upper-decile value. Night-time field strengths, on the other hand, show the opposite tendency. Furthermore, the ratio of day-time upper-decile to median values is typically 3 dB greater than the corresponding night-time ratio.

3. General aspects of the prediction of sky-wave field strength in band 5 (LF)

It is not surprising to find that comments, similar to those in the previous section, may be made in respect to predictions of sky-wave field strength in band 5 (LF). However, there are some significant departures in terms of the actual degree of variation.

In Europe the ratio of upper decile to median sky-wave field strength decreases from 4.5 dB at short distances to 1.6 dB at long distances. The standard deviation of hourly median values at midnight over a period of one year for any one transmitting station and reception site is not significantly different from that observed at medium frequencies (5.0 dB). Low frequency annual means display a considerably greater variation than medium frequency annual means and therefore more propagation paths (or reception sites) have to be investigated to obtain the same precision in locating propagation curves. The standard deviation of annual means about a common characteristic is 4.9 dB and the standard error of estimate is therefore 1.3 dB for a sample of 14 values.

TABLE I – *MF sky-wave field strength variation with time and location*

Measurements made at two locations	Measurements made at a number of locations, one of which is the base site	Standard deviation (dB)
Ratio of hourly median field strengths measured simultaneously at each site over a period of two to three weeks		1 to 2
	Median of the ratio of hourly median field strengths measured simultaneously at the base and at a site (site separation from the base not exceeding 12 km). This represents the spread of residual differences between the base and sites surrounding it.	1
	Ratio of twenty-minute medians measured at the base and at a site, the measurements being made at several sites over several nights (sites located within 3 km from the base, each site being measured once).	0.4 to 2.7

4. Information required to determine sky-wave field strength predictions

There will be an accuracy of prediction beyond which planning authorities will have little interest and therefore, from a practical point of view, there is no need to exceed this accuracy. It is difficult to set an absolute limit, but the error should be less than that which would cause a significant change in listener satisfaction within the most critical region of desired protection ratios.* It is suggested that this limit lies between ± 1.5 dB and ± 3 dB.

When making measurements to establish predictions, mean values may be determined within the required accuracy stated above by selecting samples of sufficient size as indicated in Table II. There appears to be no justification in taking more than one recording per week for a particular combination of distance and frequency, because a sample of this size will provide an annual mean with a standard error of 0.5 dB to 0.7 dB and a monthly mean with a standard error of 1.1 dB.

In addition to these errors, allowances should be made for variances introduced due to changes in receiving site environment. Typical cases are:

- where receiving antennas are in close proximity to household electric wiring, in which case the field strength may exceed that for the general area by 6 dB or more at MF,
- where the receiving site is at the coast, the field strength may be increased by up to 10 dB at MF over that received well inland (some prediction methods take account of this influence which applies to both receiving and transmitting sites), and
- residual differences observed from site to site as indicated in § 2 and Table I.

Values given in this Report can be used to estimate the minimum number of propagation paths required in a measurement campaign for a particular region. Except for the tropical region where differences are expected between N-S and E-W propagation, the standard error of estimate is between 1.3 dB and 2.5 dB in band 6 and 2.5 dB in band 5 for a sample of four annual mean values appropriate to any particular combination of distance and frequency.

Interim Working Party 6/4 has selected a prediction method intended for application in all regions. The accuracy of prediction using this method (refer to Recommendation 435) is not as great as that obtained by using methods developed specifically for individual regions. In most cases this loss of accuracy is quite acceptable and is a satisfactory tradeoff for the benefits of having a single prediction method. When applied to the 266 paths for which results are available throughout the world, the error in prediction has a standard deviation of 7 dB.

Prediction accuracy depends jointly on the accuracy of measurement at receiving and transmitting sites. Unattenuated values may be determined by field-strength measurements along the propagation path at the transmitter end. These results are used to locate an appropriate curve (ground-wave field strength E times distance d) which gives the unattenuated field strength at unit distance, when extended back to zero distance. The standard error in locating such a value is less than 0.2 dB for a sample of 14 values. In regions with a temporal variation of ground conductivity, measured values of ($E \times d$) do not alter substantially over a period of five years, provided normal operating conditions are maintained during the measurement and provided the transmitting antenna-earth system is not subjected to chemical change.

In order that a number of recordings may be considered collectively, the extraction of a single statistic from each recording requires considerable attention, as the time involved in analysis of the recordings can be the determining factor which limits the scope of a recording programme. This may not be important where continuous or automatic analysers are available but when recordings have to be analysed by inspection, the time spent on the analysis can be appreciable.

A means of reducing this time is found in the selection of a suitable field-strength statistic. Results of many measurements in the medium frequency band have shown that the variance of upper decile values is only slightly greater than the variance of median values. It therefore follows that the mean of upper decile values is determined to almost the same accuracy as that of median values for samples of equal size. The extraction of upper decile values is accomplished in considerably less time than the extraction of median values, and provides a means of measurement not significantly less accurate than the measurement of medians.

---

* For co-channel interference, an increase of 5 dB in the level of an interfering signal will reduce the percentage of listener satisfaction from 90% to 50%.

TABLE II

Recordings of half-an-hour or one hour duration	Band	Standard deviation (dB)		Standard error of mean or standard error of estimate (dB)		Origin
		A	B	A	B	
E_{10} / E_{50}	MF	1.1		0.5 for a sample of 6		Australia 1958/1959, 1963
			1.7 to 2 (1)			OIRT (Rome, 845 kHz)
	LF		1.6			OIRT (Allouis, 164 kHz)
E_{50} for any one transmitting station and any one receiving site at a particular time of night over a period of one month	MF	2.0		1.1 for a sample of 4		Australia 1963
			2.5 to 4.5 (1)			OIRT (Rome, 845 kHz)
	LF		3.7 to 5.7 (1)			OIRT (Allouis, 164 kHz)
E_{50} for any one transmitting station and any one receiving site at midnight over a period of one year	MF	3.0	4.2	0.5 for a sample of 52	0.6 for a sample of 52	Australia 1958/1959
			3.7 to 4 (1)			OIRT (Rome, 845 kHz)
			5.0		0.7 for a sample of 52	EBU (Rome, 845 kHz, to Darmstadt and Monte-Carlo, 1466 kHz to Jurbise)
	LF		5.1 to 5.5 (1)			OIRT (Allouis, 164 kHz)
			5.0		0.7 for a sample of 52	EBU (Allouis, 164 kHz to Enköping)
E_{50} annual mean, for any transmission over the period of one year	MF	1.0		0.5 for a sample of 4		Australia 1958/1959
			2.5			EBU 845 kHz, 1178 kHz, 1466 kHz
			2.6			USA 1944 and 1954
			5.0			Japan (ABU) 1970-1973
	LF		4.9		1.3 for a sample of 14	EBU 164 kHz

(1) Varies with the season.

Values under heading A refer to normal distributions (μV/m) where the standard deviation and standard error are given as ratios in decibels of (standard deviation + mean)/mean and (standard error of mean + mean)/mean. Values under heading B refer to transformed skew distributions (dB (μV/m)).

Alternatively, the standard deviation of the ratio E_{10}/E_{50} is less than the standard deviation of E_{10} over the period of one month or of one year. Since these variables are not correlated, the additional error appearing in a mean E_{50} calculated from a measured mean E_{10} and mean E_{10}/E_{50} (taken from a small sample) will be of no consequence. In most cases, it will not be necessary to take a sample of the ratio E_{10}/E_{50}, as an assumed value of 5 dB will be sufficiently accurate for the medium frequency band.

BIBLIOGRAPHY

DIXON J. M. [1977] The variation of MF sky-wave field strength. Broadcasting Engineering Division Report No. 48, Postal and Telecommunications Department, Australia.

EBERT, W. [1962] Ionospheric propagation on long and medium waves. *EBU Rev.*, Part A, 71, 3-11, 72, 68-80, 73, 109-121.

SULANKE H. and TÄUMER F. [1967] Calculation of standard deviations and errors for medians of medium and long-wave field strength recordings. Contribution to the work of International Working Party VI/4 of the CCIR.

WANG, J. C. H. [1977] Prediction of medium-frequency sky-wave field strength in North America. *IEEE Trans. Broadcasting*, Vol. BC-23, 2, 43-49.

WANG, J. C. H. [1983] Interference and sharing at medium frequency: sky-wave propagation considerations. AGARD Conf. Proc. No. 332, *Propagation Aspects of Frequency Sharing, Interference and System diversity*, 9-1 to 9-12. Ed. H. Soicher. NASA Accession No. N83-30873. National Technical Information Service, Springfield, VA 22161, USA.

CCIR Documents

[1956]: Warsaw; XII/356 (India).

[1962]: VI/88 (Australia).

[1970-74]: 6/289 (Japan).

REPORT 431-5

ANALYSIS OF SKY-WAVE PROPAGATION MEASUREMENTS FOR THE FREQUENCY RANGE 150 TO 1600 kHz

(Study Programme 31D/6)

(1970-1974-1978-1982-1986-1990)

1. Introduction

This Report describes the results of experimental work and sky-wave field-strength measurements carried out in various geographical regions. Some suggestions for future studies are given in the conclusions.

On the basis of these measurements and of theoretical studies several field strength prediction methods have been developed, applicable to a limited area or on a world-wide scale. The various methods are described in Report 575; remarks and comparisons between certain of these methods, and the results of measurements, are given here.

All measurement results and predictions presented in this Report have been normalized to a c.m.f. of 300 V. All the Figures show normalized field strength, E_0, as a function of ground distance, d.

2. Field strengths at distances of less than 300 km

There are many fewer experimental data for distances less than 300 km than for greater distances, because of the difficulty of separating the sky-wave from the ground-wave. However, a reduction of the ground-wave component can be achieved by using a transversely orientated loop antenna at the transmitting or at the receiving site, or at both sites.

Alternatively, the ground-wave can be separated from the sky-wave by the use of pulse transmissions. Reflections from the E and F regions can be identified by their time delays, as can multiple reflections, and their individual amplitudes can be measured.

2.1 *Continuous-wave measurements*

Müller [1965] has developed a method of analysis of the recordings of the combined ground-wave and sky-wave field strengths, but it can only be used when the sky-wave is the predominant component.

Measurements for a distance of 38 km have been made in Bulgaria [CCIR, 1963-66a] by means of a loop receiving antenna. They show an average reflection loss of about 12 dB at 827 kHz for the period from two hours after sunset to 2200 hours. There is, however, an important seasonal variation with stronger reflection in summer.

In April 1965, field-strength recordings were made in the Federal Republic of Germany [CCIR, 1966-69a] on 30 consecutive nights between 0000 and 0620 hours UTC. The same transmitter, which operated successively at 620, 899, 1160 and 1529 kHz for a period of 50 min at each frequency, was received simultaneously at 3 receiving sites located on a straight line at distances between 128 and 274 km. The transmitting antenna was of a small vertical type, whereas the receiving antenna was a loop at all receiving sites.

Figure 1 shows averages of the measured median field strengths.

An analysis by the Müller method of total field strength records at ranges from 150 to 230 km from a broadcast transmitter on 191 kHz in Sweden has shown good agreement with the expected reflection losses according to the method of calculation described in Report 265.

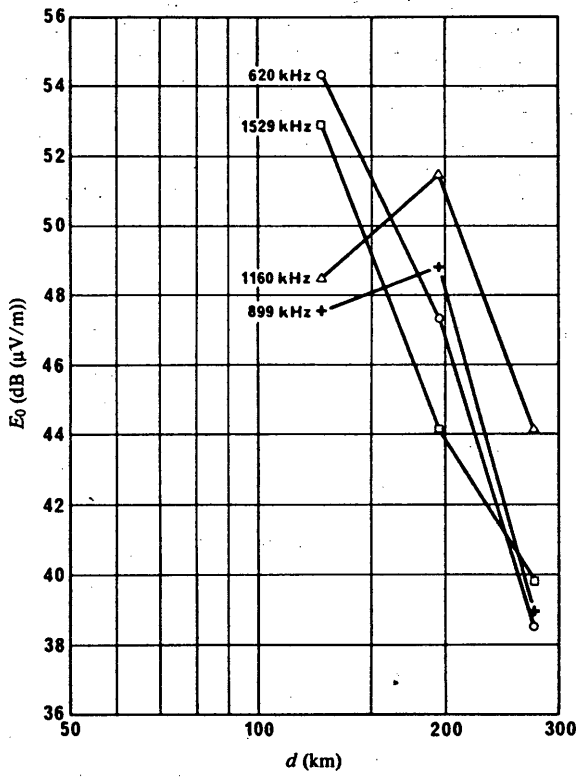


FIGURE 1 – *Field strengths measured in the Federal Republic of Germany, April 1965*

Measurements over four propagation paths with lengths of up to 315 km have been made in Japan [Mambo et al., 1986]. Loop receiving antennas, positioned to minimize the ground-wave component, were used. Field strengths at three frequencies were recorded from 2100 to 2400 (JST = UT+9) during one or two years of high solar activity; also the field strength at a single frequency was recorded from 2 hours after sunset to 2300 (JST) during one year of low solar activity. The short-term fading approximates the Rayleigh distribution. Measured median values are in fairly good agreement with values calculated by using the full-wave method applied to the International Reference Ionosphere with Es layer.

2.2 *Pulse measurements*

Pulse measurements were made in the People's Republic of Poland during 1973 to 1975 on about 170 nights using two frequencies, 786 and 1353 kHz, and over distances up to 340 km [Rau, 1978]. Propagation by means of sporadic E ionization was observed on most nights, except in spring. When F-layer reflection would otherwise occur, the presence of Es ionization results in an increase in the measured median field strength of about 8 dB. It would thus seem desirable to make all interference calculations assuming a reflection height of 100 km.

Due to the effect of Es ionization, the annual median field strength on paths of up to 200 km increases rapidly in the first hour after sunset and then remains almost constant up to midnight or even later.

Pulse measurements at vertical incidence carried out at Tsumeb (Namibia) [Elling, 1961] in the MF band were extrapolated for oblique incidence and two families of curves, for E and F reflection, were obtained for frequencies between 300 and 1100 kHz. These curves were used during the African LF/MF Broadcasting Conference [ITU, 1966]. An interpretation of the shape of the curves was given by Täumer [1968].

3. Field strengths at distances between 300 and 3500 km

3.1 *Europe*

A field-strength prediction method based on the results of measurements made in Europe by the EBU and OIRT [CCIR, 1963] has been described by Ebert [1962]. The method is intended for field-strength prediction at night in the frequency range 150 to 1600 kHz, at distances between 300 and 3500 km, in the European broadcasting area. Diurnal and seasonal variations which were observed at 845 kHz are shown in Fig. 2. Measurements at distances greater than 3000 km were rather few and were restricted to frequencies up to 845 kHz. Thus the predictions are likely to be less reliable as the frequency and range increase. The propagation formula is valid for an average ground conductivity (about 3×10^{-3} S/m) at each end of the path. The correction for a different conductivity would depend on the path length. As a first approximation for paths longer than 1000 km, a good conductivity at the transmitter site (10^{-2} S/m) would lead to a sky-wave field strength 1.5 to 2 dB greater and a poor conductivity (10^{-3} S/m) to a reduction of the same order. For a transmitter situated near the sea, an increase of about 6 dB is to be expected. Report 575 and § 2.3 of Annex I to Recommendation 435 contain further information regarding the influence of the length of path and the distance from the sea on the value of this correction.

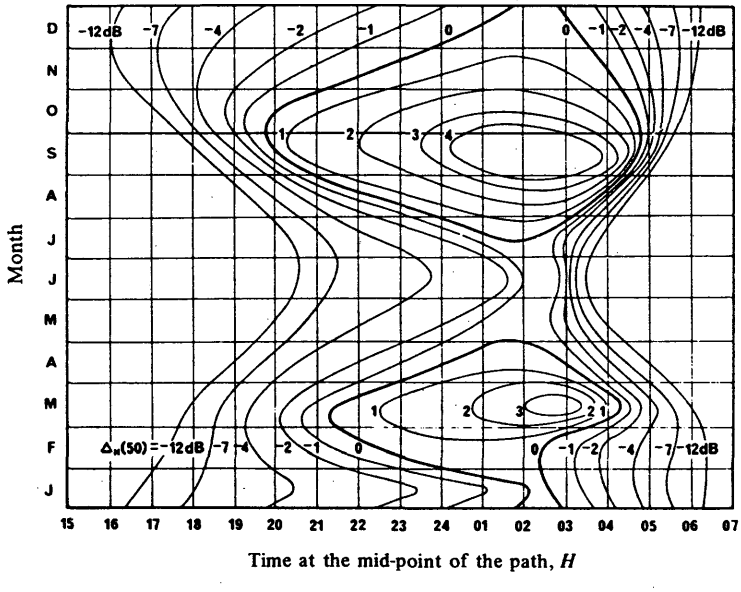


FIGURE 2 – *Correction to take account of the time at the mid-point of the path H and of the season of the year deduced from measurement results obtained in the European Broadcasting Area*
(Frequency: 845 kHz)

3.2 *Australasia*

Medium-frequency sky-wave characteristics have been studied in Australia [Dixon, 1960; CCIR, 1963-66b]. Figures 3, 4 and 5 give propagation curves developed from the results of two major measurement campaigns conducted in 1958-1959 and 1963-1965 and show the hourly median field strength exceeded on 50% and 10% of the nights of a year. A significant feature of these results is their relatively small variance from the propagation curves.

Figure 3 refers to the field strength at the second hour after sunset for paths which are predominantly north-south. Figure 4 also applies to the second hour after sunset and the period of low sunspot activity, but relates to long paths which are predominantly east-west. Figure 5 relates to the field strength at 2330 hours during the period of low sunspot activity, for paths which are predominantly north-south. These curves are not valid for reception sites with sea water in the foreground and when applied to individual cases are subject to error in accordance with the variations shown in Report 432. Figure 6 indicates the type of seasonal and diurnal variation observed. The study of these variations [CCIR, 1970-74a] and those applicable for Europe reveals characteristic features, some of which are common to both hemispheres. At mid-latitudes the maximum field strength for the year is much the same in both hemispheres but occurs at different times of night.

A detailed study of medium-frequency sky-wave propagation was made in New Zealand for transmissions across the west-east sea path between Australia and New Zealand at distances between 2000 km and 3200 km [CCIR, 1966-69b]. Figure 7 summarizes the results of 240 hours of measurement made at the second hour after sunset. The measured values at 3200 km are 6 to 7 dB higher than other field strengths measured in Australia.

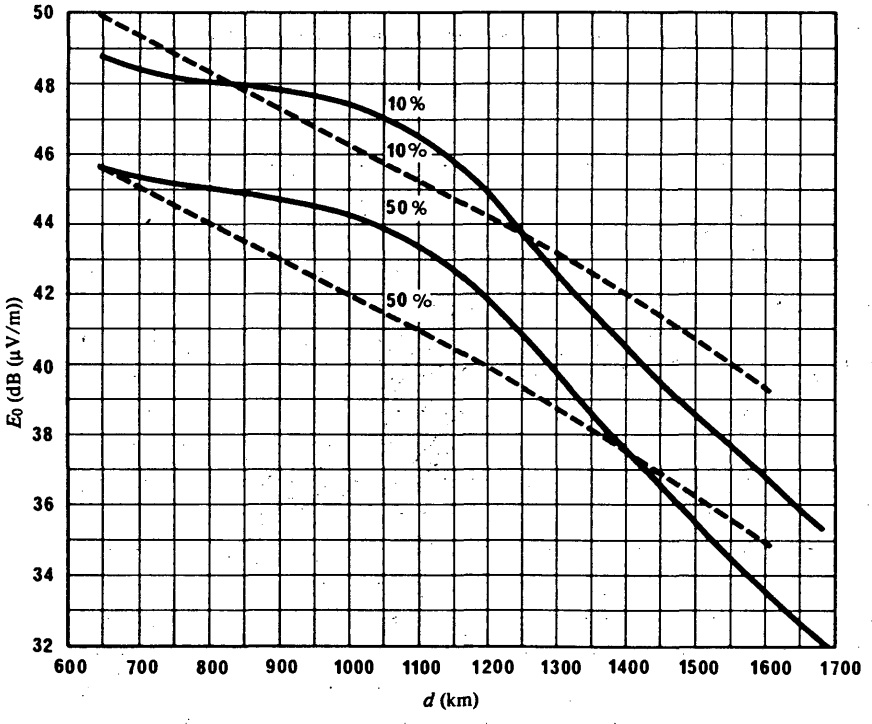


FIGURE 3 – *Australian measurement results*
Hourly median values of the field strength exceeded at 50% of locations on 50% and 10% of the nights of a year at the second hour after sunset

——— : Annual mean International relative sunspot number 10

– – – – – : Annual mean International relative sunspot number 180

North-south paths

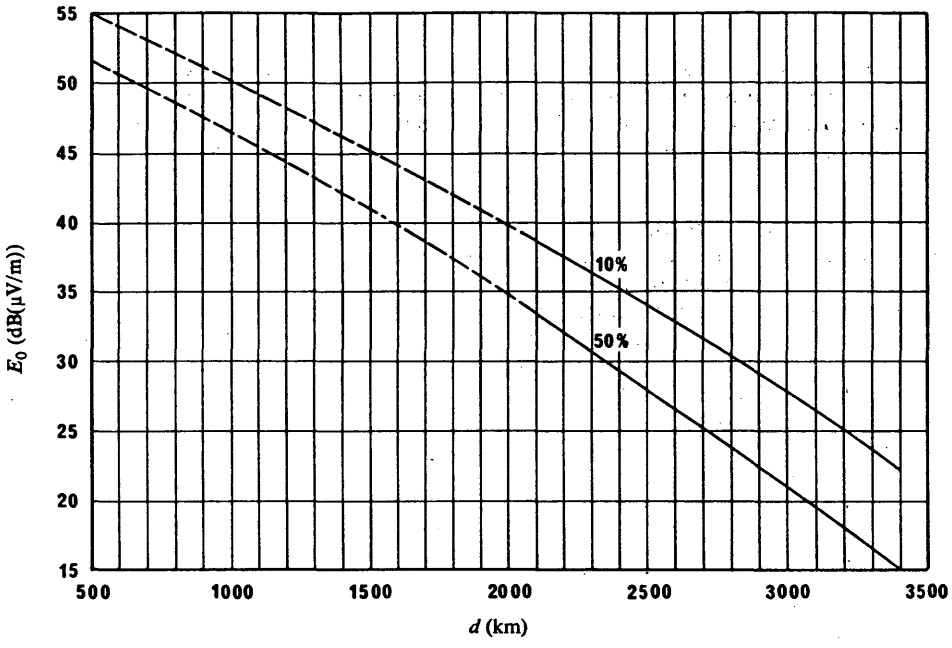


FIGURE 4 – *Australian measurement results*
Hourly median values of the field strength exceeded on 50 % and 10 % of the nights of a year at the second hour after sunset. The number of the paths investigated was not sufficient to obtain an accurate curve over the dashed section

East-West paths; annual mean International relative sunspot number 20

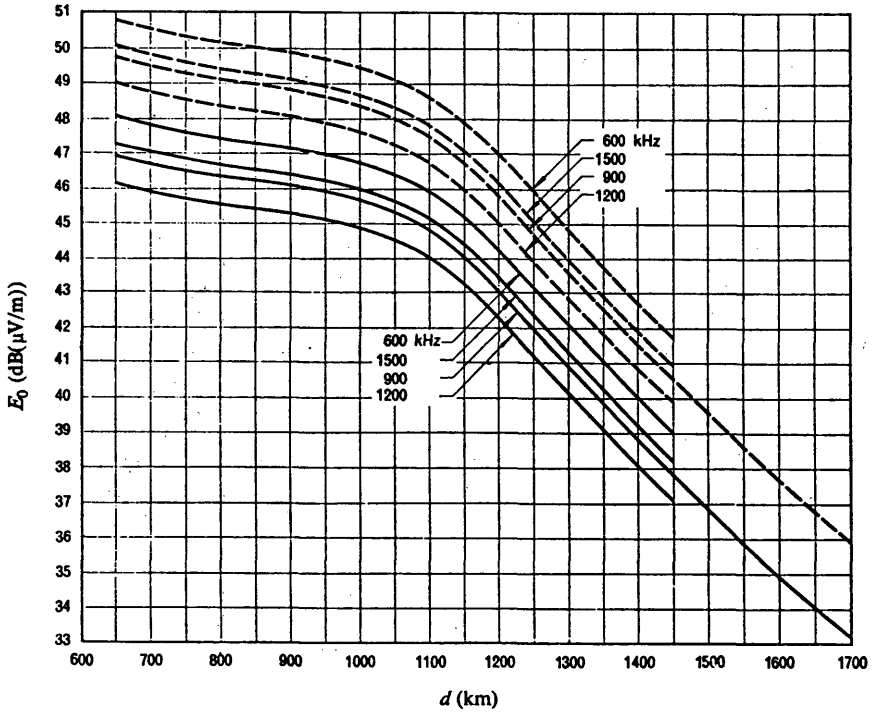


FIGURE 5 – *Australian measurement results*
Hourly median values of the field strength exceeded at 50 % of locations on 50 % and 10 % of the nights of a year at 23.30 hrs

North-South paths; annual mean International relative sunspot number 10

——— 50 %

– – – – – 10 %

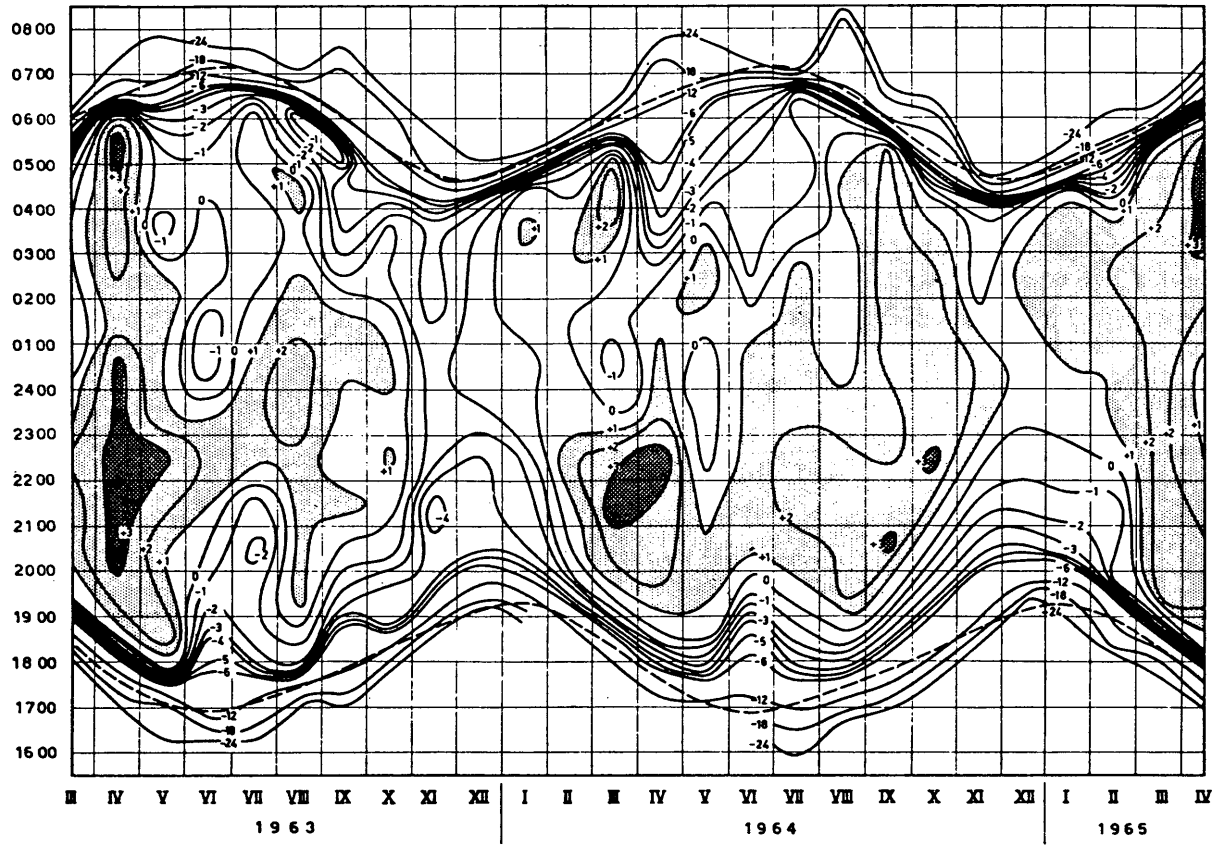


FIGURE 6 – *Field-strength variation with time of night and month of the year deduced from Australian measurement results*

Contours show the hourly median values of the field strength exceeded at 50% of locations on 50% of the nights of a month, in decibels above the hourly median value of the field strength exceeded at 50% of locations on 50% of the nights of a year (April 1964–March 1965) at the second hour after sunset. The values shown are accurate for quasi-longitudinal transmission on a path of 700 km for transmission frequencies in the range 900 kHz to 1100 kHz. Dashed lines show the times of sunset and sunrise.

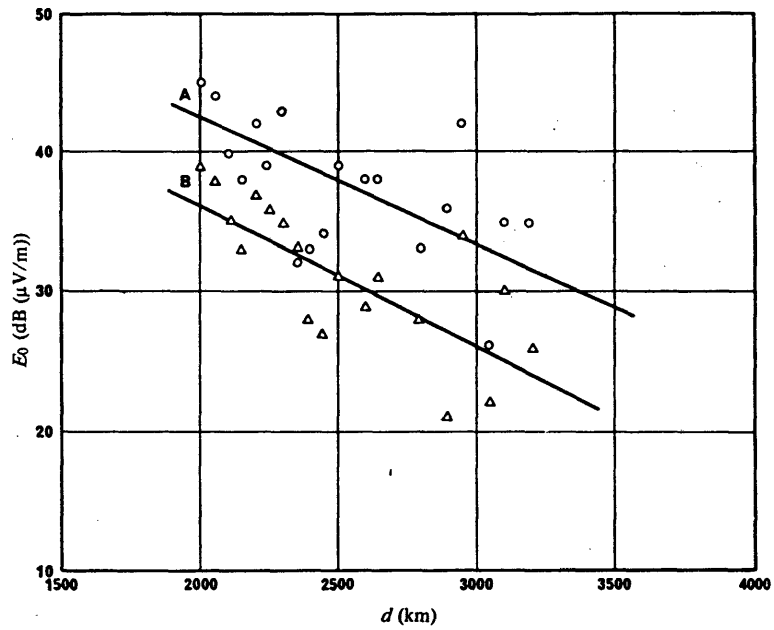


FIGURE 7 – *Field strength received for 50% and 10% of the time for 50% of locations. Overseas propagation paths between Australia and New Zealand*

West-East paths: mean International relative sunspot number 90

○: Field strengths exceeded for 10% of the time (curve A)

△: Field strengths exceeded for 50% of the time (curve B)

3.3 *Asia*

Field strengths of transmitters operating at frequencies between 550 kHz and 1560 kHz and over distances ranging from 185 km to 1760 km have been recorded in India. Field strengths in the north-south direction are about 4 to 6 dB higher than the corresponding field strengths in the east-west direction due to high polarization coupling losses on east-west propagation paths at the lower latitudes [CCIR, 1970-74b].

In China, field-strength measurements were carried out for 32 paths with distances of 380 to 8310 km in frequency range of 560 to 1390 kHz from 1974 to 1976. The geomagnetic latitudes of these paths are within the range of 16°-36° N (most of them between 20°-30° N). A comparison was made between the measurement results and the predicted values obtained with the Cairo North-South Curve and the two prediction methods adopted by the Regional Administrative LF/MF Broadcasting Conference, Geneva, 1975. The result of comparison indicates that the Cairo North-South Curve gives the least residual standard deviation, and the residual average deviations of these three methods are all negative, i.e. the predicted values are too low. A regression analysis of the measurement data in the Asian part of Region 3 shows that for low and temperate geomagnetic latitude paths no evident tendency for k_R values to decrease with lowering of geomagnetic latitude could be found, and the values of A and k_R obtained in accordance with Annex I to Recommendation 435 are somewhat higher than those obtained by regression analysis of measurement data. For geomagnetic latitude range of 8°-29° N, the values of A and k_R may be taken as constant, i.e., $A = 105$ and $k_R = 3.14$ [Pan, 1981; CCIR, 1978-82a].

Field-strength measurements of 3 circuits operating in the MF band over distances of 2840 km, 3155 km and 4380 km were carried out in India for about one decade. Analysis shows that a significant negative correlation exists between night-time field strength at MF and sunspot activity. Regression analysis of measured data gives an average value of b in the equation of loss factor k_R in Annex I to Recommendation 435, of 0.74 for these paths in this region [CCIR, 1982-86a].

3.4 *The Americas*

Extensive measurements for a complete solar cycle have been made in the United States. Data recorded at 2 hours after sunset have been published [Damelin, 1971]. Using these data, a number of field strength prediction methods, including the Region 2 method also known as the FCC curves, (see Report 575, § 7) have been developed [PoKempner, 1980]. These data have been analyzed by a number of authors. Barghausen [1966] compared the prediction methods used for the Americas and Europe [Ebert, 1962]. Wang [1977] compared all the measured data with various prediction methods including that proposed in Annex I of Recommendation 435. The latter comparison shows that, in the USA, measured field strengths on north-south paths exceed those predicted by the method of Annex I by as much as 15 dB; but for east-west paths, the measurements are 10 dB less than those predicted. At low solar activity, the method of Annex I shows better agreement with measurements than either the FCC or the European prediction method. At high solar activity none of the methods is entirely satisfactory. Furthermore, the measurements indicate that field strengths increase with frequency, in contrast to the frequency term in Annex I of Recommendation 435.

A sky-wave prediction method for North American paths developed by Wang [1977] gives the field strength as a function of frequency and geomagnetic latitude as well as solar activity and path distance. When compared to the FCC measurements, this method, the FCC curves, and the method proposed by IWP 6/4 have an overall r.m.s. deviation from the observed data of 4.8 dB, 12.9 dB, and 7.1 dB, respectively.

Crombie [1979] showed that night-time transmission loss at medium frequencies in the United States during high solar activity indicates a significant dependence on the direction of propagation. Transmission loss in the east-to-west direction is greater than predicted, and greater than the transmission loss in the opposite direction, for path lengths ranging from 300 to 2800 km. There is no significant difference between north-south and south-north paths. Short-term measurements made in various parts of the Americas including the Caribbean [Wang, 1979] and Mexico [Fernandez and Wang, 1980] have been compared with values predicted by the Cairo north-south curve, by the FCC curves and by the method described in Annex I of Recommendation 435. For the high-latitude paths (6 paths whose mid-point geomagnetic latitudes vary between 53° and 63.5° N, with path lengths between 630 and 1500 km) the measured field strengths are consistently smaller than the predicted values. For the low-latitude paths (7 paths, geomagnetic latitudes 31° to 36° N, path length 630 to 2200 km) the measured field strengths are considerably greater than predicted values. For the low latitude paths, the Cairo north-south curve and the FCC curves appear to give better results than the method of Recommendation 435. However, when solar activity is low, the measured field strengths agree well with values predicted by the method described in § 7 of Report 575. The Mexican measurements indicate that the upper decile value is only about 6 dB greater than the median value instead of the 8-12 dB observed in the United States.

During three periods (July-August 1979, March-April 1983 and July-August 1983) around 463 hours of night-time ionospheric field-strength measurements have been made in Brazil on eight circuits including distances between 352 and 1675 km and frequencies from 600 to 1510 kHz [Assis Brasil, 1979; CCIR, 1982-86b]. The geomagnetic latitude of the mid-point of these circuits is in the range of 2.1° N to 12.6° S. The measurements have been compared [CCIR, 1982-86b] with the following prediction methods:

(a) Annex I to Recommendation 435;

(b) FCC clear-channel curves;

(c) alternative method suggested by Wang [1977] for the United States of America; and

(d) modified FCC method [CCIR, 1982-86c].

Results are given in Table I. It is concluded that all prediction methods considered, underestimate the actual field-strength values.

The circuits around 380 km observed during July-August 1979 (mid-point geomagnetic latitude between 11° S and 12.6° S) showed an ionospheric absorption inversely proportional to the frequency (typical value 11 dB between 1410 and 620 kHz). Furthermore, the analysis of the results of such measurements showed a transmission loss in the West-East direction approximately 3.6 dB higher than that in the North-South direction.

TABLE I – *Mean error and standard deviation of the measurements performed by Brasil (predicted value – measured value)*

Method	Mean error (dB)	Standard deviation (dB)
(a)	−6.5	9.9
(b)	−8.4	1.1
(c)	−0.7	7.0
(d)	−1.0	7.3

3.5 *Africa*

A measurement campaign which lasted in all for about one year, from June 1963 to July 1964, was organized in Africa, although many paths were studied for shorter periods [CCIR, 1963-66c]. The results correspond to the predictions for Europe but contain a relatively large spread for which no explanation could be found.

4. Field strengths at distances greater than 3500 km

An extensive series of measurements over distances between 1500 and 12 000 km was made from 1935 to 1937 at frequencies of about 1 MHz. These measurements were used to derive the so-called Cairo curves [ITU, 1938; Knight, 1977a]. The original curves gave quasi-maximum field strengths; to enable comparisons to be made with other curves and other prediction methods, all values have been reduced by 9 dB to give median field strengths. There are two Cairo curves. The east-west curve was derived from measurements made across the North Atlantic; these measurements may have been affected to some extent by auroral absorption. The north-south curve was derived from measurements mainly between North and South America; one terminal (Buenos Aires) was situated near the sea. These curves are included in Fig. 8.

Measurements over distances between 3200 and 9300 km at frequencies between 620 and 1345 kHz have been carried out by the EBU [CCIR, 1966-69c and 1970-74c]. The Federal Republic of Germany has carried out measurements at Tsumeb, Namibia, on three north-south paths at distances of about 7000 km and frequencies of 164 kHz (Allouis), 845 kHz (Rome) and 1602 kHz (Ismaning) [Eyfrig, *et al.*, 1975]. In Fig. 8 these measurements are compared with measurements made before 1938, with the latter reduced by 9 dB to convert quasi-maximum values to median values.

The results show that field strengths observed at distances exceeding 3500 km, especially on north-south paths, are considerably higher than values obtained by extrapolating the curves for the European Area. The Cairo curve for north-south paths shown in Fig. 8 appears to be satisfactory for predicting the highest field strengths which are likely to be observed when the transmitting and receiving antennas are situated on ground of average conductivity.

Methods for field-strength measurement and analysis have been developed in the U.S.S.R. [Gadden, 1964; Vilenski *et al.*, 1970; Udaltsov, 1971; Udaltsov and Shlyuger, 1972; CCIR, 1970-74d]. Measurements were made on fourteen frequencies in the vicinity of 200, 500, 1000 and 1500 kHz at different latitudes at distances between 600 and 4500 km and the results are shown in Fig. 9 [CCIR, 1966-69d].

The U.S.S.R. curves show a much smaller dependence of field strength on frequency at middle latitudes than do the European curves. At higher latitudes, ionospheric absorption increases rapidly as the frequency increases, resulting in a much greater dependence of field strength on frequency than is found at lower latitudes.

A series of long-distance sky-wave propagation measurements in the MF band has been made by the Asian Broadcasting Union. In Fig. 10, the maximum, median and minimum field strength values are shown for each of the 25 paths under study. The values have been derived from either half-hourly or hourly cumulative distributions [CCIR, 1970-74e]. It is apparent that all of these long-term median field strengths are very close to the north-south Cairo curve [ITU, 1938], when the latter is converted from quasi-maximum to median values.

Measurements have been made in Japan since 1961 on 57 frequencies between 548 kHz and 1550 kHz. The results for frequencies near 500 kHz are plotted in Fig. 11. [CCIR, 1970-74e].

Results of two series of mobile MF field-strength measurements covering west-east/east-west and north-south propagation paths, which were carried out in June and July 1973, in the northern Pacific Ocean area on board Japanese ships, are shown in the upper two figures of Fig. 12a. The experiment was extended to the southern Pacific Ocean area until November 1973. The results obtained mainly in equinoctial months in the southern hemisphere are shown in the lowest figure of Fig. 12b. All results, regardless of the direction of propagation paths and the frequency, tend to follow the N-S Cairo curve, although the values are about 10 dB higher than those measured in the southern hemisphere [Nemoto *et al.*, 1976]. Similar results, in which the measurements also tended to support the N-S Cairo curve were made in June 1974 in the North and South Atlantic Ocean on board a ship of the Federal Republic of Germany [Schwentek and Geisweid, 1975].

Some of the measurements described in this section were made over paths between one ITU region and another. A detailed comparison has been made of predicted and measured field strengths for inter-regional paths terminating in ITU Region 2 [CCIR, 1978-82b]. A comparison of available methods for predicting medium-frequency sky-wave field strengths has also been made in the USA [Pokempner, 1980].

Long-term mobile measurements during November and December of sky-wave field strength during the night-time were carried out along north-south sea paths of approximately 10,000 km. The measurements were made along paths from a transmitter at 40°N, 140°E extending to 47°S, 180°E each year from 1973 to 1982. The results show an approximately 10 dB higher field strength than the Cairo N-S curve, as seen in Figure 12c [Nemoto et al., 1987; Kuriki et al., 1988].

A considerable number of measurements over 11 paths in the Americas ranging from 3,500 to 4,250 km and centred over geomagnetic latitudes of 32° to 57° North have been made and analysed. Measured field strengths typically fall within 5 dB of values predicted, by using the method developed by Wang [1985]. When applied to these long paths, the method described in Annex I to Recommendation 435 shows a tendency to underpredict by about 10 dB. The Cairo N-S curve and the Region 2 method, being latitude-independent, appear to be satisfactory for predicting field strengths only at low- and mid-latitudes, respectively [Wang, 1989].

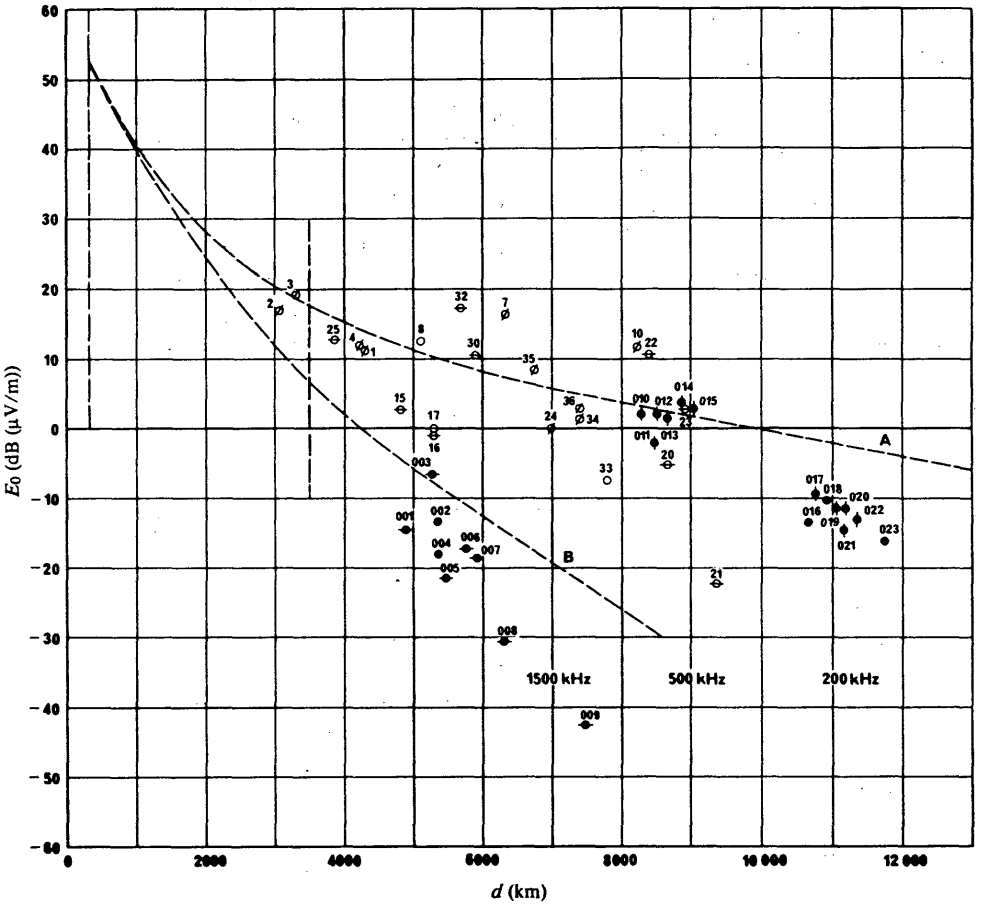


FIGURE 8 – *Sky-wave field strengths measured at distances greater than 3000 km*

A: N-S, Cairo 1938
B: E-W, Cairo

ø N/S ⊖E/W	U.E.R.
1 Riyad-Helsinki	21 Swan Island-Helsinki
2 Batra-Wittsmoor	22 Swan Island-Jurbise
3 Batra-Helsinki	23 Swan Island-Monza
4 Dakar-Limours	24 Fort de France-Jurbise
7 Batra-St-Denis	25 Kuwait-Monza
8 Harrar-Monza	30 Masirah-Limours
10 Rome-St-Denis	32 Masirah-Leucate
15 Sackville-Limours	33 Bangkok-Helsinki
16 Sackville-Châtonnaye	34 Ismaning-Tsumeb
17 Moncton-Châtonnaye	35 Rome-Tsumeb
20 Poro-Helsinki	36 Allouis-Tsumeb

♦N/S ⊖E/W U.I.R.	Nov. 1936-Jan. 1937
001 Northern Ireland-Ottawa	013 Pittsburgh-Buenos Aires
002 Rennes-Ottawa	014 Buenos Aires-Strathburn (CAN)
003 New York-London	015 Buenos Aires-Ottawa
004 Northern Ireland-Washington	016 Toulouse-Buenos Aires
005 Rennes-New York	017 Rennes-Buenos Aires
006 New York-Brussels Eindhoven	018 Nice-Buenos Aires
007 Rennes-Washington	019 Buenos Aires-London
008 New York-Berlin	020 Paris-Buenos Aires
009 New York-Moscow	021 Northern Ireland-Buenos Aires
010 Buenos Aires-Washington	022 Buenos Aires-Brussels
011 Buenos Aires-New York	023 Buenos Aires-Berlin
012 New York-Buenos Aires	

ARCHIVES U.I.T. GENÈVE

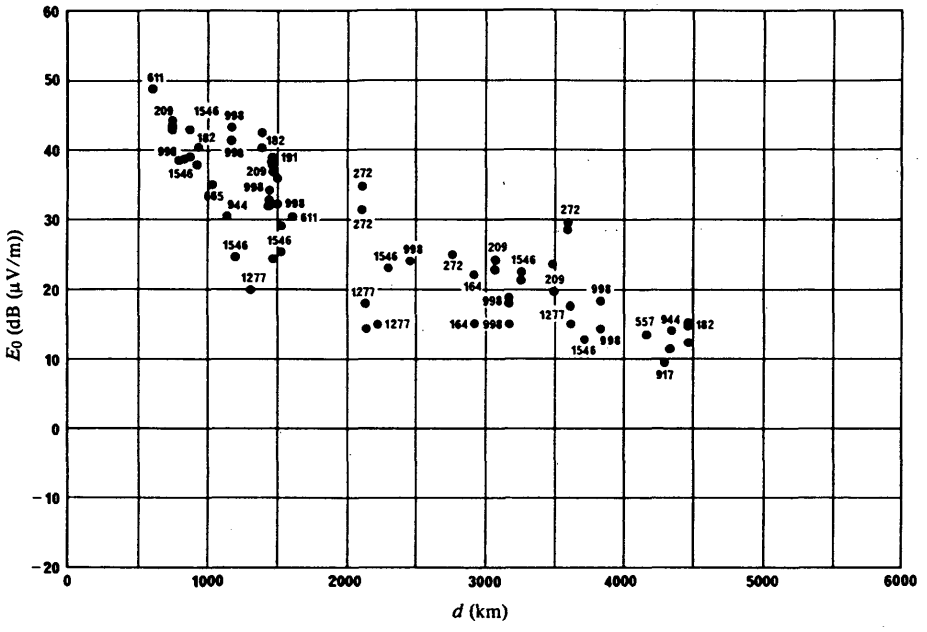


FIGURE 9 – *Results of measurements in the USSR*
(Frequencies in kHz shown beside each dot)

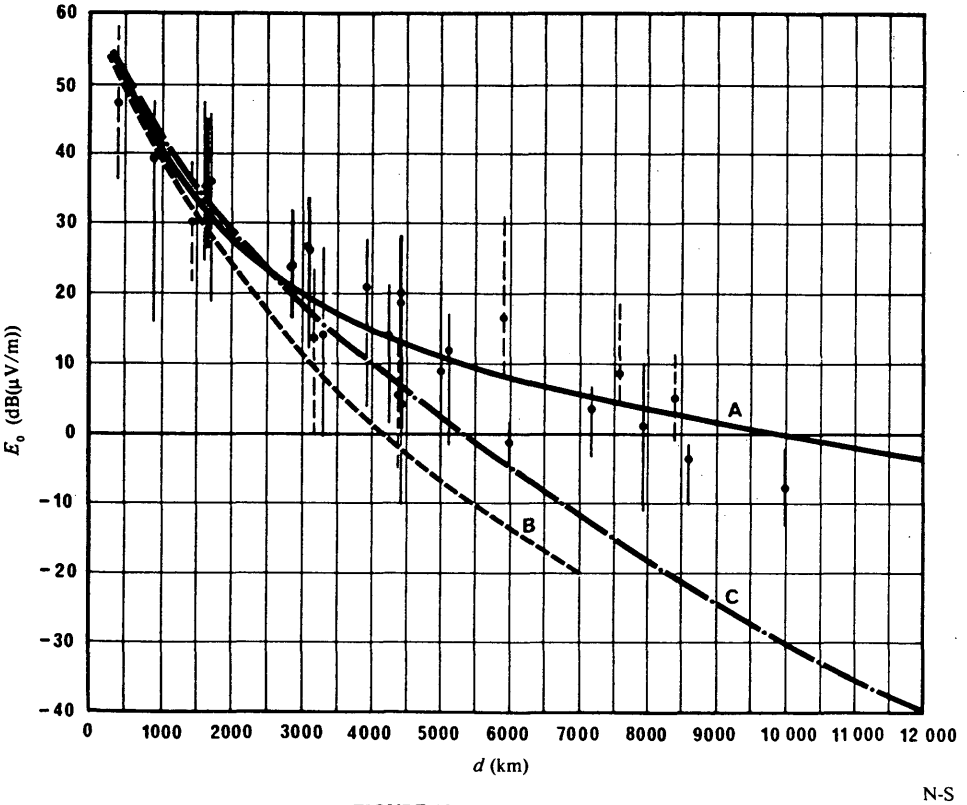


FIGURE 10 – *Asian measurements*

A: N-S curve, Cairo, 1938
B: E-W curve, Cairo, 1938
C: Curve for 1 MHz calculated from equation (5) of Report 575 for a geomagnetic latitude of 37°

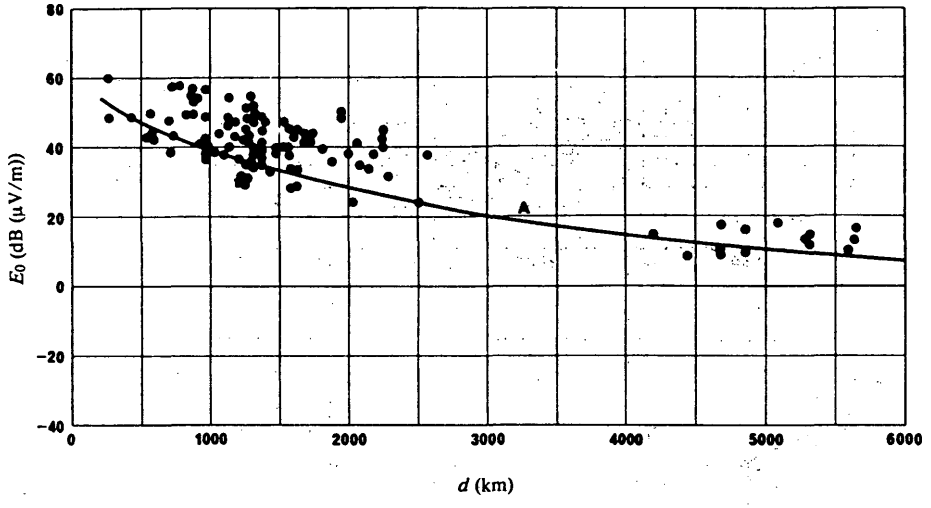


FIGURE 11 – *Japanese measurements*

Annual medians of hourly or half-hourly medians measured at frequencies around 500 kHz on East-West paths

A: N-S Cairo curve

5. Daytime propagation of the sky wave

5.1 LF Band

A study made in the United Kingdom [Bell and Knight, 1978] has shown that LF sky waves propagating over European paths during winter days are only 10 to 15 dB weaker than at night. This has been confirmed by measurements made in the United Kingdom at frequencies of 227 kHz and 251 kHz over distances of 1380 km and 1650 km respectively [Knight, 1983]. Day-time sky waves are also observed in spring and autumn, and during the spring equinox they are almost as strong as in winter. Weak day-time sky waves are observed in Europe during the summer. In India, however, the difference between summer and winter day-time field strengths is less than 6 dB [Sain *et al.*, 1968].

The conclusions stated above apply to the minimum of the sunspot cycle. It is not known how they are modified by solar activity and further measurements should be made at the peak of the next solar cycle.

5.2 MF Band

Measurements made in Germany on frequencies of 1160 kHz and 1538 kHz over distances of 610 km and 405 km respectively, showed that the annual mean value of the sky-wave field strength at noon is about 45 dB lower than the corresponding value at midnight [CCIR 1963-66d].

An analysis of the seasonal variations of the median values of the daytime field strengths over the period 1963 to 1965 was carried out by Täumer and Starick [1969]. Their results show a daytime decrease in field strength, from winter to summer, of about 18 dB at 845 kHz and 31 dB at 1466 kHz. The difference between day-time and night-time median field strengths at 845 kHz varies between about 42 dB in winter and 54 dB in summer, while at 1466 kHz the difference lies between 40 dB in winter and 65 dB in summer.

The day-time field strength at a frequency of 750 kHz and for a path length of 740 km has been recorded in Japan since 1969. The seasonal variation of the field strength at noon is similar to that of the zenith angle of the sun. The difference of the annual median field strengths at noon and at midnight during the moderate period of the sunspot cycle is 42 dB. The correction to be applied to the annual mean reference field strength valid for $R_{12} = 0$ is about $-0.055\ R_{12}$ dB, where R_{12} denotes the 12-month running average of the sunspot number [CCIR, 1970-74f].

Measurements made in the United States of America over eight propagation paths for a full solar activity cycle have been studied. The yearly analyses of the United States data, in general, agree quite well with those made in Germany and Japan. If measurements for the winter season alone are studied, however, disagreement becomes apparent. In the United States of America the difference between night-time (i.e. six hours after sunset) and day-time (i.e. noon) median field strengths during the winter usually varies between 25 and 30 dB. In the high-latitude areas, where the winter anomaly is particularly pronounced, the difference can be significantly smaller [Wang, 1983].

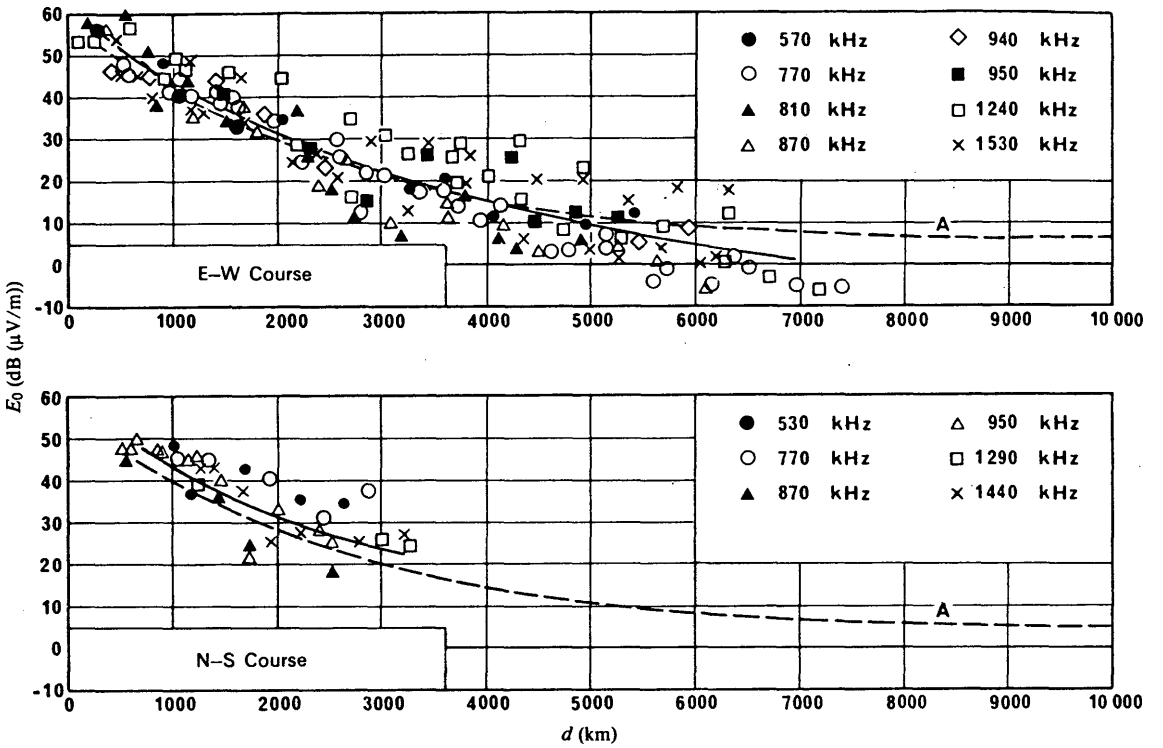


FIGURE 12a – *Night-time field strength at band 6 (MF) measured in the northern Pacific Ocean as a function of distance (Summer)*

A: Cairo N-S

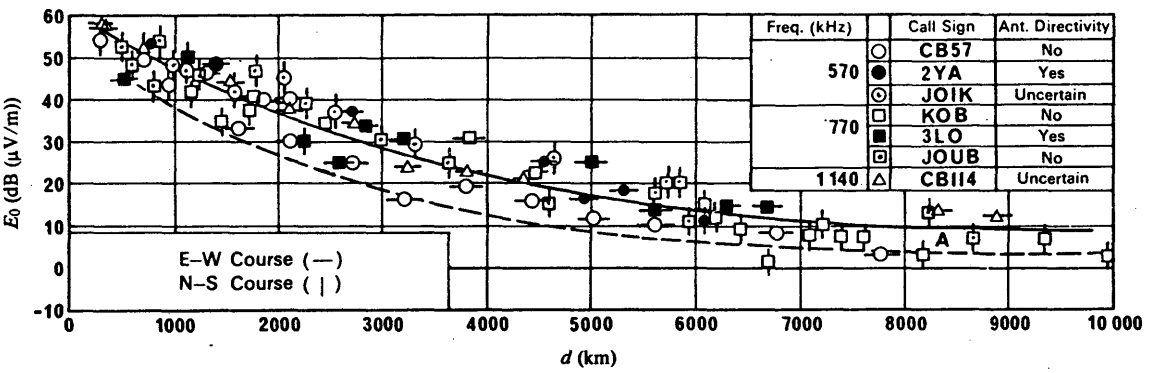


FIGURE 12b – *Night-time field strength at band 6 (MF) measured in the southern Pacific Ocean as a function of distance (Equinox)*

A: Cairo N-S

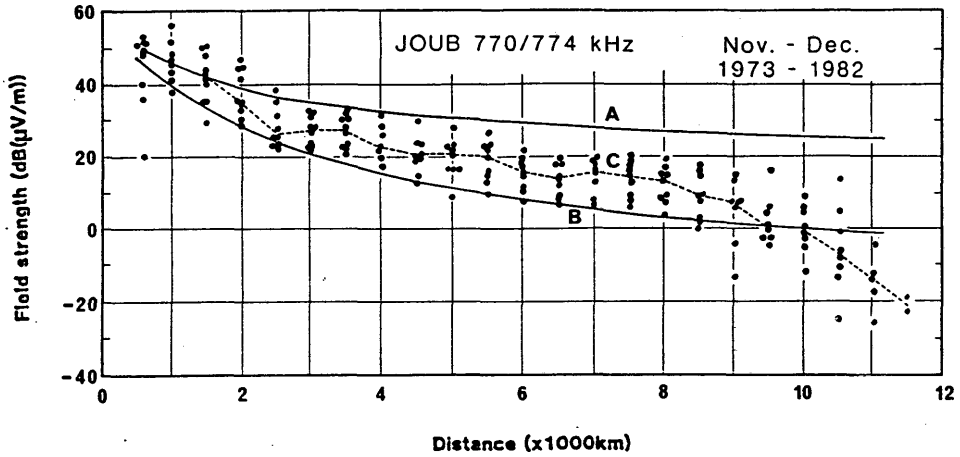


FIGURE 12c

MF sky-wave field strength during the night-time along the north-south sea paths over the east longitudes of 140°-108° (winter in the northern hemisphere)

A: free space field strength
B: Cairo N-S curve
C: median of measured field strength

6. Field-strength variations

A detailed study of LF and MF sky-wave field-strength variation has been made by Knight [1977b]. The study was based on all published sources of information, supplemented by further analysis of measured data.

6.1 *Fading rate*

Sky-wave signals vary continually in strength. The fading rate, defined as the number of times the field strength increases through the median value in a given time, is proportional to frequency and also depends on the angle of incidence at the ionosphere. On long-distance paths, E-layer reflections predominate and the fading rate for a frequency of 1 MHz is about 10 per hour in Europe; fading rates about three times greater have been measured in Japan. This comparatively slow fading is replaced by more rapid fading if F-layer reflections occur or if two propagation modes of comparable strength are received simultaneously.

6.2 *Amplitude distribution*

At the higher frequencies in the MF band, the field strength observed during two or three fading cycles usually obeys the Rayleigh distribution, see Report 266. At LF the difference between the quasi-maximum and the median is somewhat less (typically 3 dB at night and 1.7 dB during the day) and the distribution more closely resembles the log-normal.

Median field strengths measured at a given time vary randomly from night to night, with a log-normal distribution. The spread of values, measured over a period of days which is short enough to exclude seasonal and solar-cycle effects, shows no obvious dependence on frequency or path length. On most paths the difference between the field strengths exceeded on 10% and 50% of the nights lies between 3.5 and 8.8 dB; a difference of 5.5 dB may be regarded as typical. LF sky-waves propagating during the winter daytime vary from day to day in a similar manner.

Both the short-period and day-to-day variations contribute to the overall variation of the received signal. It is reasonable to assume that the field strength exceeded for 10% of the total time on a series of nights, during short periods centred on a specific time, is 6.5 dB greater at LF, and 8 dB greater at MF, than the median field strength derived from propagation curves or formulae. During similar periods on a series of days, the field strength exceeded at LF for 10% of the total time is 5 dB greater than the median field strength for that time of day.

6.3 *Diurnal variations*

At any given frequency the rates of increase of the field strength at sunset and the decrease at sunrise are almost independent of path length, although there is a slight tendency for the onset of night-time propagation to be progressively delayed as the path length increases. There is also a tendency for the onset of night-time propagation to be delayed at the lower frequencies in the MF band. In temperate latitudes the transition from day to night conditions starts in winter at least an hour before sunset but in summer the transition starts nearer to sunset and takes place more rapidly. The average diurnal-variation curve given in Fig. 3 of Annex I to Recommendation 435 is consistent with measurements [CCIR, 1970-74a; Knight and Williams, 1986].

Based on United States data, sky-wave field strength is highly frequency-dependent during transition hours [Wang, 1983]. For example, the signal of a 1530 kHz station is about 15 dB stronger than that of a 700 kHz station at sunrise or sunset. Consequently, a family of diurnal variation curves for different frequencies has been developed. When compared to the United States data, Fig. 3 (hourly loss factor) of Annex I to Recommendation 435 is most satisfactory for frequencies near 1000 kHz. Similar results are also quoted in Knight [1977b].

At LF the transition from day to night conditions in winter is very gradual in Europe, where the field strength does not reach its maximum value until about two hours before sunrise. The rapid decrease at sunrise is followed in winter by a gradual rise to a mid-day maximum which may be only 10 dB weaker than the maximum night-time field strength. In summer the field strength increases much more rapidly at sunset, and the diurnal variation resembles that observed at MF.

6.4 *Variation with season*

At night, MF sky waves propagating in temperate latitudes are strongest in spring and autumn and are weakest in summer and winter, the summer minimum being the more pronounced. The overall variation may be as much as 15 dB at the lowest frequencies in the MF band, decreasing to about 3 dB at the upper end of the band. At LF the seasonal variation at night has the opposite trend, with a pronounced summer maximum. The seasonal variation is much smaller in tropical latitudes.

Large seasonal variations are observed in daytime in Europe, where LF sky waves propagating in winter are at least 20 dB stronger than in summer and may be only 10 dB below night-time values. At MF the seasonal variation in Europe exceeds 30 dB but the winter daytime field strength is at least 10 dB lower than at LF.

Night-time MF sky-wave field strengths collected in low- and mid-latitude areas of the Americas show virtually no consistent pattern of any seasonal variation except a slight minimum in the summer. High-latitude field strengths collected in Alaska show a pronounced summer minimum and a consistent maximum in April [Hunsucker et al., 1989]. In a year of minimum sunspot number, night-time monthly median field strength for April is typically 10 to 15 dB greater than the annual median. Day-time field strengths however, show a strong maximum in the winter, similar to that observed in Europe.

6.5 *Variation with solar and magnetic activity*

In general, solar activity reduces MF night-time sky-wave field strengths. The reduction is a function of geomagnetic latitude, frequency, distance and sunspot number [Wang, 1977]. The reduction is greater in North America than in Europe and in tropical latitudes it is believed to be negligible. It has been reported [Wang, 1983, 1987] that at MF, the effect of solar activity at 2 hours after sunset is about twice as great, in terms of dB, than at 6 hours after sunset. Furthermore, recent high-latitude data collected in Alaska show that the field strength maximum tends to occur in the year immediately after sunspot minimum [Hunsucker et al., 1989]. Day-time sky-wave field strengths vary with solar activity similarly to field strengths at 2 hours after sunset.

The effect of the solar cycle at middle latitudes in Europe has an opposite influence on LF propagation (compared with MF). Increase in solar activity increases the night-time field strengths (by 2-4 dB over a solar cycle), and the increase in day-time field strength is somewhat greater [Report 265, Figure 11].

Mobile measurements along north-south sea paths [latitude 40°N to 47°S] over east longitudes of 140°-108° showed that in contrast to the results quoted above the night-time MF sky-wave field strength is influenced by solar activity. The field strength at the solar maximum was higher than that during the solar minimum by approximately 9 dB, as seen in Figure 13 [Nemoto et al., 1987; Kuriki et al., 1988].

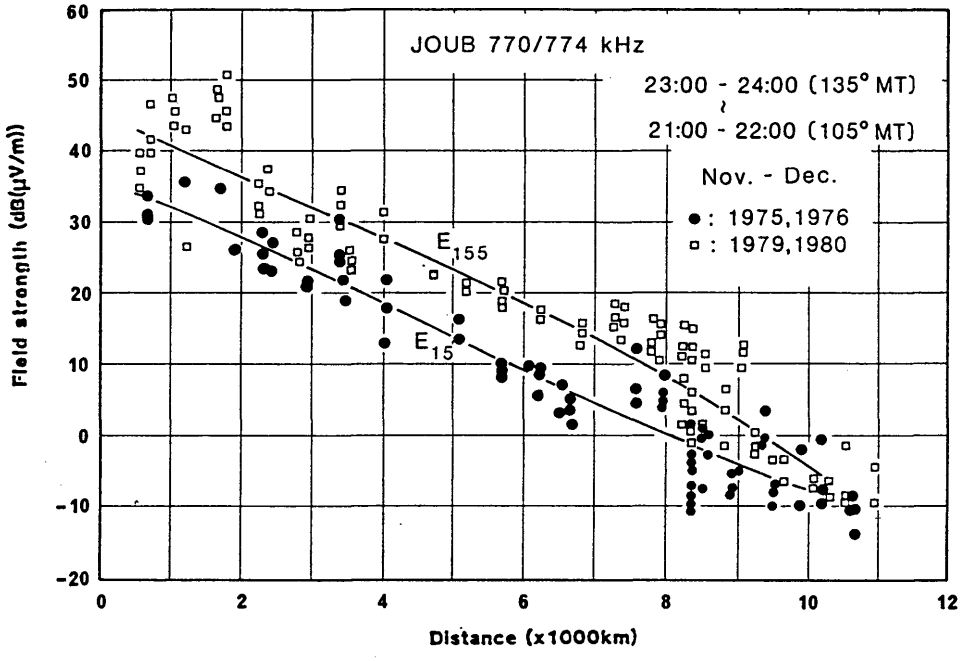
A theoretical examination of the solar activity dependence of night-time MF field strengths revealed that both the positive dependence (higher strength for higher activity) measured in the mobile experiment mentioned above and the negative dependence (higher strength for lower activity) found in North America and Europe could be consistently explained by assuming that MF waves propagate via a night-time E layer having a ledge of ionization below the peak of the layer [Kohata et al., 1989]. The ionization source for such a ledge is probably associated with magnetic storm and winter anomaly related phenomena [Hagg, 1982].

The larger variation observed on the North American paths, particularly for paths having mid- or control-points > 40° geomagnetic latitude, is probably due to their higher magnetic latitude, and to a greater magnitude of excess absorption associated with magnetic storm and post-storm effects.

Evidence based on North American data shows that the dominant factor in reducing MF night-time sky-wave field strength is the magnetic-activity-related absorption [Barghausen and Lillie, 1965; Hagg, 1982]. An additional factor which contributes sporadically to the field-strength reduction, during October to February, is the winter-anomaly-related absorption. These factors can cause large variations in median field strength.

Annual median (50%) and upper decile (10%) values of field strength are more closely related to magnetic activity than to the annual mean sunspot number *R*. Because of this interdependence on magnetic and solar activity, and since the correlation between MF field strengths on each of these factors separately is not yet established, it is at present not possible for these high geomagnetic latitude paths in North America to accurately predict the field-strength variation over the epoch of the solar cycle.

The effects of magnetic storms have a frequency dependence [Wang, 1983]. The storm-related absorption, particularly during the first few days after the onset of a storm, increases with increasing frequency.



E15: Field strength in the minimum solar activity (R_{12}=15)
E155: Field strength in the maximum solar activity (R_{12}=155)

FIGURE 13

Solar activity dependence of
MF sky-wave field strength during the night-time

7. Future work

7.1 Propagation data should be collected from those parts of the world where reliable data are not yet available.

7.2 There is a need to study and improve the accuracy of prediction by taking account of parameters such as ground conductivity not yet adequately considered.

7.3 Studies of sky-wave propagation both for short distances (less than 300 km) and for very long distances (greater than 3500 km) should be continued. The curves prepared so far have mainly been based, not on direct measurements of the sky-wave field, but on theoretical deductions. Since insufficient work has been done up to now on the critical frequency of the E layer at night, it is highly conjectural to extrapolate from vertical-incidence data to cover obliquely incident waves and thence to the calculation of sky-wave signals at short ranges. There is therefore a need to continue studies on the critical frequency of the E layer at night and on the reflection coefficient of the E and F layers for various angles of incidence at both MF and LF. If possible, direct short-distance measurements of sky waves should be made.

As regards long-distance measurements, they should help towards determining *inter alia* the influence of sunspot activity, and whether there are appreciable differences between over-sea paths and over-land paths.

7.4 There is a need for further measurements of sea gain at frequencies throughout the LF and MF bands to improve the accuracy of prediction. The variation of sea gain with ground conductivity should be studied. Measurements should also be made across sea channels of limited width to test the accuracy of the formula given in § 2.3 of Annex I of Recommendation 435.

7.5 Annex I of Recommendation 435 predicts excess polarization coupling losses of up to 28 dB per terminal on east-west paths close to the magnetic-dip equator. There is a need for further measurements to confirm these predictions.

7.6 There is a lack of detailed data on sunrise, sunset and daytime ionospheric propagation between 150 and 1600 kHz. Daytime propagation may be significant, particularly in winter months.

7.7 In Report 575 and in Annex I of Recommendation 435, geomagnetic latitudes are calculated by assuming an earth-centred dipole field model. More accurate representation of geomagnetic latitude has been derived [Hultqvist, 1958, Hakura, 1965]. More work is needed to determine to what extent the prediction will be improved by using the corrected geomagnetic latitude.

REFERENCES

ASSIS BRASIL, A. C. [1979] Absorção Ionosférica Noturna em Função da Frequência na Faixa de Radiodifusão (Night-time Ionospheric Absorption as a Function of Frequency in the MF Broadcasting Bands). MSc Thesis. Instituto Militar de Engenharia, Rio de Janeiro, Brazil.

BARGHAUSEN, A. F. [1966] Medium frequency sky-wave propagation in middle and low latitudes. *IEEE Trans. Broadcasting*, Vol. BC-12, 1-14.

BARGHAUSEN, A. F. and LILLIE, D. A. [1965] Some evidence of the influence of long term magnetic activity on medium frequency sky-wave propagation. *Proc. IEEE*, 2115-2116.

BELL, C. P. and KNIGHT, P. [1978] Daytime sky-wave propagation in the LF broadcasting band *EBU Rev. Tech.*, **167**, 2-6.

CROMBIE, D. D. [1979] Comparison of measured and predicted signal strengths of night-time medium frequency signals in the USA. *IEEE Trans. Broadcasting*, Vol. BC-25, 86-89.

DAMELIN, J. [1971] Long-term field strength measurements in the 550-1600 kHz frequency band. FCC Report No. R-7103. Supt. of Documents, US Govt. Printing Office, Washington DC 20402.

DIXON, J. M. [1960] Some medium frequency sky-wave measurements. *Proc. IRE*, Australia, Vol. 21, 407-409.

EBERT, W. [1962] Ionospheric propagation on long and medium waves. *EBU Rev.*, Part A, **71**, **72** and **73**; also EBU Technical Monograph TECH 3081.

ELLING, W. [1961] Scheinbare Reflexionshöhen und Reflexionsvermögen der Ionosphäre über Tsumeb, Südwest-Afrika, ermittelt mit Impulsen im Frequenzband von 350 bis 5600 kHz (Pulse measurements of virtual heights and reflection coefficients of the ionosphere over Tsumeb, South-West Africa in the frequency range from 350 to 5600 kHz). *AEÜ*, Vol. 15, 115-124.

EYFRIG, R., HOMUTH, H. and VOGT, K. [1975] LF and MF field strength measurements over great distances – final report. *NTZ*, Vol. 28, 30-32.

FERNANDEZ, M. and WANG, J. C. H. [1980] An analysis of the Mexican sky-wave field strength data. CITEL Doc. CARR/5-80 Add. 8.

GADDEN, K. J. [1964] Magnito-ionnaya teoriya (Magneto-ionic theory). Sbornik Geofizika i okolozemnoe kosmicheskoe prostranstvo, *Mir.*, Moscow, U.S.S.R.

HAGG, E. L. [1982] Reduction of MF skywave field strength at night due to magnetic-storm and winter-anomaly-related absorption. AGARD Conf. Proc. No. 305, *Medium, Long and Very Long Wave Propagation (at frequencies less than 3000 kHz)*, 29-1 to 29-9. Ed. J. S. Belrose. NASA Accession No. N82-27613. National Technical Information Service, Springfield, VA 22161, USA.

HAKURA, Y. [1965] Tables and maps of geomagnetic coordinates corrected by the higher order spherical harmonic terms. *Rep. Ion. and Space Res. Japan*, Vol. 19, **2**, 121-157.

HULTQVIST, B. [1958] The geomagnetic field lines in higher approximation. *Arkiv för Geofysik*, Vol. 3, **4**, 63-77.

HUNSUCKER, R.D., DELANA, B.S., and WANG, J.C.H. [1989] - Medium-frequency sky-wave propagation at high latitudes: results of a five-year study. IEEE Trans. on Broadcasting, Vol. BC-35, No. 2, 218-222.

ITU [1938] Documents of the International Radiocommunications Conference at Cairo, Vol. I, 425-433, Fig. 3. (See also Report of Committee on Radio Wave Propagation, *Proc. IRE*, Vol. 26, 1193-1234, Fig. 3).

ITU [1966] Final Acts of the African LF/MF Broadcasting Conference, Geneva, 1966.

KNIGHT, P. [1977a] LF and MF sky-wave propagation: the origin of the Cairo curves. BBC Research Dept. Report 1977/42.

KNIGHT, P. [1977b] LF and MF propagation: a study of sky-wave field-strength variation. BBC Research Dept. Report 1977/12.

KNIGHT, P. [1983] Ionospheric Propagation in the LF Broadcasting Band. BBC Research Dept. Report 1983/15.

KNIGHT, P., and WILLIAMS, W.F. [1986] - LF and MF sky-wave propagation: a comparison of measurements made at sunset and sunrise. BBC Research Department Report 1986/18.

KOHATA, H., KIMURA, I., OGAWA, T., and WAKAI, N. [1989] - Correlation of night-time MF signal strength with solar activity. Proc. International Symposium of Antenna and Propagation, 22-25 August 1989, Tokyo.

KURIKI, I., IGI, S. and WAKAI, N. [1988] - Solar activity dependence of MF sky-wave field strength in the night-time, J. Radio Res. Lab. (Japan), Vol. 35, No. 144, 43-56.

MAMBO, M., NAGANO, I., FUKAMI, T. and KAGAWA, Y. [1986] - Comparison of measured and predicted field strengths of medium frequency sky-waves over short distances in Japan. IEEE Trans. Ant. Prop., Vol. AP-34, No. 10, 1214-1222.

MÜLLER, K. [1965] Determination of the sky-wave field strength at short and medium distances from recordings of the total field on long and medium-wave transmitters. Techn. Mitt. RFZ, **9**, 89-95.

NEMOTO, C., FUJII, S. and INOUE, R. [July, 1976] Long-distance propagation characteristics of MF broadcasting waves as derived from a round-Pacific mobile experiment. *J. Radio Res. Labs.* (Japan), Vol. 22, 118.

NEMOTO, C., WAKAI, N., OSE, M. and FUJII, S. [1987] - Integrated results of the mobile measurements of medium frequency field strength along the Japan-Antarctica sailing course. Review of Radio Res. Lab. (Japan), Vol. 33, No. 168, 157-182.

PAN, Z. [1981] MF night-time sky-wave field strength prediction. *Guangbo Yu Dianshi Jishu* (Broadcasting and Television Engineering), Vol. 28, **3**, 1-6.

POKEMPNER, M. [1980] Comparison of available methods for predicting medium-frequency sky-wave field strengths. US Dept. of Commerce, National Telecommunications and Information Administration, Report 80-42, Washington, DC.

RAU, R. [1978] Propagation investigation in MF band at short distances. (In Polish). *Prace Instytutu Łączności.*

SAIN, M., RAO, M. K. and KUMAR, Y. [1968] Some studies of long-wave propagation of Radio Tashkent 164 kHz. *J. Inst.Telecomm. Engrs.* (India), Vol. 14, 533-536.

SCHWENTEK, H. and GEISWEID, K. H. [1975] Sky-wave field strength at 845 kHz observed on board a ship at distances between 1100 and 12 000 km. *NTZ*, Vol. 28, 241-244.

TÄUMER, F. [1968] Über die Ableitung von Ausbreitungskurven im Mittelwellenbereich in der afrikanischen Rundfunkregion. (On the derivation of propagation curves in the MF band for use in the African Broadcasting Area). *Techn. Mitt. RFZ*, Vol. 12, 178-182.

TÄUMER, F. and STARICK, E. [1969] Jahreszeitliche Feldstärkevariationen im Lang- und Mittelwellenbereich (Seasonal variations of field strength in the LF and MF bands). *Tech. Mitt. RFZ*, Vol. 13, 16-19.

UDALTSOV, A. N. [1971] O shirotnykh izmeneniyakh napryazhennosti poly ionosfernoi volny v nochnoe vremya (Latitudinal variations of the night-time field of the space-wave). *Geomag. i Aeronom.*, Vol. II, **5**, 912.

UDALTSOV, A. N. and SHLYUGER, I. S. [1972] Propagation curves of the ionospheric wave at night for the broadcasting range. *Geomag. i Aeronom.*, **10**, 894-896.

VILENSKI, I. M., UDALTSOV, A. N. and SHLYUGER, I. S. [1970] Field-strength of radio waves in the 150-1600 kHz range that propagate to great distances from the transmitter. *Geomag. i Aeronom.*, **10**, 204-207.

WANG, J. C. H. [1977] Prediction of medium-frequency sky-wave field strength in North America. *IEEE Trans. Broadcasting*, Vol. BC-23, 43-49.

WANG, J. C. H. [1979] Medium-frequency sky-wave propagation in Region 2. *IEEE Trans. Broadcasting*, Vol. BC-25, 79-85.

WANG, J. C. H. [1983] Interference and sharing at medium frequency: sky-wave propagation considerations. AGARD Conf. Proc. No. 332, *Propagation Aspects of Frequency Sharing, Interference and System Diversity*, 9-1 to 9-12. Ed. H. Soicher. NASA Accession No. N83-30873. National Technical Information Service, Springfield, VA 22161, USA.

WANG, J.C.H. [1985] - A sky-wave propagation study in preparation for the 1 605 - 1 705 kHz broadcasting conference. IEEE Trans. on Broadcasting, Vol. BC-31, 10-17.

WANG, J.C.H. [1987] - A study of MF sky-wave field strength data from selected paths. Proc. Ionospheric Effects Symposium, U.S. Government Printing Office, Washington, D.C. 20402.

WANG, J.C.H. [1989] - Prudent frequency management through accurate prediction of sky-wave field strengths. IEEE Trans. on Broadcasting, Vol. BC-35, No. 2, 208-217.

CCIR Documents

[1963]: Geneva; 209 (OIRT).

[1963-66]: **a.** VI/208 (People's Republic of Bulgaria); **b.** VI/205 (Australia); **c.** VI/75 (EBU-OIRT-URTNA); **d.** VI/252 (EBU).

[1966-69]: **a.** VI/186 (Federal Republic of Germany); **b.** VI/213 (New Zealand); **c.** VI/208 (EBU); **d.** VI/206 (U.S.S.R.).

[1970-74]: **a.** 6/177 (Australia); **b.** 6/295 (India); **c.** 6/97 (EBU); **d.** 10/82 (U.S.S.R.); **e.** 6/289 (Japan); **f.** 6/273 (Japan).

[1978-82]: **a.** 6/84 (China (People's Republic of)); **b.** Doc. 6/239 (Interim Working Party 6/4).

[1982-86]: ——————a. 6/211 (India); b. Doc. 105 IWP 6/4 (Brazil); c. Doc. 101 IWP 6/4 (the Chairman).

BIBLIOGRAPHY

PHILLIPS, G. J. and KNIGHT, P. [1965] Effects of polarization on medium-frequency sky-wave service including the case of multihop paths. *Proc. IEE*, Vol. 112, 31-39.

WASHBURN, J. C., RUSH, C. M. and STEWART, F. G. [1982] Development of techniques to assess interference to the MF broadcasting services. NTIA Report No. 82-90. NTIS Accession No. PB-82-194598. National Technical Information Service, Springfield, VA 22161, USA.

REPORT 265-7

SKY-WAVE PROPAGATION AND CIRCUIT PERFORMANCE AT FREQUENCIES BETWEEN ABOUT 30 kHz AND 500 kHz

(Study Programme 31D/6)

(1959-1963-1966-1970-1974-1978-1982-1986-1990)

1. Introduction

The LF band (30-300 kHz) provides for navigation and communications to intermediate distances, shorter than the global distances afforded by VLF (3-30 kHz) but longer than ground-wave distances characteristic of the MF broadcasting band (535-1705 kHz), although MF sky-wave signals propagate to great distances with relatively low loss at night. The use of frequencies in the LF band is limited by the available bandwidth and certain practical considerations, further discussed below. In this frequency range, at distances where the surface wave becomes too weak to be useful (a distance which depends on frequency, time of day, season, epoch of the solar cycle, and earth surface condition (distances of the order of 500 to 1500 km)), propagation, particularly at LF and below, continues between the Earth and the lower boundary of the ionosphere to great distances and is characterized by good reliability and stability. For a given radiated power, increased field strength is obtained with decreasing frequency, down to frequencies of 10 to 20 kHz [Watt, 1967] and the diurnal seasonal and solar cycle variations become smaller. Propagation conditions towards the top of the MF band become characteristic of the HF band. The maximum in the absorption of ionospheric radio waves lies in the frequency range 100 kHz to 1000 kHz. Owing to the long wavelengths involved, fading is characterized by spatial variations as the waves or modes add vectorially.

Comprehensive reviews of propagation in the VLF/LF range are given by Belrose [1968] and by Burgess and Jones [1975]. This subject has been overviewed and new results given at an AGARD Symposium on Medium, Long and Very Long Wave Propagation (see Bibliography and [CCIR, 1982-86a]).

Marine communications use LF and VLF, which are also used for point-to-point communications at times of severe ionospheric disturbances to HF circuits, since the lower frequencies are not in general adversely affected [Belrose and Ross, 1962], an exception being solar proton events affecting long range transpolar VLF circuits which traverse arctic or antarctic ice caps [Crombie, 1967, Reder and Westerlund, 1970]. Communication to points under the sea or beneath the ground can be achieved on these frequencies [Moore, 1967; Durrani, 1962 and 1964; Tsao and Bettencourt, 1967]. Propagation has been assumed to be essentially by way of vertical polarization, which at long distances is well preserved [Bracewell *et al.*, 1951]. A limitation, which is partly economic, is the need for large transmitting antenna installations and high transmitter powers. Another limiting factor is the increasing level of atmospheric noise with decreasing frequency (noise generated in the Earth's ionosphere can also become important at the lowest frequencies on some occasions in high latitudes), and thus, apart from the small total bandwidth available, services generally use a fairly narrow bandwidth and hence low communication rates [Belrose *et al.*, 1959].

Because of the stability of propagation (amplitude and phase), frequencies in the VLF/LF range are useful not only for communication but also for standard frequency and time broadcasts [Blair *et al.*, 1967], as well as navigation systems employing CW phase comparison [Williams, 1951] or direction-finding techniques. At frequencies above 100 kHz, where it becomes practical to isolate, in some circumstances, the ground wave by pulse and sampling techniques, highly accurate time and navigation systems can be devised [Doherty *et al.*, 1961].

Research has been concentrated on the VLF range and to a lesser extent on the LF and MF ranges. In describing propagation, it will be found useful to consider whether the transmission is by way of a once-reflected sky wave together with the surface wave, or whether waves reflected more than once from the ionosphere contribute to the received field strength. These considerations depend on frequency, distance, earth surface conditions, and ionospheric conditions [Wait, 1962].

Two methods are available for theoretically calculating the field strength of VLF and LF and MF signals.

1.1 The *"wave-hop" method* is that in which electromagnetic energy paths between a given transmitter and receiver are represented geometrically as is done in the case of HF.

This method treats radio transmission as taking place along certain paths defined by one or more ionospheric reflections, depending on whether the propagation in question involves one or more "hops". The total field is then the vectorial resultant of the fields due to each path. In view of the long wavelengths concerned, the diffraction of the waves by the earth's surface must be taken into account, which is not the case for HF. The wave-hop method may be justified by the fact that, with oblique incidence, the dimensions of the section of altitude in which propagation takes place are equal to or greater than several wavelengths.

With this method it is necessary to know the values of the reflection coefficients of the incident wave on the ionosphere. These vary greatly in altitude and the theoretical calculation of the reflection coefficients may be carried out in two different ways:

- if the ionosphere is regarded as homogeneous and as having a sharp lower edge, the reflection coefficients on the air-ionosphere interface can be calculated by the theory of rays, taking into account the polarization of the incident wave. One thereby obtains transmission and reflection matrices because, with an incident plane wave, the polarization of the reflected wave is usually elliptical;

- if we wish to use a real ionospheric model, which varies with altitude, the ionosphere must be divided into slices thin enough for the medium to be regarded as homogeneous. Since the thickness of each slice will then be small in comparison with the wavelength, the differential equations obeyed by each component of the electromagnetic field must be written out and solved below the ionosphere, taking account of boundary conditions at high altitude. If the solutions for the up and down paths are separated, the reflection coefficients can be determined. This method is usually called the "full-wave" theory.

1.2 The *"waveguide mode"* method is that in which propagation is analysed as the sum of the waves corresponding to each of the different types of propagation in the earth-ionosphere waveguide, analogous to a mode as defined for waveguides in the microwave region. The selection of the method to be used for field calculation depends on practical considerations of numerical calculation.

In the case of VLF at distances of less than 1000 km, and for LF in general, and at MF the series of modes are slightly convergent and the calculations then require adding together vectorially a large number of components. The wave-hop theory, on the other hand, requires only a limited number of paths, including the ground wave, and it is particularly convenient for the long-distance propagation of LF and MF, taking account, if possible, of the diffraction.

For VLF at distances of more than 1000 km, the wave-hop theory requires the vectorial addition of the fields due to a large number of paths whereas, since the series of modes converge rapidly, sufficient accuracy can be obtained by adding together only a small number of modes. The mode theory, therefore, is better suited to this type of propagation. Propagation at ELF also may be described in terms of a single waveguide mode.

The waveguide mode method is described in detail in Report 895.

2. "Wave-hop" propagation theory

2.1 *General description*

According to this theory, the sky-wave field (strength and phase) at a point is treated as the resultant of the fields created by different waves propagated directly from the transmitter in one or more hops. The total field at this point is then the resultant of the field due to the wave diffracted by the ground and of the field due to the sky wave.

The sky-wave field is calculated by applying the theory of rays in the regions where the methods of geometric optics are applicable and by integrating the effects of diffraction [Rydbeck, 1944; Bremmer, 1949; Wait, 1961] or by applying the full wave theory [Budden, 1961; Johler, 1962; Krasnushkin and Yablochkin, 1963; Pitteway, 1965] in regions where optics are no longer valid.

The geometry of a path comprising a single hop is shown in Fig. 1.

The surface of the Earth is defined by $r = a$ and a smooth reflecting ionospheric layer located at $r = a + h$. It is convenient to distinguish three cases. In the first, the receiving antenna located at $R_<$ is illuminated by the once-reflected sky wave for the transmitting antenna located at $T_<$, where i_g is less than $\pi/2$. In the second, the two antennas at T_c and R_c are located at the critical points where $i_g = \pi/2$. In the third case the antennas are located at $T_>$ and $R_>$ beyond the critical points such that the first sky-wave hop propagates into the diffraction or shadow zone.

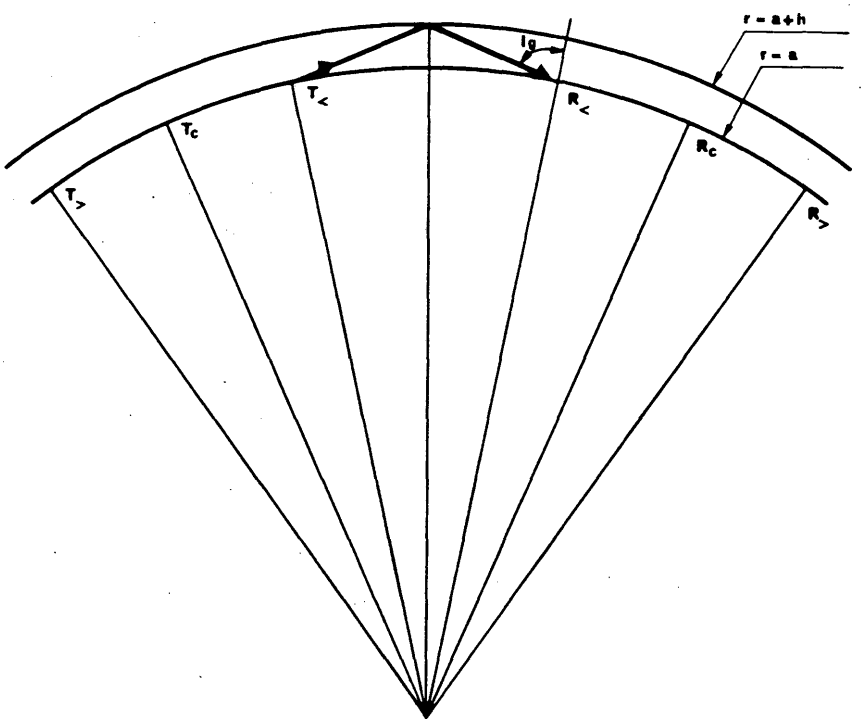


FIGURE 1 – *Ray path geometry for the wave-hop radio propagation theory (first hop sky wave)*

2.2 *Calculating the ray-path field strength*

The vertical component of electric field radiated from a short vertical electric dipole may be written as:

$$E_u \simeq 300\sqrt{p_t} \qquad \text{mV/m at 1 km} \tag{1}$$

where p_t is radiated power in kW.

The field strength of the downcoming sky wave, before reflection at the ground in the vicinity of the receiving antenna, is given by:

$$E_l = \frac{E_u}{L} \cos\psi \; {}_{\|}R_{\|} \; DF_t \qquad \text{mV/m} \tag{2}$$

where

L: sky-wave path length in km,

${}_{\|}R_{\|}$: the ionospheric reflection coefficient which gives the ratio of the electric field components parallel to the plane of incidence,

D: ionospheric focusing factor,

F_t: transmitting antenna factor,

ψ: the angle of departure and arrival of the sky wave at the ground, relative to the horizontal.

If reception is by a small in-plane loop antenna located on the surface of the Earth, the effective field strength of the sky wave is:

$$E_s = \frac{2E_u}{L} \cos\psi \; {}_{\|}R_{\|} \; DF_t \, F_r \qquad \text{mV/m} \tag{3}$$

For reception by a short vertical antenna equation (3) becomes:

$$E_s = \frac{2E_u}{L} (\cos\psi)^2 \; {}_{\|}R_{\|} \; DF_t \, F_r \qquad \text{mV/m} \tag{4}$$

where

F_r: is the appropriate receiving antenna factor.

For propagation over great distances, the wave-hop method can be extended to include skywaves reflected more than once from the ionosphere. For example for a two-hop skywave, the field strength received by a receiving loop antenna can be represented simply as:

$$E_s = 2\frac{E_u}{L} \cos\psi \; {}_{\|}R_{1\|} \; {}_{\|}R_{2\|} \; D^2 \; D_G \; {}_{\|}R_{g\|} F_t \, F_r \tag{5}$$

where

D_G: is the divergence factor caused by the spherical earth, approximately equal to D^{-1},

${}_{\|}R_{g\|}$: is the effective reflection coefficient of the finitely conducting earth,

L: is the total propagation path of the two-hop ray-path,

${}_{\|}R_{1\|}$ and ${}_{\|}R_{2\|}$: are the ionospheric reflection coefficients for the first and second reflection.

In general, the ionospheric reflection coefficients will not be equal, because the polarizations of the incident waves are not the same. However, in the simple method for calculating field strengths given here, for propagation at very oblique angles of incidence, ${}_{\|}R_{1\|} = {}_{\|}R_{2\|}$ as a first order approximation.

2.2.1 *Angles of elevation and ionospheric incidence*

The ray path geometry for determining the angles of departure and arrival of the sky wave at the ground (ψ) and ionospheric angles of incidence (i) are shown on Figs. 2 and 3. These angles are given in Fig. 2 for an effective reflection height of 70 km which corresponds to typical daytime conditions and in Fig. 3 for an effective reflection of 90 km which corresponds to typical night-time conditions. The effects of atmospheric refraction [Norton, 1960] on the departure and arrival angles are included and shown by the dashed curve although they are probably not valid for frequencies below about 50 kHz.

2.2.2 *Path length and differential time delay*

To calculate L the sky-wave path length and estimates of the diurnal phase changes, Fig. 4 is used. This shows the differential time delay between the surface wave and the one, two or three hop sky wave for ionospheric reflection heights of 70 and 90 km, corresponding to daytime and night-time conditions. A propagation velocity of 3×10^5 km/s is assumed.

2.2.3 *Focusing factor*

The ionospheric focusing factor, D, for a spherical earth and ionosphere [Wait, 1962] is shown in Fig. 5 for daytime conditions and in Fig. 6 for night-time conditions.

2.2.4 *Antenna factors*

The antenna factors, F_i and F_r, which account for the effect of the finitely conducting curved earth on the vertical radiation pattern of the transmitting and receiving antennas [Wait and Conda, 1958] are shown in Figs. 7 to 9. Factors are calculated for land, sea and ice conditions which are defined by their electrical characteristics (conductivity and permittivity), as shown in Table I:

TABLE I

	Conductivity σ (S/m)	Permittivity ε
Sea water	5	$80\ \varepsilon_0$
Land	2×10^{-3}	$15\ \varepsilon_0$
Polar ice	2.5×10^{-5}	$3\ \varepsilon_0$

where ε_0 is the permittivity of free space.

The curves were calculated assuming an effective Earth's radius, 8480 km, which is 4/3 of its actual value to take account of atmospheric refraction effects. The factors are the ratio of the actual field strength to the field strength that would have been measured if the Earth were perfectly conducting. Negative values of ψ refer to propagation beyond the geometric optical limiting range for a one hop sky wave (see Figs. 1 to 3).

2.2.5 *Ionospheric reflection coefficients* $_{||}R_{||}$

Values of the ionospheric reflection coefficient $_{||}R_{||}$ are shown in Fig. 10 for solar cycle minimum. To take account of frequency and distance changes, the values of $_{||}R_{||}$ are given as a function of $f \cos i$, where f is the transmitted frequency and i is the ionospheric angle of incidence [Belrose, 1957; Allcock, 1955; Piggott, *et al.* 1965]. Curves are shown for night, all seasons and day conditions during winter and summer seasons of the year. Measured values at vertical and oblique incidence are indicated based upon the results given in numerous reports [Allcock, 1955; Al'pert *et al.*, 1967; Bain *et al.*, 1952; Belrose, 1957 and 1963; Bickel, 1957; Bracewell, 1952; Bracewell *et al.*, 1953; Elling, 1960; Hopkins and Reynolds, 1954; Lauter and Triska, 1966; Lauter *et al.*, 1976; Sprenger and Lauter, 1966; Starick and Taumer, 1968; Straker, 1955; Weekes and Stuart, 1952].

In all cases the ionospheric reflection coefficient data given in the various references mentioned have been modified, if necessary, to account for ionospheric focusing, antenna factors, etc., so that the results of the measurements are consistent with the analysis technique given here.

The concept of an effective frequency $f \cos i$ for which reflection coefficients are constant cannot, however, always be relied on [Jones and Wand, 1969]. The curves in Figs. 10 are derived from data obtained at steep incidence ($d < 200$ km) and at more oblique incidence ($d > 500$ km) the $f \cos i$ concept is likely to be approximately correct for such distances. At intermediate distances, however, the concept of an equivalent frequency is likely to lead to substantial errors in reflection coefficient, because in such circumstances the reflection coefficient and polarization of the wave change rapidly with distance.

While many data have been incorporated into the curves in Fig. 10, which show that the ionospheric reflection coefficient varies with time of day (midnight and noon), and season, much more work is needed to establish clearly how it varies over the epoch of the solar cycle. There is clearly a solar cycle variation (see Fig. 11) in that reflection coefficients are larger in sunspot maximum years at the very low frequencies, whereas at medium frequencies they are smaller [Belrose, 1968]. The physical interpretation of this fact is as follows. During sunspot maximum years, the base of the ionosphere is lower and the electron density gradient is steeper than during sunspot minimum years. Thus, VLF waves which are reflected from this lower layer are more strongly reflected in sunspot maximum years, whereas MF waves, that are reflected above this lower layer, are more strongly absorbed. Clearly, the transition between greater and smaller reflection coefficients would be expected to be a function of frequency, time of day, season and epoch of the solar cycle; and a discontinuity in the reflection coefficient-frequency curve, at some particular frequency and time might be expected. A sharp change in the values for effective frequencies 35 to 45 kHz is apparent in the data for sunspot maximum years in summer, but this is not revealed in the presentation of the data here.

It should be noted that the frequency range of the MF broadcast band for oblique propagation lies in the range of effective frequencies where the solar cycle change in ionospheric reflectivity is opposite. That is, 1600 kHz propagated over a path of 1500 km corresponds to a $f \cos i$ of 278 kHz; whereas at 500 kHz the effective frequency is 86 kHz. An example of a calculation by the ray path method is given in Annex I.

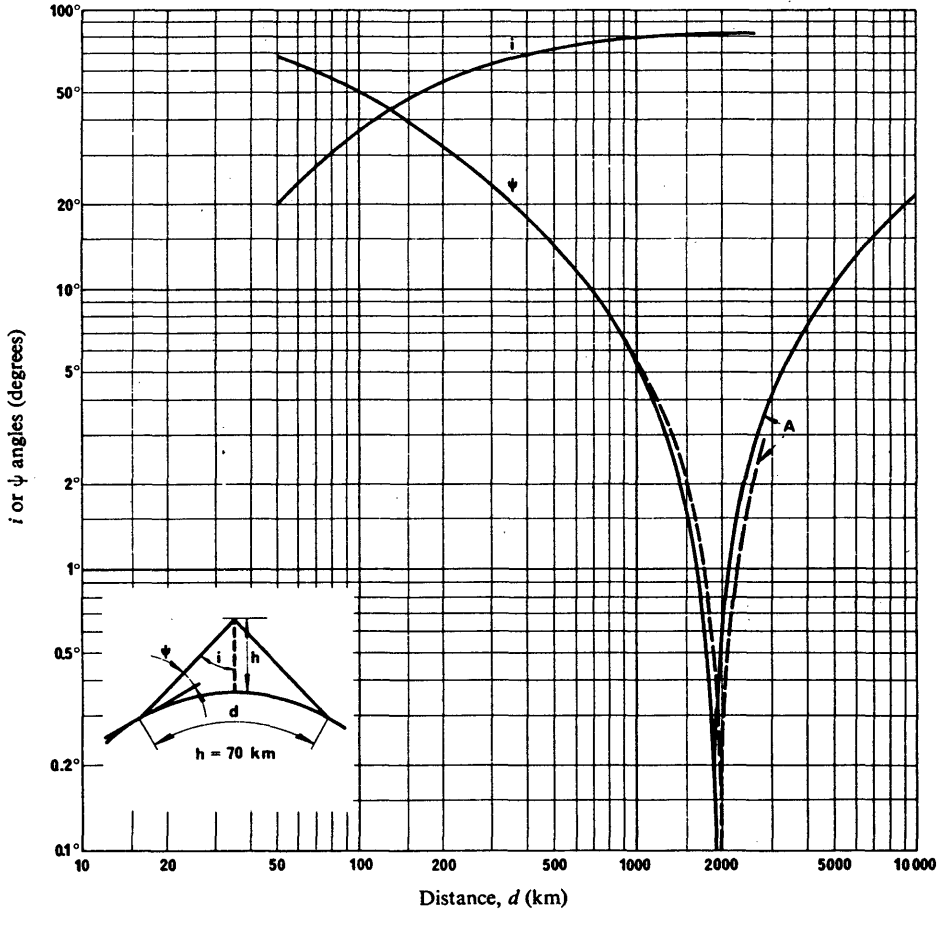


FIGURE 2 – *Departure and arrival angles (ψ) and ionospheric angles of incidence (i) for typical daytime conditions (h=70 km). The dashed curve includes the effects of atmospheric refraction*

A: negative ψ

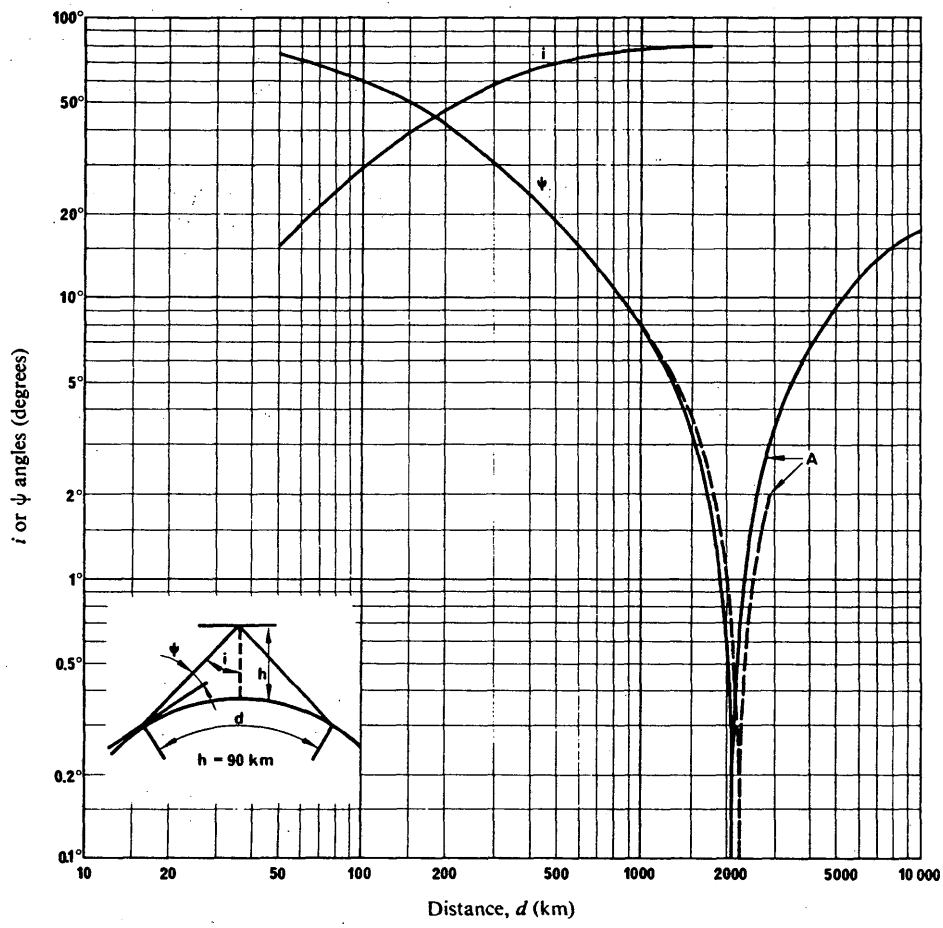


FIGURE 3 – *Departure and arrival angles (ψ) and ionospheric angles of incidence (i) for typical night-time conditions (h=90 km). The dashed curve includes the effects of atmospheric refraction*

A: negative ψ

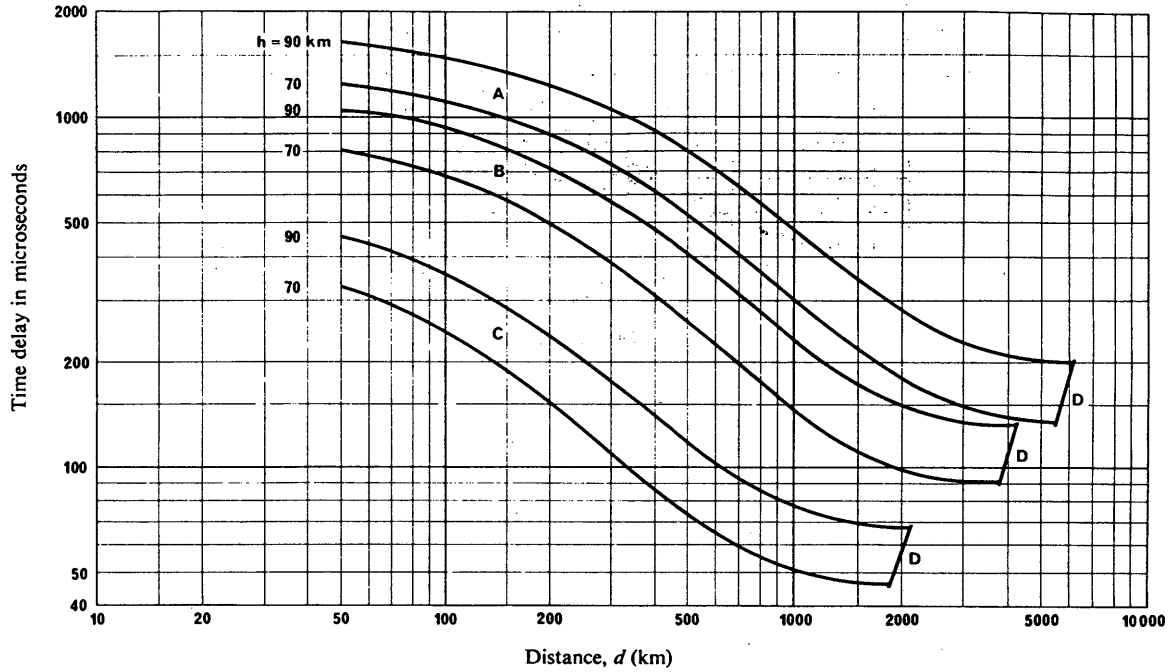


FIGURE 4 – *Differential time delay between surface wave and one, two and three hop sky waves*

A: 3 hop
B: 2 hop
C: 1 hop
D: Limiting range

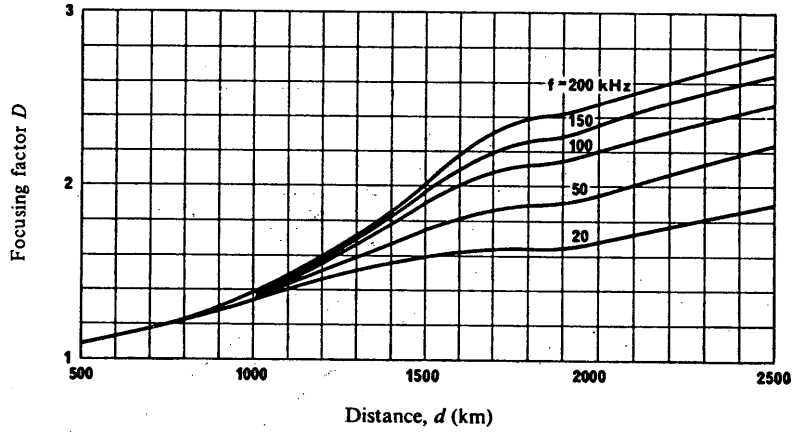


FIGURE 5 – *Ionospheric focusing factor – daytime*

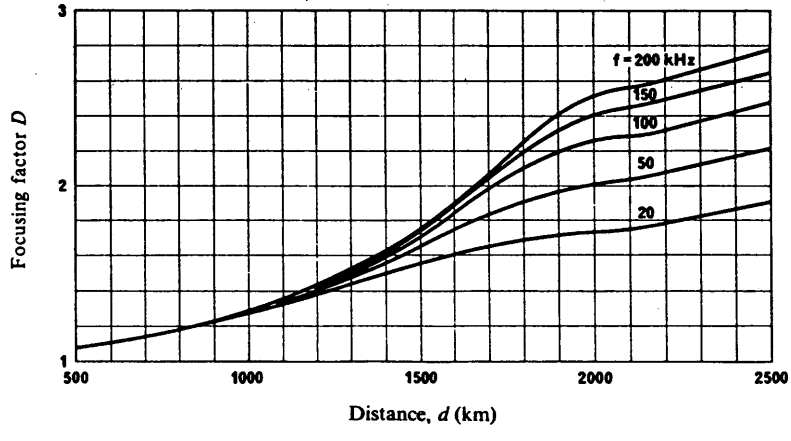


FIGURE 6 – *Ionospheric focusing factor – night-time*

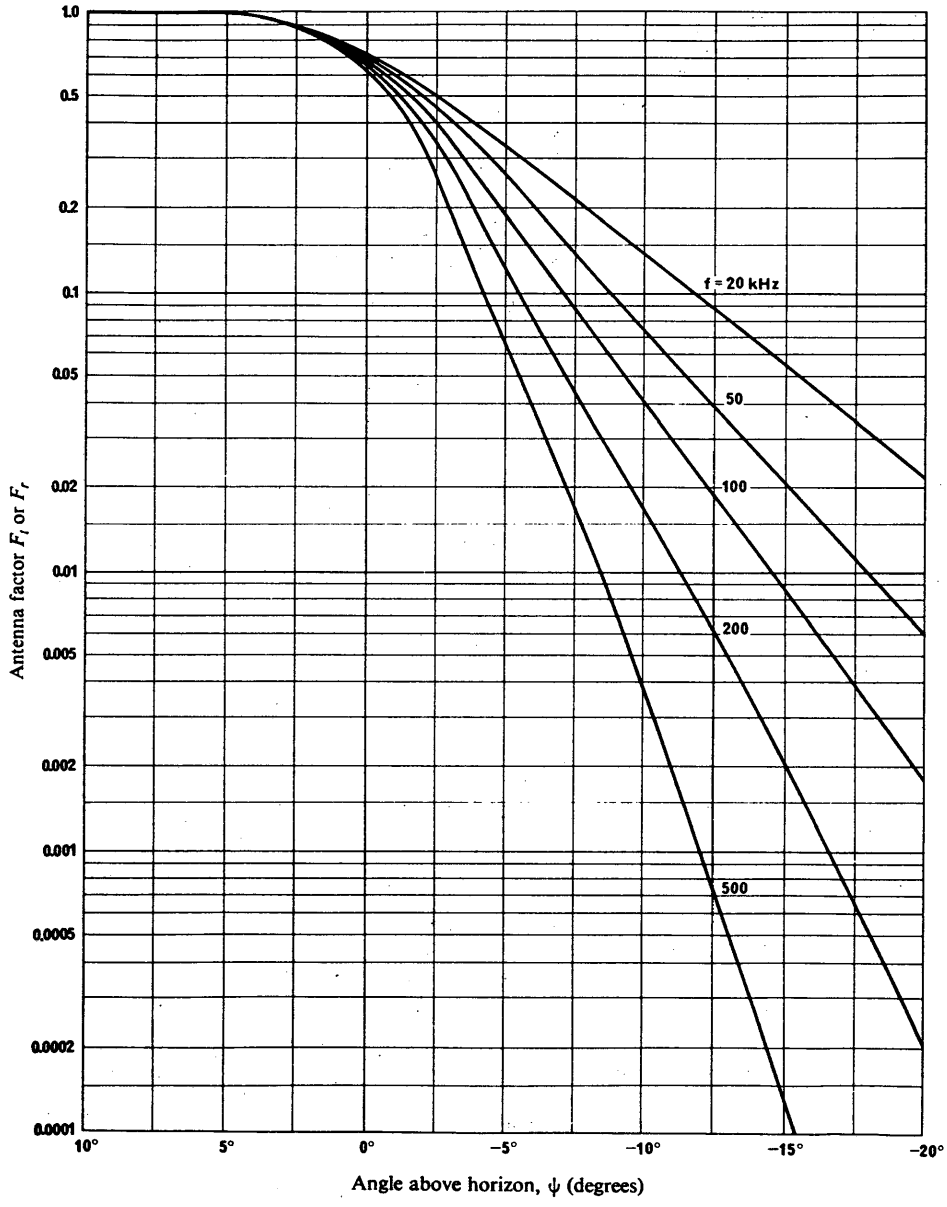


FIGURE 7 – *Antenna factor*

Sea water
$\varepsilon = 80\ \varepsilon_0$
$\sigma = 5$ S/m
$a = 4/3 \times 6360$ km

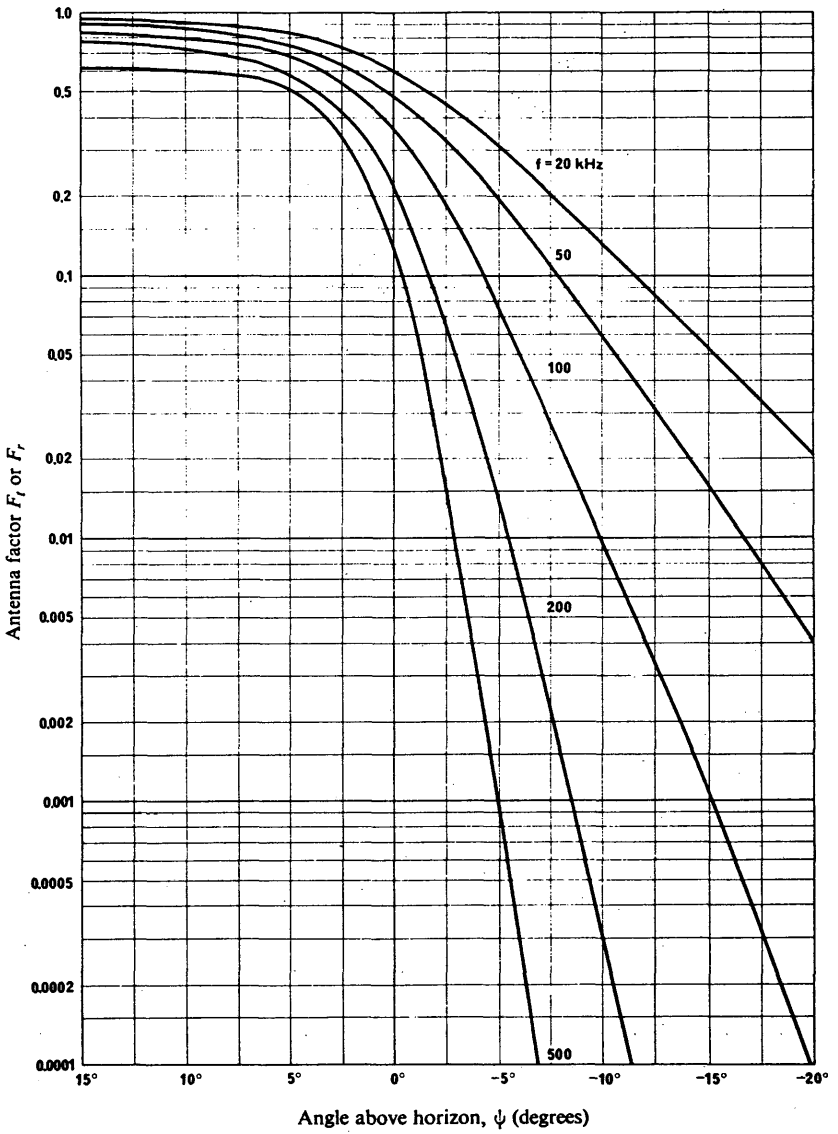


FIGURE 8 – *Antenna factor*

Land

$\epsilon = 15\ \epsilon_0$
$\sigma = 2 \times 10^{-3}$ S/m
$a = 4/3 \times 6360$ km

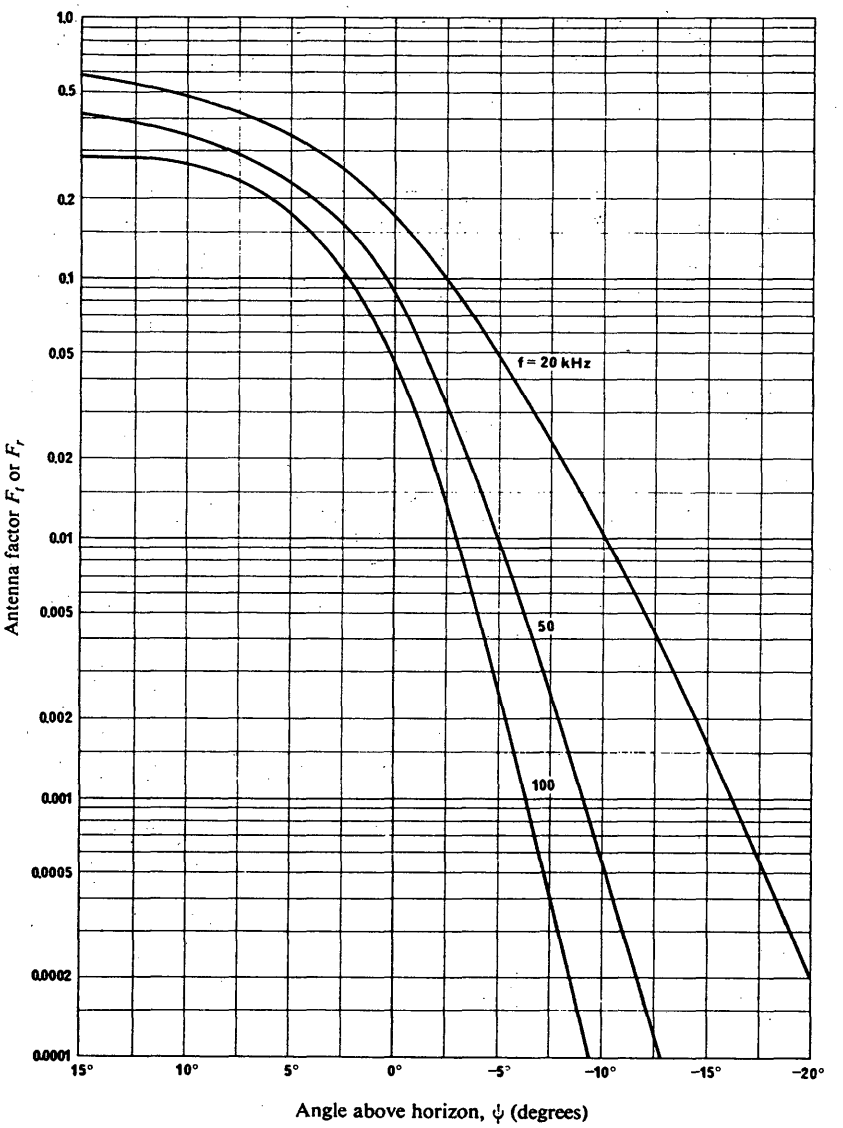


FIGURE 9 – *Antenna factor*

Ice at –4 °C

$\epsilon = 3\ \epsilon_0$
$\sigma = 2.5 \times 10^{-5}$ S/m
$a = 4/3 \times 6360$ km

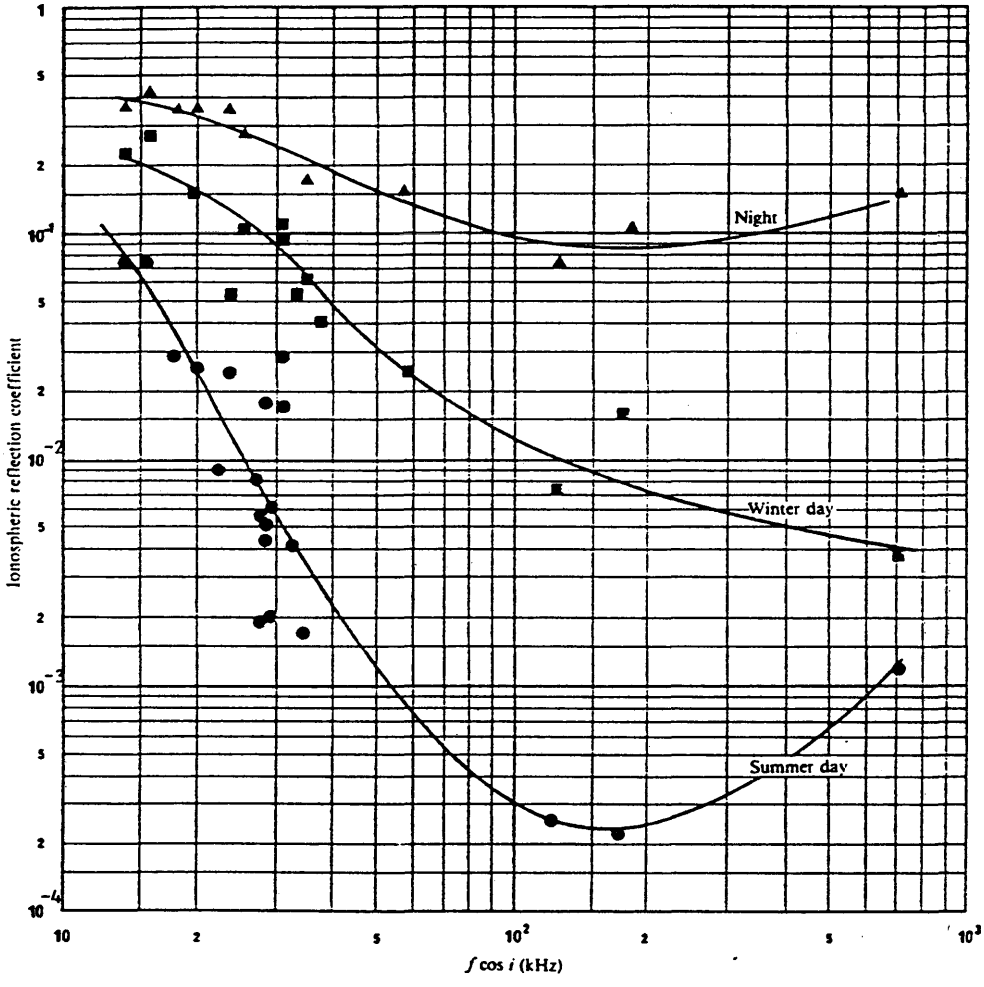


FIGURE 10 – *Ionospheric reflection coefficients – solar minimum conditions*

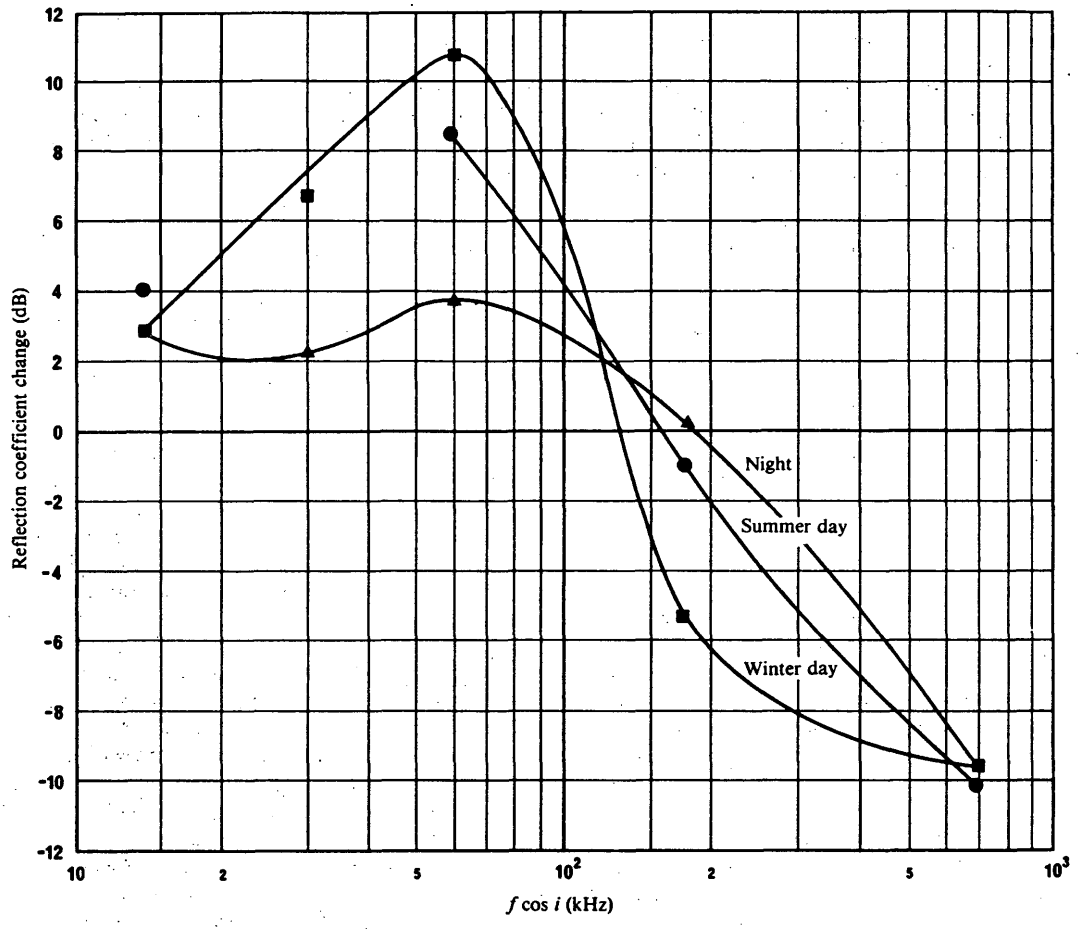


FIGURE 11 – *Change in reflection coefficient (dB) from sunspot minimum to maximum years as a function of effective frequency and time*

2.3 *Calculating the full wave field strength*

This method uses the full wave solutions for the various hops composing each path, the calculation of which has now been made possible by the existence of high-speed computers [Wait, 1961; Berry, 1964]. Berry [1967] compares the full wave method with the method described above. A report [Berry and Christman, 1965] provides curves of amplitude and phase and demonstrates a process for the separation of the effects of ionospheric reflections from those due to the diffraction propagation in a manner similar to that described for the ray-path method. A computer programme is available for these computations of field strength by means of the wave-hop method [Berry and Herman, 1971].

3. Measurements and analyses of LF sky-wave propagation

Measurements of 100 kHz signals, transmitted from Y station of the north-west Pacific chain of the Loran-C navigation system (26°36'N, 128°09'E, Okinawa, Japan) and received at Lintong, China (34°22'N, 109°13'E) (the distance 2 006 km), have been conducted continuously since 1980 and they show that the phase delay and the field strength of a 100 kHz one-hop sky-wave vary with the solar cycle, the season and the time of day. For instance, the monthly mean value of the hourly delay for noon in winter is about 2.5 μs greater than that in summer and the field strength for daytime in winter is about 2.5 dB higher than in summer for the same year. As for the same season in different

years, the delay at solar minimum is about 1 μs greater than that at solar maximum and the field strength at solar minimum is about 5 dB higher than that in solar maximum. The increments in the monthly mean value of the hourly delay corresponding to the period from 0800 hours to 1200 hours local time are about 4.5 μs, 3.5 μs and 2.5 μs for winter, spring or autumn, and summer respectively, showing regularity of variation with the solar zenith angle (Pan and Li, 1986; Pan et al., 1988).

4. Future work

The theory of radio wave propagation at VLF, LF and MF, necessary to estimate field strengths, is now becoming fairly well understood. Two competing theories are used to describe propagation in the VLF and LF bands: the wave-hop theory and the wave-guide mode theory. The solutions obtained from the wave-hop theory are generally most suitable for short distances and the higher (LF and MF) frequencies, while the wave-guide mode theory is most suitable for longer distances and the lower (VLF) frequencies.

The wave-hop theory describes the propagation using terms that correspond to physically real quantities that the radio engineer can easily visualize.

It now seems possible, at least for paths at VLF, that better propagation predictions could be made from full-wave calculations using model ionospheres than is possible by reading curves such as those in Figs. 10 and 11. Efforts to construct such model ionospheres for the D-region should be encouraged – night and noon models for various seasons, latitudes and solar activities should first be produced.

Electron density distributions which may also be useful as models under specified conditions can be found in several papers [Bain and Harrison, 1972; Belrose and Segal, 1974; Berry, 1977; Coyne and Belrose, 1972; Mechtley *et al.*, 1972; Montbriand and Belrose, 1979; Rowe *et al.*, 1974; Thomas and Harrison, 1970]. Guidance on the construction of models for other conditions has also been given [Bain, 1981; Belrose and Segal, 1974].

A more comprehensive study should be made by comparing the ray-path solutions (with diffraction corrections) and the wave-hop solutions in order to establish the validity of the approximations inherent in the former approach.

There is currently a lack of propagation data from which revised ionospheric reflection coefficients as a function of frequency, distance, time of year, solar and geomagnetic activity and other parameters can be derived. Because of this, the various theoretical treatments described above have not been adequately compared with experimental data and their usefulness is not yet fully achieved.

Concerning the reliability of the curves for reflection coefficients, Bell and Knight [1978] have noted that their measured day-time field strengths for Warsaw-Kingswood, 227 kHz/1370 km ($f \cos i = 31.6$ kHz) and for Tipaza-Kingswood, 251 kHz/1650 km (30.6 kHz), lie above those predicted by the summer, sunspot minimum curve. But they note that the summer field strengths may be influenced by ground waves since they measured the total field. On the other hand, field-strength measurements made for the paths Rome-Kolberg, 845 kHz/1143 km (154 kHz) and Monte Carlo-Kolberg, 1466 kHz/1050 km (280 kHz) have revealed that the diurnal variation observed in summer is greater than that predicted by the curves [Taumer and Starick, 1969]. It should be noted that, while Fig. 10 has been redrawn, and additional data have been included, the accuracy of the curves has not been improved. There is a scatter in the values of the summer data (by +15 dB to −8 dB for $f \cos i \sim 30$ kHz), and there is an absence of data for $f \cos i > 40$ kHz for long distance propagation. It should be noted that for all oblique incidence data except for one set of observations, ionospheric reflection coefficients have been determined from the interference maxima and minima of sky and ground waves, first determined by Bracewell *et al.* [1951] and Belrose [1957 and 1968], and also used by Starick and Taumer [1968]. Some data points have been determined from 180 kHz Loran-type pulse transmissions, from observations reported by Crichlow *et al.* [1946], and, therefore, the sky wave was clearly discernible. The analysis of propagation data at 40 kHz obtained in Japan in 1978 and 1979 shows that the sky-wave field strength of low frequency radio waves enhances during winter anomaly days of the ionospheric absorption, the increase of the reflection coefficient being 3 dB, and the monthly averaged reflection coefficient varies stepwise throughout a year, taking values 0.22 and 0.12 during winter (November to May) and summer (June to October) periods respectively [Ishimine et al., 1985; Ishimine and Echizenya, 1986].

More measurements are needed to establish differences between middle, low and high altitudes. For example, it is shown [Watt and Plush, 1959; Belrose, 1968; Morfitt, 1977] that marked effects occur due to the low ground conductivities encountered in arctic areas.

A desirable way to carry out these measurements would be to use an aircraft flying along great circles between transmitters and field receiving stations. Fixed receivers which would monitor the signals continuously could then be used to determine changes in the propagation parameters resulting from diurnal and seasonal variations and changes caused by differences in solar activity.

The other approach which is also desirable is to use measurements by rockets or ground-based techniques to determine the vertical variations of electron density in the lower ionosphere. The resulting profiles should then be used to calculate ionospheric reflection coefficients. These would then be used to calculate propagation parameters for comparison with the experimental results [Belrose and Segal, 1974]. Electron density measurements are particularly required at heights below 70 km where there are large discrepancies in existing observations, at night-time and at low latitudes.

5. Comparison with CCIR methods for predicting sky-wave field strengths at frequencies above about 150 kHz

Alternative methods to calculate night-time field strengths at LF, and above, to 1705 kHz, are given in Report 575. An intercomparison of results obtained by the methods proposed in the present Report and Report 575 should be made. Certainly field strengths predicted by the alternative methods should be consistent for frequencies and distances which are the same.

A comparison of CCIR methods for predicting sky-wave field strength above about 150 kHz has been made by Interim Working Party 6/5. It is shown that the measured values of field strength agree well with the calculated values from Report 265 for daytime in winter, but are 8 to 10 dB greater than those for daytime in summer or for night-time. Recommendation 435 (night-time only) gives the same difference [CCIR, 1986-1990].

REFERENCES

ALLCOCK, G. McK. [1955] Ionospheric absorption at low and medium frequencies. *The Physics of the Ionosphere.* The Phys. Soc. of London, 14-19.

AL'PERT. Ya. L., GUSEVA, E. G. and FLIGEL, D. S. [1967] *Propagation of LF Electro-Magnetic Waves in the Earth-Ionosphere Waveguide.* Academy of Sciences of the U.S.S.R.

BAIN, W. C. [1981] Models of the ionospheric D region at noon. IEE Conf. Proc. 195, 203-206.

BAIN, W. C., BRACEWELL, R. N., STRAKER, T. W. and WESCOTT, C. H. [1952] The ionospheric propagation of frequency 16 kc/s over distances of about 540 km. *Proc. IEE Monograph,* 37, 99 (Pt. IV), 250.

BAIN, W. C. and HARRISON, M. D. [1972] Model ionosphere for D region at summer noon during sunspot maximum. *Proc. IEEE.*, Vol. 119, 790-796.

BELL, C. P. and KNIGHT, P. [1978] Daytime propagation in the LF broadcasting band. *EBU Rev. Tech.* **167**, 3-7.

BELROSE, J. S. [1957] Some investigations of the lowest ionosphere. Ph.D. Thesis Univ. of Cambridge, first copy, 1956; revised copy.

BELROSE, J. S. [1963] The oblique reflection of low-frequency radio waves from the ionosphere. *Propagation of Radio Waves at Frequencies below 300 kc.* Ed. Blackband, AGARDograph 74, 149-165, Pergamon Press.

BELROSE, J. S. [1968] Low and very low frequency radio wave propagation. AGARD Lecture Series XXIX, NTIS Accession No. AD676788, National Technical Information Service, Springfield, Va. 22161, USA.

BELROSE, J. S., HATTON, W. L., McKERROW, C. A. and THAIN, R. S. [1959] The engineering of communication systems for low frequencies. *Proc. IRE,* Vol. 47, 661.

BELROSE, J. S. and ROSS, D. B. [1962] Observations of unusual LF propagation made during polar cap disturbance (PCD) events. *J. Phys. Soc. Japan,* **17**, Supplement A-II (Int. Conf. on Cosmic Rays and the Earth Storm), 126-130.

BELROSE, J. S. and SEGAL, B. [1974] On interpretation of CW propagation data for long radio waves. Methods of Measurements and Results of Lower Ionosphere Structure. COSPAR Symposium, Akademic-Verlag, Berlin, 77-109.

BERRY, L. A. [1964] Wave-hop theory of long distance propagation of low frequency radio waves. *NBS J. Res.*, Vol. 68D, 1275-1284.

BERRY, L. A. [1967] Wave-hop radio propagation theory. Conference on MF, LF and VLF Radio Propagation. IEE. Conf. Publ. 36, 63-69.

BERRY, L. A. [1977] A revised model of the electron density in the lower ionosphere. Command and Control Technical Centre (DCA), Tech. Rep. 111-77, NTIS Accession No. AD17883. National Technical Information Service, Springfield, Va. 22161, USA.

BERRY, L. A. and CHRISTMAN, M. E. [1965] Numerical values of the path integrals for low and very low frequencies. NBS Tech. Note No. 319. Supt. of Documents, US Govt. Printing Office, Washington, DC 20402.

BERRY, L. A. and HERMAN, J. E. [1971] A wave-hop propagation program for an anisotropic ionosphere. OT Telecom. Res. Rept. 11 (GPO Stock No. 0300-0316). Office of Telecommunications, Supt. of Documents, US Govt. Printing Office, Washington, DC 20402.

BICKEL, J. E. [1957] A method for obtaining reflection coefficients and its application to 135.6 kc/s data in the Alaskan area. *J. Geophys. Res.*, Vol. 62, 373-381.

BLAIR, B. E., CROW, E. L. and MORGAN, A. H. [1967] Five years of VLF world-wide comparison of atomic frequency standards, *Radio Sci.*, Vol. 2, (New Series), 627-636.

BRACEWELL, R. N. [1952] The ionospheric propagation of radio waves of frequency 16 kc/s over a distance of about 200 km. *Proc. IEE*, Vol. 99 (Pt. IV), 217.

BRACEWELL, R. N., BUDDEN, K. G., RATCLIFFE, J. A., STRAKER, T. W. and WEEKES, K. [1951] The ionospheric propagation of low and very low-frequency radio waves over distances less than 1000 km. *Proc. IEE*, Vol. 98 (Pt. III), 221-236.

BRACEWELL, R. N., HARWOOD, J. and STRAKER, T. W. [1953] The ionospheric propagation of radio waves of frequency 30-65 kc/s over short distances. *Proc. IEE, Monograph*, **84**.

BREMMER, H. [1949] *Terrestrial Radio Waves.* Elsevier Publishing Co., London, UK.

BUDDEN, K. G. [1961] *Radio Waves in the Ionosphere.* Cambridge University Press, Cambridge, UK.

BURGESS, B. and JONES, T. B. [1975] The propagation of LF and VLF radio waves with reference to some systems applications. *Radio and Electron. Engr.*, Vol. 45, 47-61.

COYNE, T. N. R. and BELROSE, J. S. [1972] The diurnal and seasonal variation of electron densities in the mid-latitude D region under quiet conditions. *Radio Sci.*, Vol. 7, 163-174.

CRICHLOW, W. Q., HERBSTREIT, J. W., JOHNSON, E. M. and SMITH, C. E. [1946] Measurement technique and analysis of low frequency Loran system. Report No. ORS-P-23-S. Operational Res. Staff, Washington, DC, USA.

CROMBIE, D. D. [1967] The waveguide mode propagation of VLF radio waves to great distances. IEE (London) Conf. Publ. 36.

DOHERTY, R. H., HEFLEY, G. and LINFELD, R. F. [1961] Timing potentials of Loran-C. *Proc. IRE*, Vol. 49, 1659-1673.

DURRANI, S. H. [1962] Air-to-undersea communication with electric dipoles. *IRE Trans. Ant. Prop.*, Vol. AP-10, 524-528.

DURRANI, S. H. [1964] Air-to-undersea communication with magnetic dipoles. *IEEE Trans. Ant. Prop.*, Vol. AP-12, 464-470.

ELLING, W. [1960] Scheinbare Reflexionshöhen und Reflexionsvermögen der Ionosphäre über Tsumeb, Südwest-Afrika, ermittelt mit Impulsen im Frequenzband von 350 bis 5600 kHz (Pulse measurements of virtual heights and reflection coefficients of the ionosphere over Tsumeb, South West Africa, in the frequency range from 350 to 5600 kHz). *AEÜ*, **15**, 115-124.

HOPKINS, H. G. and REYNOLDS, L. G. [1954] An experimental investigation of short distance ionospheric propagation at low and very low frequencies. *Proc. IEE*, **101** (Pt. III), 21-34.

ISHIMINE, T. and ECHIZENYA, Y. [1986] - The winter anomaly as seen in the propagation of low frequency 40 kHz waves. J Atmos. Terr. Phys. Vol. 48, 1233-1239.

ISHIMINE, T., ISHII, T. and ECHIZENYA, Y. [1985] - The seasonal variations of the D region as inferred from propagation characteristics of LF radio waves. Handbook for MAP (Middle Atmosphere Program), ed. S. Kato, Vol. 18, 15-19, SCOSTEP Secretariat, University of Illinois.

JOHLER, J. R. [1962] Propagation of low frequency radio signal. *Proc. IRE*, **50**, 404-427.

JONES, T. B. and WAND, I. C. [1969] Validity of the $f \cos i$ theorem for the absorption of very low frequency radiowaves in the ionosphere. *Nature*, Vol. 222, 462-463.

KRASNUSHKIN, P. Y. and YABLOCHKIN, N. A. [1963] *The Propagation Theory of Ultra-Long Waves.* Mathematical Institute, Academy of Sciences, Moscow, U.S.S.R.

LAUTER, E. A. and TRISKA, P. [1966] Jahresgang der ionosphärischen Absorption im Mittel- und Langwellenbereich (Ionospheric absorption of MF and LF waves throughout the year). *Veröffentlichung des National Komitees für Geophysik und Geodäsie*, II, **1**, 23-30.

LAUTER, E. A., TAUBENHEIM, J., ENTZIAN, G., BREMER, J., COSSART, G. V. and KLEIN, G. [1976] Middle atmosphere processes and lower ionosphere in winter. Heinrich-Hertz-Institut, Berlin, Report HH1-STP No. 7.

MECHTLY, E. A., BOWHILL, S. A. and SMITH, L. G. [1972] Changes of lower ionosphere electron concentration with solar activity. *J. Atmos. Terr. Phys.*, Vol. 34, 1899-1907.

MONTBRIAND, L. E. and BELROSE, J. S. [1979] Diurnal and seasonal variations of the steady state loss coefficient in the D-region. *J. Geophys. Res.*, **84**, 1921-1929.

MOORE, R. K. [1967] Radiocommunication in the sea. *IEEE Spectrum*, 4, 42-51.

MORFITT, D. G. [1977] Effective electron density distributions which describe VLF/LF propagation data. Naval Ocean Systems Center Tech. Rep. TR141, NTIS Accession No. ADA047508. National Technical Information Service, Springfield, Va. 22161, USA.

NORTON K. A. [1960] Low and medium frequency propagation. *Electro-Magnetic Wave Propagation*, 375-444. Academic Press.

PAN, L.D. and LI, D.M. [1986] - The scope of the skywave and the accuracy of time and frequency calibration. Publications of the Shaanxi Observatory, Vol. 9, No. 2, 43-50.

PAN, L.D., LI, D.M., WANG, S.Q. and MA, L.X. [1988] - Study on improving the accuracy of time information via LF sky-wave, Proceedings of the International symposium on radio propagation, Beijing, China.

PIGGOTT, W. R., PITTEWAY, M. L. V. and THRANE, E. V. [1965] The numerical calculation of wave fields, reflexion coefficients and polarizations for long radio waves in the lower ionosphere. II, *Phil. Trans. Roy. Soc.*, A-257, 243.

PITTEWAY, M. L. V. [1965] The numerical calculation of wave fields, reflexion coefficients and polarizations for long radio waves in the lower ionosphere. I, *Phil. Trans. Roy. Soc.*, A-257, 219-241.

REDER, F. H. and WESTERLUND, S. [1970] VLF signal phase instabilities produced by propagating medium – experimental results. *Phase and Frequency Stabilities in Electromagnetic Wave Propagation.* Ed. K. Davies. Technivision, Slough, UK.

ROWE, J. N., MITRA, A. P., FERRARO, A. J. and LEE, H. S. [1974] An experimental and theoretical study of the D region – II. A semi-empirical model for mid-latitude D region. *J. Atmos. Terr. Phys.*, Vol. 36, 755-785.

RYDBECK, O. E. H. [1944] On the propagation of radio waves. *Trans. Chalmers Univ. Technol. Gothenberg*, **34.**

SPRENGER, K. and LAUTER, E. A. [1966] Verfahren zur Messung der ionosphärischen Absorption nach A3 – Method im Lang- und Mittelwellenbereich (Procedures for measurements of ionospheric absorption according to the A3 method in the long-wave and medium-wave bands). *Veröffentlichung des National Komittees für Geophysicik und Geodäsie*, II, 47-66.

STARICK, E. and TAUMER, F. [1968] Die Ausbreitung der Langwellen am Tage in der D-region der Ionosphäre. (LF day-time propagation in the D-region of the ionosphere). *Techn. Mitt. RFZ*, 12 Jahrgang, Heft 2, 89-96.

STRAKER, T. W. [1955] The ionospheric propagation of radio waves of frequency 16 kHz over short distances. *Proc. IEE, Monograph*, 114.

TAUMER, F. and STARICK, E. [1969] Jahreszeitliche Feldstärkevariationen im Lang- und Mittwellenbereich (Seasonal variations of field strength in the LF and MF bands). *Techn. Mitt. RFZ*, 13 Jahrgang, Heft 1, 16-19.

THOMAS, L. and HARRISON, M. D. [1970] The electron density distributions in the D region during the night and pre-sunrise period. *J. Atmos. Terr. Phys.*, Vol. 32, 1-14.

TSAO, C. K. H. and BETTENCOURT, J. T. [1967] Subsurface radio communication. Conference on MF, LF and VLF Propagation. IEE Conf. Publ. **36**, 313-317.

WAIT, J. R. [1961] A diffraction theory for LF sky wave propagation. *J. Geophys. Res.*, Vol. 66, 1713-1724.

WAIT, J. R. [1962] Introduction to the theory of VLF propagation. *Proc. IRE*, Vol. 50, 1624-1647.

WAIT, J. R. and CONDA, A. M. [1958] Pattern of an antenna on a curved lossy surface. *IRE Trans. Ant. Prop.*, Vol. AP-6, 348.

WATT, A. D. [1967] *VLF Radio Engineering.* Pergamon Press, New York, NY, USA.

WATT, A. D. and PLUSH, R. W. [1959] Power requirements and choice of an optimum frequency for a world-wide standard frequency broadcasting station. *NBS J. Res.*, Vol. 63D (Radio Prop.), 35-44.

WEEKES, K. and STUART, R. D. [1952] The ionospheric propagation of radio waves with frequencies near 100 kc/s over short distances. *Proc. IEE*, **99** (Pt. IV), 29.

WILLIAMS, C. [1951] Low-frequency radiowave propagation by the ionosphere, with particular reference to long-distance navigation. *Proc. IEE*, **98** (Pt. III), 81-89.

CCIR Documents

[1982-86]: a. 6/228 (IWP 6/5).

[1986-90]: 6/98 (IWP 6/5).

BIBLIOGRAPHY

BELROSE, J. S. [February, 1982] Ed. AGARD Conf. Proc. No. 305, *Medium, long and very long wave propagation (at frequencies less than 3000 kHz).* NASA Accession No. N82-27613. National Technical Information Service, Springfield, VA 22161, USA.

ANNEX I

EXAMPLE OF A COMPLETE CALCULATION OF FIELD IN AMPLITUDE AND PHASE

It is required to calculate the summer day-time expected field during solar cycle minimum under the following conditions using short vertical dipole transmitting and receiving antennas:

Length of path	$d = 1911$ km
Frequency	$f = 80$ kHz
Transmitting location on land	$\sigma = 2 \times 10^{-3}$ S/m $\varepsilon = 15\ \varepsilon_0$
Receiving location on sea water	$\sigma = 5$ S/m $\varepsilon = 80\ \varepsilon_0$
Radiated power	$p_t = 0.4$ kW

The successive stages of the calculation are as follows:

Stage	Parameters	Figures	Terms calculated	Values
1	$p_t = 0.4$ kW		$E_u = 300\sqrt{0.4}$	= 190 mV/m
2	$d = 1911$ km	2	ψ	$\approx -0.36°$
			i	= 81°
3	$\psi = -0.36°$	8	F_i	= 0.36
4	$\psi = -0.36°$	7	F_r	= 0.67
5	$d = 1911$ km $c = 3 \times 10^5$ km/s	4	$L-d$ $L = 1911 + (46 \times 10^{-6} \times 3 \times 10^5)$	= 46 µs = 1925 km
6	$d = 1911$ km	5	D	= 2.16
7	$f = 80$ kHz $i = 81°$		$f \cos i = 80 \cos 81°$	= 12.5 kHz
8	$f \cos i = 12.5$ kHz solar cycle minimun day (summer)	10	$\|\|R\|\|$	= 0.11
9			E_s	$= 11.4 \times 10^{-3}$ mV/m
10	$h = 70$ km (day) $h = 90$ km (night) $d = 1911$ km (1 hop)	4	differential time delay	= 67 − 47 = 20 µs = 1.6 cycle (i.e. 576°) at 80 kHz

REPORT 895-2

RADIO PROPAGATION AND CIRCUIT PERFORMANCE AT FREQUENCIES BELOW ABOUT 30 kHz

(Study Programme 31D/6)

(1982-1986-1990)

1. Introduction

Because of the stability of propagation (amplitude and phase), frequencies in the VLF range are used for standard frequency and time broadcasts [Blair *et al.*, 1967] and a wide range of communications and navigational applications [Casselman *et al.*, 1959]. In particular, it has been found that the stability of transmission permits frequency comparison to within a few parts in 10^{12}, which is four orders of magnitude better than is possible at HF, thus permitting long-range navigation utilizing phase comparison between spaced atomic frequency-controlled or phase-locked transmissons. Navigation and location accuracies of 1 to 3 nautical miles are achieved by the Omega navigation system [Beukers, 1974]. Accuracies of an order of magnitude better than this have been obtained utilizing a differential Omega technique, in which a fixed station is utilized to establish reference corrections for diurnal and disturbance variations for a nearby mobile station [Nard, 1972; Beukers, 1973].

The ELF band (30-3000 Hz) has very serious deficiencies when compared with conventional radio communications bands. Its restricted bandwidth implies very low data rates, and because of the very large wavelength, whatever transmitting antenna could be built would be inefficient, as measured by radiated power [Burrows, 1978]. For specific applications, however, where part of the propagation path involves lossy media such as rock, earth, soil and water, ELF offers the possibility of communicating whereas conventional bands offer none. Even at VLF (3 to 30 kHz) where the wavelength is one to two orders of magnitude smaller, efficient transmitting antennas must be enormous costly structures, and transmitting powers great if global communications are desired, particularly to points under the sea and beneath the ground.

ELF transmissions are useful for global communications and for communications to points under the sea or beneath the ground [Burrows and Nielssen, 1972; Willim, 1974]. Due to the technical difficulties of radiating energy in the ELF band at high enough power to be detected at thousands-of-kilometre ranges, very little data have been gathered until quite recently. Kuhnle and Smith [1964] measured attenuation rates of a 400 Hz continuous wave signal and Davis [1976] and Bannister [1979] have measured attenuation rates as well as relative phase for ELF waves in the 40 to 50 and 70 to 82 Hz frequency bands. ELF atmospherics have been observed since 1966 [Taylor and Sao, 1970; Hughes and Theissen, 1970; Hughes, 1971; Chapman *et al.*, 1966]. A detail

quantitative description of these data is difficult because, on the one hand, the complex wave number depends upon the lower ionosphere structure, which is not uniform in position, time or direction, and on the other hand, because propagation measurements depend on naturally-occurring lightning strokes (sferics) as a signal source. One experiment was conducted to evaluate the averaging of propagation parameters of ELF waves propagating over a path in which the ionospheric environment changed within one wavelength [Hughes and Gallenberger, 1974].

Several methods (with corresponding computer programs) have been developed for calculating signal levels at ELF. Among these are those described by Johler and Lewis [1969]; Lewis and Johler [1976]; and Pappert and Moler [1974]. Barr [1971a and 1971b] has given especially complete numerical results of propagation parameters in the frequency range from 1 to 10 kHz. An extensive summary of ELF communications theory and measurement is available in Galejs [1972] and Wait [1974 and 1977].

The mode theory, which is used extensively at VLF and may be used efficiently at LF up to at least 60 kHz, is a full wave theory that includes diffraction and surface wave propagation. The waves are considered to propagate between the Earth and the ionosphere as normal modes, analogous to microwave propagation in a lossy wave-guide [Al'pert *et al.*, 1967; Budden, 1961; Galejs, 1967a and 1967b; Pappert, 1968; Volland, 1966; Wait, 1962 and 1964]. For frequencies above about 30 kHz the wave-guide is many wavelengths high, for short distances many propagating modes must be considered, but at VLF and distances greater than 1000 km only a few modes need be considered. While the physical picture of wave-guide mode theory is less easy to visualize compared with ray-paths it provides a better explanation of certain features of VLF propagation which are not readily explicable on ray-path/wave-hop theory.

VLF and LF transmitters in common use radiate a vertically polarized field. Although the ionosphere and terrestrial magnetic field may, in principle, introduce a horizontally polarized component, there is no experimental evidence which demonstrates that such fields are significant at great distances. Theoretical calculations [Snyder and Pappert, 1969; Foley *et al.*, 1973] suggest, however, that at night in low latitudes there may be considerable horizontal polarization.

Horizontal electric dipole excitation of vertical E field at the ground for 19.8 kHz radiation beneath a hypothetical daytime ionosphere and beneath a highly anisotropic ionosphere has been numerically investigated as a function of ground conductivity and source elevation [Pappert, 1970]. Results show that for source elevations comparable to or greater than a wavelength, horizontal and vertical electric dipole excitations can become comparable. Also, when one end or both ends of a propagation path are at an elevated position, gains in signal amplitude can be achieved by using transmitting and receiving antenna orientations other than vertical [Pappert and Bickel, 1970]. This property is of particular importance for air-to-air VLF and LF communications.

2. Calculating field strength by waveguide mode methods: early approaches

2.1 *Calculating field strength in a spherical homgeneous guide*

The field strength, E, from a transmitter at a distance d km, on the ground, can be calculated by [Wait, 1962]:

$$E = \frac{300\sqrt{p}}{\sqrt{a \sin d/a}} \cdot \frac{\sqrt{\lambda}}{h} e^{-i(kd+\pi/4)} \sum_n \Lambda_n e^{-ikS_n d} \quad \text{mV/m} \qquad (1)$$

where

p: radiated power (kW),

a: radius of the Earth (km),

λ: free space wavelength (km),

k: $2\pi/\lambda$,

Λ_n: excitation factor for the nth mode,

kS_n: propagation constant,

d: path distance (km),

h: height of ionosphere (70 km-day; 90 km-night).

In general, the terms Λ_n and S_n are complex. The excitation factor Λ_n gives the relative amplitude and phase of each mode of order n excited in the Earth-ionosphere wave-guide by the source. The real part of the propagation constant kS_n contains the phase information for each mode while the imaginary part determines the attenuation rate. In order to obtain the field strength the contributions of each mode must be summed giving proper attention to the relative phases of the terms. Modification is required near the antipode when $d/a \approx \pi$.

The field strength for mode n is:

$$E_n = \frac{300\sqrt{p}}{\sqrt{a \sin d/a}} \cdot \frac{\sqrt{\lambda}}{h} | \Lambda_n | e^{-\alpha_n d} e^{i(\Phi_n - kd \operatorname{Re} S_n)} \quad \text{mV/m} \qquad (2)$$

where:

Λ_n (excitation factor) $= | \Lambda_n | e^{i\Phi_n}$

α_n (attenuation factor) $= \frac{2\pi}{\lambda} \operatorname{Im} S_n$

$= -8.68 \cdot \frac{2\pi}{\lambda} \operatorname{Im} S_n$ dB/km

$\operatorname{Im} S_n$ and $\operatorname{Re} S_n$ denote the imaginary and real parts of S_n respectively. The phase velocity $V_n = c/\operatorname{Re} S_n$, where c is the free space velocity.

In most cases, it is practical to derive field strength versus distance curves [Watt, 1967]. The recommended method is to start with appropriate values of Λ_n and S_n and perform the calculations in equation (1). Where more than one mode is present, it is necessary to interpret equation (1) in amplitude and phase. In some cases (e.g., for VLF propagation during daytime from a ground-based transmitter), it is unnecessary to consider more than three modes; however more modes are needed for night-time propagation at the higher VLF frequencies [Snyder and Pappert, 1969; Bickel *et al.*, 1970; Pappert and Bickel, 1970].

The field strength due to each mode n depends on Λ_n and S_n. These factors depend on wavelength, ionosphere height, the ground electrical properties, and the spherical reflection coefficient of the ionosphere. The ionosphere reflection coefficients depend on the vertical distribution of electron density and collision frequency, the direction and magnitude of the Earth's magnetic field, the frequency, and angle of incidence. The electron density distribution is a function of latitude, season, solar cycle, time of day and whether or not ionospheric disturbances are present.

The influences of these various parameters can be broadly summarized in the following way [Al'pert *et al.*, 1967; Budden, 1961; Volland, 1966; Wait, 1964]:

- *Ground conductivity:* In general the effect of reducing the ground conductivity is to increase the attenuation rate of all modes. However, some calculations [Wait and Spies, 1965] show that when the conductivity is very low (e.g. polar ice-caps) the attenuation rate may approach a maximum and then decrease as the conductivity is lowered further. For moderate conductivities the magnitude of the excitation factor for the first order mode usually increases somewhat as the conductivity is reduced. Furthermore, as the conductivity is reduced, the phase velocity of each mode is also reduced.

- *Direction of propagation with respect to the Earth's magnetic field:* VLF model parameters show little variation with latitude or direction of propagation in the daytime. At night, there is little latitudinal variation for propagation to the magnetic east. For propagation to the magnetic west, all VLF propagation parameters show a strong latitudinal variation as the magnetic equator is approached. In particular, attenuation is greater for propagation to the west than to the east. The exact magnitude and form of the azimuthal variation in VLF propagation parameters at the magnetic equator has yet to be determined.

  Experimentally, observations of trans-equatorial anomalies over westerly trans-equatorial paths have been reported [Crombie, 1966; Lynn, 1967, 1969 and 1975; Kaiser, 1969; Chilton *et al.*, 1969; Meara, 1973; Reder, 1979] which suggest that the major variation occurs within some 15° of the magnetic equator. At Omega navigational frequencies, the diurnal phase shift on the east-to-west trans-equatorial path is 35% less than the average value at mid-latitudes [Lynn, 1975; Kikuchi, 1983]. Anomalous interference caused by a long-path signal takes place around the geomagnetic equator, indicating a large east-west asymmetry in the attenuation of propagation [Kikuchi and Ohtani, 1984]. Theoretical calculations have been presented [Gallenberger and Swanson, 1971] that show a major variation in model parameters for westward directions of propagation as the magnetic equator is approached. The frequency dependence of these effects has yet to be determined.

- *Use of conductivity parameter:* It has been shown [Wait and Spies, 1965] that useful calculations of wave-guide mode propagation can be performed by assuming the height variation of a conductivity parameter $\omega_r(z)$ to be given by:

$$\omega_r(z) = \omega_r(h) \exp [\beta (z - h)] \tag{3}$$

where $\omega_r = \omega_0^2/\nu$ for $\nu \gg \omega$; ω, ν and ω_0 are the wave angular frequency, the collision frequency, and plasma angular frequency respectively; z is the height, h is a reference height at which $\omega_r \simeq 2.5 \times 10^5\ s^{-1}$. The term β gives the vertical gradient of ω_r. Under daytime conditions, h is about 70 km and $\beta \approx 0.3$, while at night h is around 90 km and $\beta \approx 0.5$. These two parameters, h and β, provide a convenient, but approximate, means of describing the ionosphere for use in VLF calculations.

An extensive summary of specific values of the β and h parameters needed to simulate daytime and night-time VLF and LF propagated fields is given by Morfitt [1977] and by Davis and Berry [1977].

2.2 *Calculating field strength in a non-homogeneous guide*

The above calculations refer to conditions where the path properties are independent of distance. When the electron density distribution with height along the path is constant but the ground conductivity or magnetic field angle changes, it is approximately correct to use average values of the attenuation rate and phase velocity in performing the computation. For example, if the attenuation rates and phase velocities over a portion of the path of length d_m are α_{nm} and $c/\mathrm{Re}S_{nm}$ then

$$\alpha_d = \sum_m \alpha_{nm}\, d_m \tag{4}$$

$$\mathrm{Re}\, S_n\, d = \sum_m \mathrm{Re}\, S_{nm}\, d_m \tag{5}$$

When the reference heights of the ionosphere at the transmitter and receiver are different (near dawn or dusk), this procedure is not very accurate. It is then necessary, in addition, to replace Λ_n and h in equation (1) by $\sqrt{\Lambda_{nT}\,\Lambda_{nR}}$ and $\sqrt{h_T\,h_R}$ respectively, where the subscripts T and R refer to the transmitter and receiver locations [Wait, 1964; Watt, 1967].

The amplitude and phase of a single mode change smoothly in a non-oscillatory manner with distance. When two or more modes with different phase velocities are present, the field strength changes in an oscillatory manner as the various modes go in and out of phase. If only one mode is present $\Phi = \Phi_n - kd\,\mathrm{Re}S_n$. When more than one mode is present, it is suggested that calculations start with small distances and calculate new values of Φ with increasing distance.

An approximate procedure is available for calculating the diurnal field strength changes when signals are transmitted in an east-to-west or west-to-east direction and portions of the path are in daylight and darkness. This gives signal amplitudes and phases which are proportional to the combined day and night excitation factors $\Lambda_{D,N}$, attenuation rates, $\alpha_{D,N}$, and phase velocities, $V_{D,N}\,(c/\mathrm{Re}S_{D,N})$ as follows:

$$E_n \approx \sqrt{\frac{|\Lambda_D| \cdot |\Lambda_N|}{h_D \cdot h_N}}\; e^{-(\alpha_D d_D + \alpha_N d_N)}\, e^{i}\left[\frac{\Phi_N + \Phi_D}{2} - k\,(S_N d_N + S_D d_D)\right] \qquad (6)$$

Such an approach appears to account for the gross diurnal changes which are observed on long paths (approximately 10 000 km) at frequencies below about 18 kHz. The total phase delay is the sum of the phase delays along the sunlit and dark portions of the path. As the terminator (i.e. the sunrise or sunset line) moves along the path, the phase in this simple single mode model changes in proportion to the length of path in darkness giving rise to the well known trapezoidal diurnal variation [Crombie *et al.*, 1958].

At higher frequencies or on shorter paths, however, this approach is no longer adequate since it is found that the diurnal changes of phase may almost disappear, or even be reversed (i.e. phase delays are greater during the day than at night) or that the changes at sunrise and sunset may be in the same direction [Burgess, 1970]. However, when two or more modes are included in equation (1) and the calculations of phase delay are made for appropriate daytime and night-time parameters the observed patterns are obtained.

Another phenomenon [Crombie, 1964; Lynn, 1967; Walker, 1965] observed at sunrise or sunset is that instead of the phase changing smoothly, it changes in a series of steps which are accompanied by deep nulls in the field strength. This feature is observed at all frequencies in the VLF band and is not masked by the above-mentioned irregular behaviour at the lower frequencies and on long paths. The phase steps are a result of conversion of energy from one mode into another at the sunrise or sunset terminator. For example consider the case of propagation west to east at sunrise. The transmitter excites several modes of which at least the second and first are of significant amplitude at the terminator. However, because they travel with different phase velocities, they go in and out of phase along the path. The variation of mode conversion parameters with frequency has been experimentally determined by Lynn [1973].

Values of the mode parameters are best derived by fitting equation (1) to measurements of field strength versus distance taken during day and night conditions over a wide variety of paths [Wait, 1962; Watt, 1967; Bickel, 1967; Rhoads and Garner, 1967; Bickel *et al.*, 1970].

Considerable progress has been made in developing models which more correctly partition the radio energy into propagating modes through regions of rapid changes in the medium [Wait, 1968a, 1968b, 1970; Wait and Spies, 1968]. These mode conversion procedures are required for calculating the diurnal field strength changes when signals are transmitted across the daytime – night-time terminator region. Mode conversion procedures are also important when the medium changes along the propagation path (e.g., anomalous solar effects on the ionosphere or large changes in the ground conductivity).

A mode-conversion computer program has been developed which allows fully for the vertical inhomogeneity of the ionosphere as well as its anisotropy [Pappert and Snyder, 1972]. As an illustration of the potential use of the program at VLF, the sunrise amplitude of Walker [1965] was numerically modelled with allowance for four modes. Exponential profiles of varying reference height and scale height were used to simulate the terminator. Of the modelled studies, best agreement was obtained with a terminator thickness of 1000 km. Despite the multimode nature of the models, Crombie's [1964] model (where the first two night-time modes are converted into the first daytime mode) was found to be valid for the path studied because of weak conversion from the third and fourth night-time modes to the first daytime mode. Crucial to the solution of waveguide problems that involve inhomogeneity in the direction of propagation is the ability to represent the field components as an expansion in a complete set of waveguide modes [Pappert and Smith, 1972]. Evaluation of the coefficients in such an expansion generally makes use of the orthogonality of modes for the given waveguide and those of an appropriate "adjoint" waveguide.

This mode conversion program also gives good agreement to experimental sunrise results obtained with a multiple frequency VLF ionospheric sounder over a propagation path from Hawaii to southern California [Pappert and Morfitt, 1975]. Contrary to the Crombie hypothesis [Crombie, 1964], two modes were found to be influential when the receiving site was located in the daytime part of the path.

The width and the location of the change in effective waveguide height in going from day to night at sunrise and sunset are discussed by Pappert and Snyder [1972] and Lynn [1973]. Detailed calculations of sunrise phase and amplitude parameters arising from mode conversion have been compared with observation [Rugg, 1967; Mahmoud and Beal, 1971; Rinnert, 1973; Suzuki *et al.*, 1973].

The modal interference spacing (the distance over which the phase difference between two propagation modes changes by one phase cycle (2π)) is a theoretically calculable parameter which can be measured with great accuracy. Experimental determinations for the two most significant modes have been given as a function of frequency for day or night conditions [Steele and Crombie, 1967; Rawles and Burgess, 1967] and for a range of latitudes [Lynn, 1977]. Modal interference spacings determine the location of signal minima observed in aircraft flights, the timing of signal minima and of the steps in phase during sunrise and sunset, and the regular variations in diurnal phase magnitude and day-to-night signal levels with distance [Kaiser, 1969] and frequency [Araki, 1973; Lynn, 1978].

VLF radio waves propagating across Greenland are strongly affected by the very poor conductivity of the ice cap; see for example, the signal strength data of Burgess, obtained aboard aircraft flying across Greenland [Morfitt, 1977]. Experimental data show that when the ionospheric reflection height decreases, both attenuation and phase velocity increase more than normal for a seawater path [Crombie, 1967; Westerlund *et al.*, 1969]. It is found theoretically [Westerlund and Reder, 1973] that the ice affects all the important (quasi-TM) modes. Compared to seawater propagation, the first order mode has a higher phase velocity over ice, while second and third order modes have lower velocities. All three modes have higher attenuation. Mode conversion effects at the abrupt change in ground conductivity at the Greenland coast are important.

3. Calculating field strength by waveguide modes: full wave solution

In the propagation of ELF, VLF and LF terrestrial radio waves to great distances, the waves are confined within the space between the earth and the ionosphere. This space acts as a waveguide, and the "waveguide concept" is applicable for characterizing the propagated fields as a function of distance.

The waveguide mode method obtains the full wave solution for a waveguide that has the following characteristics:

- arbitrary electron and ion density distributions and collision frequency (with height) and
- a lower boundary which is a smooth homogeneous earth characterized by an adjustable surface conductivity and dielectric constant. This method also allows for earth curvature, ionospheric inhomogeneity, and anisotropy (resulting from the earth's magnetic field).

The energy within the waveguide is considered to be partitioned among a series of modes. Each mode represents a resonant condition, i.e., for a discrete set of angles of incidence of the waves on the ionosphere, resonance occurs and energy will propagate away from the source. The complex angles (θ) for which this occurs are called the eigenangles (or "modes"). They may be obtained using the "full-wave" procedures described in §§ 3.1 and 3.2 by solving the determinantal equation (i.e., the modal equation):

$$F(\theta) = \left| R_d(\theta)\, \bar{R}_d(\theta) - 1 \right| = 0 \tag{7}$$

where

$$R_d(\theta) = \begin{bmatrix} {}_{\parallel}R_{\parallel d}(\theta) & {}_{\perp}R_{\parallel d}(\theta) \\ {}_{\parallel}R_{\perp d}(\theta) & {}_{\perp}R_{\perp d}(\theta) \end{bmatrix} \tag{8}$$

is the complex ionospheric reflection coefficient matrix looking up into the ionosphere from height "d" and

$$\bar{R}_d(\theta) = \begin{bmatrix} {}_{\parallel}\bar{R}_{\parallel d}(\theta) & 0 \\ 0 & {}_{\perp}\bar{R}_{\perp d}(\theta) \end{bmatrix} \tag{9}$$

is the complex reflection matrix looking down from height "d" towards the ground.

The notation $_{\parallel}$ for the R's and $\bar{R}$'s denotes vertical polarization while the notation $_{\perp}$, denotes horizontal polarization. The first subscript on the R's referes to the polarization of the incident wave while the second applies to the polarization of the reflected wave.

The individual terms of equations (8) and (9) are:

${}_{\parallel}R_{\parallel}$: the ratio of the reflected field in the plane of incidence to the incident field in the same plane.

${}_{\perp}R_{\perp}$: the ratio of the reflected field perpendicular to the plane of incidence to the incident field perpendicular to the plane of incidence.

${}_{\parallel}R_{\perp}$: the ratio of the reflected field perpendicular to the plane of incidence to the incident field in the plane of incidence.

${}_{\perp}R_{\parallel}$: the ratio of the reflected field in the plane of incidence to the incident field perpendicular to the plane of incidence.

The ionospheric reflection matrix, R_d (equation (8)) at height, d, is obtained by numerical integration of differential equations given by Budden [1955]. The differential equations are integrated by a Runge-Kutta technique, starting at some height above which negligible reflection is assumed to take place. The initial condition for the integration, i.e., the starting value of R, is taken as the value of R for a sharply-bounded ionosphere at the top of the given electron density and collision frequency profiles. The method for obtaining this starting solution is described by Sheddy [1968]. The term R_d is calculated as described by Pappert *et al.* [1967] in terms of solutions to Stokes equation and their derivatives.

The modal equation, equation (7), is solved for as many modes (eigenangles, θ_n) as desired. From the set of θ's so obtained the propagation parameters: attenuation rate, phase velocity and the magnitude and phase of the excitation factor, can be computed [Pappert *et al.*, 1967]. These parameters are then used in a modal summation to compute the total field, amplitude and phase, at some distant point.

In many instances, the earth-ionosphere waveguide can be considered to have constant propagation properties along the transmission path. The mode sum calculations made for these cases are referred to as horizontally homogeneous. However, for propagation to great distances it is unrealistic to assume the waveguide parameters will remain constant along the whole length of the path. For example, the direction and strength of the Earth's magnetic field will vary and discontinuities can occur in the lower wall of the waveguide due to the presence of ground conductivity changes associated with various land-sea boundaries and the polar ice caps. The ionospheric conductivity also varies according to the time of day, season and the presence of the sunrise or sunset line along the propagation path.

These types of discontinuities are those which cause discrete changes in the waveguide. In these cases mode conversion effects at the discontinuity must be taken into consideration. Mode conversion implies that a single mode propagating in one region of the waveguide will produce two or more modes in the other section of the guide which then propagate to the receiver.

3.1 *The ionospheric reflection matrix, R(θ)*

A crucial step in the determination of the mode constants discussed in the previous section is the evaluation of the reflection matrix R for a vertically inhomogeneous anisotropic ionosphere. This is achieved by a numerical integration of differential equations given by Budden [1955].

The coordinate system chosen is such that the direction of z is taken positive into the ionosphere. Positive x is the direction of propagation and y is normal to the plane of propagation.

The geometry is shown in Fig. 1 where a plane wave is shown incident upon the ionosphere from below with wave vector $\vec{k}$ in the x-z plane (plane of incidence) at an angle of incidence θ_1 to the vertical (z-axis). Other variables identified in the figure are Ω, the angle of the geomagnetic field measured from the vertical ($90° < \Omega \leqslant 180°$ for the Northern Hemisphere), and ψ, the azimuth of propagation (east of magnetic north). The vector $\vec{B}$ is the earth's magnetic flux density.

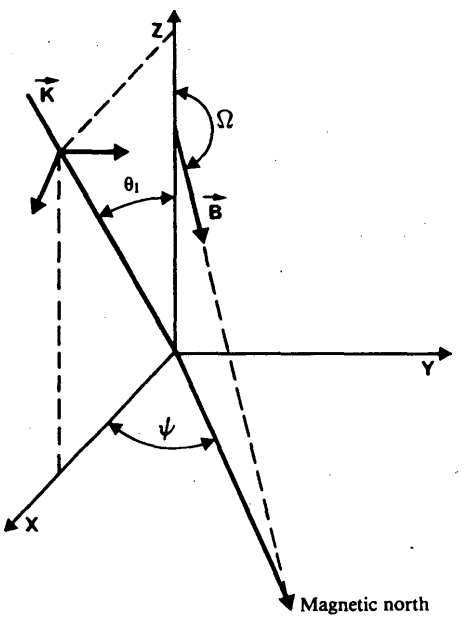


FIGURE 1 – *Wave propagation geometry*

The differential equations are integrated by a Runge-Kutta technique starting at some height above which neglible reflection is assumed to take place. The starting value of R is the value of R for a sharply bounded homogeneous ionosphere characterized by parameters at the top of the given electron, ion and collision frequency profiles. The solution used for the initial R is that described by Sheddy [1968]. Error control in the Runge-Kutta integration is by means of comparison for each step of the increments in the elements of R computed with a fourth-order Runge-Kutta method and those computed with a second-order integration step. The integration is carried out from some starting height down to the height d, where d is identified in equation (7). It is necessary only that d be chosen sufficiently low in the ionosphere that ionospheric effects are small relative to earth-curvature effects. Below level d the only effect is that of earth curvature which is included by introducing a modified permittivity which varies linearly in height.

3.2 *The ground reflection matrix,* $\bar{R}_d(\theta)$

The ground reflection coefficient matrix $\bar{R}_d$, as given in equation (9), is determined in terms of independent solutions, h_1 and h_2 to Stokes' equation

$$\frac{d^2 h_{1,2}}{dz^2} + z h_{1,2} = 0 \tag{10}$$

where the functions h_1 and h_2 are modified Hankel functions of order 1/3 (which are linearly related to Airy functions) as defined by the Computation Laboratory, Cambridge [1945]. The explicit expressions for ${}_{\|}\bar{R}_{\|}$ and ${}_{\perp}\bar{R}_{\perp}$ are given by [Pappert *et al.*, 1967].

3.3 *The mode finding method* ("MODESRCH")

Waveguide theory treats the field as being composed of one or more discrete families (modes) of plane waves confined to the earth-ionosphere waveguide. The principle objective is to find solutions to equation (7) for the eigenangles θ_n. To achieve this a method known as "MODESRCH" [Morfitt and Shellman, 1976] is employed.

The "MODESRCH" method, developed primarily for VLF and lower LF (10 kHz to about 60 kHz) propagation in the earth-ionosphere waveguide finds all modes in any physically important rectangular region of the complex eigenangle (θ_n) space. The method also finds the single mode needed for ELF propagation. The procedure is based on complex variable theory. The modal equation, equation (7), is solved for all the important eigenangles, θ_n, for the given set of earth-ionosphere parameters and propagation frequency. The search for the eigenangles is based on the fact that the lines of constant phase for any complex function, $F(\theta)$, may be discontinuous only at points where $F\theta = 0$ or $F(\theta) \rightarrow \infty$. To simplify the problem of finding the θ_n values, the function $F(\theta)$ is modified so that it contains no poles and only $F(\theta) = 0$ is considered. A solution of $F(\theta) = 0$ is denoted by θ_0, i.e., θ_0 is a zero of $F(\theta) = 0$.

Let:

$$F(\theta) = F_R(\theta_r, \theta_i) + j\, F_I(\theta_r, \theta_i) = \text{Re}\,(F) + j\,\text{Im}\,(F) \tag{11}$$

where

$$\theta = \theta_r + j\theta_i \tag{12}$$

Also

$$F(\theta) = [F_R(\theta_r, \theta_i)^2 + F_I(\theta_r, \theta_i)^2]^{1/2}\, e^{j\theta} \tag{13}$$

where

$$\varphi = \tan^{-1}\left[\frac{F_I(\theta_r,\theta_i)}{F_R(\theta_r,\theta_i)}\right] \tag{14}$$

and

$F_R(\theta)$: the real part of the complex function $F(\theta)$,

$F_I(\theta)$: the imaginary part of the complex function $F(\theta)$,

θ_r : the real part of the complex angle (θ),

θ_i : the imaginary part of the complex angle (θ).

From equation (14) if

$\varphi = 0°$ (or 180°), this implies that

$F_I(\theta_r,\theta_i) = 0$

Also if

$\varphi = 90°$ (or 270°), this implies that

$F_R(\theta_r,\theta_i) = 0$

This leads to the phase diagram of Fig. 2. A set of lines of constant phase referred to as phase contours ranging from 0 to 2π radians emanates radially (solid lines) from a simple zero. The dashed lines depict possible phase contour behaviour, in the region beyond the neighbourhood of θ_0, in order to emphasize that in this region the phase contours are generally not radial. In view of the phase behaviour near a zero of $F(\theta)$ it is conceptually useful to define a zero of $F(\theta)$ as a set of phase contours.

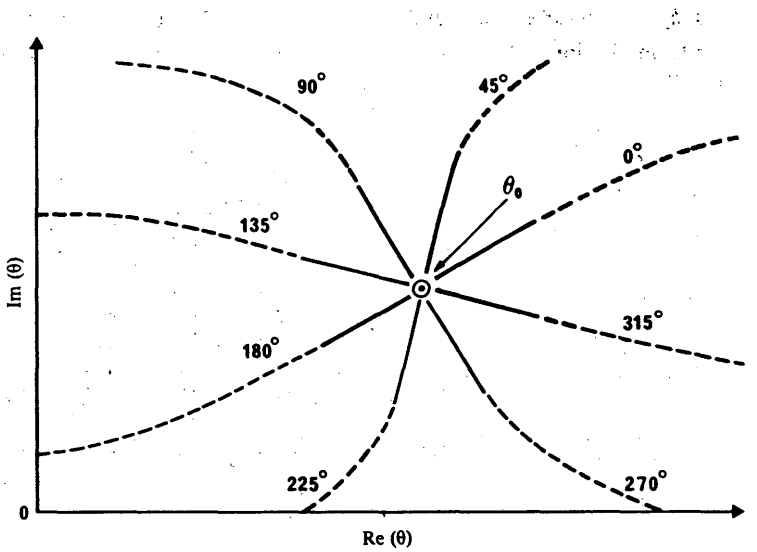


FIGURE 2 – *Phase contour behaviour near a zero of F (θ)*

——— phase contour in the neighbourhood of θ_0

– – – – phase contour beyond the neighbourhood of θ_0

Some fundamentals of the procedure to find zeros of the function, $F(\theta)$, are illustrated in Fig. 3. A search rectangle is placed about some region of the complex plane. The search rectangle is divided into a grid of mesh squares whose corners will be called mesh points. The mesh square size is optional and is usually selected according to the expected zero spacing. If $F(\theta)$ has no poles, this implies that the line of any particular constant phase value $\varphi = \varphi_c$, radiating from a zero of $F(\theta)$, must cross a closed contour containing that zero at least once. Furthermore, no other zero of $F(\theta)$ may be on this phase line. Also, the lines of constant phase around $F(\theta) = 0$ progress only in a counterclockwise direction. A line of constant phase (e.g., $\varphi = \varphi_c$) which crosses the contour may be followed inward until it leads to a zero of $F(\theta)$ or until the line again reaches the contour. Beginning at the upper left corner of the search rectangle, a boundary search for 0° and 180° phase contours is conducted in a counterclockwise direction. Any phase contour would do; however, the 0° and 180° phase contours are selected because mathematically they are easily located, occurring when Im $(F) = 0$. The search is conducted by evaluating $F(\theta)$ at the mesh points along the search rectangle boundary. When Im (F) changes sign, it indicates that a 0° or 180° phase contour has just been passed (points A, D, and G). Once either of these phase contours is located, the boundary search is temporarily halted while the 0° or 180° phase contour is traced into the interior of the search rectangle by inspection of Im $F(\theta)$ at the corners of the mesh squares (counterclockwise inspection beginning at the top left corner of each mesh square). The phase contour is followed either until a zero of $F(\theta)$ is discovered (points B and E) or until the search rectangle boundary is encountered (as would be the case for the phase contour between G and H), one of which will always occur provided no poles exist in the interior of the search rectangle. When a zero is located its location is saved. Then the phase contour is traced out the opposite side of the zero, having undergone a 180° phase change (see Fig. 2), until the search rectangle boundary is again encountered (points C and F). When the phase contour exists the search boundary, such as at points C, F, or H, the mesh square which contains this occurrence is flagged so as to avoid following the particular phase contour again at a later time during the boundary search. Also at such a point (point C, F, or H) the phase contour trace is stopped and the boundary search is resumed at the point where the last 0° or 180° phase line was encountered (e.g., points A, D, or G). Once the entire search rectangle boundary has been inspected, all the zeros of the function $F(\theta)$, located within the search rectangle will have been found.

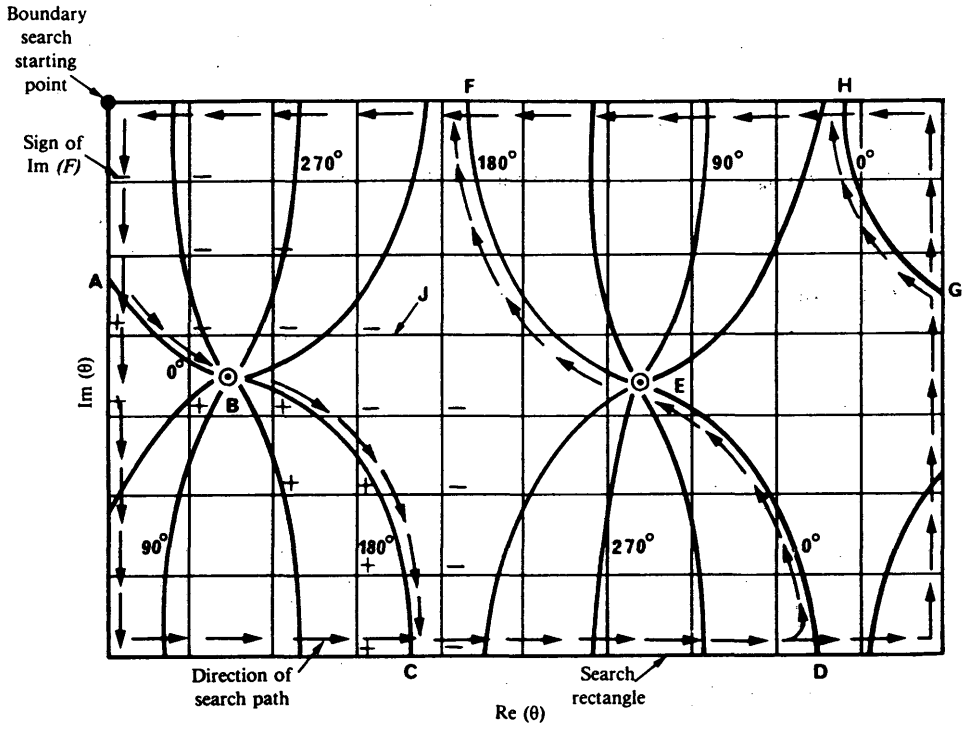


FIGURE 3 – *Mode finding method for the function F(θ)*

——— phase contours for $F(\theta)$
⊙ zeros of $F(\theta)$
J mesh square

The location of a zero is evident by the intersection of phase contours (see Fig. 2). Therefore, the intersection of the 0° or 180° phase contour with any other phase contour locates a zero of $F(\theta)$. The other phase contour chosen for this purpose is the 90° or 270° phase contour, again chosen for simplicity, as these contours are easily recognized, occurring when Re $(F) = 0$. While a 0° or 180° phase contour is being traced, Re (F) is also examined at the corners of each mesh square to locate a Re (F) sign change which indicates that a 90° or 270° phase contour has entered the mesh square. Such an occurrence indicates that a zero is probably within that mesh square or perhaps within an adjacent mesh square. Once a mesh square is known to contain a zero, a more precise location of the zero is obtained by an interpolation scheme which employs both the magnitude and phase of the function $F(\theta)$. Following this a Newton-Raphson iteration pinpoints the location of the zero.

The Newton-Raphson procedure is to use each of the eigenangle solutions, θ_n, as obtained from the "MODESRCH" grid as a starting solution θ_0 to equation (7) where $F(\theta) = 0$. The function is then re-evaluated for $\theta_0 + \delta\theta$ and the correction to θ_0 found from the equation

$$\Delta\theta = - \frac{F(\theta_0)\,\delta\theta}{F(\theta_0 + \delta\theta) - F(\theta_0)} \tag{15}$$

The correction determined by equation (15) is then evaluated and the process repeated until the quantities $|\Delta\theta_r|$ and $|\Delta\theta_i|$ are reduced to within a pre-assigned tolerance. The subscripts r and i denote the real and imaginary parts, respectively.

A computer program is available to compute these eigenangles for an arbitrary ionosphere and a homogeneous earth [Morfitt and Shellman, 1976].

4. Calculation of field strength

4.1 *Required parameters*

With the eigenangles, θ_n, known, the following quantities of physical interest are readily calculated.

$$V = \frac{c}{K(\sin\theta_n)_r} \quad = \text{phase velocity at the ground} \tag{16}$$

$$\Gamma = -8.6859kK(\sin\theta_n)_i \quad = \text{attenuation constant at the ground (in dB/megameter)} \tag{17}$$

where

$$c = 2.997928 \times 10^5 \text{ km/s} \quad = \text{vacuum speed of light}$$

$$K = \left(1 + \frac{\alpha h}{2}\right) \tag{18}$$

$$\alpha = 2/a = 3.14 \times 10^{-4}/\text{km} \tag{19}$$

Using the geometry of Fig. 1 the direction of stratification is the z direction and the direction of propagation is in the x-z plane. The direction of z is taken positive into the ionosphere. Positive x is the direction of propagation and y is normal to the plane of propagation. Thus, the fields exhibit no y dependence and a dependence on x of the form $\exp(-ik\sin\theta_x)$ where k is the magnitude of the free-space propagation vector and θ is the angle between the direction of the propagation vector and the z direction at a point in the stratified medium where the modified index of refraction is unity. All field quantities are assumed to have an $\exp(i\omega t)$ dependence where ω is the angular frequency.

The modal excitation factor and the modal height gain functions are two parameters needed in computing electric field strengths. The excitation factor formulae, are summarized in Table I. The column headings only apply to excitation of the electric field components E_z, E_y and E_x and the row headings apply to excitation by a vertical dipole (λ_V), horizontal dipole end on (λ_E) and a horizontal dipole broadside (λ_B).

R and $\bar{R}$ represent, respectively, elements of the reflection matrix looking into the ionosphere and towards the ground from the same level d within the guide. B_1 and B_2 are given by

$$B_1 = \frac{S^{5/2}}{\left.\frac{\alpha F}{\alpha\theta}\right|_{\theta=\theta_n}} \qquad B_2 = -\frac{B_1}{S} \tag{20}$$

where S is the sine of the eigenangle and the denominator is the derivative of the modal equation at the eigenangle, θn.

TABLE I — *Excitation factors*

Field component	E_z	E_y	E_x
Exciter			
λ_V	$B_1 \dfrac{(1+{}_{\parallel}\bar{R}_{\parallel})^2(1-{}_{\perp}\bar{R}_{\perp}\,{}_{\perp}R_{\perp})}{{}_{\parallel}\bar{R}_{\parallel}\,D_{11}}$	$\dfrac{-B_1}{S}\dfrac{{}_{\parallel}R_{\perp}(1+{}_{\parallel}\bar{R}_{\parallel})(1+{}_{\perp}\bar{R}_{\perp})}{D_{12}}$	$\dfrac{B_1}{S}\dfrac{(1+{}_{\parallel}\bar{R}_{\parallel})^2(1-{}_{\perp}\bar{R}_{\perp}\,{}_{\perp}R_{\perp})}{{}_{\parallel}\bar{R}_{\parallel}\,D_{11}}$
λ_E	$B_2 \dfrac{(1+{}_{\parallel}\bar{R}_{\parallel})^2(1-{}_{\perp}\bar{R}_{\perp}\,{}_{\perp}R_{\perp})}{{}_{\parallel}\bar{R}_{\parallel}\,D_{11}}$	$\dfrac{-B_2}{S}\dfrac{{}_{\parallel}R_{\perp}(1+{}_{\parallel}\bar{R}_{\parallel})(1+{}_{\perp}\bar{R}_{\perp})}{D_{12}}$	$\dfrac{B_2}{S}\dfrac{(1+{}_{\parallel}\bar{R}_{\parallel})^2(1-{}_{\perp}\bar{R}_{\perp}\,{}_{\perp}R_{\perp})}{{}_{\parallel}\bar{R}_{\parallel}\,D_{11}}$
λ_B	$B_2 \dfrac{{}_{\perp}R_{\parallel}(1+{}_{\perp}\bar{R}_{\perp})(1+{}_{\parallel}\bar{R}_{\parallel})}{D_{12}}$	$\dfrac{-B_2}{S}\dfrac{(1+{}_{\perp}\bar{R}_{\perp})^2(1-{}_{\parallel}\bar{R}_{\parallel}\,{}_{\parallel}R_{\parallel})}{{}_{\perp}\bar{R}_{\perp}\,D_{22}}$	$\dfrac{B_2}{S}\dfrac{{}_{\perp}R_{\parallel}(1+{}_{\perp}\bar{R}_{\perp})(1+{}_{\parallel}\bar{R}_{\parallel})}{D_{12}}$

The excitation factors must be supplemented with definitions of the height gains.

The field-strength calculations can be made for electric dipole exciters of arbitrary orientation located at any height within the guide. Thus, air-to-air, ground-to-air or air-to-ground VLF/LF propagation problems involving a horizontally inhomogeneous waveguide channel may be treated. Figure 4 shows the dipole orientation relative to the propagation geometry in which the z axis is always normal to the curved earth surface. The angles γ and φ measure the orientation of the transmitter relative to the x, y, z coordinate system.

From Fig. 4, $\gamma = 0°$ represents the excitation from a vertical dipole while $\gamma = 90°$ gives the excitation from a horizontal dipole. Also φ is the angle between the direction of the horizontal dipole and the direction of propagation. Explicitly, $\varphi = 0$ represents end fire and $\varphi = 90°$ represents broadside launching.

4.2 *WKB and horizontally homogeneous mode sums*

In addition to the vertical inhomogeneity of the ionosphere the guide may exhibit horizontal inhomogeneity. In particular, variability in propagation constants along the great circle path of propagation can result from either horizontal variability of the ionosphere, from variability of the ground conductivity and/or permittivity, as well as from variations in the geomagnetic field strength or orientation. In instances for which the earth ionosphere waveguide cannot be considered as horizontally homogeneous along the propagation path, a WKB form of the mode sum is used. This model is accurate when changes in the modal parameters are sufficiently gradual along the path.

In terms of the excitation factors and height gains, the WKB mode sum equations may be written as a function of propagation distance.

If the propagation path may be considered as horizontally homogeneous along its entire length, the equation becomes much simpler:

$$(\lambda_V^T = \lambda_V^R), (\lambda_B^T = \lambda_B^R) \text{ and } (\lambda_E^T = \lambda_E^R). \qquad \text{Also, } (\bar{S}_n^T = \bar{S}_n^R)$$

which may be used to compute the fields for multimode propagation at VLF and LF frequencies. These equations may also be used for ELF frequencies, however, because of the small attenuation rates which prevail in the lower ELF band, significant interference between the long and short path signals can occur.

Computer programs are available to compute these field strengths. These are for VLF/LF [Pappert and Shockey, 1971] and for ELF [Pappert and Shockey, 1972a and 1972b].

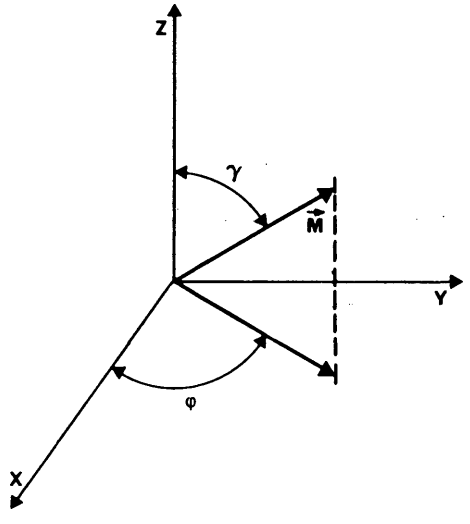


FIGURE 4 – *Dipole $\vec{M}$ orientation within the waveguide where γ is the inclination and φ the azimuthal orientation*

4.3 *Mode sums using mode conversion*

For those propagation conditions where the properties of the earth-ionosphere waveguide can not be considered as slowly varying, mode conversion techniques must be utilized. Examples, where mode conversion procedures are required for calculating field strengths, are for transmissions across the daytime-night-time terminator region or when the propagation path consists of large changes in ground conductivity, such as the transition from land to sea. The mode conversion model allows for an arbitrary number and order of modes on each side of the waveguide discontinuity. This model also allows for the calculation of the horizontal, as well as the vertical, component of the electric field at an arbitrary height in the waveguide.

The mode conversion program is based on the slab model shown in Fig. 5. Invariance in the y direction is assumed and reflection from the horizontal inhomogeneity is neglected. Subject to these assumptions and to the assumption of a unit amplitude wave in mode k incident in the transmitter region (slab NTR) the generalized mode conversion coefficient a_k^p for the p^{th} slab associated with conversion from the kth to the j^{th} mode expressed in terms of the coefficients for the previous $(p + 1)^{th}$ slab may be written in the form:

$$\sum_{j=1}^{J} a_{ik}^{p} I_{n,j}^{p,p} = I_{n,k}^{p,p+1} \qquad p = NTR - 1$$

$$= \sum_{j=1}^{J} a_{jk}^{p+1} \left[-iks_j^{p+1} (x_p - x_{p+1}) \right] I_{n,k}^{p,p+1} \qquad 1 \leqslant p < NTR - 1 \qquad (21)$$

where $i = (-1)^{1/2}$, k is the free-space wave number, S_j is the sine of the jth eigenangle for the pth slab, and J is the total number of modes assumed to be important in the total field determinations.

Critical for the solution of the system of equations (21) is the evaluation of the integral:

$$I_{jk}^{m,p} = \int_{-\infty}^{\infty} A_j^{mt} \cdot G_k^p \, dz \qquad (22)$$

where the t denotes the adjoint factor and G^p a four-element column matrix of height gains for the y and z components of the electric and magnetic field strength of the kth mode in the pth slab.

The term A_j^m is a four-element column matrix of height gains for an appropriate adjoint waveguide [Pappert and Smith, 1972].

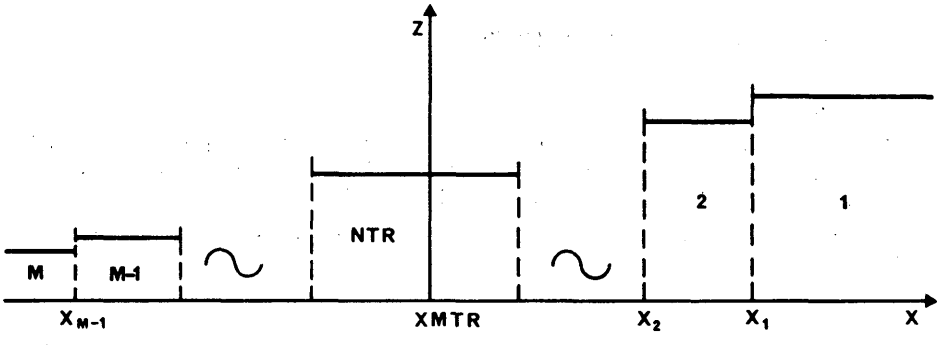


FIGURE 5 – *Mode conversion model*

Again, as in the case of the WKB mode sum procedure, the field-strength calculations can be made for electric dipole exciters of arbitrary orientation located at any height within the guide. Thus, air-to-air, ground-to-air or air-to-ground VLF/LF propagation problems in a horizontally inhomogeneous waveguide channel may be treated.

Two distinct options are available with the mode conversion procedure. One is for field calculations (amplitude and phase) as a function of range for a fixed location of the horizontal inhomogeneity. The second allows for field calculations at a distinct receiving point along a great circle path as a function of position of the horizontal inhomogeneity (this option is useful only if the ground conductivity and the geomagnetic parameters are invariant over the path). Amplitude is expressed in dB above a microvolt per metre for a one kilowatt radiator and phase in degrees relative to free space. A computer program is available for these mode conversion calculations [Pappert and Shockey, 1976].

4.4 *Ionospheric parameters*

The required ionospheric parameters needed to compute ELF/VLF/LF field strength values are the following profiles, which are functions of ionospheric height, Z. These are electron density profile, positive and negative ion density profiles, electron-neutral particle collision frequency profile and positive and negative ion-neutral particle collision frequency profiles.

A convenient parameter based on the above profiles is the ionospheric conductivity ω_r, which is a function of height, Z. This parameter is given by:

$$\omega_r(Z) = \frac{\omega_p^2(Z)}{\nu(Z)} = \frac{q^2}{\varepsilon_0}\left[\frac{N_e(Z)}{m_e \nu_e(Z)} + \frac{N_+(Z)}{m_+ \nu_+(Z)} + \frac{N_-(Z)}{m_- \nu_-(Z)}\right] \tag{23}$$

where

$\omega_p(Z)$: the plasma frequency,

q: the electron charge,

ε_0: the permittivity of free space,

ν_e: electron-neutral particle collision frequency (s^{-1}),

ν_+: positive ion-neutral particle collision frequency (s^{-1}),

ν_-: negative ion-neutral particle collision frequency (s^{-1}),

N_e: electron density (cm^{-3}),

N_+: positive ion density (cm^{-3}),

N_-: negative ion density (cm^{-3}),

m_e: mass of the electron,

m_+: mass of the positive ions,

m_-: mass of the negative ions.

For most cases of propagation at VLF or LF, only the electron density profile and electron-neutral particle collision frequency profile need to be considered. In this instance, following Wait and Spies [1965], the conductivity parameter $\omega_r(Z)$ may be considered of exponential form:

$$\omega_r(Z) = \omega_0 \exp[\beta (Z - H')] \tag{24}$$

where

β: a gradient parameter in inverse height units,

and

H': a reference height.

The ionospheric parameters needed as inputs to the multimode computer programs, then, are the electron density profile and the effective electron-neutral particle collision frequency profile. These terms may be assigned exponential relationships with height and are identified by the terms β, km^{-1} and H', km.

The value of the electron density $N(Z)$, in electrons/cubic centimetres is calculated as a function of height Z in kilometres by the equation:

$$N(Z) = \left\{1.43 \times 10^7 \times \exp(-0.15\,H')\right\}\left\{\exp[(\beta - 0.15)(Z - H')]\right\} \quad \text{el/cm}^3 \tag{25}$$

The collision frequency profile for the computations is:

$$\nu(Z) = \nu_0 \exp(-\alpha Z) \tag{26}$$

where

Z: the height in km,

ν_0: 1.82×10^{11} collisions/sec,

α: $0.15\ km^{-1}$.

This combination of electron density and collision frequency gives an ionospheric conductivity profile given by

$$\omega_r(Z) = 2.5 \times 10^5 \exp[\beta (Z - H')] \tag{27}$$

The usefulness of this simple ionospheric model is a result of its ease of application and its success in modelling experimentally measure data as demonstrated by Bickel *et al.*, [1970], Morfitt [1977], and Ferguson [1980]. The determination of the values of the β and H' parameters is achieved by comparing measured data with theoretical calculations, adjusting the parameters in the latter until acceptable agreement is obtained. The most straightforward method of comparison is obtained when the measured data are collected at a large number of points along a great circle propagation path which includes the transmitter. The easiest way to collect such data is aboard an aircraft. The data examined by Bickel *et al.*, Morfitt and Ferguson were collected in this way.

In general, the ionospheric models determined from the above procedure must be considered to represent an averaged ionosphere since the modelling assumes that the ionosphere was static during any aircraft flight period. The data fitting procedure attempts to find a calculated pattern of amplitude as a function of distance which agrees with the large scale pattern of the measured data. Thus, many small amplitude variations are averaged. It is possible that profiles of more complex forms than the exponential could be found to produce a better fit to measured data in some instances, but since the propagation paths considered are quite long, any profile determined to produce a best fit to the data is really an average profile for the total path.

Analysis of the available measured data suggests the following tables of ionospheric parameters for VLF/LF propagation predictions, Morfitt [1977] and Ferguson [1980].

The characteristic relationship, as a function for some exponential profiles is illustrated in Fig. 6 for daytime conditions and in Fig. 7 for night-time conditions.

For propagation at ELF, suggested electron and ion density profiles, [Pappert and Moler, 1974], are shown in Fig. 8.

Tables of suggested electron and ion collision profiles for ELF are given in Tables IV and V.

TABLE II — *Recommended profiles for daytime propagation at VLF/LF*

	Summer	Winter
High latitude	$\beta = 0.3$, $H' = 72$	$\beta = 0.3$, $H' = 72$
Middle latitude	$\beta = 0.5$, $H' = 70$	$\beta = 0.3$, $H' = 72$

TABLE III — *Recommended profiles for night-time propagation at VLF-LF*

	Magnetic dip range (degrees)	H' (km)		β (km^{-1})	
		F = 10-30 kHz	F = 30-60 kHz	F = 10-30 kHz	F = 30-60 kHz
Winter profiles					
High latitudes	90 to 75	76	76	$0.035F - 0.025$	1.2
Transition region	75 to 70	80	80	$0.035F - 0.025$	1.2
Middle latitudes	< 70	87	88	$0.0077F + 0.31$	$0.0077F + 0.31$
Summer profiles					
All latitudes		$H' = 87$		β (km^{-1}) = $0.0077F + 0.31$	

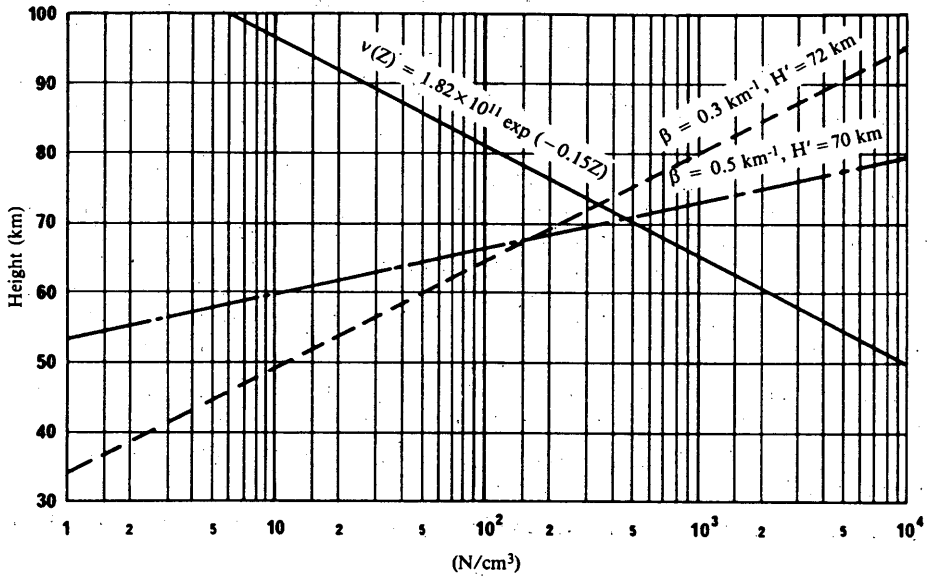


FIGURE 6 – *Daytime electron density profiles and collision frequency profile*

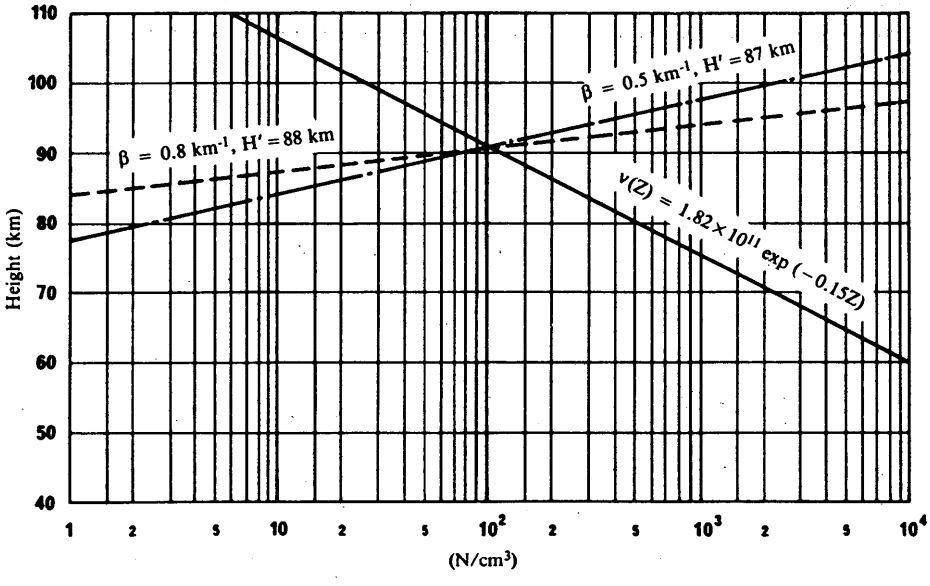


FIGURE 7 – *Night-time electron density profiles and collision frequency profile*

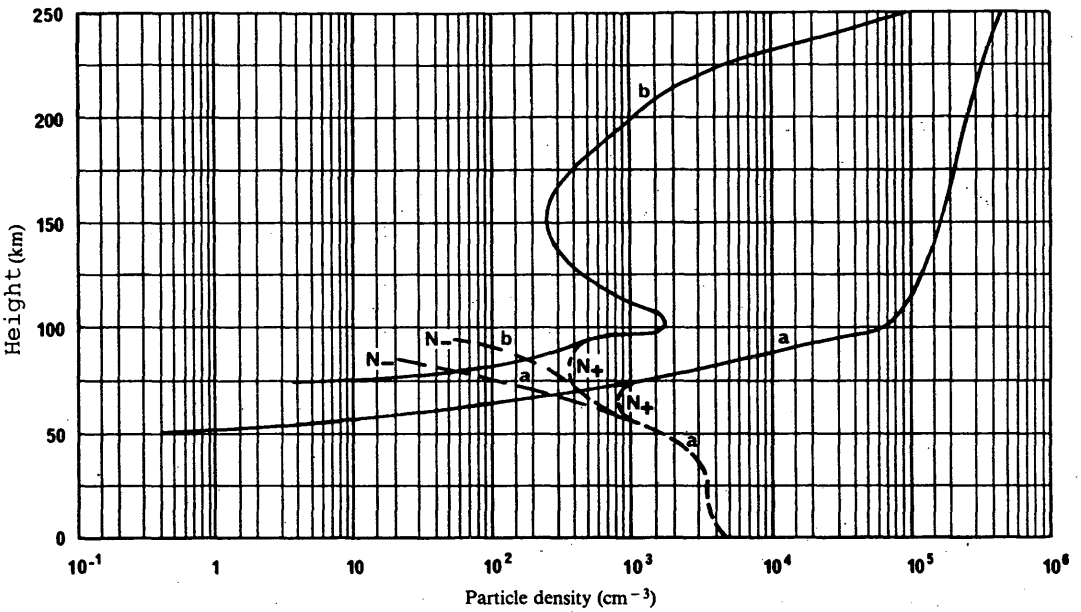


FIGURE 8 – *Ambient day and night constituent profiles*

——— electrons
– – – – ions
a day
b night

TABLE IV — *Daytime ionospheric electron and ion collision frequency in seconds^{-1} versus altitude*

Altitude (km)	Electrons	Positive ions	Negative ions
260	$6.6 \cdot 10^2$	1.02	1.02
230	$5.3 \cdot 10^2$	2.00	2.00
210	$4.8 \cdot 10^2$	3.10	3.10
200	$5.0 \cdot 10^2$	4.00	4.00
180	$6.0 \cdot 10^2$	$1.30 \cdot 10^1$	$1.30 \cdot 10^1$
170	$8.0 \cdot 10^2$	$2.40 \cdot 10^1$	$2.40 \cdot 10^1$
150	$1.6 \cdot 10^3$	$9.00 \cdot 10^1$	$9.00 \cdot 10^1$
120	$1.0 \cdot 10^4$	$6.00 \cdot 10^2$	$6.00 \cdot 10^2$
100	$3.9 \cdot 10^4$	$1.60 \cdot 10^4$	$1.60 \cdot 10^4$
0	$4.3 \cdot 10^{11}$	$2.14 \cdot 10^{10}$	$2.14 \cdot 10^{10}$

TABLE V — *Night-time ionospheric electrons and ion collision frequency in seconds^{-1} versus altitude*

Altitude (km)	Electrons	Positive ions	Negative ions
250	$1.05 \cdot 10^2$	$4.50 \cdot 10^1$	$4.50 \cdot 10^1$
225	$3.50 \cdot 10^1$	$9.00 \cdot 10^1$	$9.00 \cdot 10^1$
220	$3.00 \cdot 10^1$	1.00	1.00
210	$3.30 \cdot 10^1$	1.30	1.30
200	$4.50 \cdot 10^1$	2.00	2.00
150	$1.60 \cdot 10^3$	$4.50 \cdot 10^1$	$4.50 \cdot 10^1$
120	$1.00 \cdot 10^4$	$3.00 \cdot 10^2$	$3.00 \cdot 10^2$
100	$3.90 \cdot 10^4$	$8.00 \cdot 10^3$	$8.00 \cdot 10^3$
0	$4.30 \cdot 10^{11}$	$1.07 \cdot 10^{10}$	$1.07 \cdot 10^{10}$

4.5 *Geomagnetic and geophysical parameters*

Other parameters needed for the calculation of ELF/VLF/LF signal levels are those which describe the orientation and strength of the Earth's magnetic field along the propagation path, as well as those parameters which give the value of the Earth's complex dielectric constant as a function of propagation frequency.

The parameters which describe the Earth's magnetic field are the magnitude of the geomagnetic field, the magnetic azimuth (in degrees east of north) of the propagation direction, and the dip angle measured from the horizontal (co-dip) of the magnetic field vector. These parameters change along the propagation path and these changes are incorporated in the WKB or mode conversion formulations.

The complex relative permittivity of the Earth, N_g, is given by:

$$N_g = \varepsilon/\varepsilon_0 - i\frac{\sigma}{\omega\varepsilon_0} \tag{28}$$

where:

σ : ground conductivity,

$\varepsilon/\varepsilon_0$: relative ground permittivity,

ε_0 : permittivity of free space,

ω : angular propagation frequency.

Table VI gives recommended values for these parameters.

TABLE VI – *Conductivity and relative permittivity of the Earth*

	Conductivity σ (S/m)	Relative permittivity ε_r
Sea water	5	80
Land	2×10^{-3}	15
Polar ice cap	2.5×10^{-5}	3

5. Results of field-strength calculation

Figures 9, 10, 11 and 12 illustrate the degree to which computed field-strength values simulate measured propagation data. These figures show the vertical electric field strength as a function of propagation distance. The ionospheric profiles listed in Tables II and III were incorporated into these field-strength computations.

Figures 9 and 10 show the comparison between fields computed assuming a horizontal homogeneous ionosphere [Pappert and Shockey, 1976] and data recorded by the US Navy [Morfitt, 1977]. These data were recorded aboard inflight aircraft at various frequencies for propagation over midlatitude sea-water paths for daytime summer conditions and for night-time winter conditions. Results using the daytime ionospheric conductivity profile with $\beta = 0.5$ km^{-1} and $H' = 70$ km are shown in Fig. 9. The results obtained using the night-time profile $\beta = 0.5$ km^{-1} and $H' = 87$ km are shown in Fig. 10.

Measurements of the Omega signal (13.6 kHz) have been made during a quiet time over a path from La Réunion (22.0 S, 56.0 E) to Inubo (35.7 N, 140.9 E). Analysis of the sunrise amplitude fading and the diurnal shift in phase and amplitude gives the following waveguide parameters:

Daytime $\beta = 0.3$ km^{-1} and $H' = 75.0$ km

Night-time $\beta = 0.5$ km^{-1} and $H' = 88.5$ km

[Kikuchi, 1986].

Experimental measurements at 45 and 60 kHz have been obtained aboard an inflight aircraft during a flight over the Greenland ice cap. These transmissions originated in England and the aircraft flight path traversed the Greenland ice cap terminating at Sondrestrom, Greenland. Comparison of these field-strength measurements to computed field-strength predictions is shown in Figs. 11 and 12. The method of calculation used to construct these figures is the mode conversion program [Pappert and Shockey, 1976].

The ground conductivity was input as 5S/m for the seawater section of the path and 2.5×10^{-5} S/m for the Greenland ice cap. The profile $\beta = 0.3$ km^{-1}, $H' = 72$ km was used as input to the calculations for simulating the measured data.

6. VLF transmission phase stability

In the Earth-ionosphere waveguide the phase of the VLF field may display short-term variations caused by the irregular nature of the boundaries of the waveguide, in addition to long-term variations associated with diurnal and seasonal changes in the ionosphere. Superimposed on these regular variations are phase changes due to ionospheric disturbances caused by solar X-ray flares, and by energetic particle precipitation into the D-region, associated with geomagnetic and auroral storms, and with solar proton events. All of these phenomena affect VLF transmission phase, and they are associated with different time and space scales [AGARD, 1982].

VLF transmission phase stability is an important parameter which must be considered for such applications as VLF navigation, frequency comparison and time synchronization. For such applications, if the user has a choice of transmission paths, as for example with the Omega navigation system, those which are dominantly single mode should be employed. When two or more modes are present, the phase stability of the total field will vary with distance in a complex oscillatory manner and will clearly be worse for some ranges of distance. The use, for example, of VLF transmissions over distances less than 1,000 km should be avoided, since it is in this distance range that the first major minimum is found. This minimum in field strength is associated with an anti-phase relation between two components, a ground- and a sky-wave of almost equal amplitude. In this distance range the diurnal variation of phase can be unpredictably asymmetrical, since the direction of rotation of the phase of the resultant depends on which component is stronger at the time [Belrose, 1968].

While multi-mode propagation is particularly severe at short distances, it can be a problem at all distances. The magnitude of the effect is a function of frequency, distance, time-of-day and ground conductivity. Phase stability is clearly worse in the vicinity of field strength minima (see Figures 9 and 10).

The regular variations of VLF phase, and the changes associated with ionospheric disturbance have been studied by many researchers, and there is a great deal of information available in the literature [Belrose, 1968; AGARD, 1982]. However, there are few statistical studies that are useful for the design of systems. Short-term variations of phase are even less well documented. Watt [1967] has summarized data available at that time, and has shown how the standard deviation of phase varies as a function of frequency (for the 10 - 20 kHz band), distance (for long paths d > 1,000 km) and time-of-day (day and night conditions). More recently Pan and Tian [1988] have published results of a study in China of 12.5 kHz phase stability for 500-3,000 km North-South paths under night-time conditions. The authors have developed a mathematical expression for the standard deviation of phase that takes into account multi-mode effects and that agrees well with this experiment.

VLF transmission phase stability is a topic that needs further study.

7. Future work

The theory of radio-wave propagation at ELF and VLF, necessary to estimate field strengths, is now becoming fairly well understood. Two competing theories are used to describe propagation in the VLF bands: the wave-hop theory and the waveguide mode theory.

The solutions obtained from the wave-hop theory (see Report 265) are generally most suitable for short distances and the higher (LF) frequencies, while the waveguide mode theory is most suitable for longer distances and the lower (VLF) frequencies. More precise mode field calculations require inclusion of transverse electric (TE) as well as transverse magnetic (TM) modes and the conversion between these types of modes. The inclusion of both mode polarizations is important for the computation of both horizontal and vertical fields between elevated transmitters and receivers.

The wave guide mode theory seems to describe better certain features of VLF propagation, e.g. the phase steps at dawn which are observed on long east-to-west transmissions, than does the ray-path wave-hop theory. The calculation of field strengths can be simpler using the waveguide mode theory than the wave-hop method for many cases. More comprehensive comparisons should be made between solutions using the waveguide mode method and wave-hop method.

It has been shown that there is limited agreement between theoretical calculations and measurement. However, further experimental observations particularly at several frequencies, between 10 and 30 kHz, over sea water and land of various conductivities, and at representative latitudes are needed. There are probably sufficient measurements of phase already available, the problem here is that the data had not been systematically analysed. The observations need to be repeated sufficiently often to demonstrate their stability. With such measurements it will be possible to determine values of the excitation factors, attenuation rates and phase velocities which in themselves could be used as a basis for calculation of field strength and phase over different paths. More importantly, however, these experimental propagation parameters should be compared with theory and, if necessary, the theory should be refined or its input parameters adjusted. It is likely that greater discrepancies will be observed for night-time than for daytime conditions.

There has been, during the last few years, a renewed interest in ELF propagation and communications (see [IEEE Journal of Oceanic Engineering, 1984], AGARD [1982] and [CCIR, 1982-86]). In particular, new (and overview) information is given on ELF propagation, on ELF noise, and on modelling the ambient and disturbed ionosphere. Comparisons are made between predicted and measured field strengths.

It should be noted that these models of the ambient and disturbed ionosphere, which are reported to provide agreement between predicted and available ELF propagation data, could also be used to predict VLF field strengths, at least by those administrations who are able to make such calculations.

A number of computer programs has been developed to calculate VLF/LF (frequencies below about 60 kHz) field strength employing the waveguide mode theory. The most complete long wave prediction capability (LWPC) is the program developed by Ferguson [1988]. It is in fact a program package, that comprises a collection of programs that have been developed by the author and his colleagues over the years [Pappert and Shockey, 1971, 1972a, 1972b and 1976; Morfitt and Shellman, 1976], that are exercised separately or in sequence depending on the application. The execution of these individual programs can be set up by a driven program which automates the process. The theoretical basis for the method is exact. The model ionosphere is, however, an approximate one which characterizes the conductivity as exponentially increasing with height (see section 4.4, Tables I and II). This two parameter model can be varied step-wise if required along the great circle path. The lower boundary of the waveguide is defined by a detailed map of the world based largely on geological formations.

More measurements are needed to establish seasonal changes [CCIR, 1986-90], and to establish differences between middle, low and high latitudes. The shadowing effect of the Greenland ice cap is important. Attenuation rates for signals propagating across the Greenland ice cap are 1.3 dB/1000 km by night and 22 dB/1000 km by day. Since daytime solar proton disturbances result in a further lowering of the ionosphereric reflecting boundary, this results in attenuation rates that are still markedly greater, to such an extent that signal reception is no longer possible. Estimates of field strength for daytime paths agree well with the observed results at middle latitudes, using $\beta = 0.3$ km^{-1} and $H' = 74$ km, providing the effects of the poorly conducting ground are properly taken into account. However, at high latitudes there may be significant dependence on seasonal and solar cycle changes in ionospheric reflectivity.

At low latitudes it is not currently possible to theoretically calculate diurnal phase and amplitude variations for transequatorial paths propagating westwards. Theoretical work is needed to derive the variation of all relevant waveguide parameters, including mode conversion. The inability to calculate corrections for westward propagating transequatorial paths is severely limiting the effectiveness of OMEGA/VLF navigation. Related to this is the need for experimental definition of the variation of VLF parameters with azimuth, latitude and frequency in the vicinity of the magnetic equator.

Research employing atmospherics as natural VLF sources on frequencies below 10 kHz is being carried out by various groups. A statistical method of analysing atmospherics in this frequency range has been developed at the Heinrich-Hertz Institute in Berlin [Volland *et al.*, 1970] which permits the determination of the location of individual thunderstorms as well as of the transmission function of the ionospheric waveguide in amplitude and phase [Frisius *et al.*, 1970; Harth, 1971]. VLF atmospherics, in spite of very limited knowledge of the source characteristics, can be used for deducing empirical conductivity profiles which are useful for long path propagation prediction conditions; the method is especially valuable for studying paths where multi-frequency transmissions are not otherwise available [Hughes *et al.*, 1974; Hughes and Pappert, 1975]. In the United States of America multi-frequency pulsed and phase coherent transmissions between 9.4 and 31.25 kHz have been used for propagation studies over very short and medium paths and over the long-distance path from Hawaii to California [Morfitt, 1971 and 1973]. Observations of VLF reflectivity for a short path near Thule, Greenland have been made during several years [Pagliarulo *et al.*, 1979]. The experimental technique utilizes 100 μsec VLF pulses radiated from a 130 metre vertical antenna [Lewis *et al.*, 1973] to deduce ionospheric reflection coefficients from 6 to 35 kHz.

A desirable way to carry out these measurements would be to use an aircraft flying along great circles between transmitters and field receiving stations. In this way the mode structure at the receivers could be determined, especially at night for paths up to 5000 to 7000 km depending on frequency. The fixed receivers which would monitor the signals continuously could then be used to determine changes in the propagation parameters resulting from diurnal seasonal variations and changes caused by differences in solar activity as well as mode conversion factors.

The other approach which is also desirable is to use measurements by rockets or ground-based techniques to determine the vertical variations of electron density in the lower ionosphere. The resulting profiles could then be used to calculate ionospheric reflection coefficients. These would then be used to calculate the VLF mode parameters for comparison with the experimental results or for direct calculation of the mode parameters. Electron density measurements are particularly required at heights below 70 km where there are large discrepancies in existing observations, at night-time and at low latitudes.

ARCHIVES U.I.T. GENÈVE

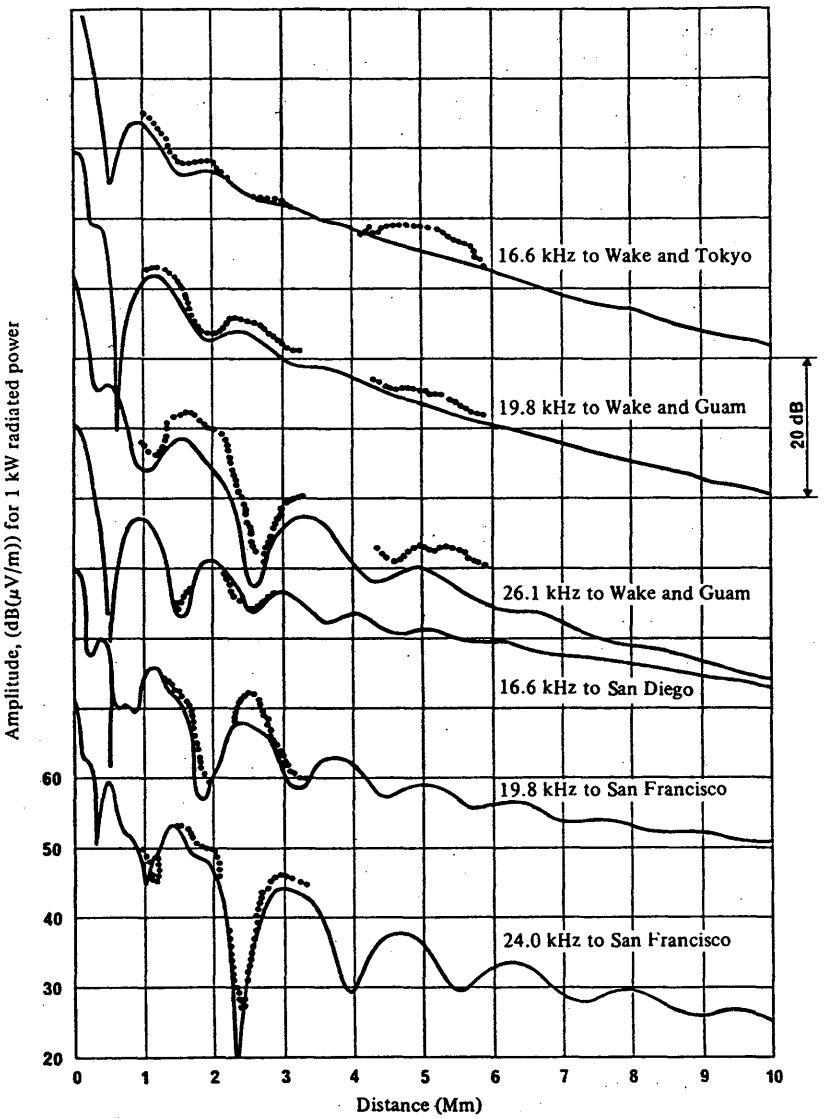


FIGURE 9 – *Propagation over the Pacific Ocean of signals transmitted from Hawaii (daytime, summer)*

——— predictions

••••••• observations

Note. – The amplitude scale applies to the lowest curve; the other curves are displaced by multiples of 20 dB.

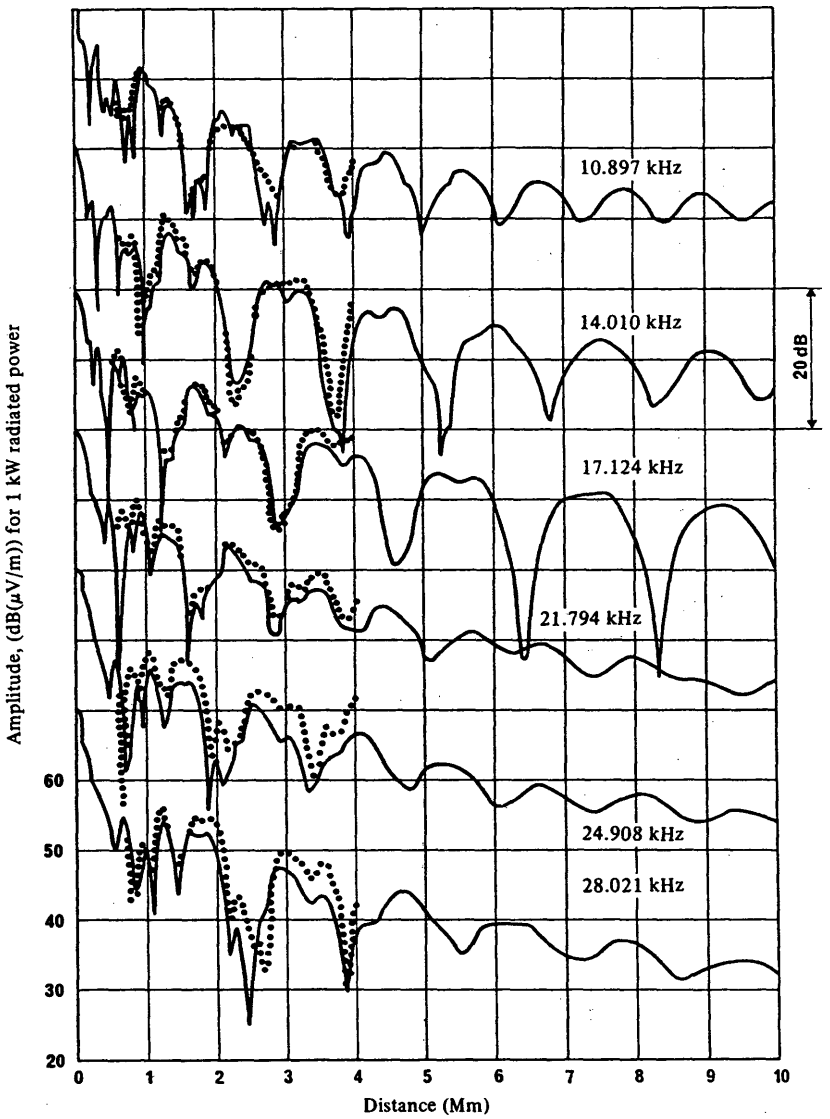


FIGURE 10 – *Propagation over the Pacific Ocean of signals transmitted from Hawaii to Southern California (night-time, winter)*

——— predictions

..... observations

Note. – The amplitude scale applies to the lowest curve; the other curves are displaced 20 dB from each other.

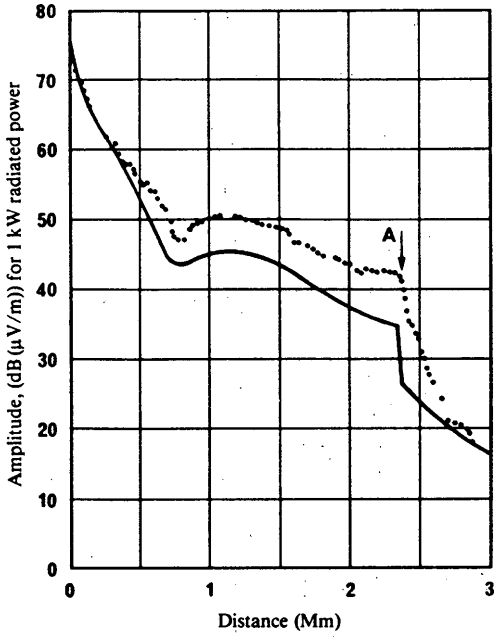


FIGURE 11 – *Daytime high latitude propagation across the Greenland ice cap (45 kHz)*

——— predictions
••••••• observations
A ice cap starts

Preston, U.K. to Sondrestrom (Greenland)
Frequency: 45 kHz
$\beta = 0.3\ km^{-1}$, $H' = 72$ km

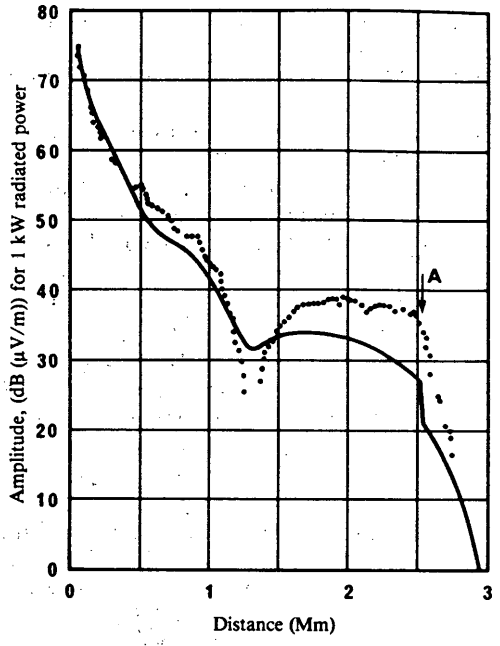


FIGURE 12 – *Daytime high latitude propagation across the Greenland ice cap (60 kHz)*

——— predictions
••••••• observations
A ice cap starts

Rugby, U.K. to Sondrestrom (Greenland)
Frequency: 60 kHz
$\beta = 0.3\ km^{-1}$, $H' = 72$ km

REFERENCES

AGARD [1982] Ed. J. S. Belrose, *Medium, Long and Very Long Wave Propagation (at frequencies less than 3000 kHz).* Conf. Proc. No. 305, NASA Accession No. N82-27613. National Technical Information Service, Springfield, VA 22161, USA.

AL'PERT Ya. L., GUSEVA, E. G. and FLIGEL, D. S. [1967] Propagation of LF electro-magnetic waveguide. Academy of Sciences of the U.S.S.R.

ARAKI, T. [1973] Anomalous diurnal changes of transequatorial VLF radio waves. *J. Atmos. Terr. Phys.*, Vol. 35, 4, 693-703.

BANNISTER, P. R. [1979] Summary of extremely low frequency (ELF) field strength measurements made in Connecticut during 1975. *Radio Sci.*, Vol. 14, 1, 103-108.

BARR, R. [1971a] The propagation of ELF and VLF radio waves beneath an inhomogeneous anisotropic ionosphere. *J. Atmos. Terr. Phys.*, Vol. 33, 343-353.

BARR, R. [1971b] The effect of the earth's magnetic field on the propagation of ELF and VLF radio waves. *J. Atmos. Terr. Phys.*, Vol. 33, 1577-1583.

BELROSE, J.S. [1968] - Low and very low frequency radio propagation. AGARD lecture series XXIX, NTIS Acces. No. AD 676788, National Technical Information Service, VA, 22161, United States.

BEUKERS, J. M. [1973] Accuracy limitations of the OMEGA navigation system employed in differential mode. *J. Inst. Nav.*, Vol. 20, 1, 81-92.

BEUKERS, J. M. [1974] A review and application of VLF and LF transmissions for navigation and tracking. *J. Inst. Nav.*, Vol. 21, 2, 117-133.

BICKEL, J. E. [1967] VLF attenuation rates deduced from aircraft observations near the antipode of NPM. *Radio Sci.*, Vol. 2, (New Series), 575-580.

BICKEL, J. E., FERGUSON, J. A. and STANLEY, G. V. [1970] Experimental observations of magnetic field effects on VLF propagation at night. *Radio Sci.*, Vol. 5, 19-25.

BLAIR, B. E. CROW, E. L. and MORGAN, A. H. [1967] Five years of VLF world-wide comparison of atomic frequency standards. *Radio Sci.*, Vol. 2, (New Series), 627-636.

BUDDEN, K. G., [1955] The numerical solution of differential equations governing reflection of long radio waves from the ionosphere. *Proc. Roy. Soc.* A227, 516-537.

BUDDEN, K. G. [1961] The waveguide-mode theory of wave propagation. Prentice Hall Inc., Englewood Cliffs, NJ, USA.

BURGESS, B. [1970] VLF phase delay variability and design of long range navigation aids. *Phase and Frequency Stabilities in Electromagnetic Wave Propagation*. Ed. K. Davies, Technivision, Slough, United Kingdom.

BURROWS, M. L. [1978] *ELF Communications Antennas.* Peter Peregrinus Ltd., Stevenage, England.

BURROWS, M. L. and NIELSSEN, C. W. [1972] ELF communication system design. IEEE International Conference on Engineering in the Ocean Environment, 95-107.

CASSELMAN, C. J., HERITAGE, D. P. and TIBBALS, M. L. [1959] VLF propagation measurements for the Radux-Omega navigation system. *Proc. IRE*, 47, 829-839.

CHAPMAN, F. W., LLANWYN JONES, D., TODD, J. D. W. and CHALLINOR, R. A. [1966] Observations on the propagation constant of the earth-ionosphere waveguide in the frequency band 8 c/s to 16 kc/s. *Radio Sci.*, Vol. 1, 1273-1282.

CHILTON, C. J., CRARY, J. H. and CROMBIE, D. D. [1969] A comparison of middle and low latitude sunrise VLF fading observed on the 1967 voyage of the Oceanographer. Proc. Third International Symposium on Equatorial Aeronomy, Ahmedabad, India, February 3-8, Vol. 1 105-113.

COMPUTATION LABORATORY AT CAMBRIDGE [1945] *Tables of the Modified Hankel Functions of Order One-Third and of their Derivatives.* Harvard University Press, Cambridge, Ma., USA.

CROMBIE, D. D. [1964] Periodic fading of VLF signals received over long paths during sunrise and sunset. *NBS J. Res.*, Vol. 68D, 27-34.

CROMBIE, D. D. [1966] Further observations of sunrise and sunset fading of VLF signals. *Radio Sci.*, Vol. 1, (New Series), 47-51.

CROMBIE, D. D. [1967] The waveguide mode propagation of VLF radio waves to great distances. IEE (London) Conf. Publ., 36.

CROMBIE, D. D., ALLAN, A. H. and NEWMAN, M. [1958] Phase variations of 16 kHz transmissions from Rugby, observed in New Zealand. *Proc. IEE*, Vol. 105B, 301-304.

DAVIS, J. R. [1976] Localized nighttime D-region disturbances and ELF propagation. *J. Atmos. Terr. Phys.*, Vol. 38, 1309-1317.

DAVIS, R. M. and BERRY, L. A. [1977] A revised model for the electron density in the lower ionosphere. Command and Control Technical Center (DCA), Tech. Rep. 111077, NTIS Accession No. AD17883. National Technical Information Service, Springfield, Va. 22161, USA.

FERGUSON, J. A. [1980] Ionospheric profiles for predicting nighttime VLF/LF propagation. NOSC TR 530, NTIS Accession No. ADA 085399. National Technical Information Service, Springfield, Va. 22161, USA.

FERGUSON, J.A. [1988] - Status of the naval ocean systems long wave propagation capability "LWPC". Paper presented at Third Workshop on ELF/VLF Radio Noise, Stanford University.

FOLEY, G., WAND, I. C. and JONES, T. B. [1973] Studies of the modal parameters of VLF radio waves propagated below the night-time ionosphere. *J. Atmos. Terr. Phys.*, Vol. 35, 2111-2122.

FRISIUS, J., HEYDT, G. and HARTH, W. [1970] Observations of parameters characterising the VLF atmospherics activity as a function of the Azimuth. *J. Atmos. Terr. Phys.*, Vol. 32, 1403-1422.

GALEJS, J. [1967a] Propagation of VLF waves below an anisotropic stratified ionosphere with a transverse static magnetic field. *Radio Sci.*, Vol. 2, (New Series), 557-574.

GALEJS, J. [1967b] Propagation of VLF waves below anisotropic ionosphere models with a dipping static magnetic field. *Radio Sci.*, Vol. 2 (New Series), 1497-1512.

GALEJS, J. [1972] *Terrestiral Propagation of Long Electromagnetic Waves.* Pergamon Press, New York/Oxford.

GALLENBERGER, R. and SWANSON, E. [1971] Variations in Omega propagation parameters. NELC/TR 1773. Naval Electronics Laboratory Center, San Diego, Calif., USA.

HARTH, W. [1971] Sudden anomalies of spectral atmospherics parameters during SID's. Proc. VLF Symposium, Ødo-Sandefjord, Norway.

HUGHES, H. G. [1971] Differences between pulse trains of ELF atmospherics at widely separated locations. *J. Geophys. Res.*, Vol. 76, 2116-2125.

HUGHES, H. G. and GALLENBERGER, R. J. [1974] Propagation of extremely low-frequency (ELF) atmospherics over a mixed day-night path. *J. Atmos. Terr. Phys.*, Vol. 36, 1643-1661.

HUGHES, H. G., GALLENBERGER, R. J. and PAPPERT, R. A. [1974] Evaluation of night-time exponential ionospheric models using VLF atmospherics. *Radio Sci.*, Vol. 9, 1109-1116.

HUGHES, H. G. and PAPPERT, R.A. [1975] Propagation prediction model selection using VLF atmospherics. *Geophys. Res. Lett.*, Vol. 2, 96-98.

HUGHES, H. G. and THEISSEN, J. F. [1970] Diurnal variations in the apparent attenuations of ELF atmospherics over two different propagation paths. *J. Geophys. Res.*, Vol. 75, 2795-2801.

IEEE JOURNAL OF OCEANIC ENGINEERING [July, 1984] Special Issue on ELF communications. Vol. OE-9.

JOHLER, J. R. and LEWIS, R. L. [1969] Extra-low frequency terrestrial radio-wave field calculations with the zonal harmonic series. *J. Geophys. Res.*, Vol. 74, 2459-2470.

KAISER, A. B. [1969] An explanation of VLF diurnal phase change observations. *Radio Sci.*, Vol. 4, 17-21.

KIKUCHI, T. [1983] Anomalous diurnal phase shifts of Omega VLF waves (10-14 kHz) on the east-west low latitude and transequatorial paths. *J. Atmos. Terr. Phys.*, Vol. 45, 743-751.

KIKUCHI, T. [1986] Waveguide model analyses of Omega VLF wave propagation at 13.6 kHz. J. Atmos. Terr. Phys., 48, 15-23 .

KIKUCHI, T. and OHTANI, A. [1984] Anomalous interference in Omega VLF wave propagation on east-to-west equatorial paths. *J. Atmos. Terr. Phys.*, Vol. 46, 697-703.

KUHNLE, P. F. and SMITH, R. D. [1964] Rome Air Development Center. Tech. Rep. RADC-TR-64-360, NTIS Accession No. ADAOC1701. National Technical Information Service, Springfield, Va. 22161, USA.

LEWIS, R. L. and JOHLER, J. R. [1976] Correction of numerical results in "ELF terrestrial radio wave field calculations with the zonal harmonic series". *Radio Sci.*, Vol. 11, 75-81.

LEWIS, E. A, RASMUSSEN, J. E., and KOSSEY, P. A. [1973] Measurements of ionospheric reflectivity from 6 to 35 kHz. *J. Geophys. Res.*, Vol. 78, 19, 3903-3912.

LYNN, K. J. W. [1967] Anomalous sunrise effects observed on a long trans-equatorial VLF propagation path. *Radio Sci.*, Vol. 2 (New Series), 521-530.

LYNN, K. J. W. [1969] Multisite observations of the VLF transequatorial propagation anomaly. *Radio Sci.*, Vol. 4, 203-211.

LYNN, K. J. W. [1973] VLF mode conversion observed at middle latitudes. *J. Atmos. Terr. Phys.*, Vol. 35, 439-452.

LYNN, K. J. W. [1975] The transequatorial reception of Omega (13.6 kHz) transmissions. *J. Atmos. Terr. Phys.*, Vol. 37, 1395-1399.

LYNN, K. J. W. [1977] VLF modal interference over west-east paths. *J. Atmos. Terr. Phys.*, Vol. 39, 347-357.

LYNN, K. J. W. [1978] Some differences in diurnal phase and amplitude variations for VLF signals. *J. Atmos. Terr. Phys.*, Vol. 40, 145-150.

MAHMOUD, S. F. and BEAL, J. C. [1971] VLF propagation parameters derived from observations of sunrise and sunset phenomena. *Proc. IEE*, Vol. 118, 1351-1357.

MEARA, L. A. [1973] VLF modal interference effects observed on transequatorial paths. *J. Atmos. Terr. Phys.*, Vol. 35, 305-315.

MORFITT, D. G. [1971] Analysis of a multimode propagation concept for predicting VLF signal strengths at night. Naval Electronics Laboratory Center Tech. Rep. TR 1798, NTIS Accession No. AD738846. National Technical Information Service, Springfield, Va. 22161, USA.

MORFITT, D. G. [1973] Computer techniques for fitting electron density profiles to oblique-path VLF propagation data. Naval Electronics Laboratory Center Tech. Rep. TR 1854, NTIS, Accession No. AD757341. National Technical Information Service Springfield, Va. 22161, USA.

MORFITT, D. G. [1977] Effective electron density distributions which describe VLF/LF propagation data. Naval Ocean Systems Center Tech. Rep. TR141, NTIS, Accession No. ADA047508. National Technical Information Service Springfield, Va. 22161, USA.

MORFITT, D. G. and SHELLMAN, C. H. [1976] MODESRCH, an improved computer program for obtaining ELF/VLF/LF mode constants. Naval Electronics Laboratory Centre Interim Rep. 771, NTIS Accession No. ADA032573. National Technical Information Service Springfield, Va. 22161, USA.

NARD, G. [1972] Results of recent experiments with differential OMEGA. *J. Inst. Nav.*, 19, 2.

PAGLIARULO, R. P., TURTLE, J. P., RASMUSSEN, J. E., COOLEY, R. L. and KLEMETTI, W. I. [1979] VLF/LF reflectivity of the polar ionosphere – September 1978 to 5 May 1979. Reports RADC-TR-79-178 and 273. Rome Air Development Center, Griffiss Air Force Base, NY, USA.

PAN WEIYAN and TIAN YUSHU [1988] - Multi-mode interference and phase stability of VLF wave propagation. Proc. 1988 International Symposium on Radio Propagation (ISRP '88), Beijing, China, 40-44.

PAPPERT, R. A [1968] A numerical study of VLF mode structure and polarization below an anisotropic ionosphere. *Radio Sci.*, Vol. 3, (New Series), 219-233.

PAPPERT, R. A. [1970] Effects of elevation and ground conductivity on horizontal dipole excitation of the earth-ionosphere waveguide. *Radio Sci.*, Vol. 5, 579-590.

PAPPERT, R. A. and BICKEL, J. E. [1970] Vertical and horizontal VLF fields excited by dipoles of arbitrary orientation and elevation. *Radio Sci.*, Vol. 5, 1445-1452.

PAPPERT, R. A., GOSSARD, E. E. and ROTHMULLER, I. J. [1967] A numerical investigation of classical approximations used in VLF propagation. *Radio Sci.*, Vol. 2, 387-400.

PAPPERT, R. A. and MOLER, W. F. [1974] Propagation theory and calculations at lower extremely low frequencies (ELF). *IEEE Trans. Comm.* Vol. COM-22, 438-451.

PAPPERT, R. A. and MORFITT, D. G. [1975] Theoretical and experimental sunrise mode conversion results at VLF. *Radio Sci.*, Vol. 10, 537-546.

PAPPERT, R. A. and SHOCKEY, L. R. [1971] WKB Mode summing program for VLF/LF antennae of arbitrary length, shape and elevation. Naval Electronics Laboratory Center Interim Rep. 713, NTIS Accession No. AD728414. National Technical Information Service, Springfield, Va. 22161, USA.

PAPPERT, R. A. and SHOCKEY, L. R. [1972a] Mode conversion program for an inhomogeneous anisotropic ionosphere. Naval Electronics Laboratory Center Interim Rep. 722, NTIS Accession No. AD743948. National Technical Information Service, Springfield, Va. 22161, USA.

PAPPERT, R. A. and SHOCKEY, L. R. [1972b] WKB fields program for lower ELF. Naval Electronics Laboratory Center Interim Rep. 731, NTIS Accession No. AD757080. National Technical Information Service, Springfield, Va. 22161, USA.

PAPPERT, R. A. and SHOCKEY, L. R. [1976] Simplified VLF/LF mode conversion program with allowance for elevated, arbitrarily oriented electric dipole anennae. Naval Electronics Laborartory Center Interim Rep. 771, NTIS Accession No. ADA033412, National Technical Information Service, Springfield, Va. 22161, USA.

PAPPERT, R. A. and SMITH, R. R. [1972] Orthogonality of VLF height gains in the earth ionosphere waveguide. *Radio Sci.*, Vol. 7, 275-278.

PAPPERT, R. A. and SNYDER, F. P. [1972] Some results of a mode-conversion programme for VLF. *Radio Sci.*, Vol. 7, 913-923.

RAWLES, A. T. and BURGESS, B. [1967] Results of the two-frequency VLF transmission experiments from Criggion GBZ. *Radio Sci.*, Vol. 2, 1295-1301.

REDER, F. [1979] Propagation effects on Omega signals and methods of reducing them. Fourth Annual Meeting of the International Omega Association, San Diego, 10-12 September, Calif., USA.

RHOADS, F. J. and GARNER, W. E. [1967] An investigation of the modal interference of VLF radio waves. *Radio Sci.*, Vol. 2 (New Series), 539-546.

RINNERT, K. [1973] Electron density profiles in the lower ionosphere deduced from long path VLF wave propagation. *Radio Sci.*, Vol. 8, 829-836.

RUGG, D. E. [1967] Theoretical investigation of the diurnal phase and amplitude variations of VLF signals. *Radio Sci.*, Vol. 2, 551-556.

SHEDDY, C. H. [1968] A general analytic solution for reflection from a sharply bounded anisotropic ionosphere. *Radio Sci.*, Vol. 3, **8**, 792-795.

SNYDER, F. P. and PAPPERT, R. A. [1969] A parametric study of VLF transequatorial propagation anomaly. *Radio Sci.*, Vol. 4, 213-226.

STEELE, F. K. and CROMBIE, D. D. [1967] Frequency dependence of VLF fading at sunrise. *Radio Sci.*, Vol. 2, (New Series), 547-549.

SUZUKI, K., BABA, K., YOSHIOKA, T. and KINOSHITA, M. [1973] Phase variation and amplitude fading of NWC – 22.3 kHz signal at dawn. *J. Geomag. Geoelect.*, Vol. 25, 403-413.

TAYLOR, W. L. and SAO, K. [1970] ELF attenuation rates and phase velocities observed from slow-tail components of atmospherics. *Radio Sci.*, Vol. 5, 1453-1460.

VOLLAND, H. [1966] Die Ausbreitung langer Wellen (propagation of long waves). *Veröffentlichungen des NKGG der DDR, Reihe II*, Vol. 2, 3-126.

VOLLAND, H., HEYDT, G. and HARTH, W. [1970] Statistical measurement of the spectral amplitude and phase of atmospherics in the VLF range. *Phase and Frequency Stabilities in Electromagnetic Wave Propagation.* Ed. K. Davies, Technivision, Slough, UK.

WAIT, J. R. [1962] *Electromagnetic Waves in Stratified Media.* Pergamon Press, New York, NY, USA.

WAIT, J. R. [1964] Two dimensional treatment of mode theory of the propagation of VLF radio waves. *NBS J. Res.*, Vol. 68D, 81-93.

WAIT, J. R. [1968a] Mode conversion and refraction in the earth-ionosphere wave-guide for VLF radio waves. *J. Geophys. Res.*, Vol. 73, 3535-3548.

WAIT, J. R. [1968b] On the theory of VLF propagation for a step model of the nonuniform earth-ionosphere wave-guide. *Can. J. Phys.*, Vol. 46, 1979-1983.

WAIT, J. R. [1970] Factorization method applied to electromagnetic wave propagation in a curved wave-guide with nonuniform walls. *Radio Sci.*, Vol. 5, 1059-1068.

WAIT, J. R. (Ed.) [1974] Special issue on extremely low frequency (ELF) communications. *IEEE Trans. Comm.*, Vol. COM-22, 4.

WAIT, J. R. [1977] Propagation of ELF electromagnetic waves and project SANGUINE/SEAFARER. *IEEE J. Ocean. Eng.*, Vol. OE-2, 2, 161-171.

WAIT, J. R. and SPIES, K. P. [1965] Influence of finite ground conductivity on the propagation of VLF radio waves. *NBS J. Res.*, Vol. 69D, 1359-1373.

WAIT, J. R. and SPIES, K. P. [1968] On the calculation of mode conversion at a graded height change in the earth-ionosphere wave-guide at VLF. *Radio Sci.*, Vol. 3, 787-791.

WALKER, D. [1965] Phase steps and amplitude fading of VLF signals at dawn and dusk. *NBS J. Res.*, Vol. 69D, 1435-1443.

WATT, A. D. [1967] *VLF Radio Engineering.* Pergamon Press, New York, NY, USA.

WESTERLUND, S. and REDER, F. H. [1973] VLF radio signals propagating over the Greenland ice-sheet. *J. Atmos. Terr. Phys.*, Vol. 35, 1475-1491.

WESTERLUND, S., REDER, F. H. and ABOM, C. [1969] Effects of polar cap absorption events on VLF transmissions. *Planet. Space Sci.*, Vol. 17, 1329-1374.

WILLIM, D. K. [1974] Sanguine, *ELF-VLF Radiowave Propagation*, 251-261. D. Reidel Publishing Co., Dordrecht, Netherlands.

CCIR Documents

[1982-86]: 6/228 (IWP 6/5).

[1986-1990]: 6/242 (Interim Working Party 6/5).

BIBLIOGRAPHY

CCIR Documents

[1978-82]: 6/242 (IWP 6/5).

SECTION 6E: IONOSPHERIC PROPAGATION PREDICTION AT FREQUENCIES BETWEEN ABOUT 1.6 AND 30 MHz

REPORT 340-6

CCIR ATLAS OF IONOSPHERIC CHARACTERISTICS

(Question 25/6)

(1966-1970-1974-1978-1982-1986)

In accordance with decisions of the XVIIth Plenary Assembly this Report is published separately.

REPORT 255-7

LONG-TERM IONOSPHERIC PROPAGATION PREDICTIONS

(Question 33/6)

(1959-1963-1966-1970-1974-1978-1982-1986-1990)

1. Prediction of the basic MUF

When considering the prediction of monthly median ionospheric propagation conditions, it is essential to consider separately the translation of vertical-incidence ionospheric data into oblique-incidence characteristics, and the prediction of vertical incidence data which is dependent on the accuracy and availability of ionospheric observations as well as predictions of other geophysical phenomena.

The prediction of ionospheric data requires:

- an accurate, reliable representation (either graphical or mathematical), and
- a known correlation with solar activity.

Regardless of the method used to represent ionospheric data, it is necessary to extrapolate into areas of the world where ionospheric observations are few or lacking. Also, the solar activity indices are rough estimates of solar activity and involve yet another prediction process. Obviously there are several potential sources of error inherent in the above process of predicting radiocommunication frequencies.

These sources of error include the following:

- the lack of data in certain geographic areas (see Report 430);
- the smoothing of basic data inherent in the mathematical representation;
- uncertain and variable relationships between the ionospheric characteristics and the solar activity index both in the rising and descending phases of the solar cycle, and also from cycle to cycle;
- unsatisfactory and inadequate methods of predicting the solar activity index or indices (see Annex I to Recommendation 371);
- the difference between basic MUF and the operational MUF (see § 2);
- the inadequacy of usable methods for taking account of the statistical variations of ionospheric parameters, including the basic MUF around the monthly median. The statistical distributions around the monthly median are often quite broad [King and Slater, 1973] and the spread of the distribution is not necessarily proportional to the value of the monthly median;
- difficulty in the translation of vertical ionosonde data to propagation predictions for operational communication circuits. The differences can be particularly large when steep horizontal gradients and inhomogeneities in ionization occur in the transmission path. Examples of this are given by Möller [1960] and Williams [1962].

2. The ratio of operational MUF to the basic MUF

2.1 In general the ratio of operational MUF to basic MUF seems to be larger for night-time than for day-time conditions, while at middle latitudes this ratio seems to be smaller in summer for both day and night than for winter nights. The largest values of this ratio for middle and high latitudes usually occur in winter. The ratio tends to increase for circuits passing near the auroral zones.

It is possible to describe this observed variation, as a first approximation, by an empirical formula based on the dynamics of the ionosphere as a function of the variation of the basic MUF [Beckmann, 1967; Beckmann and Ochs, 1969; Beckmann, 1970]. The effect of the irregularities of the ionosphere becomes more apparent as the height of the F2 layer increases and its critical frequency decreases.

Values of the ratio broadly consistent with the above information are presented in Table II of Part 3 of Report 340. It does not seem appropriate at this stage to make separate allowances for auroral paths. Use of entries appropriate to midpath conditions is suggested.

The differences between the operational MUF and the basic MUF can be explained by various ionospheric phenomena, such as scattering in the E and F regions, off-great-circle propagation, and propagation by unusual modes when horizontal gradients or ionization irregularities exist in the E and F regions. Also, spread F may be an important factor in increasing the ratio. It is also possible that some of this effect may result from inadequacies in the theoretical formulae and ray-tracing methods used. As might be expected, when comparisons are made between observed and predicted values of the MUF the differences are greater than in the case when actual ionospheric vertical incidence observations are used to calculate these values. Errors in the prediction of the basic MUF or of the operational MUF may arise from ionospheric characteristics that are not well predicted; thus an important source of error may well be the prediction of the critical frequencies and heights of the layers rather than the conversion to the basic MUF.

2.2 Spread F may be an important factor in causing the above-mentioned differences between the operational MUF and the basic MUF. Numerical maps of spread F occurrence have been developed in the United States of America for years of high and low solar activity (see Report 340).

The dispersion of the basic MUF about the monthly median exhibits variations that are similar to the variations of the probability of frequency spreading. Both the MUF-dispersion and the spread F probability show the following variations:

- a diurnal maximum in night-time hours;
- a seasonal maximum in winter or equinox at high latitudes;
- a positive correlation with solar activity at high latitudes and a negative correlation at medium and low latitudes.

The URSI Ionosonde Network Advisory Group (INAG) has issued rules for the determination of a vertical incidence spread F parameter fxI [Piggott and Rawer, 1972 and 1978]. Some administrations are investigating the application of this parameter to predictions.

3. Ionospheric models

Report 340, Part 9, contains a model of the vertical distribution of electron density in the E and F regions of the ionosphere which is specified in terms only of the routinely scaled or predicted ionospheric characteristics M(3000)F2, foF2, foE and h'F(F2) [Bradley and Dudeney, 1973]. This model (see Fig. 1) is useful for communication studies and predictions; however, it suffers from the following limitations:

- a gradient discontinuity occurs at a plasma frequency equal to foE and also at 1.7 foE;
- the profile is linear between the E and F regions;
- for the case foE > foF2/1.7 the profile reduces to a simple linear variation from hmE to hmF2.

These factors limit the applicability of the model, particularly for studies of the F1 mode of propagation.

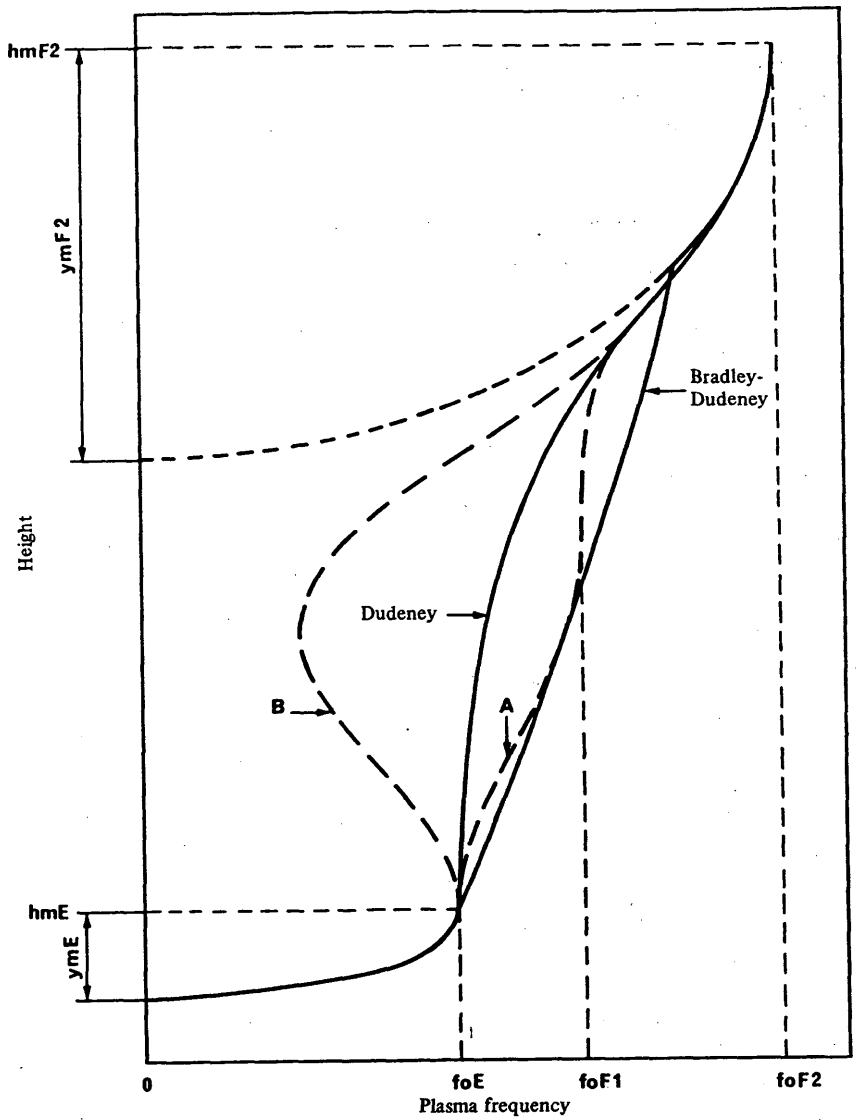


FIGURE 1 – *Comparison of the Bradley-Dudeney and Dudeney model profiles*

A: ledge option
B: valley option

A model profile which overcomes these difficulties whilst still requiring only standard ionospheric characteristics as input is available [Dudeney, 1978]. This profile is shown in comparison with the Bradley-Dudeney profile in Fig. 1. It consists of:

- a parabolic E-layer below the height of maximum hmE, with semi-thickness ymE;
- a cosine F2-layer with height of maximum hmF2 and semi-thickness ymF2;
- a secant increase in plasma frequency from hmE up to a height h_T at which the secant curve is tangential to the F2-layer curve;
- an optional cosine term between hmE and h_T, which combined with the secant curve, simulates the F1-ledge or E-F valley. To generate the ledge, the measured (or predicted) value of foF1 is required; for the valley a depth as a fraction of foE must be chosen.

The advantages of the Dudeney model are that it provides a realistic simulation of the E-F region of the ionosphere, and is hence particularly suited to studies of F1-mode propagation; and that it contains no artificial gradient discontinuities. However, it has the disadvantage that numerical techniques are required to solve for the model parameters and to generate the corresponding virtual height profile.

A multi-segment model (Lincoln and Conkright, 1981; Rawer and Bradley, 1987) given in terms of standard ionospheric characteristics and empirical relationships known as the International Reference Ionosphere (IRI) has been developed by a joint COSPAR/URSI Working Group. The IRI is specified for any given time and location using the ionospheric characteristics given in Report 340. Current work is concerned with representing this model by LAY functions (Bossy, 1987) in order to provide a smooth height variation of electron density and gradient, thereby making the model suitable for ray-tracing applications.

Models consisting of multiple quasi-parabolic and inverted quasi-parabolic segments enable the creation of profiles of arbitrary complexity [Dyson and Bennett, 1988; Baker and Lambert, 1988], which can be fitted to electron density profiles obtained either by inversion of vertical incidence ionograms or by application of the Dudeney model using scaled layer parameters. The advantage of this technique is that it leads to analytical equations for oblique raypaths [Kiyanovsky, 1972; Hill, 1979; Kiyanovsky et al., 1987].

Since the requirements of model realism and ease of use may be conflicting the simplest model commensurate with the required accuracy should be used for each application. An overall review and discussion of ionospheric models, together with current ionospheric performance prediction computer programs has been given by Rush [1986]. A comparative review of the Dudeney and other models has been given by Dudeney and Kressman [1986]. Applications of models to single-station target location have been described by McNamara [1988] and Baker and Lambert [1989].

4. Predicting the effect of F-region ionization on radiocommunications

4.1 Long-term ionospheric propagation predictions for determining the F2-layer basic MUF are available in graphical form, including the diurnal, seasonal, solar cycle, and geographical variations, for zero and 4000 km transmission distances (see Report 340, Oslo 1966). These charts were derived from mathematical representations of the vertical-incidence ionospheric observations and the representations are also available in the form of numerical coefficients for use in a computer program (see Report 340).

Studies in the United States of America and the USSR comparing the predicted monthly median foF2 with observations from ground-based ionospheric sounding stations indicate that the discrepancies in the predictions are usually less than ± 15% except in high latitudes where they are sometimes as high as 40%. A deficiency in the numerical maps of foF2 appears to be the assumption that a limited portion (five years) of solar cycle 19 can accurately predict the ionospheric state for other solar cycles. Studies in the People's Republic of China and the United Kingdom have shown that the use of the ionospherically derived index IG_{12} with the numerical maps of foF2 instead of R_{12} may be expected to overcome this deficiency and improve the accuracy of predictions [Liu *et al.*, 1983] (see Opinion 82).

India has developed a method for predicting the median foF2 three months in advance [Rao and Sain, 1965]. This method does not require a prediction of solar activity and is based on the monthly ratio (MR) for median foF2 (the ratio of the median foF2 to the median for the previous months). Predicted foF2 medians for Kodaikanal using the MR are comparable to those based on I_{F2} and better than predictions based on R_{12}.

In the USSR work is continuing on the evaluation of the accuracy of long-term foF2 predictions by different methods. The preliminary results show that the method of predicting foF2 that is based on cyclic monthly curves is more accurate than the long-term prediction based on the sunspot number [Novysh-Bylinskaya, 1966].

In the People's Republic of China, a method of predicting the monthly median foF2 and M(3000) F2 within the Asia-Oceania region has been developed and used since 1975. The method is based on the ionospheric F2 layer data of one or two solar cycles obtained at 39 ionospheric sounding stations in the region and a new index Ic derived from the foF2 of the Chong-Qing ionospheric sounding station. For the Asia-Oceania region this method provides predictions which are more accurate than those predicted by CCIR Report 340 [Sun, 1987].

In the United States of America, new global maps of foF2 have been derived by combining observations of foF2 from a network of vertical-incidence ionosondes with values of foF2 determined from a theoretical model for those areas where observations are not available (primarily oceans) [Rush *et al.*, 1983, 1984].

The variations of noon foF2 over Delhi have been studied for three solar cycles by India. Divergence in foF2 values is found to exist for similar sunspot numbers during various solar cycles. Analysis of the noon foF2-R_{12} relationship for Delhi for two solar cycles (1953-1975) suggests a significant change on a time scale that is longer that a solar cycle. This corroborates the results of Smith and King [1981]. However, a similar study of the relationship between noon foF2 and the index φ, suggests that the degree of this variation is smaller. The relationship is to be studied further for different hours and locations.

4.2 An F1-layer prediction system has been developed for transmission distances in the range 2000 to 3400 km (see Report 340). The geomagnetic influence on foF1 has been found and reduced to an empirical formula as a function of the geomagnetic latitude [Du Charme *et al.*, 1973]. A comparison of this prediction method with monthly median values of foF1 observed during 1967-69 at 28 vertical incidence sounding stations indicated that the r.m.s. deviation for most stations is about 0.2 MHz or less; the error in the equatorial regions being about 1.5 times greater than that at high latitudes. Another method for the prediction of foF1 and of the maximum solar zenith angle of foF1 occurrence [Rosich and Jones, 1973] has been developed in the United States of America. This model predicts foF1 values to a similar accuracy to that above, but also gives a better prediction of the occurrence of the F1 layer. Elkins [1973] found that foF1 at high latitude stations maximizes after local noon. The F1-layer ionization density is linearly correlated with low to moderate magnetic activity.

The USSR has developed a new method to determine foF1 directly from ionograms [Schepkin and Vinnitski, 1981].

4.3 A limited comparison of experimental MUF data for 1,700 km paths indicated good agreement with predicted values from a computational model [Millman and Swanson, 1985].

In Canada comparison has been made of the MUFs predicted by two methods with recorded MUFs from three vertical incidence stations and from three oblique incidence circuits during selected periods of high and low solar activity. One method includes F1 layer predictions as described in Part 5 of Report 340 [CCIR, 1986-90].

5. Predicting the effect of E-region ionization

5.1 The effect of the regular E layer on propagation can be determined from a series of empirical formulae expressed in terms of Φ (see Report 340). In Greece, corresponding empirical formulae in terms of R_{12} and I_{F2} have been derived by Kouris [1981a, b], which predict foE with comparable accuracy. A numerical representation of the foE developed in the USA [Leftin, 1976] predicts the day-time foE to an accuracy commensurate with the estimated error in the observations. This system provides a continuous representation of foE for all 24 hours and also a smooth representation for the transition between night and day. Simple empirical formulae and graphs for calculating foE for all 24 hours and all levels of solar activity have been developed in the USSR [CCIR, 1978-82]. For certain values of solar activity, the deviations between the observed and calculated foE do not exceed 0.1 MHz.

5.2 Because of the highly variable nature of the occurrence and intensity of sporadic-E ionization, available prediction systems are based on statistics. However, for radiocommunication purposes, the effects of sporadic E are not well understood.

Numerical maps for the world-wide occurrence of sporadic E for minimum and maximum solar activity and the blanketing sporadic E for a year of minimum solar activity are available (see Report 340). A prediction system has been developed in the USSR which calculates the probability of Es reflection at a given frequency, the frequency of the wave reflected with a given probability and the frequency at which the Es ionization acts as a screen against reflection from higher layers [Kerblaï, 1960, 1964; Chernishyev, 1968; Chernishyev and Vasiljeva, 1973-74]. A method for predicting the median fbEs for temperate latitudes has been developed by Argentina [Giraldez, 1979].

The application of vertical incidence data to oblique-incidence should be undertaken with caution. Experimental studies in the USSR [Nosova, 1973] and in the Federal Republic of Germany [Mewes and Möller, 1974] indicate that the ratio of the oblique-incidence MUF to the Es top frequency at vertical incidence is often greater than that expected from the secant law.

Equatorial sporadic E is more consistent than other types and should be included in basic MUF predictions [Kift, 1960]. During the summer day-time, the maximum observed frequency for trans-equatorial paths may be determined by Es [Mewes and Möller, 1974].

Experimental data in the United States indicate that the E_s layer is frequently tilted and that differences in small scale E_s structures can lead to considerable complexity in available propagation paths [Paul, 1986].

Analysis of oblique sounding observations over several years indicates that sporadic E was useful for propagation on a trans-atlantic path (Ottawa-The Hague) less than 1% of the time and on a trans-auroral path (Winnipeg-Resolute) only 7% of the time [Hagg and Rolfe, 1963]. The use of auroral imagery from meteorological satellites as a means of predicting and specifying the occurrence of sporadic E associated with the auroral oval has been discussed by Pike [1975]. A method for calculating sporadic-E signal strength at VHF and higher portions of the HF band is given in the Annex to Recommendation 534.

6. Propagation modes and other factors

Methods of basic MUF calculation which take modes of propagation into account can often give results which are more accurate than those which do not. In using such methods, ground scattering and reflection, and horizontal ionization gradients, must be carefully considered. The availability of high speed digital computers has stimulated the development of a wide variety of methods for ray tracing and has also made possible the incorporation of more realistic models for the ionosphere than the two or three-parabolic representations.

In order to increase the accuracy of radio path parameters, predictions of the geomagnetic parameters of $N(h)$ profiles of both the quiet and disturbed ionosphere, as well as predictions of the virtual reflection heights of the ionosphere, and of the standard deviation of these heights, are made in the USSR [Shapiero, 1960; Shapiero *et al.*, 1971a; Shapiero and Shashounkina, 1971; Shapiero, 1970; Potapova, 1971; Shapiero *et al.*, 1971b]. An analytical method of computing ray paths has been given by Chvojková [1969].

Ray trajectories in an ionosphere having a horizontal ionization gradient, as observed by Bibl [1964] and Kerblaï and Volochinova [1964], have been computed [Kerblaï and Kovalevskaïa, 1967; Kovalevskaïa and Kornitzkaïa, 1969]. A segmented quasi-parabolic method has recently been given which provides analytic ray tracing through horizontal gradients [LaBahn, 1985].

It has been shown by ray tracing that, in most cases, inhomogeneities of appropriate scale produce a basic MUF increase of several MHz and differences between the angles of departure and arrival of up to 7°; while the predicted increase in spatial attenuation caused by the inhomogeneities, especially in the high angle ray with increasing frequency, was found to be in good agreement with observed results. Angle of arrival deviations during the sunrise period have been studied by Rao and Beckwith [1974] both experimentally and theoretically. A prediction method is available in the USSR which takes account of the electron density gradient in an arbitrary direction; predictions may thus be made of the hop length, the angles of radiation and arrival, in both azimuth and elevation and of the MUF in a horizontally inhomogeneous ionosphere [Kovalevskaïa and Kerblaï, 1971]. Additional experimental studies in the United Kingdom on the effect of systematic tilts indicate that the accuracy of ray path predictions may be limited by inadequate horizontal gradient information in the ionospheric model [Tedd et al., 1985].

In considering the operational MUF, it must be remembered that its relationship to the basic MUF depends upon the type of service and the effective radiated power, as well as on the required minimum field strength.

REFERENCES

BAKER, D.C. and LAMBERT, S. [1988] - Multiparabolic ionospheric model for SSL application. Electron Lett., Vol. 24, pp. 425-426.

BAKER, D.C. and LAMBERT, S. [1989] - Range estimation for SSL HFDF systems by means of a multiquasiparabolic ionospheric model, Proc IEE, Vol. 136, pt H, 2, pp. 120-125.

BECKMANN, B. [1967] Notes on the relationship between the receiving-end field strength and the limits of the transmission frequency range MUF, LUF. *NTZ-Comm. J.*, **6**, 37-47.

BECKMANN, B. [1970] FTZ-Report A445-TBR8.

BECKMANN, B. and OCHS, A. [1969] Vorhersage der ionosphärischen Kurzwellenausbreitung (Prediction for the ionospheric short-wave propagation). *Jahrbuch des elektrischen Fernmeldewesens*, 281-365.

BIBL, K. [1964] The detection of an important anomaly in the F-region ionization above Central Europe. *Ann. de Géophys.* **20**, 447-453.

BOSSY, L. [1987] - The determination of LAY-parameters for a given profile, Advances in Space Research, Vol. 7, 6, pp. 35-37.

BRADLEY, P. A. and DUDENEY, J. R. [1973] A simple model of the vertical distribution of electron concentration in the ionosphere. *J. Atmos. Terr. Phys.*, Vol. 35, 2131-2146.

CHERNISHYEV, O. V. [1968] foEs distribution curves (in Russian). *Geomag. i Aeronom.*, **8**, 902-903.

CHERNISHYEV, O. V. and VASILJEVA, T. N. [1973-74] *Prediction of Maximum Usable Frequency* (in Russian). Nauka Publishing House, V. 1-2, Moscow, USSR.

CHVOJKOVÁ, E. [1969] Formulae for ray path in ionized layers with application to oblique ionogram and duct modes. *Radio Sci.*, Vol. 4, 23-27.

DU CHARME, E. D., PETRIE, L. E. and EYFRIG, R. [1973] A method for predicting the F1-layer critical frequency based on the Zurich smoothed sunspot number. *Radio Sci.*, Vol. 8, (New Series), 837-839.

DUDENEY, J. R. [1978] An improved model of the variation of electron concentration with height in the ionosphere. *J. Atmos. Terr. Phys.*, Vol. 40, 195-203.

DUDENEY, J.R. and KRESSMAN, R.J. [1986] - Empirical models of the electron concentration of the ionosphere and their value for radio communication purposes. Radio Science, Vol. 21, pp. 319-330.

DYSON, P.L. and BENNETT, J.A. [1988] - A model of the vertical distribution of the electron concentration in the ionosphere and its application to oblique propagation studies, J. Atmos Terr Phys, Vol. 50, pp. 251-262.

ELKINS, T. J. [1973] An empirical model of the polar ionosphere. Air Force Surveys in Geophysics, No. 267, NTIS Accession No. AD766240. National Technical Information Service, Springfield, VA 22161, USA.

GIRALDEZ, A. E. [1979] Daytime sporadic-E blanketing frequency prediction. International Solar Terrestrial Predictions Workshop Proc., Vol. IV, Boulder, CO, US Govt. Printing Office, Washington, DC 20402.

HAGG, E. L. and ROLFE, W. [1963] A study of transatlantic radio propagation modes at 41.5 MC/s. *Can. J. Phys.*, **41**, 220-233.

HILL, J.R. [1979] - Exact ray path in a multisegment quasi-parabolic ionosphere. Radio Science, Vol. 14, No. 5.

KERBLAÏ, T. S. [1960] Relation between critical Es frequencies and characteristics of apparatus (in Russian). *Ion. Studies*, **5**, 50-63.

KERBLAÏ. T. S. [1964] Instruction on calculation of HF communications reflected from the Es-layer (in Russian). *Science*, Moscow, USSR.

KERBLAÏ, T. S. and KOVALEVSKAÏA, E. [1967] Calculation of MUF in the presence of a horizontally heterogeneous ionosphere (in Russian). *Geomag. i Aeronom.*, **7**, 123-127.

KERBLAÏ, T. S. and VOLOCHINOVA, E. [1964] Estimation of the tilts of the isosurfaces of NF2 on the basis of *Nh* profiles (in Russian). *Geomag. i Aeronom.*, **1**, 61.

KIFT, F. [1960] The propagation of high frequency radio waves to long distances. *Proc. IEE*, **107B**, 127-140.

KING, J. W. and SLATER, A. J. [1973] Errors in predicted values of foF2 and hmF2 compared with the observed day-to-day variability. *Telecommun. J.*, Vol. 40, 766-770.

KIYANOVSKY, M.P. [1972] - Metod rascheta kharakteristik KV trass dlya dvumernoi modeli ionosfery (Method of calculation of HF path characteristics for a two-dimensional ionospheric model). Issledovaniya po geomagnetizmu, aeronomii i fizike solntsa, Moscow, Nauka, No. 25.

KIYANOVSKY, M.P., PRUDKOVSKY, A.G., KOTOVICH, G.V., ZASORIN, A.Z., ZYRYANOVA, L.A., KRASINA, T.Yu. and SUKHODOLSKAYA, V.E. [1987] - Metod refraktsionnogo integrala dlya dvumernoneodnorodnoi ionosfery i ego primenenie k raschetam radiotrass (Refraction integral method for a two-dimensional non-homogeneous ionosphere and its use for radio path calculation). Tekhnika sredstv svyazi, series SS, No. 5.

KOURIS, S. S. [1981a] Solar and latitude dependence of E-region critical frequency. *Nuovo Cimento C*, Vol. 4, 417-430.

KOURIS, S. S. [1981b] On the prediction of the E-layer critical frequency. *Alta Frequenza*, Vol. 50, 5, 276-278.

KOVALEVSKAÏA, E. and KERBLAÏ, T. S. [1971] *Calculation of the Length of Hop, MUF and Angles of Arrival of Radio Waves, Taking Account of the Horizontal Irregularity of the Ionosphere* (in Russian). Nauka Publishing House. Moscow, USSR.

KOVALEVSKAÏA, E. and KORNITZKAÏA, A. A. [1969] Influence of the horizontal gradients of the parameters of electron density distribution on the MUF, hop distance and angles of arrival. *Geomag. i Aeronom.*, 9, 232-235.

LABAHN, R.W. [1985] - Ray-tracing in a two-dimensional ionosphere. Radio Science, Vol. 20, pp. 972-976.

LEFTIN, M. [1976] Numerical representation of monthly median critical frequencies of the regular E-region (foE). Office of Telecommunication Rpt. 76-88, Supt. of Documents, US Govt. Printing Office, Washington, DC 20402.

LINCOLN, J.V. and CONKRIGHT, R.O. [1981] - International reference ionosphere - IRI 79, World Data Center A for Solar-Terrestrial Physics, Report UAG-82, NOAA, Boulder, CO 80303, United States.

LIU, R. Y., SMITH, P. A. and KING, J. W. [1983] A new solar index which leads to improved foF2 predictions using the CCIR Atlas. *Telecomm. J.*, Vol. 50, VIII, 408-414.

MCNAMARA, L.F. [1988] - Ionospheric modelling in support of single station location of long range transmitters, J. Atmos Terr Phys, Vol 50, pp. 781-795.

MEWES, E. R. and MÖLLER, H. G. [1974] Der Einfluss der sporadischen E-Schicht auf eine transäquatoriale Kurzwellen-Übertragung (The influence of sporadic E on transequatorial HF propagation). *Kleinheubacher Berichte*, 17, 443-447.

MILLMAN, G.H. and SWANSON, R.W. [1985] - Comparison of HF oblique transmissions with ionospheric predictions. Radio Science, Vol. 20, pp. 315-318

MÖLLER, H. G. [1960] Ergebnisse de Impulsübertragung mit veränderlicher Frequenz auf der Strecke Sodankylä-Lindau (Results of variable frequency pulse transmissions over the path Sodankylä-Lindau). *Kleinheubacher Berichte*, 7, 115-123.

NOSOVA, G. N. [1973] Character of fading of signals reflected and scattered from the sporadic-E layer (in Russian). Collection of articles; *Questions concerning short wave propagation*, IZMIRAN, USSR.

NOVYSH-BYLINSKAYA, V. N. [1966] Tsiklicheskie krivye kriticheskikh chastot sloya F2 ionesfery kak osnova dlya prognozirovaniya foF2 na lyubuyu fazu solnechnogo tsikla (Sunspot cycle curves of critical frequencies of the ionospheric F2 layer as a basis for foF2 prediction at any stage of the sunspot cycle). *Geomag. i Aeronom.*, Vol. 6, 2, 392.

PAUL, A.K. [1986] - Limitations and possible improvements of ionospheric models for radio propagation: Effects of sporadic E layers. Radio Science, Vol. 21, pp. 304-308.

PIGGOTT, W. R. and RAWER, K. [1972] URSI Handbook of Ionogram Interpretation and Reduction. World Data Center A for Solar-Terrestrial Physics, Report UAG-23, NOAA, Boulder, CO 80303, USA.

PIGGOTT, W. R. and RAWER, K. [1978] URSI Handbook on Ionogram Interpretation and Reduction (2nd Edition). Revision of Chapters 1-4. World Data Center A for Solar-Terrestrial Physics, Report UAG-23A, NOAA, Boulder, CO 80303, USA.

PIKE, C. P. (Ed.) [1975] Defense meteorological satellite program auroral ionospheric interpretation guide. Air Force Surveys in Geophysics, No. 306, NTIS Accession No. AD-A013165. National Technical Information Service, Springfield, VA 22161, USA.

POTAPOVA, N. I. [1971] Prediction of geometrical parameters for $N(h)$-profiles and $h'f$-characteristics of the quiet and disturbed ionosphere. II. Day-to-day variations of $N(h)$ and $h'f$ parameters. Published in the collection *Ionospheric disturbances and their influence on radiocommunications* (in Russian). Nauka Publishing House, 117, Moscow, USSR.

RAO, N. N. and BECKWITH, R. I. [1974] Prediction of azimuthal angle of arrival of HF waves during the sunrise period. *Radio Sci.*, Vol. 9, 617-620.

RAO, C. S. R. and SAIN, M. [1965] Prediction of critical frequency of F2-layer. *J. Inst. Telecomm. Engrs.* (India), Vol. 2, 8, 271-281.

RAWER, K. and BRADLEY, P.A. [1987] - International reference ionosphere - status 1986/87, Advances in Space Research, Vol. 7, 6, pp. 1-127.

ROSICH, R. K. and JONES, W. B. [1973] The numerical representation of the critical frequency of the F1 region of the ionosphere. Office of Telecommunciations, Report 73-22, US Dept. of Commerce.

RUSH, C.M. [1986] - Ionospheric radio propagation models and predictions - a mini-review. IEEE, Trans. on Ant. and Prop., Vol. AP-34, pp. 1163-1170.

RUSH, C. M., POKEMPNER, M., ANDERSON, D. N., PERRY, J., STEWART, F. G. and REASONER, R. [1984] Maps of foF2 derived from observations and theoretical data. *Radio Sci.*, Vol. 19, 1083-1097.

RUSH, C. M., POKEMPNER, M., ANDERSON, D. N., STEWART, F. G. and PERRY, J. [1983] Improving ionospheric maps using theoretically derived values of foF2. *Radio Sci.*, Vol. 18, 95-107.

SCHEPKIN, L. A. and VINNITSKI, A. V. [1981] O vyvedenii parametra foF1 iz ionogramm (The determination of foF1 from ionograms). *Geomag. i Aeronom.*, Vol. 21, 2, 359.

SHAPIERO, B. S. [1960] To the question of working out the predictions of geometrical parameters (hm and ym) and $h'f$ characteristics of the ionosphere (in Russian). Documents of the IZMIRAN, published by the Academy of Sciences, 17/7, 216-239, USSR.

SHAPIERO, B. S. [1970] Inter-relation of the parameters of the F2 and F1 regions and prediction of the daytime $N(h)$ profiles and $h'f$ characteristics. (In Russian) *Geomag. i Aeronom.*, 2, 344-346.

SHAPIERO, B. S., ANUFRIEVA, T. A., FREISON, A. A. and VINNIKOVA, T. A. [1971a] Prediction of geometrical parameters for $N(h)$ profiles and $h'f$ characteristics of the quiet and disturbed ionosphere. I. Regular variations of $N(h)$ and $h'f$ geometrical parameters. Published in the collection *Ionospheric disturbances and their influence on radiocommunications* (in Russian), Nauka Publishing House, 100, Moscow, USSR.

SHAPIERO, B. S., POTAPOVA, N. I., ANUFRIEVA, T. A., FREISON, A. A. and SHASHOUNKINA, V. M. [1971b] Prediction of $N(h)$ profiles and $h'f$ charcteristics of quiet and disturbed F-region. IV. Variations of the angles of arrival (A) and the hop distance (D). Published in the collection *Ionospheric disturbances and their influence on radiocommunications* (in Russian). Nauka Publishing House, 146, Moscow, USSR.

SHAPIERO, B. S. and SHASHOUNKINA, V. M. [1971] Prediction of $N(h)$ profiles and $h'f$ characteristics of the quiet and disturbed F-region. III. $N(h)$ and $h'f$ parameters during disturbances. Published in the collection *Ionospheric disturbances and their influence on radiocommunications* (in Russian). Nauka Publishing House, 135, Moscow, USSR.

SMITH, P. A. and KING, J. M. [1981] Long-term relationships between sunspots. Solar faculae and the ionosphere. *J. Atmos. Terr. Phys.*, Vol. 43, 10, 1057-1063.

SUN, X. [1987] - A method of predicting the ionospheric F2 layer in the Asia-Oceania region (in Chinese), Journal of China Institute of Communications, Vol. 8, No. 6, pp. 37-45.

TEDD, B.L., STRANGEWAYS, H.J. and JONES, T.B. [1985] - Systematic ionospheric electron density tilts (SITs) at mid-latitudes and their associated HG bearing errors. J. Atmos. Terr. Physics, Vol. 47, pp. 1085-1097.

WILLIAMS, H. P. [1962] Increase in MUF due to horizontal gradients. *Nature*, Vol. 196, 4851, 256-258.

CCIR Documents

[1978-82]: 6/64 (USSR).

[1986-90]: 6/48 (Canada).

BIBLIOGRAPHY

CHAMAN LAL [1966] The development of a formula for the seasonal and secular characteristics of F2-layer critical frequency (ΣfoF2). *Telecomm. J.*, Vol. 33, 257-262.

MESTERMAN, I., TRENTINI, F. and FENANDEZ SARMIENTO, N. [1972] Planificación de redes antárticas para telecomunicaciones en ondas decamétricas (Planning of Antarctic HF Telecommunication nets). LIARA-C18. (Also available in English). Laboratorio Ionosférico de la Armada, Argentina.

REPORT 1012-1

OPERATIONAL MODELLING OF HF RADIO PROPAGATION CONDITIONS AT HIGH LATITUDES

(Question 27/6)

(1986-1990)

1. Introduction

HF communication at high latitudes is a difficult area of study and practical application. The current state of knowledge of the high latitude ionosphere allows long-term predictions for HF communications and approximate real-time specifications of the high latitude ionosphere. The ability to provide short-term forecasts of HF communications relies on the ability to project the observed morphology forward in time. The special properties of the high latitude ionosphere affecting radio communications have been summarized in Report 886. Other reviews of the high latitude ionosphere and predictions of its properties have been published in the Solar-Terrestrial Predictions Proceedings [Donnelly, 1979, 1980] (see, for example Besprozvannaya et al. [1979], Hunsucker [1979a,b] and Vondrak [1979]), in a special issue of Radio Science [Hunsucker and Greenwald, 1983], by Tsunoda [1988] and by Belrose [1988].

2. Models of the high latitude ionosphere

The ability to predict the propagation of HF radio waves at high latitudes requires a model of the spatial and temporal distribution of electron density in the high latitude ionosphere. Because of the very definite spatial structure in the auroral and polar cap regions of the high latitude ionosphere, the specific propagation predictions may be very sensitive to the positioning and dynamic changes of the structures.

Among the high latitude ionospheric features that should be modelled for HF predictions are the following [Hunsucker, 1979b]:

(a) location and extent of the auroral oval as a function of magnetic activity;

(b) E- and F-region parameters in the auroral oval, mid-latitude trough, day-time cusp, and polar cap;

(c) profile of N_e versus height between E and F2 regions (also important for prediction of ducted propagation);

(d) auroral absorption, polar cap absorption (D-region effects);

(e) E- and F-region irregularities that cause diffuse multipath, rapid flutter fading, and off-great-circle propagation;

and also [Buchau et al., 1985]:

(f) location and extent of "patches" and sun-aligned arcs, within the polar cap, which give rise to scintillation.

For HF propagation prediction purposes, the shape of the profile and the steep gradients of the high latitude ionosphere must be represented in three dimensions. Predictions of MUF/LUF using triangulation, mode-definition and location of reflection points, may be of limited usefulness because strong horizontal gradients cause large changes in mode geometry and absorption estimates.

The present HF propagation prediction capability at high latitudes is statistical, using averaged synoptic data that ignore small scale (< 100 km) structure and transient phenomena (< 3 h). Important features such as auroral arcs and substorms are completely neglected. Some models do contain auroral E, auroral Es, auroral absorption, and F1 and F2 regions. The models incorporated into HF propagation prediction computer programs have, for the most part, not been verified with oblique path measured data.

2.1 *Available models for predictions*

The availability of high latitude ionospheric models for HF prediction purposes has been reviewed by Hunsucker [1979b]. The characteristics and process of high latitude F-region large scale (>10 km) and small scale (<10 km) irregularities have been reviewed by Tsunoda [1987] and a descriptive model has been derived. Several models are available which include features (a) to (f) above. Data accumulated with ground-based and airborne ionosondes have been used to develop a model of the structure of the high latitude ionosphere [Elkins and Rush, 1973]. This model has been further modified using incoherent-scatter radar (ISR) data [Vondrak *et al.* 1977]. The new model retains the foF2 and hmF2 values in the earlier polar model [Elkins and Rush, 1973], and incorporates an auroral E layer (essentially equivalent to blanketing Es) and a valley in the electron density profile determined from ISR data, as well as an absorption model that varies with magnetic activity.

The USSR has developed statistical models of the structure of the high latitude ionosphere [Kovalevskaya and Zhulina, 1979; Avdiushin *et al.*, 1979]. Differences have been noted between USSR and US predictions in the case of auroral absorption and foF2 in the mid-latitude trough during solar maximum. During magnetic disturbances, the USSR has identified three distinct regions of auroral absorption whereas the absorption model given by Vondrak *et al.* [1977] displays two time/latitude regions of enhanced absorption. Models also differ in describing the gradients of foF2 in the trough region at solar maximum [Miller and Gibbs, 1975].

Foppiano and Bradley [1983] have developed a method of predicting auroral absorption intensities and this is used in the CCIR method of HF field strength estimates (see supplement to Report 252). The day-to-day statistical distribution of absorption is found to be log-normal, and the probability of a given level being exceeded can be specified if one knows two parameters, the median absorption, A_m, and the probability of 1 dB being exceeded, Q_1. Foppiano and Bradley [1984] examined statistical variations of absorption data measured with a riometer on different days at a given hour. A new approximate expression was established between A_m and Q_1, and the family of amplitude distribution curves consistent with this relationship were presented. Results using this relationship and those found in earlier investigations were compared. Foppiano and Bradley [1985] have also incorporated geographical, diurnal, seasonal and solar cycle variations. Hargreaves et al. [1985] suggest that changing solar cycle activity be accounted for in the model by use of magnetic activity index (such as Ap) rather than sunspot number in view of the fact that auroral precipitation depends on solar wind rather than on sunspots directly. A method for auroral absorption intensity prediction has been developed by Zhulina *et al.* [1983]. This too, is based on an empirical model for the probability distribution of auroral absorption intensity that has been derived from observations of cosmic radio noise absorption by riometers, which for this study were located in the Euro-Asian sector of the Northern Hemisphere. In this method the space-time variations of auroral absorption are represented in the form of maps and tables [CCIR, 1982-1986a, b]. An analytical approximation of these variations in auroral absorption is given in [CCIR, 1982-1986c].

A model including a coarse F-region $N(h)$ classification of the various structural regions (trough, oval, etc.) and rather qualitative information on D and E regions effects on HF propagation has been used [Rush *et al.*, 1982] to modify monthly median ionospheric models, for specification of HF propagation conditions, and for prediction purposes.

The use of theoretical models can further the understanding of the chain of events linking activity on the Sun to modifications of the high latitude ionosphere and its effects on HF communications. Overall schemes specifying and forecasting the solar wind, the magnetosphere, the thermosphere, the geomagnetic field, and the high latitude ionosphere have been developed [Akasofu, 1981, 1982, 1983; Hakamada and Akasofu, 1982; Fuller-Rowell et al., 1987]. Theoretical models [Watkins, 1978; Sojka *et al.*, 1982] of the high latitude ionosphere alone are able to reproduce successfully many of the observed features such as the "main trough", "ionization hole," the "tongue of ionization," the "aurorally produced ionization peaks," and the "UT effects".

The descriptive model of F-region irregularities derived by Tsunoda [1987] appears to unify most of the diverse and independent high latitude observations.

2.2 *Real-time specification*

To optimize system performance, HF communication systems and HF radars require real-time specification of the main auroral/polar ionospheric features such as arcs, the mid-latitude trough, and the polar cusp. High inclination polar orbit satellites can examine the polar and auroral regions in real-time at several optical wavelengths. Ray tracing in near real-time would allow the prediction of HF propagation characteristics such as mode availability, dispersion, multimode and non-great-circle propagation.

2.3 *Short-term forecasting*

To improve existing forecasting programmes, spacecraft measurements of solar wind parameters (such as velocity, density and the interplanetary magnetic field) could be used to predict auroral oval characteristics, total magnetospheric energy input, and current system morphology [Vondrak, 1979]. High altitude satellites providing real-time global pictures of the ionospheric response to the entry of particles from the magnetosphere, could greatly aid the forecasting of detailed changes in structure, size and location of enhanced electron density regions in the ionosphere. Additional data on the high latitude ionosphere (auroral oval, cusp and polar cap) in the range of approximately 69° to 81° invariant magnetic latitude are being obtained by incoherent scatter radar [Kelly, 1983]. Within the polar cap itself, a ground-based digital sounder is supplying continuous measurements of the bottomside F layer, [Buchau et al., 1987].

REFERENCES

AKASOFU, S.-I. [1981] Energy coupling between the solar wind and the magnetosphere. *Space Sci. Rev.*, Vol. 28, 121.

AKASOFU, S.-I. [1982] Prediction of development of geomagnetic storms by using the solar wind-magnetosphere energy coupling function, ε. *Planet. and Space Sci.*, Vo. 29, 1151.

AKASOFU, S.-I. [1983] Energy flow and dynamical coupling in the solar wind-magnetosphere-ionosphere system. *Radio Sci.*, Vol. 18, 971-980.

AVD IUSHIN, S. I., DANILOV, A. D., MALISHEV, A. B., NOVIKOVA, G. N. and SVIDSKY, P. M. [1979] Forecasting ionospheric and geomagnetic conditions in the forecasting center of IAG. *STPP**, Vol. I, 104.

BELROSE, J.S. [1988] - HF Communications and remote sensing in the high latitude region. AGARD LS No. 162, Media effects on electronic systems in the high latitude regions. ISBN 92-835-0478-X, pp. 5-1 to 5-42.

* The abbreviation STPP refers to the Solar-Terrestrial Predictions Proceedings, published in four volumes by the National Oceanic and Atmospheric Administration, US Department of Commerce, and edited by R. F. Donnelly (see [Donnelly, 1979 and 1980]).

BESPROZVANNAYA, A. S., SHIROCHOV, A. V. and SHCHUKA, T. I. [1979] On the approach to forecasting polar ionospheric conditions. *STPP*, Vol. II, 528.

BUCHAU, J., REINISCH, B.W., ANDERSON, D.N., WEBER, E.J., and DOZOIS, C. [1987] - Polar cap plasma convection measurements and their relevance to the real-time modelling of the high latitude ionosphere, proceedings of the ionospheric effects symposium, the effects of the ionosphere on communications, navigation, and surveillance systems. Eds. J.M. Goodman, J.A. Klobuchar, H. Soicher, G. Joiner, US Government Printing Office, Washington D.C., 20402.

BUCHAU, J., WEBER, E.J., ANDERSON, D.N., CARLSON, Jr., H.C., MOORE, J.G., REINISCH, B.W. and LIVINGSTON, R.C. [1985] - Ionospheric Structures in the polar cap: Their origin and relation to 250-MHz Scintillation. Radio Science, Vol. 20, No. 3, 325-338.

DONNELLY, R. F. Ed. Solar-Terrestrial Predictions Proceedings:

Vol. I [1979] Prediction Group Reports. US Dept. of Commerce, US Govt. Printing Office, No. 003-023-00041-9, Washington, DC 20402.

Vol. II [1979] Working Group Reports and Reviews. US Dept. of Commerce, US Govt. Printing Office, No. 003-017-00471-6, Washington, DC 20402.

Vol. III [1980] Solar Activity Predictions. US Dept. of Commerce, US Govt. Printing Office, No. 003-017-00473-2, Washington, DC 20402.

Vol. IV [1980] Predictions of Terrestrial Effects of Solar Activity. US Dept. of Commerce, US Govt. Printing Office, No. 003-017-00479-1, Washington, DC 20402.

ELKINS, T. and RUSH, C. [1973] A statistical predictive model of the polar ionosphere. *An Empirical Model of the Polar Ionosphere*. Ed. T. Elkins. AFCRL-TR-73-0331. Air Force Cambridge Research Laboratories, Hanscom AFB, MA 01731, USA.

FOPPIANO, A. J. and BRADLEY, P. A. [October, 1983] Prediction of auroral absorption of high-frequency waves at oblique incidence. *Telecomm. J.*, Vol. 50, X, 547-560.

FOPPIANO, A. J. and BRADLEY, P. A. [1984] Day-to-day variability of riometer absorption. *J. Atmos. Terr. Phys.*, Vol. 46, 689-696.

FOPPIANO, A. J. and BRADLEY, P. A. [1985] Morphology of background auroral absorption. *J. Atmos. Terr. Phys.*, Vol. 47, 663-674.

FULLER-ROWELL, T.J., REES, D., QUEGAN, S., BAILEY, G.J. and MOFFETT, R.J. [1987] - Interactions between neutral thermospheric composition and the polar ionosphere using a coupled ionosphere-thermosphere model, J. Geophys. Res., 92, A7, 7744-7748.

HAKAMADA, K. and AKASOFU, S.-I. [1982] Simulation of three dimensional solar wind disturbances and resulting geomagnetic storms. *Space Sci. Rev.*, Vol. 31, 3.

HARGREAVES, J.K., REENEY, M.T. and BURNES, C.J. [1985] - Statistics of auroral radio absorption in relation to prediction models. AGARD-CP-321, 7.3-1 to 7.3-10.

HUNSUCKER, R. D. [1979a] Morphology and phenomenology of the high latitude E and F regions. *STPP*, Vol. II, 543.

HUNSUCKER, R. D. [1979b] High latitude E and F region ionosphere predictions. *STPP*, Vol. II, 513.

HUNSUCKER, R. D. and GREENWALD, R. A. (Guest Eds.) [1983] Including special papers: radio probing of the high-latitude ionosphere and atmosphere: new techniques and new results. *Radio Sci.*, Vol. 18, 6.

KELLY, J. D. [1983] Sondrestrom radar – initial results. *Geophys. Res. Lett.*, Vol. 10, 1112-1115.

KOVALEVSKAYA, E. M. and ZHULINA, E. M. [1979] The statistical properties of the disturbed high latitude ionosphere in radio wave propagation computations. *STPP*, Vol. III, D2-16.

MILLER, D. C. and GIBBS, J. [1975] Ionospheric analysis and modeling. Scientific Report 2, AFCRL-TR-75-0549. Air Force Cambridge Research Laboratories, Hanscom AFB, MA 01731, USA.

RUSH, C. M., ROSICH, R. K., BROOKS, C. B., LEISE, D. L. and POKEMPNER, M. [1982] A simplified model of the high latitude ionosphere for telecommunications purposes. NTIA Report 82-94. US Dept. of Commerce, US Govt. Printing Office, Washington, DC 20402.

SOJKA, J. J., SCHUNK, R. W. and RAITT, W. J. [1982] Seasonal variations of the high latitude F region for strong convection. *J. Geophys. Res.*, Vol. 87, 187.

TSUNODA, R.T. [1988] - High-latitude F-region irregularities: A review and synthesis. Reviews of Geophysics, 26, 719-760.

VONDRAK, R. R. [1979] Ionospheric predictions, magnetosphere-ionosphere interactions. *STPP*, Vol. II, 476.

VONDRAK, R., SMITH, G., HATFIELD, V., TSUNODA, R., FRANK, V. and PERREAULT, P. [1977] Chatanika model of the high-latitude ionosphere for application to HF propagation prediction. RADC-TR-78-7. Rome Air Development Center, Hanscom AFB, MA 01731, USA.

WATKINS, B. [1978] A numerical computer investigation of the polar F region ionosphere. *Planet. and Space Sci.*, Vol. 26, 559.

ZHULINA, E. M., KISHCHA, P. V., LUKASHKIN, V. M. and SHIROCHKOV, A. V. [1983] Additional energy losses on high-latitude radio links (in Russian), 208, Nauka Publishing House, Moscow, USSR.

CCIR Documents

[1982-1986]: **a.** 6/48 (USSR); **b.** 6/49 (USSR); **c.** 6/194 (USSR).

REPORT 894-2

CCIR HF PROPAGATION PREDICTION METHOD

Third CCIR computer-based method for estimation of MUF, sky-wave field strength, signal-to-noise ratio, LUF and basic circuit reliability

(Study Programme 30A/6)

(1982-1986-1990)

TABLE OF CONTENTS

1. Introduction

2. Path geometry

3. Basic and operational maximum usable frequencies

3.1 Basic MUF

3.2 Prediction of foE

3.3 E-layer basic MUF prediction

3.4 E-layer screening frequency (fs)

3.5 F2-layer data

3.6 F2-layer basic MUF prediction

3.6.1 For paths up to 4,000 km

3.6.2 For paths longer than 4,000 km

3.7 The operational MUF

4. Elevation angle

5. The prediction of the median sky-wave field strength

5.1 Method for path lengths of 0 to 7,000 km

5.2 Method for path lengths greater than 9,000 km

5.3 Method for path lengths between 7,000 and 9,000 km

6. Median available receiver power

7. Monthly median signal-to-noise ratio

8. Signal-to-noise ratios for other percentages of time

9. Lowest usable frequency (LUF)

10. Basic circuit reliability (BCR)

* * *

1. Introduction

This HF propagation prediction method derives from a method developed by CCIR Interim Working Party 6/12 for the World Administrative Radio Conference for the Planning of HF Bands Allocated to the Broadcasting Service (WARC HFBC) after reviewing some 20 field-strength prediction methods in use by different organizations.

This prediction method is a combination of a simplified Report 252 method (for path lengths of 0 to 7000 km) and the FTZ method developed in the Federal Republic of Germany (for path lengths greater than 9,000 km), with interpolation from the values obtained by the above two methods for path lengths between 7,000 and 9,000 km. The MUF prediction method used is essentially that contained in Report 340.

This composite method does not take into consideration all aspects of propagation effects, but it is simple and quick for computation, and may be convenient for operational use of the different HF services.

A computer program in both mainframe and microcomputer versions has been developed for this prediction method. Information on the availability of the program is found in Resolution 63.

2. Path geometry

Propagation is assumed to be along the great-circle path between the transmitter and receiver locations. For the lowest order F-mode the path of length D is divided into the minimum number, n, of equal hops of length d_ℓ so that d_ℓ is less than or equal to 4,000 km and $nd_\ell = D$. This hop length, d_ℓ, is used in Table I to define some of the control points at which various parameters for all F-modes are determined.

Table I Locations of control points for the determination of basic MUF, E-layer screening, reflection heights and ionospheric absorption

(i) Basic MUF

Path length D (km)	E-modes	F-modes
0 - 2000	M	M
2000 - 4000	T + 1000, R - 1000	$T + \frac{d\ell}{2}$, M, $R - \frac{d\ell}{2}$
> 4000	-	

(ii) E-layer screening

Path length D (km)	F-modes
0 - 2000	M
2000 - 9000	T + 1000, R - 1000

(iii) Reflection heights

Path length D (km)	F-modes
0 - 4000	M
4000 - 9000	$T + \frac{d\ell}{2}$, M, $R - \frac{d\ell}{2}$

(iv) Ionospheric absorption

Path length D (km)	E-modes	F-modes
0 - 2000	M	M
2000 - 4000	T + 1000, M, R - 1000	T + 1000, M, R - 1000
4000 - 9000	-	T + 1000, $T + \frac{d\ell}{2}$, M, $R - \frac{d\ell}{2}$, R - 1000

Key: M = path midpoint
T = transmitter location
R = receiver location
$d\ell$ = hop length of lowest order mode (km)

Distances are quoted in km

3. Basic and operational maximum usable frequencies

The estimation of operational MUF, the highest frequency that would permit acceptable operation of a radio service, is in two stages: first, the estimation of basic MUF from a consideration of ionospheric parameters; and second, the determination of a correction factor to allow for propagation mechanisms at frequencies above the basic MUF.

3.1 *Basic MUF*

For path lengths between 0 and 4000 km, the basic MUF of an E-mode is predicted. For all path lengths, the basic MUF for the F2-mode is predicted. Where appropriate the higher of the two values gives the basic MUF for the path.

3.2 *Prediction of foE*

For paths up to 2000 km, foE is evaluated at the path mid-point. For ranges greater than 2000 km, foE is evaluated at two control points, each 1000 km along the path from the transmitter and receiver respectively.

At these points the solar zenith angle χ, in degrees, is determined, then:

$$foE = 0.9 \left[(180 + 1.44\ R_{12}) \cos \chi'\right]^{0.25} \quad \text{MHz} \qquad (1)$$

where:

$\chi' = \chi$ for $0 \leqslant \chi \leqslant 80$;

$\chi' = 90 - \dfrac{e^{0.13(116 - \chi)}}{10.8}$ for $80 < \chi < 116$

and

$\chi' = 89.907$ for $\chi \geqslant 116$

R_{12} : 12 month running mean sunspot number.

No saturation for high values of R_{12} is assumed.

3.3 *E-layer basic MUF prediction*

The value of foE is determined at each of the control points in Table I(i) and the lower value is selected. The E mode basic MUF is given by:

$$E(d)\ MUF = foE.\ \sec i_{110} \qquad (2)$$

where i_{110} is the angle of incidence at a mid-hop reflection height of 110 km for a hop of length d.

The E-layer basic MUF for the path is the value of E(d) MUF for the minimum number of hops.

3.4 *E-layer screening frequency (f_s)*

The foE value at the middle point of the path (for paths up to 2000 km), or the higher one of the foE values at the two control points 1000 km from each end of the path (for paths longer than 2000 km), is taken for calculation of E-layer screening frequency.

$$f_s = 1.05\ foE \sec \varphi_s \qquad (3)$$

in which:

$$\varphi_s = \arcsin \left[\frac{R \cos \Delta_F}{R + 110}\right]$$

R: radius of the Earth, 6371 km,

Δ_F: elevation angle for the F2-layer mode (see § 4).

3.5 *F2-layer data*

Numerical maps of the parameters foF2 and M(3000)F2, for solar index values R_{12} = 0 and 100, and for each month are presented in Report 340. This prediction method uses the Oslo coefficients to determine the values of foF2 and M(3000)F2 for the required locations and times. At the control points given in Table I(i) the above values are determined for the solar index values R_{12} = 0 and R_{12} = 100. Linear interpolation or extrapolation is applied for the required index values between R_{12} = 0 and 150. For higher sunspot activity R_{12} is set equal to 150 in the case of foF2 only.

3.6 *F2-layer basic MUF prediction*

3.6.1 *For paths up to 4000 km*

F2-layer basic MUF is calculated from:

$$\text{F2(ZERO)MUF} = \text{foF2} + f_H/2$$

$$\text{F2(4000)MUF} = 1.1\ \text{foF2} \cdot \text{M(3000)F2}$$

where f_H is the electron gyro-frequency as given in Report 340.

Interpolation for the length of the path is applied using the relationship:

$$\text{F2(d)MUF} = \text{F2(ZERO)MUF} + [\text{F2(4000)MUF} - \text{F2(ZERO)MUF}] \times \text{M(d)} \qquad (4)$$

where:

$M(d) = 1.64 \times 10^{-7} d^2$ for $0 \leq d < 800$ and:

$M(d) = 1.26 \times 10^{-14} d^4 - 1.3 \times 10^{-10} d^3 + 4.1 \times 10^{-7} d^2 - 1.2 \times 10^{-4} d$ for $800 \leq d \leq 4000$

where d is in km.

For multihop modes d is the hop length.

This gives the median F2-mode basic MUF.

The F2-layer basic MUF for the path is the value of F2(d) MUF for the minimum number of hops.

3.6.2 *For paths longer than 4000 km*

At the control points, given in Table I(i), values of F2(4000)MUF, interpolated for sunspot number, are determined and the lower is selected. This gives the median F2-layer basic MUF for the path. It is also the basic MUF for the lowest-order F2-mode. The basic MUF for higher-order F2 modes is determined in terms of this value using eqn (4) with appropriate d for the different modes assuming in each case equal hop lengths.

3.7 The path operational MUF

The path operational MUF is the greater of the operational MUF for F2-modes and the operational MUF for E-modes. For F2-modes the operational MUF=basic MUF x R_{op} where R_{op} is given in Table II of Part 3 of Report 340. For E-modes the operational MUF is equal to the basic MUF.

An estimate of the operational MUF exceeded for 10% and 90% of the days is determined by multiplying the median operational MUF by the factors 1.15 and 0.85 respectively in the case of F-modes and 1.05 and 0.95 respectively in the case of E-modes.

4. Elevation angle

Elevation angle is taken into account in the prediction of field strength. It is given, approximately, by:

$$\Delta = \arctan\left(\cot\frac{d}{2R} - \frac{R}{R+h'}\operatorname{cosec}\frac{d}{2R}\right) \qquad (5)$$

where:

d: hop length of an n hop mode given by $d = D/n$

h': 110 km for the E-layer or h' is as given in § 5.1 for the F2-layer.

Angles determined in this way apply for frequencies below, but near to, the basic MUF. However, these angles are assumed to apply for all frequencies, including those above the basic MUF.

5. The prediction of the median sky-wave field strength

The median relates to a sample of all days and not just those days that the transmitting frequency is below the operational MUF.

5.1 Method for path lengths of 0 to 7,000 km

This method is based primarily on the method given in Report 252, with revisions of some parameters based on the Supplement to Report 252 and on more recent information.

The range and elevation angle determine which propagation modes are considered. All modes considered must have an elevation exceeding 3° as given, in the case of E modes, by mirror reflection from a height of 110 km and, in the case of F2 modes, from a height given by:

$$h_p F2 = \left[\frac{1490}{M(3000)F2} - 176\right] \text{ km or 500 km, whichever is the smaller.}$$

For path lengths up to 4,000 km the lowest-order (least number of hops) E and F2 modes meeting this minimum elevation-angle criterion are found. For these modes basic MUF's are determined according to § 3 and the field strength for the mode is evaluated for the appropriate number of hops. The two next higher-order E and the five next higher-order F2 modes are also considered. For these modes basic MUF's are determined appropriate to the hop length. For all the modes considered ray-paths are established and F2 modes screened by the E layer discounted. Field strengths for each mode are evaluated as described below allowing for transmitting antenna gain, whether or not the wave frequency is below the basic MUF. The two strongest E modes and the three strongest F2 modes are identified (number of strongest modes N = 5).

For path lengths between 4,000 and 9,000 km the lowest-order F2 mode meeting the minimum elevation angle criterion and the five next higher-order F2 modes are considered. Modes screened by the E-layer are discounted. Field strengths are evaluated and the three strongest modes identified (N=3).

The mirror height h', a function of time, location and hop length, is used for the ray-path calculations for F2 modes of all orders.

$$h' = 358 - (11 - 100a)\left(18.8 - \frac{320}{x^5}\right) + ad\left(0.03 + \frac{14}{x^4}\right) \quad \text{km} \qquad (6)$$

or 500 km, whichever is the smaller

a = 0.04 or (1/M(3000)F2) − 0.24, whichever is the larger;

x = foF2/foE, or 2, whichever is the larger.

The h' values are determined at all control points and their mean value is used.

The median field strength for mode w is given by:

$$E_{tw} = 136.6 + P_t + G_t + 20 \log f - L_{bf} - L_i - L_c - L_m - L_g - L_h - L_z \quad \text{dB}(1\mu\text{V/m}) \qquad (7)$$

where:

f: transmitting frequency (MHz);

P_t: transmitter power (dB(1 kW));

G_t: transmitting antenna gain at the required azimuth and elevation angles relative to an isotropic antenna;

L_{bf}: basic free-space transmission loss (dB) given by:

$$L_{bf} = 32.45 + 20 \log f + 20 \log p'$$

p': virtual slant range (km)

$$p' = \left[2R \sum_n \frac{\sin \frac{d}{2R}}{\cos\left(\Delta + \frac{d}{2R}\right)}\right]$$

L_i : absorption loss (dB) given by:

$$L_i = \frac{677.2 \text{ n.sec } i_{100}}{(f+f_H)^{1.98} + 10.2} \bullet \frac{1}{K} \sum_{j=1}^{K} I_j$$

with $I_j = (1 + 0.0037R_{12}).(\cos 0.881\, \chi_j)^{1.3}$

where:

i_{100} = angle of incidence at 100 km
K = number of control points (from Table I(iv))
χ_j = solar-zenith angle at j'th control point
f_H = electron gyrofrequency at midpath for path lengths up to 4000 km and for longer path lengths at the control point T+dℓ/2 or R-dℓ/2 (see Table I) where foF2 is lower.

By night I_j is assigned a minimum value of 0.1. For frequencies above the basic MUF, the absorption continues to vary with frequency and is calculated assuming the same ray-paths as those at the basic MUF.

L_c: correction term to the absorption loss for E modes, which do not penetrate the whole of the absorbing layer:

- for $f <$ E(d)MUF:
  $L_c = 1.359 + 8.617 \log_e (f/\text{E(d)MUF})$ dB
  if $L_c > 0$, $L_c = 0$ dB
  if $L_c < -9$, $L_c = -9$ dB
- For $f \geq$ E(d)MUF:
  $L_c = 0$ dB.
- For F modes:
  $L_c = 0$ dB.

L_m : 'above-the-MUF' loss. For frequency f above the basic MUF (f_b) of a given mode:

for F2 modes $L_m = 130 \left(\frac{f}{f_b} - 1\right)^2$ dB

L_m is limited to a value of 81 dB

for E modes $L_m = 81$ dB

L_g: summed ground reflection loss at intermediate reflection points.

For an n-hop mode $L_g = 2(n-1)$ dB

L_h: factor to allow for auroral and other signal losses and is obtained by subtracting 9 dB from the median values of Y_p given in Tables II and III of Report 252.

L_z: term containing those effects in sky-wave propagation not otherwise included in this method. The present recommended value is 2.8 dB (see Note (1)).

In the absence of information on receiving antenna gain, the resultant equivalent median sky-wave field strength is taken as the root sum squared field strengths for the N identified strongest modes, i.e.:

$$E_{ts} = 10 \log_{10} \sum_{w=1}^{N} \left[10^{E_{tw}/10}\right] \quad \text{dB}(1\ \mu\text{V/m}) \quad (8)$$

5.2 *Method for path lengths greater than 9000 km*

In this method predictions are made by dividing the path into the minimum number, n, of equal length hops, none of which exceeds 4000 km.

The resultant median field strength E_{tl} is given by:

$$E_{tl} = E_0 \left[1 - \frac{(f_M + f_H)^2}{(f_M + f_H)^2 + (f_L + f_H)^2} \left(\frac{(f_L + f_H)^2}{(f + f_H)^2} + \frac{(f + f_H)^2}{(f_M + f_H)^2}\right)\right] \quad (9)$$

$$-36.4 + P_t + G_{tl} + G_{ap} - L_y \quad \text{dB}(1\ \mu\text{V/m})$$

E_0 is the free-space field strength for 3 MW e.i.r.p. In this case:

$E_0 = 139.6 - 20 \log p'$, and the height used in the determination of p' is 300 km.

G_{tl}: largest value of transmitting antenna gain at the required azimuth in the elevation range 0-8°.

G_{ap}: the increase in field strength due to focusing at long distances given as

$G_{ap} = 10 \log (D/(R|\sin D/R|))$, dB

As G_{ap} from the above formula tends to infinity when D is a multiple of πR it is limited to the value of 15 dB.

L_y: term similar in concept to L_z. The present recommended value is -4.2 dB (see Note (1)).

Note 1 - It should be noted that the values of L_y and L_z are dependent on the elements of the prediction method, so that any changes in those elements should be accompanied by revision of the L_y and L_z values.

f_H: mean electron gyro-frequency at the control points given in Table I(i)

f_M: upper reference frequency. It is determined separately for the first and last hops of the path and the lower value is taken.

$$f_M = K \cdot f_g \qquad \text{MHz}$$

$$K = 1.2 + W\frac{f_g}{f_{g,\,noon}} + X\left(\sqrt[3]{\frac{f_{g,\,noon}}{f_g}} - 1\right) + Y\left(\frac{f_{g,\,min}}{f_{g,\,noon}}\right)^2$$

f_g: F2(4000) MUF for the first and last hops as appropriate.

$f_{g,\,noon}$: value of f_g for a time corresponding to local noon;

$f_{g,\,min}$: lowest value of f_g which occurs during the 24 hours.

W, X and Y are given in Table II. The azimuth of the great-circle path is determined at the centre of the whole path and this angle is used for linear interpolation in angle between the East-West and North-South values.

TABLE II – *Values W, X, Y used for the determination of the correction factor K*

	W	X	Y
East-West	0.1	1.2	0.6
North-South	0.2	0.2	0.4

f_L: lower reference frequency when the path is in daylight.

$$f_L = \left(5.3 \times I\left[\frac{(1 + 0.009\,R_{12}) \sum_{2n} \cos^{1/2}\chi}{\cos i_{90} \log_e\left(\frac{9.5 \times 10^6}{p'}\right)}\right]^{1/2} - f_H\right) \cdot A_W \qquad \text{MHz}$$

where R_{12} does not saturate for high values.

In the summation, χ is determined for each traverse of the ray path through the height of 90 km.

When $\chi > 90°$, $\cos^{1/2}\chi$ is taken as zero.

i_{90}: angle of incidence at a height of 90 km.

I is given in Table III.

A_w: winter-anomaly factor determined at the path mid-point which is unity for geographic latitudes 0 to 30° and at 90° and reaches the maximum values given in Table IV at 60°. The values at intermediate latitudes are found by linear interpolation.

As the path progressively becomes dark, the values of f_L are calculated until the time t_n when $f_L \leqslant 2f_{LN}$ where $f_{LN} = \sqrt{\frac{D}{3000}}$ (MHz). During the subsequent three hours f_L is calculated from $f_L = 2\,f_{LN}e^{-0.23t}$ where t is the time in hours after t_n. For the remainder of the night hours $f_L = f_{LN}$ until the time when the daylight equation gives a higher value.

TABLE III – *Values of I used in the equation for f_L*

Latitudes		Month											
One Terminal	Other Terminal	J	F	M	A	M	J	J	A	S	O	N	D
> 35°N	> 35°N	1.1	1.05	1	1	1	1	1	1	1	1	1.05	1.1
> 35°N	35°N - 35°S	1.05	1.02	1	1	1	1	1	1	1	1	1.02	1.05
> 35°N	> 35°S	1.05	1.02	1	1	1.02	1.05	1.05	1.02	1	1	1.02	1.05
35°N - 35°S	35°N - 35°S	1	1	1	1	1	1	1	1	1	1	1	1
35°N - 35°S	> 35°S	1	1	1	1	1.02	1.05	1.05	1.02	1	1	1	1
> 35°S	> 35°S	1	1	1	1	1.05	1.1	1.1	1.05	1	1	1	1

TABLE IV – *Values of the winter-anomaly factor, A_W, at 60° geographic latitude used in the equation for f_L*

Hemisphere	Month											
	J	F	M	A	M	J	J	A	S	O	N	D
Northern	1.30	1.15	1.03	1	1	1	1	1	1	1.03	1.15	1.30
Southern	1	1	1	1.03	1.15	1.30	1.30	1.15	1.03	1	1	1

5.3 Method for path lengths between 7,000 and 9,000 km

In this range of distance, in the absence of information on receiving antenna gain, the field strengths E_{ts} and $E_{t\ell}$ for short paths (§ 5.1) ——— and long paths (§ 5.2) ——— respectively are determined and the resultant E_{ti} is given by interpolation as follows:

$$E_{ti} = 100 \log_{10} X_i \quad \text{dB}(1\ \mu\text{V/m}) \quad (10)$$

with $$X_i = X_s + \frac{D - 7{,}000}{2{,}000} (X_\ell - X_s)$$

where $$X_s = 10^{0.01\, E_{ts}}$$

and $$X_\ell = 10^{0.01\, E_{t\ell}}$$

6. Median available receiver power

For an incident wave of r.m.s sky-wave field strength E_{tw} (dB(1 μV/m)) at frequency f(MHz) the corresponding available signal power P_{rw} (dBW) from a lossless receiving antenna of gain G_{rw} (dB relative to an isotropic radiator) in the direction of signal incidence is:

$$P_{rw} = E_{tw} + G_{rw} - 20 \log_{10} f - 107.2 \quad \text{dBW} \quad (11)$$

The resultant median available signal power P_r (dBW) is given by summing the powers arising from the different modes, each mode contribution depending on the receiving antenna gain in the direction of incidence of that mode. For N modes contributing to the summation:

$$P_r = 10 \log_{10} \sum_{w=1}^{N} 10^{Prw/10} \quad \text{dBW} \qquad (12)$$

Values of G_{rw} for the range of receiving antennas in common use are not currently available.

7. Monthly median signal-to-noise ratio

Report 322 provides values of median atmospheric noise power for reception on a short vertical lossless monopole antenna above perfect ground and Report 258 gives corresponding man-made noise and cosmic noise intensities. Let the resultant external noise factor be F_a (dB(KTb)) at frequency f(MHz) where reception is on such an ideal short lossless vertical monopole over a perfectly conducting ground plane with k the Boltzmann constant and T a reference temperature of 288 K. Then, in general, when using some other practical reception antenna the resultant noise factor may differ from this value of F_a (see Report 322). However, in the absence of complete noise measurement data for different antennas, as a first approximation, it is appropriate to assume that the same F_a applies. Hence the monthly median signal-to-noise ratio SN(dB) achieved within a bandwidth b(Hz) is:

$$SN = P_r - F_a - 10 \log_{10} b + 204 \quad \text{dB} \qquad (13)$$

8. Signal-to-noise ratios for other percentages of time

Use is made of equations (11) and (12) of § 6 of Report 266 to determine the signal-to-noise ratio for a specified percentage of time in terms of the within-an-hour and day-to-day decile deviations of the signals and the noise. Signal fading allowances are those adopted by the WARC HFBC (1987) with short-term upper decile deviation of 5 dB and lower decile deviation of 8 dB. For long-term signal fading the decile deviations are taken as a function of the ratio of operating frequency to the path basic MUF as given in Table III of Report 266.

In the case of atmospheric noise, the decile deviations of noise power arising from day-to-day variability are taken from Report 322. No allowance for within-an-hour variability is currently applied. For man-made noise, in the absence of direct information on temporal variability, the decile deviations are taken as those given in Report 258 which strictly relate to a combination of temporal and spatial variability. The combined within-an-hour and day-to-day decile variability of galactic noise is taken as ± 2 dB.

9. Lowest usable frequency (LUF)

The LUF is defined in Recommendation 373. Consistent with this definition, this is evaluated as the lowest frequency, expressed to the nearest 0.1 MHz, at which a required signal-to-noise ratio is achieved by the monthly median signal-to-noise ratio.

10. Basic circuit reliability (BCR)

BCR is determined in accordance with the procedure of method 8 of Report 892 in terms of required signal-to-noise ratio, monthly median signal-to-noise ratio and the within-an-hour and day-to-day variations. Caution is given that this approach makes no allowance for system degradation due to signal dispersion such as can be particularly important when dealing with digital transmissions.

REPORT 252-2

CCIR INTERIM METHOD FOR ESTIMATING SKY-WAVE FIELD STRENGTH AND TRANSMISSION LOSS AT FREQUENCIES BETWEEN THE APPROXIMATE LIMITS OF 2 AND 30 MHz

(Study Programme 30A/6)

(1956-1959-1963-1966-1970)

This Report has been published separately.

SUPPLEMENT TO REPORT 252-2

SECOND CCIR COMPUTER-BASED INTERIM METHOD FOR ESTIMATING SKY-WAVE FIELD STRENGTH AND TRANSMISSION LOSS AT FREQUENCIES BETWEEN 2 AND 30 MHz

(Study Programme 30A/6)

(1978-1982)

This supplement to Report 252-2 has been published separately. This supplement provides a replacement for Report 252-2; however, Report 252-2 is maintained until this supplement has been further tested.

REPORT 729-3

DEVELOPMENTS IN THE ESTIMATION OF SKY-WAVE FIELD STRENGTH AND TRANSMISSION LOSS AT FREQUENCIES ABOVE 1.5 MHz

(Study Programme 30A/6)

(1978-1982-1986-1990)

1. Introduction

For many years the CCIR has coordinated studies leading to the adoption of methods of HF field-strength estimation. The methods of Report 252 (New Delhi, 1970) and Supplement to Report 252-2 (Geneva, 1982) remain available for study and specialist investigations. However, Recommendation 533 places emphasis on the use of the method of Report 894. Decision 6 requires Interim Working Party 6/1 to effect improvements in prediction methods and the purpose of the present report is to record those aspects which appear desirable to consider particularly with regard to the further development of the method of Report 894.

2. Modelling and prediction of HF sky-wave propagation

Improvements in the representation of the standard ionospheric characteristics are needed. Studies are in progress using ground-based and satellite measurements together with appropriate theory. It is hoped that these will lead to the production of more accurate maps of foF2 over ocean regions and at high latitudes. The possibility of a representation of the auroral oval for different levels of magnetic activity appears to merit consideration. There is a need to consider improvements to the representation of foE at high latitudes and in particular to ways of allowing for particle-induced ionization at auroral latitudes. Some progress has been made on development of more sophisticated models for the high latitude region [see Reports 886 and 1012].

3. Model of the vertical height distribution of electron concentration

The existing model consists of three segments: a parabolic variation of electron concentration with height in the E and F2 regions together with a linearly varying intermediate region. The semithickness of the F2-region segment is given from empirical equations in terms of the vertical-incidence ionospheric characteristic h'F,F2. Unfortunately the accuracy of the global representation of this characteristic is not as great as is desirable because of data interpretation difficulties; also the empirical equations are only approximate for certain combinations of values of ionospheric characteristics. Some studies have been made of the relative merits of other ways of determining the F2-region semithickness [Dudeney and Bradley, 1976]. These include the use of representations of

the ratio of semithickness to height of maximum electron concentration [Lucas and Haydon, 1966] and the formulation of expressions in terms of neutral-density scale height [Rush and Elkins, 1975]. Additional work is needed to determine the optimum approach. The existing model gives discontinuities in virtual height for changes from reflection in the linear segment to the F2-region segment. New models have been produced which avoid this limitation [Dudeney, 1978; Baker and Lambert, 1988; Dyson and Bennett, 1988].

4. Propagation modes and raypaths; determination of maximum usable frequency

Further consideration should establish whether the choice of modes that are examined for the different propagation ranges is optimum. Particular attention should be paid to the case of mixed modes involving successive reflections from more than one ionospheric layer. Additional tests should be made comparing different iteration and "homing" procedures to yield raypaths between fixed terminals with the "ray-set" approach [Haydon, 1975]. The extent to which ionospheric tilts as indicated by the predictions are accurate needs assessing. If these are found to be generally realistic, tilt allowances should be employed, particularly at high latitudes where ray-tracing results reveal their extreme importance. Existing equations [Dick, 1976] should be introduced to allow for tilt modes on long-distance paths which attain a perigee with two or more ionospheric reflections without intermediate ground reflection [Hortenbach and Rogler, 1976]. The significance of off-great-circle propagation has been shown by a study of the seasonal variability of azimuthal raypath directions [CCIR, 1974-78]. Further investigations should be carried out. A procedure which allows for off-great-circle modes on long paths has been produced [Kanaya and Wakai, 1976].

Improved methods of determination of basic MUF based on ray tracing have been proposed by Huang [1977] and Lockwood [1983]. In the USSR a so-called equivalent hop method has been developed for calculation of the MUF of multihop (not necessarily uniform) paths taking into account a variation in ionospheric characteristics along the propagation path [Chernov, 1968, 1988].

Comparisons are needed between estimates of the basic MUF deduced from empirical formulae and from ray tracing and other techniques so as to determine whether the former procedure leads to estimates of adequate accuracy. Attention should be given to the validity of the two-control point method for long paths; there is still much disagreement concerning this. At present, day-to-day variability of the basic MUF is taken as being independent of propagation distance or of mode order. This needs to be confirmed.

For the planning and operation of HF radiocommunications, one of the most important parameters is the mean and standard deviation of launch and arrival angles for the path, since these angles determine the choice of the most suitable transmitting and receiving antennas, on which circuit reliability depends. CCIR Document [1986-1990a] has consolidated data (gathered in the USSR) on the statistical characteristics of angles of arrival on short to very long paths (700 - 10,000 km). Although there was a variability in the measured elevation angles on any given path and the range of this variability varies with distance, time of day and ionospheric conditions, on average the existing methods for calculating elevation angles give a sufficiently accurate representation of the observed values on real paths.

In the USSR a refraction integral method [Kiyanovsky, 1971; Kiyanovsky et al., 1987] has been developed for numerical calculation of HF paths of any length. The calculations are based on approximate representations to real electron density two-dimensional profiles, including variations along the propagation path.

5. Transmitting and receiving-antenna gain

Existing equations for antenna radiation patterns ——————— apply to antennas sited over perfect ground or take account of the effect of real earth in a rather simplified manner. Most antennas are designed to radiate or receive horizontally or vertically polarized waves along the great-circle path between the transmitter and receiver, but in other general directions such as those involved in interference calculations the response is to waves of elliptical polarization. In order to be able to calculate polarization-coupling loss, antenna expressions are needed which include this wave polarization as well as the power gain.

New improved methods for predicting the performance of antennas over real ground are becoming available [see —— Report 891]. These new more rigorous computational procedures should be included in the development of future methods for predicting HF sky-wave field strengths.

Interim Working Party 10/1 is developing a package of gain patterns for a range of antenna types in common use at HF, taking into account latest information both from theory and measurement. Computer-based representations of these patterns are needed.

6. Ionospheric absorption

The George-Bradley [1974] model for the latitude variation of regular absorption, i.e., absorption for magnetically quiet conditions disregarding auroral absorption, has been improved and extended to the high-latitude region [Izraitel et al., 1989].

Superimposed on the regular absorption are other forms of absorption, e.g., auroral absorption. A better method for taking account of auroral absorption is needed, particularly because of the recent study by Hargreaves et al., [1987], which has established that auroral absorption is much better correlated with magnetic activity than it is with solar activity. The CCIR method contained in the supplement to Report 252 is based on the earlier work of Foppiano and Bradley [1985] and it employs sunspot number as the input parameter for the prediction of auroral absorption.

7. Polarization-coupling loss

Theoretical studies for multi-hop paths have shown that under some circumstances polarization-coupling loss due to the regeneration of the magnetoionic components after wave reflection from the ground can be very large (10 dB or greater). A more complete method of allowing for this loss is available [Chernov, 1983].

8. Reflection and scattering by irregularities

Developments in knowledge of the spatial structure and temporal occurrence of sporadic-E irregularities together with a better understanding of the mechanisms responsible for wave reflection and scattering [Sinno *et al.*, 1976] indicate that improved allowances for sporadic-E reflection and obscuration losses may soon be possible. ——————— Comparisons of oblique-path signal intensities with simultaneously recorded vertical-incidence ionograms suggest that Es reflection and scattering losses may vary for the different classes of sporadic-E irregularity and so be latitude dependent.

Additional consideration should be given to ways of determining the combined influence of propagation modes involving reflection from sporadic-E irregularities and from regular ionospheric layers, taking particular account of the different probabilities of occurrence and day-to-day variations of amplitude. Further studies of the effects of irregularities in the F region on oblique-path signal intensities are needed; current procedures ignore the incidence of spread-F.

9. Spreading loss

Existing models include an inverse-square free-space loss term. Consideration should be given to the explicit computation of the spreading loss by inclusion of a term defined to include free-space loss, defocusing loss and focusing gain (skip-distance, horizon and antipodal) to provide an improved representation of total path loss. The necessary equation is available, but requires as an input, for a given mode, the derivative of the ground range with respect to elevation angle.

The importance of skip-distance focusing gain when practical antennas are used is very dependent on the gain of these antennas at low elevation angles and the relative amplitudes of the low order modes with respect to the high order modes. In all cases the importance of focusing gain is dependent on distance, elevation angle and the characteristics of the antenna employed.

10. Signal fading

Signals which propagate via the ionosphere are known to fluctuate in intensity. There are short-term as well as day-to-day variations. Present procedures allow for these variations in a compatibility assessment by the introduction of statistically suitable factors. The short-term variability arises from changes in ionospheric absorption, focusing, defocusing, and multipath. The day-to-day variability is due to corresponding variability of D- and E- and F-region ionizations. It is now recognized that day-to-day variability depends critically on the ratio of wave frequency to basic MUF [Bradley, 1983; CCIR, 1982-86a].

11. Propagation at frequencies above the basic MUF

Work in the Federal Republic of Germany and by Bradley [1989] is hoped will lead to more accurate means of assessing signal intensities at frequencies above the basic MUF. The relative importance of modes involving reflection from regular layers, reflection from Es-irregularities and sidescatter needs to be established. Experimental data [Dieminger and Rose, 1961] indicate that the rate of decrease of field strength with increase of frequency depends on path length and on whether the ionosphere is disturbed. A theoretical study of the field strength at frequencies above the basic MUF near the edge of the first skip zone was carried out in the USSR [Chernov and Zhiltsov, 1982; 1983]. It showed the field strength as a function of frequency and path length with regard to the diffuseness of the ionospheric reflecting region. At the 20 dB attenuation level the illuminated zone can be several hundred kilometres nearer the transmitter than the geometric border. Currently, no account is taken of these features.

An analysis of the measured field-strength data in CCIR Data Bank C reveals that for path lengths up to 2000 km the above-the-MUF loss is much less than for longer paths and increases only slowly with the ratio of wave frequency to MUF [CCIR, 1982-86b].

The method in Report 894 gives greatest signal intensities at the basic MUF; yet monthly median intensities derived from measurements are a maximum at a somewhat lower frequency for which signals reflected from regular layers are present on a greater fraction of the days. An improved approach to the prediction philosophy is needed to allow for the correlation between daily values of the basic MUF and of field strength.

12. Multipath probability

Multipath is judged to exist if two or more propagation modes with a difference in time delay exceeding some specified figure lead to received powers which differ by less than another specified amount. Multipath probability is deduced using estimates of the day-to-day variations in signal intensity of the different modes assuming each mode has an availability (or probability of occurrence) equal to that of the mode with the greatest availability. A procedure is needed which takes account of the separate availabilities of the different modes.

13. Predictions for long-distance paths

It seems probable that prediction accuracies require improvement for path lengths beyond about 10 000 km. The extent to which propagation modes can be predicted adequately for such distances should be examined. Observational results [Hortenbach, 1977; Hortenbach and Rogler, 1976] indicate that predictions consistent with observations can be obtained by making allowance for tilt-supported propagation modes and taking a focusing gain into account. Furthermore, the possibility of an alternative approach should be considered using simple empirical equations to give a distance dependence without regard for the modes to which it applies.

Methods of the adiabatic invariant [Gurevich and Tsedilina, 1983, 1985; Vovk et al., 1988; CCIR, 1986-1990b], and parabolic equation [Cherkashin and Chernova, 1983; Eremenko et al., 1989] have been developed in the USSR for calculating field intensity for long distance paths which take into account a variable wave guide mode of transmission.

14. Estimates of signal/noise ratio and circuit reliability

Several methods for the calculation of HF circuit reliability are described in Report 892. Verification is needed of the accuracy of current methods used in the reliability calculations. In particular, improved methods may be needed for estimating the circuit reliability of a path for which several propagation modes exist. Further, consideration ought to be given to the extension of the definition of reliability to include dispersion (due to multipath and Doppler changes), service coverage, and temporal and location variabilities [Bradley, 1983].

15. Extension to the frequency range 1.5 to 2 MHz

The prediction procedure needs extending to cover the frequency range 1.5 to 2 MHz. In particular, between 1.5 and 1.6 MHz it should give results which are consistent with those from Annex 1 of Recommendation 435.

16. Specific improvements needed in the method of Report 894

Some of the elements of the method for which improvements are specifically identified are as follows:

1) above-the-MUF loss allowance;

2) the selection of the modes for which calculations are made and the manner in which their contributions are combined;

3) the determination of the variability about the monthly median value of field strength;

4) inclusion of an allowance for the gain of all antennas in common use;

5) the frequency dependence of angle of elevation;

6) E-layer screening on paths beyond 2000 km;

7) the signal field-strength normalisation factors Lz and Ly.

REFERENCES

BAKER, D.C. and LAMBERT, S. [1988] - Multiparabolic ionospheric model for SSL application, Electronics Lettrs., Vol 24, 7, 425-426.

BRADLEY, P.A. [1983] Signal and noise variability in high frequency sky-wave radio-service planning. AGARD Conf. Proc. No. 332, *Propagation Aspects of Frequency Sharing, Interference and System Diversity*, 10-1 to 10-13. Ed. H. Soicher. NASA Accession No. N83-30873. National Technical Information Service, Springfield, VA 22161, USA.

BRADLEY, P.A. [1989] - Above the MUF loss, IEE International Conference on Antennas and Propagation. Conference Proc. 301 (pt 2) pp.257-262.

CHERKASHIN, Y.N. and CHERNOVA, V.A. [1983] - Printsip podobiya i polnomasstabnoe modelirovanie volnovykh polei metodom paraboliscHeskogo uravneniya (The similitude principle and the full-scale modelling of wave fields by means of the parabolic equation method), Rasprostranenie radiovoln v ionosfere: Sbornik nauchykh trudov, Institut zemnogo magnetizma, ionosfery i rasprostraneniya Akademii nauk SSSR (IZMIRAN), Moscow, 62-68.

CHERNOV, Yu.A. [1968] - Neskolko teorem ob ekvivalentnom skachke pri ionosfernom rasprostranenii radiovoln (Some theorems relating to the equivalent hop in sky-wave propagation). Radiotekhnika, No. 6, 13.

CHERNOV, Y. A. [1983] EnergeticHesky raschet korotkovolnovykh radiolinii (Calculation of power balance of HF radio links). *NIIR Proc.*, 4, 5-12.

CHERNOV, Yu.A. [1988] - Primenenie teoremy ob ekvivalentnom skachke k raschetu MPCh na korotkovolnykh neodnorodnykh trassakh (Application of the equivalent hop theorem to MUF calculation on non-homogeneous HF paths). Proceedings of NIIR, No. 2, 117.

CHERNOV, Y. A. and ZHILTSOV, A. U. [1982] O kaustikakh na korotkovolnovykh odnoskachkovykh radioliniyakh (About caustics on short-wave one-hop radio links). *Geomag. i Aeronom.*, Vol. 22, 3, 508.

CHERNOV, Y. A. and ZHILTSOV, A. U. [1983] Statisticheskie kharacteristiki napryazhennosty polya KV v oblasty granitsy mertvoi zony (HF field strength statistical characteristics near the border of a skip-zone), 117. Collected papers of IZMIRAN, Academy of Sciences of the USSR, Moscow.

DICK, M. I. [1976] Raypath determination with perigee condition. IWP 6/1. Doc. 36.

DIEMINGER, W. and ROSE, G. [1961] Zum Feldstärkenverlauf am Rande der toten Zone (On the variation of field strength near the border of the skip zone). *NTZ*, 14, 492-495.

DUDENEY, J. R. [1978] An improved model of the variation of electron concentration with height in the ionosphere. *J. Atmos. Terr. Phys.*, Vol. 40, 195-203.

DUDENEY, J. R. and BRADLEY, P. A. [1976] Determination of F2-layer semi-thickness. IWP 6/1. Doc. 37.

DYSON, P.L. and BENNETT, J.A. [1988] - A model of the vertical distribution of the electron concentration in the ionosphere and its application to oblique propagation studies, J Atmos Terr Phys, Vol 50, 3, 251-262.

EREMENKO, V.A., CHERKASHIN, Y.N. and CHERNOVA, V.A. [1989] - Vybor optimalnkh parametrov rastcheta kharakteristik volnovogo polya (Selection of optimum parameters for calculating wave field characteristics). Geomagnetizm i aeronomya, 29, No. 4, p. 597-603.

FOPPIANO, A.J. and BRADLEY, P.A. [1985] - Morphology of background auroral absorption, J. Atmos. Terr. Phys., 47, 663-674.

GEORGE, P. L. and BRADLEY, P. A. [1974] A new method of predicting the ionospheric absorption of high frequency waves at oblique incidence. *Telecomm. J.*, Vol. 41, 307-312.

GUREVICH, A. V. and TSEDILINA, E. E. [1983] Amplituda elektricheskogo polia korotkih radiovoln v gorizontalno-neodnorodnoi ionosfere na mnogoskachkovih trassah (Amplitude of electric field of short radiowaves in a horizontally-irregular ionosphere on many-leap lines). *Geomag. i Aeronom.*, Vol. XXIII, 764-767.

GUREVICH, A. V. and TSEDILINA, E. E. [1985] *Long-distance Propagation of HF Radio Waves*. Springer, Heidelberg, Federal Republic of Germany.

HARGREAVES, J.K., FEENEY, M.T., RANTA, H. and RANTA, A. [1987] - On the prediction of auroral radio absorption on the equatorial side of the absorption zone, J. Atmos. Terr. Phys., 49, 259-272.

HAYDON, G. W. [1975] Rayset model for oblique propagation. CCIR IWP 6/1. Doc. 16.

HORTENBACH, K. J. [1977] Einfache Korrekturformel fur Berücksichtigung der Fokussierung im Antipodenbereich bei ionosphärischen Vorhersageverfahren (Simple correction formula considering antipodal focusing in ionospheric predictions methods). *Rundfunktechn. Mitt.*, Vol. 21, 4, 169-171.

HORTENBACH, K. J. and ROGLER, F. [1976] Die Ausbreitung von Kurzwellen-Rundfunksendungen auf transantipodalen Strecken und ihre Vorhersage (Propagation of short-wave broadcasting transmissions on transantipodal paths and its prediction). *Kleinheubacher Berichte*, 20, 205-215.

HUANG HSUEH-CHING [1977] On the determination of the MUF for the propagation mode, IWP 6/1, Doc. 75.

IZRAITEL, A.G., LOBACHEVSKY, L.A., ZHULINA, E.M. and KISHCHA, P.V. [1989] - Model regulyarnogo pogloshcheniya v nizhnei ionosfere (Model of regular absorption in the lower atmosphere), Geomagnetizm i aeronomiya, No. 1, 138-140.

KANAYA, S. and WAKAI, N. [1976] Method for estimating the signal strength of ground-scatter modes at frequencies above the classical MUF for transmitter-receiver separations beyond 4000 km. IWP 6/1. Doc. 39.

KIYANOVSKY, M.P. [1971] - Metod rascheta kharakteristik KV trass dlya dvumernoi modeli ionosfery (Method of calculation of HF path characteristics for a two-dimensional ionospheric model), Moscow, Nauka, Pre-print IZMIRAN, [1971]; Issledovaniya po geomagnetizmu, aeronomii i fisike solntsa, Moscou, Nauka, [1972], No. 25.

KIYANOVSKY, M.P., PRUDKOVSKY, A.G., KOTOVICH, G.V., ZASORIN, A.Z., ZYRYANOVA, L.A., KRASINA, T.Yu. and SUKHODOLSKAYA, V.E. [1987] - Metod refraktsionnogo integrala dlya dvumerno neodnorodnoi ionosfery i ego primenenie k raschetam radiotrass (Refraction integral method for a two-dimensional non-homogeneous ionosphere and its use for radio path calculation). Teknika sredstv svyazi, series SS, No. 5.

LOCKWOOD, M. [1983] A simple M-factor algorithm for improved estimation of the basic maximum usable frequency of radio waves reflected from the ionospheric F region. *Proc. IEE*, Vol. 130F, 296-302.

LUCAS, D. L. and HAYDON G. W. [1966] Predicting statistical performance indexes for high-frequency ionospheric telecommunication systems. ESSA Tech. Rep. IER1-ITSA1, US Govt. Printing Office, Washington, DC 20402.

RUSH, C. M. and ELKINS, T. J. [1975] An assessment of the magnitude of the F-region absorption on HF radio waves using realistic electron density and collision frequency models. *Telecomm. J.*, Vol. 42, VIII, 476-488.

SINNO, K., KAN, M. and HIRUKAWA, Y. [1976] On the reflection and transmission losses for ionospheric radio wave propagation via sporadic E. *J. Radio Res. Labs.* (Japan), 23(110), 65-84.

VOVK, V.Y., MANAENKOVA, N.I., NEKRASOV, B.Y., TUSHENTSOVA, I.A., TSEDILINA, E.E. and SHUMILOV, I.A. [1988] - Sopostavlenie raschetnykh i eksperimentalnykh MPCh i ionogramm DNZ na protyazhennoi trasse Moskva-Molodezhnaya (Antarktida) dlya uslovy solntsestoyaniya. (Comparison of calculated and experimental MUF values and long-distance oblique sounding ionograms on a long-distance path Moscow-Molodezhnaya (Antarctic) for solstice conditions), Geomagnetizm i aeronomiya, Vol. 28, 1.

CCIR Documents

[1974-78]: 6/240 (Germany (Federal Republic of)).

[1982-86]: a. 6/54 (Germany (Federal Republic of)); b 6/209 (Germany (Federal Republic of)).

[1986-1990]: a. 6/35 (USSR); b. 6/36 (USSR).

REPORT 891-2

ANTENNA CHARACTERISTICS IMPORTANT FOR THE ANALYSIS AND PREDICTION OF SKY-WAVE PROPAGATION PATHS

(Question 40/6)

(1982-1986-1990)

1. Introduction

In order to analyse the observed performance of a sky-wave transmission circuit, or to predict the performance of a proposed circuit, it is important to know the radiation pattern including both polarizations, since the anisotropic ionosphere will in general depolarize the field to an unknown degree. At HF and lower frequencies, antennas are usually located close, in terms of wavelength, to the ground or to a supporting vehicle and it is also important to take account of the electrical properties and shape of nearby objects.

In analysing the effect of the antennas on the performance of a circuit, account must be taken of the fact that sky waves do not necessarily

- follow a great circle path between the transmitter and receiver;
- have the same elevation angle at both terminals;
- maintain the transmitted wave polarization;
- have a plane wave front at the receiver.

2. Antenna characteristics

2.1 *Directivity*

The directivity pattern of a transmitting antenna in free space may be calculated from the current distribution on the antenna. When the antenna is placed near to the ground the directivity pattern is modified in the vertical plane and the horizontal plane, due to the combination of the direct radiation from the antenna and that reflected in the ground. The directivity pattern of an array of antenna elements may be found by combining the pattern of each element and its ground reflection, taking account of the geometrical spacing between the element centres and of the relative phasing and amplitudes of the element currents.

For flat perfectly-conducting ground, the voltage reflection coefficient for horizontally polarized waves equals -1 for all angles of incidence. A horizontal current element thus has a reflected image in which current flows in the opposite sense, and the ground reinforcement occurs at angles of elevation for which the path difference between direct and reflected waves is a half wavelength. The dominant parameter in determining the pattern is the mean height of the active part of the antenna. If the ground is not a perfect conductor, the reflection coefficient at large angles of incidence (small elevation angles), has a smaller value but the phase remains

substantially 180° so the pattern at low elevation angles is scarcely changed. The actual reflection coefficient may lead to loss of gain, usually less than 1 dB. At large elevation angles ——————————— the reflection coefficient falls and the loss may be correspondingly greater, up to 3 dB, but even here the directive gain remains 3 dB higher than it would if the ground reinforcement were absent. For practical purposes, therefore, and particularly for antennas having small elevation angles, the effect of the imperfectly conducting ground may be ignored if the polarization is horizontal.

For vertical polarization the effects are more complex. For highly conducting ground, the reflection coefficient is approximately 1. A vertical current element above the ground has a reflected image in which the current flows in the same sense, so that reinforcement occurs at small elevation angles. This can occur in practice over ground of very good conductivity or over sea. When the conductivity is finite, the phase of the complex voltage reflection coefficient changes by 180° at large angles of incidence. Over sea, this happens at angles of incidence greater than 89° and the formation of the low angle beam is scarcely affected. Over land, the phase change occurs at angles of incidence around 75°, and the reflection coefficient falls to a low value in the region of the change. The angle at which this occurs is called the Brewster angle. Antenna performance is seriously affected, particularly as the minimum reflection occurs at angles which are comparable with the most probable arrival angles of HF sky waves for long communication paths. At small elevation angles, the ground reflection tends to cancel the direct wave, just as for horizontal polarization [Radford, 1983].

Extensive earth systems are sometimes laid beneath vertical antennas to improve ground conductivity, but while such ground systems improve the radiation efficiency, and the directive gain at large elevation angles, radial wire systems would have to extend 10 to 50 wavelengths in front of the antenna to effect improvement at small elevation angles, below about 20° [Anderson, 1965].

The ground might not be flat or horizontal. The effect of ground irregularity on antenna directivity may be modelled or studied theoretically [Knight *et al.*, 1964; Kubanov and Sheredko, 1976; Kubanov, 1980; Ott, 1971; Ott *et al.*, 1979; Ott, 1984].

Vehicles, particularly aircraft and land vehicles, may have dimensions comparable to the wavelength and to the antenna size, and it is then necessary to model or measure the radiation from the antenna and vehicle together [Hagn and van der Laan, 1970; Belrose, 1984].

The directivity pattern of an antenna is the same whether it is transmitting or receiving.

2.2 *Gain*

The power gain of an antenna is the product of the directivity and the antenna efficiency, which is the ratio of the radiated power to the transmitter power. The power radiated by an antenna near the earth is that which passes through the above-ground portion of a sphere centred on the antenna, having a radius sufficiently large such that any increase in radius does not cause a significant change in this power. The transmitter power consists of the radiated power plus the lost power: over an imperfectly conducting ground, power is lost due to induced ground currents out to many wavelengths from the antenna, as well as to the currents in the antenna conductors, insulators, and terminating or series resistors.

Imperfect ground affects not only the directivity and gain of the antenna (as discussed above), but also the input impedance. Both properties can be calculated by representing the effects of the ground by an image antenna identical to the real one and located as far below the surface of the ground as the real one is above it. The input impedance of an antenna over real earth is the input impedance in free space (self-impedance) plus the mutual impedance caused by the image antenna. In the methods devised by Barghausen *et al.* [1969], the free space mutual impedance was multiplied by the complex-ground-reflection coefficients at normal incidence. While this simple method is probably sufficiently accurate for practical calculation, improved numerical methods of determining the actual current distribution on antennas in their environment are now available e.g. the method-of-moments [Harrington, 1968; Poggio and Miller, 1973; Miller, 1984].

One method used for the prediction of interference is to assume that the radiation is never less than that from a dipole in free space radiating the same power (see Recommendation 80). An alternative approach is that adopted by the First Session of the World Administrative Radio Conference for the Planning of HF bands Allocated to the Broadcasting Service (WARC HFBC(1)) Geneva, 1984, where the radiation outside the main beam may have gain values down to a level between −8 dBi and −21 dBi, depending on antenna type.

Radio Regulation No. 154 (1988) defines the 'Gain of an antenna' for three distinct reference antennas. These definitions provide a reference for the calculation of the efficiency and directivity of practical antennas. At MF and lower frequencies, gains are usually expressed 'relative to that of a short vertical antenna' (see Reports 265 and 431 and Recommendations 435 and 683). At HF, VHF and higher frequencies, 'isotropic or absolute gain' is used as the reference (see Reports 253 and 894 and Recommendation 534). Table I of the Annex to Recommendation 341 gives information about these and other reference antennas. It should also be noted that the loop antenna, which is often used for measurement purposes, is usually calibrated according to one of these reference antennas.

2.3 *Effects of support structures and nearby antennas, towers and buildings on performance of antennas*

A great deal of work in Canada (by numerical modelling, experimental modelling and measurements at full scale) has been concerned with the re-radiation from towers, buildings and power lines on the directional pattern of MF broadcast antennas [Belrose, 1983]. This work brings out the importance of taking into account the effects of support structures and of nearby conducting objects on the patterns of MF and HF antennas.

Wire antennas such as dipoles and loops are commonly used antennas for radiocommunications in the lower HF bands. Such wire antennas are typically supported by grounded metal towers which are not intended to be a part of the antenna system. However, these support towers may be naturally resonant (heights one quarter or three-quarters of a wavelength) at, or near, the operating frequency and their presence therefore can markedly affect the antenna's directivity even for horizontal dipole antennas [Belrose, 1982].

Broadband antennas, for example the inverted cone, require a more complex support structure, and because of this and the broad frequency band of interest, great care must be taken in the electrical design to avoid resonances in the wire structures supporting such antennas (even if wooden poles and used). The performance of some inverted cone antennas of commercial manufacture clearly suffered in implementation [Wilson, 1983].

Buildings, whether conducting or non-conducting, often contain a structural steel frame, and in any case the ground wire of the electrical system for lights and appliances forms a wire grid structure, which can be resonant at MF and lower HF frequencies [Royer, 1985].

Power transmission lines are strong re-radiators at MF, since the support towers are grounded, and all the towers are usually connected at their tops by sky-wires, for lightning protection. These transmission line ground plane loops can be resonant at MF frequencies [Trueman et al., 1983, 1985, 1987].

While the effects of support structures have not been considered previously, for accurate prediction of sky-wave propagation paths, such effects can be significant, and need to be taken into account. The above-mentioned method-of-moments (MOM) can take into account these effects in a detailed numerical modelling calculation, including as well more distant conducting structures, such as unused towers, antennas, buildings and power transmission lines.

2.4 *Polarization*

Downcoming sky waves are in general elliptically polarized and, in general, receiving antennas respond to both vertical and horizontal polarization. Although an antenna responds mainly to the polarization for which it is designed when signals arrive from the intended direction, it may be more sensitive to the other polarizations when signals arrive from other directions.

The ground around the antenna also has a considerable effect in that it modifies the polarization of the received waves and therefore the antenna response to them [Bertel et al., 1987]. Similar considerations apply to transmitting antennas which are designed to radiate elliptical polarization or may do so in off-axis directions. Thus polarization information is important for the assessment of area coverage and of interference from unwanted transmissions [CCIR, 1978-82].

2.5 *Aperture*

If the signal arriving at the receiver is the resultant of several propagation modes at different angles of arrival or has been modified by ionospheric roughness, or local site effects, its wave front will not be plane. Consequently, the effective gain of an antenna whose aperture is large compared with the wavelength will be less than it would be if the wavefront were plane.

3. The minimum information required for prediction of the wanted signal

In some cases it will be possible to assume that antennas are aligned along the great circle path and that the polarizations employed are suitable for the circuit, or that the polarization coupling loss can be calculated (see Recommendation 435). It will then be possible to make a first assessment of the interference-free performance of a circuit by using only two antenna characteristics: the maximum power gain and the vertical radiation pattern in the plane of the main beam. If either the transmitting or receiving antenna is not optimized azimuthally along the great circle path, an allowance will have to be made in respect of the horizontal radiation pattern.

4. Available information

There is no readily available information which gives the performance of antennas over real ground and in their operational environments, which is required for detailed modelling and propagation studies.

4.1 Publications and computer programs available from the CCIR*

The CCIR Book of Antenna Diagrams (1978) gives the directivity and gain for arrays of vertical and horizontal thin elements over perfect ground together with correction factors for some typical values of ground constants at 1, 10 and 20 MHz. Further antenna information is given in the "Handbook on High Frequency Directional Antennae" (Geneva, 1966). A method for calculating the directional characteristics of multi-tower vertical antennas is given by Smith [1969].

4.1.1 LF and MF antennas

Recommendation 435 gives information about the vertical radiation patterns and gains of monopole antennas of realistic thickness and of various lengths over typical ground ($\sigma = 0.01$ Sm^{-1}) together with a calculation method for the effect of locating the antenna close to the sea (the "sea gain") for the LF and MF broadcasting bands. Report 265 gives "antenna factors" to allow for imperfect ground, for frequencies between 30 and 500 kHz. Similar information for frequencies between 0.2 and 1.5 MHz is given in Report 401. The CCIR Secretariat has prepared the microcomputer program LFMFANT for pattern calculations of vertical antenna arrays in these bands.

4.1.2 HF antennas

The CCIR Atlas of Antenna Diagrams (1984), gives gain and directivity performance figures for arrays of horizontal half-wave dipoles and horizontal rhombics situated on a flat, homogeneous and imperfect ground with conductivity $\sigma = 0.01$ S/m and dielectric constant $\varepsilon = 4$ (average ground) for a frequency of 10 MHz. Additionally, the CCIR Secretariat has produced microcomputer programs HFARRAYS, HFRHOMBS, HFMULSLW, HFDUASLW and HFDUASLW1.

* See Resolution 63.

4.2 Programs for the method of moments

The Method of moments (MOM) technique is particularly useful for computing the characteristics such as gain, directivity, impedance and mismatch loss of non-standard antennas over non-typical ground. This technique changes the way in which antenna problems are formulated and interpreted [Miller, 1987]. For example, the Numerical Electromagnetic Code (NEC) [Burke and Miller, 1984], which implements the method of moments, has been used in several studies to examine accepted results. The classic paper reporting on extensive tests of buried-wire-radial ground systems by Brown, Lewis and Epstein [1937] has become the standard for the design of such systems for MF broadcasting. A study using the NEC found that the unattenuated field over perfect ground gave the best agreement with the Brown et al. measurements, which evidently must have been normalized. A similar study has shown that a vertical monopole having only four quarter-wavelength radials elevated a small fraction of a wavelength above ground has a better performance than a vertical monopole mounted on the ground with 120 buried radial wires [Christman, 1988].

As presently implemented, the NEC is most suited to a mainframe computer environment, and can solve problems employing up to 300 segments. Several versions have been written; versions 2 and 3 use the Sommerfeld-Norton approach to take account of the effect of lossy ground on the impedance matrix, as well as its effect on the directivity pattern. Methods for estimating ground conductivity and permittivity developed for use in calculating ground-wave field strength (see Recommendation 527) can be used with these versions, or the electrical characteristics of the earth's surface in the vicinity of the antenna can be measured at the frequencies of interest using the methods described in Report 879.

Compact versions of the NEC with somewhat restricted capability are available for use on microcomputers. MININEC 2 can be used to predict antenna performance over perfect ground [Li et al., 1983]. MININEC 3 includes a Fresnel reflection coefficient approximation and so can be used for antennas over, but not too close to, imperfect ground [Logan and Rockway, 1986]. The latest version is available in an integrated software package with graphics and other utilities which provides an engineering environment for antenna analysis and performance prediction [Rockway et al., 1988]. Further research is planned to improve the prediction capability below HF, and to include a Sommerfeld solution capability in the framework represented by the MININEC system.

REFERENCES

ANDERSON, J. B. [1965] Influence of surroundings on vertically polarized log-periodic antennas. *Teleteknik*, Vol. IX, 2, 33-40.

BARGHAUSEN, A. F., FINNEY, J. W., PROCTOR, L. L. and SHULTZ, L. D. [1969] Predicting long-term operational parameters of high-frequency sky-wave telecommunication systems. ESSA Tech. Rep. ERL 110-ITS 78, US Govt. Printing Office, Washington, DC 20402.

BELROSE, J. S. [December, 1982] The effect of supporting structures on simple wire antennas. *QST*, Vol. LXVI, 32-35 and errata [October, 1984], Vol. LXVIII, 42.

BELROSE, J. S. [1983] VLF, LF and MF antennas. Chapter 15, *IEE Handbook of Antenna Design*, Vol. 2, 553-662. Eds. Rudge, Milne, Olver and Knight. Peter Peregrinus Ltd., London, UK.

BELROSE, J. S. [1984] On modelling and measurements in full scale. AGARD LS No. 131, *The Performance of Antennas in their Operational Environment.* NASA Accession No. N84-12367. National Technical Information Service, Springfield, VA 22161, USA.

BERTEL, L., ROJAS-VARELA, J., COLE, D. and GOURVEZ, P. [1987] - HF antenna behaviour in a receiving system. IPS Radio and Space Services, Technical Report IPS-TR-87-04.

BROWN, G.H., LEWIS, R.F. and EPSTEIN, J. [1937] Ground systems as a factor in antenna efficiency. Proc. IRE, 25, 753-787.

BURKE, G. J. and MILLER, E. K. (1984] Modelling antenna near to and penetrating a lossy interface. *IEEE Trans. Ant. Prop.*, Vol. AP-32, 10, 1040-1049.

CHRISTMAN, A. [1988] Elevated Vertical Antennas on 80 Meters. To be published in QST, 1988.

HAGN, G. H. and VAN DER LAAN, J. E. [1970] Measured relative responses toward the zenith of short-whip antennas on vehicles at high frequency. *IEEE Trans. Vehic. Tech.*, Vol. VT-19, 3, 230-236.

HARRINGTON, R. F. [1968] *Field Computation by Moment Methods.* The Macmillan Co., New York, NY, USA.

KNIGHT, P., DAVIES, R. E. and MANTON, R. G. [1964] Vertical radiation pattern of h.f. curtain arrays on plateau sites. *Proc. IEE*, Part III, 421-427.

KUBANOV, V. P. [1980] Analyses of curtain array antennas located on sloping ground of limited extent (in Russian). *Trudy NIIR*, 3, 12-17.

KUBANOV, V. P. and SHEREDKO, E. Y. [1976] Effect of ground irregularities on the characteristics of phased-array HF antennas (in Russian). *Izvestia VUZOV, Seriya Radioelektronika*, 11, 48-51.

LI, S. T., ROCKWAY, J. W., LOGAN, J. C. and TAM, W. S. [1983] *MiniNEC in "Microcomputer Tools for Communications Engineering"* 21-52. ——————— Available with software on diskette from Artech House Inc., Norwood, MA 02062.

LOGAN, J.C. and ROCKWAY, J.W. [1986] A MINI-Numerical Electromagnetic Code. Available with software on diskette from U.S. Dept. of Commerce, NTIS, Springfield, Va., 22161 (Accession No. ADA 175 800).

MILLER, E. K. [1984] Numerical modelling techniques for antennas. AGARD LS No. 131, *The Performance of Antennas in their Operational Environment.* NASA Accession No. N84-12367. National Technical Information Service, Springfield, VA 22161, USA.

MILLER, E.K. [1987] A Selective Survey of Computational Electromagnetics. Applied Computational Electromagnetics Newsletter, Vol. 2, 1, 70-123, May 1987.

OTT, R. H. [1971] An alternative integral equation for propagation over irregular terrain, 2. *Radio Sci.*, Vol. 6, 4, 429-435.

OTT, R. H. [1984] Calculation of ground wave attenuation over irregular, inhomogeneous, layer media using program Wagner. AGARD LS No. 131, *The Performance of Antennas in their Operational Environment*, 3-1 to 3-17. NASA Accession No. N84-12367. National Technical Information Service, Springfield, VA 22161, USA.

OTT, R. H., VOGLER, L. E. and HUFFORD, G. A. [1979] Ground wave propagation over irregular, inhomogeneous terrain: comparisons of calculations and measurements. US Dept. of Commerce, Research Report No. NTIA-REPORT-79-20,. NTIS Accession No. PB-298-66B/AS. National Technical Information Service, Springfield, VA 22161, USA.

POGGIO, A. J. and MILLER, D. K. [1973] Integral equation solutions of three-dimensional scattering problems. *Computer Techniques for Electromagnetics.* Pergamon Press, New York, NY, USA.

RADFORD, M. F. [1983] High frequency antennas. Chapter 16, *IEE Handbook of Antenna Design*, Vol. 2, 663-724. Eds. Rudge, Milne, Olver and Knight. Peter Peregrinus Ltd., London, UK.

ROCKWAY, J.W., LOGAN, J.C., TAM, D.W.S. and LI, S.T. [1988] The MININEC system: microcomputer analysis of wire antennas. Artech House Inc., Norwood, MA 02062, USA.

ROYER, G.M. [1985] The distortion of AM broadcast antenna patterns as caused by nearby towers and buildings. CRC Report No. 1379, Communications Research Centre, Ottawa.

SMITH, C. [1969] *Theory and design of directional antennas.* Smith Electronics Inc., Cleveland, Ohio, USA.

TRUEMAN, C.W., KUBINA, S.J. and BELROSE, J.S. [1983] Corrective measures for minimizing the interaction of power lines with MF broadcast antennas. IEEE Trans. on Elect. Comp., Vol. EMC-25, 3, 329-339.

TRUEMAN, C.W. and KUBINA, S.J. [1985] Initial assessment of radiation from power lines. IEEE Trans. on Broadcasting, Vol. BC-31, 3, 51-65.

TRUEMAN, C.W. and KUBINA, S.J. [1987] Analysis and detuning of reradiation from power lines at MF frequencies using the Numerical Electromagnetics Code. Concordia University EMC Lab. Technical Note No. TN-EMC-87-04

WILSON, Q. C. [1983] HF equipment: receivers, transmitters, synthesizers and peripherals. AGARD LS No. 127, *Modern HF Communications.* NASA Accession No. N83-30862. National Technical Information Service, Springfield, VA 22161, USA.

CCIR Documents

[1978-82]: 6/223 (USSR).

REPORT 266-7 *

IONOSPHERIC PROPAGATION AND NOISE CHARACTERISTICS PERTINENT TO TERRESTRIAL RADIOCOMMUNICATION SYSTEMS DESIGN AND SERVICE PLANNING

(Fading)

(Question 35/6)

(1953-1956-1959-1963-1966-1970-1974-1978-1982-1986-1990)

1. Introduction

Experience has shown that information concerning the mean value of the received signal is not sufficient for planning radiocommunication systems. The variations in time, space and frequency, collectively described as fading, also have to be taken into consideration. Fading has a decisive influence on the performance of radiocommunication systems and on the type of modulation that may be used effectively. It is essential to know the severity and rapidity of fading to be able to specify the power required for transmitters, the necessary protection ratio to guard against interference and, with additional knowledge of the correlation of signals at separate antennas or frequencies, to be able to determine the most efficient and economical diversity or coding systems. A discussion of the importance of fading in connection with frequency utilization, together with a treatment of various aspects of fading, is given in Reports 413, 414 and 415 (Oslo, 1966).

2. General causes of fading

Fading may be caused by several different effects, such as:

- movement of the ionosphere, and multipath changes causing interference fading;
- rotation of the axes of the polarization ellipses;
- variations of the ionospheric absorption with time;
- focusing and temporary disappearance of the signal due to MUF failure [Davies, 1965].

On an 8000 km north-south transmission path, long-term fading has been attributed to atmospheric gravity waves [Röttger, 1973].

As also remarked by Davies [1965], the period of the fading cycle depends largely upon the cause of the fading. As a result, the period for interference and polarization fading may last for a time of the order of a fraction of a second to a few seconds, focusing may last something like 15 to 30 minutes, absorption fading may last for more than an hour; MUF failure is highly irregular and occurs at times of fade-in and fadeout.

Experiments to observe the relative rate of fading of both reflected and scattered signals from the ionosphere have been performed in the USSR over path lengths of about 1000 km [Kerblaï *et al.*, 1974; Kerblaï *et al.*, 1977; CCIR, 1978-82].

Fading tends to be faster on high frequencies than on low, because a given movement in the ionosphere represents a greater phase shift at the shorter wavelengths. Motion of the ionized regions gives rise to selective fading and to a distortion of the modulation envelope of a signal. The motion produces changes in path length, and Doppler shifts of frequency on each of the individual contributing signal components.

3. Sampling periods

For the purpose of communication system analyses, it is not always essential to identify the individual contributory effects; instead, it is possible to observe the resulting time series and characterize the fluctuations of signal levels in time as a random or stochastic process [Brennan, 1961]. Characterization of the time series requires, first, the selection of an observation period T_s, long enough to include a sufficiently large number of fluctuations of the signal level. The choice of T_s, while somewhat arbitrary, is generally made to suit the objectives of the analysis. Thus, for HF paths, samples from a few minutes to an hour in length have been found suitable where the interest was in the fast fading; sampling periods of a month have been used to estimate the random variations of each hourly mean period in a day.

---

* This Report should be brought to the attention of Study Groups 3, 5, 8 and 10.

It is expedient to consider short-term and long-term fading separately. The short-term fading component includes phase interference between multipath propagation components, and rapid variations of signal strength caused by ionospheric irregularities. The long-term fading component arises from random changes in the short-term median values of the received signal. For example, long-term fading would include variations in the median field strength measured from day to day over a fixed hour. Diurnal, seasonal and solar-cycle variations are of a more systematic nature and are usually not associated with fading.

4. Severity and rapidity of short-period fading

The terms "severity" and "rapidity", as used here, refer to the characteristics of the variations of the received signal amplitude when a steady tone is emitted from the transmitter.

4.1 *Severity of fading*

The signal amplitude distribution function $P(v_0)$ conventionally employed gives the probability of finding the signal amplitude v greater than v_0. It is related to the probability density function $p(v)$ by:

$$P(v_0) = \int_{v_0}^{\infty} p(v)\, dv \tag{1}$$

Probability density functions, obtained analytically to describe the envelope of a fading signal, differ according to the different assumptions made with respect to the structure of the contributory signals. Among the most frequently used models is the one which assumes that the received signal before detection is composed of a steady sinusoidal component and a random Rayleigh component with a uniform phase probability density [McNicol, 1949; Bramley, 1951]. This leads to the Nakagami-Rice probability density function [Nakagami, 1943; Rice, 1944 and 1945]:

$$p(v) = (2\, v/v_n^2) \exp\left[-(v_1^2 + v^2)/v_n^2\right] I_0\,(2v_1\, v/v_n^2) \tag{2}$$

where:

$I_0(x)$: modified Bessel function of zero order,

v : received signal envelope voltage/$\sqrt{2}$,

v_1 : r.m.s. voltage of steady sinusoidal component,

v_n : r.m.s. value of random voltage component.

Figure 1 gives the corresponding signal amplitude distribution function $P(v_0)$. Each curve represents a constant probability $P(v_0)$ that the level v_0 (shown as the ordinate) is exceeded. The abscissa is the ratio v_n/v_1, the parameter that is needed to specify a particular Nakagami-Rice distribution. For instance, if the ratio of r.m.s. random voltage to r.m.s. steady voltage equals 1 (i.e. 0 dB), then a level that is 7.5 dB below the median will be exceeded 90% of the time.

If $v_n/v_1 \gg 1$, then equation (2) reduces to the Rayleigh density function:

$$p(v) = (2v/v_n^2) \exp\,(-v^2/v_n^2) \tag{3}$$

Figure 1 shows, however, that the actual distribution approximates closely to the Rayleigh distribution provided $v_n/v_1 > 2$ (6 dB).

If $v_n/v_1 \ll 1$, then, in the vicinity of $v = v_1$, equation (2) reduces to the normal or Gaussian distribution function

$$p(v) = \frac{1}{v_n\sqrt{\pi}} \exp\left[-\frac{(v - v_1)^2}{v_n^2}\right] \tag{4}$$

The signal then varies symmetrically about the median value v_1 with standard deviation $v_n/\sqrt{2}$. Figure 1 shows that the distribution about the median value is almost symmetrical provided $v_n/v_1 < 0.1$ (−20 dB); the distribution may therefore be regarded as approximately normal whenever this condition is satisfied.

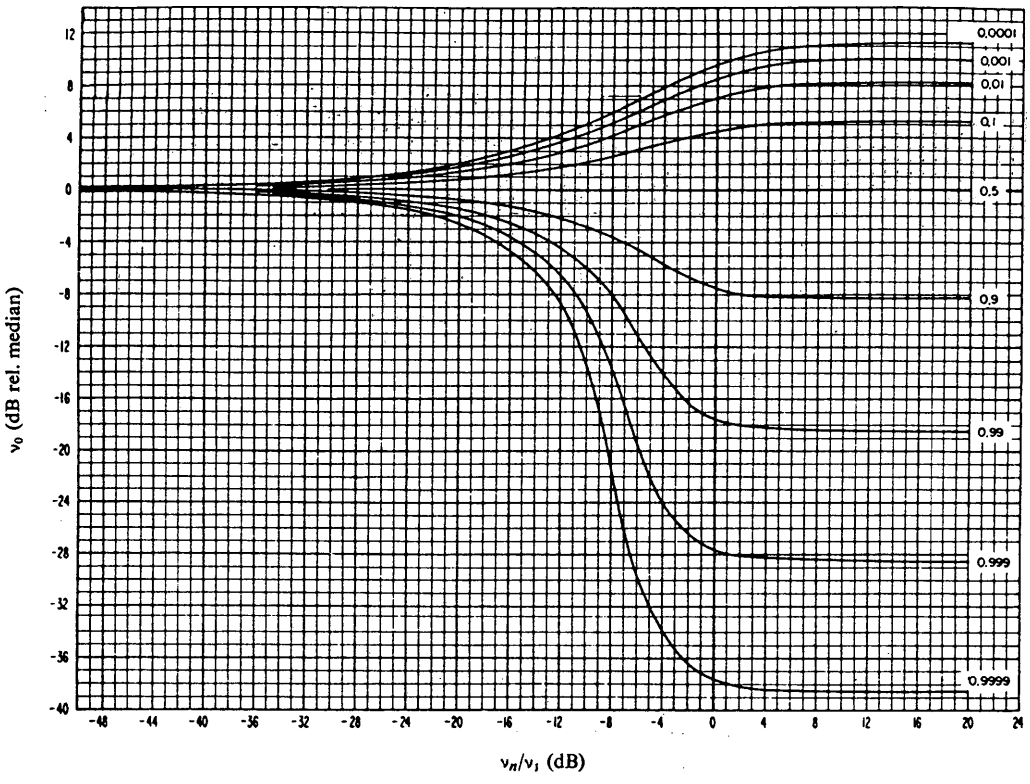


FIGURE 1 – *Distribution function P (v_0) for the Nakagami-Rice distribution*

(The values of P(v_0) are shown on the curves)

If the signal strength is expressed in decibels relative to a specified level the distribution referred to in equation (4) is known as the log-normal distribution. Both the normal and log-normal probability density functions may be expressed through one formula, as follows:

$$p(x) = \frac{1}{\sigma_x \sqrt{2\pi}} \exp\left(-\frac{x^2}{2\sigma_x^2}\right) \tag{5}$$

For the normal distribution, x is to be interpreted as $(v - v_m)$ while for the log-normal distribution in dB, x is to be interpreted as 20 log (v/v_m), where v_m is the median value of v; and σ_x is the standard deviation of x.

In addition to the above probability densities, which are bound up with certain theoretical assumptions (stationary processes, random motion of secondary radiators), there are other probability density functions worth considering, because they contain several arbitrary parameters to which values may be assigned to fit the measured data. In this connection, mention may be made of the *m*-distribution [Nakagami, 1960], which is similar to the χ^2 and gamma distributions often used in statistics. The *m*-distribution is close to a Rice distribution when m is large and close to a Rayleigh distribution when m is near unity.

In reality, the received signal on operational HF radio paths is generally the result of the interaction of several signals. If these signals have arbitrary constant amplitudes and random relative phases the amplitude distribution of the sum of the n individual signals is given by Kluyver's integral [CCIR, 1986-1990a]. Specifically, for n = 2, the distribution is given by

$$p(v) = 1 \qquad \text{for } v < |v_1 - v_n|$$

$$p(v) = \frac{1}{\pi} \arccos \frac{v^2 - \nu_n^2 - \nu_1^2}{2\nu_1\nu_n} \qquad \text{for } |\nu_1 - \nu_n| \leq v \leq (\nu_1 + \nu_n) \qquad (6)$$

$$p(v) = 0 \qquad \text{for } v > v_1 + v_n$$

If both the amplitudes and phases of the individual contributing signals are random, the envelope fading of each of the signals can be described by equation (2). For this case the amplitude distribution of the sum has been calculated by [Sergeev, 1978a].

If n > 2, the distribution of the first case approximates to a Nakagami-Rice distribution and of the second to a Rayleigh distribution. For n = 2, however, the differences are considerable. Table I gives the levels exceeded for a number of specified percentage points for the distribution according to equation (6) together with those for the theoretical distributions discussed earlier [Norton et al., 1955].

An alternative evaluation of the empirical probability density functions of a signal envelope carried out by the method of Dyakov and Kiyanovsky [1981] on single-hop and two-hop paths [Gorshkova et al., 1985] has demonstrated the possibility of describing experimental data by theoretical laws having either one parameter based on distribution shape or none at all. The probability density functions can be adequately described by a family of curves which use a family of ß distributions, having two parameters based on shape. These curves describe practically the entire range of empirical distributions of the signal envelope [Dumbrava et al., 1988].

TABLE I

Distribution	ν_n/ν_1 (dB)	Level (dB) relative to median, exceeded for the following percentage of time			
		1%	10%	90%	99%
2 waves of constant amplitudes and random relative phase	0	3.01	2.90	-13.10	-33.07
	-3	2.88	2.78	-9.87	-12.42
	-6	2.55	2.46	-6.23	-7.01
	-9	2.12	2.04	-3.97	-4.32
	-12	1.68	1.61	-2.59	-2.78
Nakagami-Rice	0	7.02	4.48	-7.53	-17.55
	-3	6.02	3.79	-6.28	-15.49
	-6	4.91	3.03	-4.57	-11.10
	-9	3.86	2.33	-3.17	-6.96
	-12	2.95	1.75	-2.18	-4.47
Rayleigh		8.22	5.21	-8.18	-18.39
Normal and log-normal		$2.326\sigma_x$	$1.282\sigma_x$	$-1.282\sigma_x$	$-2.326\sigma_x$

ARCHIVES U.I.T. GENÈVE

Frequently in radio propagation studies, the monthly median value of the signal-to-noise ratio is known, but the probability distribution of the instantaneous value is required. The median values of signal strength, expressed in decibels, for a specified time interval (e.g. 1 h) on a series of days are normally distributed, with a standard deviation of σ dB. That is, these median values are log-normal. If the distribution of the instantaneous values about the median value during each individual time interval is Rayleigh, then the total probability distributions for all the periods can be obtained from these two distributions [Spaulding, 1982]. Figure 2 [Picquenard, 1974] shows the level below which the signal falls for given percentages of the total time, for values of σ up to 20 dB. For sky-wave propagation with no interference, σ can be found from the equation for σ_{S+N} of Sailors *et al.* [1977]. For strong signal-to-noise conditions with interference present, the equation for σ_{S+N} from the same reference can be used for σ.

Spaulding [1982] has presented computational algorithms to determine the total amplitude fading distribution for a signal composed of one or more components, each of which has Rayleigh short-term fading and log-normal long-term fading of hourly median values.

Measurements in band 6 (MF) [Spaulding, 1982], tend to show that the hourly day-to-day median values of field strength, for a given night-time hour are log-normally distributed, but that the within-the-hour short-term fading can depart from the usually assumed Rayleigh distribution.

The properties of the sky-wave field-strength distribution in the LF and MF bands show that the log-normal and the Rayleigh distributions apply only in marginal cases and that the 30 min and 60 min recording intervals follow a different distribution law when performed over several years and during various seasons [Täumer and Sulanke, 1967 and 1968].

A review of information in CCIR and other publications and new analyses of available data carried out in the United Kingdom, give values of the decile deviations of signal field strength from the median values arising from within-the-hour variability. These results yield a lower decile deviation from the hourly median field strength of about 6 dB and an upper decile deviation of about 5 dB, indicating greater consistency with the log-normal distribution than with the Rayleigh or Nakagami-Rice distributions on average.

The fading distribution obtained by averaging individual experimental estimates over 2 - 3 minute periods, depends on the ray structure of the signal. As the number of rays increases, the distribution approaches Rayleigh. Also, as the observation time increases up to 30 minutes the Rayleigh distribution is approached [Sergeev, 1978b; Sergeev and Fiks, 1982].

During longer analysis intervals (30 to 60 min), the distribution seems to follow the log-normal law rather than Rayleigh. The fading range is often defined as the difference (in dB) between the signal levels exceeded for 10% and 90% of the time, and values of 13 ± 3.2 dB [Grosskopf, 1953] and 16.6 ± 3.2 dB [Konopleva, 1964] have been given for long-distance HF paths. The value does not appear to vary greatly with path length in the range 1500-6000 km, with time of day or with season [Konopleva, 1964]. For a shorter path (650 km) and a 10-minute analysis interval, a log-normal law with a fading range of about 11 dB has been reported [Gibson, 1989].

It is of interest to note that, although the form of the measured distributions may differ from the Rayleigh distribution, the observed fading range is of the same order as the value of 13.4 dB expected for the Rayleigh distribution. However, at high signal levels the fading range has been observed to fall below the Rayleigh value, possibly due to a strong constant component term arising from a specular reflection, and distributions of the Nakagami-Rice type will apply under these conditions. The deviations of the deciles of (2 to 10) minute medians from the hourly median were also studied in the USSR. For radio links operating at $f/\text{MUF} \leq 0.85$ these deviations are 5 to 7.5 dB at medium latitudes and 6.5 to 10 dB at northern latitudes [Kosikov, 1957; Khmelnitsky, 1975]. Studies have shown that the degree of fluctuation in the within-the-hour mean relative to the hourly median depends on the averaging period. For a 3000 km middle-latitude path, decile deviations from the mean hourly value of 6, 5 and 2 dB have been found for averaging times of 1, 2 and 15 min respectively [Malygin and Sergeev, 1982; Sergeev *et al.*, 1985].

Atmospheric noise data are given in Report 322. These are based on a global network of standardized measurements in which mean values were determined for a quarter-hour period each hour taken as representative of the hour in which they were made. The assumption inherent to the measurement programme is that excluding dawn/dusk transitions and local storm periods, in general there is no significant within-the-hour variation in the noise.

Information on man-made noise is given in Report 258. Mean noise power is quoted as a function of frequency for business, residential and rural environmental categories, together with the corresponding decile deviations from the hourly median field strength arising from within-the-hour variability at a fixed location. Upper decile values appropriate to HF are as given in Table II. Whereas the variability is somewhat less for rural areas at a frequency of 5 MHz, there is little difference among the other results. The median of all these values, which is also the median for residential areas, is 10.0 dB.

TABLE II – *Upper decile deviations from the hourly median field strengths for man-made noise (dB)*

Frequency (MHz)	Environmental category		
	Business	Residential	Rural
5	11.0	10.0	5.9
10	10.9	8.4	9.0
20	10.5	10.6	7.8

4.2 *Rapidity of fading*

The rapidity of fading can be characterized in different ways [McNicol, 1949; Ratcliffe, 1956; Price, 1957; Rice, 1958]. One description of fading which is useful for a number of purposes is given by the channel auto-correlation function in time or by the corresponding power spectrum.

With certain theoretical assumptions (normal distribution of the components of the velocities of the secondary radiators), a normal curve is to be expected for the auto-correlation function:

$$R(\tau) \approx R(0) \exp(-\tau^2/2\tau_0^2) \qquad (7)$$

where τ_0 is called the correlation (or coherence) time-constant of the fading channel. The corresponding power spectral density is proportional to $\exp(-\tau_0^2 f^2/2)$, a Gaussian shape with standard deviation of $1/\tau_0$. The latter is also known as the correlation (or coherence) bandwidth of the fading channel.

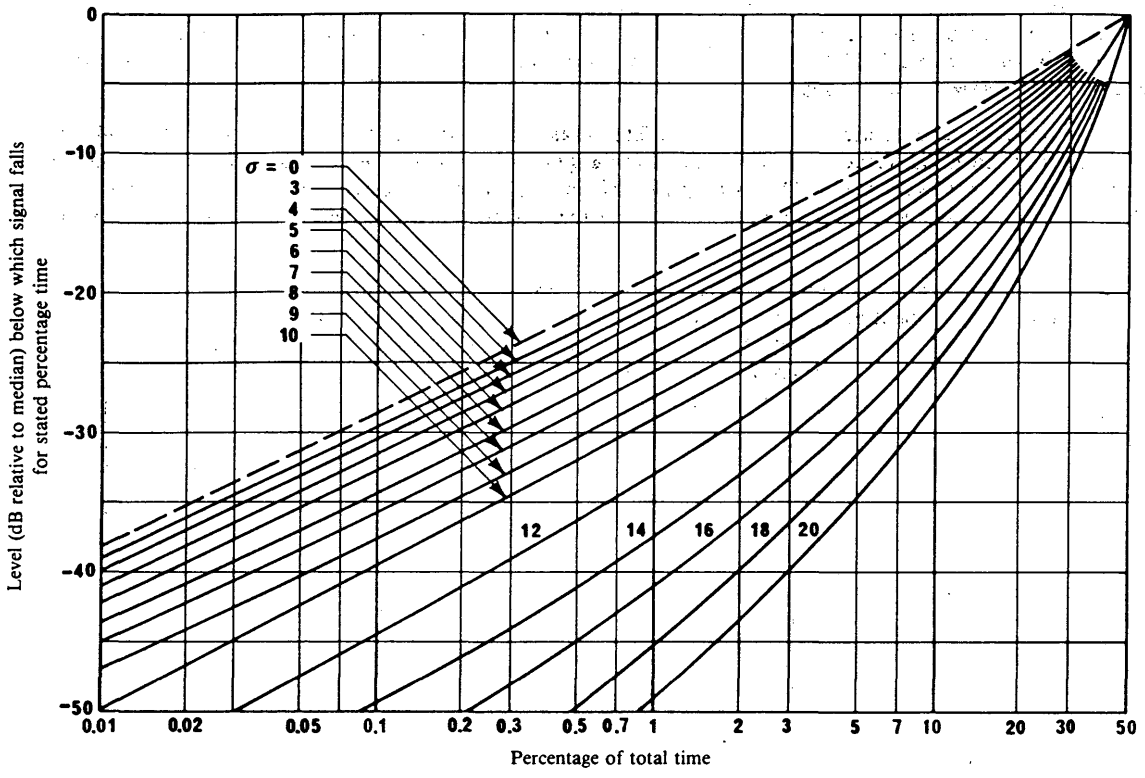


FIGURE 2 – *Level below which signal strength falls when instantaneous signal strength has a Rayleigh distribution but daily median values have a log-normal distribution, with standard deviation σ dB*

However, it is questionable whether the assumption for the velocity distribution of the secondary radiators is always justified. Therefore, the possibility of other velocity distribution functions should also be taken into consideration. These other velocity distributions can lead to other forms of the auto-correlation function as well as different Doppler spreads.

Other parameters have often been used for characterizing the rapidity of fading. There is, first of all, the fading rate defined as the number of positive crossings per unit time through any specified level.

When the signal fades according to equation (2), the fading rate through the level v is given by:

$$N(v) = (f_n v \sqrt{4\pi}/v_n) \exp[-(v_1^2 + v^2)/v_n^2] \, I_0 (2v_1 v/v_n^2) \tag{8}$$

where

f_n: r.m.s. frequency of fading obtained from:

$$f_n^2 = \frac{\int_0^\infty f^2 G(f)\, df}{\int_0^\infty G(f)\, df} = \frac{1}{4\pi^2 R(0)} \left.\frac{d^2 R(\tau)}{d\tau^2}\right|_{\tau = 0} \tag{9}$$

In equation (9), $R(\tau)$ is the autocorrelation function, $G(f)$ is the power spectrum of the fading process and f is measured from the mid-band frequency [Rice, 1948].

In the special case of the Rayleigh distribution, we can introduce the median value v_m obtaining [Rice, 1958]:

$$N(v) = 2.95 f_n (v/v_m) \exp(-0.693\, v^2/v_m^2) \quad (10)$$

where, if $v = v_m$, it follows that $N(v_m) = 1.47 f_n$. Results similar to these can be derived for various distributions of signal fading, such as the normal and log-normal distributions (equation (5)) or others. The main result is the proportionality of $N(v_m)$ to f_n.

Fading rates through the field-strength level exceeded for 90% of the time, were measured in the Federal Republic of Germany by recording on station WWV (15 MHz). The fading rates varied between 6 and 16 per min, the mean value being 11.25 per minute.

The rapidity of signal interference fading depends on the characteristics of the propagation modes which are determined to a large extent by the ratio of the working frequency to the maximum usable frequency [Sergeev, 1974, 1975; Malygin *et al.*, 1982]. Experimental data for middle-latitude paths of ranges up to 3000 km lead to values of the fading correlation time constant τ_0 of 2 to 18 s depending on working frequency and season [CCIR, 1982-86a]. The smaller figures are associated with times when there are multiple ray paths (for example, magneto-ionic splitting or with the Pedersen ray present). For multi-hop paths up to 6000 km range with complex ray structures, τ_0 = 3 to 4 s, with no dependence on working frequency.

On a certain proportion of days, HF paths in the tropics may show much more rapid fading than paths confined to higher latitudes [Osborne, 1952; Yeh and Villard, 1958; Bennington, 1960; Koster, 1963]. This phenomenon is associated with equatorial F-scattering and usually occurs, starting about 2000 h local time, for some two to four hours. It is likely to affect transmission paths with a reflection point in the F-region between magnetic latitudes ± 15°. Seasonal and sunspot-cycle variations occur, but may differ in nature with the path orientation. Long-distance paths appear to be affected more at the equinoxes and at sunspot maximum [Humby, 1959]. Besides increased fading rates, brief frequency changes of 20 to 30 Hz have been reported and there is a possibility that a lower frequency may be affected, but not a higher frequency [Davies and Barghausen, 1964]. More data are needed before a more exact account of the various fading characteristics can be given.

5. Long-period variations

In the case of long-period variations, the random component is usually analysed by taking hourly median values and evaluating the amplitude distribution over a long period. For simplicity, a log-normal distribution of the long-period variations is usually assumed, and often gives a good approximation to the actual distribution. A very full analysis, carried out in the Federal Republic of Germany [Grosskopf, 1953; 1955a and b] on long-period variations, showed that distribution curves for a sun-rotation period were closely log-normal for 50% of the 28 rotation periods examined; 25% could be split into two log-normal distributions, each valid over a different range of field strengths. The remainder could only be described in terms of the log-normal distribution if split up into more than two ranges.

Results for the spread of long-term variations have been analysed in a number of countries. Expressed in terms of the standard deviation σ_x of the log-normal distribution (equation (5)), the analyses mentioned above gave an average result of 8 dB, with some indication of greater values at night than in the daytime. USSR experiments at HF over paths of 1500, 3000 and 6000 km, for all seasons and times of day, have given values within the range 5 to 10 dB [Konopleva, 1964]. Any systematic change with season or between day and night appears relatively small. Results obtained in the United Kingdom for Accra-United Kingdom, Bombay-United Kingdom and Colombo-United Kingdom paths showed values in the range 5.5 to 7 dB. In certain regions, higher values may be obtained, e.g. a value of 10 dB or more may be found for paths crossing polar areas with high absorption.

Analyses of Bradley and Vernon [1982] based on theoretical studies and examination of measured data, suggest that latitudinal variability of the decile deviations exceeds the dependence on frequency. Different data are shown to be inconsistent, with some measurements giving a reduction in decile deviations with increase of frequency whilst others give an increase.

Studies of long-term fading have been undertaken in the USSR [Khmelnitsky, 1970a, 1975; Bogdanov and Segal, 1967; Blagoveschensky, 1981] for radio links operating at frequencies not too close to the MUF (up to 0.85) at medium and northern latitudes. At middle latitudes the deviations of deciles are equal to 4 to 5 dB over paths less than 3000 km and 6.5 to 10 dB over paths greater than 3000 km. At northern latitudes the deviations of deciles are 7.5 to 12 dB and 12.5 to 15 dB, respectively.

Other studies carried out on paths at medium and low latitudes have shown that the highest standard deviation σ is observed at frequencies close to the MUF (up to 12 - 15 dB). During the winter period an increase is found at the lower values of MUF at distances of 4,000 - 5,000 km; the standard deviation is variable, ranging from about 1 - 15 dB. On paths of length less than 3,700 km and for values of f/MUF from 0.3 to 0.85, $\bar{\sigma}$ = 3.4 dB; for values of f/MUF from 0.85 to 1.15, $\bar{\sigma}$ = 5.2 dB; for distances of 3,700 - 7,500 km and for values of f/MUF from 0.3 to 0.85, $\bar{\sigma}$ = 4.8 dB [CCIR, 1986-90b].

The results of HF field strength measurements in China during 1983 and 1984 on five paths (with distances from 1,000 to 7,000 km, frequencies 5 to 15 MHz) show that the average value of the monthly standard deviations of long-term fading (day-to-day fluctuations) is 4.4 dB [CCIR, 1986-90c].

In the USSR, a method has been developed for the calculation of the amplitude distributions of slow fades and their characteristics taking into account the fluctuations in MUF [Chernov, 1989]. An analytical expression has been obtained for the density distribution, which may have from one to three maxima depending on the real parameters of the MUF fluctuations and the fluctuations in signal levels in conditions when the MUF is far from the operating frequency.

A study was undertaken in the Federal Republic of Germany, ——— based on about 40 000 hourly monthly medians and their decile deviations of HF signal strength measurements. These include both single-hop and multi-hop paths covering all latitudes [CCIR, 1982-86b]. Long-term fading does not appear to vary greatly with path length, with time of day, with season, or with sunspot number. There is, however, a significant dependence on the ratio of the wave frequency to the monthly median basic MUF.

The Supplement to Report 252 provides representative values of the lower and upper decile deviations from the monthly median signal field strength arising from day-to-day changes. Figures have been determined from measured data and are quoted separately for path ranges less than and greater than 2500 km, as a function of midpath local time, season and midpath geomagnetic latitude. Information about long-period variations in the LF and MF bands is contained in Report 432.

Report 322 gives values of the corresponding decile deviations of atmospheric noise power as a function of frequency, season and local time.

No information is currently available on the day-to-day variability of man-made noise, but some changes might be expected with patterns of activity, e.g. reduced noise on rest days.

6. Fading allowances for service planning

A service planning method which makes use of a compatibility analysis will require:

- comparison of the strength of wanted signals with noise to establish whether a desired reception quality is achieved in the absence of interference; and
- comparison with co-channel and adjacent-channel interfering signals to determine if these are harmful.

Monthly median estimates need augmentation with appropriate fading allowances. These have to be considered separately depending on whether the background is atmospheric noise, man-made noise or an interfering signal, but in each case they depend on:

- the within-the-hour and day-to-day fading of the wanted signal;
- the within-the-hour and day-to-day fading of the background;
- the correlation between the wanted signal and background strengths; and
- the fraction of the time for which the desired reception quality must be achieved.

With the monthly median wanted signal/background for satisfactory reception given, it is convenient firstly to evaluate the enhancement or fading allowance $F_{b,90}$ necessary to achieve the desired reception quality for 90% of the time in the presence of within-the-hour and day-to-day fading of both the signals and background. Fading allowances for other percentages of the time may then be expressed in terms of $F_{b,90}$.

On the assumption that both the within-the-hour and day-to-day fading of the wanted signals and the background are uncorrelated, $F_{b,90}$ may be approximated [CCIR, 1982-86c] by:

$$F_{b,90} = \sqrt{S_{wh}^2 + S_{dd}^2 + B_h^2 + B_d^2} \quad \text{dB} \qquad (11)$$

where:

S_{wh}: wanted signal lower decile deviation from the hourly median field strength arising from within-the-hour changes (dB);

S_{dd}: wanted signal lower decile deviation from the monthly median field strength arising from day-to-day changes (dB);

B_h: background upper decile deviation from the hourly median field strength arising from within-the-hour changes (dB);

B_d: background upper decile deviation from the monthly median field strength arising from day-to-day changes (dB).

The First Session of the World Administrative Radio Conference for the Planning of HF Bands Allocated to the Broadcasting Service (WARC HFBC (1)) Geneva, 1984, adopted for short term signal fading the upper decile deviation of 5 dB and the lower decile deviation of −8 dB. For long-term signal fading the decile deviations were taken as a function of the ratio of operating frequency to the basic MUF as given in Table III.

TABLE III – *90% and 10% deviations from the predicted monthly median value of signal field strength (dB), arising from day-to-day variability*

Corrected geomagnetic latitude (1)	< 60°		≥ 60°	
Transmitting frequency/predicted basic MUF	90%	10%	90%	10%
≤ 0.8	−8	6	−11	9
1.0	−12	8	−16	11
1.2	−13	12	−17	12
1.4	−10	13	−13	13
1.6	−8	12	−11	12
1.8	−8	9	−11	9
2.0	−8	9	−11	9
3.0	−7	8	−9	8
4.0	−6	7	−8	7
≥ 5.0	−5	7	−7	7

(1) If any point on that part of the great circle which passes through the transmitter and the receiver and which lies between control points located 1000 km from each end of the path, reaches a corrected geomagnetic latitude of 60° or more, the values for ≥ 60° have to be used.

In principle, fading allowances should also take account of fading rate which can affect reception quality, but data to permit this are not yet available. The fading allowance $F_{b,x}$ for x% of time is conveniently given in terms of $F_{b,90}$ by:

$$F_{b,x} = c \cdot F_{b,90} \qquad \text{dB} \qquad (12)$$

Values of c for x in the range 50% to 90% for a log-normal distribution of signal/background ratio, a Rayleigh distribution and intermediate composite distributions, are very similar, approximating to the values of Table IV.

TABLE IV – *The parameter c*

x (%)	c
50	0
60	0.18
70	0.36
80	0.63
90	1

7. Correlation of signals in space, time, frequency and polarization

The study of correlation between two received signals as a function of their separation in position, time, frequency or polarization can provide useful information for the design of a communication system in the presence of fading.

An alternative [Stein, 1966] to the use of increased transmitter power, etc., is the utilization of techniques of modulation and reception which are less vulnerable to fading. Most widely known are multiple-receiver combining techniques classified as diversity reception. Depending upon the mechanism of the propagation, there are a variety of ways for obtaining signals for which the periods of fading occur independently of one another, such as:

- space (spaced antenna) diversity,
- frequency diversity,
- angle-of-arrival diversity,
- polarization diversity,
- time (signal repetition) diversity,
- multipath diversity (Rake).

Of these, the last two have been considered primarily for digital transmission.

It is not within the scope of this Report to discuss the details of channel characterization and diversity methods. It can be remarked, however, that most diversity analyses have been based upon slow, non-selective fading. However, in recent years, increasing attention has been directed to fast, non-selective types of fading. Very useful data on multipath ionospheric propagation have been obtained by Balser and Smith [1962] using oblique-incidence pulse sounders, which have pulse lengths of the order of 10 to 100 microseconds.

From typical data, it is deduced that any attempt to transmit serial digital streams over long distances via the ionosphere, at a rate exceeding 100 to 200 pulse/second, without specific anti-multipath measures, will tend to result in a severe intersymbol interference problem [Stein, 1966].

Operators attempt to minimize undesirable multipath effects by using frequencies near the MUF. Another approach has been the use of highly directive automatically adjustable antenna arrays, such as the MUSA [Polkinghorn, 1940], which discriminate against certain multiple-hop paths in favour of others.

For characterizing the degree of approximation to slow non-selective fading, the *spread factor* is a useful parameter [Stein, 1966]. For information pulse length T, fading is essentially non-selective if the multipath spread T_M satisfies

$$T_M \ll T \tag{13}$$

Similarly, if the Doppler spread (the width of the received power spectrum with an unmodulated carrier) is B_D, the requirement for essentially slow fading is

$$T \ll 1/B_D \tag{14}$$

Then, to approximate slow non-selective fading, T should satisfy both equations (13) and (14), and, therefore, the spread factor L, where

$$L = B_D T_M \tag{15}$$

is required to be

$$L \ll 1 \tag{16}$$

7.1 *Diversity reception*

Considering now diversity, Stein [1966] lists among the common linear methods (which are applicable both to digital and to distortionless reception of analogue transmission):

- combination of selected signals,
- combination of signals having the maximum ratio of strengths,
- combination of signals on an equal gain basis.

Stein also discusses more sophisticated methods: decision-oriented diversity for digital transmission, in which signal fidelity is abandoned as an irrelevance, and instead minimum error-rate is established as the sole goal.

It should be mentioned that limited tests in the United Kingdom of space-diversity reception of single-sideband telephone transmission indicated only a small advantage under the conditions of the test. The correlation bandwidth was too low; the "instantaneous" amplitude of the reduced carrier was a poor indicator of the speech-band transmission. On the contrary, diversity is very effective with double-sideband amplitude-modulated telephony (carrier transmitted), and on typical telegraph signals.

Normally in ionospheric propagation, the single most important limitation is multipath spread T_M. A bandwidth, Δf, may be defined in terms of the reciprocal of T_M:

$$\Delta f = 1/T_M$$

which is similar to "coherence bandwidth", "flat-fading bandwidth" or "selective-fading bandwidth" [Stein and Jones, 1967]. Multipath spread in ionospheric propagation stems from:

- O- and X-ray transit-time differences,
- high and low ray transit-time differences,
- multi-mode transit-time differences,
- irregularity (spread F, etc.) transit-time differences,
- pulse broadening in normal reflection due to dispersion.

Pickering [1975] calculated both multipath and Doppler spread for the HF ionospheric channel. The results of these calculations led to the generation of the "Doppler reduction factor" which is comparable to the "multipath reduction factor" of Bailey [1959] and of Salaman [1962] and can be used to determine the appropriate operating frequency on a given HF link.

Early investigations of space-, polarization- and frequency-diversity were carried out prior to 1940. However, the mathematical techniques for the investigation of the theoretical and empirical aspects of diversity reception have largely been developed since 1947 [Briggs *et al.*, 1950; Booker *et al.*, 1950; Glazer and Farber, 1953; Ratcliffe, 1956].

Based upon a simple, though not completely satisfactory, model of scattering from an inhomogeneous and time-varying ionosphere, a spatial correlation function $\rho(d)$, normalized to unity at $d = 0$, may be derived to show the dependence of CW signals at two antennas spaced at a distance d [Bramley, 1951, Grisdale *et al.*, 1957; Brennan, 1960; Khmelnitsky, 1960] viz.:

$$\rho(d) = \exp[-d^2/2\,x^2] \tag{17}$$

The parameter x is a function of the structure size of the ionospheric inhomogeneities, of the path length, and the frequency. At a separation $d = x$, the correlation is 0.61 and at $d = x\sqrt{2}$, it is 0.37. At even the shorter of these distances, experience and theory have shown that, for all practical purposes, substantially all the benefits of diversity have been obtained. For example, with two independently fading signals ($\rho = 0$), the diversity improvement was 14 to 15 dB at 99.9% reliability level. For $\rho = 0.61$, the diversity improvement was 13 dB. For this reason, it appears justifiable to identify the distance $d = x\sqrt{2}$ as the "diversity separation distance" or "correlation distance".

In the United Kingdom, tests made in the frequency range 6 to 18 MHz over distances of 2000 to 17 000 km indicate that the structure size, x, was between 150 and 400 m, implying diversity separation distances of 210 to 560 m (10 to 25 λ). These findings were confirmed by recordings made in the Federal Republic of Germany on station WWV (15 MHz). In addition, it was shown that the separation distances required, when specular reflection at the ionosphere is predominant, are much greater than when a substantial random component is present.

In other United States measurements below HF, the average correlation distance at 540 kHz was 29.4 $\lambda \pm$ 17.1 λ [Brennan and Phillips, 1957], while at 85 kHz [Bowhill, 1957], two distinct fading periods were observed, one of 7 min and one of 1.5 min. The correlation distance was determined to be 5 km for 7 min fading and 1 km for the 1.5 min fading.

Polarization diversity in the frequency range 6 to 18 MHz was studied in the United States of America and the United Kingdom. The antennas were at the same location, but arranged to respond to waves with mutually perpendicular polarization. The result was that the diversity action was about the same as that obtained with an equivalent space separation of 240 to 480 m [Grisdale *et al.*, 1957].

Experiments in Australia and New Guinea with nearly-vertical incidence broadcasting in the MF and HF bands have indicated that a polarization-diversity system would significantly reduce fading and distortion.

7.2 *Frequency correlation*

For the transmission of information, a band of frequencies is always required. It can be shown that, for analysis, it suffices to understand what happens to a pair of spaced tones transmitted simultaneously [Stein, 1966]. In practice, with sufficient tone spacing, the cross-correlation of the fading fluctuations at the two tone frequencies decreases toward zero. The lack of correlation in the fading of spaced tones is called *selective fading*.

An early investigation of selective fading by the use of multi-tone signals on a transoceanic path was reported in the classic paper by Potter [1930]. Other work was accomplished in the 1950's [Briggs, 1951; Price and Green, 1958].

The correlation frequency constant (correlation radius) of selective fading is generally in inverse proportion to the maximum delay between multipath rays. On middle-latitude paths up to 3000 km, the fading correlation frequency constant is between 250 and 7500 Hz depending on the ratio of wave frequency to basic MUF, reaching a maximum when that ratio is in the range 0.6 to 0.8 [Malygin and Sergeev, 1984]. However, for a 650 km path the correlation coefficient is typically 0.67 for frequency separations up to 10 kHz [Gibson, 1989].

Other studies have been carried out in China (1983 and 1984) on five paths. Analysis of the long-term fading of field strengths of different frequencies ($\Delta f \geq 900$ kHz) transmitting simultaneously shows that the average value of the correlation coefficients is 10%, with 18.4% for the same paths and 3.1% for different paths, with standard deviations of 35.1, 36.7 and 32.5% respectively. The statistical test shows that fading for different paths may be considered as being basically uncorrelated, while for the same paths there exists some correlation [CCIR, 1986-1990c].

7.3 Correlations pertinent to fading allowances for service planning

There is a need to improve the approximate expression (11) for the fading allowance $F_{b,\,90}$ to take into account correlation between the wanted signal and background strengths. Information is needed for the day-to-day fading; also data relating to the correlation of signals and noise are required. Day-to-day signal fading is probably correlated over larger separations, both spatially and in frequency, than within-an-hour fading. Preliminary measurements [Gibson, 1989] indicate a high correlation coefficient (> 99.9%) for day-to-day variations at frequencies separated by up to 10 kHz, but have not yielded significant correlation for receiving sites separated by 20-100 km.

7.4 *Signal characteristics pertinent to coding*

For modern digital communications applications, diversity schemes are invariably employed in conjunction with coding of the signals. The basic form of coding is the forward-error-correction coding, or FEC coding [Wu 1971; Diffie and Hellman 1976; Fang 1975]. For FEC coding, several common assumptions about the ionospheric channel characteristics are made. The received signal is usually modelled as having an additive white Gaussian noise (AWGN) component, a shallow, instantaneous fade (< 4 dB) and an occasional deep fade (> 4 dB).

Several parameters are of primary importance: the number of bits in deep fade duration, n_1, and the number of bits in instantaneous fade duration, n_2, both of which are related to channel data rate and the dynamics of the ionosphere. The FEC coding/time diversity techniques for this type of channel basically fall into two categories. In the first category, interleavers are used to disperse the bits transmitted during a deep fade so that every bit error seems to be independent of others. An FEC code strong enough to correct most of these errors is then applied. In the second category, an FEC code which is strong enough to correct most of the errors in the time duration without a deep fade is used to ensure a satisfactory channel during the fade-free period. Further details are given by Wu [1971], Diffie and Hellman [1976], and Fang [1975].

8. Characterization of channels for modulated signals

There has been a rigorous mathematical development of theory which encompasses the characterization of channels as time-varying filters [Zadeh and Desoer, 1963]. Such an empirical development for characterization of radio channels requires a more complete identification of the total radio environment than has been possible with the limitations in the design of propagation experiments carried out so far. Although much of the theoretical background has been developed by a number of investigators [Green, 1963; Bello, 1963 and 1964], much remains to be done.

Others have contributed to this field [Turin, 1956; Brennan, 1959; Barrow, 1963; Staras, 1956; Pierce and Stein, 1960; Wozencraft, 1961; Baghdady, 1961; Bello and Nelin, 1963].

A number of models have been used for channel characterization and Report 549 deals in detail with HF ionospheric simulators. Watterson *et al.* [1970] describe one model and its experimental confirmation. Their paper also included a comprehensive list of references. The abstract of their paper is reproduced here, as an example of work on this subject:

"Specially designed HF ionospheric propagation measurements were made and analysed to confirm the validity and bandwidth limitations of a proposed stationary HF ionospheric channel model. In the model, the input (transmitted) signal feeds an ideal delay line and is delivered at several taps with adjustable delays, one for each resolvable ionospheric modal component. Each delayed signal is modulated in amplitude and phase by a gain function for each baseband tap and the delayed and modulated signals are summed (with additive noise) to form the output (received) signal. Statistical specifications for the tap-gain functions involved three hypotheses: (1) that each tap-gain function is a complex-Gaussian process that produces Rayleigh fading, (2) that the tap-gain functions are independent, and (3) that each tap-gain function has a spectrum that in general is the sum of two Gaussian functions of frequency, one for each magneto-ionic component. Statistical tests were performed on day-time and night-time measurements confirming the validity of the three hypotheses, and thereby the validity of the model. For practical applications, the model can be considered valid over a bandwidth equal to about one fourth of the reciprocal of the effective (weighted) time spreads on the ionospheric modal components. The model should be useful both in theoretical analyses of communication system performance and for channel simulator designs."

Another approach has been made by considering propagation path models which makes more precise the quantitative assessment of the possibilities for information transmission [Konopleva and Khmelnitsky, 1970; 1972]. The accuracy of this method of assessment and the possibility of basing the calculations on real channel characteristics, with regard to the variation in both wanted signal [Khmelnitsky, 1970b] and unwanted signal [Khmelnitsky, 1969] parameters should be verified using circuits of various orientations and lengths.

In Spain, measurements made of the impulse response of an HF channel [CCIR, 1982-86d] have led to the conclusion that this approach is valid for characterizing these types of channels and could even be applied to the analysis of channels in other frequency bands.

9. Further studies desirable

Continued studies, along the lines of § 7 and 8 above, particularly as applied to ionospheric paths in various parts of the world, are desirable.

For example, among the physical causes of fading, it is felt that focusing and defocusing effects [Fok, 1950; Liakhova, 1965; Rawer, 1952; Kerblaï, 1963] merit more intensive study. Since these phenomena show considerable regularity, it may be that their description can be improved over that given by present random statistical models.

With regard to improving knowledge of the severity and rapidity of fading, different theoretical approaches to the important practical problem of longer-lasting fades and field increases associated with ionospheric irregularities are needed to supplement the random statistical theory approach. Auto-correlation methods should be helpful in studying phenomena which can be described as being between regular and random.

REFERENCES

BAGHDADY, E. J. [1961] *Lectures on Communication System Theory*. Chapters 5 and 6, McGraw-Hill, New York, NY, USA.

BAILEY, D. K. [1959] The effect of multipath distortion on the choice of operating frequencies for high-frequency communication circuits. *IRE Trans. Ant. Prop.*, Vol. AP-7, 397-405.

BALSER, M. and SMITH, W. B. [1962] Some statistical properties of pulsed oblique HF ionospheric transmissions. *NBS J. Res.*, Vol. 66D, **6**, 721-730.

BARROW, B. B. [1963] Diversity combination of fading signals of unequal mean strengths. *IEEE Trans. Comm. Systems*, Vol. CS-11, 73.

BELLO, P. A. [1963] Characterization of randomly time-variant linear channels. *IEEE Trans. Comm. Systems*, Vol. CS-11, 360-393.

BELLO, P. A. [1964] Measurement of the complex time-frequency channel correlation function. *NBS J. Res.*, Vol. 68D, 1161-1165.

BELLO, P. A. and NELIN, B. D. [1963] The effect of frequency selective fading on the binary error probabilities of incoherent and differentially coherent matched filter receivers. *IEEE Trans. Comm. Systems*, Vol. CS-11, 170.

BENNINGTON, T. W. [1960] Equatorial ionospheric effects. *Wireless World*, Vol. 66, **10**, 501-506.

BLAGOVESHCHENSKY, D. V. [1981] Rasprostronenie dekametrovykh radiovoln v vysokikh shirotakh (HF wave propagation at high latitudes), 180. Nauka Publishing House, Moscow, USSR.

BOGDANOV, S. E. and SEGAL, G. F. [1967] Statisticheskie svoistva srednikh znachenii napryazhonnosti poly a korotkovolnovykh signalov (Statistical characteristics of mean field strength values of short-wave signals). Collected papers of the NIIR, 3, (47).

BOOKER, H. G., RATCLIFFE, J. A. and SHINN, D. H. [1950] Diffraction from an irregular screen with applications to ionospheric problems. *Phil. Trans. Roy. Soc.* (London), Series A, **242**, 579.

BOWHILL, S. A. [1957] Ionospheric irregularities causing random fading of very low frequencies. *J. Atmos. Terr. Phys.*, **11**, 91-101.

BRADLEY, P. A. and VERNON, A. [1982] Decile deviations of HF daily signal strengths. IWP 6/1 Doc. 218.

BRAMLEY, E. N. [1951] Diversity effects in spaced-aerial reception of ionospheric waves. *Proc. IEE*, **98**, Part III, 19-25.

BRENNAN, D. G. [1959] Linear diversity combining techniques. *Proc. IRE*, Vol. 47, 1075-1102.

BRENNAN, D. G. [1960] The extrapolation and interpolation of spatial correlation functions. *Statistical Methods in Radio Wave Propagation*, 296-305. Ed. W. C. Hoffman, Pergamon Press, New York/Oxford.

BRENNAN, D. G. [1961] Probability theory in communication system engineering (Chapter 2); Analysis of long-term variability (Chapter 20). *Lectures on Communication System Theory.* Ed. E. Baghdady, McGraw-Hill, New York, NY, USA.

BRENNAN, D. G. and PHILLIPS, M. L. [1957] Phase and amplitude variability in medium frequency ionospheric transmission. Lincoln Lab., MIT, TR-93.

BRIGGS, B. H. [1951] An investigation of certain properties of the ionosphere by means of a rapid frequency change experiment. *Proc. Phys. Soc.*, Vol. 64B, Part 3, **375B**, 255-274.

BRIGGS, B. H., PHILLIPS, G. J. and SHINN, D. H. [1950] The analysis of observations on spaced receivers of the fading of radio signals. *Proc. Phys. Soc.*, Vol. 63B, Part 2, **362B**, 106-121.

CHERNOV, Yu. A. [1989] - Raspredelenie medlennykh zamiranii VCh signala vblizi MPCh. (Distribution of slow fades of HF signal near the MUF). Proceedings of NIIR, No. 2.

DAVIES, K. [1965] Ionospheric radio propagation. NBS Monograph No. 80.

DAVIES, K. and BARGHAUSEN, A. F. [1964] The effect of spread F on the propagation of radio waves near the equator. AGARD Ninth Meeting of the Ionospheric Research Committee, Copenhagen, Denmark.

DIFFIE, W. and HELLMAN, M.E. [1976] New directions in cryptography. *IEE Trans. Inf. Theory*, Vol. 22, 644-654.

DUMBRAVA, Z.F., GORSHKOVA, E.Z., KIYANOVSKY, M.P. and MASHKOVA, E.A. [1988] - Approksimatsiya empiricheskikh raspredelenii amplitudy — dekametrovogo signala. (Approximation of the empirical distribution of the HF signal amplitude.) Issledovaniya po geomagnetizmu, aeronomii i fizike solntsa, Moscow, Nauka, No. 80.

DYAKOV, A.V. and KIYANOVSKY, M.P. [1981] - Metodika alternativnoi otsenki prinadlezhnosti statisticheskoi vyborki k konkretnym zakonam raspredeleniya. (Alternative evaluation of statistical selection as a specific distribution law.) Issledovaniya po geomagnetizmu, aeronomii i fizike solntsa, Moscow, Nauka, No. 55.

FANG, R. J. [1975] DIVEC, a combined diversity and error control scheme. *COMSAT Tech. Rev.*, Vol. 5, 105-133.

FOK, V. A. [1950] Obochtchenie otrajatelnykh formul na slutchaï otrajeniia proïzvolnoï volny ot poverkhosti proïzvolnoï formy (Generalization of reflection formulae for the case of the reflection of an arbitrary wave by a surface of arbitrary shape). *Journ. Eksp. Teoret. Fisiki*, **20**, 961.

GIBSON, A.J. [1989] - Measurements of fading on HF communication links. Proc. 6th Intl. Conf. on Antennas and Propagation (ICAP 89), IEE Conf. Pub. No. 301 (Part 2) 23-30.

GLAZER, J. and FARBER, L. [1953] Evaluation of polarization diversity performance. *Proc. IRE*, Vol. 41, 1774-1778.

GORSHKOVA, E.Z., DUMBRAVA, Z.F., DYAKOV, A.V., KIYANOVSKY, M.P. and PISAREVA, L.Y. [1985] - Alternativnaya otsenka prinadlezhnosti empiricheskikh raspredelenii k konkretnym teoreticheskim zakonam. (Alternative evaluation of empirical distributions as specific theoretical laws.) Issledovaniya po geomagnetizmu aeronomii i fizike solntsa, Moscow, Nauka, No. 73.

GREEN, P. E. Jr. [1963] Time-varying channels with delay spread. *Monograph on Radio Waves and Circuits*. Ed. S. Silver, Elsevier, London, UK.

GRISDALE, G. L., MORRIS, J. G. and PALMER, D. S. [1957] Fading of long-distance radio signals and a comparison of space- and polarization-diversity reception in the 6-18 Mc/s range. *Proc. IEE*, Vol. 104B, **13**, 39-51.

GROSSKOPF, J. [1953] Statistical studies of short-wave transmission paths. *NTZ*, **6**, 373-378.

GROSSKOPF, J. [1955a] Feldstärkemessungen im Kurzwellenbereich, I. Teil (Field-strength measurements in the short-wave band, Part I). *NTZ*, **8**, 114.

GROSSKOPF, J. [1955b] Feldstärkemessungen im Kurzwellenbereich, II. Teil (Field-strength measurements in the short-wave band, Part II). *NTZ*, **8**, 146.

HUMBY, A. M. [1959] Equatorial sunset effect. *Wireless World*, Vol. 65, **7/8**, 343-345.

KERBLAÏ, T. S. [1963] Vliianiа gorizontalnykh gradientov elektronnoï kontsentratsii v ionosphere na velitchinou MPTCH (Influence of horizontal electron-concentration gradients on the value of the MUF). *Geomag. i Aeron.*, Vol. 3, 772.

KERBLAÏ, T. S., NOSOVA, G. N., ALLABERDIEV, D. and POROSNAYA, A. P. [1974] O kharactere zamiranii signala pri razlichnikh sposobakh rasprostranenia radiovoln (On the characteristics of the signal fading depending on propagation mode). *Geomag. i Aeronom.*, Vol. 14, **6**, 1024.

KERBLAÏ, T. S., NOSOVA, G. N., MINULLIN, R. G. and KURGANOV, R. A. [1977] Periodi fluktuatsii signalov obuslovlennikh ionosfernim rasseianiem i otrageniem ot sloia Es na chastotakh 27.8 i 40.3 MHz (Fluctuation periods of the signal, caused by ionospheric scattering and reflection from Es layer at frequencies 27.8 and 40.3 MHz). *Geomag. i Aeronom.*, Vol. 17, **2**, 231.

KHMELNITSKY, E. A. [1960] *Raznessennyi priem i opredelenie ego effektivnosti* (Diversity reception and assessment of its effectiveness). Sviazizdat, Moscow, USSR.

KHMELNITSKY, E. A. [1969] Veroyatnost sboya na kv liniyakh svyazi pri pomekhakh ot sosednikh po chastote stantsii (Probability of error on short-wave circuits due to interference from stations operating on adjacent frequencies). *Elektrosviaz*, **4**, 22-30.

KHMELNITSKY, E. A. [1970a] Sravnenine eksperimentalnykh i raschotnykh znachenii urovnya signala v KV diapazone (Comparison between experimental and calculated values of signal levels in the short-wave range). *Elektrosviaz*, **6**, 45-51.

KHMELNITSKY, E. A. [1970b] Otsenka kachestva kv kanala svyazi dlya peredachi diskretnykh signalov (Assessment of the quality of a short-wave channel for discrete signal transmission). *Elektrosviaz*, **10**, 18-32.

KHMELNITSKY, E. A. [1975] Otsenka realnoi pomekhozashchisshchennosti priyema signalov v KV diapazone (Evaluation of real protection against interference of signal reception in the short-wave range). Sviaz, Moscow, USSR.

KONOPLEVA, E. N. [1964] Reliability of communications and necessary signal/noise ratio in short-wave radio channels (in Russian). *Elektrosviaz*, **5**, 3-8.

KONOPLEVA, E. N. and KHMELNITSKY, E. A. [1970] Vozmozhnye sostoyaniya kv kanala svyazi po usloviyam raspostraneniya radiovoln (Possible states of a short-wave channel depending on propagation conditions). *Elektrosviaz*, **12**, 19-24.

KONOPLEVA, E. N. and KHMELNITSKY, E. A. [1972] Modeli rasprostraneniya radiovoln na kv liniyakh svyazi neoptimalnoi protyazhennosti (Propagation models for short-wave circuits of non-optimum length). *Elektrosviaz*, **1**, 33-38.

KOSIKOV, K. M. [1957] Zamiranie signala (Signal fading). Collected papers of the NIIR, **2**(6), 42-45.

KOSTER, J. R. [1963] Some measurements on the sunset fading effect. *J. Geophys. Res.*, Vol. 68, 2571-2578.

LIAKHOVA, L. N. [1965] Otsenka effekta fokoussirovky pri rasprostranenii radiovoln po rikochetirouemoï traiektorii (Evaluation of the focusing effect in the propagation of radio-waves over ricochet paths). *Geomag. i Aeronom.*, Vol. 5, 351.

MALYGIN, V. B. and SERGEEV, O. I. [1982] Rezultaty eksperimentalnoi otsenki korrelyatsionnoi i spektralnoi funktsii ogibayushchei KV-signala (Results of experimental evaluation of the correlation and spectral functions of the short-wave signal envelope). *NIIR Proc.*, **2**.

MALYGIN, V. B. and SERGEEV, O. I. [1984] Otsenka intervalov chastotnoy korrelyatsii ogibayushchei KV-signala pri razlichnykh usloviyakh rasprostraneniya (Evaluation of frequency correlation intervals of short-wave signal envelope in various propagation conditions) *Radiotekhnika*, **10**.

MALYGIN, V. B., SERGEEV, O. I. and CHERNOV, Yu. A. [1982] Otsenka mnogoluchevosti KV-signala po rezultatam impulsnogo naklonnogo zondirovaniya (Evaluation of multipath characteristics of short-wave signals from the results of impulsive oblique sounding). *Radiotekhnika*, Vol. 37, **5**.

McNICOL, R. W. E. [1949] The fading of radio waves of medium and high frequencies. *Proc. IEE*, Part III, **96**, 517-524.

NAKAGAMI, M. [1943] Statistical character of short-wave fading. *J. Inst. Elec. Comm. Engrs. Japan*, **27**, 145.

NAKAGAMI, M. [1960] The m-distribution: a general formula of intensity distribution of rapid fading. *Statistical Methods in Radio Wave Propagation*, 3-36. Ed. W. C. Hoffman, Pergamon Press, New York/Oxford.

NORTON, K. A., VOGLER, L. E., MANSFIELD, W. V. and SHORT, P. J. [1955] The probability distribution of the amplitude of a constant vector plus a Rayleigh distributed vector. *Proc. IRE*, Vol. 43, 1354-1361.

OSBORNE, B. W. [1952] Note on ionospheric conditions which may affect tropical broadcasting after sunset. *J. Brit. IRE Radio Engrs.*, **12**, 110.

PICKERING, L. W. [1975] The calculation of ionospheric Doppler spread on HF communication channels. *IEEE Trans. Comm.*, Vol. COM-23, 526-537.

PICQUENARD, A. [1974] *Radio Wave Propagation.* Halsted Press, John Wiley and Sons, New York, NY, USA.

PIERCE, J. N. and STEIN, S. [1960] Multiple diversity with non-independent fading. *Proc. IRE*, Vol. 48, **1**, 89-104.

POLKINGHORN, F. A. [1940] A single-sideband Musa receiving system for commercial operation on transatlantic radiotelephone circuits. *Proc. IRE*, Vol. 28, **4**, 157-170.

POTTER, R. K. [1930] Transmission characteristics of a short-wave telephone circuit. *Proc. IRE*, Vol. 18, 581-648.

PRICE, R. [1957] The autocorrelogram of a complete carrier wave received over the ionosphere at oblique incidence. *Proc. IRE*, Vol. 45, 879-880.

PRICE, R. and GREEN, P. E. [1958] A communication technique for multipath channels. *Proc. IRE*, Vol. 46, 555-570.

RATCLIFFE, J. A. [1956] Some aspects of diffraction theory and their application to the ionosphere. *Reports on Progress in Physics*, **19**, 188, Proc. Physical Society, London, UK.

RAWER, K. [1952] Calculation of sky-wave field strength. *Wireless Engineer*, Vol. 29, 287-301.

RICE, S. O. [1944, 1945] Mathematical analysis of random noise. *BSTJ*, Vol. XXIII, 282 and Vol. XXIV, 46.

RICE, S. O. [1948] Statistical properties of a sine wave plus random noise. *BSTJ*, Vol. XXVII, 109-157.

RICE, S. O. [1958] Distribution of the duration of fades in radio transmission: Gaussian noise model. *BSTJ*, Vol. XXXVII, **3**, 581-635.

RÖTTGER, J. [1973] Langperiodisches Fading von Kurzwellensignalen (Long-periodic fading of shortwave signals). *Kleinheubacher Berichte*, **16**, 167-178.

SAILORS, D. B., KUGEL, C. P. and HAYDON, G. W. [1977] Predicting the compatibility of high frequency sky-wave communication systems. *IEEE Trans. Electromag. Compt.*, Vol. EMC-19, 332-343.

SALAMAN, R. K. [1962] A new ionospheric multipath reduction factor (MRF). *IRE Trans. Comm. Systems*, Vol. CS-10, 220-221.

SERGEEV, O. I. [1974] Rezultaty eksperimentalnoi otsenki kharakteristik vybrosov KV-signala (Results of experimental evaluation of shortwave signal rapid-fading characteristics). *NIIR Proc.*, **2**.

SERGEEV, O. I. [1975] Rezultaty izmereniya skorosti interferentsionnykh zamiranii KV-signala pri razlichnykh usloviyakh rasprostraneniya (Measurement data on rapidity of shortwave signal interfering fades in different propagation conditions). *NIIR Proc.*, **1**.

SERGEEV, O.I. [1978a] - Resultaty teoreticheskogo issledovaniya raspredeleniya ogibayushchei interferentsionnykh zamirany KV signala (Results of theoretical studies of the distribution of the interference fading envelope of SW signals), Trudy NIIR,1.

SERGEEV, O.I. [1978b] - Eksperimentalnye otsenki raspredeleniya ogibayushchei KV signala (Experimental evaluations of the distribution of the SW signal envelope), Trudy NIIR, 4, pp. 13-18.

SERGEEV, O. I., DOTOLEV, V. G., ZHILTSOV, A. U., PELEVIN, Y. V. and CHERNOV, Y. A. [1985] K voprosu ob eksperimentalnoi otsenke srednego urovnya ogibayushchei KV-signala (Concerning the experimental evaluation of the mean shortwave signal envelope level). *NIIR Proc.*, **4**.

SERGEEV, O.I. and FIKS, Y.A. [1982] - Otsenka veroyatnosti oshibok v radiokanale s zamiraniyami pri ogranichennom intervale nablyudeniya (Estimating error probability in a radio channel subject to fading with a limited observation interval, Elektrosvyaz, 9.

SPAULDING, A. D. [June, 1982] Fading signals in the MF band. National Telecommunications and Information Administration Report 82-102. NTIS Accession No. PB 82-262916. National Technical Information Service, Springfield, VA 22161, USA.

STARAS, H. [1956] Diversity reception with correlated signals. *J. Appl. Phys.* (Lett.), Vol. 27, **1**, 93-94.

STEIN, S. [1966] Part III of *Communication Systems and Techniques*, by Schwartz, Bennett and Stein, McGraw-Hill, New York, NY, USA.

STEIN, S. and JONES, J. J. [1967] *Modern Communication Principles.* McGraw-Hill Book Co., New York/London.

TÄUMER, F. and SULANKE, H. [1967 and 1968] Die Eigenschaften von Häufigkeitsverteilungen der Raumwellenfeldstärke im Frequenzbereich von 150-1600 kHz (The properties of sky-wave field strength distribution in the bands 5 and 6). *Techn. Mitt. RFZ*, Vol. 11, **4**, 192-195 and Vol. 12, **1**, 32-39.

TURIN, G. L. [1956] Communication through noisy, random-multipath channels. *IRE Nat. Conv. Record*, Part 4, 154.

WATTERSON, C. C., JUROSHEK, J. R. and BENSEMA, W. D. [1970] Experimental confirmation of an HF channel model. *IEEE Trans. Comm. Tech.*, Vol. 18, 792-803.

WOZENCRAFT, J. M. [1961] Sequential reception of time-variant transmissions. Ch. 12. *Lectures on Communication Theory.* Ed. E. Baghdady, McGraw-Hill, New York, NY, USA.

WU, W. W. [1971] Applications of error-coding techniques to satellite communications. *COMSAT Tech. Rev.*, Vol. 1, 183-219.

YEH, K. C. and VILLARD, O. G. [1958] A new type of fading observable on high-frequency radio transmission propagated over paths crossing the magnetic equator. *Proc. IRE*, Vol. 46, 1968-1970.

ZADEH, L. A. and DESOER, C. A. [1963] *Linear System Theory.* McGraw-Hill, New York, NY, USA.

CCIR Documents

[1978-82]: 6/63 (USSR).

[1982-86]: **a.** 6/187 (USSR); **b.** Doc. 6/54 (Germany (Federal Republic of)); **c.** IWP 6/12 Doc. D14 (IWP 10/5 Doc. 58); **d.** 6/212 (Spain).

[1986-90]: a) 6/182 (Germany (Federal Republic of)); b) 6/37 (USSR); c) 6/237 (China).

REPORT 892-2*

COMPUTATION OF RELIABILITY FOR HF RADIO SYSTEMS

(Question 35/6)

(1982-1986-1990)

1. Introduction

The basic parameter given by most HF propagation prediction methods is the predicted signal power or field strength. However, as is pointed out, for example in Report 729 and in the Supplement to Report 252, signal-strength data are not sufficient to fully quantify the performance of a radio service.

A parameter of an HF radio system which may be used as a figure of merit is the predicted reliability. Reliability, in general, is defined as the probability that a specified performance will be achieved by the system. More specific definitions of the different types of reliability are given in Appendix I. A term related to reliability, circuit compatibility, is discussed in Report 657.

Predicted reliabilities are valuable in antenna-design optimization, selection of preferred combinations of frequencies, and necessary transmitter powers to achieve a desired performance. Hence accurate methods are required to estimate reliabilities and to apply these estimates in assessing radio system performance. This Report outlines the various computational methods in use. Almost all of these methods require assumptions or approximations since there are insufficient data available regarding correlation among the various modes which may simultaneously exist over a given circuit.

The reliabilities discussed in this Report form a hierarchy as illustrated in Figure 1. Mode reliability is discussed in § 3, circuit reliability in §§ 4 and 5, reception reliability in § 6 and service reliability in § 7. Path and communications reliabilities, which are relevant to HF networks, are discussed in § 9.

---

* This Report is brought to the attention of Study Groups 3, 8 and 10.

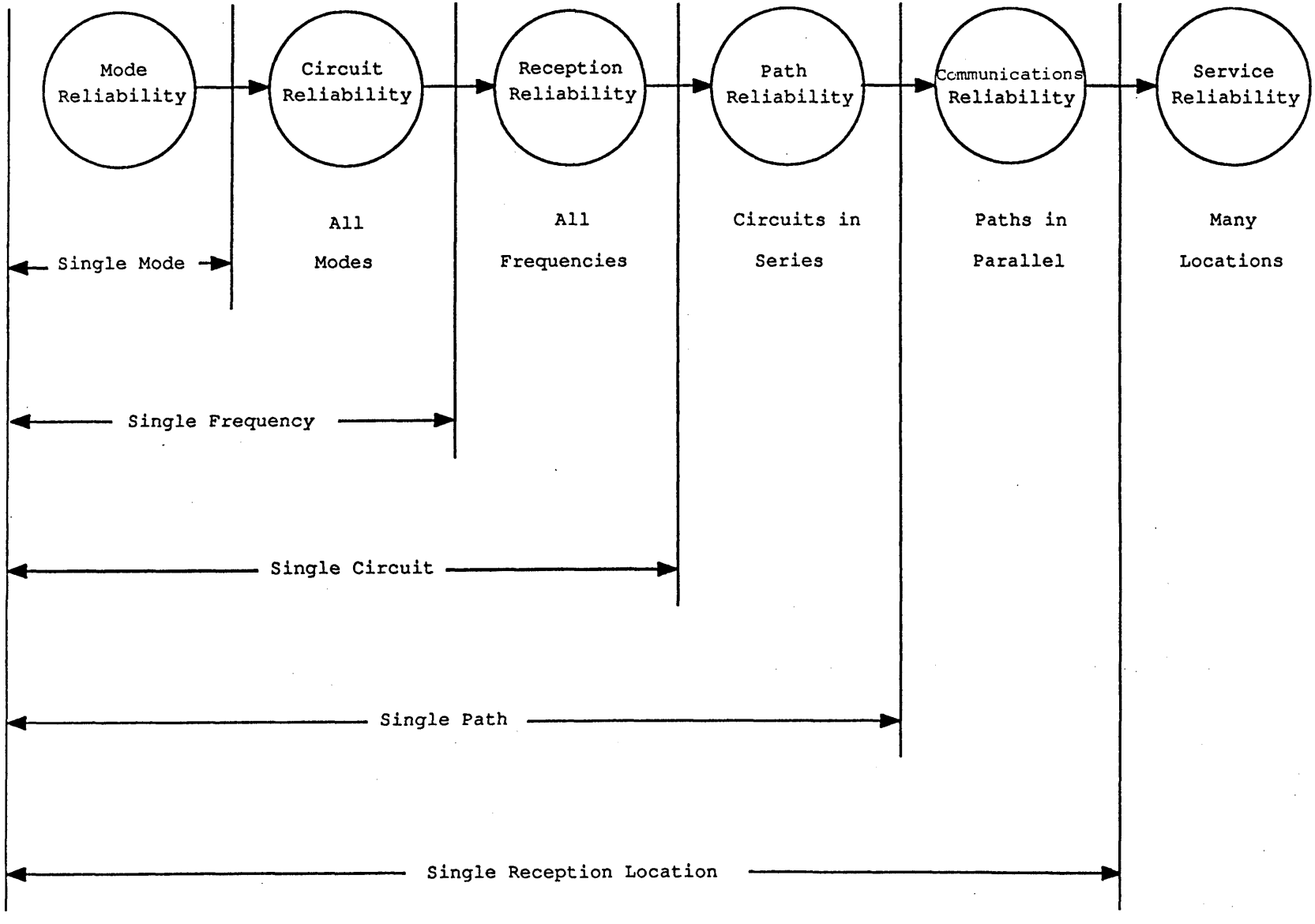


FIGURE 1 - Chart of reliabilities

2. Inputs to reliability computation

The computation of the various reliabilities requires the following inputs:

- estimates of received power for each mode at a given location or the total received power from the modes that are predicted to propagate at the specified hour for a given frequency. This power is expressed as the monthly median of the hourly medians. Methods to estimate this are contained in Report 252, the Supplement to Report 252 and Report 894;
- estimates of the received noise power at the given location for a given frequency and bandwidth expressed as monthly median of hourly medians. Estimation methods are given in Reports 322 and 258;
- estimates of the variability of signal and noise power. These are expressed as upper and lower decile deviation from the median values. Methods to estimate these are contained in Reports 266, 322 and 258;
- estimates of the signal-to-noise ratio required to provide specified performance. This required signal-to-noise ratio is the hourly median ratio taken under stable conditions. Recommendation 339 provides a tabulation of such required signal-to-noise ratios;
- estimates of the signal-to-interference ratio required to provide specified performance. This required signal-to-interference ratio is taken under stable conditions. Report 525 provides methods of obtaining the required signal-to-interference ratio.

3. Computation of basic mode reliability

Mode reliability, R_m, is defined in Appendix I. On the assumption that the probability of mode reflection is independent of signal strength:

$$R_m = q \cdot P_{S/N} \tag{1}$$

where q is the mode availability and $P_{S/N}$ is the conditional probability of equalling or exceeding the required signal-to-noise power, given that the mode exists. Equation (1) may be used to estimate R_m where $P_{S/N}$ is determined from a signal-strength prediction procedure giving the median field strength for a sample restricted to those cases when reflection is judged to occur (e.g. the method of Report 252). Alternatively where the signal prediction gives the median for the whole of the time of interest (e.g. the methods of Report 894 and the Supplement to Report 252):

$$R_m = P'_{S/N} \tag{2}$$

where $P'_{S/N}$ is the fraction of time that the signal-to-noise ratio exceeds the required value.

q is given in § 4.2 of the Supplement to Report 252. The equations of Bradley and Bedford [1976] may be applied to obtain $P_{S/N}$ in the following way:

- for $S/N \leqslant (S/N)_m$

$$P_{S/N} = 1.3 - \frac{0.8}{1 + \left(\dfrac{(S/N)_m - S/N}{G_l} \right)} \tag{3a}$$

When the value obtained is greater than 1, use the value 1.

- for $S/N > (S/N)_m$

$$P_{S/N} = \frac{0.8}{1 + \left(\dfrac{S/N - (S/N)_m}{G_u} \right)} - 0.3 \tag{3b}$$

When the value obtained is negative, use the value 0.

where:

S/N: required signal-to-noise ratio (dB); and

$(S/N)_m$: estimated monthly median signal-to-noise ratio (dB).

On the assumption that the signal and noise amplitude variations are uncorrelated:

$$G_u = \sqrt{S_{uh}^2 + S_{ud}^2 + N_{lh}^2 + N_{ld}^2} \quad \text{(dB)} \tag{4a}$$

and

$$G_l = \sqrt{S_{lh}^2 + S_{ld}^2 + N_{uh}^2 + N_{ud}^2} \quad \text{(dB)} \tag{4b}$$

with:

$S_{uh}(N_{uh})$: signal (noise) upper decile deviation from the hourly median field strength arising from within-the-hour variations (dB);

$S_{lh}(N_{lh})$: signal (noise) lower decile deviation from the hourly median field strength arising from within-the-hour variations (dB);

$S_{ud}(N_{ud})$: signal (noise) upper decile deviation from the monthly median field strength arising from day-to-day variations (dB);

$S_{ld}(N_{ld})$: signal (noise) lower decile deviation from the monthly median field strength arising from day-to-day variations (dB).

Calculations showing the dependence of mode reliability on frequency have been presented by Bradley and Lockwood [1982] for the case when signal transmission loss includes a term for "above-the-MUF" loss dependent on the ratio of the wave frequency to the mode basic MUF, and another term for the absorption loss in decibels inversely proportional to the square of frequency. The analysis provides a way of combining the effects of day-to-day changes in basic MUF affecting mode support with the day-to-day changes in the other loss terms. Bradley [1983] has shown that for frequencies above the monthly median basic MUF, mode support is the dominant factor controlling mode reliability.

Another approach to the computation of mode reliability is to compare the monthly median of hourly median signal level with the monthly median of hourly median noise to estimate the monthly median of hourly median S/N ratio. The day-to-day distribution of hourly median S/N ratios may be estimated by combining this median with the upper and lower deciles. This day-to-day distribution may be entered with any specified hourly median S/N ratio to obtain an estimate of the percentage of days within the months that this specified ratio is expected to be achieved or exceeded. This percentage may be assumed to equate to the probability that the specified hourly median S/N ratio may be achieved at a given time.

4. Computation of circuit reliability

An expression may be given [Liu and Bradley, 1985] for the general case of n possible modes, showing that circuit reliability depends on the extent of the correlation among both mode occurrences and mode strengths. The likelihood of three or more modes with comparable amplitudes, each mode contributing significantly to the circuit reliability, is considered to be low. In practice, a simplification of the general case to only two modes is considered. In this case, the expression becomes:

$$R_c = q_1 P_1 + q_2 P_2 + q_{12} P_{12} \tag{5}$$

where R_c is the circuit reliability, q_{12} is the probability that both modes 1 and 2 are simultaneously present and P_{12} is the probability that modes 1 and 2 together, when present, lead to the required signal-to-noise ratio being exceeded. The parameters q_1 and P_1 are the mode availability and mode performance achievement, respectively, when only mode 1 is present; q_2 and P_2 are the mode availability and mode performance achievement, respectively, when only mode 2 is present.

Simplified and approximate methods for calculating circuit reliability are listed below.

4.1 *Method 1 (HFMUFES)*

Barghausen *et al.* [1969] compute the circuit reliability as the product of the maximum value for each of P_r and $P_{S/N}$. The two values P_r and $P_{S/N}$ used in the computation do not need to be associated with the same mode of propagation.

4.2 *Method 2 (IONCAP)*

In the IONCAP [Teters *et al.*, 1983] prediction programme, the combined signal power for all modes is computed by summing the powers in each mode. This summation assumes that the signals propagated via different modes exhibit random phases with respect to each other. The signal-to-noise ratio is taken to have as its mean value the difference of the means for the signal and the noise, and as its variance the sum of the variances of the signal and the noise. The circuit reliability is calculated as the percentage of days within a month that the signal-to-noise ratio equals or exceeds that required. In this method no account is directly taken of the fraction of days when the modes are reflected by the ionosphere. The assumption inherent in this conveniently simple approach is that adopted values of day-to-day variations of signal power based on observed data automatically include allowances for ionospheric variability affecting mode support.

4.3 *Method 3*

In the method described by Chernov [1969], circuit reliability (versus noise and/or interference) is calculated assuming that the interference is significantly greater than the noise. The statistical laws of signal and interference distributions are taken into consideration as well as prediction uncertainties in estimates of the median power flux-densities of both the signal and interference. The mean value of circuit reliability $\bar{T}$ is given by:

$$\bar{T} = \frac{1}{\sqrt{2\pi}} \int_{-\infty}^{\gamma} e^{-\frac{x^2}{2}} \, dx \qquad (6)$$

where $$\gamma = \frac{E_s - \rho_b - \langle E_i \rangle}{\sqrt{\sigma_s^2 + \sigma_i^2 + \sigma_{\bar{s}}^2 + \sigma_{Ms}^2 + \sigma_{Mi}^2}}$$

and

σ^2_s, σ^2_i : variances of signal and interference levels caused by attenuation,

$\sigma^2_{\bar{s}}$, $\sigma^2_{\bar{I}}$: variances of monthly median values of signal and interference for the set of stations of the wanted network and the network of interfering stations,

σ^2_{Ms}, σ^2_{Mi} : error variances in the method of calculating monthly median signal and interference levels,

$\langle E_s \rangle$, $\langle E_i \rangle$: average median values of signal levels for the wanted network and interfering network set,

ρ_b: specified signal-to-interference ratio limit,

E_s: median value of signal level for the wanted circuit.

All the above values are expressed in decibels.

To evaluate the mean circuit reliability when the wanted network comprises several or many circuits, in the equation for γ, the value E_s is replaced by $\langle E_s \rangle$ and the term $\sigma^2_{\bar{s}}$ is added under the square root in the denominator.

4.4 *Method 4*

In this method, basic circuit reliability is calculated by averaging between two extremes, one of which is an under-estimate and the other of which is an over-estimate. The under-estimate is the reliability $P_r \cdot P_{S/N}$ of the single mode with the largest reliability, ignoring all other modes. The over-estimate is the assumption that all modes are statistically independent, so that the probability of successful communication by at least one mode is equal to one minus the product of the probabilities that each mode fails to provide communication. In the absence of adequate information concerning the correlation between modes, averaging these two estimates appears to provide a reasonable single estimate of basic circuit reliability.

4.5 *Method 5 (CRC)*

A method used with the CRC (Canadian) prediction system combines the modes being propagated in a different way [Petrie, 1981]. Based on the premise that reflection of a high order hop necessitates reflection of lower order hops, the probability density of signal power can be computed for various combination of modes. The mean signal power for each combination is determined by summing the appropriate individual powers. This summation assumes that the signals propagated via different modes are independent.

The resultant distribution function for the signal power $P(S)$ for all combinations of modes is determined by summing the distribution functions for each of the combinations. From a knowledge of the distribution function of the noise power $P(N)$ the circuit reliability is computed for a required signal-to-noise ratio, based on the assumption that $P(S)$ is independent of $P(N)$. Signal and noise powers are both assumed to have normal distributions.

4.6 *Method 6 (Maslin)*

Maslin [1978] has discussed possible approaches to the summation of mode reliabilities for different modes in order to give estimates of circuit reliability. Signal powers are additive assuming the separate components have random relative phases. In general, a correct allowance for ionospheric reflection of the signal must assume some degree of correlation between the different modes which depends on the spatial correlation between day-to-day ionization changes. Expressions are given for the case of uncorrelated modes and modes of given correlation coefficient.

4.7 *Method 7*

This method [Liu and Bradley, 1985] assumes that daily values of basic MUF and S/N ratio (expressed in decibels) follow a normal distribution. An approximation is applied for the bivariate normal distribution and the signal power from the separate modes is assumed to sum, ignoring any correlation in strength. The fraction of occasions that the S/N ratio exceeds that specified when the separate mode contributions do not is also ignored. When the mode MUFs have correlation coefficient ρ_{12}, then equation (5) becomes [Thompson, 1974]:

$$R_c = Q_1 P_1 + Q_2 P_2 \left\{1 - \left[\rho_{12}^2 + (1 - \rho_{12}^2)\, Q_1\right] P_1\right\} \qquad (7)$$

Here Q_1 is the probability that mode 1 is present either alone or together with mode 2 and is given by $Q_1 = q_1 + q_{12}$. The term Q_2 is similarly defined and given by $Q_2 = q_2 + q_{12}$. The modes are chosen so that Q_1 exceeds Q_2.

In the case of two F2 modes it is suggested that equation (7) be used with $\rho_{12} = 0.8$.

For modes reflected from different layers (except the case of the E and F1 layers), these are taken as uncorrelated ($\rho_{12} = 0$) giving:

$$R_c = Q_1 P_1 + Q_2 P_2 (1 - Q_1 P_1) \qquad (8)$$

For two completely correlated modes ($\rho_{12} = 1$), such as two E modes or an E and F1 mode, then equation (7) simplifies to:

$$R_c = Q_1 P_1 + Q_2 P_2 (1 - P_1) \qquad (9)$$

4.8 *Method 8*

This method, developed at the First Session of the WARC HFBC, involves a knowledge of median signal field strength together with the upper and lower decile deviations of signal long-term (day-to-day) and short-term (within-the-hour) fading. For the noise background, consideration is given to atmospheric noise, man-made noise and intrinsic receiver noise, with the median noise field strength being evaluated as the greatest of these three components. Variability of the noise is ignored and the decile deviations of S/N ratio are taken as the r.m.s. sum of the respective day-to-day and within-the-hour signal deviations, where all quantities are expressed in decibels. In estimating the percentage of time that the required S/N ratio is achieved, S/N ratio expressed in decibels is assumed to follow a pair of normal distributions below and above the median value.

4.9 Method 9

This method, developed and adopted at the First Session of the WARC HFBC, is similar to method 8 of § 4.8 in so far as the determination of the decile values of signal amplitude arising from combined day-to-day and within-the-hour variability are concerned. Signal intensity is then assumed to follow a pair of normal distributions below and above the median value and basic circuit reliability is given as the percentage of time that the minimum usable field strength (see Recommendation 499) is exceeded.

5. Comparison of methods of determining circuit reliability

For assumed χ^2 variations of day-to-day values of basic MUF and of the composite of all other loss factors, comparisons of values of circuit reliability given by the method of Bradley and Lockwood [1982] in the case when only one mode is present, have been compared with corresponding figures given by methods 1 and 2. Results for method 2 generally agree to within 0.1, but method 1, based on the product of two probabilities, seriously underestimates the reliability at frequencies above the monthly median of basic MUF.

The circuit reliabilities calculated by methods 1, 4 and 5 were compared for a variety of assumed signal levels and signal-to-noise ratios for 2 or 3 modes. For ease of computation, a normal distribution function was used to describe the day-to-day variation of the signal power about the monthly median value for all three methods. In all computations the monthly standard deviations of the signal and of the noise were each assumed to be 7 dB. The median difference and its associated upper and lower decile range between the reliability computed by method 5 and by both of the other methods are as follows:

TABLE I

	Method 5-Method 1	Method 5-Method 4
Median difference	+0.01	0.00
Upper decile range	0.06	0.03
Lower decile range	0.13	0.06

While the median differences are small for both cases, the decile ranges for method 1 are nearly double those for method 4. The computation time for method 5 is considerably longer than that for methods 1 and 4.

Method 3, which takes the interference into account, gives lower values of reliability than other methods which do not allow for interference.

6. Computation of reception reliability

HF reception reliability is analogous to circuit reliability, but assumes that a combination of frequencies may be used. Several methods which have been suggested for the calculation of reception reliability are outlined below.

6.1 *Method 3*

When transmitting the same information at several frequencies simultaneously, this method estimates the probability of satisfactory reception on at least one frequency by supposing that the signal/(noise and interference) ratios at the different frequencies are uncorrelated [Chernov, 1982]. This assumption holds particularly when interference from other stations is present.

Reception reliability when there are n frequencies operating simultaneously may be calculated from the following approximation:

$$T_n = 1 - (1 - \bar{T})^n \qquad (10)$$

where $\bar{T}$ is determined using the equations in § 4.3.

6.2 *Method 4*

In a manner analogous to the calculation of circuit reliability, pessimistic and optimistic estimates of reception reliability are computed for each set of frequencies being considered for a HF circuit.

For each set, the circuit reliabilities possible on each frequency are examined for a specific period and the maximum reliability is selected. This underestimates the reception reliability because it assumes no contribution from any other frequency. An optimistic value of the reception reliability can be computed by assuming that the circuit reliabilities for each frequency are independent. The estimated reception reliability is taken as the average of these two values.

6.3 *Method 5*

To compute reception reliability for various combinations of frequencies, this method uses basic mode information, based on the additional assumption that reflection at one frequency via a given mode implies reflection at a lower frequency via the same mode.

6.4 Method 9

Reception reliability is calculated in terms of circuit reliability by assuming that the contributions from different frequencies are uncorrelated. Measurements in China show that for frequency separations of at least 900 kHz, the average value of the correlation coefficient for long-term fading is less than 20% (see Report 266, — section 5). It is shown by approximate analysis that the impact of this correlation on the basic reception reliability is small and the calculation may —— be made as for uncorrelated fading [CCIR, 1986-1990b].

7. Computation of basic service reliability

The computation of basic service reliability requires the selection of sample reception locations within the geographic area of interest and a selective combination of the values of basic reception reliability determined for each of these locations. Several forms of combination are possible:

- the mean or median of the values of basic reception reliability for the separate sample reception locations;
- the fraction of such locations for which the basic reception reliability exceeds some specified required value;
- the basic reception reliability exceeded at some specified required fraction of locations.

The optimum approach to adopt will depend on the operational requirement and may therefore vary with service application.

8. Computation of overall circuit, reception and service reliability

The computation of overall circuit reliability parallels the computation of basic circuit reliability except the received powers from the potentially interfering transmitters are summed and compared with the available signal to determine the within-the-hour and the day-to-day distribution of hourly median S/I ratios. This distribution is entered with the hourly median S/I ratio required for the specified performance to determine the fraction of time within the month the circuit can be expected to operate successfully in the presence of interference only. This percentage is compared with the basic circuit reliability, and the overall circuit reliability is the lower of these percentages. (A more precise computation involves the combination of the noise and interference to determine the distribution of the $S/(N + I)$ ratio, but, until required $S/(N + I)$ ratios associated with specified performance become available, this approach is not considered practical.)

In a similar way to the methods used in computing the basic reception and service reliabilities from S/N ratios, the overall reception and service reliabilities may also be computed from the assumed distributions of hourly median S/I or $S/(N + I)$ ratios.

9. Reliability estimation in HF networks

Extensions of these reliability concepts may be used, for example for application to an HF network consisting of a number of circuits connected by relay sites. There are in general several paths between source and receiver, and each path, or series of circuits, may contribute to the reliability of communications between the two terminals. The concepts defined above are not adequate for the computation of the reliability of communications between two terminals in such a network, which requires the combination of circuits in both series and parallel.

Two additional types of reliability may be applied to networks. Path reliability is the reliability of a path consisting of one or several contiguous circuits, and communications reliability is the reliability between two terminals considering all contributing paths. One may also consider a special type of service reliability of communications between a single source and several specified reception locations.

In the case where there is only one circuit, the path reliability equals the reception reliability for that circuit. Note that path reliability differs from the others in that it consists of reception reliabilities in series. Using the philosophy of method 4, which takes an average of optimistic and pessimistic estimates, for two or more circuits, an assumption of independence of the reception reliabilities gives a reasonable pessimistic estimate. It is computed as the product of the reception reliabilities for all the circuits on the path. On the other hand, an optimistic estimate is that communications cannot be better than that over the poorest circuit, i.e. that events are correlated, given by the minimum reception reliability over the path [CCIR, 1986-1990a].

10. Operational use of reliability estimates

The reliability information obtained in one of the above ways may be used to choose appropriate frequency bands for the required high frequency service. The optimum single frequency band is determined by computing for each frequency band the circuit reliability for the time periods considered and selecting the frequency band having the maximum average reliability.

The optimum one-, two-, three-band, etc. complement, without considering interference, is chosen to be the one that has the maximum reception reliability over the trial periods being considered. The reliabilities determined for these complements may then be compared. That complement which achieves the required reliability with the minimum number of frequency bands may be selected to satisfy the particular high frequency service requirement.

For frequency assignment, the effect of interference must be considered and overall circuit and reception reliabilities may be used (see Appendix I).

Basic broadcast reliability, which is an adaptation of basic service reliability for the HF broadcasting service, (see Final Acts of the WARC-HFBC, Geneva 1987), is taken as the value of basic reception reliability equalled or exceeded at 80% of test points, calculated on an hourly basis.

11. Summary

Several methods to compute reliabilities of a HF radio system have been reviewed in this report. These methods require further investigation, concerning both their accuracy and the ease with which they may be implemented in prediction methods.

REFERENCES

BARGHAUSEN, A. F., FINNEY, J. W., PROCTOR, L. L. and SCHULTZ, L. D. [1969] Predicting long-term operational parameters of high-frequency sky-wave telecommunication systems, ESSA Tech. Rep. ERL 110-ITS 78, US Govt. Printing Office, Washington, DC 20402.

BRADLEY, P. A. [1983] Signal and noise variability in high frequency sky wave radio service planning. ARARD Conf. Proc. No. 332, *Propagation Aspects of Frequency Sharing, Interference and System Diversity*, 10-1 to 10-13. Ed. H. Soicher. NASA Accession No. N83-30873. National Technical Information Service, Springfield, VA 22161, USA.

BRADLEY, P. A. and BEDFORD, C. [1976] Prediction of HF circuit availability. *Electron. Lett.*, **12**, 32-33.

BRADLEY, P. A. and LOCKWOOD, M. [1982] Simplified estimation of HF sky-wave signal intensity and mode reliability. IEE Conf. Proc. No. 206, 60-67.

CHERNOV, Yu. A. [1969] Nadiodznost kanala radioveshania (Broadcasting channel reliability). *Trudy NIIR*, **1**, 131-139.

CHERNOV, Yu. A. [1982] Neobkhodimoe chislo chastotnykh kanalov v HF diapazone dlya peredachi odnoy programmy s zadannoy nadyozhnostyu (Necessary number of HF frequency channels for transmission of the same programme with a given reliability). *Proc. NIIR*, **3**, 66-72.

LIU, R. Y. and BRADLEY, P. A. [1985] Estimation of HF basic circuit reliability from modal parameters. *Proc. IEE*, Vol. 132, Part F, 111-118.

MASLIN, N. M. [1978] The calculation of circuit reliability when a number of propagation modes are present. CCIR WP 6/1, Doc. 79.

PETRIE, L. E. [1981] Selection of a best frequency complement for HF communications. Communications Research Centre, Dept. of Communications Contract Report No. OER80-00339, Ottawa, Ontario, Canada.

TETERS, L. R., LLOYD, J. L., HAYDON, G. W. and LUCAS, D. L. [1983] Estimating the performance of telecommunication systems using the ionospheric transmission channel. *Ionospheric Communications Analysis and Prediction Program User's Manual.* NTIA Report 83-127, NTIS Accession No. PB 85212942. National Technical Information Service, Springfield, VA 22161, USA.

THOMPSON, A.S. [1974] - The multivariate normal distribution as applied to EMC problems. IEEE Trans. Electromagn. Compt., EMC-19, 115-125.

CCIR Documents

[1986-90]: a. 6/217 (Canada); b. 6/237 (China).

APPENDIX I

The following definitions are given for the purposes of this Report:

1. Terms relevant to the operation and design of HF radio systems

Reliability

Probability that a specified performance is achieved.

Circuit reliability

Probability for a circuit that a specified performance is achieved at a single frequency.

Reception reliability

Probability for a circuit that a specified performance is achieved by taking into account all transmitted frequencies associated with the desired signal.

Path reliability

Probability for a pair of terminals that a specified performance is achieved over a single path between the terminals consisting of one or more contiguous circuits, by taking into account all transmitted frequencies.

Communications reliability

Probability for a pair of terminals that a specified performance is achieved by taking into account all the paths between them and all frequencies associated with the desired signals.

Service reliability

Probability for a service area that a specified performance is achieved by taking into account all transmitted frequencies.

Note 1. – In the above terms circuit means a transmission link from one transmitter to one receiving location with or without diversity.

Note 2. – The above terms are preceded by the word "basic" when the background is noise alone and by "overall" when the background is noise and interference.

Note 3. – When the background is noise and interference, the above terms may relate either to the effects of a single interferer or to multiple interference from co-channel and adjacent-channel transmissions.

Note 4. – For many applications it is convenient to adopt a given value of signal-to-background ratio as the specified performance.

Note 5. – The above terms relate to one or more periods of time which should be stated.

Note 6. – For a given radio service the definitions contained above may need to be adapted to the requirements of that service. For example, for broadcasting applications, the term service reliability is replaced by the term broadcast reliability, and is calculated for a specified number of test points within the service area (Final Acts of the WARC-HFBC, Geneva, 1987).

2. Terms relevant to prediction techniques

Mode reliability

Probability for a circuit that a specified performance is achieved by a single mode at a single frequency.

Mode availability

Probability for a single circuit that a single mode at a single frequency can propagate by ionospheric refraction alone.

Mode performance achievement

Probability for a single circuit that a specified performance is achieved by a single mode at a single frequency given that the mode can propagate by ionospheric refraction alone.

Note 1. – Notes 4 and 5 of § 1 apply.

SECTION 6F: IONOSPHERIC PROPAGATION PREDICTION AND APPLICATIONS AT FREQUENCIES ABOVE ABOUT 30 MHz

REPORT 263-7

IONOSPHERIC EFFECTS UPON EARTH-SPACE PROPAGATION

(Question 37/6)

(1963-1966-1970-1974-1978-1982-1986-1990)

1. Introduction

In the design of Earth-space radio links, ionospheric and tropospheric effects must be considered for frequencies from HF to SHF. The effects of the non-ionized atmosphere are treated in Report 564.

A radio signal which penetrates the ionosphere is modified by the medium due to the presence of electrons and the Earth's magnetic field. Both large scale changes due to the variation of electron density as well as smaller scale irregularities affect the signal. The effects include scintillation, absorption, variation in the direction of arrival, propagation delay, dispersion, frequency change, and polarization rotation. These effects on transmissions mainly above about 20 MHz are treated in the succeeding sections.

2. Scintillation

2.1 *Introduction*

Scintillations as discussed in this Report are variations of amplitude, phase, polarization and angle-of-arrival produced when radio waves pass through electron density irregularities in the ionosphere. The phenomena are produced by one of two causes [Fang and Liu, 1984]: i) sufficiently high electron density fluctuations at scale sizes comparable to the Fresnel zone dimension of the propagation path, or ii) sharp gradients of ambient electron density, especially in the direction transverse to the direction of propagation. Either cause is likely to occur in the ionosphere and the scintillations can become quite severe and may represent a practical limitation for some communication systems. Data showing scintillation have been observed on frequencies from about 10 MHz to about 12 GHz.

For systems applications, scintillations can be characterized by the depth of fading and fading period. The use of the Fresnel zone concept enables an estimate of these characteristics to be made under conditions of weak scintillation, i.e., peak to peak fluctuations in amplitude less than 8 dB. The implications of using the Fresnel zone for both weak and strong scintillations have been discussed in detail by many workers [Yeh *et al.*, 1975; Crane, 1977]. A useful index to compare scintillation data is the scintillation index, S_4, which is defined as the standard deviation of received power divided by the mean value of the received power [Briggs and Parkin, 1963].

The fading period of scintillation varies over quite a large range and can be as long as several minutes [Koster, 1966]. The fading period depends both upon the apparent motion of the irregularities relative to the ray path, and in the case of strong scintillation, on its severity. For strong scintillation the fading period is shorter than for weak scintillation with the same relative velocity. The fading period of gigahertz scintillation ranges from approximately 2 to 15 s [Sessions, 1972; Paulson and Hopkins, 1973; Taur, 1973]. However, long period (of the order of tens of seconds) components of saturated scintillation (S_4 approaches 1) at VHF bands have been observed at Ascension Island [Franke and Liu, 1987]. The gigahertz measurements were in the weak scintillation limit and were made when both the transmitter and receiver were stationary; therefore the observed fading periods reflect the motion of the ionospheric irregularities. A more precise measure of fading can be defined by the power spectra as shown by ground measurements of synchronous satellites [Taur, 1976; Whitney and Basu, 1977; Ott, 1977; Umeki *et al.*, 1977a; Fang *et al.*, 1978; Fang, 1980; Fang and Liu, 1984] and by ground measurements of low altitude satellites [Crane, 1976; Fremouw *et al.*, 1978].

In addition to the normal randomly varying type of amplitude scintillation, a fading pattern known as "quasi-periodic" or "Fresnel" type scintillation is sometimes observed, which is usually symmetrical about a deep central minimum in the time domain. The fade duration varies widely from a few seconds to several minutes. There are many reports of this type of scintillation at VHF [Slack, 1972] and it has also more recently been observed, particularly at early night-time in early summer at 1.5 and 4 GHz [Karasawa et al., 1985; Moriya et al., 1985; Karasawa, 1987]. Although it remains uncertain whether quasi- periodic scintillation occurs in the ionospheric E- or F-Region, the existence of small scale columnar irregularities with extremely high ionization is an indispensable condition for the occurrence of quasi-periodic scintillations, particularly at frequencies above 1 GHz [Karasawa, 1987].

Small-scale ionospheric irregularities which produce amplitude scintillation also give rise to angular scintillation. In middle latitudes the magnitude of these is typically a few tenths of a milliradian at 136 MHz [Bramley, 1974], but larger values may be expected in the equatorial and high-latitude zones of stronger scintillation. These angular fluctuations again decrease with increasing frequency, but in a way which depends on the size and distance from the receiver of the ionospheric irregularities, and the detailed frequency dependence has not yet been established experimentally or theoretically.

2.2 *Frequency dependence of scintillation*

If results from direct measurement are not available, an $f^{-1.5}$ frequency dependence of S_4 is suggested for engineering application.

Observations [Fremouw *et al.*, 1978] employing ten frequencies between 138 MHz and 2.9 GHz, transmitted from the same satellite, show a consistent $f^{-1.5}$ behaviour in amplitude for S_4 less than about 0.4, where f is the frequency. The frequency dependence is less steep for stronger scintillation, with S_4 attaining a maximum value near unity with a few exceptions. This is consistent with theoretical predictions taking into account the saturation effect due to multiple scattering [Yeh *et al.*, 1975; Umeki *et al.*, 1977b]. The same observations show that the phase scintillation index, σ_Φ (defined as the standard deviation of phase in the fluctuation-spectral range containing intensity scintillations), varies as f^{-1}, a result also obtained by Crane [1976].

Multi-frequency amplitude scintillation data at about 1.5 and 3.9 GHz from the equatorial region at Ascension Island [Franke *et al.*, 1984] reveal a frequency dependence between $f^{-1.6}$ and $f^{-1.9}$ with $f^{-1.7}$ as the average. These values are believed to be related to a two-component power-law irregularity spectrum as observed in the *in situ* and radar observations of the night-time F region [Basu *et al.*, 1980].

Measurements with beacons of the ETS-II geostationary satellite during two months from the end of April to the end of June 1978 made at Kashima (geographic coordinates, 35°57′ N, 140°40′ E; geomagnetic latitude, 25°37′ N) show frequency dependences of S_4 scintillation indices between 136 MHz and 1.7 GHz as, on the average, $f^{-1.4}$ for the night-time and $f^{-1.5}$ for the day-time. The frequency dependence varies with time at night in accordance with the temporal variation in the structure of electron density irregularities after the F-layer sunset [Fujita *et al.*, 1982].

In the GHz frequency range, amplitude observations of 1.7, 4 and 11.5 GHz signals transmitted from Japanese geostationary satellites, show the dependence of f^{-1} for $1.7 \leqslant f \leqslant 4$ GHz and of f^{-2} for $4 \leqslant f \leqslant 11.5$ GHz at the time of severe scintillations during the geomagnetic storm on 15 February, 1978. At that time, S_4 at 136 MHz was greater than unity, indicating focusing [Ogawa *et al.*, 1980].

2.3 *Geometrical considerations*

The intensity at which scintillations are observed depends upon the position of the observer relative to the irregularities in the ionosphere that cause the scintillation. Keeping both the thickness of the irregularity region and ΔN, the electron density deviation of the irregularity, constant, geometrical factors have to be considered to evaluate data and to predict scintillation effects at a particular location. Among these are:

2.3.1 zenith angle of the propagation path at the ionospheric layer. One study [Wand and Evans, 1975] found the intensity of scintillation may be related approximately to the zenith path values by the secant of the zenith angle to 70°; at lower elevation angles a dependence ranging between 1/2 and first power of the zenith angles should be used;

2.3.2 propagation angle relative to the Earth's magnetic field. Evaluation of scintillation demands the use of an irregularity configuration and the consideration of Gaussian or a power-law model for the spectrum of the irregularities. At auroral latitudes, irregularities are elongated along the Earth's magnetic field in sheet-like configurations [Rino, 1978]. For equatorial latitudes this elongation ratio may be of the order of 50 to 100 [Koster, 1963]; at mid-latitudes, measurements at 136 MHz during the summer of 1981 have suggested that ionospheric irregularities at 300 km altitude, which are responsible for VHF to UHF scintillations, are elongated along the Earth's magnetic field with an elongation factor of 10 [Sinno and Minakoshi, 1983]. The level of scintillation is found to increase considerably when the direction of propagation through the ionosphere lies close to the direction of the Earth's magnetic field. Spaced-receiver scintillation measurements at mid-latitude using three antennas give the mean value of an elongation factor of 24 [Kumagai and Ogawa, 1986]. The correlation distance of irregularities decreases with increasing scintillation strength [Kumagai, 1987].

2.4 *Morphology*

The variations in scintillation can be divided into components that depend on geomagnetic latitude, longitude, and local time. A review of morphology is contained in Aarons [1982]. A summary of scintillation characteristics is given in Table I.

Equatorial ionospheric scintillation is primarily a night-time phenomenon, with more severe fluctuations occurring pre-midnight. Scintillation activity peaks near the equinoxes in the South American and African sectors, but the seasonal variation at other longitudes is not yet certain. Equatorial scintillation, the boundary of which lies between 20° and 30° geomagnetic latitude [Taur, 1973], exhibits a long-term positive correlation with sunspot number [Taur, 1974; Aarons, 1977]. The sunspot number dependence is illustrated in Fig. 1 based on data collected at selected INTELSAT earth stations over a ten-year period [Fang, 1980; Fang and Pontes, 1981; Fang and Liu, 1983, 1984].

At mid-latitudes there is a variation with time of day and with latitude as well as season and epoch of the solar cycle. High latitude scintillation shows a sharp equatorward boundary, the position of which depends on time of day and magnetic activity. Poleward of the boundary, scintillations maximize over aurora.

Figure 2 [Basu et al., 1988] is a generalized map of the night-time hemisphere showing depth of fluctuation as a function of local meridian time for a year of relatively high solar activity. The depth of fluctuation is proportional to the shading density of the figure. This map was derived primarily from measurements made at L-band (about 1.6 GHz).

2.4.1 *Equatorial scintillation*

Fading to 6 GHz has been noted on long-term observations in the equatorial region [Taur, 1973; Skinner *et al.*, 1971]. The equatorial latitudes show greater depth of scintillation than the high-latitude auroral regions. The occurrence of scintillation is positively correlated with solar flux and shows a tendency to be inversely correlated with magnetic activity [Koster, 1972; Mullen, 1973]. The equatorial scintillation region expands in geographic extent and intensity with increasing phase of the solar cycle. The most intense scintillation in years of high solar activity occurs in the evening hours after local sunset in the region within ± 20° of the geomagnetic equator where high electron densities are observed [Aarons *et al.*, 1981; Aarons, 1982; Fang and Pontes, 1981; Fang and Liu, 1983].

It should be noted that scintillation in the equatorial region displays a marked longitudinal behaviour [Basu and Khan, 1976]. A seasonal occurrence pattern for two longitude regions, 0 to 70° W and the Guam-Kwajalein region at 135 to 180° E is shown in Fig. 3 [Aarons *et al.*, 1980]. For gigahertz signals, there is a clear equinoctial maximum with the lower frequency signals frequently showing a scintillation index approaching unity. The seasonal occurrence pattern for other longitude regions can be significantly different. Tsunoda [1985] has shown that the seasonal maxima in scintillation activity correspond closely to times of the year when the solar terminator is most nearly aligned with geomagnetic flux tubes.

In Kuwait, large scintillations at 4 GHz, whose magnitudes were greater than 10 dB peak-to-peak with the duration exceeding 2 hours, were observed in the spring of 1980. The rate of fluctuation was found to decrease gradually during an observation period [Karasawa and Yasukawa, 1981].

For applications in international communications employing a synchronous satellite at 4 GHz, the cumulative effect of ionospheric scintillations can be assessed by Fig. 4 [Fang and Pontes, 1981].

TABLE I – *Solar-geophysical and temporal dependence of ionospheric scintillation*

			High-latitude	
Parameter	Equatorial	Mid-latitude	Auroral	Polar
Activity level	Exhibits greatest extremes	Generally very quiet to moderately active	Generally moderately active to very active	Great intensity in high sunspot years
Diurnal	Maximum-night-time Minimum-day-time	Maximum-night-time Sporadic-day-time	Maximum-night-time Maximum-day-time (not within polar cap)	Maximum-night-time
Seasonal	Longitud e dependent Peaks in equinoxes Accra, Ghana Maximum-November and March Minimum-solstices Huancayo, Peru Maximum-October to March Minimum-May to July Kwajalein Islands Maximum-May Minimum-November and December	Maximum-spring Minimum-winter Tokyo, Japan Maximum-summer Minimum-winter	Pattern a function of longitude sector	Pattern a function of longitude sector
Solar cycle	Occurrence and intensity increase strongly with sunspot number	Tokyo, Japan Occurrence in night-time decreases with sunspot number; Occurrence in daytime has little dependence	Occurrence and intensity increase strongly with sunspot number	Occurrence and intensity increase strongly with sunspot number
Magnetic activity	Longitude dependent Accra, Ghana Occurrence decreases with K_p Huancayo, Peru March equinox Occurrence decreases with K_p June solstice Occurrence increases with K_p September equinox 0000-0400 h (local time) Occurrence increases with K_p	Independent of K_p	Occurrence increases with K_p	Occurrence increases only slightly with K_p

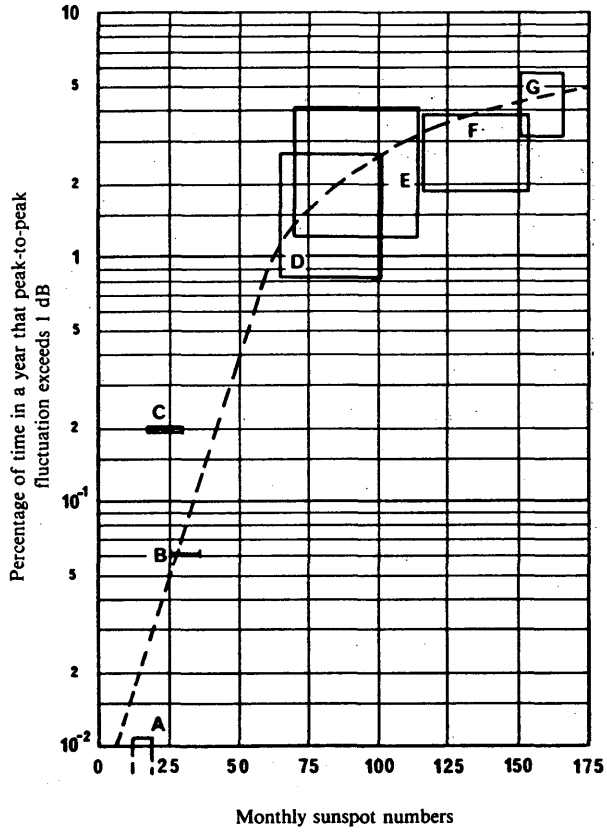


FIGURE 1 – *Dependence of 4 GHz equatorial ionospheric scintillations on monthly average International relative sunspot number*
[Fang, 1980; Fang and Pontes, 1981]

The bars and squares are the ranges of variations over a year for different carriers.

A: 1975-1976, Hong-Kong and Bahrein, 15 carriers
B: 1974, Longovilo, 1 carrier
C: 1976-1977, Taipei, 2 carriers
D: 1970-1971, 12 stations, > 50 carriers
E: 1977-1978, Hong-Kong, 12 carriers
F: 1978-1979, Hong-Kong, 10 carriers
G: 1979-1980, Hong-Kong, 6 carriers

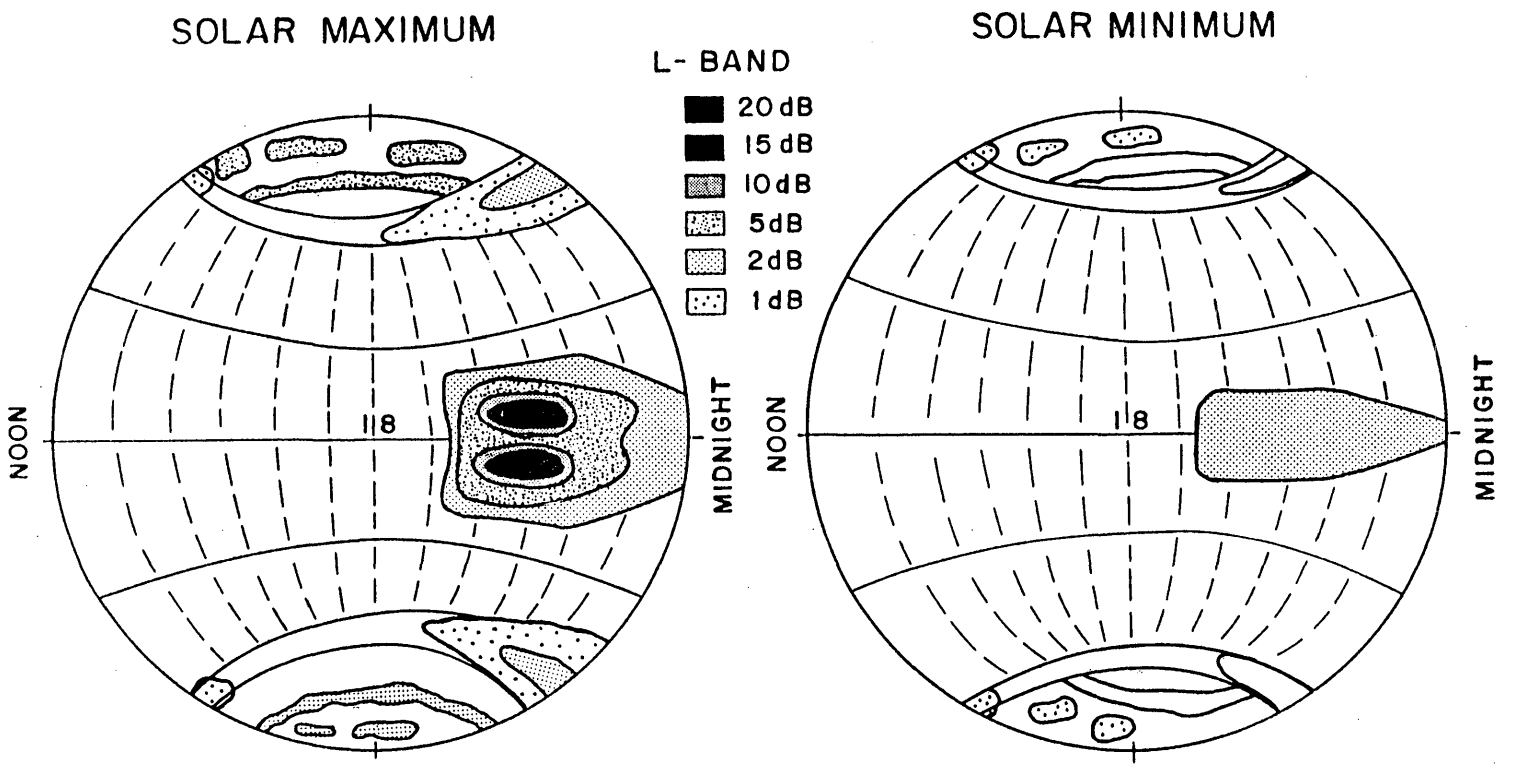


FIGURE 2

Illustrative picture of scintillation occurrence based on observations at L-Band (1.6 GHz)

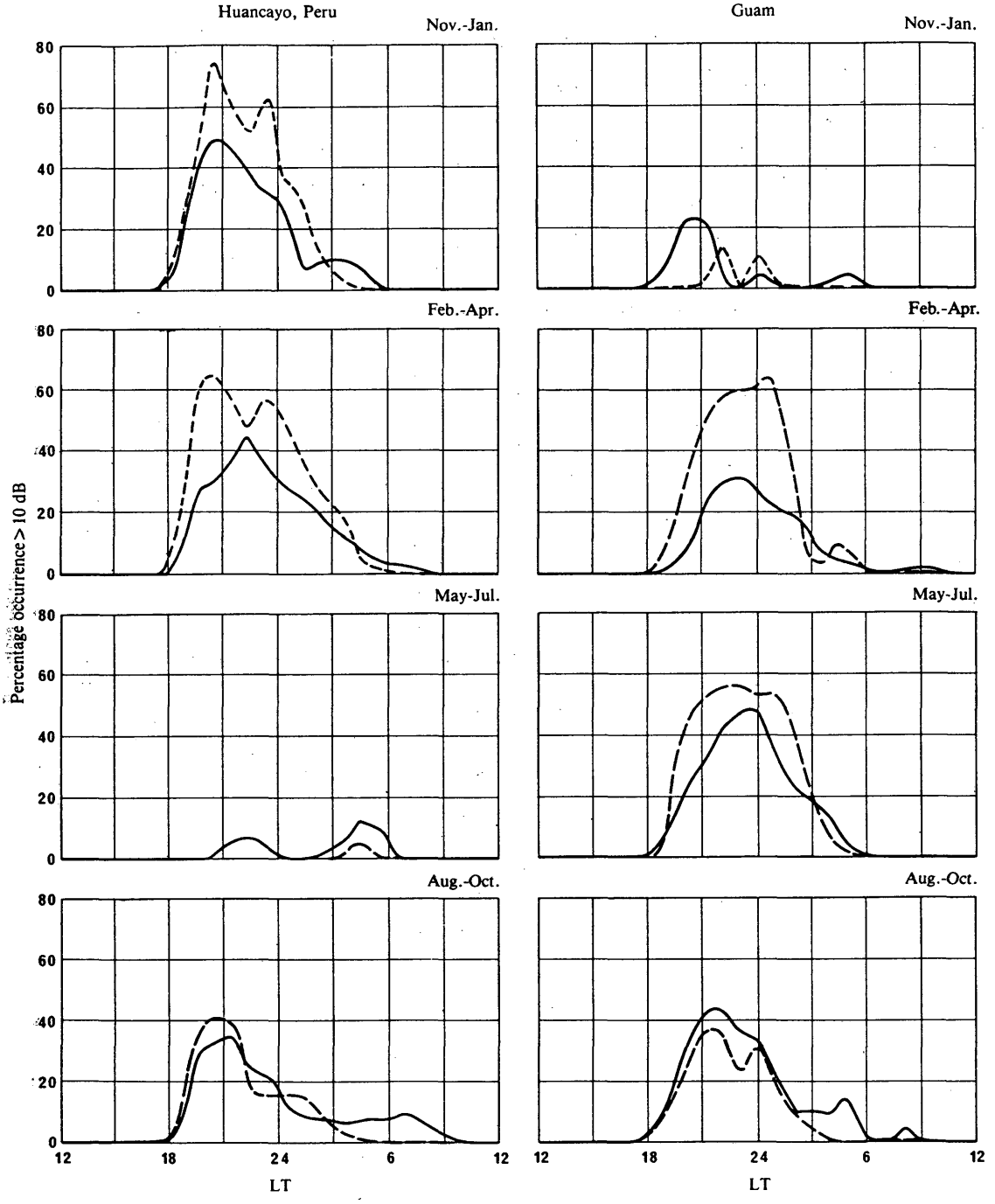


FIGURE 3 – *Seasonal occurrence pattern of scintillations for two longitudinal regions near equator*

– – – $K_p = 0 - 1^+$

——— $K_p = 3^+ - 9$

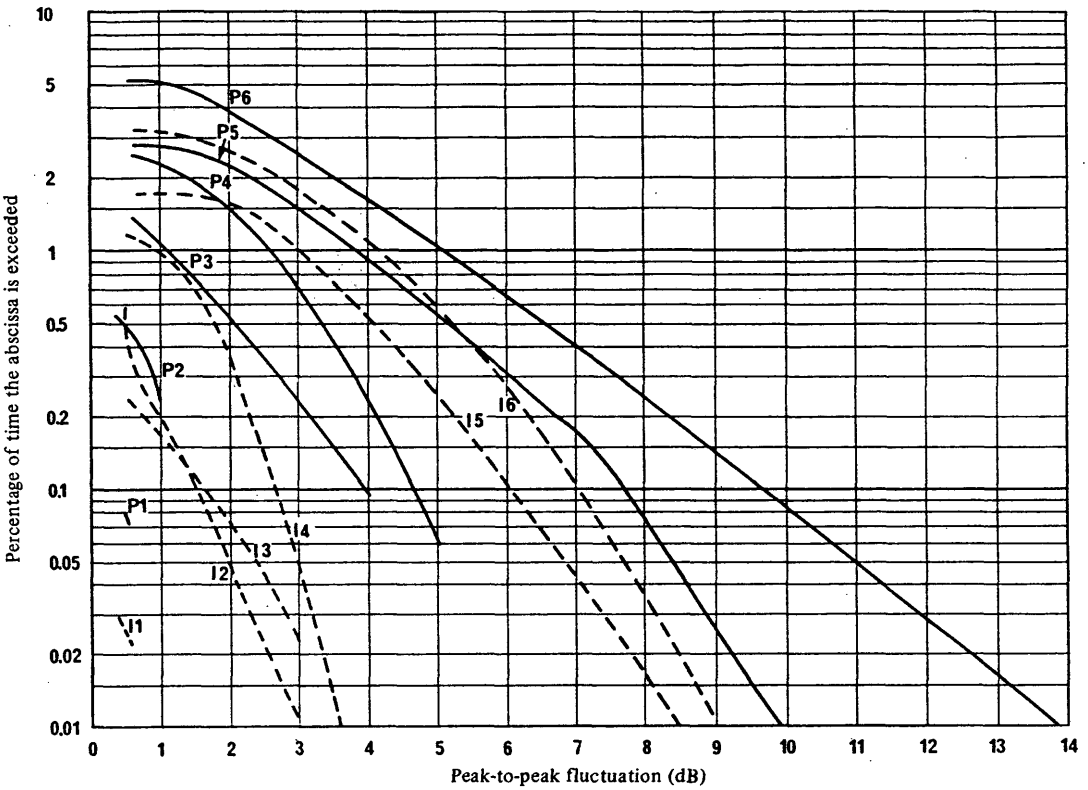


FIGURE 4 – *Annual statistics of 4 GHz ionospheric scintillation observed at Hong Kong earth station (Curves I1, P1, I3-I6, P3-P6) and Taipei earth station (Curves P2 and I2)*

P curves refer to a 20° elevation angle pointing to an eastward synchronous satellite while I curves refer to a 30° elevation angle pointing to a westward synchronous satellite [Fang and Pontes, 1981]

Curve	Period	SSN range
I1 P1	March 75-76	10-15
I2 P2	June 76-77	12-26
I3 P3	March 77-78	20-70
I4 P4	October 77-78	45-110
I5 P5	November 78-79	110-160
I6 P6	June 79-80	153-165

2.4.2 *Mid-latitude scintillation*

The diurnal variation of mid-latitude scintillations shows a well-established maximum near midnight which correlates with the occurrence of ionospheric spread F. A second maximum around midday has also been found in some sets of observations. This is most pronounced in summer, and there is evidence for its association with sporadic E [Aarons and Whitney, 1968; Cornec, 1978]. Data collected during quiet and disturbed magnetic conditions indicate little correlation between mid-latitude scintillation and magnetic activity [Bramley, 1974; Wand and Evans, 1975; Aarons and Martin, 1975].

Observations in and around Tokyo, Japan (invariant latitude of the propagation path at the F2 peak = 26°) show a pronounced maximum in summer and a minimum in winter (Table I). The percentage occurrences of scintillations in summer, equinox and winter are listed in Table IIa for 136 MHz signals from ETS-II [Fujita *et al.*, 1978; Sinno and Kan, 1980]. Night-time scintillation has a slight negative correlation with sunspot number, but daytime scintillation has little correlation [Minakoshi, 1988]. Strong ionospheric scintillations have been observed in Japan for the microwave signals from geostationary satellites. In particular, during the geomagnetic storm on 22 March, 1979, scintillation observed at 4 GHz reached 10 dB peak-to-peak and at 12 GHz reached 3.5 dB peak-to-peak [Ogawa *et al.*, 1980; Minakoshi *et al.*, 1981]. These strong scintillations are associated with a duct structure which forms along the mid-latitude field lines [Ogawa and Kumagai, 1985]. Penetration of the magnetospheric electric field toward low latitudes plays an important role in the formation of these ducts [Tanaka, 1981, 1986].

2.4.3 *High latitude scintillation*

The effects differ between the auroral and polar regions. Compared to mid-latitude levels, scintillation increases considerably when the ray path traverses the high-latitude region. The increase starts with the boundary of low-level irregularities located at night in the same region as the ionospheric trough [Houminer *et al.*, 1981]. Scintillations maximize above the aurora [Fremouw and Rino, 1973]. During periods of magnetic activity, auroral scintillation levels increase dramatically with local excursions of the magnetic field. Statistically, scintillation levels increase with the planetary magnetic index K_p [Basu, 1975; Basu and Aarons, 1980]. For definition of K_p see [Davies, 1965].

Observations of synchronous satellites from Ottawa (a station near the scintillation boundary at night) have shown peak-to-peak fades at 230 MHz in excess of 2 dB for less than 1% of the time and in excess of 10 dB for less than 0.1% of the time [Maynard, 1972a and b].

Other studies of synchronous satellites from Ottawa and Ft. Churchill, Canada of ionospheric fading margins have shown that these fading margins vary not only with the required system reliability but also with the operating frequency and geomagnetic latitude [Maynard, 1976; Ponnappa, 1973]. From the measurements of the signals from the LES-6 and ATS-5 satellites, it was found that for a 99.9% propagation reliability, an ionospheric fading of 1.5 to 3 dB was required at Ottawa on 254 MHz whereas at Churchill a margin of 8 to 14 dB is required. Increasing the frequency to 1500 MHz changes the above values to 0.2 to 0.3 dB at Ottawa and 0.35 to 0.8 dB at Churchill.

At polar latitudes, scintillation is high during years of high sunspot number, particulary during the dark months. During sunlit months the level decreases in solar maximum years. Polar scintillations (at latitudes greater than 82° Corrected Geomagnetic Latitude) are produced by polar arcs traversing this region and have shown levels greater than 28 dB peak-to-peak for hours at 250 MHz [Aarons *et al.*, 1981]. Occurrence of polar scintillation increases only slightly during magnetic activity.

Amplitude and phase scintillation measurements have been made by the UK at a high-latitude site in northern Europe during a two-year period. Transmissions from the polar-orbiting multi-satellite NNSS system have been used to achieve both latitudinal and temporal coverage of the observations, with more than 12000 satellite passes being monitored to yield in excess of 400,000 values of each of the S_4 and σ indices for amplitude and phase scintillation respectively. The importance of propagation geometry to high-latitude scintillation observations is clear from the observations, and estimates of the geometrical factors in both S_4 and σ for different irregularity anisotropies have been computed. A seasonal effect is apparent (Fig. 5) with more scintillation activity from May to September than in other months [Kersley et al., 1988]. The initial analysis of early observations from a sub-auroral location in northern UK provides confirmation of this seasonal effect at European longitudes.

Tables IIb and IIc give the percentage of occurrence of scintillations at selected high latitude stations.

TABLE IIa – *≥ 10 dB peak-to-peak scintillations at 136 MHz mid-latitude*

Site	Season	Day (0600-1800 LT)	Night (1800-0600 LT)
Tokyo, Japan (Invariant lat. 26°)	Summer Equinox Winter	0.7 0.1 0.0	10.5 0.7 0.4

TABLE IIb – *≥ 12 dB peak-to-peak scintillations at 137 MHz, sub-auroral and auroral latitudes*

Site	K_p	Day (0500-1700 LT)	Night (1700-0500 LT)
Hamilton (Massachusetts)	0 to 3+ > 3+	0 0.1	1.4 2
Goose Bay (Labrador)	0 to 3+ > 3+	0.1 1.6	1.8 6.8
Narssarssuaq (Greenland)	0 to 3+ > 3+	2.9 19	18 45

TABLE IIc – *≥ 10 dB peak-to-peak scintillations at 254 MHz, auroral latitudes*

Site	K_p	Day (0600-1800 LT)	Night (1800-0600 LT)
Goose Bay (Labrador)	0 to 3+ > 3+	0.1 0.3	0.1 1.2
Narssarssuaq (Greenland)	0 to 3+ > 3+	0.1 2.6	0.9 8.4

LT: local time.

2.5 *Signal characteristics*

2.5.1 *Signal statistics*

The intensity of the scintillation may be characterized by the variance in received power or by the variance in the logarithm of received power. The measure σ_χ is the standard deviation of the variance of the logarithm of the received power [Tatarski, 1967]. For periods of scintillation having a constant value of either one of these measures, the signal level fluctuations may be described by an empirical probability density function (pdf). Sample empirical pdfs are given in Fig. 6 for several S_4 values. The phase of the received signal also may vary. Empirical pdfs for phase fluctuations are given in Fig. 7 for the same cases shown in Fig. 6. The data depicted in Figs. 6 and 7 were obtained at a mid-latitude station at 150 MHz [Crane, 1974].

Attempts have been made to model the observed amplitude pdf. Whitney *et al.* [1972] have constructed model distribution functions based upon the use of the Nakagami-*m* distribution ($m = (S_4)^{-2}$) and have shown that the models provide a reasonable approximation to their observed empirical distribution functions. Whitney *et al.* [1972] and Rino and Fremouw [1973] have shown that the log-normal distribution is not a good model for ionospheric scintillation. Crane [1974] showed that the Nakagami-*m* model provided a a reasonable approximation for use in relating S_4 to σ_χ and for interpreting the many reported sets of observations. Also the Rayleigh pdf provided a good fit to the data under conditions of very strong scintillation ($S_4 > 0.9$). The relationships between the most commonly used measures of scintillation have been deduced assuming that the pdf of amplitude is a Nakagami-*m* distribution [Bischoff and Chytil, 1969; Chytil, 1967]. Nakagami [Hoffman, 1960] derived the relationship between the Nakagami-*m* distribution and the Nakagami-Rice distribution function given in Report 266. The Nakagami-*m* distribution is a Rayleigh distribution for $m = 1$ (strong scintillation), and is a log-normal distribution for $m \gg 1$ (weak scintillation).

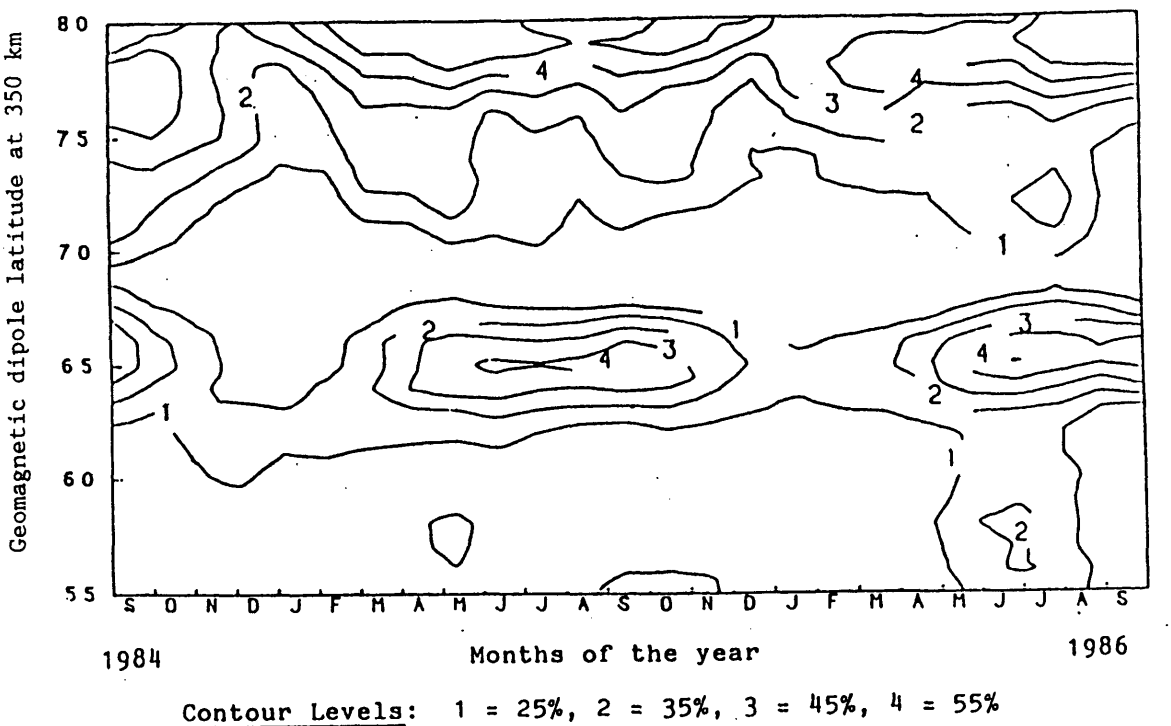


FIGURE 5

Scintillation occurrence by month (S4 > 0.2) observed at Kiruna (64.3 N, 102.8 E CGM) from September 1984 to September 1986

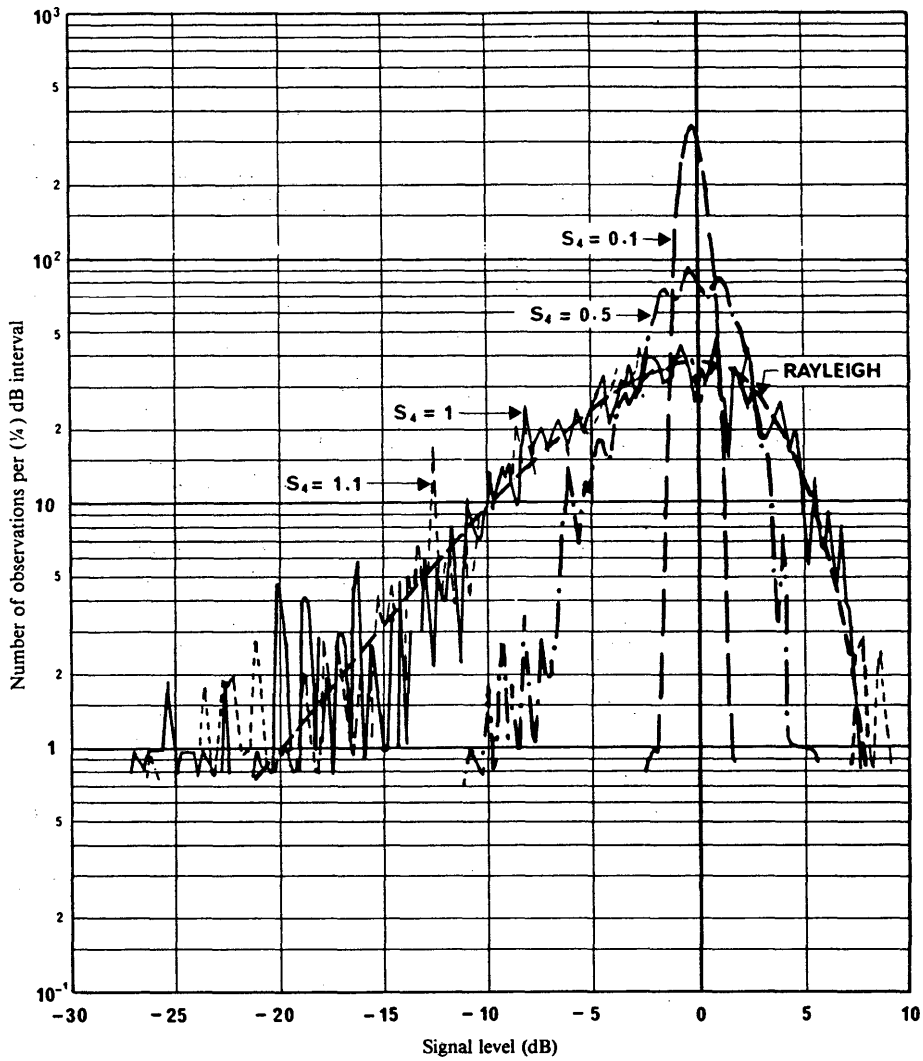


FIGURE 6 – *Empirical amplitude probability density functions*

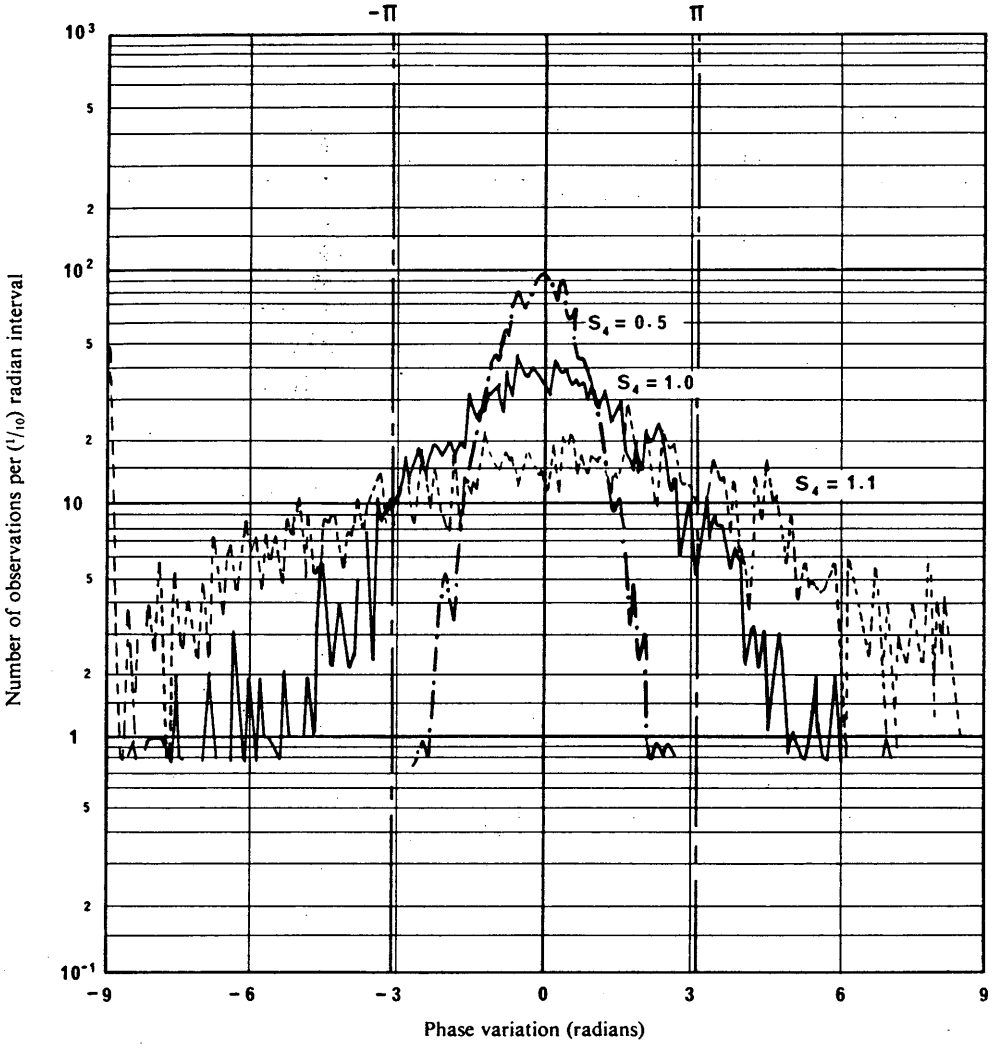


FIGURE 7 – *Empirical phase probability density functions*

The log-normal and Nakagami-*m* distributions are both characterized by a single parameter which can be related to either S_4 or σ_χ. More complex models exist with more parameters that can be adjusted to fit the data. A leading candidate from models in this class is the complex Gaussian statistics model [Rino and Fremouw, 1973]. The in-phase and quadrature components of the received signal are modelled as joint-dependent zero-mean Gaussian processes providing three parameters for use in fitting the empirical pdfs, namely, the variances for the two components, and the correlation between them. For strong scintillation, the variances for the two components are equal, and their correlation is zero (Rayleigh process). A simpler model, based on the Nakagami distribution for intensity and normal distribution for phase, is found to be equal or superior to a two component model [Fremouw *et al.*, 1980].

2.5.2 *Spectrum of amplitude and phase fluctuations*

The signal fluctuations may also be described by spatial or temporal power spectra [Rufenach, 1972]. Temporal power spectral density was estimated by Crane [1975] for scintillation observed at 150 and 400 MHz and compared with a theoretical model based upon an irregularity power-law spectrum giving weak scintillation. The comparison shows that the spectra for log-amplitude fluctuations peak at a frequency near $f = 0.4\ v/r_0$ where v is the relative velocity of the irregularities normal to the line of sight (drift velocity) at the location of maximum fluctuations in the electron density, and r_0 is the size of the first Fresnel zone at the same point ($r_0 = (\lambda Z)^{1/2}$, with λ = wave length and $Z = \rho(L - \rho)/L$ where L = path length and ρ = distance at which irregularities are found). The power spectrum for log-amplitude fluctuations decreases with increasing frequency as f^{-3} (the high-frequency asymptote). The data have this form until masked by modulation noise. A number of power spectra obtained for equatorial scintillation of 4 GHz signals from the geostationary Intelsat-IV satellite is depicted in Fig. 8 [Fang and Pontes, 1981; Fang and Liu, 1984].

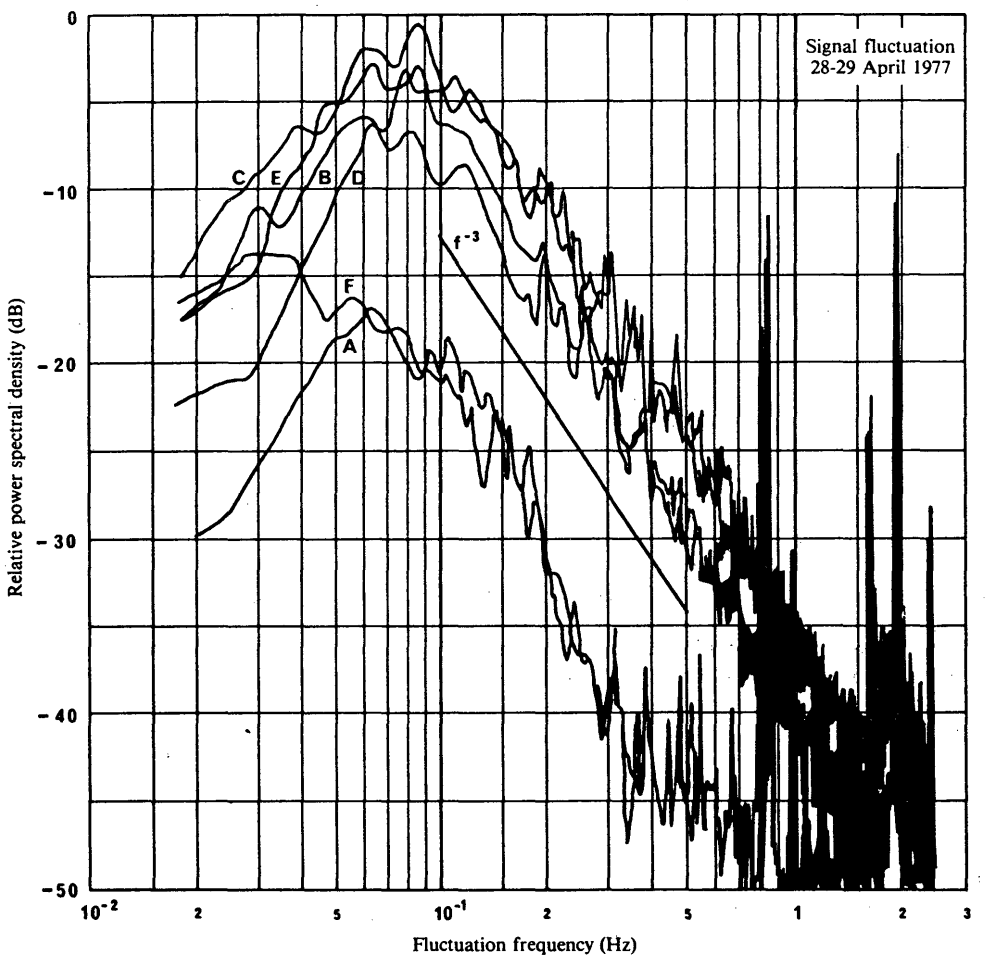


FIGURE 8 – *Power spectral density estimates for a geostationary satellite (Intelsat-IV) at 4 GHz*

The scintillation event was observed during the evenings of 28-29 April 1977 at Taipei Earth Station

A: 30 minutes before event onset
B: at the beginning
C: 1 hour after
D: 2 hours after
E: 3 hours after
F: 4 hours after

In the equatorial region, the spectra of intense amplitude scintillations at 250 MHz and 1.6 GHz are characterized by a single power law having a steep roll-off with power law indices of -5 to -7 [Basu et al., 1987]. At 4 GHz, a uniform power spectral density does not always occur, as two slopes are often observed. The transition frequency, separating the low frequency and high frequency slopes, increases and the high frequency slope may also increase to as much as f^{-4}. The increase in the transition frequency, often referred to as a spectrum broadening, is due to multiple scattering [Umeki et al., 1977a].

Closely related to the spectra of the scintillation and relevant to the diversity schemes are the correlation functions of the amplitude and phase. Of special interest is the correlation time, defined as the time interval for the correlation to decrease from its maximum value to one half of the maximum. In the case of weak scintillation, the size of the first Fresnel zone determines the correlation distance of the amplitude scintillation, which is proportional to the correlation interval. Therefore the correlation time varies as $f^{-1/2}$ in the weak scintillating regime. As the strength of scintillation increases, the signal becomes decorrelated due to multiple scattering. For a given ionospheric condition, the scintillation becomes stronger as the frequency decreases and eventually the signal undergoes decorrelation resulting in a smaller correlation interval [Umeki *et al.*, 1977b]. The correlation interval for the phase scintillations does not have strong frequency dependence since the major contributions of phase fluctuations are from large size irregularities. However, decorrelation may still play a role as the scintillation intensifies [Myers *et al.*, 1979].

2.5.3 *Diversity schemes*

Diversity schemes attempt to reduce the effects of fading during a scintillation event by combining two signals that are fading independently. For a Rayleigh process, signal fades below median level are greater than 18.4 dB for one percent of the time. For two independent Rayleigh processes, the larger of the two signals at any sample point fades below 8.2 dB for one percent of the time yielding a gain in protection against fading of about 10 dB. In general, the diversity gain depends upon the correlation between the two samples of the fading process. If the correlation coefficient is less than 0.6, the diversity gain is 8 dB or better. A correlation coefficient of 0.6 may be used as a threshold for satisfactory diversity action although the quoted gain of 8 dB strictly applies only to Rayleigh fading (strong scintillation). In the limit of weak scintillation, a correlation coefficient less than 0.6 occurs between observations at two frequencies for signals propagating along the same path only if the carrier frequencies are separated by more than a factor of three, suggesting that frequency diversity is not generally effective in combating scintillation [Crane, 1977]. Simultaneous fluctuations on orthogonal-polarized channels are also highly correlated for frequencies above 100 MHz [Koster, 1966; Whitney and Ring, 1971; Crane, 1977]. Occasional exceptions may occur under conditions of extreme scintillation. Measurements of the 136 MHz signal from the ETS-II satellite [Sinno and Kan, 1978] showed decreasing correlation between the two linearly polarized components when scintillation was accompanied by rapid variation in Faraday rotation. Observations under conditions of equatorial GHz scintillation [Fremouw *et al.*, 1980] have shown reduced correlation across relatively narrow bands at lower frequencies. In particular, total decorrelation of phase and partial decorrelation of intensity have been observed between 390 and 436 MHz. Visual inspection of UHF records as narrowly spaced as 11.5 MHz also has revealed decorrelation, but quantitative analysis has not yet been performed.

Two diversity schemes are viable for both weak and strong scintillation conditions: time and space. For a two-station configuration, time diversity requires that the same message be sent at two different times separated far enough for the correlation coefficient to be less than 0.6. Space diversity requires that the same message be detected at two receiving points separated far enough for the coefficient to be less than 0.6. The correlation function may be calculated from the power spectrum for the received signal fluctuations. The time separation corresponding to a correlation coefficient of 0.6 as computed for the spectra described in § 2.5.2 is given by $\tau = 0.3\ r_0/v$. For space diversity, the distance for a correlation coefficient of 0.6 is $l = 0.3\ r_0 z_2/(z_2 - z_1)$ for a direction normal to the line-of-sight and normal to the field, and $l = 0.3\ r_0 \alpha z_2/(z_2 - z_1)$ for a direction normal to the line-of-sight in the direction of the field, where α = axial ratio of the irregularities. For oblique incidence, the projection of these distances onto the ground is required for the estimation of diversity distance.

Diversity schemes are normally only required to overcome the effects of intense scintillations; weak scintillations are offset by a reasonable fade margin. In the equatorial zone, measurements of the spatial cross-correlation function for strong scattering conditions have given typical values for the correlation coefficient of 0.6 for 300 m antenna separation and 0.3 for 1000 m separation [Paulson and Hopkins, 1977]. The corresponding drift velocity of the irregularities was approximately 50 m per second. It was measured with E-W antenna baselines which would be parallel to the expected drift velocity vector. Other antenna orientations would require greater baselines to achieve the necessary decorrelation. Therefore space diversity seems only practical for fixed ground stations.

2.5.4 Simultaneous occurrence of ionospheric scintillation and rain fading

Ionospheric scintillation and rain fading are two impairments of completely different physical origin. For C-band (6/4 GHz) in equatorial regions at years of high sunspot number, the simultaneous occurrence may have an annual percentage time that is significant to system design. According to Fang and Allnutt [1987], who analyzed 17-month, 4 GHz satellite signal data starting from October 1980 at Djutiluhar earth station in Indonesia, the cumulative simultaneous occurrence time was about 0.06% annually.

Fang and Allnutt reported that the simultaneous events have signatures that are often vastly different from that when only a single impairment, either scintillation or rain alone, is present. For example, while ionospheric scintillation alone is not a depolarization phenomenon, and rain fading alone is not a signal fluctuation phenomenon, the simultaneous events produce a significant amount of signal fluctuations in cross-polarization channel. Attention to these simultaneous events is needed for applications to satellite-earth microwave systems which require high availability.

3. Absorption

3.1 *Introduction*

When direct information is not available, ionospheric absorption loss can be estimated from available models according to the (sec i)/f^2 relationship, for frequencies above 30 MHz where i is the zenith angle of the propagation path at the ionosphere.

The lower limit of the usable radio-frequency spectrum is determined by ionospheric reflection and absorption which, in general, increase with decreasing frequency [Davies, 1965]. For equatorial and mid-latitude regions use of frequencies above 70 MHz will assure penetration of the ionosphere without significant absorption.

In addition to the generally predictable seasonal and solar activity variations of the ionosphere, there are less predictable variations arising from short term changes in solar activity. These short term variations have their greatest effect at high latitudes——————————————

maximum [Hook, 1968]. Absorption in the northern hemisphere is a maximum in the Russian-Alaskan sector [Agy, 1975]. Absorptions occurring in the morning hours in winter are found to be twice those for summer [Basler, 1966]. Assuming that the absorption experienced by VHF signals at oblique incidence is proportional to (sec i)/f^2, and using empirical equations which have been fitted to measured riometer absorption data as given in Supplement to Report 252, the absorptions to be expected at the location and period of greatest auroral absorption are as shown in Table III. Absorptions exceeded for different percentages of the time are quoted for a frequency of 127 MHz and for angles of elevation of 20° and 5°.

These results confirm that at VHF auroral absorption is only significant for a small percentage of the time.

TABLE III – *Auroral absorption at 127 MHz, dB*

Percentage of the time	Angle of elevation	
	20°	5°
0.1	1.5	2.9
1	0.9	1.7
2	0.7	1.4
5	0.6	1.1
50	0.2	0.4

3.3 *Polar cap absorption*

At geomagnetic latitudes greater than 64° another source of attenuation is polar cap absorption which occurs on relatively rare occasions [Bailey and Harrington, 1962]. It usually occurs in discrete, though sometimes overlapping, events which are nearly always associated with discrete solar events. The absorption is long-lasting and is detectable over the sunlit polar cap [Davies, 1965; Ortner *et al.*, 1962]. Polar cap absorption occurs most usually during the peak of the sunspot cycle, when there may be 10 to 12 events per year. Such an event may last up to a few days. This is in contrast to auroral absorption, which is frequently quite localized, with variations in periods of minutes. The absorption is due to bombardment of the upper atmosphere by solar protons, which are focused by the Earth's magnetic field to the polar regions.

The absorption is produced by ionization at heights greater than about 30 km. Due to the high collision frequency between electrons and neutral molecules at heights between 30 km and 90 km, this additional ionization results in considerable attenuation principally in the HF and lower VHF range.

A remarkable feature of a polar cap absorption event is the great reduction in the absorption during hours of darkness for a given rate of electron production. Figure 9 is a hypothetical model of the diurnal variation of polar cap absorption following a major solar flare based upon riometer observations at various latitudes.

Table IV, produced from an analysis of oblique-path forward-scatter measurements and from riometer absorption data [Bailey, 1964] gives the number of polar-cap events over the period 1952-1963 leading to absorption greater than 2.5 dB at vertical incidence for a frequency of 30 MHz. Also included for the events of each year are the average duration together with the average and greatest peak absorptions at 30 MHz for vertical incidence.

Polar-cap absorption observed at 30 MHz at near-vertical incidence may be extrapolated to other frequencies and angles by the (sec i)/f^2 relationship. This relationship with frequency is only strictly valid for absorption at heights above that where the angular wave frequency exceeds the electron collision frequency. Although during polar-cap events some of the absorption will occur at lower heights, this is unlikely to produce significant error.

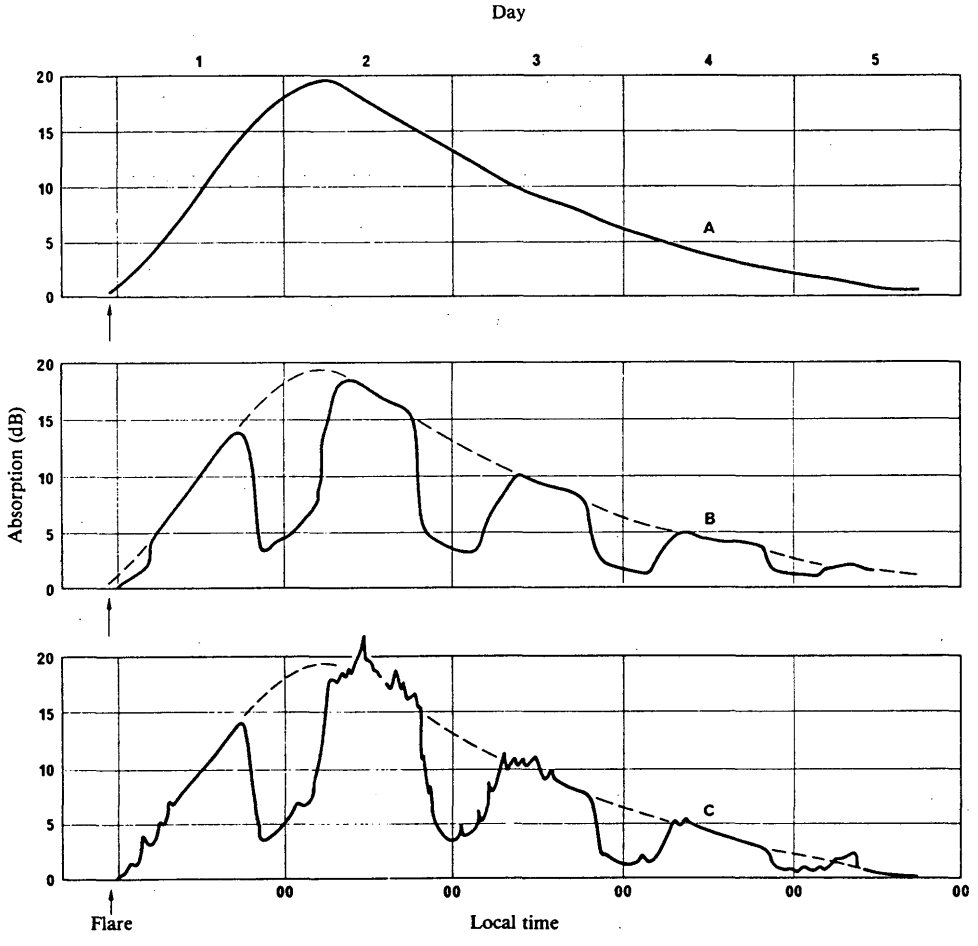


FIGURE 9 – *Hypothetical model showing polar cap absorption following a major solar flare as expected to be observed on riometers at approximately 30 MHz*

A: high latitudes – 24 hours of daylight
B: high latitudes – equal period of day and night
C: auroral zone

TABLE IV – *Polar cap absorption events*

Year	1952-1955	1956	1957	1958	1959	1960	1961	1962	1963
Mean smoothed Zurich sunspot number	6 to 38	142	190	188	160	114	55	38	28
Number of events	0	4	13	9	5	12	3	0	2
Average duration (hours)	-	104	60	76	149	54	69	-	72
Average peak absorption (dB)	-	7	5	10	18	7	9	-	4
Greatest peak absorption (dB)	-	13	9	24	24	20	17	-	5

In events recorded at stations where the day/night ratio is near unity, the absorption (measured in decibels) normally decreases on the second day of the event to about half the maximum value of that on the first day and a further reduction by half is evident on the third day. Using this model and 12 hours of daylight, Table V is constructed. The duration of the day within the polar cap can vary greatly depending on latitude and season.

TABLE V – *Numbers of hours of polar cap absorption for various levels (1952 to 1963 inclusive)*

Absorption (dB) 127 MHz (10° elevation)	Number of hours
7-8	36
6-7	48
5-6	24
4-5	12
3-4	144
2-3	96
1-2	480

4. Effects depending on total electron content

4.1 *Introduction*

A single parameter of the ionization distribution which is very significant in determining ionospheric effects on communication and navigation systems is the integral $\int n_e \, ds$, which is the integrated or total electron content (TEC) along the ray path from transmitter to receiver. A number of these effects, such as refraction, dispersion and group delay, are in magnitude directly proportional to the TEC; Faraday rotation is also approximately proportional to TEC, with the contributions from different parts of the ray path weighted by the longitudinal component of magnetic field. A knowledge of the TEC thus enables many important ionospheric effects to be estimated quatitatively. When used without qualification TEC is usually taken to mean the content of a vertical column of unit cross-section, but for practical applications it is generally the content along a slant path which is required; thus in any particular case it is important to make clear whether slant or vertical values are being quoted. Further information about the TEC is given in Report 725.

4.2 *Radiowave group delay*

For radiowave propagation along a station-satellite link, the presence of free electrons along the ray path causes the radiowave to travel with a group velocity less than the in-vacuo speed of light, thereby increasing the travel time over that expected from a free space geometry. This retardation suffered by the radiowave is commonly called the "group delay" which affects the accuracy of satellite navigation systems. For high-precision, delay must be compensated for either by prediction techniques or by direct measurement. If the precision required is of a considerable order of magnitude, e.g. 1 m over a distance of 5000 km or 1 mm per second when measuring speed by Doppler effect, no model is yet capable of achieving such precision [Papet-Lépine, 1978]. The problem can nonetheless be solved in real time by exploiting the dispersive effect of the ionosphere by combining the ionospheric effects on several carefully chosen frequencies.

Magnetoionic theory, neglecting the geomagnetic field and collisions, shows that the ionospheric group delay depends inversely on the square of the frequency used and directly upon the integral of the number of electrons along the ray path. Functionally, the relation is:

$$\Delta\tau \approx \frac{1.33 \times 10^{-7}}{f^2} \int_s n_e\,(s)\ \mathrm{d}s = \frac{1.33 \times 10^{-7}}{f^2} N_s \qquad (1)$$

where $\Delta\tau$ is the group delay due to the presence of free electrons measured in seconds, f is the frequency in hertz, and $\int_s n_e(s)\mathrm{d}s$ is the integrated electron concentration along the slant ray path (N_s) expressed in units of electron/m^2. Figure 10 is a plot of time delay ($\Delta\tau$) versus frequency (f) for several values of electron content along the ray path (N_s).

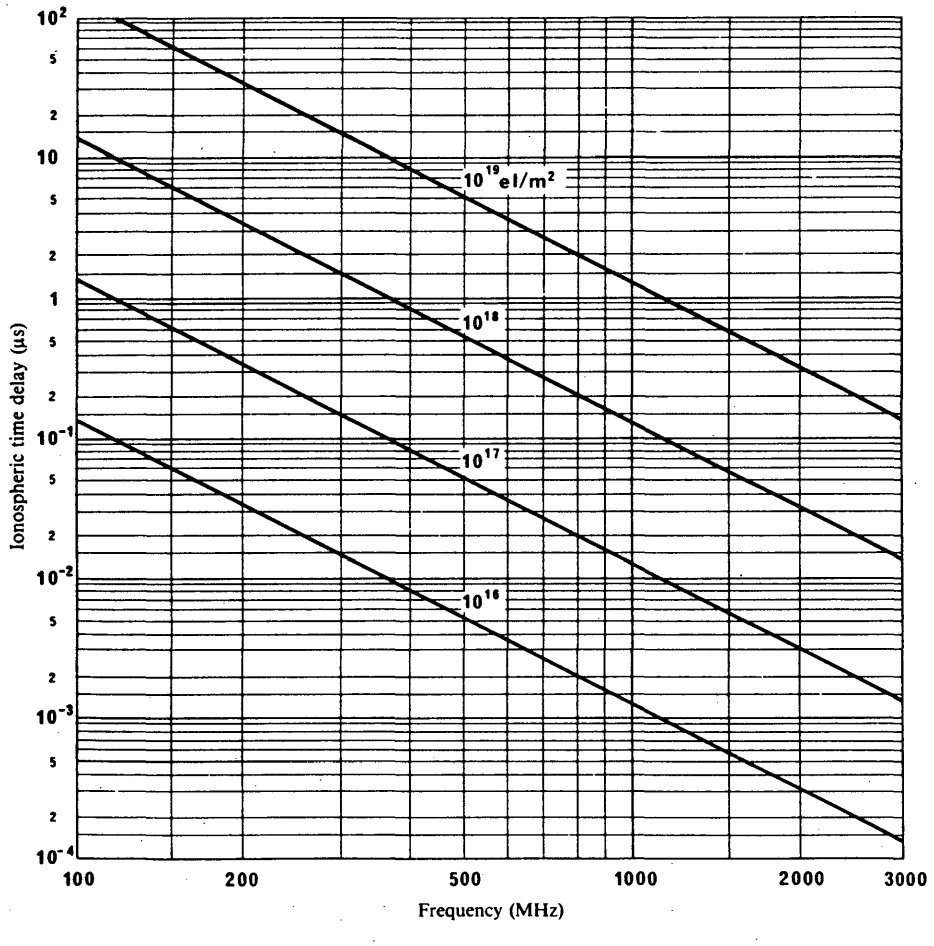


FIGURE 10 – *Ionospheric time delay versus frequency for various values of electron content*

For a band of frequencies around 1600 MHz the signal group delay varies from approximately 0.5 to 500 ns, for TEC from 10^{16} to 10^{19} electrons/m^2. Figure 11 shows the yearly percentage of daytime hours that the time delay will exceed 20 ns at a period of relatively high solar activity using a total electron content model developed by Bent *et al.* [1975].

In cases where frequency diversity schemes are adopted for satellite communications, it is necessary to know the propagation delay between the two channels used. Measurement of the delay time by using the 11 and 4 GHz bands of Japanese CS satellite communication loop showed 1.16 ns per 10^{17} electron/m^2 in N_s. This result agrees very well with the theoretical value estimated by equation (1) [Kosaka *et al.*, 1979].

4.3 *Dispersion*

When trans-ionospheric signals occupy a significant bandwidth the propagation delay (being a function of frequency) introduces dispersion. The differential delay across the bandwidth is proportional to the integrated electron density along the ray path. For a fixed bandwidth the relative dispersion is inversely proportional to frequency cubed. Thus, systems involving wideband transmissions must take this effect into account at VHF and possibly UHF. For example, for an integrated electron content of 5×10^{17} electron/m^2 a signal with a pulse length of 1 μs will sustain a differential delay of 0.02 μs at 200 MHz while at 600 MHz the delay would be only 0.00074 μs. (See Fig. 12 [Millman, 1967].) For pulse transmission, ionospheric dispersion causes distortion of the signal amplitude, envelope, pulse length, modulation and phase [Millman and Olsen, 1980].

4.4 *Frequency change*

The effect of the ionosphere upon the apparent frequency of a radio signal from a satellite produces only a second-order effect. However, the dispersive Doppler effect and the related phase-modulation techniques are of considerable interest as a tool for measuring the electron content of the ionosphere and exosphere [Alpert, 1963; Rawer, 1964].

In the course of systematic observations of the Doppler effects at 48° N at 20 and 40 MHz, numerous ionospheric effects were found [Joint Satellite Studies Group, 1965]. Deformations of the curve of Doppler frequency as a function of time, due to refraction, were found to be strong, increasing considerably the inaccuracy of the determination of the time of closest approach [Arendt *et al.*, 1965].

4.5 *Polarization*

The performance of Earth-space communication systems may be significantly affected by ionospheric Faraday rotation. This phenomenon seriously affects any VHF space communication system which uses linear polarization. Faraday rotation may also be important at higher frequencies in systems proposing frequency re-use where linear polarization is employed. It also provides the basis for an accurate and sensitive technique to measure the total electron content of the ionosphere. The cross-polarization discrimination for aligned antennas, XPD in dB, is related to the Faraday rotation angle, I, by:

$$XPD = -20 \log (\tan I) \qquad (2)$$

When a linearly polarized radio wave traverses the ionosphere, it separates into two independent components both elliptically polarized with opposite senses of rotation. The waves approach circular polarization as the frequency increases. Since the two waves progress inside the ionized medium with different velocities of propagation, their phase relationships are continously being altered. On emerging from the ionosphere the waves recombine to form a linearly polarized wave whose plane of polarization has been rotated with respect to that of the incident wave. This phenomenon, which is commonly referred to as the Faraday effect, is brought about by the interaction of the electromagnetic wave with the electrons in the presence of the Earth's magnetic field.

The Faraday rotation is inversely proportional to the square of frequency and directly proportional to the integrated product of the electron density and the component of the Earth's magnetic field along the propagation path (Report 725). Its median value at a given frequency exhibits a very regular diurnal, seasonal, and solar cyclical behaviour that can be predicted. This regular component of the Faraday rotation can therefore be compensated for by a manual adjustment of the polarization tilt angle at the earth-station antenna. However, large deviations from this regular behaviour can occur for small percentages of the time as a result of geomagnetic storms and, to a lesser extent, large-scale travelling ionospheric disturbances. These deviations cannot be predicted in advance. Intense and fast fluctuations of the Faraday rotation angles of VHF signals have been associated with strong and fast amplitude scintillations respectively, at locations situated near the crests of the equatorial anomaly [Lee *et al.*, 1982].

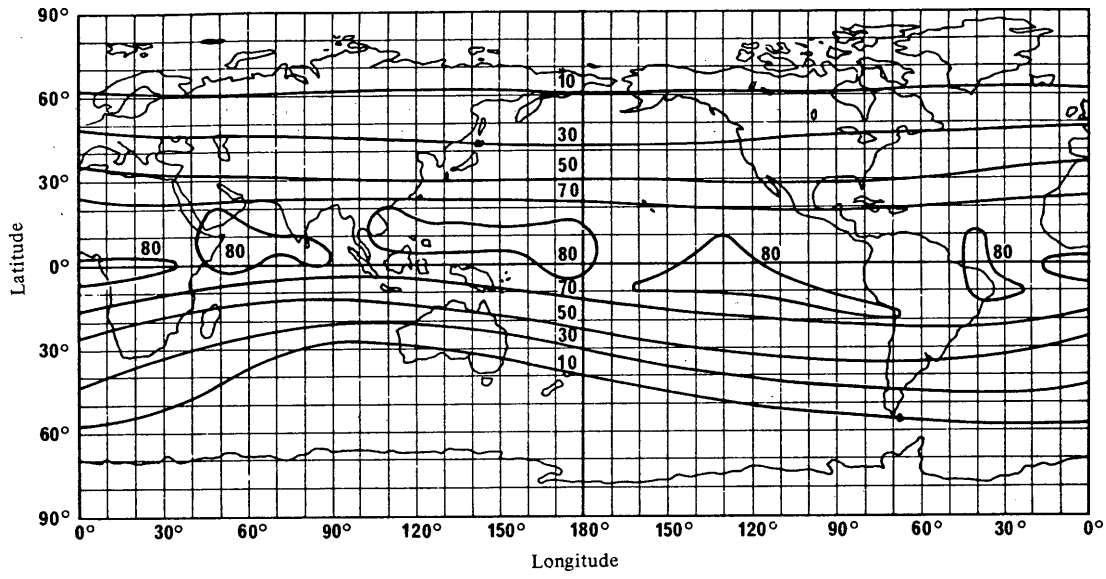


FIGURE 11 – *Contours of percentage of yearly average daytime hours when time delay at vertical incidence at 1.6 GHz exceeds 20 ns (sunspot number = 140)*

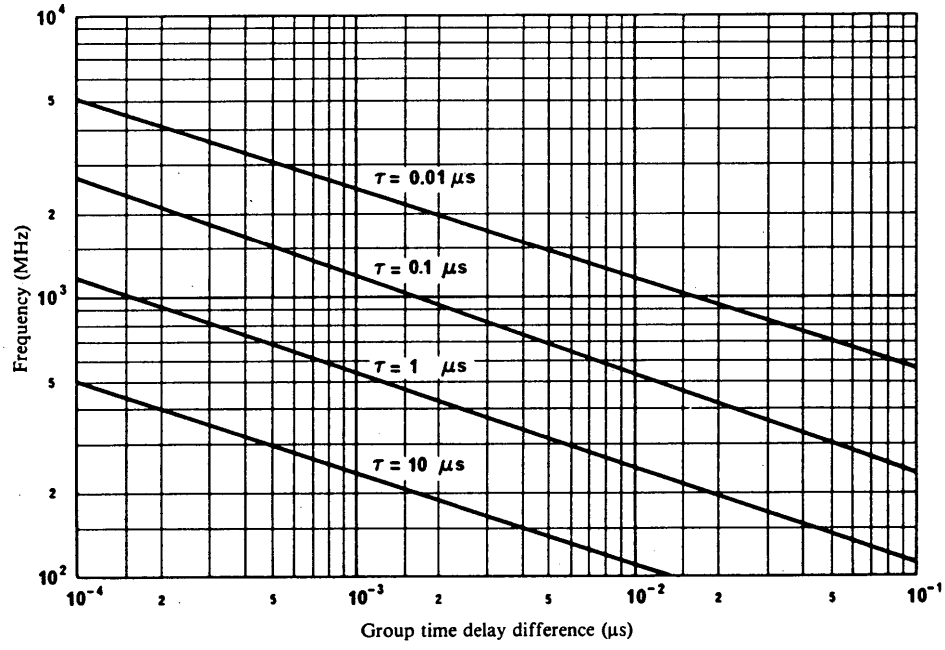


FIGURE 12 – *Difference in the time delay between the lower and upper frequencies of the spectrum of a pulse of width transmitted through the ionosphere, one-way transmission path [Millman, 1967]*

$\int n_e \, ds = 5 \times 10^{17}$ electrons/m^2

τ: pulse length

Near the maximum of a solar cycle (sunspot number of about 100), peak daytime rotations of about 2° at 4 GHz (cross-polar discrimination = 29 dB) can be expected at some locations in North America [Lee, 1977]. A somewhat higher peak value, 9° at 4 GHz is quoted in Report 555.

Table VI gives values of the magnitude which may be involved in a typical situation of communications between a mid-latitude station and a geostationary satellite. The values were derived from measurements at Tokyo (35°42′ N, 139°29′ E) using transmissions from the satellite ETS-II at 130° E. The zenith angle of the path at 300 km height was 40.5°. The Table gives the Faraday rotation in degrees which would be exceeded for the stated percentages of time, at a frequency of 1 GHz, during a complete year of observation, at both sunspot maximum and minimum periods.

TABLE VI — *Faraday rotation at 1 GHz exceeded for given percentages of time*

Time percentage	99	90	50	10	1	0.1	0.01	Period	R_{12}
Rotation (degrees)	3	7	23	43	64	75	82	1979-80	157
	1	2	7	14	30	41	47	1977-78	42

5. Refraction effects and variations in the direction of arrival

When radio waves propagate obliquely through the ionosphere they undergo refraction, mainly due to the electron density gradient. Since the gradient is itself often spatially inhomogeneous, a multiplicity of wave paths will occur. Each path has an amplitude and a time delay different from any other. The resultant effect of refraction and multipath will in general increase the apparent elevation angle of a radio source, and consequently introduce an error in the angular position of the source. There are two cases in which the multipath is significant. One is the case of low elevation angle propagation where the horizontally stratified layers of electron density irregularities in the ionosphere cause the refraction of the waves. In this case, the most noticeable effect is the change of the angle of arrival. At a constant altitude between 300 and 1000 km, this effect attains a maximum value of the order of a few milliradians at an elevation angle between 3° and 5° at 100 MHz, and decreases with increasing height and increasing elevation angle [Millman, 1967]. It is also inversely proportional to frequency squared and varies diurnally with changes in electron content.

The other case is the propagation at a direction along the geomagnetic field lines where large-scale irregularities are generally aligned with the magnetic field. Variations in refraction, and thus in the direction of arrival of transionospheric signals, also arise from the movement across the line of sight of medium- or large-scale ionospheric irregularities. These irregularities, which range from tens to hundreds of kilometres in size, are frequently associated with travelling disturbances and give rise to fluctuations in the direction of arrival, with periods from about 15 minutes up to an hour or more [Vitkevich, 1958; Wild *et al.*, 1959; Lawrence and Jespersen, 1961; Bramley, 1974]. They are most commonly observed in daytime. The magnitude of the fluctuation is typically of the order of 1 milliradian at 100 MHz and is again inversely proportional to the square of the frequency.

6. Summary of terrestrial ionospheric effects

The magnitude and behaviour of ionospheric effects have been described. Each effect may be an important consideration in the design of different kinds of Earth-space links. The effects decrease with increasing frequency; several can be mitigated even in frequency ranges where they would otherwise present severe problems.

Table VII estimates maximum values for ionospheric effects at a frequency of 1 GHz. It is assumed that the total zenith electron content of the ionosphere is 10^{18} electron/m^2 column. An elevation angle of about 30° is also assumed. The values given are for the one-way traversal of the waves through the ionosphere.

ARCHIVES U.I.T. GENÈVE

In anticipation of the coming era of Integrated Services Digital Network (ISDN) for global communications, system design engineers have to face ionospheric effects for applications in long distance ISDN connections using satellite links. The current ISDN description for the bit error rate (BER) allocation for a Fixed Satellite Service (FSS) transmitting 64 kbit/s digital messages over a Hypothetical Reference Digital Path (HRDP) has been provided in CCITT Study Group XVIII [CCITT, 1988].

TABLE VII – *Estimated maximum ionospheric effects at 1 GHz for elevation angles of about 30° one-way traversal*

Effect	Magnitude	Frequency dependence
Faraday rotation	108°	$1/f^2$
Propagation delay	0.25 μs	$1/f^2$
Refraction	< 0.17 milliradians	$1/f^2$
Variation in the direction of arrival	0.2 min of arc	$1/f^2$
Absorption (polar cap absorption)	0.04 dB	$\sim 1/f^2$
Absorption (auroral + polar cap absorption)	0.05 dB	$\sim 1/f^2$
Absorption (mid-latitude)	< 0.01 dB	$1/f^2$
Dispersion	0-4 ns/MHz	$1/f^3$
Scintillation	See § 2 of the Report	See § 2 of the Report

7. Extraterrestrial propagation effects

Propagation effects due to ionized media occur when the path transits the solar corona. These effects for a path at 4 solar radii from the centre of the Sun at a frequency of 2.3 GHz are summarized in Table VIII [Smith and Edelson, 1979].

TABLE VIII

Effect	Magnitude
Faraday Rotation	20-200°
Group Delay	17 μs
Angular Broadening	0.02-2 min of arc
Spectral Broadening	7-16 Hz
Absorption	negligible
Dispersion	10 ns/MHz
Intensity Scintillation	saturates (m = 1)

REFERENCES

AARONS, J. [1977] Equatorial scintillations: A review. *IEEE Trans. Ant. Prop.*, Vol. AP-25, **5**, 729-736.

AARONS, J. [1982] Global morphology of ionospheric scintillations. *Proc. IEEE*, Vol. 70, 360-378.

AARONS, J. and MARTIN, E. [1975] The effects of the August 1972 magnetic storms on ionospheric scintillation. *Radio Sci.*, **10**, 547-554.

AARONS, J., MULLEN, J. P., KOSTER, J. R., DaSILVA, R. F., MEDEIROS, J. R., MEDEIROS, R. T., BUSHBY, A., PANTOJA, J., LANAT, J. and PAULSON, M. R. [1980] Seasonal and geomagnetic control of equatorial scintillations in two longitudinal sectors. *J. Atmos. Terr. Phys.*, Vol. 42, **9-10**, 861-866.

AARONS, J., MULLEN, J. P., WHITNEY, H. E., JOHNSON, A. L. and WEBER, E. J. [1981] UHF scintillation activity over polar latitudes. *Geophys. Res. Lett.* Vol. 8, **3**, 227-280.

AARONS, J. and WHITNEY, H. E. [1968] Ionospheric scintillations at 136 MHz for a synchronous satellite. *Planet and Space Sci.*, Vol. 16, 21-28.

AGY, V. [1975] On the geographic distribution of auroral absorption. *J. Atmos. Terr. Phys.*, Vol. 37, 681-685.

ALPERT, J. L. [1963] An investigation of the upper atmosphere on the basis of measurements of Doppler effect in satellite signals at coherent frequencies (in Russian). *Geomag. i Aeronom.*, Vol. 3, **1**, 10-24.

ARENDT, P. R., PAPAYOANOU, A. and SOICHER, H. [1965] Determination of the ionospheric electron content utilizing satellite signals. *Proc. IEEE*, Vol. 53, 268-277.

BAILEY, D. K. [1964] Polar cap absorption. *Planet and Space Sci.*, **12**, 495-541.

BAILEY, D. K. and HARRINGTON, J. M. [1962] A survey of polar cap absorption events (solar proton events) in the period 1952 through 1960. *J. Phys. Soc. Japan*, **17**, Supplement A-II, 334.

BASLER, R. P. [1966] Annual variation of auroral absorption. *J. Geophys. Res.*, Vol. 71, 982-984.

BASU, S. [1975] Universal time seasonal variations of auroral zone magnetic activity and VHF scintillations. *J. Geophys. Res.*, Vol. 80, 4725-4728.

BASU, S. and AARONS, J. [1980] The morphology of high-latitude VHF scintillation near 70° W. *Radio Sci.*, Vol. 15, **1**, 59-70.

BASU, S. and KHAN, B. K. [1976] Model of equatorial scintillations from in-situ measurements. *Radio Sci.*, Vol. 11, 821-832.

BASU, S., McCLURE, J. P., BASU, S., HANSON, W. B. and AARONS, J. [1980] Coordinated study of equatorial scintillation and *in situ* and radar observations of night-time F region irregularities. *J. Geophys. Res.*, Vol. 85, 5119.

BASU, S., MACKENZIE, E. and BASU, S. [1988] - Ionospheric constraints on VHF/UHF communication links during solar maximum and minimum periods. Radio Sci., Vol. 23, 363-378.

BASU, S., MACKENZIE, E., BASU, S., COSTA, E., FOUGERE, P., CARLSON, H. and WHITNEY, H. [1987] - 250 MHz/GHz scintillation parameters in the equatorial, polar and auroral environments. IEEE J. of Selected Areas in Communications, Vol. SAC-5, 102-115.

BELLCHAMBERS, W. H., PIGGOTT, W. R. and BARCLAY, L. W. [1962] *Royal Society I.G.Y. Expedition. Halley Bay*, 2, 209. Royal Society, London.

BENT, R. B., LLEWELLYN, S. K., NESTERCZUK, G. and SCHMID, P. E. [1975] The development of a highly-successful world-wide empirical ionospheric model and its use in certain aspects of space communications and world-wide total electron content investigations. Proc. Symposium of the Effect of the Ionosphere on Space Systems and Communications, Naval Research Laboratory, Arlington, Va., USA, 23-38.

BISCHOFF, K. and CHYTIL, B. [1969] A note on scintillation indices. *Planet. and Space Sci.*, Vol. 17, 1059-1066.

BRAMLEY, E. N. [1974] Fluctuations in direction and amplitude of 136 MHz signals from a geostationary satellite. *J. Atmos. Terr. Phys.*, Vol. 36, 1503-1513.

BRIGGS, B. H. and PARKIN, I. A. [1963] On the variation of radio star and satellite scintillations with zenith angle. *J. Atmos. Terr. Phys.*, Vol. 25, 334-365.

CCITT Blue Book, Vol. III, Facsicle III.4, Study Group XVIII document, Recommendation G.821, IXth Plenary Assembly, Melbourne, November 1988.

CHYTIL, B. [1967] The distribution of amplitude scintillation and the conversion of scintillation indices. *J. Atmos. Terr. Phys.*, Vol. 29, 1175-1177.

CORNEC, J. P. [1978] Amplitude scintillations of ATS-6 radio signals in Lannion. Proc. Symposium COSPAR Satellite Beacon Group on Beacon Satellite Measurements of Plasmaspheric and Ionospheric Properties, Florence, May 1978. Published by l'Instituto di Ricerca sulle Onde Elettromagnetiche, Consiglio Nazionale delle Ricerce (CNR), Florence, Italy, 40-1 to 40-14.

CRANE, R. K. [1974] Morphology of ionospheric scintillation. Tech. Note 1974-29, Lincoln Laboratory MIT, Lexington, Mass., USA.

CRANE, R. K. [1975] Spectra of amplitude and phase scintillation. Proc. IES Symposium, Naval Research Laboratory, Arlington, Va., USA.

CRANE, R. K. [1976] Spectra of ionospheric scintillations. *J. Geophys. Res.*, Vol. 81, **13**, 2041-2050.

CRANE, R. K. [1977] Ionospheric scintillation. *Proc. IEEE*, Vol. 65, 180-199.

DAVIES, K. [1965] Ionospheric radio propagation. NBS Monograph 80. (Also available from Dover Press, New York, NY, USA.)

DRIATSKIY, V. M. [1966] Study of the space and time distribution of auroral absorption according to observations of the riometer network in the arctic. *Geomag. i Aeronom.*, **6**, 828-834.

FANG, D. J. [1980] 4/6 GHz ionospheric scintillations measurements. AGARD Conf. Proc. No. 284. Propagation Effects in Space/Earth Paths, 33-1 to 33-12.

FANG, D.J. and ALLNUTT, J.E. [1987] - Simultaneous rain depolarization and ionospheric scintillation impairments at 4 GHz. IEE Conference Publication No. 274, Part 2, Proceedings of the fifth International Conference on Antennas and Propagation, pp. 281-284.

FANG, D. J., KENNEDY, D. J. and DEVIEUX, C. [1978] Ionospheric scintillations at 4/6 GHz and their systems impact. IEEE Electronics and Aerospace Systems (EASCON '78), Publ. No. CH1352-4/78/0000 0385, Washington, DC 20402, USA.

FANG, D. J. and LIU, C. H. [1983] A morphological study of gigahertz equatorial scintillations in the Asian region. *Radio Sci.*, Vol. 18, 241-252.

FANG, D.J. and LIU, C.H. [1984] - Statistical characterizations of equatorial scintillation in the Asian region. Radio Science, Vol. 19, pp. 345-358.

FANG, D. J. and PONTES, M. S. [1981] 4/6 GHz ionospheric scintillation measurements during the peak of sunspot cycle 21. *COMSAT Tech. Rev.* Vol. 11, **2**, 293-320.

FRANKE, S.J. and LIU, C.H. [May, 1987] Analysis of a long period fading component in saturated VHF amplitude scintillation observed at Ascension Island. J. Atmos. Terr. Phys., Vol. 49, 5, 421-431.

FRANKE, S. J., LIU, C. H. and FANG, D. J. [1984] Multifrequency study of ionospheric scintillation at Ascension Island. *Radio Sci.*, Vol. 19, 695-706.

FREMOUW, E. J. LIVINGSTON, R. C. and MILLER, D. A. [1980] On the statistics of scintillating signals. *J. Atmos. Terr. Phys.*, Vol. 42, 717-731.

FREMOUW, E. J., LIVINGSTON, R. C., RINO, C. L., COUSINS, M., FAIR, B. C. and LEADABRAND, R. L. [1978] Complex-signal scintillation – early results from the DNA-002 coherent beacon. *Radio Sci.*, Vol. 13, 167-187.

FREMOUW, E. J. and RINO, C. L. [1973] An empirical model for average F-layer scintillation at VHF/UHF. *Radio Sci.*, Vol. 8, 213-222.

FUJITA, M., OGAWA, T. and KOIKE, K. [1978] 1.7 GHz scintillation measurements at midlatitude using a geostationary satellite beacon. *J. Atmos. Terr. Phys.*, Vol. 40, 963-968.

FUJITA, M., SINNO, K. and OGAWA, T. [1982] Frequency dependence of ionospheric scintillations and its application to spectral estimation of electron density irregularities. *J. Atmos. Terr. Phys.* Vol. 44, 13-18.

HARGREAVES, J. K. [1966] On the variation of auroral radio absorption with geomagnetic activity. *Planet. and Space Sci.*, Vol. 14, 991-1006.

HARGREAVES, J. K. and COWLEY, F. C. [1967] Studies of auroral space absorption. *Planet. and Space Sci.*, Vol. 15, 1571-1585.

HARTZ, T. R. [1972] Morphology of radio-radar polar propagation effects. NATO Advisory Group for Aerospace Research and Development. Conference Proc. AGARD-CP-97, 1-1 to 1-18. Technical Editing and Reproduction Ltd., London, UK.

HARTZ, T. R., MONTBRIAND, L. E. and VOGAN, E. L. [1963] A study of auroral absorption at 30 Mc/s. *Can. J. Phys.*, **41**, 581-595.

HOFFMAN, W. C. [1960] *Statistical Methods in Radio Wave Propagation*, 3-36. Pergamon Press, New York, NY, USA.

HOLT, C., LANDMARK, B. and LEID, F. [1961] Analysis of riometer observations obtained during polar radio blackouts. *J. Atmos. Terr. Phys.*, Vol. 23, 229-243.

HOOK, J. L. [1968] Morphology of auroral zone radiowave absorption in the Alaska sector. *J. Atmos. Terr. Phys.*, Vol. 30, 1341-1351.

HOUMINER, Z., AARONS, J. and RICH, F. [1981] Production and dynamics of high-latitude irregularities during magnetic storms. *J. Geophys. Res.*, Vol. 86, 9939.

IIDA, T., MURATA, K. and ISHIDA, T. [1973] Measurement of the attenuation of 9.303 MHz waves from ISIS-II through the ionosphere. *J. Radio Res. Labs.* (Japan), Vol. 20, 17-33.

IIDA, T. and YAMAYA, K. [1976] Method of direct reception of swept-frequency topside sounder signals from ISIS-II through the ionosphere. *J. Radio Res. Labs.* (Japan), Vol. 23, 111-138.

JOINT SATELLITE STUDIES GROUP [1965] A synoptic study of scintillations of ionospheric origin in satellite signals. *Planet. and Space Sci.*, Vol. 13, 51-62.

KARASAWA, Y. [1987] - Interpretation of quasi-periodic scintillation at frequencies above 1 GHz. Trans. IEICE (Japan), E70, pp. 768-774.

KARASAWA, Y. and YASUKAWA, K. [1981] Gradual change of power spectrum of ionospheric scintillation. *Trans. Inst. Electron. Com. Engrs. Japan*, Vol. E64, 9.

KARASAWA, Y., YASUKAWA, K. and YAMADA, M. [May/June, 1985] Ionospheric scintillation measurements at 1.5 GHz in mid-latitude region. *Radio Sci.*, Vol. 20, 3.

KERSLEY, L., PRYSE, S.E. and WHEADON, N.S. [1988] - Amplitude and phase scintillation at high latitudes over Northern Europe. Radio Sci., Vol. 23, 320.

KOSAKA, K., AWAKA, J. and OTSU, Y. [1979] Measurement of relative propagation delay between C- and K-band satellite loops. *IEEE Trans. Ant. Prop.*, Vol. AP-27, 893-895.

KOSTER, J. R. [1963] Some measurements of the irregularities giving rise to radio star scintillations at the equator. *J. Geophys. Res.*, Vol. 68, 9, 2579-2590.

KOSTER, J. R. [1966] Ionospheric studies using the tracking beacon of the Early Bird synchronous satellite. *Ann. de Géophys.*, Vol. 22, 435-439.

KOSTER, J. R. [1972] Equatorial scintillations. *Planet. and Space Sci.*, Vol. 20, 1999-2014.

KUMAGAI, H [1987] - Spatial correlations in intense ionospheric scintillations: Comparison between numerical computation and observation. Radio Sci., 22, pp. 439-448.

KUMAGAI, H. and OGAWA, T. [1986] - Behaviour of mid-latitude F-Region irregularities deduced from spaced-receiver VHF scintillation measurements. J. Atmos. Terr. Phys., 48, pp. 221-230.

LAWRENCE, R. S. and JESPERSEN, J. L. [1961] Refraction effects of large-scale ionospheric irregularities observed at Boulder, Colorado. Space Research II, Proc. 2nd International Space Science Symposium, 227.

LEE, M. C., DAS GUPTA, A., KLOBUCHAR, J. A., BASU, S. and BASU, S. [March-April, 1982] Depolarization of VHF geostationary satellite signals near the equatorial anomaly crests. *Radio Sci.*, Vol. 17, 2, 399-409.

LEE, M. K. [1977] Cross-polarization performance of the RCA Satcom system. *RCA Rev.*, Vol. 38, 2, 171-210.

MAYNARD, L. A. [1972a] L-Band ionospheric fading measurements at Ottawa. Paper presented at IMCO Panel of Experts for Maritime Satellites.

MAYNARD, L. A. [1972b] Ionospheric fading margins at 1550 MHz at Churchill. Paper presented at IMCO Panel of Experts for Maritime Satellites.

MAYNARD, L. A. [1976] Channel fading on air mobile satellite communications links. AGARD Conf. Proc. No. 173, Radio Systems and the Ionosphere, Athens, Greece.

MILLMAN, G. H. [1967] A survey of tropospheric, ionospheric and extraterrestrial effects on radio propagation between the earth and space vehicles; Propagation Factors in Space Communications, AGARD Conf. Proc. No. 3, 3-55, Technivision.

MILLMAN, G. H. and OLSEN, K. A. [1980] Ionospheric dispersion effects on wideband transmissions. AGARD Conf. Proc. No. 284, Propagation Effects in Space/Earth Paths, 26-1 to 26-12.

MINAKOSHI, H. [1988] - Observation of ionospheric scintillation in the Asian northern mid-latitude region. (To be published in J. Comm. Res. Lab. (Japan)).

MINAKOSHI, H., SINNO, K., KAN, M., KURIHARA, H. and FURUTA, O. [1981] Severe ionospheric scintillation associated with magnetic storm on March 22, 1979. *J. Radio Res. Labs.* (Japan), Vol. 28, **125/126**, 1-9.

MORIYA, Y., IWATA, Y. and SAKURADA, H. [1985] - New type of ionospheric scintillation at L-band. Int. Symp. Antennas & Propagation (ISAP'85). IECE of Japan, Kyoto, pp. 1011-1014.

MULLEN, J. P. [1973] Sensitivity of equatorial scintillation to magnetic activity. *J. Atmos. Terr. Phys.*, Vol. 35, 1187-1194.

MYERS, W. J., GJELDUM, R. J., LIU, C. H. and YEH, K. C. [1979] A study of ionospheric scintillations of phase and quadrature components. *J. Geophys. Res.*, Vol. 84, 2039-2048.

OGAWA, T. and KUMAGAI, H. [1985] - Deep depletions of total electron content associated with severe mid-latitude gigaherts scintillations during geomagnetic storms. J. Geophys. Res., 90, pp. 6652-6656.

OGAWA, T., SINNO, K., FUJITA, M. and AWAKA, J. [1980] Severe disturbances of VHF and GHz waves from geostationary satellites during a magnetic storm. *J. Atmos. Terr. Phys.*, Vol. 42, 7, 637-644.

ORTNER, J., HULTQVIST, B., BROWN, R. R., HARTZ, T. R., HOLT, O., LANDMARK, B., HOOK, J. L. and LEINBACH, H. [1962] Cosmic noise absorption accompanying geomagnetic storm sudden commencements. *J. Geophys. Res.*, Vol. 67, 4169-4186.

OTT, R. H. [1977] Observed temporal amplitude and phase spectra from ATS-6 radio beacon experiment at 40, 140 and 360 MHz. *Radio Sci.*, Vol. 12, 2, 319-325.

PAPET-LEPINE, J. [1978] Influence de l'ionosphère sur la précision des mesures en géodésie par satellite artificiel. (Effect of the ionosphere on the precision of geodetic measurements by artificial satellite.) Operational modelling of the aerospace environment. AGARD Conf. Proc. No. 238, Vol. 1, 24-1 to 24-19.

PAULSON, M. R. and HOPKINS, R. U. F. [1973] Effects of equatorial scintillation fading on Satcom signals. Naval Electronics Laboratory Center, TR-1875, San Diego, Calif., USA.

PAULSON, M. R. and HOPKINS, R. U. F. [1977] Spatial diversity characteristics of equatorial scintillation for satellite signals at UHF and L-band. Naval Ocean Systems Center, TR113, NTIS Accession No. ADA040628, National Technical Information Service, Springfield, Va. 22161, USA.

PONNAPPA, P. [1973] High latitude ionospheric fading measurements at 254 MHz (VHF) and 1550 MHz (L-Band) at Churchill, Manitoba. TER-RD-254 Telecommunications and Electronics Branch Air, Ministry of Transport, Ottawa, Canada.

RAWER, K. [1964] Erforschung der Ionosphäre mit Radiowellen von Satelliten und Raketen. Phasenverfahren (Investigation of the ionosphere with radio waves from satellites and rockets; phase methods). *Space Sci. Revs.*, 3, 380-432.

RINO, C. L. [1978] Evidence for sheetlike auroral ionospheric irregularities. *Geophys. Res. Lett.*, 5, 1039-1042.

RINO, C. L. and FREMOUW, C. L. [1973] Statistics for ionospherically diffracted UHF/VHF signals. *Radio Sci.*, 8, 223-233.

RUFENACH, C. L. [1972] Power-law wavenumber spectrum deduced from ionospheric scintillation observations. *J. Geophys. Res.*, Vol. 77, 4751-4772.

SESSIONS, W. B. [1972] Amplitude fading of simultaneous transionospheric L-band and VHF signals received at the geomagnetic equator. NASA X-810-72, 282 Goddard Space Flight Center, National Aeronautical and Space Administration. Greenbelt, Md., USA.

SINNO, K. and KAN, M. [1978] Mid-latitude ionospheric scintillation of VHF radio signals associated with peculiar fluctuations of Faraday rotation. *J. Atmos. Terr. Phys.*, Vol. 40, 503-506.

SINNO, K. and KAN, M. [1980] Ionospheric scintillation caused by spread-F and sporadic-E over Kokubunji, Japan. *J. Radio Res. Labs.* (Japan), Vol. 27, 53-77.

SINNO, K. and MINAKOSHI, H. [1983] Experimental results on satellite scintillations due to field-aligned irregularities at mid-latitudes. *J. Atmos. Terr. Phys.*, Vol. 45, 563-567.

SKINNER, N. J., KELLEHER, R. F., HACKING, J. B. and BENSON, C. W. [1971] Scintillation fading of signals in the SHF band. *Nature Phys. Sci.*, Vol. 232, 19-21.

SLACK, F. F. [1972] Quasiperiodic scintillation in the ionosphere. *J. Atmos. Terr. Phys.*, Vol. 34, 927-939.

SMITH, E. K. and EDELSON, R. E. [1979] Radio propagation through solar and other extraterrestrial ionized media. JPL Publications 79-117. Jet Propulsion Laboratory, California Institute of Technology, Pasadena, Calif. 91109, USA.

TANAKA, T. [1981] - Severe ionospheric disturbances caused by the sudden response of evening sub-equatorial ionospheres to geomagnetic storms. J. Geophys. Res., 86, pp. 11335-11349.

TANAKA, T. [1986] - Low-latitude ionospheric disturbances: Results for March 22,1979 and their general characteristics. Geophys. Res. Lett., 13, pp. 1399-1402.

TATARSKI, V. I. [1967] *Radio Propagation in a Turbulent Medium.* English translation by P. Silverman. McGraw Hill, New York, NY, USA.

TAUR, R. R. [1973] Ionospheric scintillation at 4 and 6 GHz. *COMSAT Tech. Rev.*, Vol. 3, 1, 145-163.

TAUR, R. R. [1974] Ionospheric scintillation at frequencies above 1 GHz. *COMSAT Tech. Rev.*, 4, 461-476.

TAUR, R. R. [1976] Simultaneous 1.5 and 4 GHz ionospheric scintillation measurements. *Radio Sci.*, Vol. 11, 1029-1036.

TSUNODA, R.T. [1985] - Control of the seasonal and longitudinal occurrence of equatorial scintillations by the longitudinal gradient in integrated E-region Pederson conductivity. J. Geophys. Res., Vol. 90, 447-456.

UMEKI, R., LIU, C. H. and YEH, K. C. [1977a] Multifrequency spectra of ionospheric amplitude scintillations. *J. Geophys. Res.*, Vol. 82, 2752-2770.

UMEKI, R., LIU, C. H. and YEH, K. C. [1977b] Multifrequency studies of ionospheric scintillations. *Radio Sci.*, Vol. 12, 311-317.

VITKEVICH, V. V. [1958] Investigation of ionospheric inhomogeneities by radioastronomical methods. *Radiotekhnika i Elektronika*, **3**, 478-486.

WAND, R. H. and EVANS, J. V. [1975] Morphology of ionospheric scintillation in the auroral zone. Proc. IES Symposium, Naval Research Laboratory, Arlington, Va., USA.

WHITNEY, H. E., AARONS, J., ALLEN, R. S. and SEEMANN, D. R. [1972] Estimation of the cumulative amplitude probability distribution function of ionospheric scintillation. *Radio Sci.*, Vol.7, 1095-1104.

WHITNEY, H. E. and BASU, S. [1977] The effect of ionospheric scintillation on VHF/UHF satellite communication. *Radio Sci.*, Vol. 12, 123-133.

WHITNEY, H. E. and RING, W. F. [1971] Dependency of scintillation fading of oppositely polarized VHF signals. *IEEE Trans. Ant. Prop.*, Vol. AP-19.

WILD, J. P., SHERIDAN, K. V. and NEYLAN, A. A. [1959] An investigation of the speed of the solar disturbances responsible for Type III radio bursts. *Austral. J. Phys.*, **12**, 369-398.

YEH, K. C., LIU, C. H. and YOUAKIM, M. Y. [1975] A theoretical study of the ionospheric behaviour caused by multiple scattering. *Radio Sci.*, Vol. 10, 97-106.

REPORT 259-7*

VHF IONOSPHERIC PROPAGATION

(Question 41/6)

(1951-1953-1956-1959-1963-1966-1970-1974-1978-1982-1986-1990)

1. Introduction

The ionosphere, while primarily responsible for reflection of radio waves below 30 MHz, is capable of producing reflections in the VHF band (30 - 300 MHz) under some conditions, during relatively short periods of time and in certain areas of the world.

This report describes the conditions under which the E- and F-Regions produce such reflections, subdivided into normal and abnormal, in the sense that normal propagation can be forecast as a function of long range geophysical or solar parameters with a high degree of predictability on a daily basis, while abnormal means that its predictability is low on a daily basis, and only long term statistics provide some assessments of its behaviour.

It should be noted that ranges in excess of 1000 km may also result from the effects of anomalous tropospheric propagation through the non-ionized medium. Should it be necessary, or desirable, to identify the mode of an interfering signal, reference should be made to —— § 4, where the principal characteristics are tabulated.

2. F-Region

In this section, the F-Region is considered in relation to normal and abnormal propagation.

2.1 Normal F-Region propagation

Near the peak of the solar cycle long-distance transmissions via the F2 layer in —— mid- latitudes can occur for a significant fraction of the time up to 50 MHz or more. In low latitudes regular transmission will occur around 30 to 40 MHz, and such transmission can occur at 60 MHz and above. The lowest frequency at which interference due to such propagation becomes so infrequent as to be negligible is about 60 MHz for stations in mid- latitudes, and 70 MHz for stations at low latitudes (see Figs. 1, 2, 3).

* This Report is brought to the attention of Study Groups 5, 8 and 10.

A report of normal propagation of television signals at very high frequencies has been produced in India [Saksena, 1979]. Also, propagation of VHF TV signals at about 60 MHz over a 3100 km path from Bangkok has been observed in India at Rohtak, particularly during equinoctial months and during a period of high solar activity due to propagation via the ionospheric F-layer at frequencies greater than the basic MUF. This signal reception was centred at 2000 local time with durations between one and two and a half hours [CCIR, 1982-86].

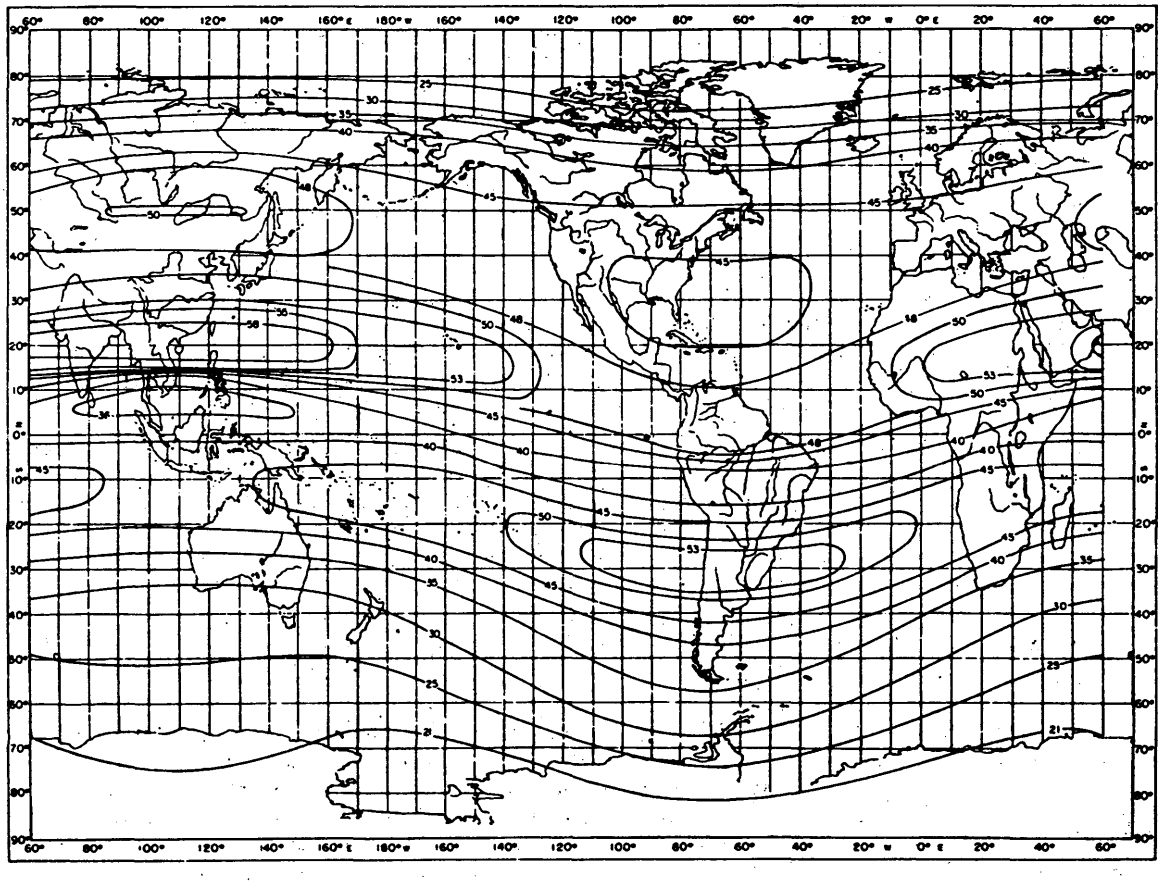


FIGURE 1 – *F2 (4000) MUF exceeded during 1 % hours – December solstice; sunspot maximum*

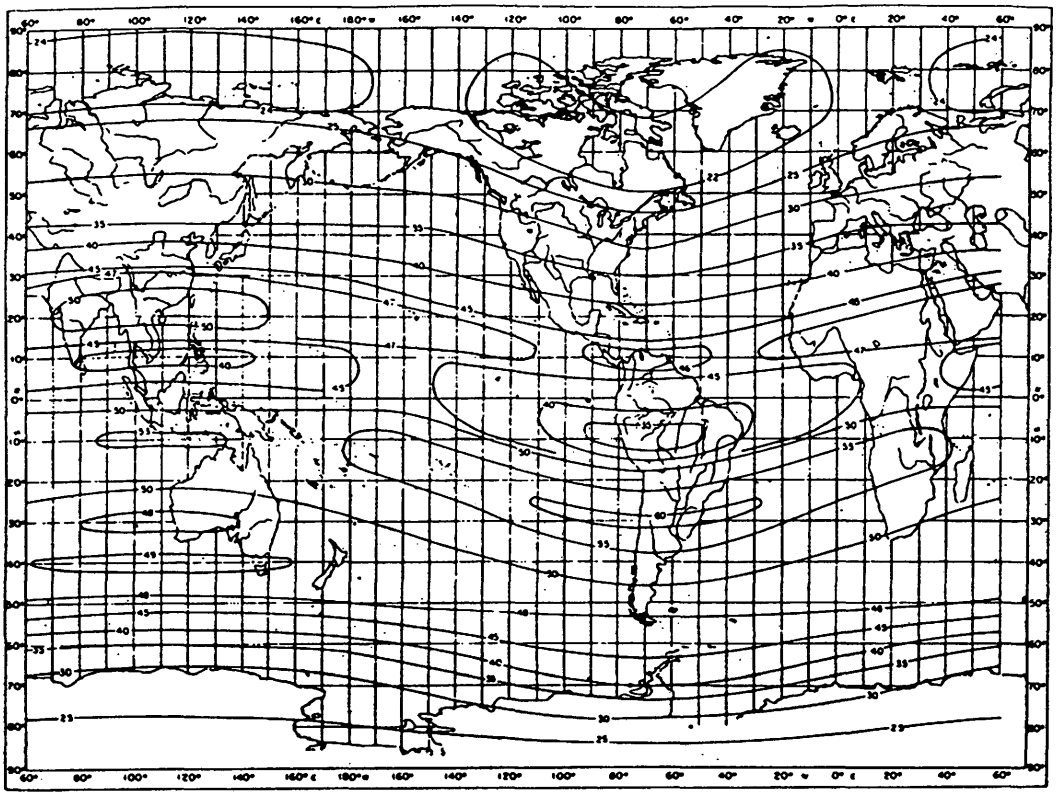


FIGURE 2 – *F2 (4000) MUF exceeded during 1 % of hours – June solstice; sunspot maximum*

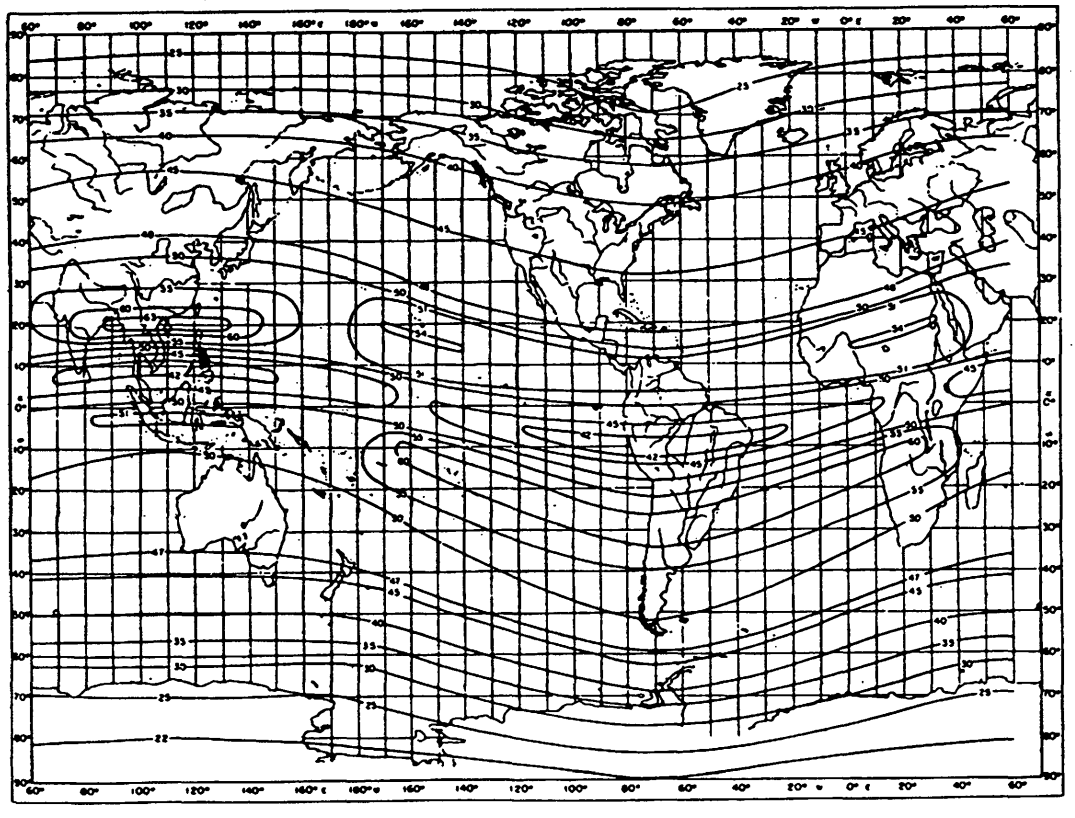


FIGURE 3 – *F2 (4000) MUF exceeded during 1 % of hours – Equinox; sunspot maximum*

2.2 Abnormal F-Region propagation

2.2.1 *Trans-equatorial propagation (TEP)*

Recent studies indicate that strong transmission can occur, particularly during high sunspot years, over long North-South paths spanning the magnetic equator. Most observations have been made by radio amateurs at a frequency of 50 MHz for paths of the order of 4000 to 9000 km; paths between South America-North America, Africa-Europe and Japan-Australia have been noted.

According to the experiment carried out between Australia and Japan during about one cycle of solar activity (1965-1974) at frequencies 32, 48 and 72 MHz, and during about a half-cycle of the activity (1969-1974) at additional frequencies 88 and 102 MHz, it was found that trans-equatorial propagation occurred at 32 MHz during a large part of the day (except a few hours in the morning) even in years of low solar activity. The hours of reception were increased with solar activity. At frequencies of 48, 72, 88 and 102 MHz, trans-equatorial propagation occurred after around 2000 h local time during both equinoctial periods and lasted for 6-8 h at 48 MHz, and 2-4 h at 102 MHz. Long-term variations of basic transmission losses at VHF which propagated over the trans-equatorial path are shown in Fig. 4 [Tao *et al.*, 1970; Kuriki *et al.*, 1972; Tanohata *et al.*, 1980]. On the basis of the signal levels observed on these four frequencies, the received signal power, normalized to 1 kW e.r.p. and using transmitting and receiving dipole antennas, is inversely proportional to a value between the 10th and 12th power of the frequency [Kuriki *et al.*, 1972].

It seems that propagation in the daytime is by the 2F mode, based on the equatorial anomaly; the night-time signal which exhibits rapid shallow fading is due to a scattering process associated with the equatorial spread-F [Tao *et al.*, 1970].

There appear to be two types of trans-equatorial propagation characterized by the times of peak occurrence, fading characteristics and modes of propagation. General reviews of TEP have been written by McCue and Fyfe [1965] and by Nielson and Crochet [1974].

The first type of TEP, which is called the afternoon type, has the characteristics:

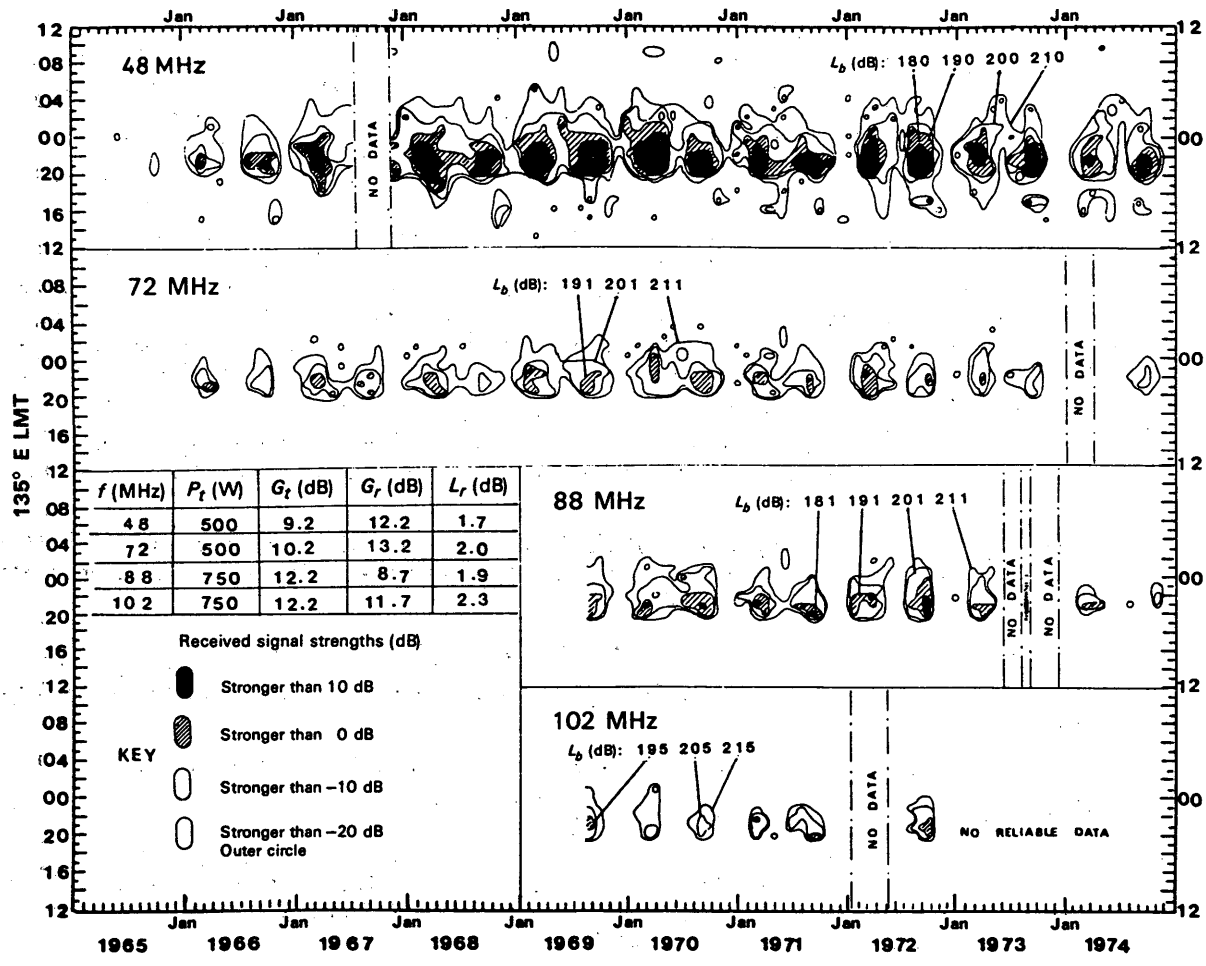
- a peak occurrence around 1700-1900 h LMT, the time being measured at the point where the circuit cuts the magnetic equator;
- normally strong steady signals with a low fading rate and a small Doppler spread (about ± 2-4 Hz);
- path lengths of about 6000-9000 km and sometimes longer.

It has been suggested by Gibson-Wilde [1969] that, in the Australasian zone at least, these signals probably travel by the "super-mode" or FF mode proposed by Villard *et al.* [1957]. Propagation by this mode involves two F-region reflections without an intervening ground reflection.

The second type of TEP, which is called the evening type, generally supports higher frequencies than the afternoon type and has very different characteristics:

- a peak occurrence around 2000-2300 h LMT;
- high signal strenghts but with deep and rapid fading at rates up to about 15 Hz and a large Doppler spread which sometimes exceeds 40 Hz;
- path lengths usually shorter than for the afternoon-type mode, being about 3000-6000 km.

The propagation mode for evening-type TEP is still uncertain. Different mechanisms have been proposed to explain this type of TEP; detailed explanations can be found in Bowen *et al.* [1968], Tao *et al.* [1970], Kuriki *et al.* [1972], McNamara [1973], Heron and McNamara [1979], Winkler [1981] and Ferguson and Booker [1983].



f (MHz)	P_t (W)	G_t (dB)	G_r (dB)	L_r (dB)
48	500	9.2	12.2	1.7
72	500	10.2	13.2	2.0
88	750	12.2	8.7	1.9
102	750	12.2	11.7	2.3

FIGURE 4 – *Basic transmission losses (L_b) and received signal strengths (V_r) indicated by open circuit antenna voltage*

P_t: transmitter power
G_t: transmitter antenna gain
G_r: receiver antenna gain
L_r: loss of receiving feeders.

Received signal strength is in dB(1 μV).

2.2.2 Other mechanisms of abnormal propagation

The studies indicate that there may, at times, occur bodies of ionization at heights different from those of any of the recognized ionospheric layers. Such ionization irregularities may occasionally give rise to reflections of waves in the 30 to 300 MHz range, the principal case being that of reflection from the edges or sides of magnetic-field aligned irregularities which occur within or near the auroral zone. Such reflections may constitute a source of interference to stations working in the 30 to 300 MHz range [Czechowsky, 1970].

Reflections have been observed via the F region, at frequencies appreciably above the F2 basic MUF but at intensity levels well below free-space. These reflections have been observed in the Far East, in South America and in Africa and appear to be a phenomenon of high sunspot years [Bateman *et al.*, 1959]. The equinoctial months appear to be favoured.

Enhanced MOFs are observed at night on Guam to N.W. Cape and Manila to N.W. Cape circuits during equinoctial months at high solar activity. The MOFs exceed the 2F MOF and often exceed 32 MHz, the upper limit of the equipment. They have been explained in terms of a two-hop propagation mode by McNamara [1974b]. Propagation on the first hop is deduced to be by scattering from field-aligned irregularities. The length of the first hop is assumed to be less than half the total circuit length, with the second hop being via the F layer and having a greater MUF than the second hop of a normal 2F mode.

2.2.3 *Ground and ionospheric side-scatter*

VHF radio waves propagated via the ionosphere have been observed to arrive at azimuths which differ considerably from the great circle direction. The signals are predominantly the result of multihop modes of propagation in which side-scatter occurs from irregularities at the surface of the Earth (Report 726). The intensity levels of the signals are well below free-space values and exhibit fading frequencies which are less than 1 Hz.

3. E-Region

VHF propagation by way of the regular E layer is unlikely at any time, whereas propagation by way of meteoric ionization or sporadic-E clouds can be significant.

3.1 Meteoric ionization propagation

Studies have been made in Canada, the Federal Republic of Germany, the United Kingdom, the United States of America and elsewhere, of the reflections which occur from meteor trails. Report 251 gives a bibliography on this subject.

Although of irregular occurrence, daily predictions of the durations of openings in the low VHF band can be made and, because of the daily occurrence, the openings are used for data transmission on dedicated networks.

3.2 Sporadic-E ionization

Sporadic-E ionization ———— appears as an intensification in ionization in the form of a horizontal sheet of about 1 km average thickness and a horizontal dimension of the order of 100 km. The height is commonly 100 to 120 km. The sheets appear in a random manner but show distinct preference for certain times of day and months of the year (see also Reports 725 and 255). There are three major sporadic-E zones, in low, middle and auroral latitudes.

The low latitude zone is subdivided into two sub-zones, the equatorial zone and the sub-equatorial zone (see Recommendation 534). The equatorial zone is a belt centred on the magnetic equator, extending about 6° in magnetic dip on either side of it. The edge of the belt shifts by approximately 1° of dip latitude between summer and winter, being at its greatest distance from the magnetic equator in the summer solstice. A highly transparent form of sporadic E (*q*-type) is a regular occurrence on the day-side of the belt and can be shown to be associated with the equatorial electrojet. Vertical incidence echoes produced by the equatorial Es layer, at frequencies above 7 MHz may be observed for a large percentage of the time, with substantial differences between the various continents [Giraldez, 1980]. Though there is no significant seasonal variation in the occurrence pattern, there is a tendency for the occurrence of equinoctial peaks for stations close to the dip equator, and solstitial peaks for stations a few degrees from it [Oyinloye, 1988]. Propagation of VHF signals via *q*-type Es is by scattering. The sub-equatorial zone extends on both sides of this belt up to ±20° dip latitude.

The mid-latitude zones cover most of the Earth and extend from the low latitude zone to a geomagnetic latitude of about 60° (actually to the line at which the occurrence of aurora is 15% of its maximum). The most dominant feature in the mid-latitude zone is the summer maximum in occurrence of intense sporadic E, which becomes more distinct as one moves to higher latitudes until it is sharply altered by auroral zone influences. Sporadic E rarely occurs between the hours of midnight and 0600h local time. It normally peaks around 1000h local time and in some areas exhibits a second peak in the afternoon or the evening. The sporadic-E layer is often very dense in the daytime. There are considerable longitude as well as latitude variations in the occurrence of sporadic E in the mid-latitude zones. The world-wide maximum is confirmed as being located between 120 and 160° east longitude and between 15 and 40° north latitude, geographic coordinates [Li Zanju, 1988]. A mechanism associated with wind shear appears most promising as an explanation for intense sporadic E at mid-latitudes.

In the auroral zones, the dominant feature is the night-time peak in the occurrence of sporadic E. The summer peak observed at mid-latitudes disappears entirely at the zone of maximum visible aurora. The auroral zones, like the equatorial zone, are regions of heavy current flow in the lower ionosphere. In addition, they are regions where ionized layers can be formed through the precipitation of charged particles. It appears that both of these phenomena may be responsible for the production of sporadic E. The occurrence of sporadic E in the high latitude zones is closely tied to the instantaneous auroral oval [Wagner *et al.*, 1973]. The role of charged particle precipitation, ionospheric currents and the wind shear mechanism in creating sporadic-E ionization and the morphology and structure of this ionization have been described by Hunsucker [1975], Wilson *et al.* [1976] and Wright and Hunsucker [1983]. The dominant production mechanism appears to be auroral particle (1-10 keV electron) precipitation. Hagg et al., [1959] found an interesting local time vs. latitude variation in the maximum occurrence frequency of sporadic E. (Note that present-day knowledge shows their explanation of the phenomenon to be incorrect.) At about 20 hours local time this maximum occurs at about 72° geomagnetic latitude; as local time increases the maximum swings gradually equatorward, reaching about 60° geomagnetic latitude at 03 hours local time.

3.3 Sporadic-E propagation

The occurrence of sporadic-E propagation decreases with increasing frequency. It might be considered a negligible factor above 100 MHz except as a source of interference to circuits with high reliability requirements.

3.3.1 Low latitudes

The reception of television signals in the band between 47 and 68 MHz in India has also been analysed [Saksena, 1979]. In addition, radio amateurs show great interest in Es activity and communications via Es up to frequencies of 144 MHz are often reported [CCIR, 1978-82].

Combination propagation modes, in which one hop is via the equatorial sporadic-E layer while the other is a normal, but long-distance, F-layer hop, have been deduced to exist on circuits between Guam and N.W. Cape (Australia) and between Manila and N.W. Cape [McNamara, 1974a]. During daylight, both of these circuits support an Es-F mode with an MOF often in excess of 32 MHz (the upper limit of the oblique sounder) and a 2Es-F mode with a somewhat lower MOF. The Manila-N.W. Cape circuit appears to support the normal 2F and 3F modes as well, but the 2F mode may not exist on the Guam-N.W. Cape circuit because of Es screening.

Results from a sub-equatorial 1985 km path (East-West) between Sao Paulo (Brazil) and Tucuman (Argentina) for a TV (audio) frequency of 59.75 MHz, effective transmitter power in the direction of reception of 9 kW, reception antenna gain 6 dB (horizontal polarization, 14 m height) [Moro, 1984] show the following characteristics:

- high percentage of occurrence during night-time (2000-0100 local time);
- for field strength greater than 5 μV/m, the occurence is normally distributed with a maximum (70 h/month) in late spring and a minimum (1 h/month) in late autumn;
- for the period spring/summer, 60% of the days have been reported to have contacts lasting 2 h for field strength $\geq$ 5 μV/m;
- percentage of hours/month decreases very rapidly with growing field strength, changing from one maximum in late spring to two maxima in early spring and early autumn (September and March) for field strength higher than 10 μV/m. Figure 5 summarizes observed hours/month reception as function of month and field strength level.

3.3.2 Mid latitudes

Preliminary studies in the South American sector indicate that the behaviour of oblique propagation via sporadic E in that sector can be acceptably described by the characteristics given below for the European sector.

Oblique-incidence pulse soundings between Greece and the Federal Republic of Germany (1700 km) [Reinisch, 1965] showed that the MOF was often determined by Es reflections from May to September, the average daytime occurrence (0600 to 1800 hours local time) being about 10% at 22 MHz decreasing to almost zero at 30 MHz. An examination of the oblique-incidence data obtained on the Ottawa-The Hague (5500 km) and Winnipeg-Resolute Bay (2800 km) circuits indicate that the sporadic-E mode at times controls the operational MUF, but sporadic-E layer propagation seldom occurs at frequencies greater than 30 MHz over these paths [Stevens, 1968].

Minullin [1988] and Minullin et al.[1988] have elucidated and analytically described the space-time variations of the limiting frequencies foEs for the middle latitudes, which makes it possible to calculate the probability of specific values of foEs for a selected latitude, season and time of day. Variations in the reflection coefficient for the Es layer in the case of oblique incidence have been obtained as a function of its limiting frequency of the sporadic-E layer and the critical frequency of the regular E layer.

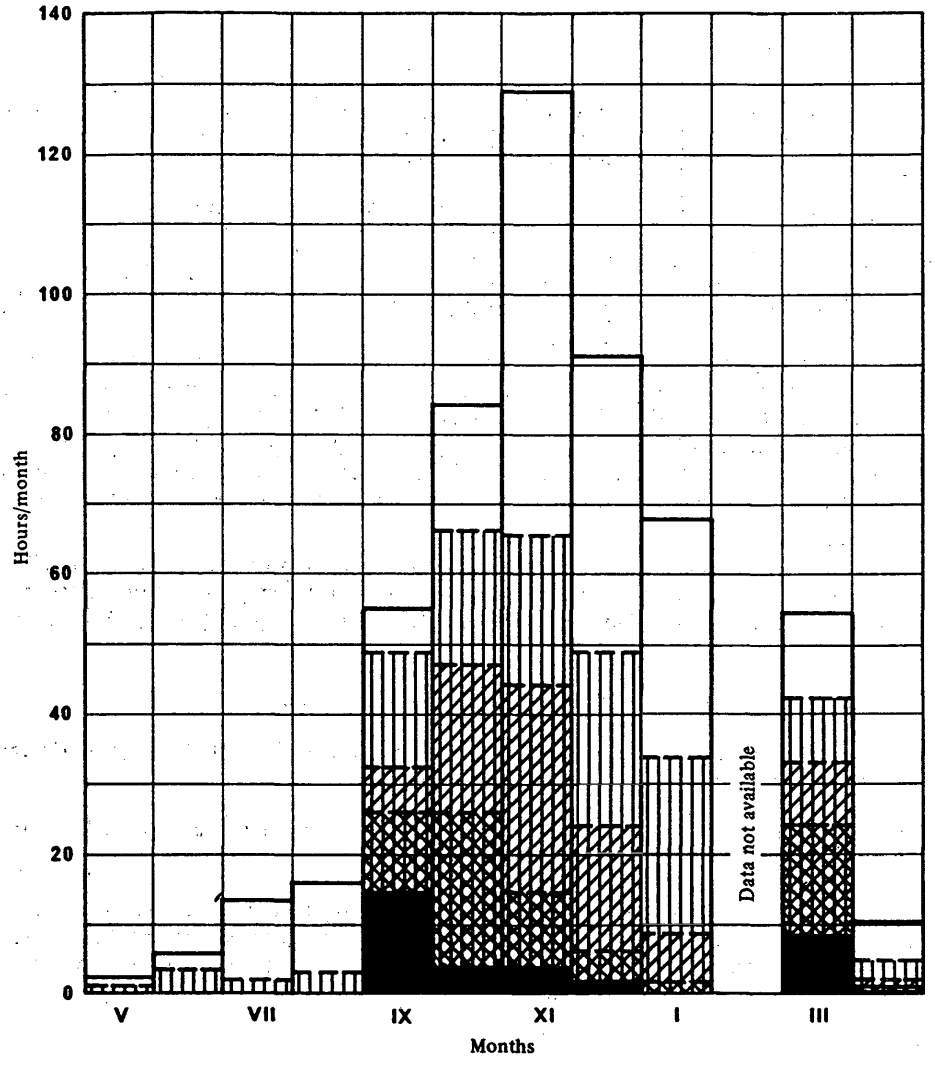


FIGURE 5 – *Cumulative number of hours/month for given field-strength intensity (1980-1981)*

E > 2 μV/m

E > 5 μV/m

E > 10 μV/m

E > 20 μV/m

E > 50 μV/m

Roman numbers indicate month number (I = January)

Effective radiated power in the receiver direction: 9 kW

Since 1962, the EBU has recorded data on 23 paths [Lari *et al.*, 1967], varying in length between 900 and 2510 km, and which are situated in different locations in Western Europe. Daily measurements were taken at five frequencies in the range 41 to 59 MHz between 0800 and 2300 UTC from April to October of each year. The results may be summarized as follows:

- considerable year-to-year variation exists, differences in field strengths of up to 35 dB were observed;
- the month of maximum sporadic-E ionization varied between the end of spring and the end of summer;
- for a given path this month varied from year-to-year, and for a given year it changed for the various paths;
- studies of the variation in field strength with distance showed maximum field strengths (exceeded for 1% of the time) occurring at a distance of approximately 1400 to 1500 km; at these ranges the field strength exceeded for 5% of the time was about 15 to 30 dB lower. At 2500 km the corresponding field strengths were only 10 to 20 dB less than those at 1500 km. This result suggests that, at VHF, atmospheric refraction and the use of elevated antennae may extend the maximum range for one-hop ionospheric propagation beyond that normally experienced at lower frequencies.

The observations made during a complete solar cycle of 11 years, indicate that there is no simple long-term correlation between solar activity * and VHF propagation via Es. However, it became apparent that the yearly variations are rather regular and tend to be similar for different paths.

Table I shows the years when maxima and minima of the field strength were observed.

TABLE I

Path	f (MHz)	Field-strength maxima	Field-strength minima
Divis—Enköping	41·465	1964, 1966, 1971	1965, 1967/8
Divis—Châtonnaye	41·465	1964, 1966, 1971	1965, 1967/8
Meldrum—Enköping	58·215	1963/4, 1966	1965
Divis—Monte-Lauro	41·465	1964, 1968/9, 1971	1963, 1965/6, 1970

Analysis of several years of VHF recordings made at Aberystwyth, United Kingdom, of the received signal level on three frequencies, has allowed statistics to be compiled of the temporal behaviour of observed sporadic-E events [Edwards *et al.*, 1984]. The statistics relate to some nine years of recordings on 59.25 and 62.25 MHz, and to some six years of recordings on 77.25 MHz. The signals originate from broadcasting stations located mainly in central and eastern Europe at distances between 1000 and 2000 km and having effective radiated powers between 50 and 100 kW. Analysis has been confined to the time period 0600-2300 h UTC each day, there being few regular transmissions outside of these hours.

* Sunspot-maximum: 1968-69; minimum: 1964-65.

Cumulative distributions, indicating the percentage of total duration of sporadic-E occurrence in summer time as a function of event duration, are shown in Fig. 6 for 62.25 MHz. These demonstrate that the total duration of all events is due largely to the duration of the longest events. At the 3 dB(μV/m) reference level, 75% of the total duration was contributed by events lasting longer than 5 min and at the 13 dB(μV/m) level, by events lasting longer than 4 min. Similar distributions were obtained for 59.25 and 77.25 MHz.

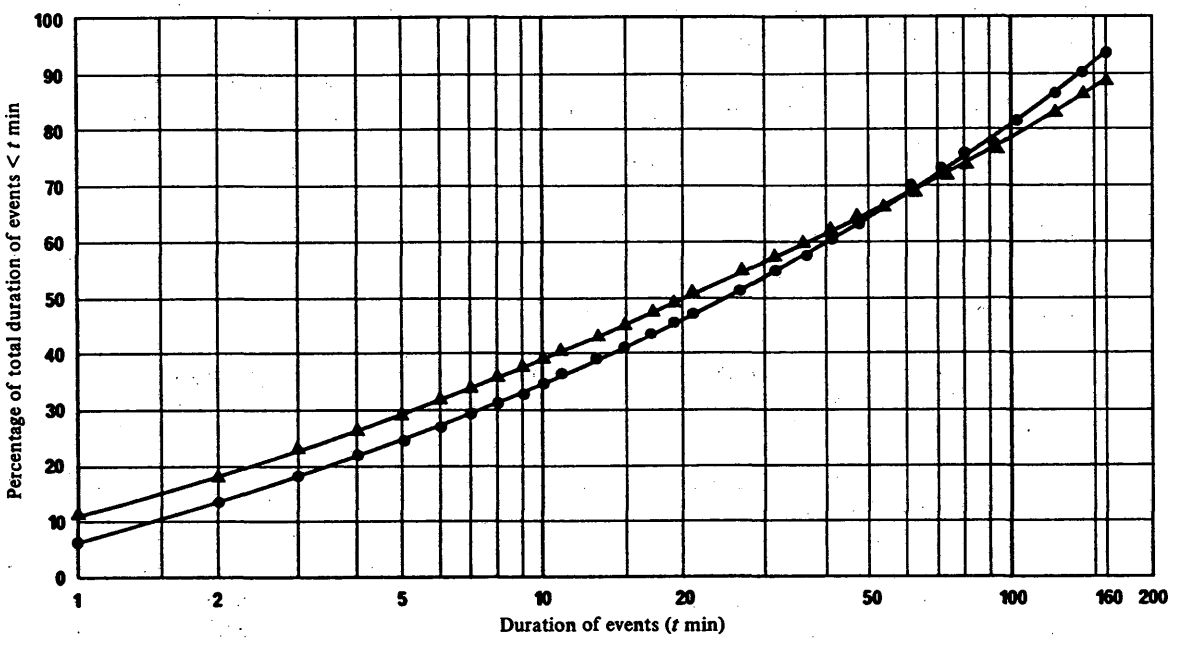


FIGURE 6 – *Cumulative percentage duration of events in summer time as a function of event duration for the two threshold levels observed at Aberystwyth at 62.25 MHz*

Threshold level (μV/m):
● 3 dB
▲ 13 dB

Figures 7 a) and 7 b) show the average total durations of sporadic-E events for the three frequencies plotted by month. The two figures relate to events exceeding field-strength levels of 3 dB(μV/m) and 13 dB(μV/m) respectively. A well-defined seasonal variation is apparent, showing sporadic-E as essentially a summer-time phenomenon, with very little activity between September and April. The greater occurrence of sporadic-E events on 62.25 MHz as compared with 59.25 MHz is a notable feature, contrary to the generally accepted frequency dependence of sporadic-E propagation. However, in a comparison of this kind, it is important to consider the geographical distribution of the transmission sources on each frequency as well as the number. Although fewer stations are to be found on 62.25 MHz than 59.25 MHz, they cover a considerably wider arc centred on Aberystwyth, and thus the number of potential propagation paths for 62.25 MHz might be expected to exceed that for 59.25 MHz.

Figures 7 a) and 7b) indicate that the greatest activity occurs in June, and the percentages of total time analyzed for which sporadic-E events were observed at each frequency are summarized in Table II.

TABLE II – *Maximum observed average time percentages of sporadic-E propagation*

	59.25 MHz	62.25 MHz	77.25 MHz
3 dB (μV/m)	8	12	2
13 dB (μV/m)	5	6	1.3

Figures 8 a) and 8b) show the average diurnal variation of sporadic-E event duration for the summer months May to August.

The distributions exhibit a twin peaked structure at 59.25 and 62.25 MHz, but only a single evening peak at 77.25 MHz. However, considerable variation was apparent in the diurnal patterns for individual months.

Distributions of the durations of events in summer-time exceeding the two field-strength thresholds for 62.25 MHz are shown in Fig. 9. The distributions indicate that:

- the events having the shortest duration occur most frequently; some 75% of the events observed above the 3 dB(μV/m) level had durations of less than 3 min, and 75% of those observed above the 13 dB(μV/m) level, less than 4 min;
- the stronger events (i.e. those observed above the 13 dB(μV/m) level), tend to be of longer duration than those observed above the lower level (3 dB(μV/m)).

Similar distributions were obtained for 59.25 and 77.25 MHz, revealing a slight frequency dependence with a tendency towards shorter events at the highest frequency. Further studies of event duration revealed enhancements in the numbers of the shorter events coincident with recurrent meteor showers, thereby indicating a contribution from propagation associated with long-lived meteor trails.

A similar distribution to that in Fig. 9 was obtained in a brief study undertaken by the EBU on three paths for June, 1971. The distribution was found to be largely independent of path length [EBU, 1976].

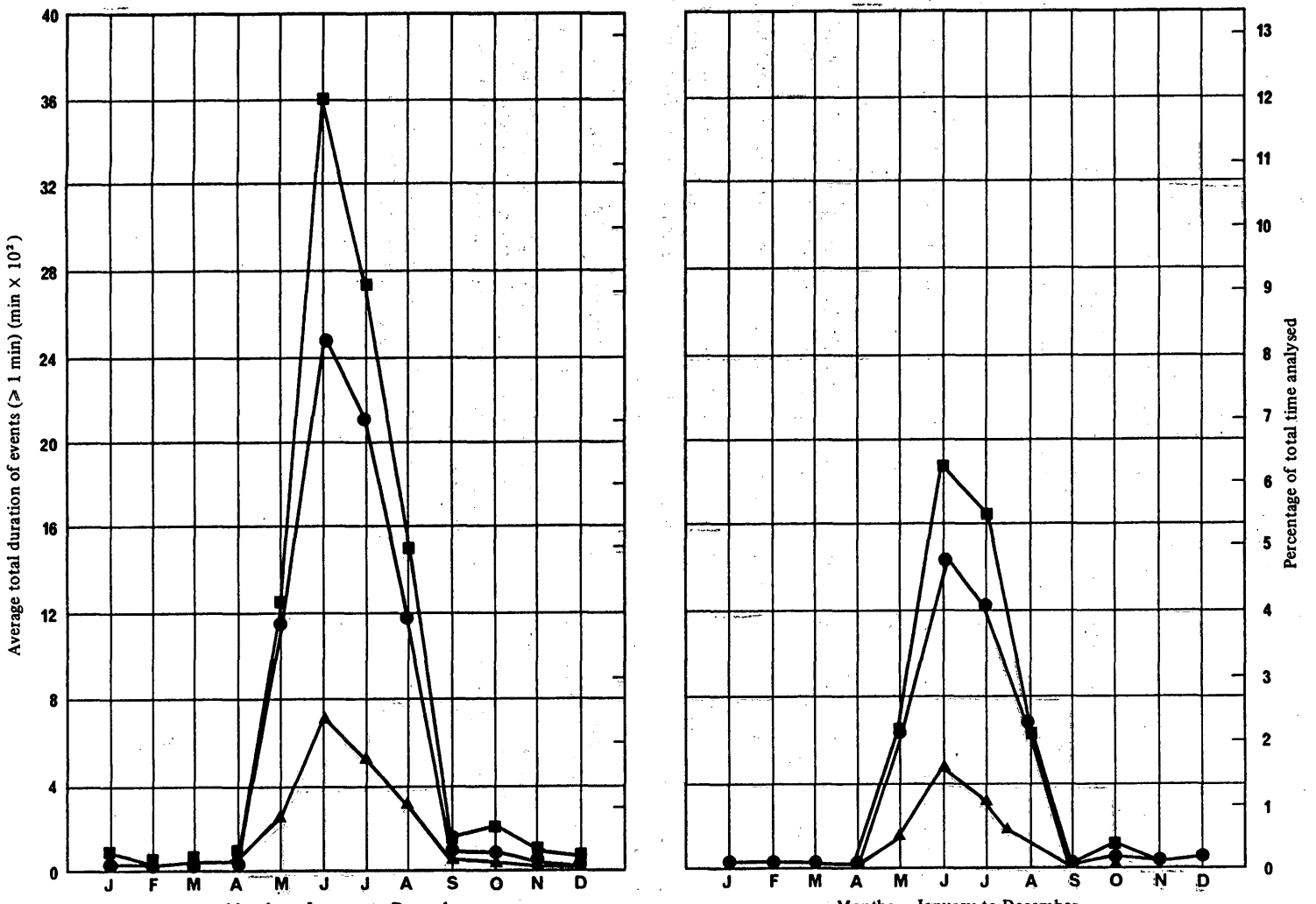


FIGURE 7 – *Seasonal variations of average total duration of events exceeding field strengths of 3 dB(μV/m) and 13 dB(μV/m)*

Frequency (MHz):

● 59.25 ■ 62.25 ▲ 77.25

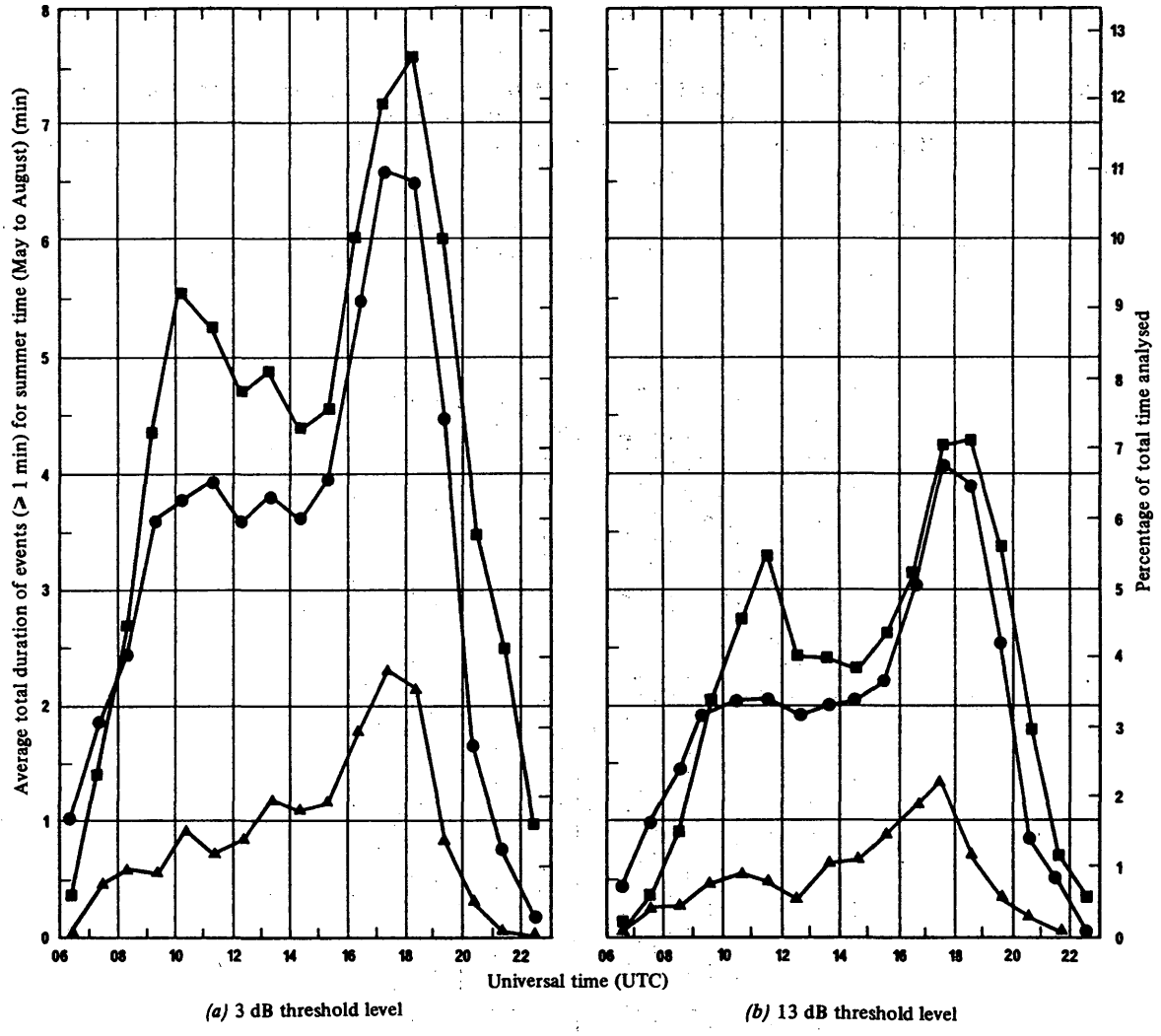


FIGURE 8– *Diurnal variations of average total duration of events exceeding field strengths of 3 dB(μV/m) and 13 dB(μV/m)*

Frequency (MHz):

● 59.25

■ 62.25

▲ 77.25

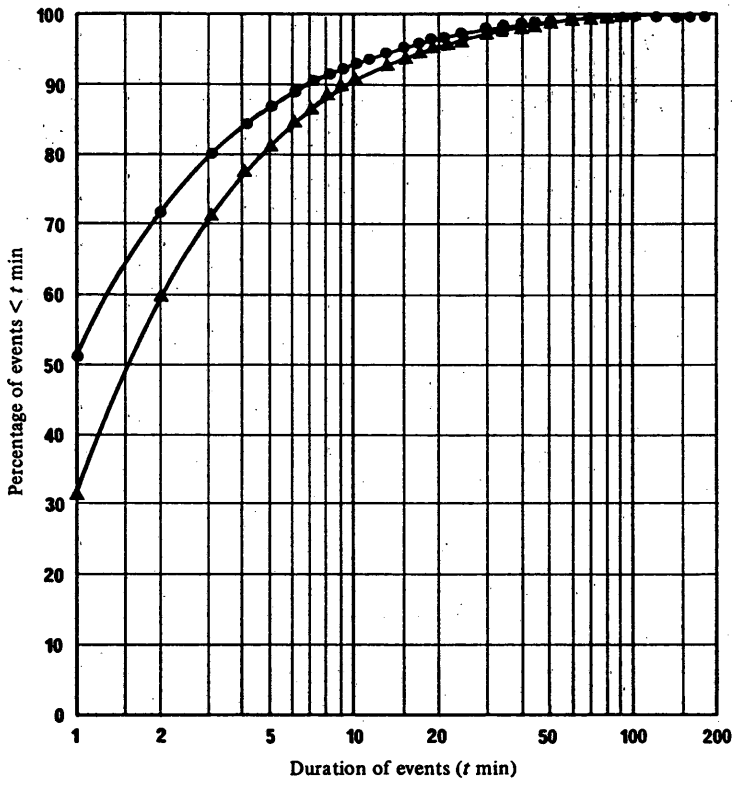


FIGURE 9 – *Cumulative distribution of events in summer time as a function of event duration for the two threshold levels observed at Aberystwyth at 62.25 MHz*

Threshold level (μV/m):
● 3 dB
▲ 13 dB

Detailed reports on amateur radio observations at frequencies as high as 144 MHz over Europe during occurrences of intense sporadic E have been summarized by Canivenc [1988].

3.3.3 High latitudes

Plasma frequencies as high as 14.9 MHz at 100 km altitude have been recorded near Fairbanks, Alaska [Wilson *et al.*, 1976]. For an assumed earth-curvature-limited secant factor of 5, this implies a MUF of 74.5 MHz. Sporadic-E propagation over polar paths as long as 5000 km have been observed with MUFs as high as 46 MHz [Hunsucker, 1979].

3.4 Sporadic-E propagation field strength estimation

The only comprehensive and continuing source of sporadic-E data is the world-wide network of ionosonde stations. It is important therefore to develop quantitative methods for estimating the oblique-incidence transmission characteristics from the vertical-incidence data. A consideration of this question for the United States is found in Davis *et al.* [1959].

A study of this problem in Japan has been carried out by Miya and Sasaki [1966] and by Miya *et al.* [1978]. Sporadic E is first classified by its reflection coefficient, Γ, as observed on VHF oblique-incidence circuits. The study suggests that if $\Gamma \leqslant 45$ dB, then the sporadic-E reflections are specular in nature, while if 45 dB $< \Gamma <$ 70 dB, a scattering mechanism is involved. Curves are available for calculating Γ in terms of the ratio f/foEs, where f is the transmission frequency in question and foEs is the vertical-incidence critical frequency of the ordinary wave for sporadic E taken from ionosphere observations. Estimates are available for both single-hop (0 to 2600 km) and two-hop (2600 to 4000 km) sporadic-E modes. An important feature of the method is the inclusion of antenna-to-medium coupling loss.

The Interim Working Party 6/8 has treated reflection loss of the sporadic-E signal applying the same analysis as used in the Japanese study described above. Many data for the temperate zone have been employed in the study including data of the EBU measurement campaign, 1962 to 1972 [EBU, 1976]. The IWP 6/8 method for calculating VHF sporadic-E signal strength at certain percentages of time of occurrence, is shown in Annex I to Recommendation 534. This method is applicable not only to VHF but is expected to be valid also for the upper half of the HF band if non-deviative D-region absorption is taken into account [CCIR, 1974-78].

A series of measurements was carried out in Italy in 1973 and 1974 of television transmitters at distances between 1000 km and 2500 km to determine the interfering field strength at about 55 MHz caused by sporadic-E layer propagation. The results showed a flat maximum of field strength at a distance of around 1800 km and proved to be in good agreement with that predicted by the method described by Miya *et al.* [1978].

A method has been developed in the USSR for calculating the horizontal Es layer inhomogeneity characterized by the angle of inclination of isolines of electron density based on vertical sounding data. It was used to calculate the focusing and defocusing effects of waves reflected from the Es layer [Kerblai and Kishcha, 1985].

Analysis of data from the equatorial belt shows that the percentage of time of Es occurrence is much higher for paths whose reflection point is in the equatorial belt and is found to exhibit an approximately linear relationship with the maximum frequency of vertical reflection instead of the well-known logarithmic relationship (Phillips law) accepted for middle latitudes.

Studies by the Max-Planck-Institute [Möller, 1963] using HF pulse transmissions with different transmitter powers over a 1965 km path in middle latitudes indicate the possibility that propagation by the sporadic-E layer may be power sensitive. This could result, for a 10 dB change in transmitter power, in modest differences (6 to 8%) is Es MOF. During the summer months, the power sensitivity appears to vary as a function of the time of day, indicating a possible correlation with the physical structure of the sporadic-E layer (see Report 255).

As a consequence of a study made in the USSR on oblique-incidence propagation over paths of about 1000 km in length and at frequencies of 4.5 to 40 MHz, with ionosondes near the path midpoints, the following conclusions were drawn [Kerblaï *et al.*, 1973, 1979]:

- the fading rate during Es propagation by specular reflection is slow (0.01 to 0.1 Hz), but increases when the scattering type of reflection sets in (0.05 to 0.4 Hz);
- while the secant law relating vertical-incidence values of foEs to oblique-incidence conditions is in satisfactory agreement in the HF band, it gives values 1.2 to 1.3 times too low at VHF;
- values of the focusing and defocusing effects during Es propagation are on average 2-4 dB and 5-7 dB respectively; in some cases (4% of the total number of Es cases), defocusing reaches values of 10-13 dB.

4. Main causes of interference to stations working at frequencies between 30 and 300 MHz

Cause of interference	Latitude zone	Period of severe interference	Approximate highest frequency with severe interference (MHz)	Approximate frequency above which interference is negligible (MHz)	Approximate range of distances affected (km)	Principal distinguishing features
Regular F-layer reflections	Mid	Day, equinox and winter, solar-cycle maximum	50	60	E-W paths 3000-6000 or N-S paths 3000-10 000	Occurrence broadly in accordance with regular-layer morphology
	Low	Afternoon to late evening, solar-cycle maximum	60	70		
Sporadic-E reflections	High	Night	70	90	500-4000	Principally during summer months in mid latitudes. Sudden onset and conclusion, beginning later and ending earlier with increase of operating frequency. Area concerned relatively small and mobile. Duration minutes or hours. No associated signal enhancements at short range
	Mid	Day and evening, summer	60	83-135 (1)		
	Low	Day	60	90		
Sporadic-E scatter	Low	Evening to midnight	60	90	Up to 2000	
Reflections from meteoric ionization	All	Particularly during showers	May be important anywhere in the range		Up to 2000	Signal bursts with durations from a fraction of a second to several minutes. Marked diurnal variation, maximum 0600 h local time, minimum 1800 h. Some activity present at all times, but considerable increases during predictable shower periods
Reflections from magnetic field aligned columns of auroral ionization	High	Late afternoon and night				Associated with geomagnetic disturbances, typically when local K-index reaches 5 or more. Characteristic rasping note due to multiple Doppler shifting. Normal duration a few hours, often afternoon to midnight.
Scattering in the F region	Low	Evening to midnight, equinox	60	80	1000-4000	
Special transequatorial effects	Low	Evening to midnight	60	80	4000-9000	Paths generally aligned symmetrically across the dip equator. Generally around equinoctial periods with regular occurrences. Strong signals. Refer to main text for further details.
Anomalous(2) tropospheric propagation	All	Any season or time	May extend into UHF	Generally beyond VHF band	Up to 2000 km	Associated with high atmospheric pressure. Effects cover wide area with a slow movement, gradual build-up and decline, with enhancement of normal signals at shorter ranges. May extend over several days. Comparable effects over a wide range of frequencies, usually beyond those affected by sporadic E.

(1) For 0.1% of the time during the hours 0800-2300 LT for May to August (111 min total) the following frequencies may be derived from the Annex I to Recommendation 534 for a distance of 1800 km and $\Gamma = 30$ dB for temperate zone:

Region A (Europe and North Africa)	83 MHz
Region B (North America)	93 MHz
Region C (Asia)	135 MHz
Region D (Average for northern hemisphere)	115 MHz

(2) See Recommendation 370.

REFERENCES

BATEMAN, R., FINNEY, J. W., SMITH, E. K., TVETEN, L. H. and WATTS, J. M. [1959] IGY observations of F-layer scatter in the Far East. *J. Geophys. Res.*, Vol. 64, 403-405.

BOWEN, E. D., FAY, W. J. and HERITAGE, J. L. [1968] VHF characteristics of the transequatorial ionosphere. *J. Geophys. Res.*, Vol. 73, 2469-2476.

CANIVENC, S. /1988/ Propagation via la couche E sporadique et propagation sur les irrégularités alignées sur le champ magnétique terrestre. Analyse générale de quinze années d'observation dans la bande VHF. Radio REF, 01, 20-23; 02, 18-21; 03, 16-19.

CZECHOWSKY, P. [1970] Berechnung eines Stromsystems in der polaren E-region (Calculation of a current system in the polar E-region). *Z. für Geophysik.*, Vol. 36, 647-650.

DAVIS, R. M., SMITH, E. K. and ELLYETT, C. D. [1959] Sporadic E at VHF in the USA. *Proc. IRE*, Vol. 47, 762-769.

EBU [1976] Ionospheric propagation in Europe in VHF television Band T. EBU Technical Document TECH 3214, Vols. I and II, Technical Centre, 32, Avenue Albert-Lancaster, 1180-Brussels, Belgium.

EDWARDS, K.J., KERSLEY, L. AND SHRUBSOLE, L.F. [1984] - Sporadic-E propagation at frequencies around 70 MHz. Radio and electronic engineer, Volume 54 (5), 231-237.

FERGUSON, J. A. and BOOKER, H. G. [1983] A scattering theory of VHF transequatorial propagation. *J. Atmos. Terr. Phys.*, Vol. 45, 641-657.

GIBSON-WILDE, B. C. [1969] Relation between the equatorial anomaly and transequatorial VHF radio propagation. *Radio Sci.*, Vol. 4, 797-802.

GIRÁLDEZ, A. E. [1980] Equatorial belt sporadic-E statistics. LIARA C-30. Laboratorio Ionosférico de la Armada, República Argentina.

HAGG, E.L., MULDREW, D.B. and WARREN, E.S. [1959] Spiral occurrence of sporadic-E. J. Atmos. Terr. Phys., 14, 345-347.

HERON, M. L. and McNAMARA, L. F. [1979] Transequatorial VHF propagation through equatorial plasma bubbles. *Radio Sci.*, Vol. 14, 897-910.

HUNSUCKER, R. D. [1975] Chatanika radar investigation of high latitude E-region ionization structure and dynamics. *Radio Sci.*, Vol. 10, 277-288.

HUNSUCKER, R. D. [1979] Morphology and phenomenology of the high-latitude E- and F-regions. *Solar-Terrestrial Predictions Proceedings*, Vol. II, Working Group Reports and Reviews, 543-561. Ed. R. F. Donnelly. US Dept. of Commerce, US Govt. Printing Office, No. 003-017-00471-6, Washington, DC 20402.

KERBLAÏ, T. S., and KISHCHA, P. V. [1985] Calculation of the horizontal Es layer inhomogeneity and its effects on radiowave field attenuation. *Geomag. i Aeronom.*, 3, 495-497.

KERBLAÏ, T. S., MINULLIN, R. G. MAKARENKO, S. F., NASYROV, A. M., NASYROV, G. N., NOSOVA, G. N. and PODOLSKAYA, T. Y. [1979] The azimuthal angles of Es layer-reflected radio waves. *Questions of Radio Wave Propagation in High and Medium latitudes*, 71-77 (in Russian). IZMIRAN, Academy of Sciences of the USSR, Moscow.

KERBLAÏ, T. S., NOSOVA, G. N., MINULLIN, R. G. and KURGANOV, R. A. [1973] Periody fluktuatsŭ signalov s chastotoi 27.8 MGts. otrazhennykh ot intensivnykh sloev Es (Fluctuation periods of signals with a frequency 27.8 MHz reflected from intense Es layers). Collection of articles *Questions concerning short-wave propagation*, IZMIRAN, Academy of Sciences of the USSR, Moscow.

KURIKI, I., TANOHATA, K., SAKAMOTO, T. and IGUCHI, M. [1972] Propagational mode deduced from signal strength in the VHF band on the trans-equatorial path. *J. Radio Res. Labs.* (Japan), Vol. 19, 175-195.

LARI, G., TAGHOLM, L. F. and BELL, C. P. [1967] Research on VHF ionospheric propagation (Band I). EBU Technical Document TECH 3085-E, EBU Technical Centre, 32, Avenue Albert-Lancaster, 1180-Brussels, Belgium.

LI ZANJU [1988] - On the geographic occurrence of ionospheric Sporadic-E in the Far East. Proceedings of International Symposium on Radiopropagation, Beijing, China (pp. 189-190).

McCUE, C. G. and FYFE, D. F. [1965] Transequatorial propagation. Task Bridger introductory review. *Proc. IREE* (Australia), Vol. 26, 825-835.

McNAMARA, L. F. [1973] Evening-type transequatorial propagation on Japan-Australia circuits. *Austral. J. Phys.*, Vol. 26, 521-543.

McNAMARA, L. F. [1974a] Sporadic E propagation modes on transequatorial circuits. Report IPS-R25, Ionospheric Prediction Service, Sydney, Australia.

McNAMARA, L. F. [1974b] Unusual night-time propagation modes on the Guam and Manila-N.W. Cape Circuits. Report IPS-R27, Ionospheric Prediction Service, Sydney, Australia.

MINULLIN, R.G. [1988] - Periodichnosti v variatsiyakh mediannykh znacheny predelnykh chastot sloya Es (Periodicities in the variations of the median values of Es layer limiting frequencies). Geomagnetizm i aeronomiya, Vol. 28, 969-975.

MINULLIN, R.G., NAZARENKO, V.I. and SHERSTYUKOV, O.N. [1988] - Vysoty i koeffitsienty otrazheniya ot sloya Es (Heights and coefficients of reflection from the Es layer). Ionosfernye issledovaniya, Moscow, No. 44, 48-55.

MIYA, K. and SASAKI, T. [1966] Characteristics of ionospheric Es propagation and calculation of Es signal strength. *Radio Sci.*, Vol. 1, (New Series), 99-108.

MIYA, K., SHIMIZU, K. and KOJIMA, T. [1978] Oblique incidence sporadic-E propagation and its ionospheric attenuation. *Radio Sci.*, Vol. 13, 3, 559-570.

MÖLLER, H. G. [1963] Impulsübertragungsversuche mit schräger Inzidenz und veränderlicher Frequenz über Entfernungen zwischen 1000 km und 2000 km (Pulse transmission tests at oblique incidence and variable frequency made over distances between 1000 km and 2000 km). *Forschungsberichte des Landes Nordrhein-Westfalen* Nr. 1149.

MORO, E. S. M. [1984] Anomalous VHF propagation. *Contributions on Radiopropagation and Electromagnetic Compatibility 1982-1984.* SECYT, Secretaria de Ciencia y Técnica, Buenos Aires, Argentina.

NIELSON, D. L. and CROCHET, M. [1974] Ionospheric propagation of HF and VHF radio waves across the geomagnetic equator. *Rev. Geophys.*, Vol. 12, 688.

OYINLOYE, J. [1988] - Ionospheric characteristics and radio propagation in the equatorial region. Telecommunication Journal Volume 55-5, (pp. 322-335).

REINISCH, B. [1965] Die Bedeutung von Echos an der sporadischen E-Schicht bei Impulsfernübertragung über 1700 km (Athen-Breisach) (The influence of sporadic-E echoes using pulse transmission for a distance of 1700 km (Athens-Breisach)). *AEÜ*, Vol. 19, 361-366.

SAKSENA, R. C. [1979] Anomalous long distance TV reception at Delhi. *Indian J. Radio and Space Phys.*, Vol. 8, 351-356.

STEVENS, E. E. [1968] The significance of sporadic E propagation in determining the MUF. *Ionospheric Radio Communications*, 289-293. Ed. K. Folkestad, Plenum Press, New York, NY 10011, USA.

TANOHATA, K., KURIKI, I., IGUCHI, M., YAMASHITA, K. and SAKAMOTO, T. [1980] The results of long-term experiment of transequatorial VHF wave propagation. *Rev. Radio Res. Labs.*, (Japan), Vol. 26, 885-897.

TAO, K., OCHI, F., YAMAOKA, M., WATANABE, S., WATANABE, C. and TANOHATA, K. [1970] Experimental results on VHF transequatorial propagation. *J. Radio Res. Labs.* (Japan), Vol. 17, 83-101.

VILLARD, D. G. Jr., STEIN, S. and YEH, K. C. [1957] Studies of transequatorial ionospheric propagation by the scatter-sounding method. *J. Geophys. Res.*, Vol. 62, 399-412.

WAGNER, R. A., SNYDER, A. L. and AKASOFU, S. I. [1973] The structure of the polar ionosphere during exceptionally quiet periods. *Planet. and Space Sci.*, Vol. 21, 1911-1922.

WILSON, C. R., HUNSUCKER, R. D. and ROMICK, G. J. [1976] An auroral infrasonic substorm investigation using Chatanika radar and other geophysical sensors. *Planet. and Space Sci.*, Vol. 24, 1155-1175.

WINKLER, C. [1981] Radio wave guidance at VHF through equatorial plasma bubbles. *J. Atmos. Terr. Phys.*, Vol. 43, 307-316.

WRIGHT, J. W. and HUNSUCKER, R. D. [1983] Estimation of turbulent energy dissipation, winds and ionospheric structure from dynasonde measurements. *Radio Sci.*, Vol. 18, 988-994.

CCIR Documents

[1974-78]: 6/251 (USSR).

[1978-82]: 6/74 (IWP 6/8).

[1982-86]: 6/231 (India).

BIBLIOGRAPHY

BAILEY, D. K. [1962] Ionospheric forward-scattering. *Monograph on Ionospheric Radio*, 189-199. Ed. W. J. G. Beynon, Elsevier, London, UK.

COLLINS, C. and FORSYTHE, P. A. [1959] A bistatic radio investigation of auroral ionization. *J. Atmos. Terr. Phys.*, Vol. 13, 315-345.

DIEMINGER, W., ROSE, G. and WIDDEL, H. U. [1963] On the probability of co-channel interference in VHF bands I, II and III in Africa, caused by scatter and reflection from the E and F layers. *Telecomm. J.*, Vol. 30, 251-256.

REPORT 251-5*

COMMUNICATION BY METEOR-BURST PROPAGATION

(Question 41/6)

(1959-1963-1966-1978-1982-1986-1990)

1. Introduction

Scattering from ionization caused by meteor trails provides a means of communication at HF and VHF. Experimental two-way telecommunications circuits have been operated with frequencies between 30 and 100 MHz over ranges up to 1300 km. The communication relies on bursts of propagation during the occurrence of meteor trails and supports data rates up to 100 bauds when averaged over several minutes.

Modern communication techniques, such as the use of mini-computers to carry out interactive operations between transmitting and receiving terminals, have made meteor-burst communication relatively more attractive for special applications where time delays of possibly a few minutes can be tolerated. Among such applications are the intermittent transmission of information to a central station from a large number of remote stations, transmissions to and from mobile terminals, and order-wire transmissions for engineering liaison in support of medium-length short-wave circuits.

The earliest indication that meteors could cause ionization in the upper atmosphere came from the observed correlation of trans-Atlantic HF signals with meteor showers [Pickard, 1931]. In 1943 the continuous monitoring of distant VHF stations in the USA showed that bursts of undistorted signals sometimes could be received at distances as great as 2200 km [Allen, 1948]. These bursts had durations up to one second and a diurnal variation in frequency of occurrence which correlated with the known incidence of visual meteors and with theoretical estimates.

Subsequent experiments used both back-scatter and forward-scatter techniques. Together with theoretical studies, a considerable amount of information on meteor-burst propagation was obtained by the mid-1950's. This activity culminated in an important set of papers which includes descriptions of two trial communication systems [Forsyth *et al.*, 1957; Vincent *et al.*, 1957].

The next decade saw further work which permitted better estimates to be made of the probable performance of a meteor-burst communication system. Summaries of the state-of-the-art appeared in the form of a book [McKinley, 1961] and an extensive review article [Sugar, 1964]. A more sophisticated experimental communication system employing automatic repeat transmission in the presence of errors (ARQ) and diversity reception gave a minimum transmission rate of 50 bauds over a 1000 km circuit [Bartholomé and Vogt, 1968]. Kokjer and Roberts [1986] have described networked meteor-burst communication system implementations. A historical perspective of meteor-burst communication system

---

* This Report is brought to the attention of Study Group 3.

development is provided by [Cannon and Reed, 1987] who have also reviewed the background theory and fundamentals of meteor-burst propagation. Those special properties which distinguish meteor-burst communication from other radiocommunication modes are highlighted and, within this framework, the evolution of meteor-burst communication systems is traced.

Tests in Canada showed that even at frequencies as high as 104 MHz meteor-burst circuits were not, as had been hoped, entirely free from black-outs in Arctic regions [Maynard, 1968]. However, at lower latitudes in Norway no such difficulties were encountered [Ince *et al.*, 1978]. These differences may relate to the occurrence of exceptionally large solar flares during the period of sunspot maximum when the former set of tests were carried out. Santeford [1976] reported winter test results on the Alaska meteor burst system which indicated multipath effects due to auroral ionization approximately 8% of the time. These multipath effects were correlated with large magnetic disturbances. The exploitation of meteor-burst links now centres more on the use of circuits demanding only occasional communication such as the transmission of weather information [Smith, 1978], of time signals [Minullin *et al.*, 1971], or as an order-wire system [Brown and Williams, 1978]. The exceptionally wide coherence bandwidth of meteor-burst signals [Akram *et al.*, 1977] has not yet been exploited.

A meteor-burst communications model developed by Haakinson [1983] predicts the reliability of a meteor-burst communications system. The waiting times required to complete the transfer of messages from a master to a remote station are predicted as a function of system parameters, station separation and temporal conditions.

A more advanced meteor scatter communication model developed by Weitzen [1986] defines the relationship between arrival rate of usable meteors and antenna patterns, link parameters, Faraday rotation loss and polarization. The model can be used to determine (1) the range dependence of meteor communication, (2) the effect of various antenna patterns on system performance and (3) the performance tradeoffs related to the use of vertical and horizontal polarization. A review of advances in the state of knowledge of meteor scatter phenomena has been given by Weitzen and Ralston [1988].

This Report summarises the principal factors which determine the characteristics of meteor scatter and which should be considered in the design of communication systems relying on this propagation mechanism.

2. Distribution of meteors

At certain times of the year meteors occur in the form of showers and may be prolific over durations of a few hours. There is, however, a general background of meteors incident upon the Earth from all directions and it is appropriate to consider only these sporadic meteors for communication-planning purposes.

The distribution of sporadic meteors according to mass is such that the number exceeding a given mass is approximately inversely proportional to that mass. Meteors occur in all parts of the world at all hours but statistical information is incomplete on their geographical distribution and trail directions.

An estimate of the number of meteors incident on the atmosphere can be derived from observational data and theory [Eshleman and Manning, 1954]. The annual average flux of meteors incident per unit area and producing electron-line densities q exceeding a threshold q_0 per metre, $I(q > q_0)$, is given as:

$$I(q > q_0) = \frac{160}{q_0} \text{ m}^{-2} \text{ s}^{-1} \quad (1)$$

It is known [Manning and Eshleman, 1959] that for sporadic meteors at mid-latitudes there is a roughly sinusoidal diurnal variation of incidence with a maximum at 0600 h and a minimum at 1800 h local time. The ratio of maximum to minimum averages about four. There is a seasonal variation of similar magnitude with a minimum in February and maximum in July [Sites, 1978]. Considerable day-to-day variability exists in the incidence of both sporadic and shower meteors. Some combined statistics of the daily incidence of the two types are given by Millman [1978].

3. Positions of regions of optimum scatter

The scattering properties of straight meteor ionisation trails are strongly aspect sensitive. To be effective, it is necessary for the trails approximately to satisfy a specular reflection condition. This requires the ionized trail to be tangential to a prolate spheroid whose foci are at the transmitter and receiver terminals (see Fig. 1). The fraction of incident meteor trails which are expected to have usable orientations is approximately 5% in the area of the sky which is most effective [Eshleman and Manning, 1954]. Figure 2 shows the estimated percentages of useful trails for a terminal separation of 1000 km. It may be seen that the optimum scattering regions are situated about 100 km to either side of the great circle, independent of path length.

This feature, together with the fact that the trails lie mainly in the height range 90-110 km, serve to establish the two "hot-spot" regions towards which both antennas should be directed. The two hot spots vary in relative importance according to time of day and path orientation [Eshleman and Manning, 1954]. Generally antennas used in practice have beams broad enough to cover both hot spots. Thus the performance is not optimized, but on the other hand the need for beam swinging does not arise. However, trial systems have been used with a split beam and a null along the great-circle path [Davis *et al.*, 1957].

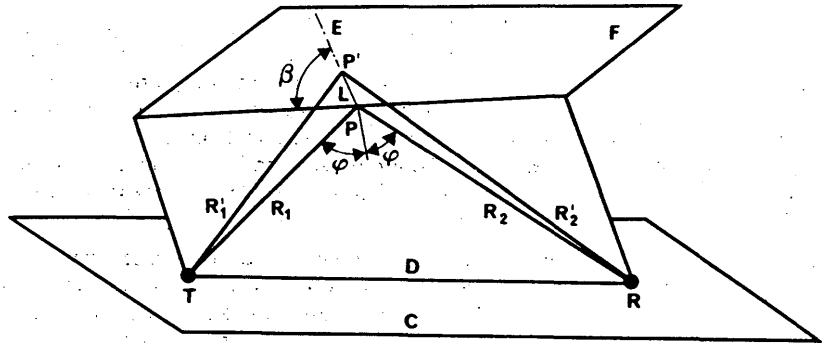


FIGURE 1 – *Ray geometry for a meteor-burst propagation path*

C: Earth's surface
D: plane of propagation
E: trail
F: tangent plane
β: angle between the trail axis and the plane of propagation
T: transmitter
R: receiver

(For the terms L, P, P′, R_1, R_2, R'_1, R'_2 and φ see § 5)

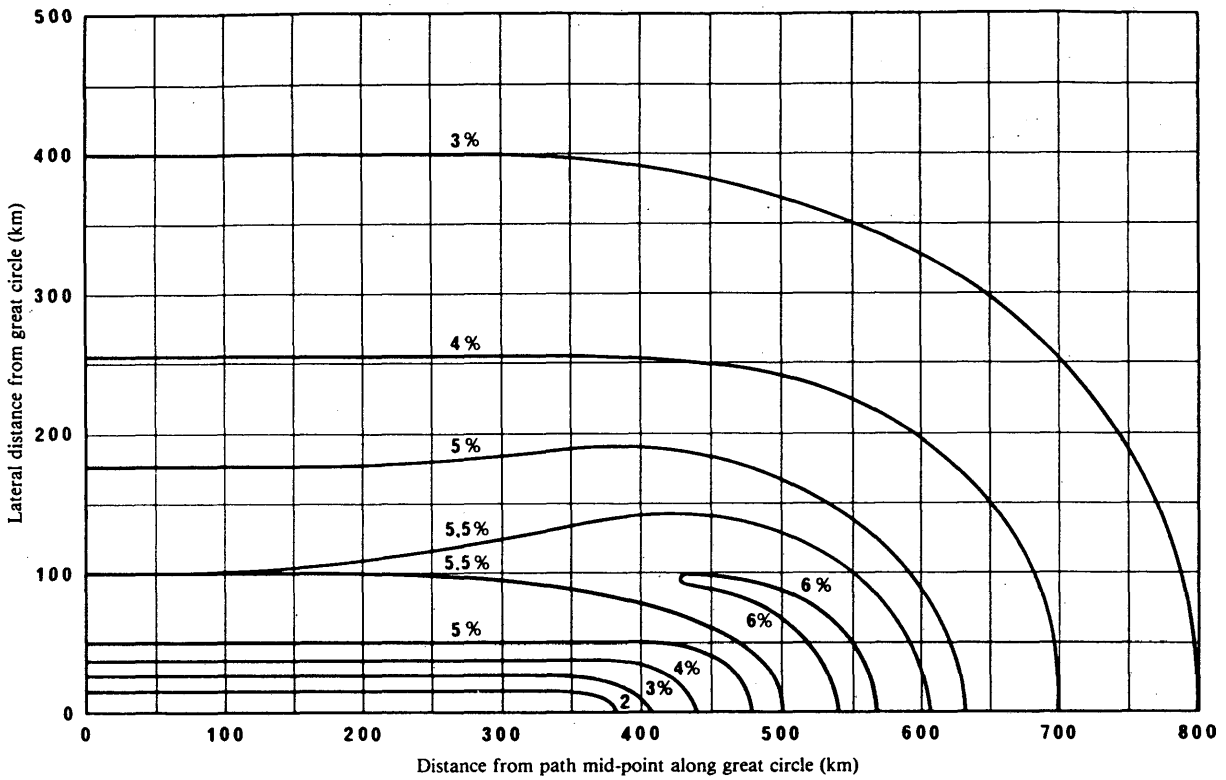


FIGURE 2 – *Estimated percentages of useful trails as a function of scattering position for a terminal separation of 1000 km [Eshleman and Manning, 1954]*

4. Underdense and overdense trails

The ionized trails caused by meteors can be classified as underdense or overdense according to the intensity of the ionization. The amplitude of signals scattered from underdense trails may be calculated by summing the scattered field arising from each individual electron. Overdense trails are those for which the coupling between electrons cannot be ignored, in which case, the reflecting properties are calculated as if the trail were a long metallic cylinder. The division between the two cases occurs for line densities of approximately 2×10^{14} electrons per metre. At frequencies used in practice the echoes from underdense trails show an abrupt start followed by an exponential decay, whereas those from overdense trails have more rounded envelopes and are of longer duration [Sugar, 1964]. The relative proportions of underdense and overdense echoes will depend on the system sensitivity.

The peak amplitudes of the reflections from underdense and overdense trails vary as q and $q^{1/4}$ respectively, where q is the electron-line density. Since q is proportional to the mass of the meteor, and since the rate of incidence of sporadic meteors exceeding a given mass is approximately inversely proportional to that mass, the number of signals, N, observed in a given time with peak amplitudes greater than some level, A, is as follows:

for underdense trails: $N \sim A^{-1}$ (2)

for overdense trails: $N \sim A^{-4}$ (3)

Thus the relative frequency of occurrence of reflections as a function of signal amplitude depends on the sensitivity of the system. A common experimental result in the systems used so far is that $N \sim A^{-1.2}$, showing that the echoes were predominantly from underdense trails. The same result may be expressed as:

$$D_C \sim p_R{}^{-0.6} \quad (4)$$

where

D_C: duty cycle (proportion of time exceeding the threshold A)

p_R: received power corresponding to the threshold A.

The duty cycle may therefore also be expressed as:

$$D_C \sim p_T^{0.6} \tag{5}$$

where

p_T: transmitter power.

5. Effective length, average height and radius of meteor trails

Consider the ray geometry for a meteor-burst propagation path as shown in Fig. 1 between transmitter T and receiver R. P represents the tangent point and P' a point further along the trail such that $(R'_1 + R'_2)$ exceeds $(R_1 + R_2)$ by half a wavelength. Thus PP' (of length L) lies within the principal Fresnel zone and the total length of the trail within this zone is $2L$. Provided R_1 and R_2 are much greater than L, it follows that:

$$L = \left[\frac{\lambda R_1 R_2}{(R_1 + R_2)\ (1 - \sin^2 \varphi \cos^2 \beta)}\right]^{\frac{1}{2}} \tag{6}$$

where

φ: angle of incidence

β: angle between the trail axis and the plane of propagation

and

λ: wavelength.

In order to evaluate the scattering cross section of the trail it is usual to assume that ambipolar diffusion causes the radial density of electrons to have a Gaussian distribution and that the volume density is reduced while the line density remains constant. These assumptions lead to an equation for the volume density, N_v, in electrons per cubic metre as a function of radius, r, and time from the instant of formation, t, which is:

$$N_v(r,t) = \frac{q}{\pi(4Dt + r_0^2)} \exp\left[\frac{-r^2}{(4Dt + r_0^2)}\right] \tag{7}$$

where

q: electron line density per metre

D: ambipolar diffusion coefficient in $m^2\ s^{-1}$

and

r_0: initial radius of trail in metres.

Both D and r_0 are marked functions of height. From experimental results [Greenhow and Hall, 1960] the following empirical formula for evaluating the average height of trails, which is a function of frequency (see § 8) can be derived:

$$h = -17 \log f + 124 \tag{8}$$

where

h: average trail height (km)

and

f: wave frequency (MHz).

The average trail height is a function of other system parameters in addition to frequency. However equation (8) is a good approximation.

Various empirical relationships have been derived between the initial trail radius, and the meteor height. An average expression given by Brown and Williams [1978] is:

$$\log r_0 = 0.035\ h - 3.45 \tag{9}$$

6. Ambipolar diffusion constant

A good estimate of the ambipolar diffusion constant is provided by the expression [Greenhow and Neufeld, 1955; McKinley 1961]:

$$\log D = 0.067\ h - 5.6 \tag{10}$$

Based on the results of Greenhow and Hall [1960] the ratio of the ambipolar diffusion constant D to the velocity of the meteor V (required in the evaluation of received power) can be approximated by:

$$D/V = [0.0015\ h + 0.035 + 0.0013\ (h - 90)^2]\ 10^{-3} \tag{11}$$

where

V: velocity of the meteor in m/s.

7. Received power

7.1 *Underdense trails*

The received power $p_R(t)$ after scattering from underdense trails at frequencies used in practice is given [McKinley, 1961; Sugar 1964] as follows:

$$p_R(t) = \frac{p_T\ g_T\ g_R\ \lambda^2\ \sigma\ a_1\ a_2(t)\ a_2(t_0)\ a_3}{64\pi^3\ R_1^2\ R_2^2} \tag{12}$$

where

λ: wavelength (m)
σ: echoing area of the trail (m^2)
a_1: loss factor due to finite initial trail radius
$a_2(t)$: loss factor due to trail diffusion
a_3: loss factor due to ionospheric absorption
t: time in seconds measured from the instant of complete formation of the first Fresnel zone
t_0: half the time taken for the meteor to traverse the first Fresnel zone
p_T: transmitter power (W)
$p_R(t)$: power available from the receiving antenna (W)
g_T: transmit antenna gain relative to an isotropic antenna in free space
g_R: receive antenna gain relative to an isotropic antenna in free space
(Lossless transmitting and receiving antennas are assumed)

The echoing area σ is given as

$$\sigma = 4\ \pi\ r_e^2\ q^2\ L^2 \sin^2 \alpha \tag{13}$$

where

r_e: effective radius of the electron $= 2.8 \times 10^{-15}$ m

α: angle between the incident electric vector at the trail and the direction of the receiver from that point.

Since L^2 is directly proportional to λ, the echoing area, σ, is also proportional to λ and hence the received power for underdense trails varies as λ^3. Horizontal polarization normally is used at both terminals. The $\sin^2 \alpha$ term in equation (13) is then nearly unity for trails at the two hot spots.

The loss factor a_1 is given by:

$$a_1 = \exp\left[-\frac{8\pi^2\ r_0^2}{\lambda^2 \sec^2 \varphi}\right] \tag{14}$$

It represents losses arising from interference between the re-radiation from the electrons wherever the thickness of the trail at formation is comparable with the wavelength.

The factor $a_2(t)$ allows for the increase in radius of the trail by ambipolar diffusion. It may be expressed as:

$$a_2(t) = \exp\left[-\frac{32\pi^2 Dt}{\lambda^2 \sec^2 \varphi}\right] \tag{15}$$

The increase in radius due to ambipolar diffusion can be appreciable even for as short a period as is required for the formation of the trail. The overall effect with regard to the reflected power is equal to that which would arise if the whole trail within the first Fresnel zone had expanded to the same extent as at its mid-point. Since this portion of trail is of length $2L$ the mid-point radius is that arising after a time lapse of L/V seconds. Calling the time lapse t_0 gives, for trails near the path mid-point ($R_1 \approx R_2 = R$):

– For trails at right angles to the plane of propagation ($\beta = 90°$):

$$t_0 \simeq \left(\frac{\lambda R}{2V^2}\right)^{\frac{1}{2}} \tag{16}$$

– For trails in the plane of propagation ($\beta = 0$):

$$t_0 \simeq \left(\frac{\lambda R}{2}\right)^{\frac{1}{2}} \times \frac{\sec \varphi}{V} \tag{17}$$

Substituting t_0 from equation (16) into equation (15) gives for the $\beta = 90°$ case:

$$a_2(t_0) = \exp\left[-\frac{32\pi^2}{\lambda^{3/2}}\left(\frac{D}{V}\right)\left(\frac{R}{2}\right)^{\frac{1}{2}}\frac{1}{\sec^2 \varphi}\right] \tag{18}$$

For $\beta = 0°$ the exponent in this expression is sec φ times greater.

$a_2(t)$ is the only time-dependent term and gives the decay time of the reflected signal power. Defining a time constant T_{un} for the received power to decay by a factor e^2 (i.e. 8.7 dB) leads to:

$$T_{un} = \frac{\lambda^2 \sec^2 \varphi}{16\pi^2 D} \tag{19}$$

With reflection at grazing incidence $\sec^2 \varphi$ will be large and hence so is the echo-time constant. The echo-time constant is also increased by the use of lower frequencies.

7.2 *Overdense trails*

The formula for the received power in the case of overdense meteor trails is usually based on the assumption of reflection from a metallic cylinder whose surface coincides with the region for which the dielectric constant is zero [McKinley, 1961; Sugar 1964]. The effect of refraction in the underdense portion of the trail is usually ignored. As in the underdense case, the received power varies as λ^3 and again the echo duration varies as λ^2. However, the maximum received power is now proportional to $q^{1/2}$ in contrast to q^2 for underdense trails. Thus the increase in received signal power with ionization intensity is more modest.

7.3 *Typical values of basic transmission loss*

Since any practical meteor-burst communication system will rely mainly on underdense trails, the overdense formulae are of less importance. Satisfactory performance estimates can be made using formulae for the underdense case with assumed values of q in the range 10^{13} to 10^{14} electrons per metre according to the prevailing system parameters.

Basic transmission loss curves derived from equation (12) with $q = 10^{14}$ electrons per metre are given in Fig. 3. As the angle β can take any value between 0° and 90° only these two extreme cases are shown. The advantage of lower propagation loss at the lower frequencies is clearly seen. Average meteor heights given from equation (8) have been used in deriving the curves. It should be noted that the prediction of system performance depends critically on the heights assumed.

8. The underdense echo ceiling

Both the initial trail radius, r_0, and the ambipolar diffusion constant, D, increase with altitude. Consequently, the loss factors a_1 and $a_2(t_0)$ combine to reduce the number of underdense meteors occurring near the top of the meteor region which are useful for communication purposes. This effect is usually referred to as the underdense echo ceiling. Similar constraints have been observed to exist in the monostatic case. Figure 4 shows the measured height distribution of underdense echoes using various radar frequencies given by McKinley [1961]. It can be seen that the lowest altitude at which underdense echoes occur is 85 km, and that the altitude distribution is approximately Gaussian at any frequency. A procedure for estimating the number of detectable meteor bursts based on an assessment of the underdense echo ceiling is given by Milsom [1979].

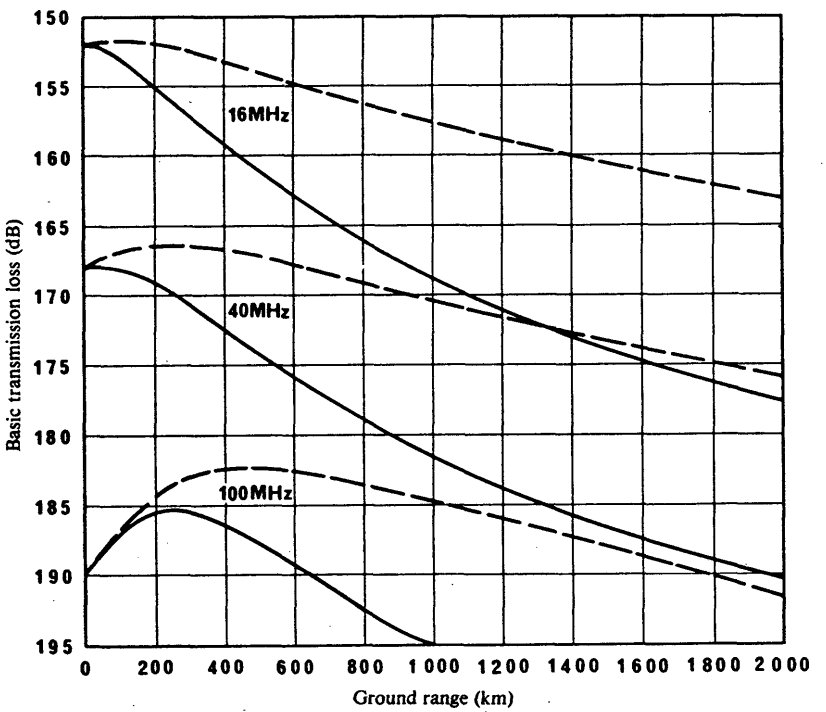


FIGURE 3 – *Basic transmission loss for underdense trails given by equation (13) with $q = 10^{14}$ electrons/m and horizontal polarization*

——— trails at right angles to the plane of propagation (β = 90°)

— — trails in the plane of propagation (β = 0°)

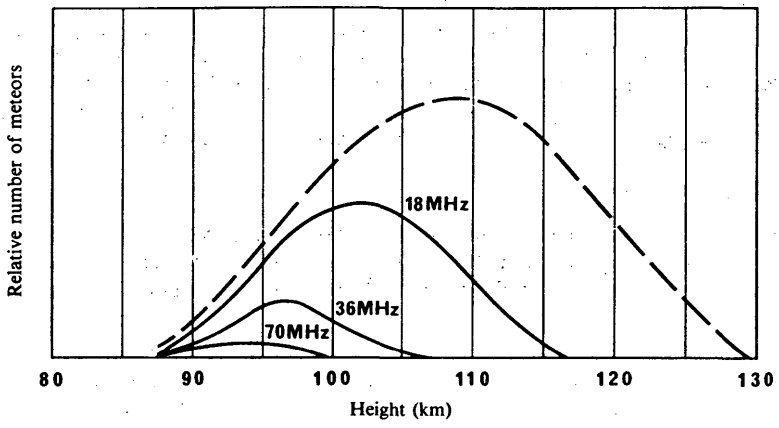


FIGURE 4 – *Height distribution of underdense meteors providing echoes at frequencies of 18, 36 and 70 MHz* [McKinley, 1961]

— — estimated distribution of meteor trails

9. Wavelength dependence of information duty cycle

The wavelength dependences of the maximum received power, $p_{R_{max}}$ and the duty cycle, D_C, as implied by equation (12) are such that for fixed transmitter power and antenna gains:

$$p_{R_{max}} \sim \lambda^3 \tag{20}$$

This relationship holds for both underdense and overdense trails. The effect on the duty cycle will depend on the relative occurrence rate of these two types of trail. Assuming an intermediate relationship between those of equations (2) and (3) of the form $N \sim A^{-2}$, then $N \sim p_{R_{max}}^{-1}$ and the duty cycle varies with wavelength as follows:

$$D_C \sim p_{R_{max}} T_{un} \sim \lambda^5 \tag{21}$$

In very quiet receiving locations the predominant noise at frequencies above 25 MHz is cosmic noise and the intensity of this varies as $\lambda^{2.3}$. Hence the information duty cycle, I_C, for a given bandwidth, i.e. the proportion of time a given signal/noise ratio is exceeded, varies with wavelength as follows:

$$I_C \sim \lambda^{2.7} \tag{22}$$

A fuller discussion of this relationship under various assumptions is given by Eshleman [1957]. Since noise power is proportional to bandwidth B, the use of equation (4) leads to:

$$I_C \sim B^{-0.6} \tag{23}$$

The average channel capacity, C, is the product of the signalling rate and the information duty cycle. The former term may be assumed to be proportional to the bandwidth. Therefore the average channel capacity is related to the bandwidth as follows:

$$C \sim B^{0.4} \tag{24}$$

For maximum information transfer the bandwidth should be as large as possible.

Apart from questions of bandwidth availability, the increased noise in a wider bandwidth and hence the decreased availability of the required signal/noise ratio, leads to a reduction in the information duty cycle; this in turn implies longer message delays. Moreover, a point is reached where the system has to rely on overdense trails in which case equation (4) no longer holds, as can be seen by comparing exponents of N in equations (2) and (3). When the exponent of p_R to which D_C is proportional becomes less than -1 there is no advantage in speeding up the rate of signalling [Montgomery and Sugar, 1957]. It may be noted that the exponent is liable to fall below -1 for frequencies below 40 MHz on account of ionospheric scatter signals masking the weaker meteor-burst signals.

The usable bandwidth is not likely to be limited by the coherence bandwidth, since this is of the order of several megahertz for the main part of the burst [Akram *et al.*, 1977]. Even during the tails of the bursts, where there is fading on account of wind shears, the coherence bandwidth is some hundreds of kilohertz.

10. Practical considerations in the choice of frequency

The choice of frequency in a meteor-burst communications system is constrained by several factors. Firstly, equation (22) has shown that the information duty cycle is increased by reducing the frequency. Secondly, the high path loss associated with meteor-burst communication signals requires that the level of interfering signals be kept to a minimum. As a consequence, the operating frequency should be above that at which normal ionospheric modes propagate. Thirdly, absorption should be minimized, which also requires the use of as high a frequency as possible. This is particularly of concern for systems operated at high latitudes, where auroral and polar cap absorption can attenuate and even totally absorb the signal if the operating frequency is too low [Maynard, 1968]. Lastly, Cannon [1986] has shown that, at certain times, Faraday rotation of linearly polarized meteor-burst communication signals will severely reduce the communications link capacity for frequencies below about 40 MHz. Evidently, the first constraint is in conflict with the latter three, and when making his frequency choice the system designer must judge the appropriate weightings to be assigned to each.

11. Doppler effects

Reflection from the head of a meteor gives rise to Doppler frequency shifts which may span the whole of the audio band. The Doppler frequency shift from a meteor trail is the result of ionospheric wind motions and could be of the order of 20 Hz at a frequency of 40 MHz [Millman, 1978].

REFERENCES

AKRAM, F., SHEIKH, N. M., JAVED, A. and GROSSI, M. D. [1977] Impulse response of a meteor-burst communications channel determined by ray-tracing techniques. *IEEE Trans. Comm.*, Vol. COM-25, 467-470.

ALLEN, E. W. Jr. [1948] Reflections of very-high frequency radio waves from meteoric ionization. *Proc. IRE*, Vol. 38, 346-352.

BARTHOLOMÉ, P. J. and VOGT, I. [1968] COMET – A new meteor-burst system incorporating ARQ and diversity reception. *IEEE Trans. Comm.*, Vol. COM-16, 268-278.

BROWN, D. W. and WILLIAMS, H. P. [1978] The performance of meteor-burst-communications at different frequencies. *Aspects of Electromagnetic Wave Scattering in Radio Communications.* Ed. A. N. Ince. AGARD Conf. Proc. 244, 24-1 to 24-26.

CANNON, P. S. [1986] Polarization rotation in meteor burst communication systems. *Radio Sci.*, Vol. 21, 3, 500-510.

CANNON, P.S. and REED, A.P.C. [1987] - The evolution of meteor-burst communications systems. J. Institution of Electronics and Radio Engineers, Vol. 57, No. 3, 101-112.

DAVIS, G. W. L., GLADYS, S. J., LANG, G. R., LUKE, L. M. and TAYLOR, M. K. [1957] The Canadian "JANET" system. *Proc. IRE*, Vol. 45, 1666-1678.

ESHLEMAN, V. R. [1957] On the wavelength dependence of the information capacity of meteor-burst propagation. *Proc. IRE*, Vol. 45, 1710-1717.

ESHLEMAN, V. R. and MANNING, L. A. [1954] Radio communication by scattering from meteoric ionization. *Proc. IRE*, Vol. 42, 530-536.

FORSYTH, P. A., VOGAN, E. L., HANSEN, D. R. and HINES, C. O. [1957] The principles of JANET – a meteor burst communication system. *Proc. IRE*, Vol. 45, 1642-1657.

GREENHOW, J. S. and HALL, J. E. [1960] The importance of initial trail radius on the apparent height and number distributions of meteor echoes. *Monthly Notices Roy. Astron. Soc.*, Vol. 121, 183-196.

GREENHOW, J. S. and NEUFELD, E. L. [1955] The diffusion of ionised meteor trails in the upper atmosphere. *J. Atmos. Terr. Phys.*, Vol. 6, 133-140.

HAAKINSON, E. J. [1983] Meteor burst communications model. NTIA Rep. 83-116, PB83-194134. US Dept. of Commerce, Office of Telecommunications, Institute for Telecommunication Sciences, Boulder, CO, USA.

INCE, A. N., VOGT, I. M. and WILLIAMS, H. P. [1978] A review of scatter communications. AGARD Conf. Proc. No. 244, *Aspects of Electromagnetic Wave Scattering in Radio Communications*, 21-1 to 21-31. Ed. A. N. Ince. NASA Accession No. N79-10299. National Technical Information Service, Springfield, VA 22161, USA.

KOKJER, K.J. and ROBERTS, T.D. [1986] - Networked meteor-burst data communication. IEEE Communications Magazine, 24, 11, 23-29.

MANNING, L. A. and ESHLEMAN, V. R. [1959] Meteors in the ionosphere. *Proc. IRE*, Vol. 47, 186-199.

MAYNARD, L. A. [1968] Meteor-burst communications in the Arctic. *Ionospheric Radio Propagation*, 165-173. Plenum Press, New York, NY, USA.

McKINLEY, D. W. R. [1961] *Meteor Science and Engineering*. McGraw-Hill Book Co. Inc., New York, NY, USA.

MILLMAN, G. H. [1978] HF scatter from overdense meteor trails. *Aspects of Electromagnetic Wave Scattering in Radio Communications*. Ed. A. N. Ince. AGARD Conf. Proc. 244, 6-1 to 6-14.

MILSOM, J. D. [1979] Some aspects of meteor-burst communications system design. Marconi Survey Series 79/9A.

MINULLIN, R. G., PALII, G. N., SIDOROV, V. V., SUKHOTSKII, A. V. and IVANOVA, Yu. D. [1971] Time measurements – locking in to the state standard of time by using reflections from meteors. 1971 Consultants Bureau, Plenum Publishing Corp., New York, Trans. from *Izmeritelnaya Tekhnika*, **1**, 22-24.

MONTGOMERY, G. F. and SUGAR, G. R. [1957] The utility of meteor bursts for intermittent radio communication. *Proc. IRE*, Vol. 45, 1684-1693.

PICKARD, G. W. [1931] A note on the relation of meteor showers and radio reception. *Proc. IRE*, Vol. 19, 1166-1170.

SANTEFORD, H. S. [1976] Meteor burst communication system: Alaska winter field test program. NOAA Tech. Memo NWS-Hydro-30, PB-260 449/4. National Oceanic and Atmospheric Administration, National Weather Service, Boulder, CO 80303, USA.

SITES, F. J. [1978] Communications via meteor trails. *Aspects of Electromagnetic Wave Scattering in Radio Communications*. Ed. A. N. Ince. AGARD Conf. Proc. 244, 25-1 to 25-21.

SMITH, H. C. [1978] Meteor-burst data communication system. 28th Annual Conference of the IEEE Vehicular Technology Society, 22-24 March, Denver, Colo., USA, Conf. Record, 497-502.

SUGAR, G. R. [1964] Radio propagation by reflection from meteor trails. *Proc. IEEE*, Vol. 52, 116-136.

VINCENT, W. R., WOLFRAM, R. T., SIFFORD, B. M., JAYE, W. E. and PETERSON, A. M. [1957] A meteor-burst system for extended range VHF communications. *Proc. IRE*, Vol. 45, 1693-1700.

WEITZEN, J.A. [1986] - Predicting the arrival of meteors useful for meteor burst communication. Radio Science, Vol. 21, 1009-1020.

WEITZEN, J.A., and RALSTON, W.T., [1988] Meteor scatter - an overview. IEEE Trans. Ant. and Prop., Vol. 36, No. 12, 1813-1819.

REPORT 260-3

IONOSPHERIC SCATTER PROPAGATION

(Question 28/6)

(1956-1959-1963-1966-1970-1978)

Ionospheric scatter propagation refers to a propagation mode used to communicate over distances of 800 to 2000 km by means of scattering from ionospheric irregularities at a height of around 85 km. Operating frequencies are in the 30 to 60 MHz range. The lower frequency is set by absorption during sudden ionospheric disturbances (SIDs) and polar cap events and by the desirability of avoiding signals propagated by the F2 layer normal and side-scatter modes.

The upper limit of frequency is fixed by mainly economic considerations. Since, as a rough guide, the signal intensities may be taken as varying inversely as the 7.5 power of the frequency, for scaled antennas with equal input power, while the cosmic noise intensities vary inversely as about the 2.5 power of the frequency, the signal-to-noise ratio varies inversely as approximately the 5th power of the frequency. With this frequency dependence of the signal-to-noise ratio and using scaled antennas, 15 dB more transmitter power is required at 60 MHz than at 30 MHz to give the same signal-to-noise ratio.

The signal, while weak compared to the normal ionospheric modes, is persistent (in most areas of the world); and high-powered ionosphere scatter systems were used in the 1950s and 60s for high-reliability voice and data traffic. Communication systems employing ionospheric scatter propagation are rarely used today and hence the rather extensive discussion contained in earlier versions of this Report (1956-1974) has been abbreviated in this document after the XIVth Plenary Assembly, Kyoto, 1978. The bibliography contains the readily accessible citations from the previous text.

A related communication mode, meteor-burst propagation, is treated in Report 251.

BIBLIOGRAPHY

ABEL, W. G., de BETTENCOURT, J. T., CHISHOLM, J. H. and ROCHE, J. F. [1955] Investigations of scattering and multipath properties of ionospheric propagation at radio frequencies exceeding the MUF. *Proc. IRE*, Vol. 43, 1255-1268.

BAILEY, D. K. [1962] Ionospheric "forward" scattering. General survey to the XIIIth General Assembly of URSI, London, September 1960, in *Monograph on Ionospheric Radio*, 189-199. Elsevier, London, UK.

BAILEY, D. K, BATEMAN, R., BERKNER, L. V., BOOKER, H. G., MONTGOMERY, G. F., PURCELL, E. M., SALISBURY, W. W. and WIESNER, J. B. [1952] A new kind of radio propagation at very high frequencies observable over long distances. *Phys. Rev.*, Vol. 86, 141-145.

BAILEY, D. K., BATEMAN, R. and KIRBY, R. C. [1955] Radio transmission at VHF by scattering and other processes in the lower ionosphere. *Proc. IRE*, Vol. 43, 1181-1230.

BAIN, W. F. [1963] Solar-induced effects on VHF ionospheric propagation at low magnetic latitudes. Agardograph 59. The effect of disturbances of solar origin on communications, 185-192. Pergamon Press, New York/Oxford.

BLAIR, J. C., DAVIS R. M. and KIRBY, R. C. [1961] Frequency dependence of D-region scattering at VHF. *NBS J. of Res.*, Vol. 65-D, 417-425.

BRAY, W. J., SAXTON, J. A., WHITE, R. W. and LUSCOMBE, G. W. [1956] VHF propagation by ionospheric scattering and its application to long-distance communications. *Proc. IEE*, Vol. 103, Part B, 236-260.

HALLEY, P., DUBOC, J. and THUILLIER, J. [1961] Etude des limites supérieures des fréquences susceptibles d'être réfléchies par l'ionosphère en Europe (Study of the upper limits of frequency that can be reflected by the ionosphere in Europe). *Ann. des Télécomm.*, Vol. 16, 5-6.

KOCH, J. W. [1959] Factors affecting modulation techniques for VHF scattter systems. *IRE Trans. Comm. Systems*, Vol. CS-7, 2, 77-79.

In addition to the above, attention is drawn to substantial parts of issues of journals as follows:

IRE Transactions on Communications Systems [March, 1956] Vol. CS-4.

Proc. IEE [May, 1958] Vol. 105, Part B, containing, under Session I, the papers and discussion of a symposium on "Ionospheric forward scatter propagation".

Proc. IRE [October, 1955] Vol. 43.

Proc. IRE [January, 1960] Vol. 48, 7-31. Report of JTAC on "Radio transmission by ionospheric and tropospheric scatter".

SECTION 6G: IONOSPHERIC PROPAGATION MEASUREMENTS AND DATA

REPORT 253-5*

MEASUREMENT OF SKY-WAVE SIGNAL INTENSITIES AT FREQUENCIES ABOVE 1.6 MHz

(Question 42/6)

(1963-1966-1974-1978-1982-1990)

1. Introduction

Measurements of sky-wave signal intensities, if undertaken in a carefully controlled manner, are of value in assessing the accuracy of methods for estimating field strength and transmission loss. Such measurements may also yield an indication of sources of error in existing prediction methods and may be used either to improve these methods or as a basis for developing new methods. Recommendation 378 states that, provided appropriate procedures are adopted, measurement accuracies of ± 2 dB should be attainable. Hence, assuming transmitter radiated powers can be determined to this same accuracy, differences between measured and predicted values in excess of 4 dB are significant. Ideally, the requirements are for measurements to be carried out systematically over as wide a range of conditions as possible at a series of frequencies over paths of different lengths in all regions of the world. Measurements are needed at each hour of the day in the separate seasons and for different solar epochs.

Since 1962 the CCIR Secretariat (in conjunction with Interim Working Party 6/1) has maintained a Data Bank of measurements provided to it by administrations and other organisations. Existing data have already proved useful, but ——————————————————— further data are needed. Whilst it is recognized that opportunities to make measurements for particular circuits often arise only incidentally, with transmission schedules and system parameters such as the choice of antennas being determined by operational considerations, nonetheless useful results can be obtained in such cases. However, it is evident that data have their greatest value when measurements are carried out under standardized conditions and when uniform analysis and tabulation procedures are followed. This Report presents the desirable criteria to be adopted to the extent that other constraints permit. Related information is contained in Reports 227 and 273.

A field-strength measurement campaign intended for future improvements in prediction methods, particularly those used for HF broadcasting, is described in Report 1149. This involves synchronous coded emissions from a network of up to 9 globally distributed transmitters. Darnell et al [1988] have proposed complementary measurements using such transmitters to determine other propagation parameters besides field strength.

* This Report is brought to the attention of Study Group 1.

2. Choice of circuits and periods of operation

Signal-intensity data are required from circuits of different ranges in all geographical regions. In practice, the selection by a particular organization of circuits for recording is likely to be influenced by:

- the relevance of the measured data to communication or other systems involving ionospheric propagation operated by the organization or its collaborators: the extent to which it is anticipated that the data will provide monitoring information which can be used to assess and, if necessary, improve the performance of the associated systems or that they are of value as a general indication of propagation conditions, and
- the availability of suitable transmitters or of site facilities for the establishment of transmitters.

In general, propagation tends to be most readily understood for short-distance paths (< 2500 km ground range) so that the likelihood of being able to make useful deductions from data is greatest for these; also, with the replacement of many HF point-to-point communication circuits by satellite and cable links, a large proportion of existing HF circuits now involve short paths. Synoptic short-distance path data are of additional scientific value for investigating propagation features associated with specific geographical regions (e.g. winter-anomaly absorption). Middle-latitude circuits usually experience the most stable and regular propagation conditions, whereas at high latitudes and over trans-equatorial paths there is appreciable day-to-day variability which serves to make data interpretation rather more difficult. For medium-distance paths (2500 to 8000 km range) multiple-hop signals involving more than one ionospheric reflection position occur and there are changes in the dominant mode; hence the study of the results obtained is correspondingly complicated. Long-distance paths (greater than 8000 km range) tend to be characterized by off-great circle propagation and by marked variations in propagation on different occasions, with both large systematic and day-to-day changes. For transmitter-receiver separations greater than 15 000 km and at certain times of day, depending on the antennas employed, the strongest signals may propagate via the longer great-circle path.

Recordings of a given transmission should be made for as many hours as possible every day. The objective should be to derive the median and other percentile values of the day-to-day distribution of signal intensity over all days of the month. Where it is not feasible to carry out measurements every day uncertainties arise in estimates of these values. Assuming a log-normal law of variation with decile deviation from the median of D(dB), the standard error E in the median based on a sample of N days within a month of 30 days (see Fig. 1) is:

$$E = \frac{D}{1.28}\sqrt{\frac{1}{N} - \frac{1}{30}} \quad \text{(dB)} \qquad (1)$$

Clearly the standard error increases as the number of days of recording decreases. Whilst there is no limiting sample size giving an abrupt increase in error, as a general rule 10 or more measurements are required for the calculation of the medians, 14 for the quartiles and 18 for the deciles.

It is seldom feasible to embark on a measurement programme extending over a significant part of a solar cycle but to ease data interpretation and to be statistically meaningful, measurements should cover a minimum period of one year at a given fixed frequency. There are particular advantages in attempting to record signals simultaneously over a path at a series of different frequencies, both to aid the understanding of propagation effects and to permit quantitative data to be obtained by night when maximum usable frequencies are low, as well as by day when there is much absorption at the lower frequencies so that signals are masked by background noise.

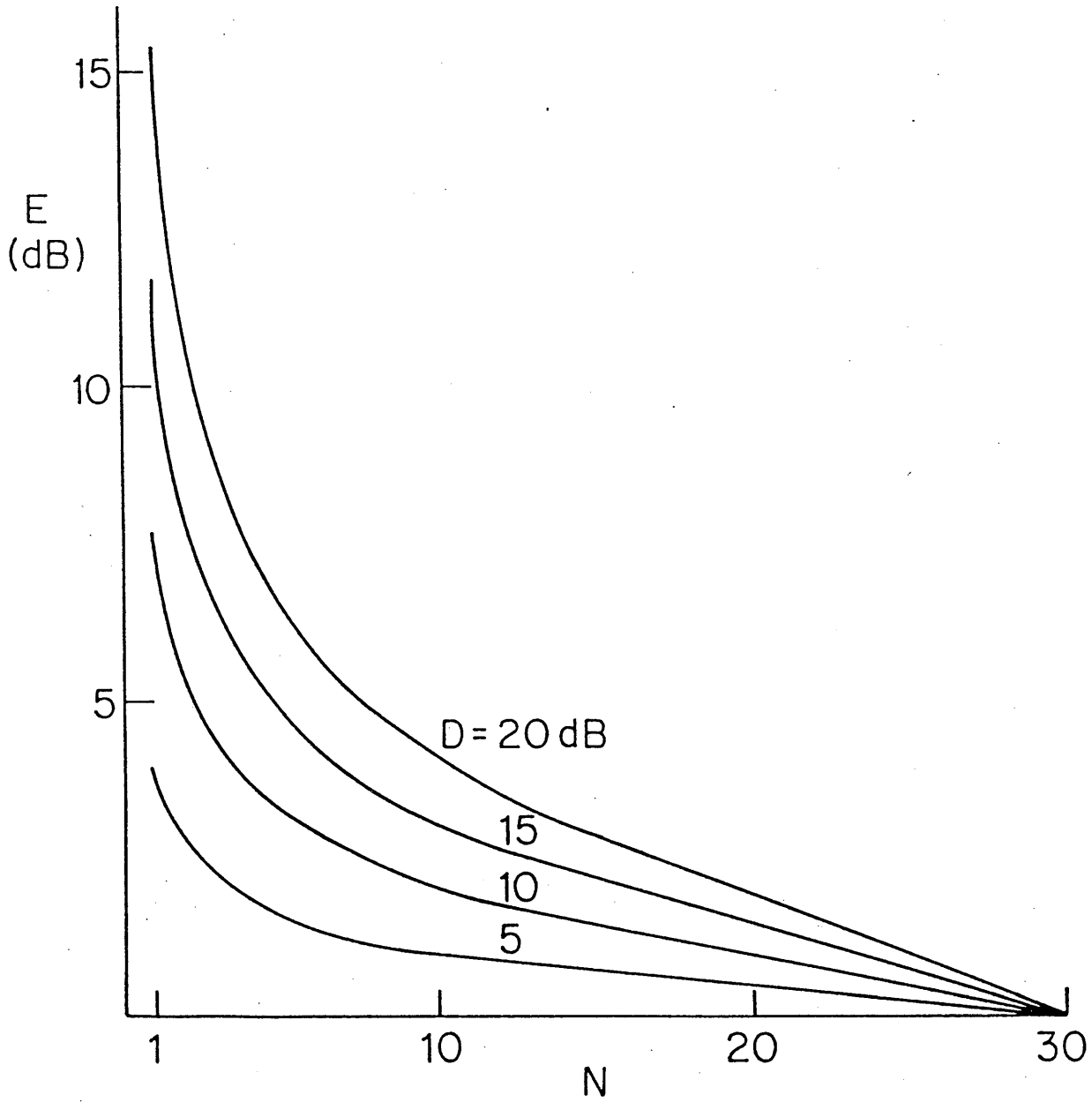


FIGURE 1

Standard error in monthly median (E) as a function of number of days sampled (N) for different decile deviations from the median (D)

3. Transmitter and transmitting antenna

The transmitter may be already in use or especially commissioned for the purpose. In either case it should be unambiguously identifiable so as to be sure that what is recorded is the wanted transmission and not co-channel signals, adjacent channel signals, or interfering noise. It is useful if the signals are interrupted at some periodic rate, say for 5 minutes once every hour, both as an aid to transmitter identification and to determine received background levels as confirmation that there is no significant signal contamination. The transmitter should operate preferably for 24 hours per day. It must be stable in both frequency and radiated power, and these two parameters must be known accurately. For reception over short paths it should desirably have a radiated power in excess of 1 kW and over medium-distance and long paths a power of 10 kW or more. Where a special transmitter is operated, this would normally radiate continuous waves, although pulsed signals may also be used with receiver time-gating to study the characteristics of individual propagation modes. If use is made of commercial transmitters carrying modulated signals, it is important that the type of modulation should be constant and the mean percentage modulation should not vary. Narrowband transmissions (approximately 1 kHz bandwidth or less) or a narrowband component of a composite signal are most appropriate to record. Wider-bandwidth signals are liable to interference contamination. Standard-frequency transmissions, as listed in Report 267, ——— have been employed in the past, but in many receiver locations there is now serious interference between signals from different transmitters operating this service and sharing the same frequency, except that some stations in the USSR are alleviating the problem by adopting offset frequencies of ±4 kHz. ——— Nevertheless, interference can be avoided to some extent by means of a narrowband receiver capable of resolving the different audio modulation frequencies of each co-channel transmitter. Transmitters for point-to-point telephony or telegraphy services offer the advantages of providing channels which are relatively free from interference, and a detailed log of transmission schedules is usually available. On the other hand, these transmitters often employ high-gain antennas, which tends to be a disadvantage.

A suitable category of transmitters meeting nearly all of the above criteria is weather-chart (FAX) transmitters using frequency shift-keying (+/- 400 Hz). As there are numbers of receivers (ships) with unknown position, these transmitters use omnidirectional antennas and transmit mostly for 24 hours per day. Some of these transmitters are listed by Damboldt and Suessmann [1987]. Receiving systems should be very sensitive especially when recordings are made for very long paths.

Inspection of the International Frequency List maintained by the IFRB is of value in the selection of suitable transmitters to monitor. In particular, this usually gives information concerning transmitter radiated power, form of modulation and period of the day of operation. Sometimes it also yields details of the antenna type and orientation. The International Frequency List is useful additionally in providing a list of co-channel and adjacent-channel transmitters which should be considered further to assess the likelihood of possible interference. However, before embarking on a programme of systematic measurements it is recommended that after selecting a potentially suitable transmitter in this way, firstly a series of monitoring measurements should be carried out at various times over a period of about a month to determine the order of signal intensities encountered, the time coverage over which such signals can be detected, and the amounts of interference experienced. Then, a direct approach should be made to the organization operating the transmitter to verify the International Frequency List entries, to supply such additional details as are required – for example, concerning the type of antenna used and the associated ground properties. In particular, it should be checked that the radiated power is maintained constant, that different antennas are not used by night and day, and that the transmitter is not part of a network of transmitters operating at the same frequency from geographically separated sites – a procedure adopted in the HF broadcasting services in some countries. It is important to confirm also that it is proposed that the transmitter will remain operational throughout the whole period for which it is intended to make measurements. Only then should a decision be reached to carry out systematic recordings of the transmissions. Whilst ideally it would be desirable to receive details of the transmitter log, noting in particular any malfunctions or temporary changes in technical characteristics which might influence the measurements, it is rarely feasible to obtain such data and to apply variable corrections to results in retrospect. Instead, every effort should be taken at the outset to avoid the monitoring of transmitters whose characteristics are known to fluctuate.

For a particular transmitter to be suitable for signal-intensity measurements, the performance of its transmitting antenna needs to be known accurately. Transmitters coupled to antennas with little directivity have advantages over those with highly-directional antennas because radiation patterns usually approximate more closely to theory, because the relative strengths at the receiving site of signals travelling via different modes are then determined mainly by propagation effects, and because valid deductions may be made with a single allowance for transmitting-antenna gain in the absence of a knowledge of wave launch directions. Unfortunately though, low-gain transmitting antennas are seldom used for other applications. Most point-to-point HF land-fixed communication circuits employ high-gain rhombic or log-periodic antennas; for sky-wave broadcasting, arrays of horizontal dipoles, also with significant directivity, are popular. The exception is with standard-time transmitters which aim to provide all-round azimuthal coverage by means of vertical half-wavelength dipoles. These transmissions are particularly suitable for monitoring purposes. Radiation patterns for a vertical-dipole antenna may be estimated fairly accurately, except at low elevation angles where the particular ground constants control signal intensities. However, even at low angles the performance is known more accurately than for most other types of antenna. If no such transmitter is conveniently positioned for use, then before monitoring transmissions from a directional antenna it should be checked that the great-circle path to the receiver does not involve reception of side-lobe signals. If propagation is over medium or long distances, ideally the antenna vertical polar diagram for elevation angles less than 20° should approximate that of a reference short vertical radiator sited over average ground (see Fig. 2*a*).

Where a special transmitter is operated, a short vertical antenna is to be preferred. Alternatively, for short paths a horizontal dipole aligned for broadside radiation along the great-circle direction may be used. For greater ranges corresponding to low elevation angles, the direct and ground-reflected components of the sky wave nearly cancel one another so that a horizontal antenna is very inefficient unless elevated to a great height and should be avoided.

Transmitting-antenna gain (like receiving-antenna gain) is best determined from near-site measurements in the far-field region, but it is recognized that these rarely form part of the normal programme of work at a transmitting installation and that it is not generally possible to be able to arrange for such measurements to be carried out at a remote location, not under the control of the receiving organization. Accordingly, transmitting-antenna gain must usually be calculated from theoretical relationships in terms of the known antenna geometry, and by making certain assumptions concerning the type of ground involved.

4. Receiving antenna, receiver and recording techniques

Since existing methods of prediction of signal intensities do not take account of field distortion effects due to local features at the receiving site such as undulating ground, obstacles like buildings and foliage and adjacent antennas which act as re-radiating structures, it is important to site the receiving antenna so that these effects are kept to a minimum. The ground should have a slope not exceeding 2° out to a distance of five wavelengths and no obstacles should subtend an angle from the horizontal at the centre of the antenna in excess of 5°. The separation from other antennas should be not less than ten times the antenna length.

It is more important that the receiving-antenna performance should be known accurately than that it should have high gain. Except at the lower frequencies during the daytime when there is much ionospheric absorption, threshold levels for signal detection will normally be determined by external noise intensities whatever receiving antenna is used. In general, the greater the antenna gain, the more likely the possibility of error in assessing its performance. Accordingly, a short vertical active antenna or a grounded vertical monopole antenna not exceeding a quarter wavelength high as proposed in Recommendation 378 or a small loop antenna are most appropriate to employ. The loop antenna would normally be aligned in a vertical plane containing the great-circle direction to the transmitter. For long-distance paths where off-great circle propagation is likely to be important, the vertical-monopole antenna is preferable since this provides omnidirectional azimuthal pick-up. If several transmissions from different azimuths are recorded with one antenna, only a vertical antenna should be used. Some organizations use vertical monopoles for

signal measurements but standardize results by means of calibration data involving comparisons for selected sample signals with the pick-up indicated by a portable "field-strength" meter incorporating an integral loop-receiving antenna (see Report 227 for further details).

Figure 2*a* shows the variation with elevation angle of the term $E_0 - E$ (a measure of the signal pick-up resulting from a downcoming sky-wave of constant intensity and its associated ground-reflected wave, defined in § 6.2) for a short vertical grounded monopole and a loop antenna, both situated over average ground. For elevation angles below about 30° the monopole and loop antennas have very similar polar diagrams but at higher elevation angles the loop-antenna pattern is preferable since the pick-up is relatively insensitive to angle. Fig. 2*b* shows the effect of antenna siting over-ground of different properties. Signal pick-up for wet ground exceeds that for very dry ground by some 2-6 dB with the largest differences occurring at low elevation angles. The marked dependence of the pick-up on the ground constants and on the elevation angle when this is low, which have been discussed already with regard to the transmitting antenna, lead to particular data interpretation difficulties for long paths where elevation angles are not known accurately. In principle, the use of an artificial ground screen would lead to a receiving system performance less dependent on weather conditions which affect ground water content. The screen would improve the ground constants and so increase the signal pick-up, but to be effective in this role it would need to have dimensions of the order of tens of wavelengths and this is rarely practicable. On the other hand, short screens of length up to about five wavelengths can be implemented and are of value in stabilizing antenna impedances to improve circuit matching. If a screen is used, it is desirable to assess its effect by carrying out near-site calibration measurements with signals radiated in the far-field region from an airborne transmitter.

Horizontal half-wave dipoles for single-frequency operation or terminated dipoles for multiple-frequency measurements are sometimes suitable for reception of signals on short paths. In particular, pick-up is not strongly dependent on the ground constants. However, for medium distance and long paths when elevation angles are low, these antennas provide only limited pick-up, again markedly dependent on elevation angle, unless they are elevated to great heights. They should not be used for these paths because of calibration difficulties.

Some organizations are equipped to make measurements using special antenna systems, such as rhombic arrays, designed for specific circuits to improve signal/noise ratios and to enable measurements to be made under conditions where a simple antenna would be unusable. It is difficult to interpret the results obtained on an extended antenna system in the presence of a complex field built up of several waves incident at different angles, but measurements made with such antennas may be acceptable for the purpose in hand, if they can be related consistently to those that would be obtained at the same time on a standard antenna. In making a choice between antennas responding either to vertical or horizontal polarization, it is prudent to check (e.g. see [Bradley, 1968]) that, if propagation paths involve waves with markedly non-circular polarization, reception (or transmission) is predominantly that of the stronger ordinary wave.

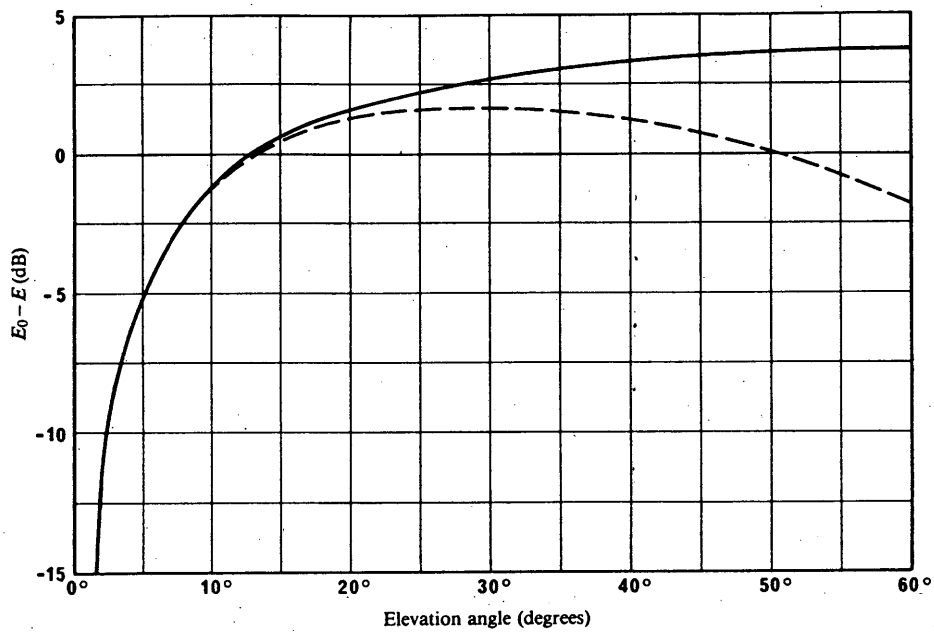
The receiving antenna should be connected to the receiver via a buried coaxial cable and appropriate matching circuitry. This latter may take the form of a transformer or a wideband pre-amplifier. The receiver bandwidth should be as narrow as possible consistent with the bandwidth of the transmitted signals, in order to optimize the received signal/noise ratio. For continuous-wave signals and for the monitoring of the steady tone sideband signals of standard-time transmissions, bandwidths of the order of 100 Hz or less are suggested [Wakai *et al.*, 1971].

Received signal intensity depends on radiated power within the receiver bandwidth. This is a function of the carrier, modulation and recording arrangement. For a receiver bandwidth which encompasses the carrier and all sidebands, the operative radiated power is equal to the sum of that of the carrier and all other components. Figures for different types of modulation are given in Recommendation 326. In the case of narrowband reception of a single sideband of a standard time transmission of carrier power P where the amplitude modulation depth is m, the sideband power is $m^2P/4$.

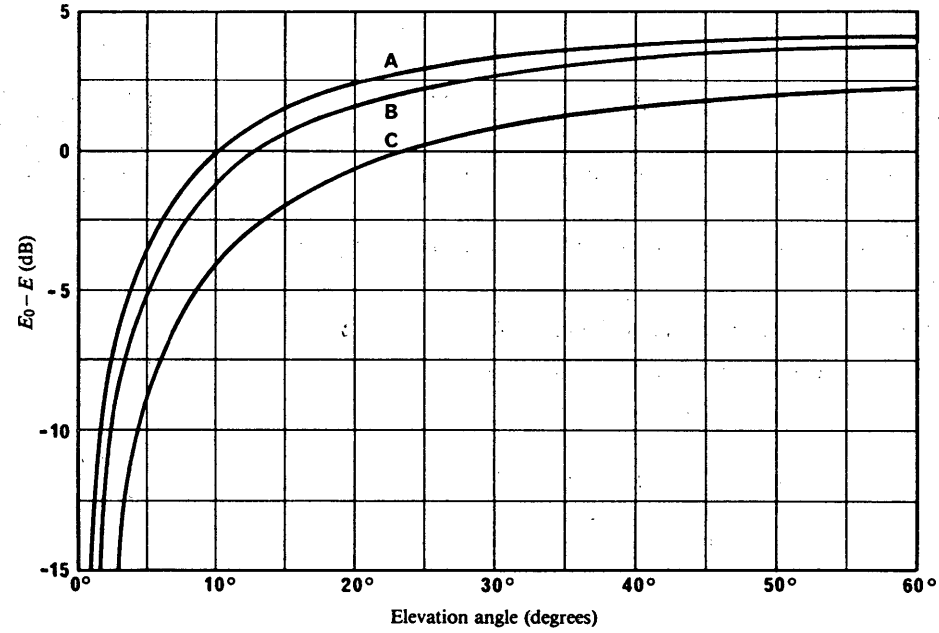
Signals should be detected, applied to appropriate integration-smoothing circuitry, and then recorded in suitable form.

Some organizations monitor signals over oblique paths in order to note the occurrence of events like sudden ionospheric disturbances (SIDs) and magnetic storms, or to study fading statistics. In these cases, special recording procedures may be necessary. Where, however, the prime requirements are to collect representative hourly signal-intensity data, measurements are best made using a pen-chart recorder with a logarithmic amplitude scale (i.e. linear in decibels) and a chart speed of about 2 cm per hour. The integration time constant should be about 20 s. This arrangement provides a convenient length of record for manual smoothing whilst at the same time permitting the rejection of sections shown to be contaminated by interfering signals or strong atmospherics. It is often simpler to record the automatic gain-control voltage from a commercial receiver after modifications to equate and lengthen the rise and decay time constants to the 20 s noted above. However, this approach may lead to unacceptable errors under some conditions, even after continuous-wave calibration of the response. Output voltage is usually approximately proportional to the logarithm of the input voltage, but since this non-linearity is associated with the detection process and occurs prior to integration, recordings give the mean logarithm of the signal intensity and not the mean in logarithmic units as required. These quantities differ when there is signal fading present. An alternative acceptable form of recording involves digital quantization of instantaneous amplitudes at a convenient sampling rate so as to cover the known periodicity of typical fading components (with fading durations up to about 20 min). Representative values may then be determined by computer processing. Apart from identification problems, the use of a computer to control the measuring receiver can greatly accelerate and simplify both measurements and statistical analysis [Lehtoranta, 1987]. It cannot be emphasized too strongly though that with these techniques some form of regular check must be introduced to ensure that what is measured is the wanted transmission.

Hourly figures each day are best expressed in the form of median values. With chart recording it is preferable to derive the median directly as that amplitude which is exceeded for a total of half the recording duration (i.e. 30 min for hourly medians). This procedure is independent of the chart amplitude scale. When a precise logarithmic amplitude scale is used for recording, the median may alternatively be given approximately by two-thirds the chart deflection between the quasi-minimum value (exceeded for Q% of the time, say, where $Q \geqslant 90$%) and the quasi-maximum value (exceeded for (100 – Q)% of the time), assuming that fading follows a Rayleigh distribution (see Report 266). With computer recording and processing it is suggested in Report 1149 that a minimum of 12 independent samples are needed to produce representative hourly median values. The samples should ideally be distributed uniformly throughout the hour, but if switched recording of signals from several transmitters is required, groups of 4 samples within 4 minutes, repeated three times during the hour, are acceptable.



(a) Sited over average ground of conductivity σ = 0,01 S/m, relative dielectric constant ε = 15



(b) Sited over wet, average and very dry ground

FIGURE 2 – *Difference between r.m.s. equivalent-incident field strength, E_0, and r.m.s. sky-wave field strength, E, for short vertical monopole and for loop antenna at a height of 1 m. Frequency: 15 MHz*

Curves A: wet ground σ = 0.02 S/m, ε = 20
B: average ground σ = 0.01 S/m, ε = 15
C: very dry ground σ = 0.002 S/m, ε = 5

— — — — monopole

———— loop

5. Calibration measurements

Pen-chart recorder deflections or computer-recorded data should be related to the associated voltages injected directly into the receiver from a signal generator. Periodic calibration measurements are needed to express r.m.s. signal-generator voltage readings in terms of the corresponding amplitudes of the recorded sky waves. Two approaches are possible. In the one, cable, mis-match and coupling losses, together with antenna impedance measurements, are needed so that signal data may be expressed as available receiver powers and associated field strengths. In the other, appropriate only to reception of vertically-polarized wave components, a direct comparison is made with meter values indicated by a portable "field-strength" measuring system incorporating a vertical loop antenna. In this case, it is important to be certain what assumptions have been made in calibrating the meter and what field strengths are quoted (see § 6.2).

6. Conversion of measured data to mean available receiver power and r.m.s. sky-wave field strength

The existing methods of Report 894, Report 252 and its Supplement for estimating sky-wave signal intensities give values of mean available receiver power in the absence of receiving-system losses and r.m.s. sky-wave field strength. Hence, conversion relationships are needed between the measured voltages developed across the receiver input terminals and these quantities.

6.1 *Mean available receiver power*

The relationship between measured receiver input voltage when fed from a practical antenna and the available power from an idealized lossless receiving antenna coupled to a matched load depends on the receiving-system losses and the impedances of the antenna and receiver. In general, the receiving-system losses and the antenna impedance are frequency-dependent factors. In particular, the relationship is not a function of the wave-arrival directions or polarizations.

Consider first the idealized case of a lossless receiving antenna feeding a matched load.

Let

P_a: available power from receiving antenna (dBW),

V_0: r.m.s. voltage developed across matched load (dB(1 μV))

r: antenna load resistance (ohms).

Then

$$P_a = V_0 - 10 \log r - 120.$$

In particular for $r = 50\ \Omega$

$$P_a = V_0 - 137.0 \quad \text{(dB)} \tag{2}$$

Now consider the practical case of an antenna coupled to a receiver via a feeder cable and a transformer or other matching circuitry, but where some matching losses arise, r is then the load resistance presented by the receiver.

Let

V: r.m.s. voltage developed across receiver input terminals (dB(1 μV)),

L: cable loss (dB)

T: mis-match and coupling losses (dB).

In general, the evaluation of T involves a knowledge of the antenna impedance. T includes losses in transformers and other antenna-matching circuitry, and losses associated with the matching of the feeder cable to the receiver. Then

$$V_0 = V + L + T$$

so that, from (2):

$$P_a = V + L + T - 137.0 \qquad \text{(dB)} \tag{3}$$

Now for reception of fading sky-wave signals where P_a represents the mean available power (in dBW) and V is the hourly median receiver input voltage (dB(1 μV)), a fading allowance must be included in equation (3). Assuming Rayleigh fading, the r.m.s. voltage is 1.6 dB greater than the median, so that:

$$P_a = V + L + T - 135.4 \qquad \text{(dB)} \tag{4}$$

Equation (4) may be used to relate measured values of V to P_a provided the various system losses are known. If it is not possible to determine L and T as, for example, where calibration is by standardization with a portable field-strength meter, then alternatively P_a may be given in terms of E, the r.m.s. sky-wave field strength (dB(μV/m)), when this is known (see § 6.2), by

$$\begin{aligned} P_a &= E + G_r - 120 + 10 \log \left(\frac{\lambda^2}{480 \pi^2} \right) \\ &= E + G_r - 20 \log f - 107.2 \qquad \text{dB} \end{aligned} \tag{5}$$

λ is the wavelength in metres and f the frequency in MHz. G_r is the receiving antenna gain (expressed in decibels relative to an isotropic radiator in free space) which, in particular, depends on wave-arrival direction. This direction is not usually measured but must be predicted. Hence, this means of deriving P_a is less appropriate, since it does not lead to independent data to test the accuracy of the predictions.

6.2 *R.m.s. sky-wave field strength*

Measured receiver input voltages may be expressed in terms of the corresponding voltages induced in the receiving antenna, and thence as associated field strengths. In the case of simple configurations such as a vertical monopole antenna and a broadside or end-on dipole or loop antenna responding to waves with a single (horizontal or vertical) polarization, it is convenient to introduce the concept of an equivalent-incident field strength. This refers to a resultant field with the same polarization as that to which the antenna responds. It may be regarded as the sum of a downcoming sky wave and a ground-reflected wave. Portable commercial field-strength meters are usually calibrated to indicate equivalent-incident field strength. On the other hand, for extended antennas composed of separate limbs with different orientations, such as the horizontal rhombic antenna, the term "equivalent-incident field strength" has no physical significance. The signal pick-up and the resultant field vary for the different limbs. In the case of the off-axis pick-up on a simple antenna like a dipole or a loop antenna, the equivalent-incident field concept also is not particularly useful. The antenna then responds to waves of elliptical polarization, and induced voltages depend not only on the wave strengths, but also on the match between the wave polarizations and the polarizations to which the antenna responds for the particular directions of incidence. Waves of different polarization and intensity incident from the same direction may then produce the same induced voltage.

The relationship between equivalent-incident field strength and voltage induced in the receiving antenna is a function of frequency, but unlike the corresponding relationship for sky-wave field strength, it is independent of wave-arrival direction and ground constants. In both cases the conversion factor has the dimensions of length, so that where the concept of an equivalent-incident field strength is meaningful, it is convenient to refer to two different antenna effective lengths. Let l_{ei} be the effective length relating equivalent-incident field strength to antenna induced e.m.f., and l_{es} be the effective length relating sky-wave field strength to antenna induced e.m.f. To compare equivalent-incident field strength and sky-wave field strength, which is the same as to relate l_{ei} to an appropriate l_{es}, is usually complicated and involves assumptions about the prevailing wave-field component amplitudes, polarizations and arrival angles; also a knowledge of the antenna polar diagram is required.

Let

E_0 : r.m.s. equivalent-incident field strength (dB(μV/m)),

V: median voltage developed across receiver input terminals (dB(1 μV))

and let l_{ei} be expressed in metres. Then again assuming Rayleigh fading:

$$E_0 = V + L + T - 20 \log (l_{ei}) + 7.6 \qquad \text{(dB)} \tag{6}$$

For a vertical monopole of physical length l (metres)

$$l_{ei} = \frac{\lambda}{2\pi} \tan \frac{\pi l}{\lambda} \tag{7}$$

and in particular for $l \ll \lambda$, $l_{ei} \simeq \frac{l}{2}$

For a small n-turn loop antenna of area A aligned in the plane of incidence:

$$l_{ei} = \frac{2\pi nA}{\lambda} \tag{8}$$

Now if E is the r.m.s. sky-wave field strength (dB(μV/m)), and l_{es} is expressed in metres, then comparison with equation (6) leads to:

$$E = V + L + T - 20 \log (l_{es}) + 7.6 \qquad \text{(dB)} \tag{9}$$

But l_{es} is given in terms of the antenna gain relative to an isotropic antenna in free space g_r and radiation resistance $r_a(\Omega)$ by

$$l_{es}^2 = \frac{g_r \lambda^2 r_a}{120\pi^2} \tag{10}$$

so that with $G_r = 10 \log g_r$ and f in MHz, E may be expressed alternatively as:

$$E = V + L + T - G_r - 10 \log r_a + 20 \log f - 11.2 \qquad \text{(dB)} \tag{11}$$

The difference between equivalent-incident field strength and sky-wave field strength is given from equations (6) to (11) by equating values of V. This is shown in Fig. 2 for the cases of a short vertical grounded monopole and a loop antenna.

6.3 *Preferred signal-intensity parameter for comparison of measured data with predictions*

It has been seen in § 6.1 and 6.2 that whereas measured data are related to available receiver power in terms of the receiving-system parameters only, to express the measurements as corresponding sky-wave field strengths involves a knowledge of wave-arrival directions and polarizations. Since these directions are not normally measured but must be predicted, it follows that, where possible, the preferred signal-intensity parameter for the purpose of comparison exercises with predictions is the available receiver power.

7. Data-tabulation procedures

Four types of data-tabulation sheet may be prepared, depending on whether it is the wish of the organization undertaking measurements to quote values in:

- received power in dBW (without correcting for receiving antenna effects),

- receiver input voltage in dB (μV) (without correcting for receiving antenna effects),
- incident field strength in dB (μV/m) (receiving antenna allowance ignores reflection of the downcoming sky-wave near the receiving antenna),
- sky-wave field strength in dB (μV/m)

Although received power would be the most suitable parameter, presently it is desirable to use incident field strength because the receiving antenna allowance is probably better known at the receiving site.

7.1 Circuit and operating details

A sample sheet for the technical information needed is contained in Table I. Tables II and III provide a brief amplification of what is asked for in Table I. The purpose of these three Tables is that they be used by organisations undertaking HF signal-amplitude measurements.

7.2 Monthly tabulation sheets of signal-amplitude measurements

Table IV contains a sample sheet for recording the hourly and monthly values of signal-amplitude measurements. Table V explains Table IV. Table IV is required for each frequency and month, whereas Table I is only needed once for each frequency.

The evaluation of count, upper and lower deciles, upper and lower quartiles and median is done by a computer or, if not available, by means of the procedure described in Table VI.

Hourly median values should be expressed to the nearest 1 dB. Where for some reason values are believed only correct within 2 to 4 dB they should be accompanied by an appropriate descriptive letter and qualified as uncertain. If an estimate to within 4 dB cannot be made, then only a descriptive letter and no numerical value should be quoted. The following letters are to be used:

- qualifying letters (preceding numerical values)

  D: to indicate that the numerical value is a lower-limit value;

  E: to indicate that the numerical value is an upper-limit value;

  U: to indicate that the numerical value is uncertain;

- descriptive letters (following numerical values or alone)

  C: no measurement was carried out or was possible because of technical trouble;

  S: measurements influenced or impossible because of interference or atmospherics;

Medians, quartiles and deciles should not be quoted if these figures are not more than 2 dB above the received background noise intensity.

If more than half of all possible daily numerical values within a month are qualified for any reason, then the median, the quartile and the decile values should be qualified by U and accompanied by the relevant descriptive letter, being that appropriate to the majority of the missing and qualified data. When the median, quartile or decile is only between 2 and 4 dB greater than the noise background, it should also be qualified by U and described by S.

7.3 Tabulation of data for computer processing

If signal-intensity measurements are made with the aid of a computerized system, the data exchange should be in accordance with the procedure described in Table VII.

TABLE I

Technical information sheet

CCIR data bank of HF signal-amplitude measurements		
This technical information sheet must accompany the hourly data sheets		
Kind of Information	**Transmitter**	**Receiver**
Location		
Geographical latitude	N/S	N/S
Geographical longitude	E/W	E/W
Name and address of station		
Ground conductivity	S/m	S/m
Ground permittivity		
Antenna: type		
polarisation		
hor. beam	Deg.	Deg.
vert. beam	Deg.	Deg.
gain	dBi	dBi
length	m	m
height	m	m
groundscreen		
number of elements		
Frequency	kHz	———
Call sign		———
Class of modulation		———
Carrier power	kW	———
Power at antenna feed point	kW	———
Hours of operation	UTC	———
Source of information		———
Reliability of information		———
Receiver type	———	
Recording time	———	min/h
Receiver bandwidth	———	kHz
Hourly parameter reported (please tick which)	———	median mean RMS
Units reported (please tick)	———	
Received power	———	dBW
Receiver input voltage	———	dB (uV)
Incident field strength	———	dB (uV/m)
Skywave field strength	———	dB (uV/m)
Data reduced to 1 kW (yes/no)	———	
TX-antenna reduced to isotropic (yes/no)	———	
Assumed elevation angle	Deg.	Deg.

TABLE II

Explanation of the technical information sheet (part 1)

CCIR data bank of HF signal-amplitude measurements
Explanations of the technical information sheet
location: name of transmitter/receiver site
geographical latitude: latitude of transmitter/receiver in degrees and minutes
geographical longitude: longitude of transmitter/receiver in degrees and minutes
name and address of station: name of the organisation that is responsible for the transmitter /receiver and mailing address and/or telephone/telexnumber
ground conductivity: at the transmitter/receiver site
ground permittivity: at the transmitter/receiver site
antenna: type (dipole, log-periodic, curtain ...), horizontal or vertical polarisation horizontal main beam direction in degrees vertical main beam direction in degrees gain in dBi in the main lobe length in m height in m groundscreen, if any - provide details number of elements
frequency: in kHz
call sign: if any
class of modulation: broadcast, rtty, fax ...
carrier power: nominal power of the transmitter in kW
power at antenna feed point: carrier power minus cable and matching loss between transmitter and antenna in kW
hours of operation: in UTC

TABLE III

Explanation of the technical information sheet (part 2)

CCIR data bank of HF signal-amplitude measurements
Explanations of the technical information sheet
source of information: Where is the information about the transmitter from?
reliability of information: subjective judge of the reliability of the above information. Most reliable is direct information from the transmitting station. Rather unreliable e.g. is information from the International Frequency List.
receiver type: manufacturer, type of receiver
recording time: how many minutes per hour are recorded to derive the hourly value?
receiver bandwidth: in kHz
hourly parameter recorded: are the measured data median, mean or rms values?
units reported: are the values measured received power in dBW (without correction for receiving antenna effects) or receiver input voltage in dB (uV) (without correction for receiving antenna effects) or incident field strength in dB (uV/m) (receiving antenna allowance ignores reflection of the downcoming sky-wave near the receiving antenna) or sky-wave field strength in dB (uV/m)?
data reduced to 1 kW: are the measured data reduced to 1 kW radiated power?
TX-antenna reduced to isotropic: are the measured values reduced to an isotropic transmit antenna?
assumed elevation angle: how was the elevation angle of the incoming wave calculated (or assumed), when the transmit antenna gain was deduced or when the measured data were converted to sky-wave field strength?

TABLE IV - Sample sheet for hourly and monthly signal-amplitude measurements

CCIR data bank of HF signal-amplitude measurements												Circuit:					Frequency:		kHz	Month:		Year:		
Time UTC / Day	00.30-01.30	01.30-02.30	02.30-03.30	03.30-04.30	04.30-05.30	05.30-06.30	06.30-07.30	07.30-08.30	08.30-09.30	09.30-10.30	10.30-11.30	11.30-12.30	12.30-13.30	13.30-14.30	14.30-15.30	15.30-16.30	16.30-17.30	17.30-18.30	18.30-19.30	19.30-20.30	20.30-21.30	21.30-22.30	22.30-23.30	23.30-00.30
1																								
2																								
3																								
4																								
5																								
6																								
7																								
8																								
9																								
10																								
11																								
12																								
13																								
14																								
15																								
16																								
17																								
18																								
19																								
20																								
21																								
22																								
23																								
24																								
25																								
26																								
27																								
28																								
29																								
30																								
31																								
Count																								
Upper decile																								
Upper quartile																								
Median																								
Lower quartile																								
Lower decile																								

Qualifying letters: E : receiver input below recording threshold D : receiver input above recording maximum U : uncertain value

Descriptive letters: C : no measurement carried out or technical trouble S = interference

TABLE V

Explanations for the hourly and monthly signal-amplitude measurements

CCIR data bank of HF signal-amplitude measurements	
Explanation of the tabular sheet for the hourly measurements	
circuit:	Name of transmitting/receiving station
hourly values:	For continuous transmissions, the average signal from 30 minutes before the hour to 30 minutes after the hour is to be taken. If a transmission lasts 60 minutes, from one hour to the next full hour, it will be split into two 30-minute periods and two hourly values shall be entered into the table. For hours where there was no measurement the letter C shall be entered into the table. For hours where there was a measurement but this is judged to be influenced by interference or atmospherics the letter S shall be entered into the table. For hours where there was a measurement but the wanted signal was below the recording threshold that threshold and the letter E shall be entered into the table. For hours where there was a measurement but the wanted signal was above the recording maximum that maximum and the letter D shall be entered into the table. For hours where there was a measurement but the wanted signal was uncertain due to any reason the measured value and the letter U shall be entered into the table. All daily and monthly summary amplitudes shall be quoted only to the nearest integer decibel.
count:	The number of hours with numerical values and with letters D, E and U is the "count".
deciles, quartiles and medians:	all measured values should be sorted in order of reducing amplitude. D-values have to appear at the upper end and E-values at the lower end. Deciles, quartiles and medians are yielded according to Table VI.

TABLE VI

Table for deriving deciles, quartiles and medians

CCIR data bank of HF signal-amplitude measurements

Table for deriving deciles, quartiles and medians

In the table below, the procedure how to calculate deciles, quartiles and medians is given.

If the sorted table contains 31 values the 4th from the top is the upper decile, half of the sum of the 8th and 9th value is the upper quartile and the 16th value is the median.

If the sorted table contains 30 values, the upper decile is taken as 9 times the 4th value plus the 3rd value divided by ten etc.

Upper deciles and quartiles are counted by starting at the upper end of the table. Lower deciles and quartiles are counted by starting at the lower end of the table.

count	Values to be used in the calculations: decile	quartile	median
31	4th	(8th+9th)/2	16th
30	(9*4th+3rd)/10	(3*8th+9th)/4	(16th+15th)/2
29	(4*4th+3rd)/5	8th	15th
28	(7*4th+3*3rd)/10	(3*8th+7th)/4	(15th+14th)/2
27	(3*4th+2*3rd)/5	(7th+8th)/2	14th
26	(3rd+4th)/2	(3*7th+8th)/4	(14th+13th)/2
25	(2*4th+3*3rd)/5	7th	13th
24	(3*4th+7*3rd)/10	(3*7th+6th)/4	(13th+12th)/2
23	(4th+4*3rd)/5	(6th+7th)/2	12th
22	(4th+9*3rd)/10	(3*6th+7th)/4	(12th+11th)/2
21	3rd	6th	11th
20	(9*3rd+2nd)/10	(3*6th+5th)/4	(11th+10th)/2
19	(4*3rd+2nd)/5	(5th+6th)/2	10th
18	(7*3rd+3*2nd)/10	(3*5th+6th)/4	(10th+9th)/2
17		5th	9th
16		(3*5th+4th)/4	(9th+8th)/2
15		(4th+5th)/2	8th
14		(3*4th+5th)/4	(8th+7th)/2
13			7th
12			(7th+6th)/2
11			6th
10			(6th+5th)/2

TABLE VII

Explanation of the computerized data-exchange sheet

CCIR data bank of HF signal-amplitude measurements

Explanations of computerized data exchange

Technical Information must also accompany the measurements if the data exchange is by computer. The daily and monthly measured values, however, will have the following format:

Columns 1-3 Circuit and frequency code

Column 5
1 = daily values
2 = upper deciles
3 = upper quartiles
4 = medians
5 = lower quartiles
6 = lower deciles

Column 7
1 = median
2 = mean
3 = RMS

Column 8
1 = available receiver power in dBW
2 = receiver input voltage in dB (uV)
3 = incident field strength in dB (uV/m)
4 = sky-wave field strength in dB (uV/m)

Columns 10-11 Year (two digits)

Columns 13-14 Month (two digits)

Columns 16
1 = 01-12 UTC
2 = 13-24 UTC

Columns 18-19 Day number

Remaining columns from 21 to 80: 5 columns each for 12 hours
column 1: qualifying letter (or space if none)
column 2: data value - hundreds
column 3: data value - tens
column 4: data value - units
column 5: descriptive letter (or space if none)

Data should be written on a magnetic tape (1600 BPI, 9-Tracks, logical record length 80, block size 80, EBCDIC- or ASCII-Code, no label) or on diskettes (5 1/4" 360 KByte MS-DOS-Format).

REFERENCES

BRADLEY, P. A. [1968] Wave polarization and its influence on the power available from a radio signal propagated through the ionosphere – 2. *Proc. IEE*, **115(6)**, 777-781.

DAMBOLDT, T. and SUESSMANN, P. [1987] - Characteristics of transmissions suitable for recording of field strength. IWP 6/1 Doc 310.

DARNELL, M., HAGUE, J. and CHAN, A. [1988] - A global common-user system for the provision of HF propagation data in "Propagation effects and circuit performance of modern military radio systems with particular emphasis on those employing band spreading", AGARD Conf., Paris, October.

LEHTORANTA, V. [1987] - Field strength measurements automation with personal computers. IWP 6/1, Doc. 302.

WAKAI, N., FUJII, S. and MIYAMOTO, Y. [1971] Measurement of the field intensity of HF radio waves by means of a narrow band receiver *J. Radio Res. Labs.* (Japan), Vol. 18, 183-190.

REPORT 1150

STANDARDIZED PROCEDURE FOR COMPARING PREDICTED AND OBSERVED HF SKY WAVE SIGNAL INTENSITIES AND RESULTS OF SUCH COMPARISONS

(Question 42/6)

(1990)

1. Introduction

This Report describes a preliminary standardized procedure for comparing predicted and observed sky-wave signal intensities at frequencies between 2 and 30 MHz. Such comparisons provide information on the accuracy of prediction methods and on desirable improvements to them. It is important that administrations and organizations keep the CCIR informed on the current status of their comparisons. Some sample results of comparisons are contained in this Report.

2. General

In order to obtain comparable results, the same data set and the same procedure should be applied when making comparisons between predicted and observed field strengths. The most recent data base should be used. This is a CCIR-agreed data set and provides a wide range of observations with respect to distance, month, sunspot number, frequency and geographical zone (Suessmann, 1989a).

The output from the comparisons should be:

- count
- mean difference (dB) and
- standard deviation (dB).

"Count" indicates the number of samples used in the comparisons. The "mean difference" provides a measure of the deviation between predicted and observed monthly median field strengths. The most important parameter for assessing the accuracy of the monthly median field strength given by a particular prediction method is the standard deviation (see equations 1 and 2) but it should be cautioned that this provides no information about the accuracy on individual days .

In order to find systematic deviations (e.g. as a function of distance or geographical zone) of a particular prediction method, comparisons should be made for a variety of different subsets of data. The purpose of the detailed subsets of comparisons is to give hints for the detection of systematic weaknesses of the method under consideration. The choice of a certain prediction method should not be based on favourable results obtained for a particular subset (e.g. distance range).

3. Subsets for which comparisons should be made

Different comparisons, i.e., the calculation of mean difference and standard deviation (see Annex), should be made for the following parameters:

3.1 Frequencies, f

single frequency
all frequencies of the same circuit
frequency groups

$2 \leqslant f \leqslant 5$ MHz
$5 < f \leqslant 10$ MHz
$10 < f \leqslant 15$ MHz
$15 < f \leqslant 30$ MHz

3.2 Path great-circle distance, D

$0 < d < 1\,000$ km
$1\,000 \leqslant d < 2\,000$ km
$2\,000 \leqslant d < 3\,000$ km
$3\,000 \leqslant d < 4\,000$ km
$4\,000 \leqslant d < 5\,000$ km
$5\,000 \leqslant d < 7\,000$ km
$7\,000 \leqslant d < 9\,000$ km
$9\,000 \leqslant d < 12\,000$ km
$12\,000 \leqslant d < 15\,000$ km
$15\,000 \leqslant d < 18\,000$ km
$18\,000 \leqslant d < 22\,000$ km
$22\,000 \leqslant d \leqslant 40\,000$ km

3.3 Geomagnetic latitude, Φ (north or south, at path midpoint)

$0^\circ \leqslant \Phi \leqslant 20^\circ$
$20^\circ < \Phi \leqslant 40^\circ$
$40^\circ < \Phi \leqslant 60^\circ$
$\Phi > 60^\circ$

3.4 Sunspot numbers, R_{12}

$0 < R_{12} < 15$
$15 \leqslant R_{12} < 45$
$45 \leqslant R_{12} < 75$
$75 \leqslant R_{12} < 105$
$105 \leqslant R_{12} < 150$
$R_{12} \geqslant 150$

3.5 Season (at path midpoint)

Month	Season	
	Northern Hemisphere	Southern Hemisphere
November, December, January, February	Winter	Summer
March, April	Spring	Autumn
May, June, July, August	Summer	Winter
September, October	Autumn	Spring

3.6 Local time h (at path midpoint)

$00 < h \leqslant 04$
$04 < h \leqslant 08$
$08 < h \leqslant 12$
$12 < h \leqslant 16$
$16 < h \leqslant 20$
$20 < h \leqslant 24$

3.7 Origin of data

This information can be helpful in finding a possible geographical dependence.

3.8 Ratio of transmitted frequency to predicted monthly median basic MUF

This ratio should also be calculated for all subsets as indicated in sections 3.1 to 3.7.

only below path monthly median basic MUF
only above path monthly median basic MUF
below and above path monthly median basic MUF.

4. Comparison procedure

4.1 Prediction program requirements for parameters to be predicted

If the prediction program allows a minimum elevation angle to be specified as an input parameter, it should be set to 3 degrees to be consistent with the data bank.

The following parameters should be transferred from the prediction program to the comparison program:

- general information: month, year, sunspot number
- circuit information: circuit identifier, frequency, great-circle distance, geographical coordinates, geomagnetic latitude at path midpoint,
- 24 predicted hourly values (always monthly median values) of:

  (i) sky-wave field strength in $dB\mu V/m$ (all values below -99 dB are set to -99 dB in order to store 24 values in an 80 column line with 3 digits each)

(ii) path basic MUF (in tenths of a MHz in order to store 24 values in an 80 column line with 3 digits each)

(iii) the percentage of days per month when the frequency is below the path basic MUF (in order to store 24 values in an 80 column line with 3 digits each) if the predictions do not give monthly median field strength for all days of the month.

4.2 Comparison program

Differences are calculated as the predicted monthly median sky-wave field strengths minus values derived from measurements (i.e. predicted minus measured). Note that cases where there is a prediction but no valid measurement and cases where there is a measurement but no prediction are disregarded.

The following parameters must be evaluated:

- Count (number of cases where measured and predicted values are available for comparison)
- Mean difference $= \dfrac{\Sigma\,(p - m)}{n}$ (1)

p = predicted
m = measured
n = count

- Standard Deviation $= \sqrt{\dfrac{\Sigma\,(p - m)^2 - \dfrac{(\Sigma\,(p - m))^2}{n}}{n - 1}}$ (2)

Table I provides an example of summary comparisons between Data Bank D1 and the prediction method of Report 894.

4.3 Graphic representation

In the histograms in Tables II and III, columns of 5 dB are generated (e.g. -2.5 to 2.5 dB, 2.6 to 7.5 dB, 7.6 to 12.5 dB ...) in the range -32.5 dB to +32.5 dB together with two additional columns for >32.5 dB and <-32.5 dB. Each subset listed in § 3 should be accompanied by a histogram.

4.4 Measures to be taken if a prediction does not give the median field strength for all days of the month

In some cases where predictions give the median field strength only for a certain "fraction of days" per month (expressed as a percentage (see section 4.1 (iii)), the measured and predicted values cannot be compared directly. Only if the fraction of days is 99%, measured and predicted values are directly comparable. In all other cases a conversion procedure must be applied to the measured values. If the fraction of days is, for example, 50%, proper ionospheric reflection occurs on 15 days of the month and the predicted median field strength is valid for those 15 days only. The prediction does not give any information on the field strength on the other 15 days of the month. A measured monthly median, however, is derived from 30 daily values (including the 15 days without proper reflection). Consequently, the measured monthly median is likely to be lower than the predicted median.

If a data bank contains all daily values the measured value corresponding to the predicted fraction of days can be derived by determining the median value for the predicted fraction of days. (Note that Data Bank D1 does not contain daily values). The following procedure describes how the measured (30-day) monthly median field strength can be converted to the same fraction of days per month as that given for the predicted field strength:

Step 1: Calculate the f/(path basic MUF) ratio

Step 2: If the data bank does not contain deciles (Data Bank D1 does not) take the measured value as the 50% value and calculate 10% and 90% values by means of Table III of Report 266 "90% and 10% deviations from the predicted monthly median value of signal field strength (dB), arising from day-to-day variability". This table requires information about the ratio f/(path basic MUF) and whether or not the great-circle path crosses the 60 degree corrected geomagnetic latitude (north or south). The actual ratio should be interpolated linearly between the values contained in the table.

Step 3: Calculate the Gaussian distribution from the 10%, 50%, and 90% values of measured field strength from Step 2. Read a "corrected measured" value from this Gaussian distribution applying half of the value of "fraction of days" per month given by the prediction.

Step 4: Compare the field strength of the prediction with the corrected measured value derived in Step 3.

5. Comparison results

For the following prediction methods (see also Resolution 63) comparisons with Data Bank D1 have been made by IWP 6/1:

Method	count	mean difference (dB)	standard deviation (dB)
REP894	16268	0.0	14.3
SUP252	14775	2.4	17.3
FTZ (Damboldt, 1976)	16268	-1.2	9.9
MINIFTZ4 (Damboldt and Suessmann, 1989)	16268	-1.0	10.1
REP252	13678	-1.1	14.1

Further details are given in Suessmann (1989b)

REFERENCES

DAMBOLDT T (1976) A comparison between the Deutsche Bundespost ionospheric HF radio propagation predictions and measured field strengths, AGARD Conf Proc. No 173, Radio Systems and the Ionosphere, 12-1 to 12-7. Ed W T Blackband, NASA Accession No N77-20302, National Technical Information Service, Springfield, VA 22161.

DAMBOLDT T and SUESSMANN P (1989) The FTZ HF propagation model for use on small computers and its accuracy, AGARD Conf. Proc. Operational decision aids for exploiting or mitigating electromagnetic propagation effects, San Diego, May.

SUESSMANN P (1989a) Data Bank D1, IWP 6/1 Doc 331.

SUESSMANN P (1989b) Results of applying the standardised procedure for comparing HF predictions and measurements, IWP 6/1 Doc 324 (Rev 1) + Corr 1 + Adds. 1 and 2.

ANNEX I
ALTERNATIVE APPROACH

In the standardised procedure for comparison described in this report the mean and the standard deviation of the differences between the monthly medians of predicted and observed field-strength values are used as a figure of merit for the different data subsets (§ 4.2). It is recognised that these figures of merit do not take into account the day-to-day variability of the signal and thus do not reflect the complete statistics of the compared magnitudes.

A different method of comparison based on monthly means and variances of both predicted and measured daily data has been proposed (Hortenbach, 1989) which provides statistics often of more direct application. It has been shown that using this method the mean differences of the different data subsets are similar to those obtained by the method described in this Report. The standard deviations, however, exceed the results of the present method by typically 3 dB but may become considerably larger depending on the data subset.

As the new method requires not only the means but also the variances of the daily measured data it cannot be used with the present CCIR Data Banks which only contain monthly medians. Its adoption will be postponed until Data Banks containing either daily values or a measure of the day-to-day variability become available.

REFERENCE

HORTENBACH, J. (1989) On the comparison of random data, IWP 6/1 Doc 334.

ANNEX II

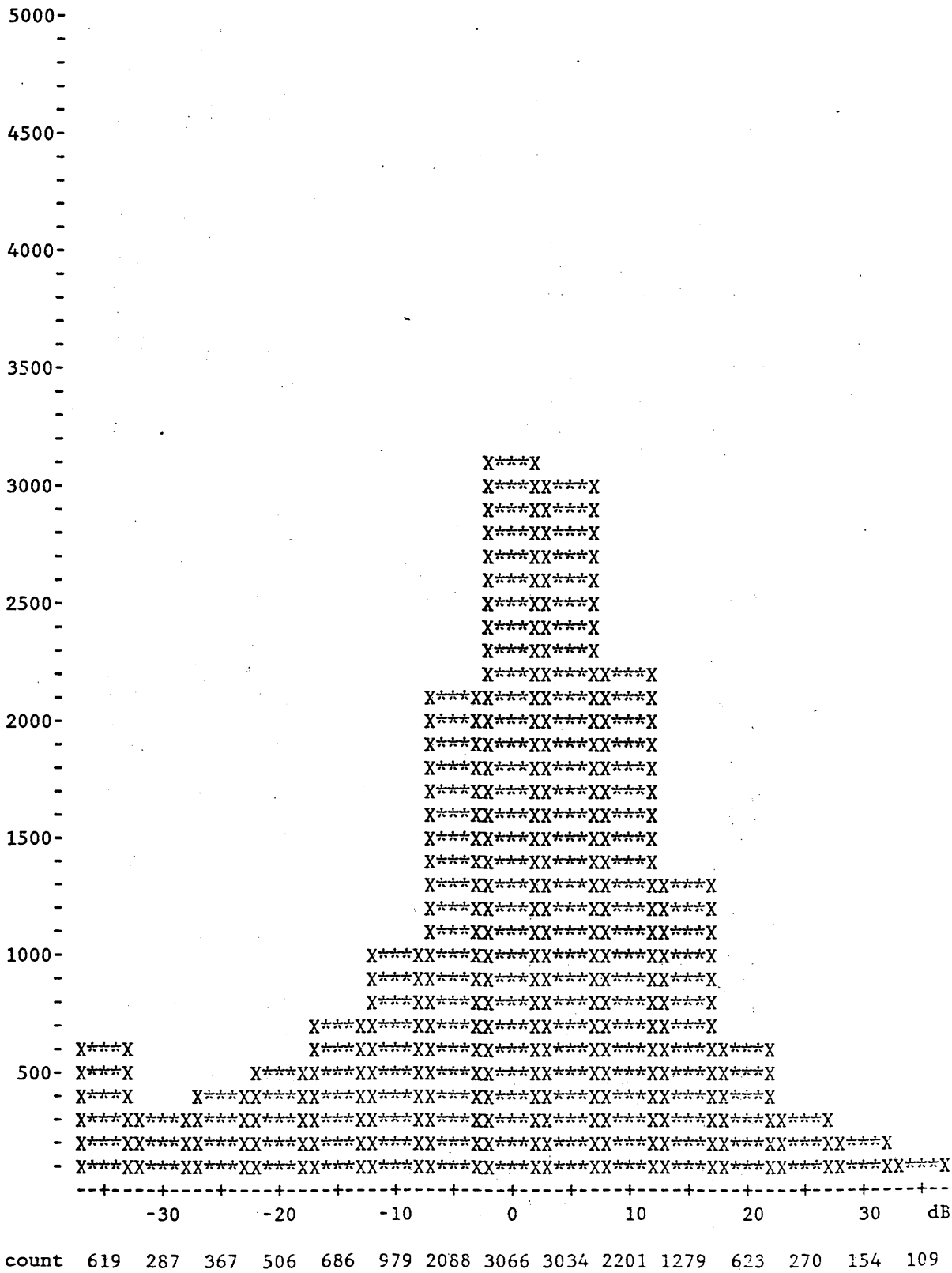
TABLE I - REP894-2 predicted field strength versus data bank D1

subset	below and above MUF	count	mean. diff. dB	standard-deviation dB
frequency groups	2 - 5 MHz	4030	3.3	10.0
frequency groups	>5 - 10 MHz	4004	1.5	13.6
frequency groups	>10 - 15 MHz	5270	-3.2	14.7
frequency groups	>15 - 30 MHz	2964	-0.8	17.8
distance	0 - 999 km	6439	-2.8	16.9
distance	1000 - 1999 km	1144	1.5	12.7
distance	2000 - 2999 km	151	6.7	6.4
distance	3000 - 3999 km	975	6.3	9.4
distance	4000 - 4999 km	126	4.1	8.7
distance	5000 - 6999 km	2785	3.2	13.9
distance	7000 - 8999 km	59	-0.4	8.4
distance	9000 -11999 km	2223	-1.1	10.9
distance	12000 -14999 km	607	0.9	9.5
distance	15000 -17999 km	1093	3.2	9.1
distance	18000 -21999 km	0	0.0	0.0
distance	22000 -40000 km	666	-2.1	12.1
geom. lat.	0-20 deg. path midp.	2806	1.8	10.7
geom. lat.	>20-40 deg. path midp.	4158	3.4	7.5
geom. lat.	>40-60 deg. path midp.	7188	-3.9	16.9
geom. lat.	>60 deg. path midp.	2116	4.2	15.5
sunspot number	0 - 14	1333	-2.0	15.8
sunspot number	15 - 44	5229	2.4	13.4
sunspot number	45 - 74	2969	0.2	13.3
sunspot number	75 - 104	2121	-4.3	16.2
sunspot number	105 - 149	2789	-0.1	13.0
sunspot number	>149	1827	-0.4	15.0
winter		3915	0.8	15.4
spring		4016	-0.1	14.3
summer		4169	-1.2	13.9
autumn		4168	0.5	13.6
local time	>00-04 LT at path midp.	3370	-0.6	13.7
local time	>04-08 LT at path midp.	2246	-1.2	15.0
local time	>08-12 LT at path midp.	2505	-0.3	14.1
local time	>12-16 LT at path midp.	2493	1.4	14.2
local time	>16-20 LT at path midp.	2365	0.6	14.9
local time	>20-24 LT at path midp.	3289	0.3	14.1
origin of data:	Germany	10499	-1.4	16.2
origin of data:	Japan	4119	2.3	8.2
origin of data:	China	428	6.6	9.3
origin of data:	India	182	2.2	10.2
origin of data:	Deutsche Welle	783	2.4	14.3
origin of data:	BBC/EBU	161	2.2	13.1
origin of data:	Australia	96	1.1	6.2
all data		16268	0.0	14.3

TABLE II - Histogram of REP894-2 predicted field strength versus Data Sample D1

all data below and above MUF

count: 16268 mean difference: 0.0 dB standard deviation: 14.3 dB

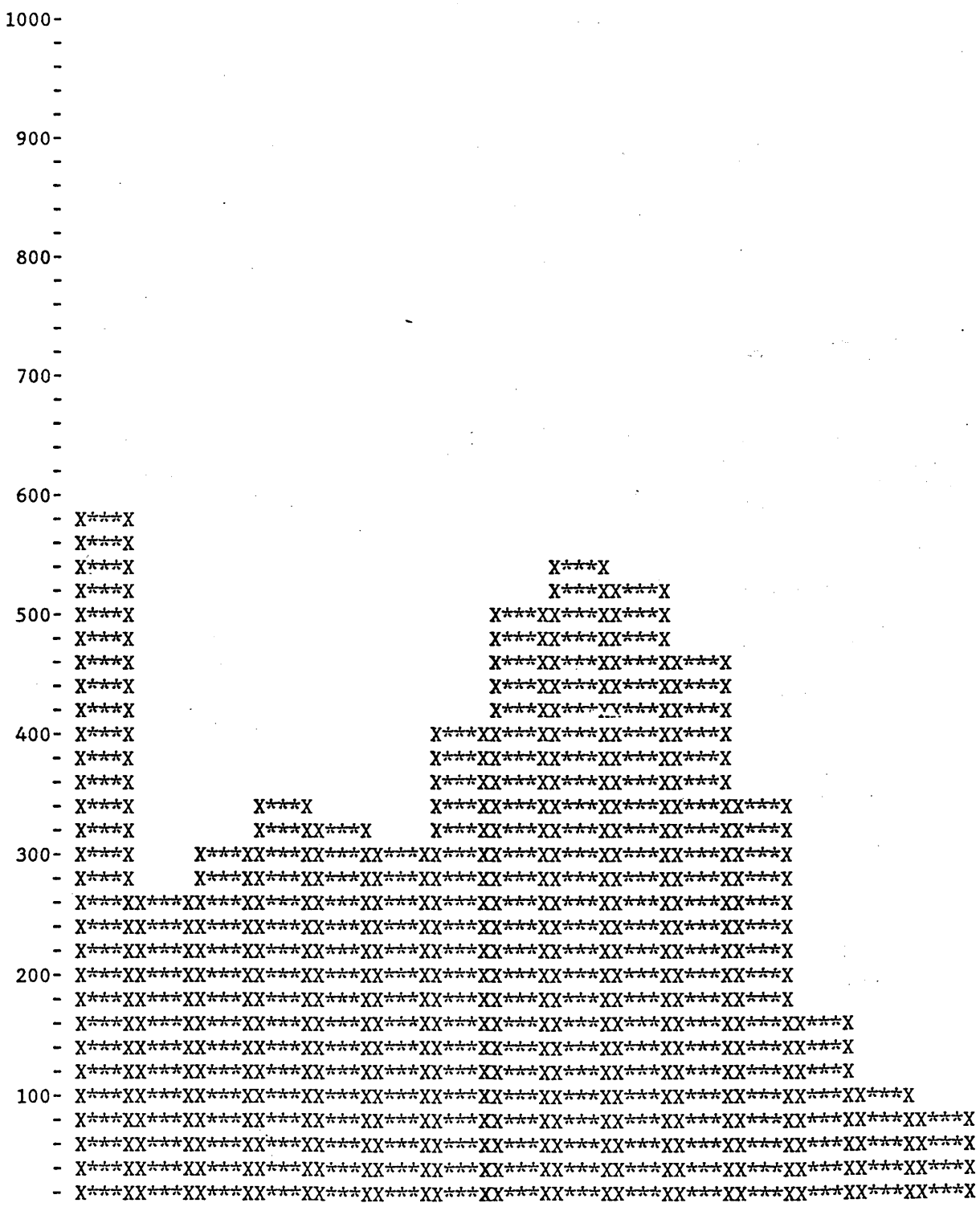


count	619	287	367	506	686	979	2088	3066	3034	2201	1279	623	270	154	109

TABLE III - Histogram of REP894-2 predicted field strength versus data sample D1

all data frequencies above MUF

count: 5199 mean difference: -4.7 dB standard deviation: 20.3 dB



count	582	263	303	340	321	299	407	492	541	513	466	335	150	106	81

REPORT 571-4

COMPARISONS BETWEEN OBSERVED AND PREDICTED SKY-WAVE SIGNAL INTENSITIES AT FREQUENCIES BETWEEN 2 AND 30 MHz

(Question 42/6)

(1974-1978-1982-1986-1990)

1. Introduction

This Report gives a brief summary of comparisons between observed and predicted sky-wave signal intensities at frequencies between 2 and 30 MHz. Such comparisons provide information on the reliability of various prediction methods and on desirable improvements to introduce to CCIR procedures. It is important that administrations and organizations keep the CCIR informed on the current status of their comparisons.

2. Signal intensity at vertical incidence

In the U.S.S.R. [CCIR, 1970-74a] a comparison has been made of calculated and observed values of vertical incidence signal intensity attenuation using four different prediction methods. The comparisons showed large differences among prediction methods, up to 25 dB at 2.4 and 4.0 MHz and up to 20 dB at 4.5 MHz at a distance of 50 km [CCIR, 1978-82a] between calculated and observed values of signal intensity attenuation.

3. Signal intensity at oblique incidence

3.1 *Temperate latitudes*

3.1.1 Comparison of field strength values calculated using the method set out in § 7 of Report 729 [Chernov, 1983] with values measured on 4,000 - 14,000 km paths at night-time has shown a close correlation and has revealed a regular signal level fluctuation along the transmission path within the first and second hops [CCIR, 1986-1990a].

3.1.2 A field strength prediction method [Damboldt, 1976] was developed by the Telecommunications Engineering Centre (FTZ) in Germany (Federal Republic of) that predicts the field strength for a circuit including the case for frequencies exceeding the basic MUF. Comparisons with CCIR Data Bank D1 are available [Suessmann, 1989].

3.1.3 Comparison between experimental field strength values obtained during the equinox in 1975-1976, with f = 15 MHz, over the paths Fort Collins-Hiraiso, WWV (about 9,200 km) and Hawaii-Hiraiso, WWVH (about 6,000 km) and the calculated values obtained using the adiabatic invariant method has shown that the two sets of values are in good agreement when the path is fully illuminated [CCIR 1986-1990b]. This corresponds to the CCIR method (Report 894), (Manaenkova and Tsedilina, 1989). For night-time and twilight conditions, the calculated values are higher than the experimental values, on average by ~30 dB. In particular this is due to the fact that the theoretical calculation method does not take ionospheric scattering into account [Tsedilina, 1989].

3.2 *Low latitudes*

Field-strength measurements made in Delhi on the lowest frequency bands allocated to HF broadcasting, from some regional HF transmitters of All India Radio, have indicated that the correlation between the measured and the calculated values of the field-strength is better with AIR method [Rao, 1969] than with the CCIR first Interim method as given in Report 252, when the propagation is via F layer. The field strength calculated by AIR method tends to deviate more and more as the frequency of the transmission is lowered and the mode of propagation changes from F to E layer. The difference between the measured and the calculated values by the CCIR method when propagation is via E layer is also significant [CCIR, 1974-78a].

4. Comparisons using the methods of estimation of Report 252 and its Supplement

4.1 *General comparisons*

4.1.1 A comparison between field strength values calculated by the CCIR interim method and experimental data has been carried out in the U.S.S.R. The circuits involved cover distances between 2000 and 14 000 km and operating frequencies between 2.5 and 15 MHz. The results exhibit considerable discrepancies (10 dB on average).

4.1.2 The measured values of field strength at Delhi from some of AIR's regional HF transmitters have been compared with those calculated from the formula given in the second CCIR computer-based Interim Method as described in the Supplement to Report 252. The comparison indicates good correlation both when propagation is via F layer and via E layer. This second CCIR Interim method, therefore, appears to be quite promising and may also be suitable for application to circuits in the Tropical Zone. However, the compared data being meagre, it is not possible to form a final opinion [CCIR, 1974-78b].

4.1.3 A comparison has been made in the USSR, between predicted HF energy losses on high-latitude radio links due to auroral absorption and values deduced from measurements [CCIR, 1982-86a]. Calculations have been carried out by two methods: by the Foppiano method included in the CCIR method (see Supplement to Report 252), and by the method developed in the USSR [Zhulina *et al.*, 1983; CCIR, 1982-86b]. Results show that the first method gives errors in the estimated absorption expressed in decibels in excess of 40% in approximately 45% of the cases compared with approximately 10% of the cases for the second method.

4.2 *Comparisons using the CCIR Data Bank*

4.2.1 Interim Working Party 6/1 has carried out an analysis between r.m.s. sky-wave field strengths and mean available receiver powers determined from measurements and values estimated by the method of Report 252. A representative sample of the measured data deposited in the CCIR Data Bank for 16 paths (Table I) with ranges of 450-16 200 km has been studied. The calibration procedures used in deriving these data have been examined and measurements have been normalized to give the corresponding monthly median field strengths and powers for 1 kW radiation from an isotropic transmitting antenna.

Separate comparisons of measured field strengths with predictions by the method of Report 252, based on the use of the computer program HFMLOSS, have been undertaken in Argentina [Pérès, 1978], the Federal Republic of Germany and the United Kingdom. Results of these comparisons are in complete agreement. Attention has been restricted in the analyses to cases when the signals are measured and also the predictions indicate that these are present for more than half the days of the month. There is some evidence that the differences between predictions and measurements vary with time-of-day, season and path range with a greater tendency for the predicted intensities to exceed those which are measured by night and in the winter; also for discrepancies to be greater on the longer paths. However, the effects are not large by comparison with the scatter in the results.

Other corresponding comparisons in terms of receiver power have been made in the United Kingdom [Dick and Hurst, 1980] with the aid of the computer program RIM1A (an extended version of HFMLOSS including antenna gains) produced by the specialized staff of the IFRB. This program includes the calculation of receiving-antenna gain to avoid the need for adoption of values based on assumed average wave-arrival directions. Data for circuits 1 to 15 of Table I have been used. Tests provide only limited evidence supporting minor, systematic variations of prediction discrepancies with frequency, time-of-day and season. There are no clear changes with path length.

The best summary of the results is a combined histogram of differences for all hours, frequencies, months and circuits grouped together (see Fig. 1). For the field-strength comparisons the median discrepancy corresponds to a predicted field strength 3 dB greater than measured. 70% of the discrepancies are less than 10 dB and 90% are less than 20 dB. For the power comparisons the median discrepancy corresponds to a predicted power 1.5 dB greater than measured, 60% of the discrepancies are less than 10 dB and 85% less than 20 dB.

As examples of comparisons between predictions and measurements for paths in different geographical regions with data for all hours and months combined, Fig. 2 presents histograms of the (predicted minus measured) receiver power for sample circuits traversing the Tropical Zone and at middle and high latitudes. The sample count is indicated, together with the mean and r.m.s. differences.

TABLE I — *Representative sample of the measured data deposited in the CCIR Data Bank*

No.	Circuit	Range (km)	Frequencies (MHz)	Year
1	Tokyo—Akita	448	5.0, 2.5	1971
2	Bracknell—Luchow	846	18.3, 9.2, 4.8, 2.6	1975
3	Shannon—Luchow	1 346	5.5	1973
4	Moscow—Luchow	1 707	15.9, 7.7, 5.4, 3.9	1976
5	Halifax—Luchow	5 301	22.4, 12.8, 8.5, 6.4	1974
6	Kauai—Hiraiso	5 908	15.0	1974
7	New York—Luchow	6 174	20.9, 16.2, 13.6	1973
8	Maui—Hiraiso	6 271	15.0	1969
9	Brazzaville—Luchow	6 383	22.0	1972
10	Nairobi—Luchow	6 494	17.4, 9.0	1972
11	Tokyo—Luchow	8 994	22.8, 13.6, 10.0, 3.6	1971
12	Fort Collins—Hiraiso	9 146	15.0	1974
13	Mauritius—Luchow	9 287	22.6, 13.0, 8.6	1975
14	Washington—Hiraiso	10 797	15.0	1966
15	Honolulu—Luchow	11 677	13.9	1974
16	Canberra—Luchow	16 200	19.7, 13.9, 11.0, 5.1	1975

4.2.2 A comparison between the field intensities predicted by the CCIR interim method and those measured at three frequencies (5, 10 and 15 MHz) in four seasons for different epochs of solar activity, can be seen from a Table in [CCIR, 1970-74b]. The predicted and observed values are generally in good agreement. However, it is suggested from the comparison that the following points have to be taken into account in the revision of Report 252:

- at 5 MHz as an example of relatively short distance propagation, predicted values are higher (less than 5 dB) than those measured;
- at 10 MHz, also in short distance propagation (about 1000 km), the predicted values are lower than those measured for minimum solar activity, and for maximum solar activity the exponent of cos χ in the absorption equation is too low;
- at 15 MHz on the WWVH-Hiraiso path (about 6300 km), good agreement is seen, except in spring when the predicted values are lower (less than 5 dB) than those measured;
- at 15 MHz on the WWV-Hiraiso path (about 10 000 km), good agreement is also seen. However, measured intensities suggest that improvements are required in the calculation of MUF, since high field intensities are observed even when the operating frequency exceeds the basic MUF of the circuit. It is to be noted that a part of this discrepancy can be removed when the contribution of the long path signal to the received field intensities is taken into account.

4.2.3 Comparisons have been carried out in the United Kingdom [Dick,1987] between field strengths calculated by the method of the Supplement and the values of Data Bank D.14704 data pairs where predicted and measured values exist yielded the results given in Table II.

TABLE II - Difference statistics for the method of the Supplement to Report 252

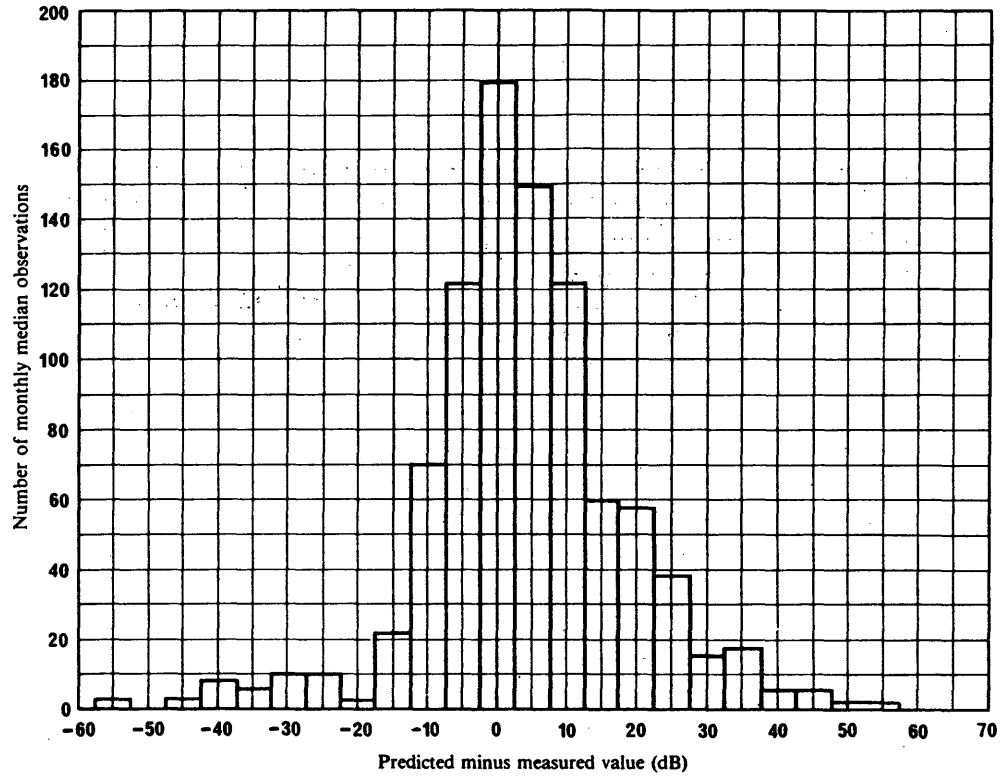
	n	$\bar{x}$	σ
All data	14704	9.9	19.1
Frequencies below MUF	10331	10.3	12.7
Frequencies exceeding MUF	4373	9.0	29.2

n - sample size
$\bar{x}$ - mean difference (predicted minus measured field strength (dB))
σ - standard deviation (dB).

5. Comparisons using methods of estimation developed from Report 252 and its Supplement

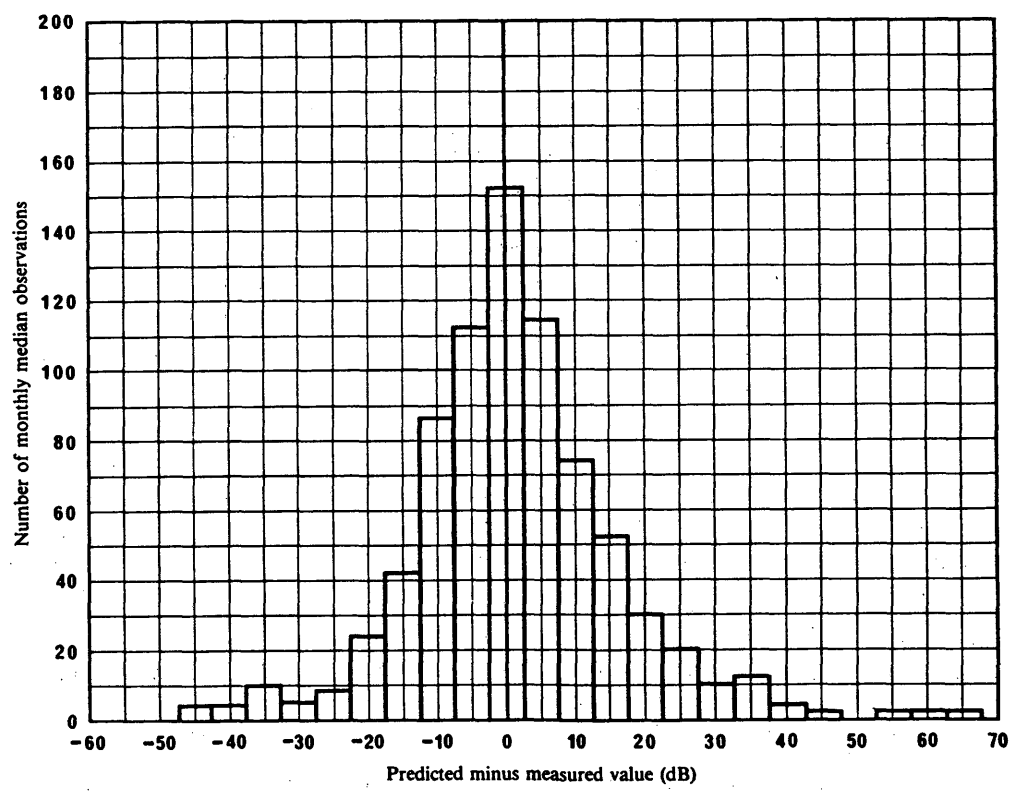
5.1 *General comparisons*

Field-strength measurements made in India of a number of Indian and foreign transmitters in the frequency range of 3 to 12 MHz and at distances from 300 to 3000 km [CCIR, 1978-82b] have been compared by All India Radio using a method [CCIR, 1978-82c] which is a simplified manual adaptation of the CCIR method of the Supplement to Report 252 for single-hop circuits. This method takes into account transmitting antenna gain, spatial attenuation, focusing gain, deviative and non-deviative absorption and a constant polarization-coupling loss of 3 dB. Sporadic-E losses and above-the-MUF losses are not considered. In most of the cases the measured values have been found to be within ± 3 dB of the calculated ones. It has been concluded that the prediction method is adequate for use in the Tropical Zone.



(*a*) Field-strength comparison (results of studies in Argentina)

A = 922 B = 3 C = 15



(*b*) Receiver-power comparison (results of studies in the United Kingdom)

A = 922 B = 1.5 C = 14

FIGURE 1 – *Differences between values given by prediction method of Report 252 and measured data contained in the CCIR Data Bank*

A: sample count; B: mean difference (dB); C: rms difference (dB)

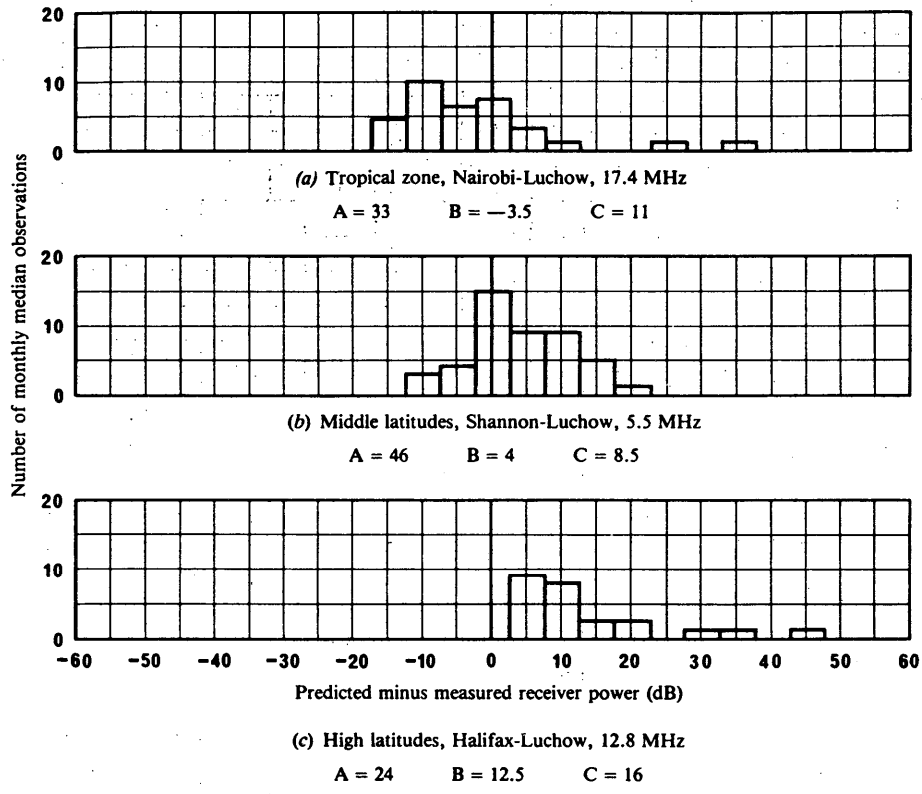


FIGURE 2 – *Comparisons between measured receiver power and values predicted by the method of Report 252 for sample data for circuits traversing the Tropical Zone and at middle and high latitudes*

A: sample count
B: mean difference (dB)
C: r.m.s. difference (dB)

5.2 *Comparisons using the CCIR Data Bank*

5.2.1 Other comparisons have been made in Argentina [Pérès and Finkelberg, 1981] between measured field-strength data for circuits 1 to 15 of Table I and values estimated by a modified version of the method given in Report 252. This version differs only in that it employs the absorption evaluation procedure contained in the Supplement to Report 252. There is a general tendancy for the predicted values to be larger than the measured values; the median discrepancy for all circuits, frequencies and times is 6 dB. By comparison, values calculated using the method of Report 252 without modification are generally in better agreement with the measured values, as shown in Fig. 1(a). On the other hand, the scatter of discrepancies is less using the modified procedure.

5.2.2 Comparisons of a similar nature have been made in Australia between field-strength data for some circuits of Table I (circuits 2, 3, 4, 5, 9 and 13) and those calculated by a procedure which involves the following basic features of the Supplement to Report 252 [Caruana, 1980]: the MUF formulae, the absorption factor, ground reflection and polarization loss; the procedure does not take into account auroral absorption, sporadic-E, or above-the MUF loss and makes use of Australian ionospheric data. In general, the calculated field strengths were found to be 10 to 20 dB greater than those measured.

6. Comparisons using an estimation method based on Report 894-1 (Dubrovnik, 1986)

6.1 General comparisons

Comparisons have been made in China between the measured field strength (for 11 paths with distances from 939 to 9,830 km, 1981-1984) and the values predicted by the propagation prediction method which was approved by WARC-HFBC-87 and which is based on Report 894-1 (Dubrovnik, 1986) with some modifications (see Final Acts of WARC-HFBC-87). The results of the comparisons show that for path lengths less than 7,000 km, the rms differences between the predicted and measured values of the monthly median field strengths are relatively small (9.1 dB); for path lengths longer than 7,000 km, the rms differences are considerable (14 dB) and the predicted values are too low (-9 dB in average). The long-term (day-to-day) fading of hourly median field strength values depends on the ratio of the transmission frequency to the MUF. The upper decile values of long-term fading are 2-7 dB, and the lower decile values are 3-12 dB [Pan and Ji, 1988].

6.2 Comparisons using the CCIR Data Bank

The measured data in CCIR Data Bank C and the values predicted by the WARC-HFBC-87 method and by the Report 252 method have also been compared in China. It was found that the rms difference of 15.9 dB between the measured values and the values predicted by the WARC-HFBC-87 method was smaller than the 26.8 dB difference between the measured values and the values predicted by the Report 252 method.

For path lengths less than 7,000 km, the measured field strength data for frequencies above the MUF were selected from CCIR Data Bank C and compared with the values predicted by the WARC-HFBC-87 method. It was found that if the upper limit of the "above the MUF" loss is reduced from the originally used value of 81 dB to 40 dB, the rms differences between the measured and predicted values were also reduced from 25.6 dB to 13.1 dB. The accuracy of prediction is thus evidently improved [Pan and Ji, 1988].

REFERENCES

CARUANA, J. [1980] Comparisons between measured and computed HF field-strengths. CCIR, IWP 6/1, Doc. 15.

CHERNOV, Yu. A. [1983] Energetichesky raschet korotkovolnovykh radiolinii (Calculation of the power balance of HF radio links), NIIR Proceedings No. 4, page 5.

DAMBOLDT, T. [1976] A comparison between the Deutsche Bundespost ionospheric HF radio propagation predictions and measured field strengths. AGARD Conf. Proc. No. 173, Radio Systems and the Ionosphere, 12-1 to 12-7. Ed. W.T. Blackband. NASA Accession No. N77-20302. National Technical Information Service, Springfield, VA 22161, USA.

DICK, M.I. [1987] Accuracy of field-strength prediction method Supplement to Report 252-2. IWP 6/1 Document 309.

DICK, M. I. and HURST, E. [1980] Results of comparisons between measured HF mean available receiver power data and values estimated by the method of Report 252-2, IWP 6/1, Doc. 106.

MANAENKOVA, N.I. and TSEDILINA, E.E. [1989] - Sopostavlenie raschetnykh i eksperimentalnykh znacheny napryazhennosti polya na sredneshirotnykh protyazhennykh trassakh (Comparison of calculated and experimental field strength values on mid-latitude long distance paths), Vzaimodeistvie radiovoln S ionosferoi, Institut zemnogo magnetizma, ionosfery i rasprostraneniya radiovoln Akademii nauk SSSR, Moscow, 112.

PAN ZHENZHONG and JI PING [1988] HF Field Strength Measurement in China and Test of HF Propagation Prediction Methods (digest) Proceedings of the International Symposium on Radio Propagation, Beijing, 1988.

PÉRÈS, M. [1978] Results of comparisons between measured HF field strength data and values estimated by the method of Report 252-2. IWP 6/1, Doc. 76.

PÉRÈS, M. and FINKELBERG, L. [1981] Evaluation of the absorption prediction methods of the CCIR. *Geoacta*, Vol. XI.

RAO, M. K. [1969] Nomographs for calculation of field strength. *J. Inst. Telecomm. Engrs.* (India), 15, 729.

SUESSMANN, P. [1989] - Results of applying the standardized procedure for comparing HF predictions and measurements. IWP 6/1 Document 324(Rev.1).

TSEDILINA, E.E. [1989] - Vliyanie terminatora i solnechnoi aktivnosti na napryazhennost polya korotkikh radiovoln na protyazhennykh trassakh (Influence of terminator and sunspot activity on short-wave field strength over long-distance paths), Geomagnetizm i aeronomiya, 29, No. 6.

ZHULINA, E. M., KISHCHA, P. V., LUKASHKIN, V. M. and SHIROCHKOV, A. V. [1983] Dopolnityelnye energeticheskiye poteri na vysokoshirotnykh radioliniyakh (Additional energy losses on high-latitude radio links), 208. Nauka Publishing House, Moscow, USSR.

CCIR Documents

[1970-74]: **a.** 6/89 (USSR); **b.** 6/65 (Japan).

[1974-78]: **a.** 10/56 (India); **b.** 10/323 (India).

[1978-82]: **a.** 6/223 (USSR); **b.** 6/77 (India); **c.** 6/76 (India).

[1982-86]: **a.** 6/51 (USSR); **b.** 6/48 (USSR).

[1986-1990]: a. 6/34 (USSR); b. 6/198 (USSR).

REPORT 1149

HF FIELD STRENGTH MEASUREMENTS

Specifications for a field strength measurement campaign intended for future improvements in prediction methods, particularly those used for HF broadcasting

(Question 42/6)

(1990)

1. Introduction

The World Administrative Radio Conference for the planning of the HF bands allocated to the broadcasting service (HFBC-87) invited the CCIR to undertake studies of the HF propagation prediction method adopted by the Conference, and to recommend both improvements in the method and later, if necessary, an improved method to be used in the future for the HF bands allocated to the broadcasting service. It also recommended that administrations should conduct HF field strength measurement programmes and should contribute data in a form suitable for study to the CCIR.

The data set currently available to the CCIR has been examined by IWP 6/13 and by IWP 6/1. Although some improvements of predictions may still be possible, it seems unlikely that any major improvements will be achieved until a further substantial body of reliable measurement data becomes available.

The current data bank incorporates all available, calibrated measurement data and examination of this data bank shows that the existing data do not adequately cover some path lengths and geographical regions which are important for a world-wide prediction method. A substantial quantity of new data is required and there is a particular shortage of data for low latitude and southern hemisphere paths. These data are required if any improvements to the prediction method are to be investigated in time for future world administrative radio conferences associated with HF spectrum usage. There would also be a significant benefit if the measurements could be continued in years with other levels of solar activity.

Major difficulties arise in HF field-strength measurements in the positive identification of transmissions and in the characteristics of equipment and antennas available for those measurements. Thus it is proposed that a network of new computer-controlled transmitters and receivers be installed with the characteristics described in this report. These arrangements will minimize the uncertainties, ensuring data of high quality, and should permit a large number of moderately priced receiving installations to be provided around the world.

2. The HF field-strength measurement campaign

The required data cannot be achieved unless new transmitters and receivers are installed. It is proposed that these transmitters should be frequency agile, each radiating on five frequencies sequentially according to a predetermined schedule. In each case there should be a period of steady signal emission for manual measurements and coded sequences permitting aural identification of the source, computer identification of the source and computer evaluation of the intensities of both the signal and the background noise or interference.

To minimize the possibility of interference, the transmissions should be on assigned frequencies probably in the fixed service bands.

A number of receiver implementations are possible, meeting the specification given below, but a single standard for the receiving antenna is proposed. Each receiver should operate on a rapid measuring sequence, dwelling on each frequency for up to 12 seconds, and will be able to measure signal levels on many of the 45 transmitted frequencies during each hour. At least one model of receiver, including the interface, computer and software, is available and it is hoped that some administrations will provide some equipments on loan to those developing countries where there is a great need for new measurement data.

3. Transmitter

3.1 Transmitter locations

In order to collect data representative of HF propagation conditions on a world-wide scale, preferably there should be at least nine transmitters. These should be located in the northern and southern hemispheres at middle latitudes and in the tropics in Regions 1, 2 and 3:

TABLE I

	Region 1	Region 2	Region 3
N. Hemisphere	North/Central Europe	North America	Asia
Tropics	Tropical Africa	Caribbean Area	South East Asia
S. Hemisphere	Southern Africa	South America	Australasia

3.2 Transmitter power

Transmitter power should be in the range of 5 - 10 kW.

3.3 Transmitting antennas

Transmitting antennas should be omnidirectional in azimuth and should have a broad elevation pattern. In order to avoid the necessity for frequent switching of high rf powers, a single broadband monopole or conical structure is preferable. However, such antennas usually have a changing vertical radiation pattern (vrp) for frequencies greater than about 3 times the lowest design frequency, which is

when the antenna height is approximately $\lambda/4$, and the characteristics of particular proposed antennas should be studied carefully before implementation. The criterion for the vrp is that at the higher operating frequencies the pattern should not depart by more than 3 dB from the vrp of a $\lambda/2$ monopole (the mid-band case) over the range of elevation angles up to 65°. A possibility is to select a broadband antenna which is operating at about three times its lowest design frequency at the highest operating frequency and that operation on the lowest operating frequency is permitted by the use of a frequency selective matching network.

The antenna should be installed on flat ground of no more than 2° slope and should be located on an unobstructed site with obstacles of not higher than 4° elevation (see Report 253).

3.4 Frequencies and transmitter schedules

Transmissions from one location should take place in five frequency bands on frequencies, preferably in the fixed service bands, near 5.5, 8, 11, 15 and 20 MHz. The emissions on each frequency should be radiated sequentially commending at 0, 4, 8, 12 ... etc. minutes after each hour. The frequency schedule should be communicated to the Director, CCIR, for dissemination to all participants in the measurement campaign.

Should more than five transmitters operate simultaneously, more than one frequency will be needed in all bands if mutual interference is to be avoided. Six to 10 transmitters require two frequencies in each band, 11 to 14 require three per band, etc.; the number required for n transmitters is $\lfloor (n-1)/5 \rfloor + 1$. Table II shows a schedule for nine transmitters that use two frequencies, 1 and 2, in each band A to E.

TABLE II - Frequency schedule for nine transmitters

Transmitter \ Minutes	0	4	8	12	16	20
1	A1	B1	C1	D1	E1	
2	B1	C1	D1	E1	A2	
3	C1	D1	E1	A2	B2	
4	D1	E1	A2	B2	C2	
5	E1	A2	B2	C2	D2	
6	A2	B2	C2	D2	E2	
7	B2	C2	D2	E2	A1	
8	C2	D2	E2	A1	B1	
9	D2	E2	A1	B1	C1	

3.5 The transmitted signal

3.5.1 The emission should be of class F1B with a frequency shift of 850 Hz. In accordance with Recommendation 246 the "mark" should be on the lower frequency i.e. 425 Hz below the assigned frequency.

Note - If the emission is generated using suppressed carrier single sideband techniques then it may be convenient to use, for example, as a reference frequency, a suppressed carrier frequency 1225 Hz below the assigned frequency, in conjunction with upper sideband modulation frequencies of 800 Hz for the "mark" frequency and 1650 Hz for the "space" frequency.

3.5.2 The transmitted sequence on each frequency should be as described below having a duration of 12 s. The sequence should be repeated for four minutes, curtailing the final repetitions as necessary so as to allow time for the transmitter frequency change.

a) FSK preamble at 100 bit/s for one second, comprising signal reversals commencing on the mark frequency.

b) a pause of 50 ms

c) an identification signal in morse code on the higher frequency (see Recommendation 246) contained within a period not exceeding 3.3 s

- the dot length of the morse code should be specified by the transmitting organization

- if permissible this identification signal could with advantage be based on the international locator code used by radio amateurs, provided that the signal can be contained within the period specified

d) a pause of 50 ms

e) a 256-bit complementary sequence transmitted at 1200 bit/s as follows:

Sequence 1:
1110010000101000000101001101100000011011001010001110101111011000000110
1111010111000101001101100011100100110101111110101111011000000110111101
0111111010110010011100011011001010001110101111011000111001000010100011
1010110010011111110010011010111111010111101100

f) a pause of 50 ms

g) a second 256-bit complementary sequence transmitted at 1200 bit/s, as follows:

Sequence 2:
0001101111101011111101011001001111110010011010111000101000010011100011 0
1111010111000101001101100011100100110101111110101111011000111001000010
1000000101001101100011100100110101110001010000100111111001000010100011
1010110010011111110010011010111111010111101100

h) a pause of 50 ms

i) a series of FSK reversals, comprising 400 bits at 100 bit/s, commencing on the lower frequency

j) a constant signal on the higher frequency for a duration of at least 3 s, which should continue until the total time for the sequence is 12 s.

3.6 Log-keeping

Detailed logs containing information on the status of the transmitter and particularly on the transmitter power should be completed at all sites and should be forwarded periodically to the Director, CCIR.

4. Receiver

4.1 Receiver locations

There should be as many receiving stations for the recording of the 9 proposed transmitters as possible. Due to the null in the elevation pattern of vertical transmitting antennas, measurements should not be made at ranges shorter than about 500 km.

4.2 Antennas and siting

Short vertical active antennas are recommended for use with field-strength measurements according to the specifications given in Annex A. The antennas should be installed on flat ground of no more than 2 degrees slope and should be located on an unobstructed site of at least 25 m radius, with more distant obstacles not higher than 4 degrees elevation, measured at ground level. The antenna should be situated away from electric power lines and other metallic structures. The antenna may be protected against damage by a wooden fence or stockade not higher than 2 m at a distance of at least 3 m. It is preferable that the site should be in an area of good and homogeneous ground conductivity; in any case the conductivity needs to be known for use in the analysis of results.

In the USSR comparisons were carried out among a number of simple receiving antennas [Zhiltsov and Chernov, 1989]. It was found that the antenna providing the smallest difference in measured field strength ΔU when compared with that of a standard loop antenna was that described in Annex A. Figure 1 shows the variation of ΔU over the approximate frequency range 7-17 MHz.

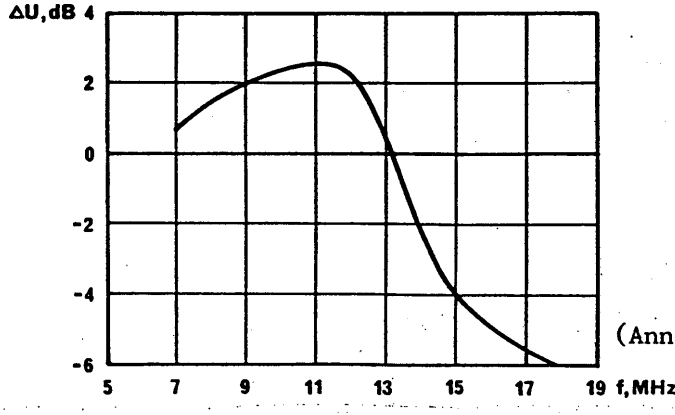


FIGURE 1 - Frequency dependence of the differences in measured field strength between a vertical antenna (Annex A) and a standard loop antenna

4.3 Receiver specifications and calibration

The field-strength measuring receiver should meet the following minimum performance requirements:

1. Synthesiser control (10 Hz step)
2. External bus available for computer control
3. Frequency accuracy $\pm$ 1 part in 10^6
4. Synthesiser noise sidebands: Reciprocal mixing performance better than 70 dB in a bandwidth of 3 kHz at 20 kHz offset
5. Sensitivity SSB 1.0 µV terminated for at least 10 dB (S+N)/N for a bandwidth of 3 kHz
6. Unwanted spurious responses (e.g. image, I.F.) better than 70 dB
7. Selectivity:
   Approx. 3 kHz bandwidth, shape factor -60dB to -6dB 2:1
8. Linearity: 3rd-order intercept, 20 kHz spacing, +10dBm
9. True average measuring capability within 4 seconds
10. Timing accuracy within the receiver system should be maintained within one second.

4.4 Receiver measurement sequence

Within the 12 second code sequence transmitted, only four seconds are required for computer measurement, allowing sufficient tolerance for timing differences.

Section 5 indicates that 12 samples are required to establish a median signal level within a one-hour interval. Thus it is sufficient to measure four samples within four minutes, repeating three times in the hour using the 20-minute cycle of transmission. In this way measurements can be accommodated on five frequencies within four minutes and on 25 frequencies within one hour. The sequence is illustrated in Fig. 2.

Organizations operating only one receiver may select up to 25 transmissions for measurement from the potentially available 45 transmissions in order to meet the above requirement. Alternatively, two receivers can be operated in parallel, to monitor more than 25 transmissions. Advice on the selection of suitable transmissions should be available from the "international group" as recommended in § 6

4.5 Recording units and calibration

Use of a standardized receiving antenna and receiving system permits a common conversion to field strengths to be applied for all sites during data analysis. Measured amplitudes should be expressed in terms of corresponding receiver input voltages by injecting a reference calibration signal ideally once each day. This should be of fixed amplitude giving approximately full-scale receiver output. The strength of the calibration signal should be noted in the station log together with a record of any input attenuation used and the receiver output level should be recorded on floppy disk.

5. Signal and background noise measurement and data processing

This section describes the basic procedures to be applied to yield signal amplitudes for inclusion in a future CCIR Data Bank. The transmitter signal format (§ 3.5.2) is designed to also permit additional measurements to be carried out for other types of propagation studies if desired.

5.1 Sampling

For each selected circuit (transmitter/receiver/frequency combination) the receiver records sufficient amplitude samples within each hour to permit statistically meaningful estimates of the hourly medians of both the signal and noise intensities to be determined in relation to the likely within-an-hour fading. Using either analogue or digital signal processing, average voltage amplitudes over a period of 4 s within each 12 s transmission cycle should first be determined. A minimum of 12 such samples within a given hour on a given day should be taken, these to be distributed approximately uniformly over the period that the transmitter is radiating. This results in a standard error due to sampling of less than 2 dB.

5.2 Input attenuation

To allow for the varying signal amplitude on different circuits and at different times of day, it is suggested that a switched attenuator under computer control may be inserted between antenna and receiver, values of attenuation to be recorded on floppy disk along with the signal and noise data.

5.3 Data recording

Data should be dumped to floppy disk in an agreed format (Annex B). Hourly medians are to be calculated centrally. Rules for dealing with samples in which the signal is not discernible from noise and interference are given in Annex C.

5.4 Determination of monthly medians and deciles

Monthly medians and upper and lower decile values of signal amplitude should be calculated by combining together the hourly median signal-amplitude data at a given hour for the different days. Rules for dealing with daily samples in which the signal is below the noise are given in Report 253.

5.5 Data normalisation

Data provided from the separate receiving sites should be accompanied by corresponding receiver and antenna system calibration factors for each circuit. Using this information together with that from the transmitter logs, centralised data normalisation will be applied to the different daily/hourly values for incorporation in the Data Bank.

6. Data handling, quality assurance and training

The scheme envisages a large number of receiving locations (some operating in areas where there is a severe shortage of skilled engineers), with a large quantity of data, probably in floppy-disk format, being sent to a central agency for compilation and processing. Such a scheme will work only if adequate attention is given to organisation and training.

It is recommended that an international group should be set up to oversee the measurement programme and to provide guidance and assistance to participants. It is further recommended that ITU support should be provided to receive and process the data in consultation with the group.

The necessary tasks are to:

(i) collect and validate measured data provided from the different receiving sites,

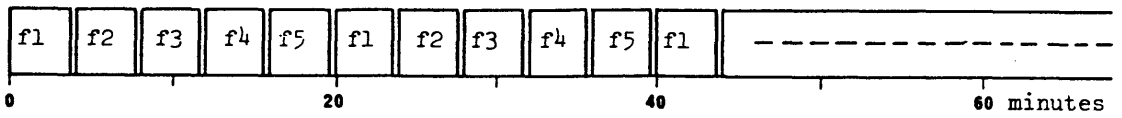
(ii) create and maintain summary files of daily hourly median field strengths,

(iii) normalise these results in accordance with the known transmitting and receiving system performance, generate a definitive Data Bank, and

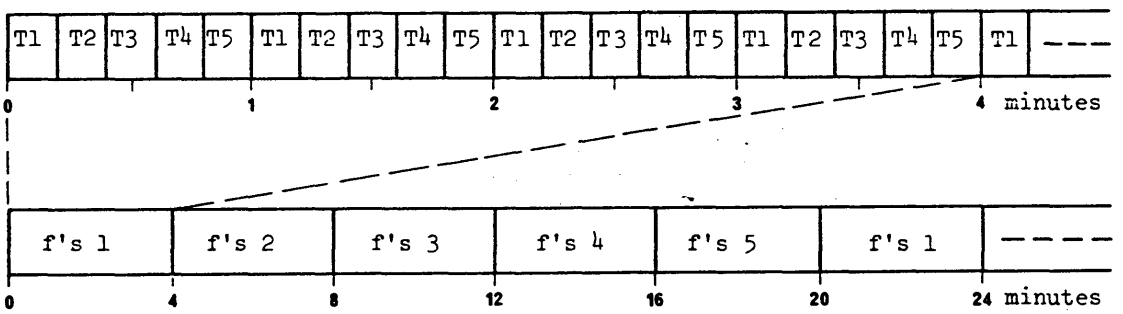
(iv) arrange training workshops in various parts of the world so as to ensure the satisfactory operation of receiving systems.

It is suggested that all Administrations and Organisations contributing to the data should have access to all data for additional studies, and arrangements for this should be made as required.

TRANSMITTER SCHEDULE



RECEIVER SCHEDULE



SIGNAL FORMAT

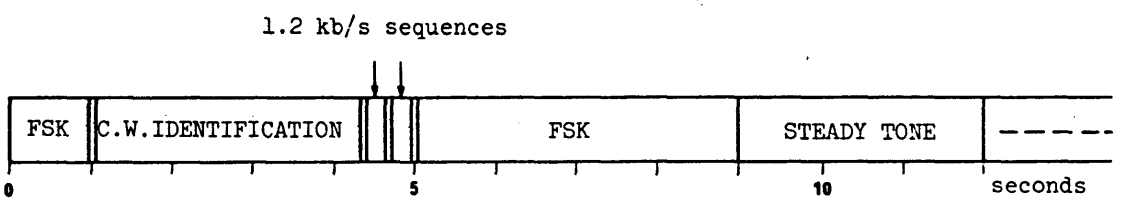


FIGURE 2 - Schedules and formats

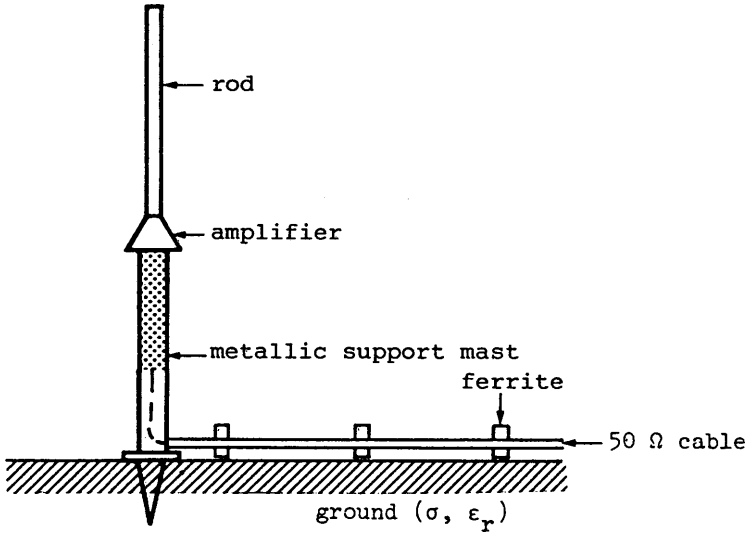
REFERENCES

ZHILTSOV, A.U. and CHERNOV, Yu.A. [1989] - Sravnitelnaya effektivnost prostykh priemnykh korotkovolnovykh antenn (Comparative performance of simple HF receiving antennas). Proceedings of NIIR, No. 3.

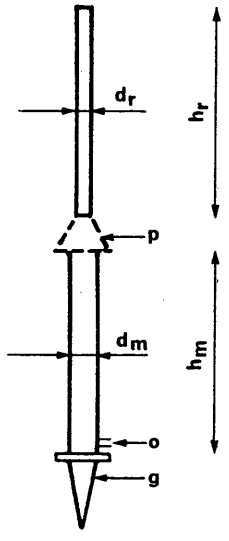
ANNEX A

SPECIFICATIONS FOR A VERTICAL ANTENNA AS A FIELD PROBE FOR FIELD STRENGTH MEASUREMENTS

1. General outline



2. Geometrical Structure



h_r: 1m (rod)

d_r: 5 to 10mm

d_m: about 5cm (tube)

h_m: 1m (tube)

p: plastic housing for shielded amplifier

o: outlet for 50Ω cable

g: ground stake

Figure 1: Geometrical structure of active antenna

3. Amplifier of active antenna

3.1 Basic schematic

For example an FET source follower and bipolar emitter follower could be used. The DC power could be fed through the inner conductor of the coaxial cable.

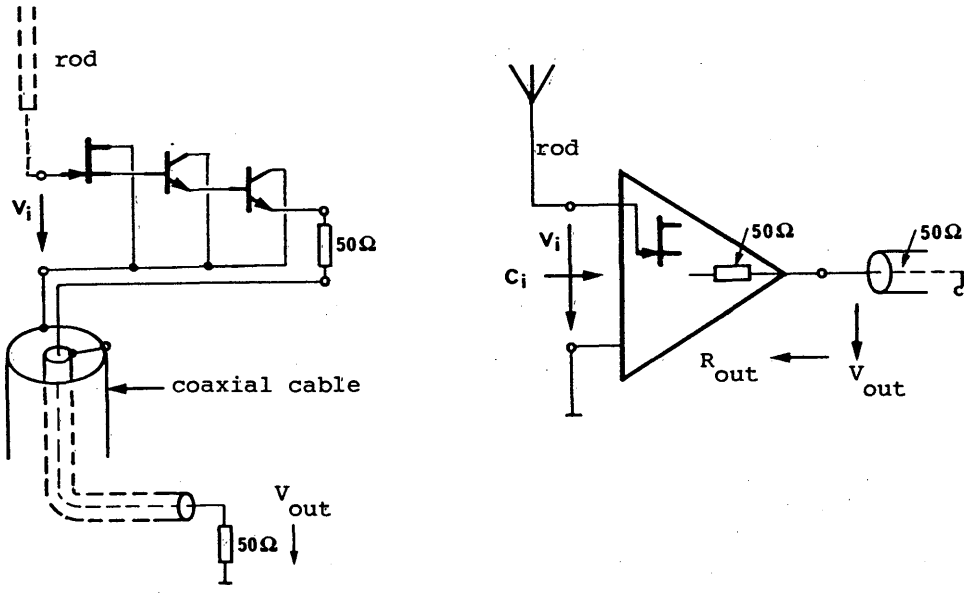


FIGURE 2 - Basic schematic of active antenna

3.2 Electric characteristics of active antenna

- Amplification: $V_{out}/V_i \approx 1/2 \mathrel{\hat{=}} -6dB$
- Input impedance: $C_i = 15$ pF
- Output resistance: $R_{out} = 50\ \Omega$, VSWR $\leq$ 2
- Noise figure measured at output:

  $F_{out} \leq 15 \mathrel{\hat{=}} 11.8dB$

  (Available noise power measured at the output of the shielded antenna or at the output of the amplifier when loaded with C_A = 10pF at the input.)
- Linearity range (Signal level for 1dB compression)

  $V_{comp,out} \geq 1.2$ Volts (at a load of 50 Ω) measured with dummy antenna
- Intermodulation characteristics:

  Intercept point 2nd order, measured at the output:

  IPOP2 $\geq$ 50 Volts (or 47dBm)

  (with dummy antenna)

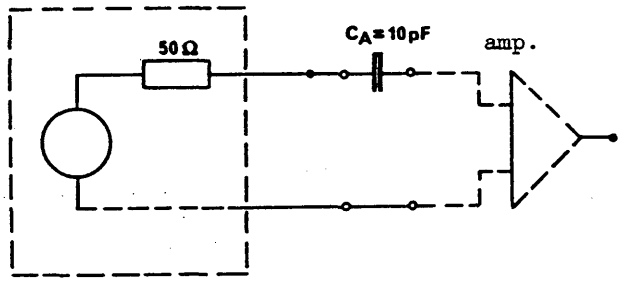
Intercept point 3rd order, measured at the output:

IPOP3 $\geq$ 5 Volts (or 27 dBm)

(with dummy antenna)

The intercept points to be measured by the method of two signal generators.

- Dummy antenna for measurements on the amplifier

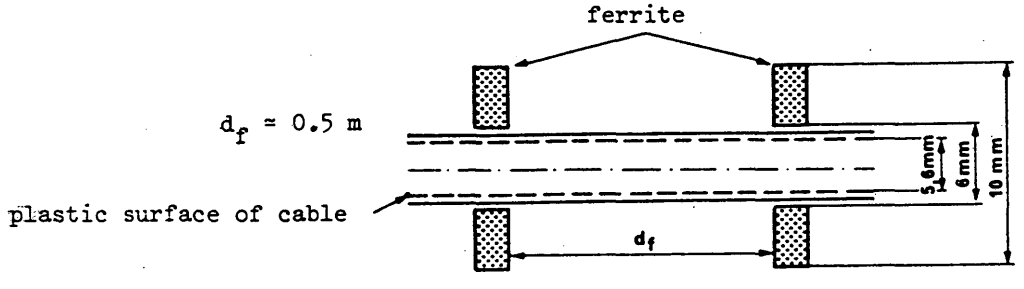


- Antenna Factor: The antenna factor (as a function of frequency and ground conductivity) for conversion of measured signal strengths (μV) to incident field intensities (μV/m) is yet to be determined. The dependence of this factor on ground contact resulting from the ground stake (Figure 1) has also to be established, although this effect will be less than 3.5 dB.

  (There may be a problem with seasonal changes in ground contact when the soil freezes and when using the recommended antenna in places where there is deep snow in winter. In such cases a counterpoise may provide a more stable ground system and will make it possible to elevate the antenna. Some research needs to be done to optimize the size of the counterpoise required.)

4. Antenna cable

- Characteristic impedance Z_c = 50
- Suppression of currents on the outer conductor by ferrite rings



- type of ferrite: A_l = 3000 to 5000 n H/turn^2

6. Lightning protection

The amplifier should be protected against discharge by means of diodes and a spark gap at the input.

The antenna should withstand a transient electric field of

$$\left|\frac{dE}{dt}\right| \geq 500 \quad \frac{kV}{m \cdot sec}$$

ANNEX B

RECORDING OF SIGNAL AND NOISE AMPLITUDES AND RELATED INFORMATION

1. *INTRODUCTION*

Individual 4s average signal and noise amplitudes are to be recorded on diskettes. Whilst this will lead to the need for greater subsequent data processing by the international team than if hourly median amplitudes were recorded *it will avoid the requirement for off-line data analysis at remote sites and will permit changes in analysis procedures to be introduced if subsequently found necessary.*

2. *GENERAL DATA ORGANIZATION*

The signal and noise amplitudes will be stored in individual files, each covering a period of one hour.

Calibration information will constitute a separate file.

There will also be a general description file that contains information like disk titles, etc.

Data having predetermined values will be coded and organized into tables in order to save space and facilitate some verification throughout the process.

3. *TABLES*

3.1 *Receiver Table*

Each record contains:

- *Receiver numeric code* *Max. value* 65536 *(binary)*	*2 bytes*
- *Receiver name* *20 characters*	*20 bytes*
Expected number of records:	-------

3.2 *Transmitter Table*

Each record contains:

- *Transmitter numeric code* *Max. value* 65536 *(binary)*	*2 bytes*
- *Transmitter Call Sign* *5 Characters*	*5 bytes*
- *Transmitter Name:* *20 Characters*	*20 bytes*
Expected number of records:	-------

3.3 *Frequency table*

Each record contains:

- *Frequency (binary)* centre*frequency quoted to the nearest* 100 Hz	2 bytes
Expected number of records:	25

4. *File Formats*

4.1 *General Description File*

Only one record that contains

- *Title* *containing the string* *"IWP 6/14 HF MEASUREMENTS"*	*32 characters*
- *Remarks* *(for incorporation of general pertinent information)*	*50 Characters*

4.2 *Calibration file*

Each record contains:

- *Date and time of calibration (binary)*	*4 bytes*
- *One calibration signal for all 25 frequencies 1 byte for each frequency*	25 bytes
Total	29 bytes

The number of records depends on the number of calibrations that take place during the weekly period (there is one record per calibration).

4.3 *Measurements File (for each hour and circuit)*

- *Date and time (binary)*	*4 bytes*
- *Transmitter Code (binary)*	*2 bytes*
- *Frequency Identification (index of the frequency tables)*	*1 byte*
- Input attenuation (dB)	*1 byte*
- *Signal and noise Values 12 times* (binary)	
. *Signal Amplitude*	*1 byte*
. *Signal qualifying* or descriptive letter	*1 byte*
. *Noise Amplitude*	*1 byte*
Total	**44 bytes**

5. *Diskettes Organization*

Each diskette will contain data *for a period of one week (7days)* consisting of the following:

- *1 General description file*
- *1 Calibration file*
- *168 hourly signal and noise files.*

6. *Storage Considerations*

Double side double density diskettes of 5.25 inches with a 360 kbytes capacity should be used to collect the data.

The data corresponding to one week of recording fit in one of these diskettes occupying approximatively 50% of total space available.

7. *Remarks*

- *All receiving stations should register their activity with the international* coordination *group and be given* an identification *code.*

- Date and time - a binary number (4 bytes) that contains the elapsed seconds since 00:00:00 UT, 1 January 1970, according to the system clock and permits calculation of the actual date and time.

- *Qualifying letters are given in Report 253.*

- *Rules for qualifying numerical values as uncertain are given in Report 253.*

- Signal and Noise Amplitudes will be recorded as integer values.

ANNEX C

RULES FOR DETERMINING HOURLY MEDIAN SIGNAL AMPLITUDES

For a particular circuit there will normally be 12 signal amplitude samples within a given hour on a given day. If all these samples have unqualified numerical values the median is readily determined by ranking them in ascending order and taking the average of the two middle numbers.

However, complications arise when some sample values are qualified or are accompanied or replaced by descriptive letters. The following qualifying and descriptive letters are proposed (see also Report 253):

D - to indicate that the numerical value is lower than or equal to the true value (as for example when exceeding receiver full scale)

E - to indicate that the numerical value is greater than or equal to the true value (below the composite background of receiver noise, atmospheric noise and man-made noise and interference)

U - uncertain. A numerical value is classified as uncertain when it is not believed accurate to within $\pm$ (2 to 4 dB)

C - no measurement was possible because of technical trouble

S - measurement influenced by or impossible because of interference or atmospherics

Every measured signal amplitude is accompanied by an associated amplitude of the composite background with which it is compared in selecting letters E and U.

Cases of C or S do not contribute to the signal sample count but numerical values accompanied by qualifying letters do.

When there are some data values accompanied by qualifying letters a first trial median is determined ignoring all qualifying letters. If then it is found that all values accompanied by D are greater than this median and all accompanied by E are less than this median, then the first trial median is the final median. Otherwise a second trial median is produced by moving all E values to the bottom of the list and all D values to the top. The final median is then the average of the first and second trial medians. If these differ by more than 2 dB then the final median is qualified by U.

If more than half of the signal samples are qualified by E (or D) the median is determined in the normal way and is also qualified by E (or D).

REPORT 430-5

IMPROVEMENT IN THE WORLD-WIDE IONOSPHERIC OBSERVING PROGRAMME FOR NUMERICAL MAPPING PURPOSES

(Question 42/6)

(1970-1974-1978-1982-1986-1990)

1. Introduction

Improvements in long- and short-term predictions of ionospheric conditions depend upon the availability of new sources of ionospheric observations as well as upon improved methods of ionospheric mapping and predictions. Significant improvement might be possible by expanding the existing network of ground-based ionosondes and by supplementing vertical-incidence ionization measurements with ionospheric parameters obtained with satellites and by other appropriate techniques. Ionospheric data from back-scatter and oblique-incidence sounding programmes may also be of value.

2. Geographical distribution of ground-based ionosondes

The ionosonde network in existence when Report 340 was prepared has provided a reasonable sample of basic data for about one-third of the Earth's surface. Since that time, new ionosondes have begun operation and the data from these observing stations should be incorporated into the numerical maps. However, gaps remain in ionosonde coverage in the ocean areas and sparsely populated land area, especially the equatorial anomaly region, the South Atlantic magnetic anomaly region, the Antarctic magnetic anomaly region, the Antarctic region, and the sub-auroral region. It might be possible to cover these regions using unattended ionosonde equipment which would automatically measure, scale, process and transmit pertinent ionospheric parameters in digital form. Unattended operation (with periodic maintenance) of digital ionosondes is now feasible by using remote control to convey the digital output [Bibl and Reinisch, 1978]. Computer processing of ionosonde output is facilitated by the use of digital ionosondes [Reinisch, 1986; Poole, 1985; Poole and Evans, 1985] permitting in many cases the automatic scaling of standard parameters and automatic conversion to true-height electron density profiles [Reinisch and Huang, 1982a].

Wright [1981] proposed a global network based on 88 stations that took into account limitations due to oceans and deserts. It is probable that many more stations would be needed in zones where the ionosphere changes rapidly with position unless the complex mixture of vertical and oblique sounding was available at all stations.

To use a ground-based network for short-term predictions, [Rush, 1976], following the work of Gautier and Zacharisen [1965] found that foF2 observations every 1000 km in the north-south direction and 2000 km in the east-west direction are needed to reduce the error in the prediction of daily values of foF2 at a remote location by 50%. An observation network needed to achieve this degree of improvement in the mid-latitude ionosphere requires ionospheric measurements approximately every 10° of latitude and every 20° of longitude. Such a network could easily be implemented using existing ionosonde locations in Western Europe and the USSR with little modification. It would be necessary, however, to coordinate the observations and forward them with a short time delay to a central location for dissemination to all users.

3. Quality of data

Constant vigilance is required for adequate quality control of data from ionospheric sounding stations. The statistical significance of data reported from a given ionospheric station depends entirely on careful following of the established rules for scaling and reporting and adequate continuity of records to provide sufficient data for meaningful monthly medians.

The Ionosonde Network Advisory Group (INAG) of URSI Commission G is responsible for considering the scientific problems associated with the ground-based vertical-incidence network, and, when necessary, for recommending appropriate action. INAG [Piggott and Rawer, 1972 and 1978; Piggott, 1975] has recommended a number of modifications in the rules previously used for scaling ionograms.

4. Use of top-side sounding and other satellite data

The availability of top-side data from satellite soundings can provide possible improvements in ionospheric predictions by establishing information on:

- world-wide information of foF2 which would improve the ground-based information through capability of collecting data more uniformly distributed in latitude and longitude;
- mean gradients of foF2 and hmF2 in order to improve the extrapolation of data from ground ionosonde stations to remote locations;
- geographic or magnetic coordinate systems which would enable ionospheric characteristics to be represented more accurately by numerical mapping methods;
- the extent to which the changes in vertical incidence ionospheric characteristics depend upon changes in the positions of localized features such as the peaks and troughs in F2 in equatorial and high-latitude regions. Ancillary data such as electron density and temperatures, total ionospheric electron content and ionization gradients may also be applicable to mapping problems, especially if these measurements are simultaneous.

Many of the features observed by top-side sounders and relevant to ionospheric mapping problems have been reviewed in the Proceedings of the IEEE [IEEE, 1969]. Australia and Japan using data from the Alouette satellites [Nishizaki and Nagayama, 1969] and Australia, Japan and the United Kingdom using data from the ISIS-1 and ISIS-2 satellites are examining the compatibility of ground-based and top-side sounder data. Sample maps of foF2 at constant local times have been produced from such top-side sounder data at equatorial, middle and polar latitudes [Burge *et al.*, 1973].

In the USSR bottomside ionospheric profiles and world maps of foF2 were derived from data obtained by the satellites Intercosmos-19 and Cosmos-1809 using a new transionospheric sounding method [Danilkin, 1985]. The method makes it possible also to determine the MUF for radiocommunication and to obtain information on horizontal gradients and ionospheric inhomogeneities.

In Japan, world-wide maps of foF2 have been produced from ISS-b satellite data [Matuura *et al.*, 1981, Wakai and Matuura, 1980]. Numerical mapping techniques developed in the United States of America [Jones and Obitts, 1970, Jones and Stewart, 1970; Flattery and Ramsay, 1975] permit the integration of ground based data with top-side sounder data.

Progress has also been reported on the development of a digital top-side sounding project with automatic processing of the top-side ionograms [Mathwick *et al.*, 1981; Reinisch and Huang, 1982b]. Three to five digital top-side sounders together with a global ground-based network of remotely controlled modern ionosondes could provide a continuously updated global ionospheric model.

Plasma frequency observations from the Ariel-3 satellite [Piggott, 1970; Sayers, 1970] indicate that the ratio of plasma frequency to foF2 at different longitudes for the same local time is approximately constant from day-to-day. This feature is of potential use in deducing ionospheric conditions in remote areas in terms of available ground-based observations. On the other hand, a small number of theoretical calculations suggest that the extrapolation of satellite data to values of foF2 is markedly dependent on electron temperature and local time [King, 1973]. A theoretical relationship has been established between neutral-air winds and electron density distributions [Rishbeth and Kelley, 1971]. The theory can be used to deduce changes in height of maximum ionization with longitude and thereby to yield values of foF2 from the observed plasma frequencies at the satellite.

Other types of data, e.g. airglow observations [Daniell *et al.*, 1985; McCoy and Anderson, 1985] could provide additional useful information on spatial variations of ionization. Maps of predicted airglow intensity have been produced from the numerical coefficients of M(3000)F2 and foF2 and these have been compared with observational data obtained using the OGO-4 and OGO-6 satellites [Thuillier *et al.*, 1976]. The observed variations (for example, the longitudinal fine structure) over ocean areas, particularly those in the southern hemisphere, reveal features which differ somewhat from those indicated by the CCIR predictions. Comparisons of this type, and the introduction of relevant ionospheric theory, could be used to improve the accuracy of the predictions.

It should be appreciated, however, that satellite observations are limited in the distance to which they can be extrapolated away from the sub-satellite point. To achieve significant improvement in predictions in inaccessible areas, particularly for short-term predictions, numerous spacecraft requiring sophisticated ground-support equipment would be required. Observations from satellites have been shown to be extremely useful in ascertaining sharp, well-defined features in the structure of the ionosphere, particularly those associated with gradients in electron density related to the equatorial anomaly and mid-latitude trough [Piggott, 1969]. These observations are particularly valuable in regions inaccessible to ground-based observations.

The availability of very large scale photographs of the aurora, by the US DMSP satellites, promises to permit mapping F-region irregularity zones, and the mid-latitude trough. This satellite imagery is available from the archives of the National Geophysical and Solar-Terrestrial Data Center, National Oceanic Atmospheric Administration (NOAA) Boulder, Colorado 80303, USA.

An ionospheric model for North America has been developed for foF2 and spread-F using about 10^6 Alouette-1 ionograms [Muldrew *et al.*, 1978; Gladwin, 1980]. Magnetic tapes of reduced data and computer (FORTRAN) programs are available. Gladwin [1980] has developed a model giving a rough estimate of layer thickness using 10^4-10^5 electron density profiles and a simple bottomside model. For the northern hemisphere between 180° W and 45° W (excluding the low latitude Pacific Ocean region), foF2, a spread-F index, and layer thickness can be obtained for each hour of local time; the required inputs are month, K_p, sunspot number, and location.

5. Total electron content

Maps of total electron content (TEC) are needed for predicting ionospheric effects on satellite-Earth links. Measurements of total electron content have been made at many stations by observations of the Faraday rotation or the Doppler effect on signals from low orbiting and geostationary satellites. Maps of total electron content have been prepared for a mid-latitude ionosphere [Amayenc *et al.* 1971; Klobuchar, 1973; Soicher and Gorman, 1984]. Observations of the latitudinal variations of TEC in different equatorial regions have been described [Physical Research Laboratory, 1969; Golton and Walker, 1971]. More information on total electron content is contained in Report 263.

The spatial variability in TEC values has been described [Soicher, Klobuchar and Doherty, 1984], indicating complexity in the task of providing an accurate world-wide map.

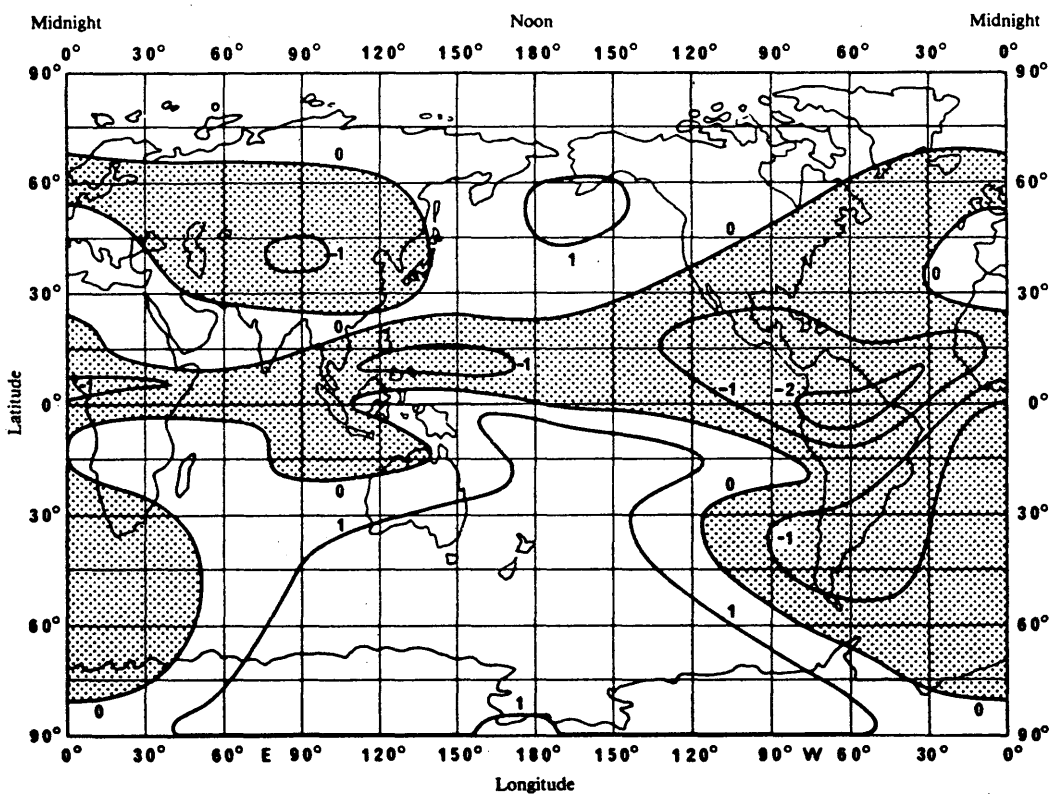


FIGURE 1 – *UTC-map of the frequency difference* Δf *(=fISS - fCCIR)* (MHz)

Shaded portion indicates the area of negative Δf 0000 UTC 11 August, 1978-12 December, 1978

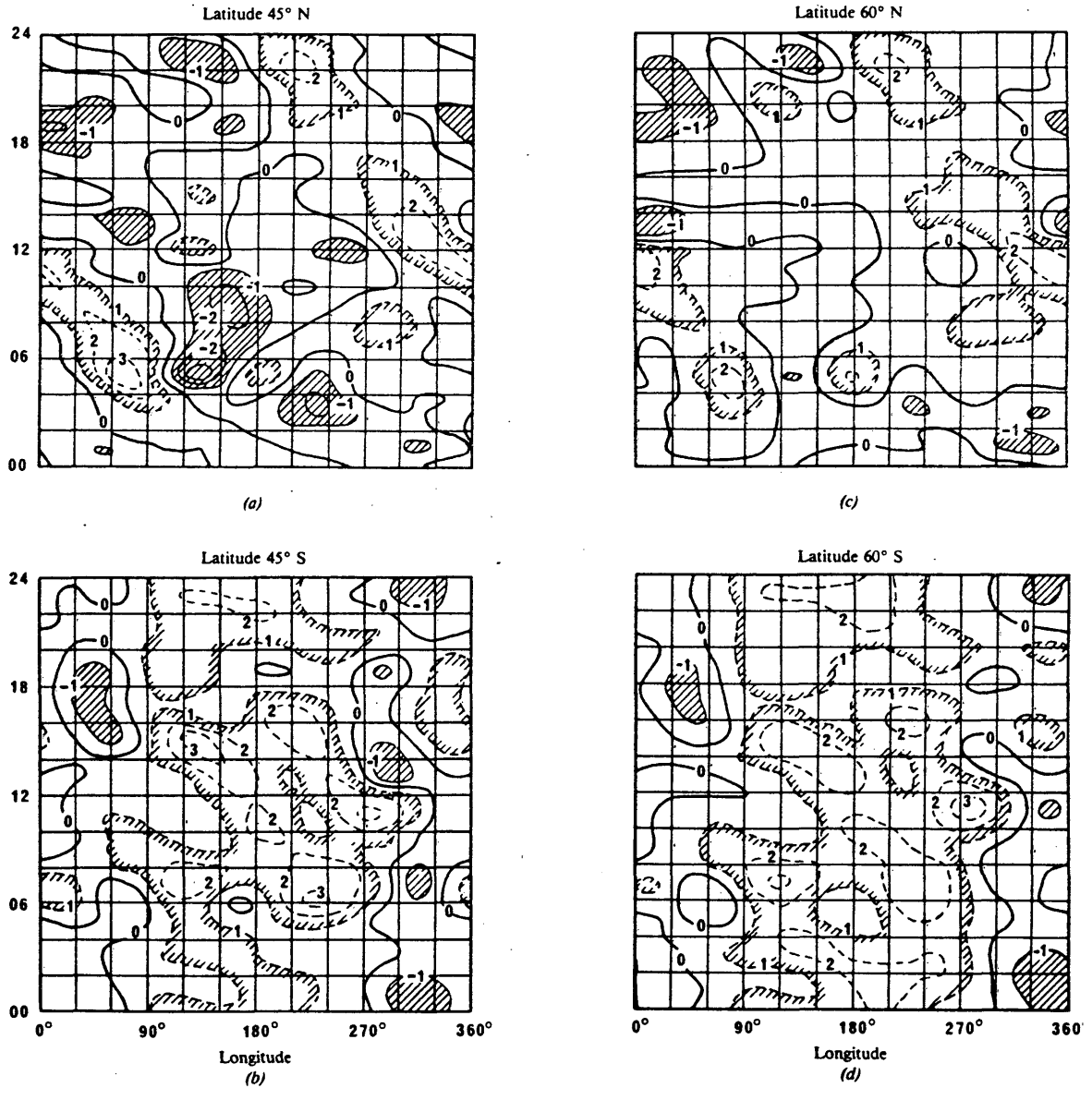


FIGURE 2 – *Distribution of the frequency difference $\Delta foF2$ ($=f_{ISS} - f_{CCIR}$) with respect to the geographic longitude versus UTC, for latitudes (a) 45° N, (b) 45° S, (c) 60° N and (d) 60° S. Contours in every 1 MHz of $\Delta foF2$, thick continuous curves for $\Delta foF2 = 0$, hatched portion for $\Delta foF2 \leqslant -1$ MHz, and partly hatched portion with broken curves for $\Delta foF2 \geqslant 1$ MHz*

6. Accuracy of the CCIR numerical maps of foF2 and hmF2

Comparisons made [Burge *et al.*, 1973; King, 1973] between satellite observations of plasma frequencies and the numerical maps of foF2 reveal that average discrepancies are generally small, but that in some ocean regions, notably the South Pacific and in the southern hemisphere, in the night-time, the predictions are in error by as much as a factor of 2.

Departures from predicted median or mean values of foF2 are generally determined when measurements from an observational network are used in the short-term prediction of propagation performance. The final improvement in the prediction of propagation performance is then dependent in part on the difference between the observed daily and predicted monthly values of foF2.

The world-wide mapping analysis has been applied to the differences between the observed value of foF2 given by ISS-b and the value of foF2 predicted by the CCIR method at each observation point. The results shown in Fig. 1 and Fig. 2 for the period 11 August 1978-12 December 1978 indicate that, in the area of the South Pacific Ocean, the observed foF2 tends to exceed the prediction, but tends to be the reverse in the areas of South America, the South Atlantic Ocean and near the magnetic equator [Matuura, 1980], and also indicate that, in the northern hemisphere, the areas where the frequency differences are appreciable tend to appear on fixed local time [Matuura *et al.*, 1981].

In situ measurements of ionospheric electron density on board Aeros-A and B when compared with the CCIR numerical maps have also shown rather large differences in those areas where the data input from ground stations was insufficient. Major discrepancies are found above the Pacific and at lower latitudes in the equatorial belt [Sheikh *et al.*, 1978].

New global maps of foF2 have been developed by Rush *et al.*, [1984] by combining monthly median vertical incidence observations of foF2 with values of foF2 derived from the time-dependent continuity equation for ions (and electrons) for locations where data were not available. In regions inaccessible for routine observations, the new numerical maps yield values of foF2 that differ significantly from those obtained from the CCIR numerical maps. Limited tests of validity indicate that the new numerical maps yield much improved values of foF2 for these inaccessible regions.

7. Parameter variability

A second type of improvement which the world-wide data base of ionosonde measurements could provide is the mapping of parameter variability, in addition to the present maps of the monthly median parameter values. This type of mapping would also benefit from an improved geographical distribution of ionosondes, but even the current world-wide data base of ionosonde measurements could provide maps useful in improving communication system predictions.

Recent studies of the day-to-day percentage variability in foF2 within a given month and hour show a dependence of this parameter on both monthly effective sunspot number (IG) and magnetic activity [Sowers and Pokempner, 1989]. For the mid-latitude stations studied, a significant positive correlation with IG was found during the summer daytime hours while during the summer evening and winter daytime hours a negative correlation is likely. Correlations with IG were also derived using only those periods which were magnetically quiet ($AP \leqslant 12$). The magnetically quiet IG correlations show similar results with somewhat stronger dependencies.

REFERENCES

AMAYENC, P., BERTIN, F., PAPET-LEPINE, J. [1971] Sur l'évolution latitudinale du contenu électronique de l'ionosphère (On the latitudinal evolution of the electron content of the ionosphere). *Ann. de Géophys.*, **27**, 345-357.

BIBL, K. and REINISCH, B. W. [1978] The universal digital ionosonde. *Radio Sci.*, Vol. 13, 519-530.

BURGE J. D., KING, J. W. and SLATER, A. J. [1973] Mapping of foF2 by means of top-side sounder satellites. *Telecomm. J.*, **40**, 356-363.

DANIELL Jr., R. E., STRICKLAND, D. J. and JASPERSE, J. R. [1985] Global monitoring of the ionosphere by optical techniques. *The Ionospheric Effects Symposium*, Ed. J. M. Goodman, 276-287 , Library of Congress Catalog Card No. 85-600558.

DANILKIN, N.P. [1985] - "Prosvechivanie ionosfern na granitse diapazona radioprozrachnosti" ("Illumination of the ionosphere at the limit of the radiotransparency range") - Radiotekhnika, No. 9, page 3.

FLATTERY, T. W. and RAMSAY, A. C. [1975] Derivation of total electron content for real-time global applications. Proc. Symposium on the Effects of the Ionosphere on Space Systems and Communications, Naval Research Laboratory, Arlington, VA, USA.

GAUTIER, T. N. and ZACHARISEN, D. H. [1965] Use of space and time correlations in short-term ionospheric predictions. Conf. Rec., First Annual IEEE Communications Convention.

GLADWIN, J. C. [1980] An F-layer model of the ionosphere for North America. Communications Research Centre Report, No. 1337, Dept. of Communications, Ottawa, Ontario, Canada.

GOLTON, E. and WALKER, G. O. [1971] Observations of ionospheric electron content across the equatorial anomaly at sunspot minimum. *J. Atmos. Terr. Phys.* **33**, 1-11.

IEEE [1969] Topside sounding and the ionosphere. *Proc. IEEE*, **57**, 859-1171.

JONES, W. B. and OBITTS, D. L. [1970] Global representation of annual and solar cycle variation of foF2 monthly median 1954-1958. Telecommunications Research Report OT/ITSRR3, Boulder, CO, USA.

JONES, W. B. and STEWART, F. G. [1970] A numerical method for global mapping of plasma frequency. *Radio Sci.*, **5**, 773-784.

KING, J. W. [1973] The determination of foF2 and hmF2 from satellite-borne probe data. *Telecomm. J.*, **40**, 364-368.

KLOBUCHAR, J. A. [1973] Total electron content studies of the ionosphere. Report TR-73-0098, Air Force Cambridge Research Labs., Bedford, MA, USA.

MATHWICK, H. R., AUBERT, D. E., MARTZ, A. F., BIBL, K., REINISCH, B. W. and LEWIS, D. [1981] An advanced mission to map the worldwide topside ionosphere. *Effects of the Ionosphere on Radiowave Systems*. Ed. J. M. Goodman. US Govt. Printing Office, Library of Congress, Catalog No. 82-600510.

MATUURA, N. [1980] Characteristics on global distribution of foF2 based on topside sounding by ISS-b. Highlights of the Japanese IMS Programme, Institute of Space and Aeronautical Science, University of Tokyo, 239-247.

MATUURA, N., KOTAKI, M., MIYAZAKI, S., SAGAWA, E. and IWAMOTO, I. [1981] ISS-b experimental results on global distributions of ionospheric parameters and thunderstorm activity. *Acta Astronautica*, Special Issue of the 31st IAF Congress, Tokyo, Vol. 8, **5-6**, 527-548.

McCOY, R. P. and ANDERSON Jr., D. E. [1985] Ultraviolet remote sensing of the F2 ionosphere. *The Ionospheric Effects Symposium*, Ed. J. M. Goodman, 295-302 , Library of Congress Catalog Card No. 85-600558.

MULDREW, D. B., GLADWIN, J. C. and JAMES, H. G. [1978] An F-layer model for North America and its application to the Search and Rescue Satellite Programme. Proc. Symposium of the COSPAR Satellite Beacon Group on Beacon Satellite Measurements of Plasmaspheric and Ionospheric Properties, Florence, May, 1978, coordinated by Professor P. F. Checcacci, Instituto di Ricerca sulle Onde Elettromagnetiche, Cosiglio Nazionale delle Ricerche (C.N.R.), Florence, Italy, Paper 42.

NISHIZAKI, R. and NAGAYAMA, M. [1969] Analysis of observational data obtained by Alouette II. V. Comparison of foF2 from two observational methods of top-side sounding and ground-based sounding. *J. Radio Res. Labs.*, (Japan), **16**, 227-234.

PHYSICAL RESEARCH LABORATORY, Ahmedabad [1969] Proc. of Third International Symposium on Equatorial Aeronomy, India.

PIGGOTT, W. R. [1969] The acquisition and use of ionospheric data for prediction and other practical applications. *Telecomm. J.*, **36**, 273-279.

PIGGOTT, W. R. [1970] The use of satellite data for prediction purposes in ionospheric forecasting. AGARD Conf. Proc. No. 49.

PIGGOTT, W. R. [1975] High latitude supplement to URSI handbook of ionogram interpretation and prediction. World Data Center A for Solar Terrestrial Physics, Report UAG-50, NOAA, Boulder, CO 80303, USA.

PIGGOTT, W. R. and RAWER, K. [1972] URSI handbook of ionogram interpretation and reduction (2nd Ed.), World Data Center A for Solar-Terrestrial Physics. Report UAG 23. NOAA, Boulder, CO 80303, USA. Spanish text available from LIARA (Argentina), and French text available from CNET (France).

PIGGOTT, W. R. and RAWER, K. [1978] URSI handbook of ionogram interpretation and reduction (2nd Ed.). Revision of Chapters 1-4. World Data Centre A for Solar-Terrestrial Physics. Report UAG-23A, NOAA, Boulder, CO 80303, USA.

POOLE, A.W.V. [1985] - Advanced sounding 1. The FMCW alternative. Radio Sci., Vol. 20, 1609-1616.

POOLE, A.W.V. and EVANS, G.P. [1985] - Advanced sounding 2. First results from an advanced chirp sounder. Radio Sci., Vol. 20, 1617-1623.

REINISCH, B. W. and HUANG, X. [1982a] Automatic calculation of electron density profiles from digital ionograms, 3. Processing of bottomside ionograms. *Radio Sci.*, Vol. 17, 837-844.

REINISCH, B. W. and HUANG, X. [1982b] Automatic calculation of electron density profiles from digital ionograms, 1. Automatic O and X trace identification for topside ionograms. *Radio Sci.*, Vol. 17, 421-434.

REINISCH, B.W. [1986] - New techniques in ground-based ionospheric sounding and studies. Radio Sci., Vol. 21, 331-341.

RISHBETH, H. and KELLEY, D. M. [1971] Maps of the vertical F-layer drifts caused by horizontal winds at mid-latitudes. *J. Atmos. Terr. Phys.*, **33**, 539-545.

RUSH, C. M. [1976] An ionospheric observation network for use in short-term propagation predictions. *Telecomm. J.*, **43 (8)**, 544-549.

RUSH, C. M., POKEMPNER, M., ANDERSON, D. N., PERRY, J., STEWART, F. G. and REASONER, R. [1984] Maps of foF2 derived from observations and theoretical data. *Radio Sci.*, Vol. 19, 1083-1097.

SAYERS, J. [1970] In situ probes for ionospheric investigation. *J. Atmos. Terr. Phys.*, **32**, 663-691.

SHEIKH, N. M., NESKE, E., RAWER, K. and REBSTOCK, K. [1978] Comparison of peak electron densities of the F2-layer derived from in situ measurements with CCIR predictions. *Telecomm. J.*, **45**, 225-227.

SOICHER, H. and GORMAN, F. J. [1984] Faraday rotation observations near solar maximum at midlatitudes. *The Ionospheric Effects Symposium*, Ed. J. M. Goodman, 213-220.

SOICHER, H., KLOBUCHAR, J.A. and DOHERTY, P.H. [1984] - Spatial variability of total electron content in the Eastern Mediterranean region. Radio Sci., Vol. 19, 757-764.

SOWERS, M. and POKEMPNER, M. [1989] - The dependence of the critical frequency of the F2 region on the effective sunspot number (IG) and magnetic activity (to be published).

THUILLIER, G., KING, J. W. and SLATER, A. J. [1976] An explanation of the longitudinal variation of the O^1D (630 nm) tropical nightglow intensity. *J. Atmos. Terr. Phys.* **38**, 155-158.

WAKAI, N. and MATUURA, N. [1980] Operational and experimental results of the Ionosphere Sounding Satellite-b. *Acta Astronautica*, Vol. 7, 999-1020.

WRIGHT, J. W. [1981] Global real-time ionospheric monitoring. *Effects of the Ionosphere on Radiowave Systems.* Ed. J. M. Goodman. US Govt. Printing Office, Library of Congress, Catalog No. 82-600510.

PAGE INTENTIONALLY LEFT BLANK

PAGE LAISSEE EN BLANC INTENTIONNELLEMENT

DECISIONS

DECISION 6-7

SKY-WAVE FIELD STRENGTH AND TRANSMISSION LOSS AT FREQUENCIES ABOVE 1.6 MHz

(Study Programme 30A/6)

(1956-1959-1963-1966-1970-1974-1976-1978-1981-1983-1985-1988-1989)

CCIR Study Group 6,

CONSIDERING

(a) that there is a need for the production of improved propagation prediction methods which are as simple as possible consistent with the requirements of accuracy for practical purposes;

(b) that Recommendation No. 514 (HFBC-87) invited the CCIR to undertake studies of the HF propagation prediction method adopted by the Conference and to recommend both improvements in the method and later, if necessary, an improved method to be used in the future for the HF bands allocated exclusively to the broadcasting service,

DECIDES

1. to maintain IWP 6/1, with the following terms of reference:

- the production of improved prediction methods for computerized implementation;
- to liaise with the activities of IWP 6/15 in order to ensure that data banks of HF signal strength measurements are in suitable validated form for use in prediction/measurement campaigns;
- cooperation with administrations and international organizations by assisting in making predictions of field strengths for circuits under study by the methods of the CCIR or by any other method;

2. that IWP 6/1 shall be composed as shown in Annex I;

3. that the Director, CCIR, shall communicate any changes to Annex I which may come to his attention, to the Chairman and Vice-Chairmen of Study Group 6, as well as to the Chairman of IWP 6/1, without such changes being considered as modifications to the present Decision;

4. that IWP 6/1 shall report to the next meeting of Study Group 6 and, in particular, propose new CCIR texts and/or modifications to existing ones, relating to its terms of reference.

List of participants in IWP 6/1:

Chairman:

Mr. P. A. Bradley (United Kingdom)
Rutherford-Appleton Laboratory
Chilton
Didcot
Oxfordshire, OX11 OQX
United Kingdom

Administrations:

Germany (Federal Republic of)
Argentina
Australia
Brazil
Chile
China (People's Republic of)
Cuba
Spain
United States of America
Finland
France
India
Iran (Islamic Republic of)
Japan
Qatar
United Kingdom
USSR
Yugoslavia (Socialist Federal Republic of)

International Telecommunication Union:

IFRB

International Organisations and Recognized Private Operating Agencies:

Deutsche Welle
EBU
Telefonica

DECISION 9-5

RADIO PROPAGATION AND CIRCUIT PERFORMANCE AT FREQUENCIES BELOW ABOUT 500 kHz

(Study Programme 31D/6)

(1963-1966-1970-1974-1976-1978-1981-1985-1989)

CCIR Study Group 6,

CONSIDERING

(a) that IWP 6/5 has developed methods of estimating sky-wave field strength at frequencies below about 500 kHz (see Reports 265 and 895);

(b) that although the methods contained in these Reports are intended to be broadly applicable in the various regions of the world, it is likely that their precision could be improved for specific application in some regions, since the methods have been largely based on observations in the Euro-Asia ITU Region,

DECIDES

1. to maintain Interim Working Party 6/5, with the following terms of reference:

- to refine the ionospheric model to be used with the waveguide mode method (Report 895), in particular through analysis of new data presently being collected at high latitudes in ITU Region 2; and

- to foster development of a computer program that can be used to automate the present numerical-graphical procedures of the wave-hop method (Report 265), which predicts sky-wave field strength. Such a program should be a part of an integrated software package and graphics that includes the ground-wave, and the vector sum of ground- and sky-waves, i.e. the total field;

2. that IWP 6/5 shall be composed as shown in Annex I; however, administrations interested in this study should be encouraged to participate in the work;

3. that the Director, CCIR, shall communicate any changes to Annex I which may come to his attention, to the Chairman and Vice-Chairmen of Study Group 6, as well as to the Chairman of IWP 6/5, without such changes being considered as modifications to the present Decision;

4. that IWP 6/5 shall report to the next meeting of Study Group 6 and, in particular, propose new CCIR texts and/or modifications to existing ones, relating to its terms of reference.

ANNEX I

List of participants in IWP 6/5:

Chairman:

Dr. J. Belrose (Canada)
Communications Research Centre
Department of Communications
Shirley Bay
P.O. Box 11490, Station H
Ottawa, Ontario K2H 8S2
Canada

Administrations:

Canada
United States of America
Japan

DECISION 11-6

VHF AND UHF PROPAGATION BY SPORADIC E AND OTHER IONOSPHERIC REGIONS

(Question 41/6)

(1970-1974-1976-1978-1981-1983-1985-1989)

CCIR Study Group 6,

CONSIDERING

that VHF and UHF propagation by sporadic E and other ionospheric regions is often responsible for serious interference to sound and television broadcasting services, mobile services, and to systems employing tropospheric and ionospheric scattering, and, if ignored, can sometimes seriously affect estimates of system reliability,

DECIDES

1. to maintain IWP 6/8, with the following terms of reference:
- to study the VHF and UHF propagation aspects of sporadic E and other natural ionospheric regions;
- to improve the existing method for estimating the field strength or transmission loss at VHF resulting from propagation by sporadic-E reflections placing emphasis on the study of foEs in the equatorial zone, southern mid-latitude zone and high-latitude zones;
- to develop methods for estimating the field strength or transmission loss at VHF and UHF resulting from propagation by sporadic-E reflections and F-region reflections;

2. that IWP 6/8 shall be composed as shown in Annex I;

3. that any other administration or organization participating in the work of Study Group 6 which would like to join in the work of this Interim Working Party should make known to the Director, CCIR, the name and address of their expert member;

4. that the Director, CCIR, shall communicate any changes to Annex I which may come to his attention, to the Chairman and Vice-Chairmen of Study Group 6, as well as to the Chairman of IWP 6/8, without such changes being considered as modifications to the present Decision;

5. that IWP 6/8 shall report to the next meeting of Study Group 6 and, in particular, propose new CCIR texts and/or modifications to existing ones, relating to its terms of reference.

ANNEX I

List of participants in IWP 6/8:

Chairman:

Dr. Alberto Giráldez (Argentina)
Laboratorio Ionosférico de la
Armada Argentina (LIARA)
Avenida Libertador No. 327
1638 Vicente Lopez
Buenos Aires
Argentina

Administrations:

Germany (Federal Republic of)
Argentina
Australia
Brazil
United States of America
India
Japan
Nigeria
United Kingdom
Sweden
USSR

International Organizations:

European Broadcasting Union (EBU)
International Amateur Radio Union (IARU)

DECISION 57-2

SKY-WAVE PROPAGATION AT FREQUENCIES BETWEEN 150 AND 1 700 kHz

(Study Programme 31D/6)

(1983-1985-1989)

CCIR Study Group 6,

CONSIDERING

(a) that there is a need for an accurate method of estimating sky-wave field strength at frequencies between 150 and 1 700 kHz suitable for world-wide applications;

(b) that in preparation for recent ITU conferences, IWP 6/4 has analysed existing methods and developed a number of new methods which are described in Recommendation 435 and Report 575;

(c) that, although these methods are intended to be broadly applicable in all geographical regions of the world, different methods are being used in different regions of the ITU,

DECIDES

1. to maintain Interim Working Party 6/4 with the following terms of reference:

- to analyse available field-strength prediction methods and to compare these methods against data collected in all parts of the world;
- to carry out the studies listed in Study Programme 31D/6;
- to study further existing methods and propose refinements, and/or new methods, if necessary, for world-wide application;

2. that IWP 6/4 shall report to the next meeting of Study Group 6, and in particular, propose new CCIR texts and/or modifications to existing ones, relating to its terms of reference;

3. that IWP 6/4 shall be composed as shown in Annex I;

4. that the Director, CCIR, shall communicate any changes to Annex I which may come to his attention, to the Chairman and Vice-Chairmen of Study Group 6, as well as to the Chairman of IWP 6/4, without such changes being considered as modifications to the present Decision.

ANNEX I

List of participants in IWP 6/4:

Chairman:

Mr. J. C. H. Wang (United States of America)
Federal Communications Commission
2025 M Street, NW
Washington, DC 20554
United States of America

Administrations:

Argentina
Brazil
Canada
Cuba
United States of America
India
Italy
Mexico
United Kingdom

DECISION 83

HF MEASUREMENTS AND DATA BANKS

(Question 42/6)

(1989)

CCIR Study Group 6,

CONSIDERING

(a) that Report 253 discusses techniques for the measurement of sky-wave signal intensities at frequencies above 1.6 MHz and identifies some transmissions suitable for such measurements;

(b) that Report 1149 details proposals for a measurement campaign using a specially designed modulation format and dedicated receivers;

(c) that there continues to be a need for the development and extension of data banks, with adequate safeguards for calibration and data integrity,

DECIDES to establish Interim Working Party 6/15 with the following terms of reference:

1. to improve the information available on measurement techniques and calibration;

2. to establish new and extended data banks, taking account of the requirements of IWP 6/1;

3. that IWP 6/15 shall report to the next meeting of Study Group 6, and in particular, propose new CCIR texts and/or modifications to existing ones, relating to its terms of reference;

4. that IWP 6/15 shall be composed as shown in Annex I;

5. that the Director, CCIR, shall communicate any changes to Annex I which may come to his attention, to the Chairman and Vice-Chairmen of Study Group 6, as well as to the Chairman of IWP 6/15, without such changes being considered as modifications to the present Decision.

ANNEX I

List of participants in IWP 6/15

Chairman: Professor N. Wakai (Japan)
Tokai University
2-28 Tomigaya
Shibuya-ku
TOKYO 151

Professor Wakai is supported in this work by the Communications Research Laboratory, Japan.

Administrations: Germany (Federal Republic of)
Australia
United States of America
France
India
Iran (Islamic Republic of)
Italy
Japan
United Kingdom
USSR

DECISION 84

THE POTENTIAL FOR AN HF FIELD-STRENGTH MEASUREMENT CAMPAIGN TO PROVIDE A SIGNIFICANT MEASUREMENT DATA BANK IN TIME FOR PREPARATIONS FOR A WARC HFBC IN 1993

(1989)

CCIR Study Group 6,

CONSIDERING

(a) that Report 1149 provides a sufficient specification of the aspects of transmitter and receiver installation and operation for the purposes of HF field-strength measurement;

(b) that design details and hardware for the transmitter modulator and for the receiver/computer interface are available;

(c) that Resolution 111 recommended administrations to conduct HF field-strength measurement programmes and that this was given wide distribution in the CCIR Circulars AC/293 and AC/299,

BUT NOTING ALSO

(d) that even if a full scale measurement campaign were to start immediately there is scarcely time for the collection of sufficient data and for analysis with a view to refining the prediction methods of WARC HFBC-87 and Report 894 in time for submission to a conference to be held early in 1993;

(e) that firm proposals for the provision of transmitters in the immediate future have been received from two administrations, and that, while such provision will be most beneficial in improving the data banks in the longer time, this number does not meet the minimum criteria identified by the Study Group for an intensive, one year, campaign;

(f) that submissions made to Interim Working Party 6/14 included Recommendations that the measurement campaign should, in any case, be carried out over a longer period;

(g) that the establishment and operation of stations would be the responsibility of administrations,

DECIDES

1. to discontinue the attempt to conduct a short-term intensive campaign in 1990;

2. to continue to urge administrations to provide transmissions and make measurements over a longer period, with due regard for the need for training and guidance;

3. that the work of IWP 6/14 should be terminated since it has fully met its objectives and has provided sufficient information in Report 1149 to initiate a measurement campaign.

DECISION 85

STUDIES OF THE PROPAGATION PREDICTION METHOD FOR HF BROADCASTING

(1989)

CCIR Study Group 6,

CONSIDERING

(a) that Recommendation 514 (HFBC-87) invites the CCIR to undertake studies of the HF propagation prediction method adopted by the Conference and to recommend both improvements in the method and later, if necessary, an improved method to be used in the future for the HF bands allocated exclusively to the broadcasting service;

(b) that Recommendation 512 (HFBC-87) recommends that the propagation prediction method and the associated software to be used in application of Recommendation 514 (HFBC-87) shall be those applied by the IFRB during the intersessional period;

(c) that Resolution 514 (HFBC-87) resolves that following each CCIR Plenary Assembly, the IFRB shall review its Technical Standards relating to the technical parameters of HF broadcasting in the light of new or modified CCIR Recommendations, and shall circulate to all administrations the results of its review, indicating the reasons for its proposed actions,

DECIDES

1. that Interim Working Party 6/1 shall undertake studies of the propagation prediction method applied by the IFRB in accordance with Recommendation 512, shall compare the predictions with the most appropriate data bank of measurements and shall recommend improvements where appropriate in particular possible changes to the values of L_z and L_y and of the interpolation procedure;

2. that IWP 6/1 shall report, through the Chairman of Study Group 6, direct to the Plenary Assembly of CCIR in 1990 and, if appropriate, shall draft Recommendations for improvement;

3. that, following the Plenary Assembly, the studies shall be continued and a full report prepared 17 months prior to the date of commencement of the WARC HFBC (1993).

DECISION 86

PREPARATION OF A CCIR HANDBOOK ON HF RADIO SYSTEMS DESIGN

(1989)

CCIR Study Group 6,

CONSIDERING

(a) the existence and development of computer-based methods associated with HF radio systems within the CCIR Study Groups;

(b) that there is a need for a single CCIR Volume encompassing the many aspects of HF radio systems and their design,

DECIDES

1. to establish a group of experts within Study Group 6 to prepare an appropriate handbook on HF radio systems design aspects within the competence of that group;

2. to invite Study Groups 3, 8 and 10 to nominate one or more experts familiar in the design and operation of radio systems to join this group of experts;

3. that the group of experts shall report to the next meeting of Study Group 6 on the preparation and progress relating to the production of the new handbook.

[redacted]